DIAGNOSTIC AND PROOF LOAD TESTS ON BRIDGES

EDITED BY: Fikret Necati Catbas and Eva Lantsoght

frontiers Research Topics

About Frontiers

Frontiers is more than just an open-access publisher of scholarly articles: it is a pioneering approach to the world of academia, radically improving the way scholarly research is managed. The grand vision of Frontiers is a world where all people have an equal opportunity to seek, share and generate knowledge. Frontiers provides immediate and permanent online open access to all its publications, but this alone is not enough to realize our grand goals.

Frontiers Journal Series

The Frontiers Journal Series is a multi-tier and interdisciplinary set of open-access, online journals, promising a paradigm shift from the current review, selection and dissemination processes in academic publishing. All Frontiers journals are driven by researchers for researchers; therefore, they constitute a service to the scholarly community. At the same time, the Frontiers Journal Series operates on a revolutionary invention, the tiered publishing system, initially addressing specific communities of scholars, and gradually climbing up to broader public understanding, thus serving the interests of the lay society, too.

Dedication to Quality

Each Frontiers article is a landmark of the highest quality, thanks to genuinely collaborative interactions between authors and review editors, who include some of the world's best academicians. Research must be certified by peers before entering a stream of knowledge that may eventually reach the public - and shape society; therefore, Frontiers only applies the most rigorous and unbiased reviews.
Frontiers revolutionizes research publishing by freely delivering the most outstanding research, evaluated with no bias from both the academic and social point of view. By applying the most advanced information technologies, Frontiers is catapulting scholarly publishing into a new generation.

What are Frontiers Research Topics?

Frontiers Research Topics are very popular trademarks of the Frontiers Journals Series: they are collections of at least ten articles, all centered on a particular subject. With their unique mix of varied contributions from Original Research to Review Articles, Frontiers Research Topics unify the most influential researchers, the latest key findings and historical advances in a hot research area! Find out more on how to host your own Frontiers Research Topic or contribute to one as an author by contacting the Frontiers Editorial Office: researchtopics@frontiersin.org

DIAGNOSTIC AND PROOF LOAD TESTS ON BRIDGES

Topic Editors:
Fikret Necati Catbas, University of Central Florida, United States
Eva Lantsoght, Universidad San Francisco de Quito, Ecuador

Table of Contents

Editorial: Diagnostic and Proof Load Tests on Bridges

Eva O. L. Lantsoght [1,2]*

[1] Politécnico, Universidad San Francisco de Quito, Quito, Ecuador, [2] Concrete Structures, Department of Engineering Structures, Civil Engineering and Geosciences, Delft University of Technology, Delft, Netherlands

Editorial on the Research Topic

Diagnostic and Proof Load Tests on Bridges

The load testing of bridges is a practice as old as bridge engineering. In the past, load testing was used when a new bridge was built and was a means of demonstrating that the structure was safe for the traveling public. Over time, engineers have developed different practices for load testing, many of which follow on from these traditions as they are based on practical experience, a practice that has influenced current codes and guidelines for load testing. These codes and guidelines use limits based on experience, which may differ across countries, and which may not directly be related to the philosophy of the safety of these design codes. Procedures for the field testing of new and existing bridges have been developed, and over time the range of applications of load tests have grown significantly from simply demonstrating that a bridge is safe for use to determining particular aspects of structural behavior, such as the contribution of non-structural elements (barriers, curbs, etc.) to the overall stiffness of the structure, or transverse load distribution.

There are two main types of load test, diagnostic load tests and proof load tests. Diagnostic load testing is used to evaluate and update the analytical models for the design and assessment of bridges. For new bridges, diagnostic tests can be used to demonstrate that the bridge behaves as designed. For existing bridges, diagnostic tests can be used to update the model that is employed for some sort of decision-making, for example determining the load rating of the bridge, load permits for special loads. Proof load testing is used to demonstrate that a given bridge can safely carry the loads prescribed by the governing code or a specification. A load corresponding to the load combination prescribed by the governing code or specification is applied to the bridge. If the bridge can carry this load without signs of distress, the test is considered to show that the bridge can fulfill specified load requirements.

This Research Topic includes a number of case studies, examples of the load testing of bridges, and discusses potential ways of expanding knowledge of the subject. One of the ways in which load testing has evolved is in terms of the tools that are used to interpret optimal field test results. A contribution by Commander shows the evolution of diagnostic load testing in the US. This article shows how the lines between field testing, structural health monitoring, and non-destructive testing have been blurred, and how these techniques are becoming more and more intertwined. The author illustrates how a bridge engineer can select the right tools in response to test objectives and discusses emerging technologies. From a European perspective, a study by Olaszek and Casas offers practical advice for static and dynamic load tests. This article examines the factors that can result in errors in interpreting test results compared to target values or values derived from a numerical model. Such errors can lead to errors in bridge assessment, and ultimately, wrong decisions.

Another contribution by Shahsavari et al. considers the synergy between structural health monitoring and load testing using the Memorial Bridge as a case study.

This bridge has a structural health monitoring system in place, and the study examines the bridge using numerical models. A load test was carried out to calibrate the finite element models and to define post-processing and decision-making tools related to structural performance. Al-Khateeb et al. explore the combination of structural health monitoring and load testing based on the Indian River Inlet Bridge, which has been subject to six load tests since 2012. The authors focus on how a structural health monitoring system can be valuable for repeat diagnostic load tests, giving insights into bridge performance. The authors indicate how repeated diagnostic load tests form an integral aspect of the bridge operation and maintenance strategy. In another case study, Duvnjak et al. discuss a damaged steel railway bridge in Croatia, which was monitored during strengthening works. In this example load testing was used to update the finite element of the bridge, to evaluate its ability to carry the design loads, and to determine the dynamic parameters of the structure.

In recent years load testing is often combined with finite element modeling. Wolert et al. detail a case study of a 100-year-old reinforced concrete flat slab bridge, of which no plans, reinforcement details, or records from the time of construction are available. The contribution shows how the field test results were used to develop a field-verified finite element model of the structure, after which the structure could be load rated. In another article, Lantsoght, de Boer et al. show the advantages and challenges associated with combining proof load testing results and non-linear finite element results, based on the case study of Viaduct De Beek. When compared to linear finite element modeling, the presented method requires more time and effort but may result in a sharper assessment and avoid unnecessary strengthening actions.

Nowadays, load tests on new bridges are not required before they open. However, for bridges using novel materials or structural systems, it is good practice to conduct a load test to verify its performance upon completion of construction. Alahmari et al. present a case study that involved the diagnostic and proof load testing of a prestressed concrete bridge using high performance concrete girders in span 2 and locally developed ultra-high performance concrete girders in span 1. These field tests allowed for a direct comparison between the high performance concrete girders and ultra-high performance concrete girders. Additionally, the test results provided a baseline of performance, and repeated tests can be used to study durability and possible changes in load distribution over time. Hernandez and Myers report another case study in which diagnostic load testing was conducted on a bridge with self-consolidating concrete (SCC) girders and high-strength self-consolidating concrete girders. The focus of the study is the transverse load distribution, and the results from the field test are compared to distribution factors obtained with a finite element model and AASHTO LRFD Bridge Design Specifications. The authors show that the distribution factors from AASHTO LRFD result in larger values than the field test and that no difference in behavior can be observed between the SCC and conventional concrete members.

Wenner et al. show the results of load testing of the Itz Valley Railway Viaduct. The goal of this case study was to determine the longitudinal pier stiffness, to show whether load testing can also be used to learn more about the properties of the substructure.

For this purpose, diagnostic load tests and breaking tests were carried out, and the results of these experiments were compared to numerical predictions. Diagnostic load tests can be used to identify composite action, as demonstrated by the three case studies presented in Yarnold et al.. In many existing bridges the level of composite action may be unknown, and the authors explored how load testing can be used to identify composite action, discussing the advantages and disadvantages of these diagnostic load tests. Dong et al. show a case study of a concrete highway bridge, where a static load test was used to determine the live load distribution factor and the load rating factor, and the characteristics of the model were determined through the use of different truck-load and speed cases. Zhou and Guzda show a case study of proof load testing on a prestressed girder bridge, where uncertainties arose with regard to the shear capacity of the dapped ends of the prestressed girders.

Over time, the importance of measurements during load testing has also increased. While traditional load testing may be limited to a single deflection measurement, one can now find reports from load tests with more elaborate instrumentation, which can address a number of elements of structural behavior. When undertaking proof load testing, the importance of measurements lies is connected to verifying the stop criteria, as shown by Lantsoght, Yang et al.. This research study examines current stop criteria for proof load tests for flexure, and derives new stop criteria for strain and crack width to avoid a flexural failure during a proof load test. The proposed stop criteria were verified by field tests and the results from laboratory experiments.

To align the safety philosophy of design codes with the practice of bridge load testing, concepts of structural reliability are combined with load testing. Schmidt et al. show how concepts of structural reliability can be used to develop an approach to probabilistic decision analysis. This approach encompasses two parts: (1) providing a basis for decision-making during a proof load test to ensure a safe and efficient execution; and (2) identifying efficient strategies for bridge reclassification, accounting for the available information obtained for load testing, monitoring, and modeling.

The papers in this Research Topic present practical insights into the current state of bridge load testing and show how this practice has evolved.

AUTHOR CONTRIBUTIONS

The author confirms being the sole contributor of this work and has approved it for publication.

ACKNOWLEDGMENTS

suggesting this Research Topic and his advice and guidance during the development of this collection of articles.

Conflict of Interest: The author declares that the research was conducted in the absence of any commercial or financial relationships that could be construed as a potential conflict of interest.

Identification of Composite Action Through Truck Load Testing

Matthew Yarnold[1]*, Thomas Golecki[2] and Jeffrey Weidner[3]

[1] Zachry Department of Civil Engineering, Texas A&M University, College Station, TX, United States, [2] Pennoni Associates, Intelligent Infrastructure Systems, Philadelphia, PA, United States, [3] Department of Civil Engineering, The University of Texas at El Paso, El Paso, TX, United States

The continual increase of truck weights on our transportation system is a growing concern among bridge engineers. The load carrying capacity of the structures within the system must withstand this ever-growing demand. For multi-girder steel bridges, the load carrying capacity is heavily influenced by the presence of composite action between the girders and the concrete deck slab. While detailing to ensure reliable composite action is typically included in new designs, for many existing structures, the owner may not fully know the level of composite action. This may be due to administrative issues like insufficient original construction drawings or mechanical issues like breakdown of the shear transfer components. Even in situations where composite action was not intended there exists some partial interaction due to chemical bond and friction. Clearly understanding the presence and reliability of composite action in multi-girder structures is key to managing these structures effectively. This paper explores how load testing has been utilized to identify the level of composite action for existing bridges. The challenges associated with field identification of composite action are presented. In addition, three case studies of truck load testing are discussed. The first case utilized uncontrolled ambient truck measurements of an instrumented structure to field determine the composite behavior. The second and third cases perform a controlled load test with variations in truck weights and positions. Overall, the paper illustrates the advantages and disadvantages of truck load testing for identification of composite action and provides recommendations for future studies.

Keywords: load testing, composite action, bridges, capacity, neutral axis

INTRODUCTION

Bridge load testing is a valuable method engineers utilize for the evaluation of existing structures. Typically, load testing is implemented when analytical rating methods indicate insufficient vertical load capacity. There are two general forms of bridge load testing. The first is diagnostic testing. Diagnostic testing includes the measurement of load effects in bridge members and compares these results with an analytical model (AASHTO, 2018). The tests allow for model calibration and more accurate structural analysis (typically through load ratings). Proof testing is the second form of load testing. In this case, loads that exceed the desired operational load level are applied to the bridge and observations are made to determine if the bridge carries these loads without damage. Loads are applied in increments and the bridge is monitored to provide an early warning of possible distress or non-linear behavior (AASHTO, 2018).

Substantial research has been performed on bridge load testing that specifically address composite action. National Cooperative Highway Research Program (NCHRP) funded a study (Report 306) to correlate bridge load capacity estimates with test data (Burdette and Goodpasture, 1988). A section of the project was dedicated to unintended composite action in beam and slab bridges. Eleven comprehensive experimental studies were compiled that included laboratory and field tests to ultimate capacity. The results indicated that the bond between the beam and deck slab was the most important factor in determining whether a bridge built non-composite could be counted on to act composite. Even though this bond was shown to be very effective in transmitting horizontal shear, the reliability was questioned. It also concluded that the degree of composite action is difficult to quantify and should be regarded as a 'bonus'.

NCHRP 12-28(13)A was another large study on non-destructive load testing (Lichtenstein, 1993). The study indicated that without mechanical shear connection, some composite action exists between the beams and deck slab due to friction and chemical bond. Similar to the prior NCHRP study, it found that chemical bond had significantly more of an effect on composite behavior compared to friction. They indicate that, except for a field test, there is no practical way to ascertain if bond exists and that if the "top flange of a girder is partially embedded in the deck slab, the bond resistance is very effective in promoting the composite action." Bakht and Jaeger (1992) found exception to this during their ultimate load test where the top flanges were partially embedded and no mechanical connection to the deck was provided. In their test, the composite action that existed at service loads broke down at loads approaching failure and did not achieve the ultimate strength of the fully composite section. NCHRP 12-28(13)A presents recommended bond strengths for bridges not load tested. In addition, an analytical method is provided for calculating proof load levels from the results of diagnostic testing.

Chajes et al. (1997) performed experimental diagnostic load testing on a steel girder bridge that was designed as non-composite. Five factors were presented for consideration of unintended composite action in a load rating. This include the current condition, past traffic history, future traffic, structural redundancy and potential for future non-destructive testing. In the bridge they studied, composite action was recommended for the final rating with a higher frequency of inspections to be performed that examine the deck-girder interface.

Jauregui et al. (2000) evaluated two non-composite steel girder bridges through testing to failure. Partial composite action was not only measured through girder strains, but horizontal girder-slab differential displacements. Partial composite action was observed with more composite action present in the exterior girders due to the larger curb and railing. Heavier load had no significant impact on the load distribution and partial composite action of the girder. The transverse load position of the test trucks had a larger impact on the composite behavior.

Work by Barker et al. (1999) for the Missouri Department of Transportation aimed to quantify field test behavior for rating steel girder bridges. The study indicates that unintended composite action may not be reliable during the bridge's service life. As a result, an approach is presented for removal of measured composite action for load rating purposes. Other more recent studies have also evaluated unintended composite action through diagnostic load testing such as Breña et al. (2013), James and Yarnold (2017), and Sigurdardottir and Glisic (2013).

The presented study aims to further the state-of-knowledge with regard to field identification of composite action of steel girder bridges using load testing. An emphasis was placed on quantifying the variability of neutral axis locations and the resulting level of composite action between the beams and deck slab. This research was conducted through three case studies that includes three bridges, designed non-composite, composite, and composite only in the positive moment regions, respectively. Conclusions and recommendations are provided from these three case studies along with review of substantial prior research.

INFLUENCE OF COMPOSITE BEHAVIOR

Truck load testing has repeatedly shown to provide information that can significantly increase the understanding of a structures live load behavior. For a conventional steel girder bridge, there are several areas of uncertainty where a load test can provide refined information. This includes:

- lateral load distribution
- span continuity
- boundary condition stiffness
- dynamic amplification (impact factor)
- section dimensions
- composite behavior

The focus of this paper is the composite behavior between the girders and concrete deck slab. For structures where composite action is in question, load testing can provide valuable information. Two general situations are confronted in a live load test of a girder bridge. The first is a bridge where the girders were not mechanically connected to the deck slab. The intention of the designer is to produce non-composite behavior where the girders and slab act independently, as shown in **Figure 1C**. However, in reality there is some form of partial composite action due to the chemical bond and friction between the girders and deck. The partial composite and full composite strain distributions are illustrated in **Figures 1A,B**, respectively. The second situation is a bridge where mechanical connection of the girders to the deck slab was originally provided. Nevertheless, the concrete deck slab may be degraded or there may be fatigue issues of the shear studs. In this case, a fully composite strain distribution may have been assumed, but in reality slip is occurring producing a partially composite situation.

Identifying the level of composite action can substantially influence the assessment of vertical load capacity of a bridge (typically expressed through load ratings), fatigue life estimate or serviceability checks. Most load tests on assumed non-composite bridges have concluded the structure was composite to some degree, which can increase the load rating (e.g., Chajes et al., 1997; Breña et al., 2013; James and Yarnold, 2017). As stated earlier, the reliability of this composite action at ultimate strength is

questionable (Bakht and Jaeger, 1992; Barker, 2001). Therefore, bridge owners differ in their willingness to accept full or partial composite action for ultimate strength without quantifiable interface shear strength for bridges with unknown connection details.

To further illustrate the impact of composite action between the steel girders and concrete deck slab, a sensitivity study was conducted by the authors to determine the ultimate (plastic) moment capacity of a section as a function of varying levels of composite action. The horizontal shear transferred between the girders and slab (V') was varied for the girder geometry shown later in each case study, denoted here as CS1, CS2, and CS3. Each case study has different girder dimensions, girder spacing and deck slab thickness. They cover a wide range of configurations. Overall, the purpose of the sensitivity study is to illustrate the relative increase in flexural capacity for different levels of composite action. The specific results for each case study are provided in section Case Studies.

The sensitivity study was performed by setting an interface shear force between non-composite, zero interface shear, and fully composite, when interface shear matches the minimum of the steel or concrete strength. In practice this level of composite behavior is determined by the relative stiffness of the interface. This ratio (V'/V) can be considered the level or percentage of composite action. The ultimate strength is then computed as follows. Because the steel section is considered to be at yield stress throughout the cross section, and the net axial force is assumed to be zero, the interface shear is essentially the net axial force in the deck. A neutral axis location can then be found which balances the tension and compression. Finally, the depth of the compression region is determined by assuming a rectangular stress block at $0.85f'_c$ through a thickness necessary to produce a net compression value equal to the assumed interface shear. This stress distribution is then used to determine the resulting flexural moment, i.e., partially composite capacity (M) of the section.

Figure 2 illustrates the relative results, where M_{fc} is the fully composite flexural capacity, V is the fully composite shear force, the minimum of $A_s F_y$ and $0.85f'_c\ b_e t_s$ where A_s is the steel cross-sectional area and F_y is the steel yield stress f'_c is concrete strength, t_s is slab thickness and b_e is the effective deck width. In Case Study 1, the composite section is governed by the steel section, meaning it has a relatively thick deck. The other two case studies are governed by the slab. Because of this, the

change in strength from non-composite to fully composite is more significant for the Case Study 1 cross section. The flexural capacity is roughly 100% greater for the fully composite vs. the non-composite condition in CS1 and roughly 50% greater for CS2 and CS3. Overall, the non-linear relationship shown in **Figure 2** indicates that even a relatively small amount of shear transfer can provide a significant increase in moment capacity, especially for cross sections with thicker decks.

CHALLENGES FOR FIELD IDENTIFICATION OF COMPOSITE ACTION

Measurement of composite action through field instrumentation is more challenging than one might expect. The conventional approach is to measure the longitudinal strain response at multiple positions along the height of a girder cross-section. These measurements are then utilized to identify the neutral axis. It can be observed in **Figure 1** that the neutral axis changes with the composite nature of the system. The increase in composite action causes the neutral axis to move up the cross-section, resulting in a more efficient section. Some studies have measured the relative slip between the girders and deck to identify composite action. However, this has achieved only limited success. The main challenges associated with identifying the neutral axis and resulting level of composite action are listed below followed by a brief discussion of each. Recommendations for dealing with these challenges are included at the end of the paper.

- environmental conditions
- material properties
- geometry
- test setup

Environmental Conditions
Typically, a load test is conducted over a short period in time. As the duration of measurements increase, the level of uncertainty increases due to varying environmental conditions. These conditions can naturally change the behavior. For example, the stiffness of an asphalt wearing surface varies with temperature change. In addition, moisture and humidity can cause corrosion that further restrains bearings producing additional axial force effects.

FIGURE 1 | Strain distribution for **(A)** full-composite, **(B)** partial-composite, and **(C)** non-composite behavior.

FIGURE 2 | Change in moment capacity vs strength of shear interface.
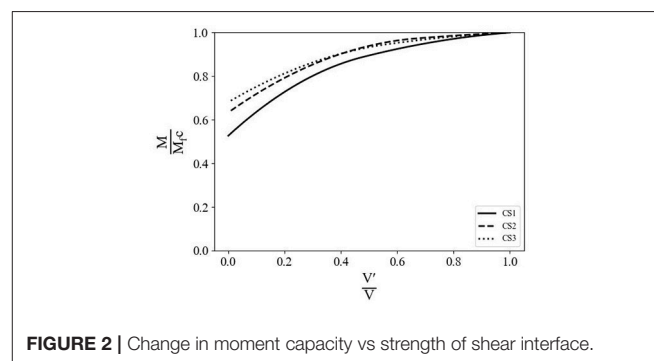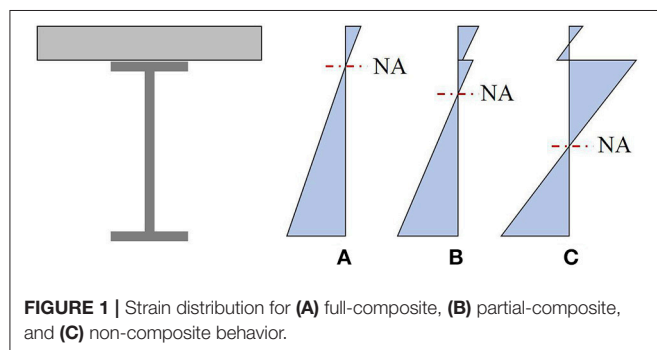
Material Properties

The material properties of concrete and steel can vary from the original design drawings. These properties may have a significant impact on the composite action, both in stiffness and strength. The strength of the concrete is of importance as it affects the plastic neutral axis and total moment capacity of the section. Concrete strength is understood to vary with time resulting in a challenge to predict. The stiffness of the material is also of interest, as it will affect the elastic neutral axis location. In addition, calculation of the transformed section properties using the modular ratio will vary. However, material properties should have minimal impact on the variability of composite action over a short timeframe.

Geometry

Many aspects of the geometry are a challenge. The uncertainty will vary based on the quality of plans available. For field identifying composite action, the deck and girder dimensions are critical. This partly relates back to environmental conditions and if the dimensions have changed over time. Steel girders can have corrosion-induced section loss with breakdown of the paint system. The deck thickness could be different than the plans due to the initial construction, rehabilitations or wear on the top surface from traffic. In addition, the haunch thickness might not be stated on drawings and typically varies in the field, as well as at changes in girder geometry such as cover plates. This is a critical dimension as it determines the "moment arm" between the girder and the deck, and therefore effects both stiffness and strength of the composite section. Additionally, steel sections embedded into the deck can be considered to have a negative haunch. Care should be taken when using traditional capacity equations with these sections as the geometry may make these inapplicable.

The overall geometry of the bridge system adds further aspects to consider. Curved, skewed or even straight bridges in some cases can produce out-of-plane bending or torsion in the girders that must be considered. Another geometric aspect that complicates field testing is the barriers. This and any other elements cast on the deck (sidewalk, median, etc.) can heavily influence the results.

Test Setup

Selection of the local strain gauge locations in each girder cross-section is a major decision for the load test. The literature shows a variety of arrangements. Overall, the design of an instrumentation system needs to consider both composite and non-composite behaviors as a possibility. Placement of a gauge near the neutral axis can produce minimal response. In this situation, it is difficult to confirm the gauge functionality and confirm results with a poor signal-to-noise ratio.

The global spatial resolution needed to identify composite action is another difficult question when designing the instrumentation. The number of cross-sections along a given girder and/or number of girders to instrument can significantly vary based on the objectives of the load test, type of structure and the resources of the project.

Load magnitude is also something that should be considered for evaluating composite action. At higher load levels the

response can be non-linear (Lichtenstein, 1993), increasing the complexity for data interpretation. However, the AASHTO Manual for Bridge Evaluation does not recommend conducting load tests outside the linear elastic range (AASHTO, 2018). In addition, the load position can have an impact on composite action and should be considered (Jauregui et al., 2000). The effective slab width can vary with different load levels due to the transverse spread of the load.

Other challenges for testing can be sensor noise and sensor orientation errors. The gauge resolution varies based on the manufacturer and model selected. The greater the resolution the more difficult it will be to identify reliable strain profiles. The orientation of the sensor can be an issue in harsh environments. If care is not taken to align the sensors parallel to the longitudinal axis of the girders, then this must be accounted for in the future data interpretation.

CASE STUDIES

Presented below are three case studies demonstrating different methods for identification of composite action and the resulting variability of the level of composite action observed. Case Study I illustrates a load test that utilized ambient traffic data to evaluate composite action where no mechanical connection was provided between the girders and deck slab. Case Study II presents a controlled proof load test for a structure designed with shear studs. Finally, Case Study III also conducted the evaluation through a controlled load test, but shear studs are only provided for the positive moment region of the two span continuous girders.

Case Study I

Background and Motivation

The first case study structure is a three span highway bridge, located in Tennessee, USA. The two lane rural bridge, constructed in 1975, spans a total of 40 m (131 ft) and includes eight steel girders, spaced at approximately 1.0 m (40.3 in), with no skew. **Figure 3** shows a typical section of the structure along with the girder numbers.

The motivation to use this structure as a test bed is primarily due to the uncertain composite action present between the steel girders and concrete deck slab. No mechanical connectors (e.g., shear studs) are shown on the design drawings. However, the top flange of the girders is embedded within the deck slab. The owner preferred to consider the bridge as composite, prior to field testing.

Approach

The approach to identify the level of composite action was to instrument two girders (#2 and #4) with the configuration shown in **Figure 4**. Then measurements were recorded during ambient traffic (uncontrolled) for 10 days with a trigger threshold of 20 $\mu\varepsilon$ in either girder. Note that ambient temperature changes induce variations in strain so the trigger threshold was based off a moving average. In the post-processing phase, a zeroing algorithm was implemented so only the relative strain measurements were used for each truck event.

FIGURE 3 | Case Study I bridge typical section.

FIGURE 4 | Strain gauge setup for **(A)** Girder #2 and **(B)** Girder #4.
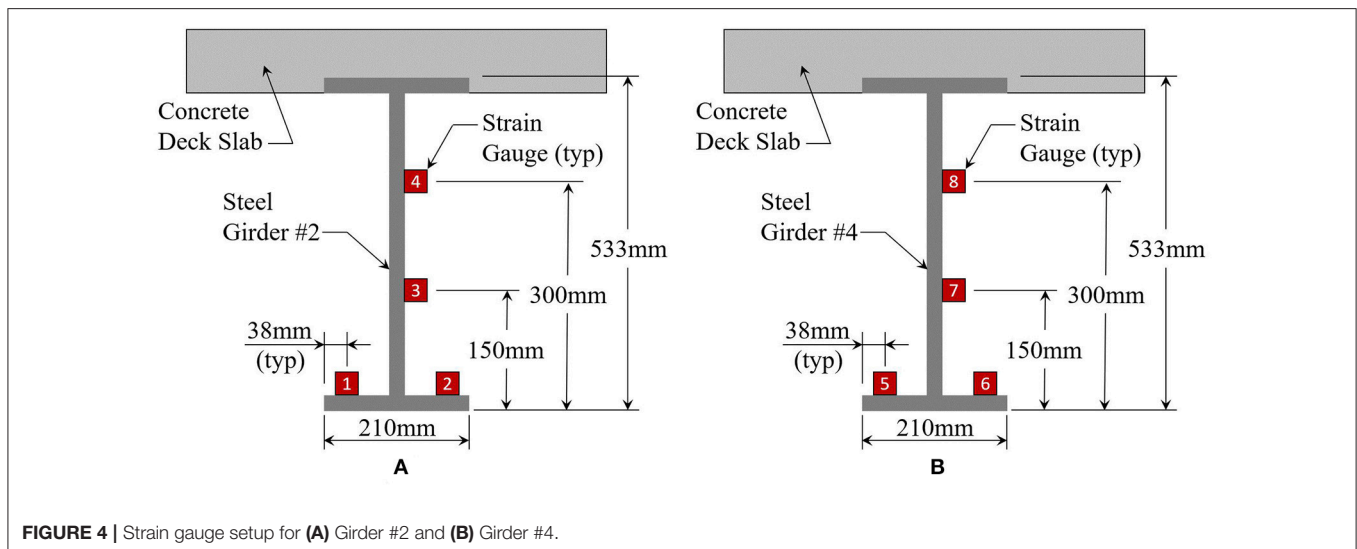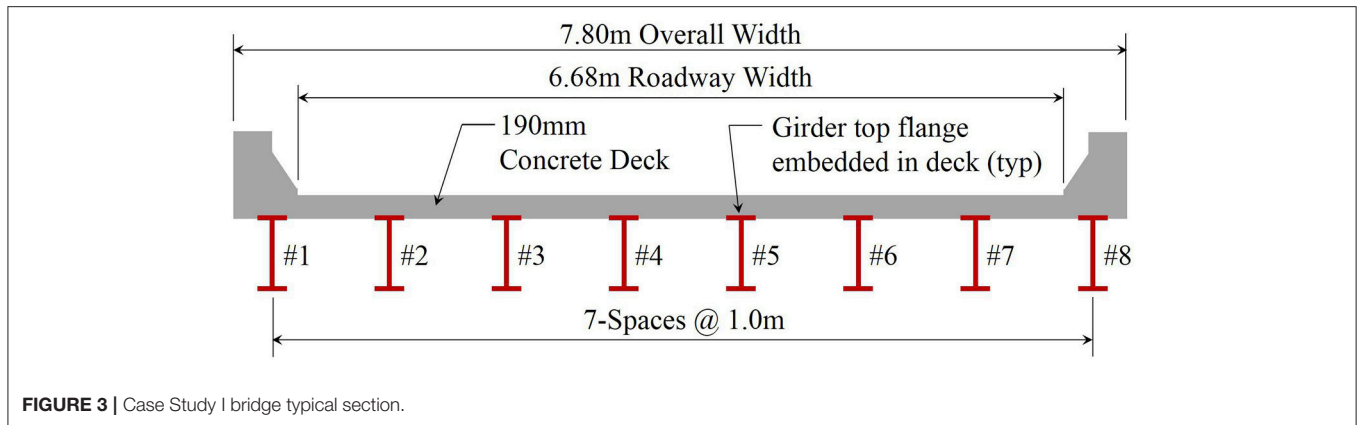
Vibrating wire (VW) strain gauges (SG) were utilized for this study (Geokon Model 4000), which has a resolution of 1.0 με. **Figure 5** shows a photo of one instrumented girder. Campbell Scientific data acquisition equipment was used (CR3000) with dynamic vibrating wire analyzers (CDM-VW305). This allowed for a sampling rate of 50 Hz, which was more than sufficient for the relatively slow vehicle speeds. Power was provided through a 90-watt solar panel that charged a 12-volt battery.

Results

The Case Study I Bridge exhibited composite behavior under ambient loading. This was determined from over 150 recorded truck events (each response >20 με) over the 10 days of measurements. The largest response was 104 με in strain gauge #5 (SG5). **Figure 6** shows the time history plot from this data set (unfiltered). This plot illustrates the quality of data recorded. In addition, the paired response from SG1/SG2 and SG5/SG6 indicates minimal out-of-plane bending was induced.

The conventional approach for identification of the neutral axis using ambient truck traffic is to plot the strain gauge profiles during a significant truck event. Then these lines are projected to find the vertical axis intercept. **Figure 7** represents measurements

from the average of SG5 and SG6 along with SG7 and SG8 over different time intervals during the largest truck events. The height of the girder is 533 mm (21 in) so the neutral axis is clearly in the deck slab indicating composite behavior despite having no shear studs. This would be the common conclusion drawn for most load tests. However, the results from a single truck event are deceiving and do not illustrate the variability of the field identified neutral axis.

To comprehensively evaluate the composite nature of the structure, the neutral axis was projected for all truck events at both girders. The objective was to quantitatively determine the distribution of neutral axis location and the variability in composite action. **Figure 8** provides the overall results. The left side of the figure shows the strain profile for each truck event for both girders (over 300 strain profiles). The projected neutral axis location (y-axis intercept) is also identified. A wide spread of results can be observed. As a frame of reference the plastic neutral axis of the composite section (PC), elastic neutral axis of the composite section (EC), and the neutral axis of the non-composite section (NC) are provide in the center of the figure. In addition, the right side of **Figure 8** provides a histogram of the neutral axis locations. The data indicates a mean neutral

axis location of 534 mm (21 in) with a standard deviation of 52 mm (2.1 in), thus a coefficient of variation (COV) of 0.10. The magnitude of loading subjected to the bridge was in the elastic range so the comparison of measured neutral axis should be with EC and NC. The results indicate composite behavior under service level truck loading. The variability comes from a number of uncertainties (many discussed earlier in the paper). In this particular case some of the primary uncertain parameters are the concrete material properties and fixity of the bearings (which can induce axial force), and the presence of a large concrete barrier near one of the measured girders. Conclusions and recommendations taking into account these results are provided at the end of the paper.

Case Study II
Background and Motivation
The second case study focuses on a typical highway structure in the eastern United States. The structure is a multi-span, simply-supported steel multi-girder bridge with varying span geometries (i.e., straight, skewed, and straight-skewed combination, as shown in **Figure 9**) and lengths [ranging between 21 and 40 m (70 and 130 feet)]. The adjacent twin spans were built in 1983 and include variable, built-up section properties. The structure was designed composite with 152 mm (6 in) tall, 19 mm (3/4 in) diameter shear studs in groups of two to three at a spacing of 380 to 530 mm (15 to 21 inches).

This bridge was selected for field testing for several reasons. Unlike the other case studies presented herein, this test was not conducted specifically to determine whether the bridge behaved in a composite fashion, nor was the test specifically conducted to load rate the structure. The bridge was selected for an international study on bridge assessment. As the bridge was going to be accessed by numerous teams of researchers from around the globe, access was a critical driver. Additionally, the bridge exhibited many performance problems that are common on many operating structures in the United States (e.g., fatigue cracking, bearing deterioration, deck and joint deterioration), making it an ideal candidate for the international study. For the sake of simplicity, testing was limited to one span (identified on **Figure 9**) of a total of eight available spans.

Approach
The instrumentation and testing approach utilized for the structure was in line with the overarching goal of the international study which was to conduct a round robin test on single structure using best practices from other countries. The results presented here were to be considered the "ground-truth." The instrumentation was laid out in a grid, with the following general desired outcomes:

- Provide situational awareness during the live load testing (i.e., safety)
- Function within the situational constraints of the test (i.e., budget, time on site, etc.)
- Facilitate both direct and model-based interpretation of the test results
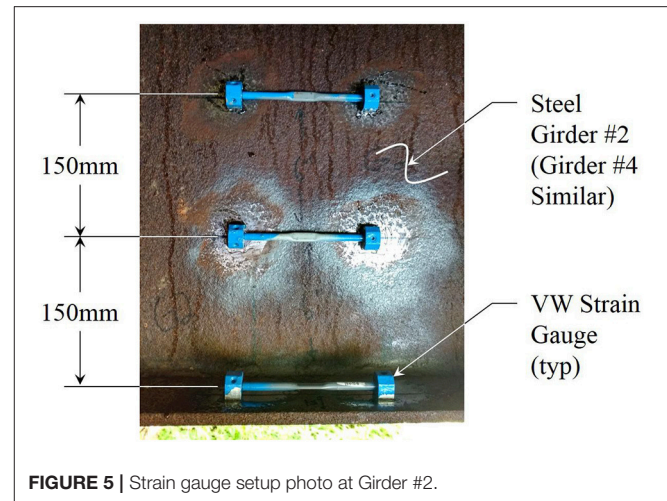
FIGURE 5 | Strain gauge setup photo at Girder #2.

Figure 10 illustrates the instrumentation plan, with sensor configurations at each node that allows for data interpretation at the system, component, and material levels. To that end, each main grid location had two or three longitudinal strain gages to identify demand on the cross section, and level of composite action, as these are good indicators of both system and component level behavior.

The strain sensors were 25.4 mm (1 in) weldable, quarter bridge strain gages from Hitec Products. The sensors were installed per manufacturer specifications on the top of one side of the bottom flange, and 508 mm (20 in) up the height of the web, as shown in **Figure 11**. The budget for the testing did not allow for sensors on both sides of the flange and web, and the time on site prevented installation of sensors on the bottom of the bottom flange. This sparse cross-sectional instrumentation creates uncertainty related to both axial force and out-of-plane bending, but unavoidable in this situation. Due to the unique geometry, each girder has a different overall length with different start and end points for flange transitions on the top and bottom flanges, shown generally in **Figure 12**. This results in seven different cross-section configurations out of a total of 12 instrumented locations. Testing itself consisted of three load stages of three to six dump truck at various load levels, and positions across the deck. The final load level achieved exceeded the proof level load as required by the AASHTO Manual for Bridge Evaluation (AASHTO, 2018), meaning the test served as a proof level load test. Note that after each load stage, the sensor outputs returned to zero, indicating an elastic test.

Results
Longitudinal strains at each location were plotted vs. position on the height of the cross-section. The strain profile was assumed to be linear, and extrapolated to the neutral axis. This analysis was carried out for each load level and load position on the bridge. **Figure 13** shows the linearity plots, a girder cross-section with the location of the elastic neutral axis (EC), plastic neutral axis (PC), and non-composite elastic neutral axis (NC) plotted for reference, and a histogram for experimental neutral axis location
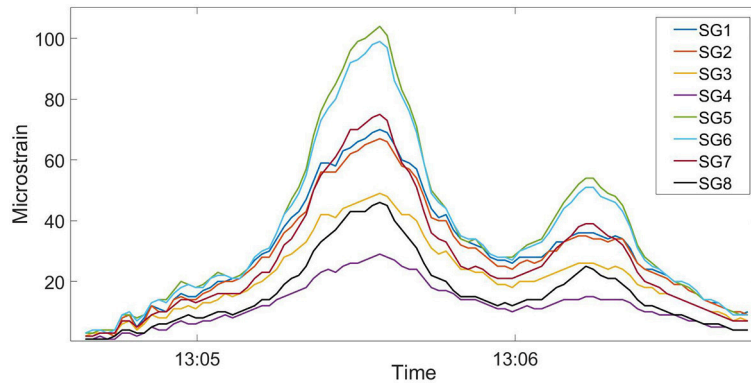
FIGURE 6 | Time history from the largest truck event.
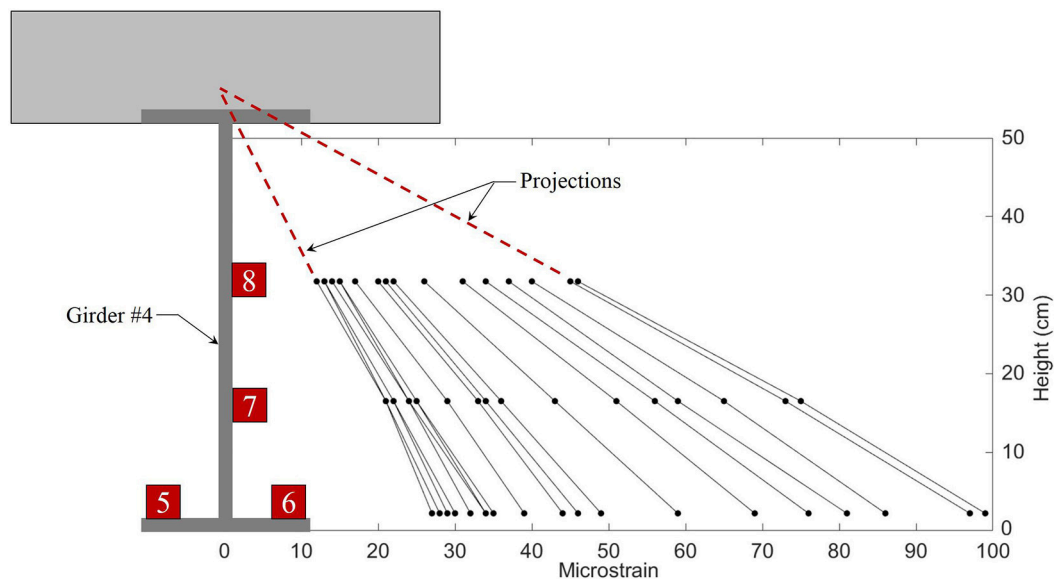
FIGURE 7 | Strain measurements at Girder #4 for the maximum truck event.

at all load stages for the sensors along Girder 1 (the longest exterior girder). These sensors produce consistent composite results across load levels and positions, with the experimental mean occurring almost directly at the composite elastic neutral axis.

The responses at three quarter span for Girder 3 are shown in **Figure 14**. At this location, it can be observed that the neutral axis location is shifted toward the elastic, non-composite neutral axis which indicates a partial loss of composite action. Given that all load levels and positions produced neutral axis location results consistently between the elastic composite and non-composite neutral axis locations, it can be concluded that there was a reduction in composite action at this location that was not observed along Girder 1. This can be concluded in spite of the uncertainty stemming from the sparse cross-sectional instrumentation. There is additional uncertainty in the distribution of neutral axis location which may stem from

material properties, load location and magnitude, the presence of non-structural components, as well as the aforementioned out-of-plane behavior and axial components. At the cross-sectional level, much of this could be reduced by adding additional sensors along the height of the girder and on both sides of the flange and web. In practice, the spatial variation of composite action observed here makes a strong case for a dispersed instrumentation grid where it may be infeasible to heavily instrument every cross-section location.

Case Study III
Background and Motivation
The third case study bridge consists of a two-span continuous structure with spans of roughly 24.4 m (80 ft). The concrete deck is supported on nine kinked steel girders with a spacing that varies from 2.20 m (7 ft 2.5 in) to 2.05 m (6 ft 8.75 in). The variable girder spacing is the result of a tapering lane from an

FIGURE 8 | Measured strains vs height (left), schematic of girder (center), histogram of neutral axis locations (right).

FIGURE 9 | Plan view schematic of Case Study II bridge showing varying span geometry, direction of traffic (red arrows) and test span.

FIGURE 10 | Instrumentation layout of Span 2 Southbound, showing sensor grid (Locations with blue squares are presented in this paper).

FIGURE 11 | Girder cross-section showing sensor locations (typical for all instrumentation locations).

FIGURE 12 | Schematic elevation of girder showing flange transitions with four different section properties per girder.

onramp right before the bridge. The girders are supported by a fixed bearing at the center pier and by expansion bearings at the ends. The concrete deck was initially 190 mm (7.5 in) thick, rehabilitation drawings indicate the top 50 mm (2 in) has been removed and replaced with a 65 mm (2.5 in) thick concrete overlay. A typical girder elevation is shown in **Figure 15**. Note that the positive moment regions are designed as composite with shear studs while the negative moment regions have no shear studs and are indicated as non-composite.
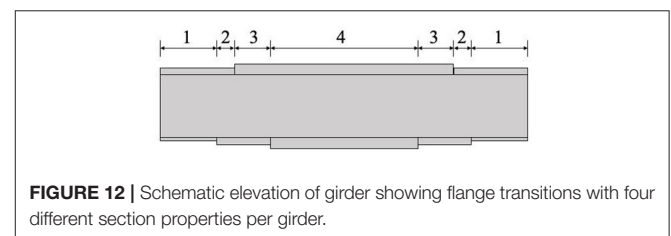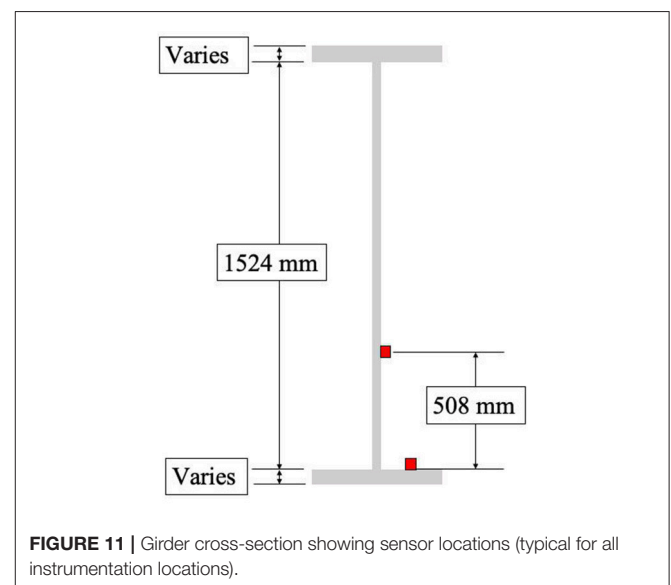
Approach

A load test of this structure was carried out with the intent of capturing moment distribution among the girders to compute a more accurate load rating. In order to achieve this, two cross
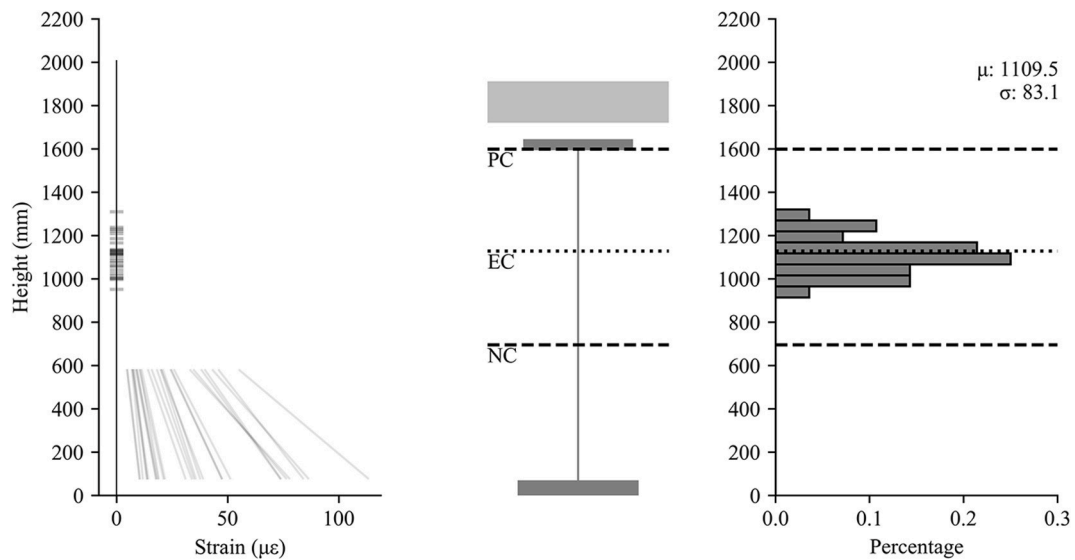
FIGURE 13 | Measured strains vs. height (left), schematic of girder (center), histogram of neutral axis locations (right) for Girder 1.
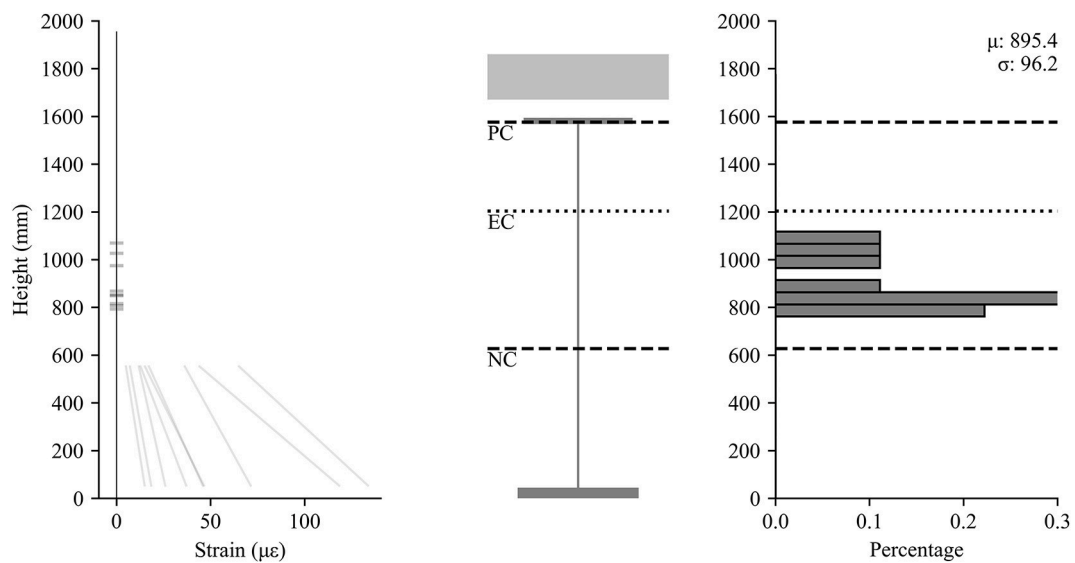
FIGURE 14 | Measured strains vs. height (left), schematic of girder (center), histogram of neutral axis locations (right) for Girder 3 at ¾-span.
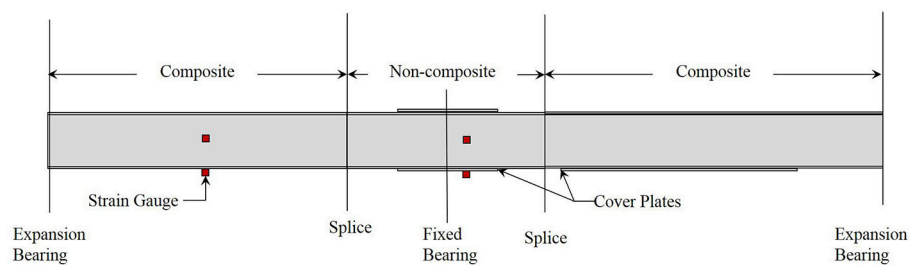
FIGURE 15 | Typical girder elevation (shear studs are only present in the positive moment regions).

sections of the bridge were instrumented with Geokon Model 4000 vibrating wire strain gauges (**Figure 16**). Each girder in the cross section was instrumented as shown in **Figure 17**. The placement of three gauges on the cross section was selected to measure primary bending strains while being able to exclude any out-of-plane moment of the girder webs. This instrumentation also allows for an evaluation of composite action of each girder by linearly projecting strain values to find the neutral axis. Results presented herein focus on composite action, rather than moment distribution.

The load test was conducted using three axle dump trucks with their rear axles placed at quarter-span locations in each lane.

Multi-truck cases were also considered, by placing all three trucks side by side at quarter span locations, and by placing one truck at the center of each span in the same lane. A total of 31 different vehicle placement locations were included in the load test using empty dump trucks. The trucks were then loaded with salt and all tests were repeated. This provided some indication of response linearity while maintain the vehicle configuration. In addition, the variability of composite action with load level was evaluated.

Results

Load test results are shown in **Figures 18**, **19** as strain profiles in each of the nine instrumented girders in the positive and negative
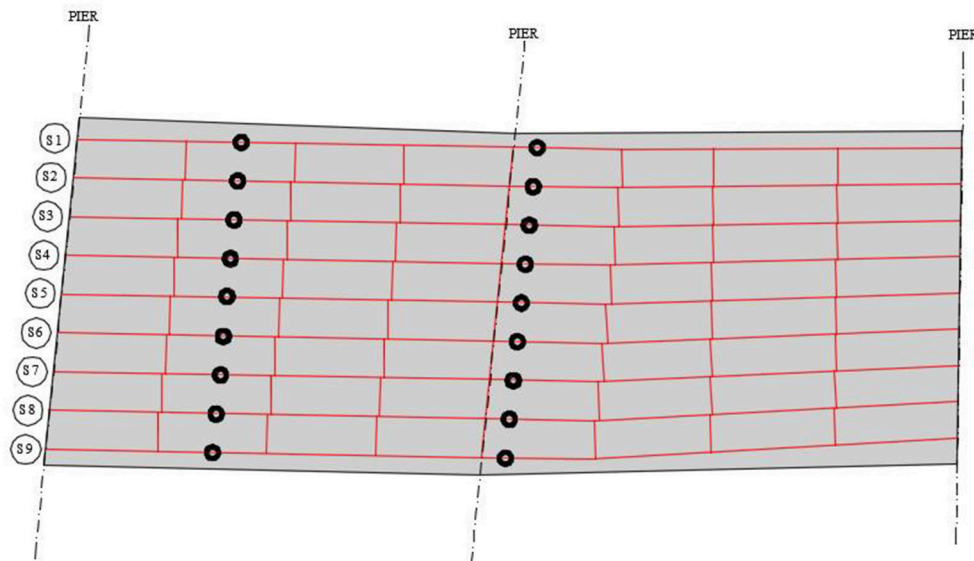
FIGURE 16 | Plan view showing instrumented locations.
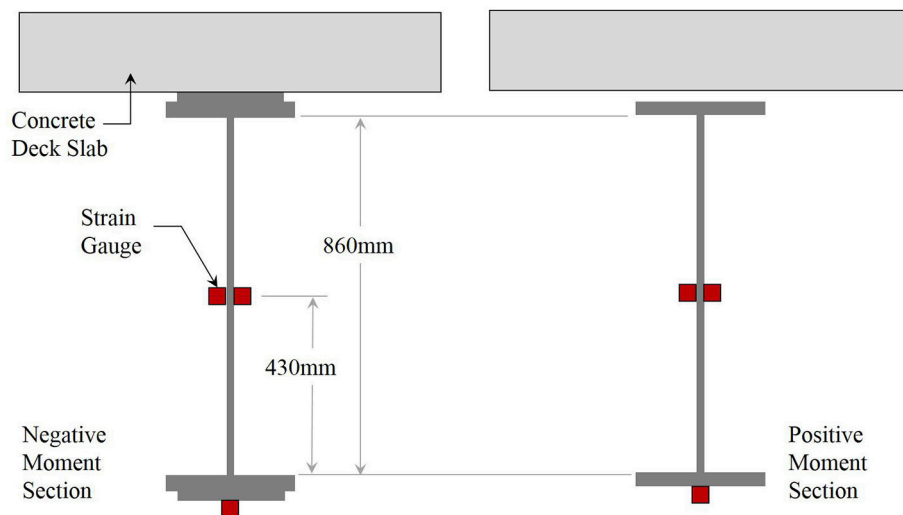
FIGURE 17 | Instrumented cross section details.
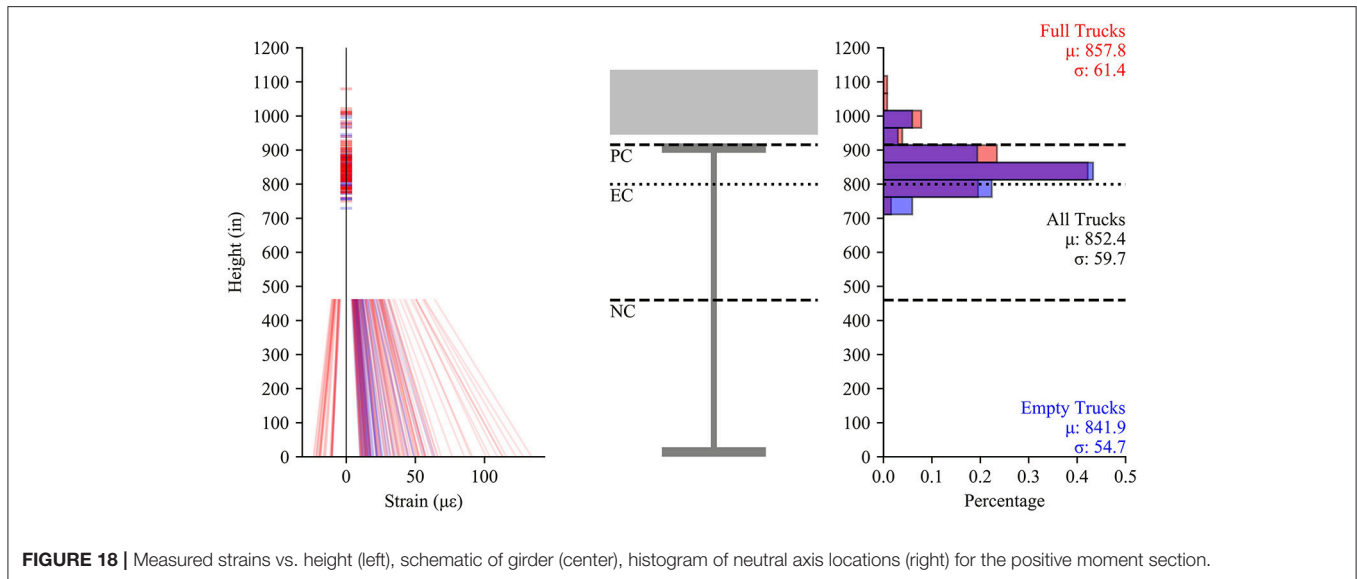
FIGURE 18 | Measured strains vs. height (left), schematic of girder (center), histogram of neutral axis locations (right) for the positive moment section.
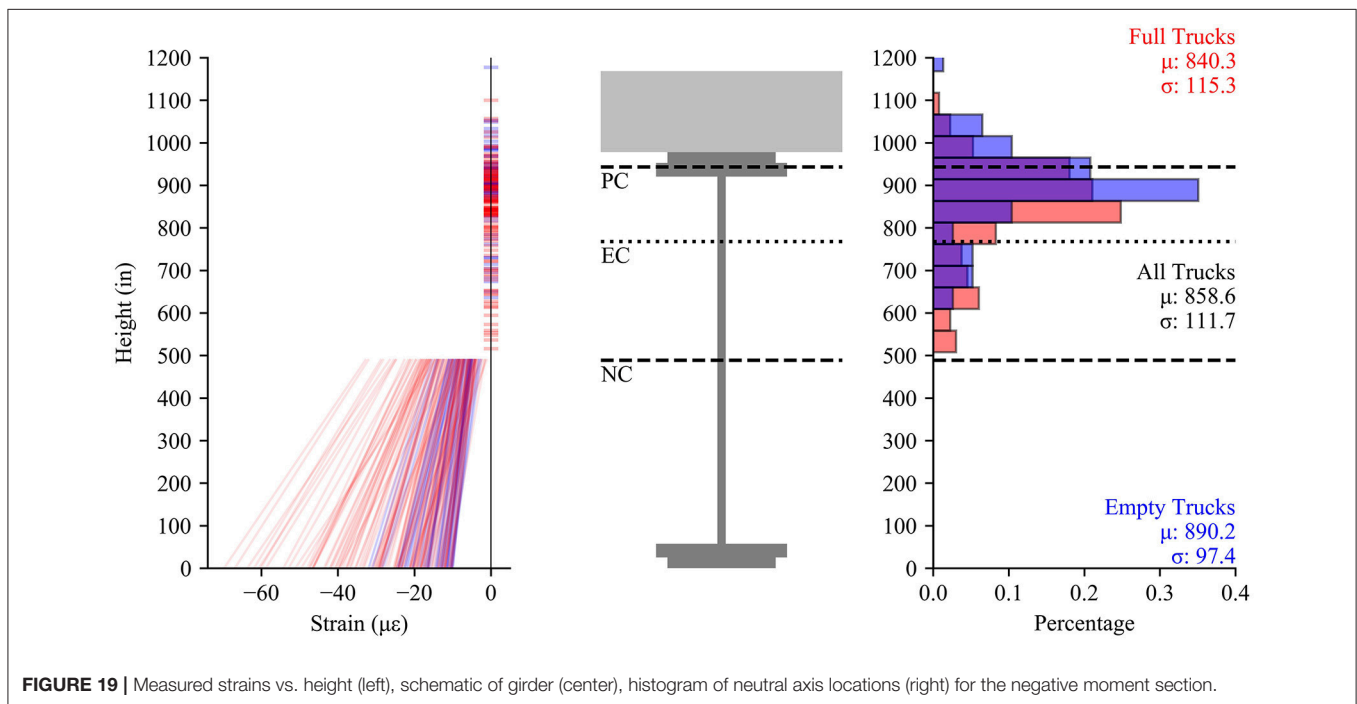
FIGURE 19 | Measured strains vs. height (left), schematic of girder (center), histogram of neutral axis locations (right) for the negative moment section.

moment regions, respectively for load cases which generated at least 10 $\mu\epsilon$ in the bottom flange. From **Figure 18** it is seen that the positive moment region is primarily composite. The neutral axis locations are consistently near the bottom of the top flange with a coefficient of variation (COV) of 0.07. The negative moment region (**Figure 19**) also behaves with essentially composite behavior in most girders but with a wider variation, COV of 0.13. In both **Figures 18**, **19** reference lines are drawn indicating the location of the non-composite neutral axis (NC), elastic neutral axis (EC), and plastic neutral axis (PC). The first interior girders are the closest to non-composite with neutral

axis locations in the upper half of the web, but in all other girders, the neutral axis location is near the bottom of the top flange. The lack of shear studs in the negative moment region did not create non-composite behavior in this region. Rather, the reinforced concrete deck stiffness in tension and bond to girders was adequate to exhibit essentially composite behavior. Both regions show an average neutral axis location between the theoretical elastic and plastic neutral axes. Comparing this data between the full and empty trucks (approximately twice the total loading) shows linear behavior, and similar neutral axis trends.

CONCLUSIONS

The level of composite action between the steel girders and deck slab can have a significant impact on the assessment of vertical load capacity. Truck load testing has been utilized to field identify composite action (or lack thereof) for bridges with capacity concerns. The literature and three case studies performed as part of this research have shown varying degrees of success for reliably identifying the composite nature of girder bridges. Even simple structures, such as Case Study I, show appreciable variability in the results.

Variability in field identified composite action results comes from a wide range of parameters. These include environmental conditions, material properties, geometry and the test setup itself. Reducing uncertainty due to environmental conditions is typically mitigated through relatively short test durations. Material property uncertainties can be addressed with specimen testing (e.g., concrete cylinder tests) or non-destructive evaluation techniques. The desired accuracy and resources of the project will dictate if this should be performed. Uncertainties associated with the geometry and the test setup itself can be dealt with through carefully designed field measurement strategies. General recommendations are provided below as a result of a substantial literature review and the three case studies performed.

RECOMMENDATIONS

These recommendations are intended to provide a strategy for field identification of composite action using truck load testing. Recommendations are provided for local measurement of the girders, global measurement across the structure, truck loading, and data processing. These recommendations are intended to be comprehensive and minimize uncertainties to a significant extent, while maintaining a realistic instrumentation plan. The authors realize resources, access, etc. vary per project and all components described below may not be addressed (similar to the case studies). However, it is beneficial to understand the capabilities of different test setups for planning and future data interpretation.

Local Measurement

The girder cross-sections instrumented should address the potential for out-of-plane bending and signal-to-noise levels. Out-of-plane bending is more prevalent in curved and skewed structures; however, it may not be negligible for girders with slender elements. Therefore, it is recommended to place sensors on opposite sides of the flange and web (**Figure 20**). This allows future averaging of the data. Note that if resources are limited the bottom flange can be instrumented at the center of the bottom. The setup utilized for Case Study II is not recommended because it was susceptible to issues with out-of-plane bending.

Measurement signal-to-noise ratios can be an issue if sensors are placed near the neutral axis. The design of an instrumentation system should consider both composite and non-composite behaviors as a possibility, therefore measuring strain in the upper half of the web or on the bottom of the top flange (for interior girders) can inadvertently locate a gauge near the neutral axis

FIGURE 20 | Recommended strain gauge locations to identify the neutral axis for **(A)** interior steel girders and **(B)** exterior steel girders with symmetric cross-sections.
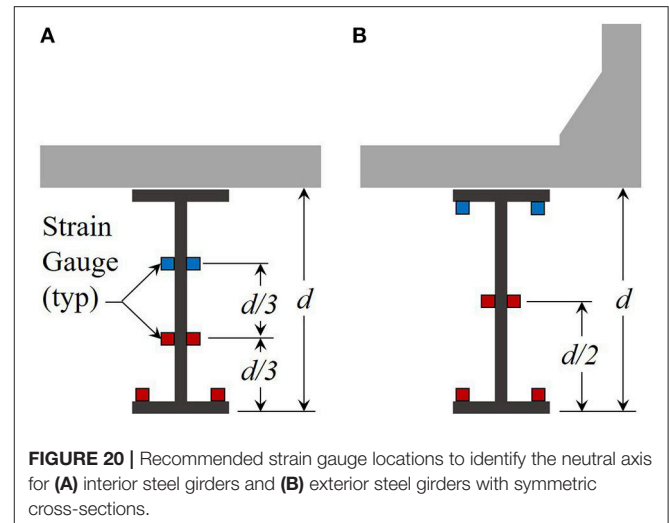
producing very little response. This makes it difficult to confirm the gauge functionality. The minimal response also introduces more error in the projection of the strain profile to identify the neutral axis.

For example, it is recommended for a steel interior girder with a symmetric section to implement strain gauges on both sides of the top surface of the bottom flange along with a pair of gauges on the web at approximately 1/3 the girder depth (*d*) from the bottom flange. **Figure 20A** illustrates this setup with the sensors shown in red. Ideally, another gauge pair would be placed at 2/3 the web depth if resources allow (**Figure 20A** blue sensors). For the exterior girder, it is recommended to move the web gauges up the height of the web due to the presence of a barrier (**Figure 20B** red sensors). Even minimal composite action will move the neutral axis high on the section so signal-to-noise should be adequate at that location. This should allow for better linear interpolation and identification of the neutral axis, minimizing the effects of sensor noise. Again, a second pair of gauges may be placed on the web if resources allow (**Figure 20B** blue sensors).

Note that if the girders are not symmetric due to different flange sizes, then the web gauges should be adjusted accordingly to avoid potential neutral axis locations.

Global Measurement

Spatial location of the instrumented girder cross-sections is a critical aspect of the load test. It is recommended to provide locations that have sufficient response (e.g., mid-span of a simple span structure). The literature shows that this is commonly applied with the exception of tests that had access restrictions. The spatial resolution of the testing is also important and widely varies among studies. It is recommended to instrument at least two different girders and to provide measurements at a minimum of two different bridge cross-sections for identification of composite action. Following the local measurement recommendation provide above, that would equate to a minimum of 16 strain gauges. This is very realistic to incorporate into a load test.

The girders can be subjected to axial forces from live loading in cases where the bearings are restrained. The eccentricity of the support conditions can induce axial forces from vertical loading. In these cases, it is recommended to consider placement of another strain gauge setup near the end of the girder to minimize flexure. This should allow for measurement of the axial contribution (Barker, 2001). Another option to identify the bearing stiffness is to leave the setup but include thermistors to measure the temperature changes. Then record measurements throughout several days and compare the thermal input with the strain responses (Yarnold and Dubbs, 2015). Mechanical strain measurements will indicate the magnitude of boundary condition restraint.

Truck Loading

For a controlled truck load testing (diagnostic or proof) it is recommended to vary the truck magnitudes and positions. There is variability in the data and it is best to have statistically sufficient data for future processing. The final truck weight should be well above service load levels. As stated earlier, the reliability of the composite action results are up to the magnitude of test truck. It is recommended to utilize the heaviest truck that can safely be justified for the test.

If controlled truck load testing is not possible, then ambient data can be utilized as illustrated in Case Study I. The results are more limiting in that the magnitude of vehicles crossing the structure are not controlled. In addition, the vehicle weight is not known for each recorded truck event. However, estimates can be back-calculated. Another option worth considering in this situation is to orchestrate a heavy vehicle to make passes across the structure with the bridge operational. This will supplement the ambient data and ensure several truck events with sufficient response.

Data Processing

Once strain data is acquired, care should be taken in data processing to ensure accuracy in the analysis. Depending on the location of loading and the location of instrumentation,

there may be test data with very low magnitude responses, as in the case studies above. Data points of less than a specific threshold strain in the bottom flange are not used because poor signal quality can introduce errors in locating the neutral axis. It is also recommended to choose a consistent axis system between all instrumented locations that is maintained through changes in cross section configuration. Selecting the bottom of web as a reference location avoids the need to adjust the height of gauges relative to different bottom flange thicknesses. This is another benefit to instrumenting on the top of the bottom flange. Lastly, care should be taken in computing cross section parameters such as reference neutral axis locations and section strengths, especially when the cross section configuration is non-standard. For example, when the top flange is embedded in the deck, this is essentially a negative haunch which may invalidate some of the standardized equations.

AUTHOR CONTRIBUTIONS

All authors have contributed to the contents within this paper. The lead for Case Study I, II, and III was MY, JW, and TG, respectively. The literature review was mostly performed by MY. Statistical analysis and figure development was primarily conducted by TG. All the authors developed the overall challenges, conclusions, and recommendations.

FUNDING

REFERENCES

AASHTO (2018). *The Manual for Bridge Evaluation, 3rd Edn*. Washington, DC.

Bakht, B., and Jaeger, L. (1992). Ultimate load test of slab-on-girder bridge. *J. Struct. Eng.* 118, 1608–1624. doi: doi: 10.1061/(ASCE)0733-9445(1992)118:6(1608)

Barker, M. G. (2001). Quantifying field-test behavior for rating steel girder bridges. *J. Bridge Eng.* 6, 254–261. doi: 10.1061/(ASCE)1084-0702(2001)6:4(254)

Barker, M. G., Imhoff, C. M., McDaniel, W. T., and Frederick, T. L. (1999). *"Field Testing and Load Rating Procedures for Steel Girder Bridges,"* in RDT99-004. (MoDOT).

Breña, S., Jeffrey, A., and Civjan, S. (2013). Evaluation of a noncomposite steel girder bridge through live-load field testing. *J. Bridge Eng.* 18, 690–699. doi: 10.1061/(ASCE)BE.1943-5592.0000398

Burdette, E. G., and Goodpasture, D. W. (1988). *NCHRP Report 306: Correlation of Bridge Load Capacity Estimates with Test Data*. Washington, DC: Transportation Research Board.

Chajes, M., Mertz, D., and Commander, B. (1997). Experimental load rating of a posted bridge. *J. Bridge Eng.* 2, 1–10. doi: 10.1061/(ASCE)1084-0702(1997)2:1(1)

James, E. D., and Yarnold, M. T. (2017). Rapid evaluation of a steel girder bridge: case study. *J. Bridge Eng.* 22:05017013. doi: 10.1061/(ASCE)BE.1943-5592.0001151

Jauregui, D. V., Yura, J. A., Frank, K. H., Wood, S. L., and Jirsa, J. (2000). "Measurement-Based Evaluation ofNoncomposite Steel Girder Bridges," in *FHW A/TX-0-1746-1*.

Lichtenstein, A. G. (1993). *NCHRP 12-28(13)A: Bridge Rating Through Nondestructive Load Testing*. Washington, DC: Transportation Research Board.

Sigurdardottir, D. H., and Glisic, B. (2013). Neutral axis as damage sensitive feature. *Smart Mater. Struct.* 22:075030. doi: 10.1088/0964-1726/22/7/075030

Yarnold, M. T., and Dubbs, D. C. (2015). Bearing assessment using periodic temperature-based measurements. *Transport. Res. Record J. Transport. Res. Board* 2481, 115–123. doi: 10.3141/2481-15

Practical Considerations Regarding Results From Static and Dynamic Load Testing of Bridges

Piotr Olaszek[1]* and Joan Ramon Casas[2]

[1] *Road and Bridge Research Institute, Warsaw, Poland,* [2] *Department of Civil and Environmental Engineering, Universitat Politècnica de Catalunya-BarcelonaTech, Barcelona, Spain*

Bridge tests are a helpful tool for bridge assessment and evaluation. Both in the case of a static and dynamic load testing, each element of the test: the load selection and application, the creation of a numerical model to follow the progress of the test or to check the validity of the test results, the measurement process itself and the comparative analysis of experimental results and calculations could be a source of errors in the bridge final evaluation if these errors and uncertainties are not properly considered. The article presents some of the most important factors that may bring errors in the interpretation of the test results and their comparison to targeted values or values derived from a numerical model. This, at the end, may result in the adoption of decisions that are not accurate and appropriate. The selected sources of feasible errors are presented with the division into static and dynamic loading tests. The presented examples of bridge load testing show how the use of improper test methods could lead to significant errors in bridge assessment and evaluation and, consequently, to wrong decisions.

Keywords: bridges, diagnostic, proof, static, dynamic, load testing, errors, uncertainty

INTRODUCTION

The role of the test loading research in the bridge management system is significant in the world. The publication (Casas, 2006; Wiśniewski et al., 2012) presented the current situation and future trends related to the assessment of the condition and bearing capacity of a structure. The importance of diagnostic test loading was emphasized to be the most accurate tool to assess the structure's bearing capacity. The method of bridge bearing capacity assessment which integrates analytical methods with experimental tests is particularly useful and is verified by test loading research (Wang et al., 2011).

The basic division of test loading is made on the basis of the load variations in time:

- static load testing,
- dynamic load testing.

There are three types of tests distinguished due to the method and purpose of testing:

- diagnostic load testing (also called supplementary load testing) carried out in order to assess the carrying capacity of a bridge structure in service, based on an integration of the structure numeric analysis results and load tests-(Institution of Civil Engineers and National Steering Committee for the Load Testing of Bridges, 1998).
- proof load testing carried out in order to assess the carrying capacity of a bridge structure in service, based on testing the structure under increasing load until the structure's non-linear response to the increasing load can be observed (Faber et al., 2000; Casas and Gomez, 2010; Casas and Gómez, 2013; Wiśniewski et al., 2012).

- acceptance tests carried out before a bridge structure is approved for use; it's similar to diagnostic load testing due to the method of the results analysis, and similar to proof load testing but with the level of the load reaching the design load and not going beyond this point.

Regardless of the type of bridge tests and the purpose of performing these tests, it should be strongly taken into account that the test results are always subject to undesired errors. The impact of these errors on the outcome of the final evaluation of the bridge depends on many factors. An important element of the research is to find the causes of errors and to estimate their influence on the final uncertainty of the bridge evaluation, or to try to avoid them by taking the appropriate solutions during the execution and analysis of the test results.

Analyzing the causes of errors related to various elements of the bridge evaluation process by a loading test, some of them appear during the preparation and execution of the test, meanwhile others are derived in the posterior analysis of the results. We can distinguish the following causes:

- measurement errors related to the measuring equipment used;
- method errors related to inaccuracies in the definition (standardization) of a particular test method;
- modeling errors in the numerical model used for comparison in diagnostic and acceptance tests;
- environmental errors related to disturbances from changes in temperature or external vibrations unrelated to the load of the tested bridge;
- analysis of the results from the measurements.

The individual errors may be random or systematic. Based on the recognition of error sources, it is possible to estimate the uncertainty of individual elements of the loading test (Guide, 2010).

Figure 1 presents a block diagram of static test loading process during diagnostic tests of a bridge structure with marked sources of the bridge assessment uncertainty, while **Figure 2** shows analogous scheme in case of dynamic test loading. The diagrams were developed by analogy or on the basis of the diagram presented in the norm (ISO 18649, 2004).

UNCERTAINTY DURING LOAD TESTING

Moon and Aktan (2006) discuss the state of the art related to the structural identification of constructed civil systems. They pointed out that constructed civil systems cannot be isolated from sources of uncertainty during the structural identification process. Dynamic and static load testing is one of common experimental technologies applied for structural identification. In Goulet and Smith (2013) is presented the fact when system identification methodologies are used to interpret measurement data taken from structures, uncertainty dependencies are in many cases unknown due to model simplifications and omissions.

In this article, attention is paid to some errors of the preliminary measurement data analysis that may bring errors in the interpretation of the test results and their comparison to

FIGURE 1 | Block diagram of static test loading process during diagnostic tests of a bridge structure; developed by analogy with the diagram from the norm (ISO 18649, 2004).

FIGURE 2 | Block diagram of dynamic test loading process during acceptance tests of a bridge structure; developed on the basis (ISO 18649, 2004).
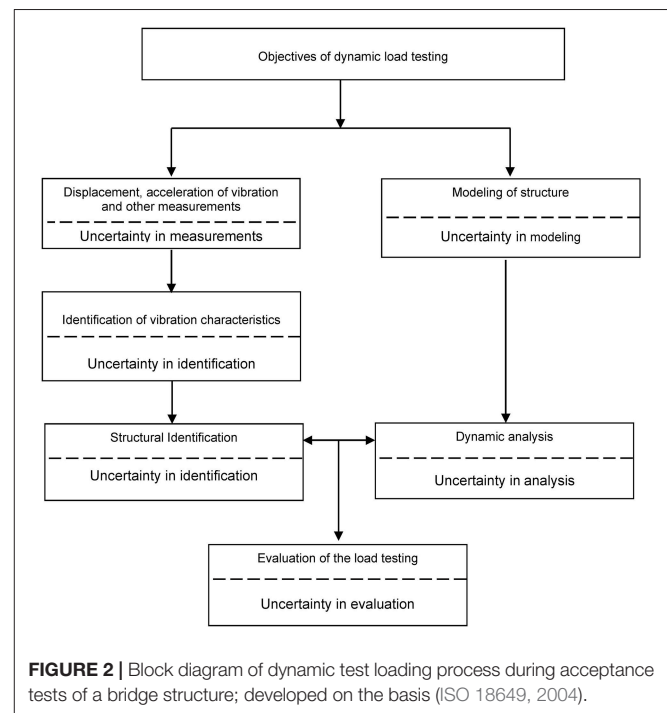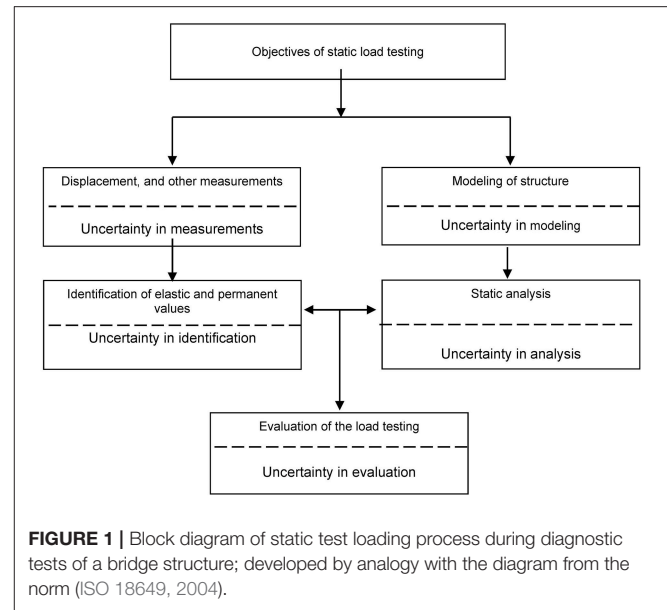
targeted values or values derived from a numerical model. Many of those kinds of errors are not dealt with in other publications.

The notion of measurements uncertainty is relatively well-known and often taken into account. All factors should be taken into consideration while analyzing the uncertainty of tests.

In the case of static tests, load application can last for long time periods and, therefore, the environmental effects with their inherent uncertainty should be considered in the analysis. For dynamic tests, although environmental, and other external effects

will almost not affect the results of a particular test, due to the short time of application of the load, other uncertainties regarding the load level, load frequency,... must be considered. This is particularly true in the case that the excitation is achieved by means of vehicle passages or by ambient vibration (wind, ambient traffic,....). Of course, it should be noted that for the particular test at a defined point in time, the dynamic characteristics of the bridge have been determined under specific environmental conditions and may be different under different conditions of temperature and humidity. Therefore, appropriate corrections should be carried out when comparing dynamic parameters obtained in particular tests performed in different times of the year.

The execution of a numerical model to design the test and to analyse the results afterwards is also subject to several uncertainties regarding the mechanical properties of the materials as well as the inherent simplifications assumed in the modeling.

While selecting measurement methods for the static load testing it is important to consider not only the measurements uncertainty, but also the possibilities of making an analysis of the structure's displacements in on-line mode. The load is applied in accordance to a loading scheme and held for a certain time period. The duration of the test and the accuracy of the results will depend on the time the load should be held until stabilization of the outputs. The early removal of the load before the permanent or stationary value is reached can lead to important errors.

UNCERTAINTY OF MEASUREMENTS AND THEIR RESULTS ANALYSES

At the beginning it is necessary to mention one of the basic rules of metrology—completely accurate measurements do not exist—in practice their results are affected by errors whose sources are of numerous characters. Taylor (1997) points out that errors in scientific measurements are not mistakes, you cannot eliminate them by being very careful. The best you can hope to do is to ensure that errors are as small as reasonably possible and to have a reliable estimate of how large they are.

A measurement makes sense only when the inaccuracy of its result can be determined. It is possible to assess the uncertainty of individual measurements on the basis of recognized sources of errors, and this is widely known and applied (Guide, 2010). Basic error categories related to measurement equipment include:

- assembly errors–resulting from the inaccuracies in assembly of transducers, for example: shifting of measurement points in relation to theoretical ones or non-parallel transducer positioning to the measuring direction;
- instrument adjusting errors (the process of instrument adjusting is often determined as a pre-adjustment calibration)-resulting from application of inaccurate standards (calibrators) or adjusting in the points of measuring range different from real measuring points;
- non-linearity errors–resulting from the deviation of the sensor output curve from straight line specified during adjustment

process; that error can be decreased by applying adjustment curve instead of straight line;
- environmental errors–resulting from the uncontrolled influence of the temperature, sunshine or wind to measurement equipment.

The authors' own experience leads to the conclusion that the errors directly related to the measurement equipment are not the basic measurement-related reason of possible inappropriate assessment of a bridge. Other reasons might be more significant, for example those related to environmental conditions or, in the case of displacement measurements, to the selected point of reference (considered as of null displacement).

There are various systems of transmitting the displacements of the examined girder to the point of the sensor location which are used in case of the measurement of displacements and application of mechanical sensors located in the area under the tested span. The most popular ones include:

- a wire attached at one end to a girder and the other end to a spring fixed at the sensor location point,
- a wire attached at on end to a girder, while the other end is loaded with a weight hung at the sensor,
- special scaffolding erected under the bridge where a sensor reaching the girder is mounted.

In the first system, errors were observed resulting from not taking into account the change in the force pulling the wire from the stretched spring and the change in the wire length resulting from that. The errors related to not taking into account the change in the wire length height—all resulting from the changes in temperature—can be observed in all the systems.

In case of the measurement of displacements by geodetic methods considerable errors can result from taking only a tripod (of a total station or a leveling instrument) as a reference point, without control readout of prisms or reference level staff.

Environmental errors are connected with the state of surrounding conditions during the tests. In case of static load tests temperature can have a particular impact on the measurement system as well as on the measured levels. In case of dynamic load tests, any errors caused by temperature changes during the tests can be ignored due to basically short time of the performed tests. However, it should be analyzed carefully the comparison of results from dynamic tests carried out at different times during the year. Temperature and humidity may affect the value of the dynamic parameters that are usually taking for damage detection.

In case of static load testing considerable errors might be also related to an error in determining the bridge stabilization time while identifying the permanent and elastic values (it will be discussed in detail on the example of static tests in chapter 4).

Other errors include the use of simplifications such as determining the deflection of girders only on the basis of the measurement of their displacements without any correction taking into account the displacement of the bearing points. This is important when conducting tests with a considerable level of load (proof loading tests) and comparing the deflection values obtained during the measurements with the calculated values.

In case of dynamic load testing the reasons of possible inappropriate bridge structure assessment are more complex. They result from two sources: one related to the incorrect or simplified method of research/measurements and the other related to the incorrect or simplified analysis of the measurements results. In addition, it should be noted that considerable errors might also be caused by difficulties in distinguishing the global and local responses of the bridge structure. This applies to both methods of research/measurements and methods of measurements results analysis.

The authors' experience shows that in case of measuring the accelerations by means of accelerometers the errors related to wrong selection of filters as well as the influence of local elements vibrations might be of dominating character, as discussed in detail on the first example of dynamic tests in chapter 4).

The last 30 years have been the time of intensive development of digital measurement methods and digital signal processing, which especially contributed to the development of dynamic load testing. The application of the digital measurement methods as well as the digital signal processing can have both positive and negative influence on the results of assessing a bridge structure.

The positive influence can be observed mainly in:

- eliminating the excessive errors connected with "manual" readout of analog devices;
- easier control of the measurement system correctness in order to assess the influence of other factors on the measurement results,
- possibility of applying the digital signal processing methods in order to:

  - eliminate the influence of the noise on the registered measurement signals,
  - use digital filtration,
  - make spectral analysis of the measured signals,

- possibility of applying the innovative measurement methods which make it possible to measure the qualities which were practically unmeasurable by means of analog methods (visual, interference, inertial methods, etc.).

Negative influence, i.e., increased measurement error uncertainty, of applying the digital measurement methods and digital signal processing can be observed, for example, in:

- applying wrong sampling and initial filtration of the measured signals especially in the case of acceleration records,
- creating innovative methods to measure displacements which do not take into account the errors resulting from the location of the point of reference, based only on a device tripod; which is for example essential in case of vision methods (Olaszek, 1999),
- estimation of the quasi-static value on the basis of the displacements registered during vehicle rides at the speeds close to the maximum ones in-stead of the speed of approximately 10 km/h, (crawl test) can result in significant errors, as will be discussed in detail in the second example of dynamic tests in chapter 4.

FIGURE 3 | The road bridge view—the extreme span at the foreground; from Olaszek (2015) permission was granted by The Committee on Civil Engineering and Hydroengineering of the Polish Academy of Sciences.

LOAD TEST EXAMPLES

The presented examples concern practical cases where the use of improper test methods could lead to significant errors in bridge evaluation if not properly detected. The first case concerns static load testing in a highway bridge and shows how significant errors in the bridge evaluation may appear when analyzing the bridge deflection stabilization time while identifying the permanent and elastic values. The next two cases concern dynamic load testing of two railway bridges. The second example shows that in case of measuring the accelerations by means of accelerometers the errors related to wrong selection of filters as well as the influence of local elements vibrations might be of dominating character in the comparison to the results of the analytical calculation. The third example shows how significant errors in the bridge evaluation could appear when estimating the quasi-static value of the displacements registered during train rides at speeds close to the maximum ones instead of the speed of approximately 10 km/h.

Example of Static Load Testing

The tested bridge consists of three simply supported spans with span length of 29.00 + 21.20 + 29.00 m. It had to undergo repair because of its poor technical condition with destroyed wooden deck and limitation of carrying capacity to 3.5 tones. The structure of the bridge after its repair is shown in **Figure 3**. The presented case took place at the extreme spans. Each of the spans consist of three steel double-tie girders to which the bottom flanges and cross bars making a grate are added. During repair a composite-reinforced concrete deck slab was made on the steel span girders. All steel joints were designed as friction joints with high strength friction grip bolts (**Figure 4**).

During the first static test in the original repaired bridge, significant deflection values were observed at the end span right after two trucks entered the bridge. However, since the registered

FIGURE 4 | Bottom view of the extreme span–visible details of the added structure during the renovation; from Olaszek (2015) permission was granted by The Committee on Civil Engineering and Hydroengineering of the Polish Academy of Sciences.
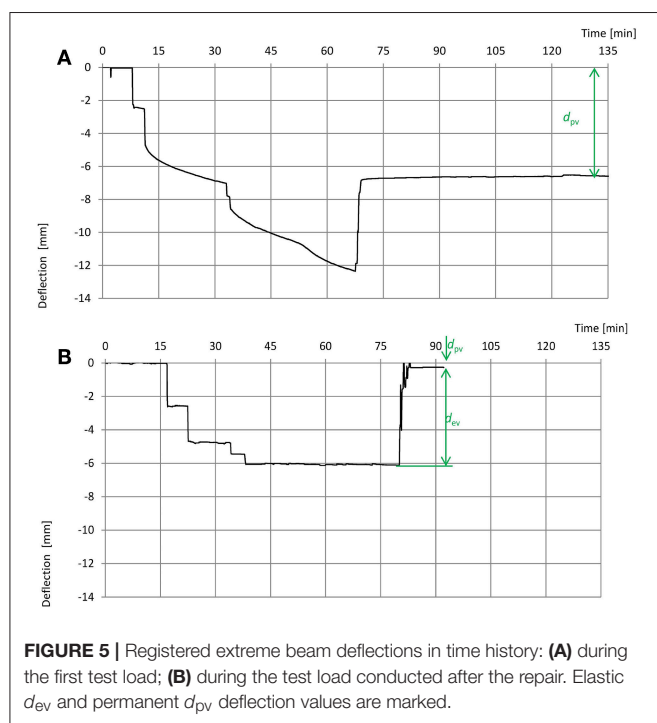
FIGURE 5 | Registered extreme beam deflections in time history: **(A)** during the first test load; **(B)** during the test load conducted after the repair. Elastic d_{ev} and permanent d_{pv} deflection values are marked.

measured deflection values were considerably lower in relation to the calculated ones, two more trucks were introduced. Because of the registered increment deflection values (**Figure 5A**), the test was stopped before these values got stabilized. It was possible to determine only the permanent value of the displacement d_{pv}; which attained a very large value.

The correct diagnosis of the observed bridge behavior and the stop of the load test before an irreversible damage was made in the bridge, was given on the basis of continuous and

on-line observation of the deflections– time history. Summing up the results from the measurements and the information provided by the Contractor, it could be stated that the Contractor made compression joints with incomplete carrying capacity. Fortunately, the test was stopped and the spans were unloaded. If the process of loading had been continued, clearances between the bolts of friction joints and the holes in structure elements could have disappeared. On the basis of the above analysis the repair of the joints was made—independent welded joints were introduced between structure elements which until that moment had been connected with frictional joints. More details about the load testing and the analysis of inappropriate behavior of the structure are presented in Olaszek et al. (2014b).

A second load test was conducted after the joints had been repaired. Test results proved that after the repair the structure worked properly. Exemplary deflection time history during test load of an extreme span is presented in **Figure 5B** and it is characterized by a fast stabilization of displacements both after applying a load and after removing it. It was possible to determine the elastic values of the displacement d_{ev} and the permanent values of the displacement d_{pv}. In this case, the permanent value of the displacement d_{pv} was very small, close to zero.

In the presented case (the first test loading), we can see an exceptional behavior where significant deflection increments and no tendency of displacements stabilization after the application of the load were observed. On the contrary during the test after repair we can see very fast stabilization of displacements both after applying a load and after removing it. During execution of the static load testing on different type of bridges different speeds of stabilization can be observed. This is a very important factor to take into account in the execution of a static diagnostic load test and the duration of the test and the accuracy of the results will depend on the time the load should be hold until stabilization of the outputs. The early removal of the load before the permanent or stationary value is reached is a common error that can lead to important errors of the test results and adoption of wrong decisions. A more detailed presentation of different speeds of stabilization for different types of concrete and steel bridges is available in Olaszek and Casas (2019).

Examples of Dynamic Load Testing

The first example of the dynamic load testing is a bridge that consists of two structures each one for a single railway line. Each bridge was designed as a steel free-ends truss with parallel chords (**Figure 6**). Bottom chords consist of two plate girders with composite reinforced concrete ballast pan. The truss structure was welded and riveted. The span length is 93.00 m. Railway track is the characteristic feature of this viaduct, because the track is curved over the whole length of the span with a radius of curvature $R = 2,600$ m (**Figure 7**). The problem of modeling dynamic analysis of high-speed trains running over curved in-plan bridges was presented in literature (Xia et al., 2008; Dimitrakopoulos and Zeng, 2015). The presented here example is related to the issue of comparing the measured acceleration values with the values determined analytically. The reliability of this comparison can be assumed if the measured acceleration values correspond only to the vibrations of the structure elements

FIGURE 6 | Lateral view of the first presented railway bridge; from Olaszek (2015) permission was granted by The Committee on Civil Engineering and Hydroengineering of the Polish Academy of Sciences.

FIGURE 8 | Geometry of the numerical model of the bridge, marked the elements of bridge structure modeled with a 1-D beam elements: ST-element of steel truss, SS-steel strut beam, SC-steel cross beam, CD-element of reinforced concrete deck; (Olaszek et al., 2013) permission was granted by Waldemar Szaniec (author of the model).

FIGURE 7 | View of the bridge from the railroad level-visible curved railway track; from Olaszek (2015) permission was granted by The Committee on Civil Engineering and Hydroengineering of the Polish Academy of Sciences.

sleepers, track and balustrades was estimated and distributed between the elements of deck model.

The mobile load (inertial, sprung) was modeled as concentrated forces moving on the structure. Due to the fact that horizontal forces should always be combined with vertical railway traffic load, the calculations were executed in two steps. In the first case the calculation was executed for a straight track, and in the second case for curved track with given radius. In the second case the components involved in the action of horizontal forces were added to the vector of vertical action.

The bridge model was calibrated to deflection time histories and later on the accelerations were computed with the calibrated model. It was necessary to predict acceleration time histories to check the maximally acceptable value of the acceleration of the bridge at different speeds of a train (EN, 2003, 2005).

The comparative analysis of the displacement time history measured during a train ride at 200 km/h and determined analytically with the numerical model explained above, shows high compliance of the measurement results with the calculation results–about 99%. The example of measured and calculated time histories of vertical displacements for drive of a special train (two locomotives and four passenger railcars placed between them) with the speed of 200 km/h are shown in **Figure 9**.

Significantly, different compliance appears when comparing the acceleration time history registered and determined with the theoretical model at the same point of the tested structure girder during the same train ride. The ratio of the extreme measured positive and negative acceleration amplitudes to the calculated ones was between 131 and 288% in case of using a 20 Hz Bessel filter signal measurement during the test (**Figure 10A**). This important difference resulted from the high frequency vibrations in the measured time history (**Figure 10B**). The most probable reason of the lack of the high frequency content in the calculated acceleration time history is the non-modeling of tracks and barriers. After using a 10 Hz Bessel filter a ratio close to the displacement compliance was obtained—in the range from 103 to 112% (**Figure 10C**). This example is a proof of the

that are included in the calculations. As a rule, dynamic structure calculations do not take into account elements such as railway tracks, barriers, rails, etc. Even if an acceleration transducer is located very carefully, undesired vibrations of the elements excluded from the calculations can be registered. The main vibration frequencies of these elements are as a rule higher than the fundamental frequencies of girders, and reliable comparison to the calculated values can be possible only after using proper filtration of the registered acceleration time history.

The numerical model of the bridge (**Figure 8**) was a three-dimensional frame comprised of elements with 6 degrees of freedom in node (Olaszek et al., 2013). All elements of truss and the cross beams of the deck were modeled as 1-D beam elements. The composite reinforced concrete deck was also modeled as a grid of beam elements. The model consists of 249 nodes and 526 elements. The weight of additional components such as ballast,
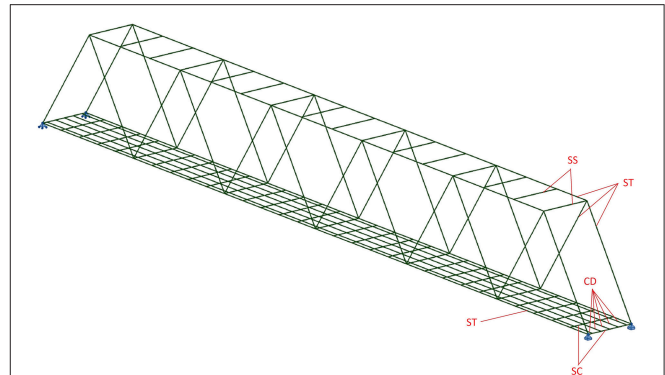
FIGURE 9 | Measured and calculated time histories of vertical displacement for the passage of a special train (two locomotives and four passenger railcars placed between them) at 200 km/h.
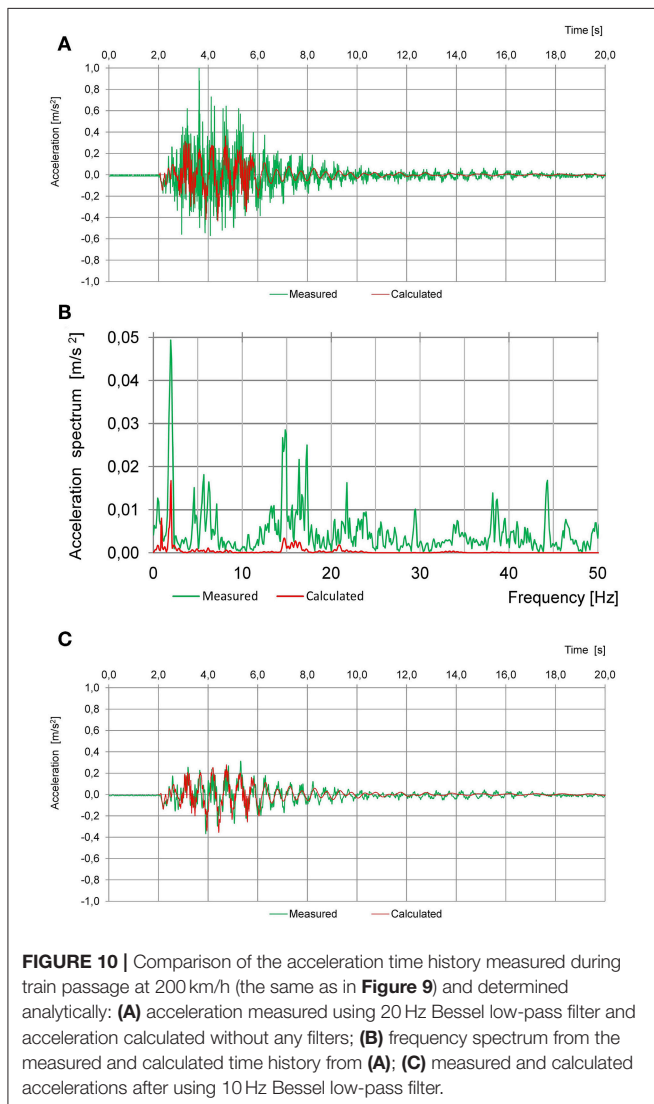
FIGURE 10 | Comparison of the acceleration time history measured during train passage at 200 km/h (the same as in **Figure 9**) and determined analytically: **(A)** acceleration measured using 20 Hz Bessel low-pass filter and acceleration calculated without any filters; **(B)** frequency spectrum from the measured and calculated time history from **(A)**; **(C)** measured and calculated accelerations after using 10 Hz Bessel low-pass filter.

importance of using proper filters while measuring and analyzing the bridge vibration accelerations and also about the need of accurate theoretical models to obtain the predicted values, or,

the importance of knowing perfectly the main limitations of the models due to the adopted hypotheses and simplifications of the reality. A more detailed presentation of the importance of using proper filters while measuring and analyzing the bridge vibration accelerations is presented in Olaszek (2015).

The second example of the dynamic load testing is also a bridge with two parallel structures each for a single railway line. Each structure is a steel arch bridge with reinforced concrete bridge deck. The span length is 75 m and the height of the arch is 15 m (**Figure 11**). The hangers are made from steel bars and welded to the arch and tie of the arch (**Figure 12**). During the acceptance diagnostic load test high values of the dynamic amplification factor were observed, which resulted from the bridge's dynamic susceptibility. The bridge shows a high level of vibration in the hangers both for forced and free vibration cases. An example of the recorded time-histories of the horizontal accelerations of hangers for two passages (10 and 200 km/h) of a special train are shown in **Figure 13**. We can see there how accelerations largely increase with the speed and also different behavior is observed between along and crosswise accelerations depending on the train speed. Similar excessive vibrations of the hangers caused by resonance during train passages are presented in Andersson and Karoumi (2012).

This example presents a possible application of digital signal processing techniques for extrapolation of measurement results during dynamic testing of high-speed railway bridges. Different methods were tested to estimate the quasi-static value of the displacement on the basis of the displacements registered during the train rides at the speeds close to the maximum ones instead of the speed of approximately 10 km/h. The error of using different alternatives was investigated.

The real values of the dynamic amplification factors d_{av} should be calculated as:

$$d_{av} = \frac{d_{vmax}}{d_{vsta}}$$

where d_{vmax} is extreme deflection value at speed of v_{max} and d_{vsta} is extreme deflection value at speed of v_{sta}.

The dynamic tests were conducted using a special train consisting of two locomotives and four passenger railcars placed between them. The train rides were at speeds from $v_{sta} = 10$ km/h to $v_{max} = 200$ km/h, with intermediate speeds of $v_i = 80$, 120, 160, and 180 km/h. The examples of measured time-histories of the vertical displacement at ¼ span length (the point with the maximum deflections) during the train passage with speeds v_{10} and v_{200} are presented in **Figure 14A**.

The quasi-static displacement time-history $d(v_{sta},t)$ was made on the basis of the displacements time-history $d(v_{max},t)$ registered during the train ride at the maximum permissible speed $v_{max} = 200$ km/h.

In case of road bridges, the method of obtaining quasi static displacements history by means of filtering was presented in Paultre et al. (1992). According to this publication, a low pass digital filter, applied to the recorded data, is used to smooth out the dynamic frequencies in the signal. The filtering can be done with a moving average filter or finite-impulse response filters. The

FIGURE 11 | Lateral view of the second railway bridge.

FIGURE 12 | View of the bridge from the railroad level–visible hangers made from steel bars.

applied filter must have a passband of f_{pb} frequency:

$$f_{pb} = \frac{v}{L}$$

where v is the vehicle speed, L is the span length. The stopband with a cut-off frequency f_{co} must be below the bridge's first fundamental frequency f_{F1}:

$$f_{pb} < f_{co} < f_{F1}$$

In order to analyse the effectiveness of the filtering method in the case of railway bridges, three types of low pass filters, significantly different in frequency characteristics, were tested (Smith, 2003; Lyons, 2011):

- Bessel filter (BF),
- Finite Impulse Response (FIR) filter,
- Moving average filter (MAF).

The results in case of the Bessel Filter, FIR filter and Moving Average Filter were analyzed using the method of successive approximations (filtering using variable cut-off frequency) in order to get no free vibration in the filtered signal. **Figure 14B** present examples of train passage results obtained after using Bessel, FIR filters and Moving average filter with the cut-off frequencies to get no free vibration in the filtered signal. The extreme level of displacements registered during the train ride at 10 km/h is also shown. The best result (≈0% relative deviation) was obtained by using the FIR filtration and the worst result (−83% relative deviation) was obtained after using the moving average. The dynamic amplification factor determined on the basis of train rides at 10 and 200 km/h was 1.23. After the filtration used to estimate the quasi-static value two filters gave overvalued values of the dynamic amplification factor equal to 1.85 and 7.19 and one estimated value is close to the real value. A more detailed presentation of different methods of extrapolation for dynamic tests in railway bridges is presented in Olaszek and Casas (2019).

HOW TO MANAGE WITH UNCERTAINTIES AND ERRORS IN BRIDGE LOAD TESTING

As shown in the previous chapters, uncertainty and errors are inherent to the execution and analysis of results from bridge load tests. If this is not taken appropriately, it may derive in wrong decisions regarding the bridge safety (lack of stiffness,....) and/or serviceability (excess of vibration, permanent deflections, dynamic amplification factor,....). The first step to avoid such errors is by knowing them. In this sense, the experience given by a large number executed tests provides a valuable background. The experiences shown in the present paper and others, are of extreme value regarding the adoption of measures in particular tests and finally they may be the basis for the adoption of a Guideline for correct tests execution and analysis. Of course, the final objective would be the derivation of Standards and Codes.
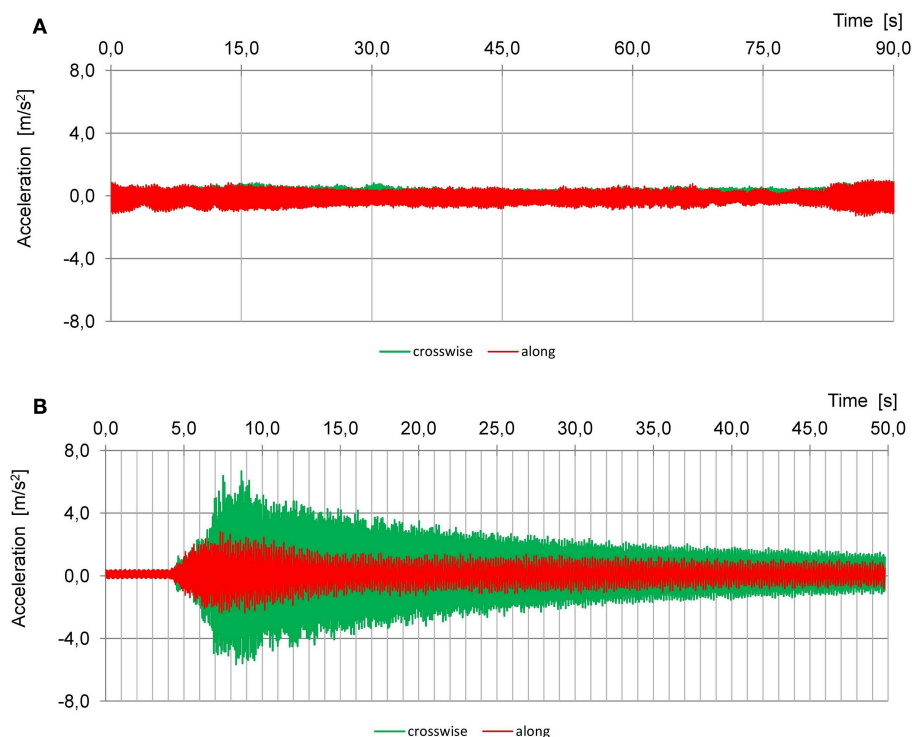
FIGURE 13 | Measured time-histories of the horizontal accelerations of hangers for passage of a special train (two locomotives and four passenger railcars placed between them): **(A)** at the speed v = 10 km/h, **(B)** at the speed v = 200 km/h; the directions of horizontal accelerations: crosswise and along are given relative to the track direction.

Standardization is an essential element of the tests. Standard (ISO/IEC 17025, 2017), used by research laboratories, specifies the general requirements for the competence, impartiality and consistent operation of laboratories. Research laboratories which want to have their competences confirmed by accreditation issued by an authorized accreditation unit in a given country must apply this norm. Currently, its version of 2005 is in force, and from 2020 its version of 2017 will become effective—which is regulated internationally by ILAC [International Laboratory Accreditation Cooperation (ILAC, 2018)].

Important elements of the Standard (ISO/IEC 17025, 2017) are, among others, related to:

- Personnel;
- Facilities and environmental conditions;
- Equipment;
- Metrological traceability;
- Selection, verification and validation of methods;
- Handling of test or calibration items;
- Evaluation of measurement uncertainty;
- Ensuring the validity of results;
- Reporting of results.

Interlaboratory comparisons are carried out as an important check for assuring the quality of tests and the avoidance of errors. Olaszek et al. (2014a) presented interlaboratory comparisons which enabled to verify the methods of measuring bridge deflections used by laboratories. The examination proved that the system of transmission of displacements of the tested girder to the transducer location point by means of a wire and a weight is appropriate for both static and dynamic load tests, but only in the case of low frequency vibrations. The system does not work in case of higher frequencies of vibrations and strong impulse functions.

The norm was elaborated in order to guarantee the quality of research in all kinds of laboratories. It does not take into account the specifics of bridge load testing. Because of that, a document (Polish Centre for Accreditation, 2017) was developed in Poland which includes specific requirements related to bridge tests, such as:

- scope and requirements for research methods applied to test bridge structures under test loading;
- limit values of measurements uncertainty and required components of a measurements uncertainty budget;
- requirements related to the quality assurance program for laboratory research results;
- standard scope of accreditation in case of tests of railway bridges, road bridges and footbridges;
- required minimal research program in case of railway bridges, road bridges and footbridges.
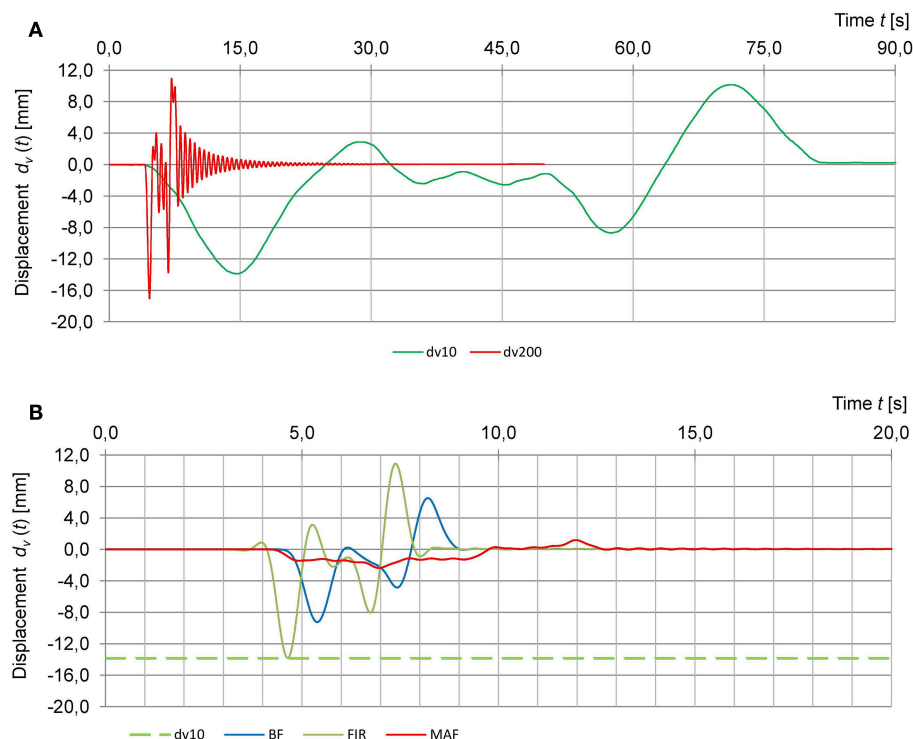
FIGURE 14 | Measured and extrapolated time-histories of the vertical displacements for train passages (the same as in **Figure 13**): **(A)** measured vertical displacements at the speed v = 10 km/h and v = 200 km/h; **(B)** the quasi-static value estimation using the low-pass BF, Bessel filter; FIR, FIR filter; and MAF, moving average filter.

The document was developed in cooperation with the Accreditation Expert Group for laboratories which carry out tests of engineering structures, especially bridges. The document was reviewed by the Ministry of Infrastructure and Construction, General Directorate for National Roads and Highways and Polish State Railways S.A. Similar initiatives would be of interest in order to eliminate sources of errors both in the acquisition, analysis and comparison of results in bridge load tests carried out by different laboratories worldwide.

CONCLUSIONS

The paper presents the practical considerations regarding several sources of error in the execution and analysis of results from static and dynamic load testing of bridges. Attention was paid to different reasons of uncertainty of bridge evaluation during load testing. At the case of measurements, it is possible to assess the uncertainty of individual measurements based on recognized sources of error. The main causes of errors related to different measurement methods are presented.

The use of improper test methods could lead to significant errors in bridge evaluation. This is shown in the three examples of load testing described in the paper. The first case from static load testing shows how significant errors in the bridge evaluation may appear when analyzing the bridge deflection stabilization time while identifying the permanent and elastic values. The

next examples are from dynamic load testing. The second one shows how in the case of measuring the accelerations by means of accelerometers significant errors in the bridge evaluation may appear due to wrong selection of filters. The third example shows how significant errors in the bridge evaluation could appear during determination dynamic amplification factor by estimating the quasi-static value of the displacements from records obtained at high speeds.

The application of appropriate international standards or national regulations, based on compendium of experiences as the ones shown in the paper, becomes necessary to correctly manage the uncertainties and errors in bridge load testing and to compare results provided by different agents or laboratories. In fact, the same experimental records can derive on very different testing results due to the application of different techniques. These techniques should, therefore, be properly calibrated to avoid any presence of errors.

Not all aspects from load testing are adequate for standardization. But at least, the standardization should primarily include the load levels, the range and the accuracy of measurements and the methods of preliminary data analysis. Because of different types, situations and state of tested bridges, the standardization is difficult to apply and in some cases could not go beyond the application of sound engineering judgement rules based on the background built after many years of experience.

AUTHOR CONTRIBUTIONS

PO and JC prepared the conception of the paper. PO prepared examples of bridge testing and wrote the first draft of the manuscript. JC wrote sections of the manuscript and edited final revision. Both authors read and approved the submitted version.

ACKNOWLEDGMENTS

REFERENCES

Andersson, A., and Karoumi, R. (2012). "Attenuating resonant behavior of a tied arch railway bridge using increased hanger damping," in *6th International Conference on Bridge Maintenance, Safety and Management* (Stresa: Taylor & Francis Group).

Casas, J. R. (2006). "Bridge management: actual and future trends," in *Bridge Management, Life Cycle Performance and Cost,* ed. P. J. S. Cruz, D. M. Frangopol, and L. C. Neves (Taylor & Francis), 21–30. doi: 10.1201/b18175-6

Casas, J. R., and Gomez, J. D. (2010). "Bridge capacity assessment by combined proof-loading and WIM data," in *Proceedings of IABMAS'10* (Philadelphia, PA).

Casas, J. R., and Gómez, J. D. (2013). Load rating of highway bridges by proof-loading. *KSCE J. Civil Eng.* 17, 556–567. doi: 10.1007/s12205-013-0007-8

Dimitrakopoulos, E. G., and Zeng, Q. (2015). A three-dimensional dynamic analysis scheme for the interaction between trains and curved railway bridges. *Comput. Struct.* 149, 43–60. doi: 10.1016/j.compstruc.2014.12.002

EN 1990:2002/A1 (2005). Eurocode - Basis of structural design. European Committee for Standardization, Brussels.

EN 1991-2 (2003). *Eurocode 1: Actions on Structures-Part 2: Traffic Loads on Bridges.* Brussels: European Committee for Standardization.

Faber, M. H., Val, D. V., and Stewart, M. G. (2000). Proof load testing for bridge assessment and upgrading. *Eng. Struct.* 22, 1677–1689. doi: 10.1016/S0141-0296(99)00111-X

Goulet, J. A., and Smith, I. F. (2013). Structural identification with systematic errors and unknown uncertainty dependencies. *Comput. Struct.* 128, 251–258. doi: 10.1016/j.compstruc.2013.07.009

Guide (2010). *Evaluation of Measurement Data-Guide to the Expression of Uncertainty in Measurement.* Paris: Joint Committee for Guides in Metrology; International Organization of Legal Metrology.

ILAC (2018). Available online at: https://ilac.org/

Institution of Civil Engineers, and National Steering Committee for the Load Testing of Bridges (1998). *Guidelines for the Supplementary Load Testing of Bridges.* London: Thomas Telford Ltd.

ISO 18649 (2004). *Mechanical Vibration-Evaluation of Measurement Results from Dynamic Tests and Investigations on Bridges.* Geneva: International Organization for Standardization.

ISO/IEC 17025 (2017). *General Requirements for the Competence of Testing and Calibration Laboratories.* Geneva: International Organization for Standardization.

Lyons, R. G. (2011). *Understanding Digital Signal Processing. 3rd Edn.* Upper Saddle River, NJ: Pearson, Prentice Hall.

Moon, F. L., and Aktan, A. E. (2006). Impacts of epistemic (bias) uncertainty on structural identification of constructed (civil) systems. *Shock Vibrat. Digest.* 38, 399–422. doi: 10.1177/0583102406068068

Olaszek, P. (1999). Investigation of the dynamic characteristic of bridge structures using a computer vision method. *Measurement* 25, 227–236. doi: 10.1016/S0263-2241(99)00006-8

Olaszek, P. (2015). *Application of Digital Measurement Methods to Bridge Research (in Polish - Cyfrowe Metody Pomiarowe w Zastosowaniu do Badan Mostów).* Warszawa, Polska Akademia Nauk Komitet Inzynierii Ladowej i Wodnej.

Olaszek, P., and Casas, J. R. (2019). "Diagnostic load testing of bridges – Background and examples of application," in *Load Testing of Bridges (Structures and Infrastructures)* ed. E. Lantsoght (CRC Press, Taylor & Francis Group).

Olaszek, P., Cieśla, J., and Szaniec, W. (2013). Investigation of horizontal forces result in railway viaduct with curved truck (in Polish - Badanie skutków oddziaływan bocznych na wiadukcie kolejowym lezacym na łuku). *Budown. Arch.* 12, 47–54.

Olaszek, P., Łagoda, M., and Casas, J. R. (2014b). Diagnostic load testing and assessment of existing bridges: examples of application. *Struct. Infrastruct. Eng.* 10, 834–842. doi: 10.1080/15732479.2013.772212

Olaszek, P., Mazanek, M., Janas, L., Salamak, M., and Matysek, A. (2014a). The essence of interlaboratory comparisons - quality of the load tests (in Polish:Istota porównan miedzylaboratoryjnych–jakość badan pod próbnym obciazeniem). *Mosty* 2, 32–35.

Paultre, P., Chaallal, O., and Proulx, J. (1992). Bridge dynamics and dynamic amplification factors-a review of analytical and experimental findings. *Can. J. Civil Eng.* 19, 260–278. doi: 10.1139/l,92-032

Polish Centre for Accreditation (PCA) (2017). *Accreditation of Research Laboratories Performing Load Testing of Bridges DAB-15.* Available online at: https://www.pca.gov.pl/publikacje/dokumenty/pca/dokumenty- dotyczace-laboratoriow-badawczych/ (in Polish).

Smith, S. W. (2003). *Digital Signal Processing: A Practical Guide for Engineers and Scientists.* Amsterdam: Newnes, Elsevier Inc.

Taylor, J. (1997). *Introduction to Error Analysis, the Study of Uncertainties in Physical Measurements.* Sausalito, CA: University Science Books.

Wang, N., O'Malley, C., Ellingwood, B., and Zureick, A. (2011). Bridge rating using system reliability assessment. I: assessment and verification by load testing. *J. Bridge Eng.* 16, 854–862. doi: 10.1061/(ASCE)BE.1943-5592.0000172

Wiśniewski, D., Casas, J. R., and Ghosn, M. (2012). Codes for Safety assessment of existing bridges- current state and further development. *Struct. Eng. Int.* 22:2. doi: 10.2749/101686612X13363929517857

Xia, H., Guo, W. W., Wu, X., Pi, Y. L., and Bradford, M. A. (2008). Lateral dynamic interaction analysis of a train–girder–pier system. *J. Sound Vibrat.* 318, 927–942. doi: 10.1016/j.jsv.2008.05.002

Structural Health Monitoring of a Cable-Stayed Bridge Using Regularly Conducted Diagnostic Load Tests

Hadi T. Al-Khateeb[1], Harry W. Shenton III[2], Michael J. Chajes[2]* and Christos Aloupis[2]

[1] Jacobs Engineering, New York, NY, United States, [2] Department of Civil and Environmental Engineering, University of Delaware, Newark, DE, United States

The management and maintenance of cable-stayed bridges represents a major investment of human and financial capital. One possible approach to reducing the cost while simultaneously improving the process is by utilizing structural health monitoring (SHM) systems to enable diagnostic load tests to be regularly and efficiently conducted. The Indian River Inlet Bridge (IRIB), a 533-m long cable stayed bridge, was opened for traffic in 2012. From the very early stages of the design process, the Center for Innovative Bridge Engineering (CIBrE) at the University of Delaware (UD) worked with the Delaware Department of Transportation (DelDOT) and their design-build team of Skanska and AECOM to plan and install a comprehensive structural health monitoring (SHM) system. The SHM system is a fiber-optic based design with more than 120 sensors of varying type distributed throughout the bridge. The system, which not only collects data continuously during normal operation, has also been utilized during regularly scheduled controlled diagnostic load tests being used to monitor ongoing bridge performance. This paper presents results from a unique series of six diagnostic load tests which have been performed over the first 6 years of the bridge's service life (just prior to the bridge's opening, and then again at 6 months, 1, 2, 4, and 6 years). The results of this extended set of diagnostic load tests have enabled the bridge's baseline performance to be rigorously established. This in turn has provided the opportunity to develop a process for conducting future biennial tests to and adding their results to an evolving database, thereby enhancing DelDOT's ability to operate and maintain the bridge.

Keywords: diagnostic, load, test, structural, health, monitoring, cable-stayed, bridge

INTRODUCTION

In order to ensure the structural integrity of a bridge throughout its life, it is essential that the structural components of the bridge are routinely inspected and evaluated. Inspections results and ensuing evaluations are used to classify the physical and functional condition of the bridge. The data generated from observational inspections are qualitative and rely on the inspector's experience, skill, and primarily focus on components of the bridge that can be readily seen. Other evaluation methods can be used, along with visual techniques, to improve the load rating process such as non-destructive evaluation technologies of bridge load testing. In a bridge load test, instruments such as strain gauges tilt meters, deflection devices, or other instruments are strategically located and attached to the bridge. A load, typically a heavily loaded vehicle, is then placed or driven across the bridge and the bridge response is measured.

Bridge load tests are often categorized into the categories of (1) proof tests, (2) diagnostic tests, and (3) in-service tests. Proof load tests are used in verifying the load carrying capacity of the bridge. A truck, weighing the load the bridge is intended to be able to carry safely, crosses the bridge. If the load crosses the bridge without damage and within the designated acceptable stress range, it was deemed as proof the bridge can carry the load. Diagnostic load tests are used to quantify a bridges response to heavy loads, and the response is then used to either directly evaluate the bridge or calibrate a numerical model which is in turn used to evaluate the bridge. In an in-service load test, instrumentation is used to measure the response of the bridge due to ambient traffic over a specified amount of time. Statistical analyses are then used to correlate the collected data to the traffic loading. In all of these different types of load tests, the response of the bridge to the load is used to determine an acceptable load rating for the bridge, and that rating is ultimately compared to the rating calculated using conventional methods.

The following publication provide both guidelines for using load tests to evaluate bridges as well as provide numerous applications (Pinjarkar et al., 1990; Fu and Tang, 1992; Moses et al., 1994; Lichtenstein, 1995; Nowak and Saraf, 1996; Chajes et al., 1997, 1999, 2000; Fu et al., 1997; NCHRP, 1998; The Institution of Civil Engineers, 1998; AASHTO, 2003; Chajes and Shenton, 2006; Schiff et al., 2006; Jeffrey et al., 2009; Hosteng and Phares, 2013; Olaszek et al., 2014; Peiris and Harik, 2016; Al-Khateeb et al., 2018). Most recently, Bayraktar et al. (2017), has employed static and dynamic field testing on a cable-stayed bridge.

Historically, bridges have undergone "one-off" load tests for specific reasons (i.e., low rating, damage, load carrying capacity validation, numerical model validation, assessment of repair effectiveness, lack of construction drawings, etc.) and have been instrumented with temporary sensors for a specific test. As such, there is little documented history of owners conducting a series of controlled load tests to quantify and monitor bridge health. This paper documents the initiation of a long-term monitoring program involving regularly conducted load tests used in combination with other long-term monitoring, all performed utilizing a comprehensive SHM system.

SHM has been a topic of intense research for some time; an early review of research in this area can be found in Doebling et al. (1996). The literature review was updated through 2001, in Sohn et al. (2003). Carden and Fanning (2004) also provided an updated review on vibration based SHM, picking up where Doebling et al. (1996) left off. More recent updates on SHM research include Das et al. (2016), Mesquita et al. (2016), and Seo et al. (2016). Finally, Li and Ou (2016) provide a detailed review of SHM of cable-stayed bridges which is particularly relevant here. Their paper includes a list of significant cable-stayed bridges that have installed on them SHM systems; many are located in Asia. The paper outlines the many uses for SHM data in the operation and maintenance of a cable-stayed bridge including the use of diagnostic load tests.

SHM systems have primarily been used for long-term in-service monitoring. In this paper, the focus is on demonstrating how SHM systems can make it possible to collect data during regularly performed diagnostic load tests.

Delaware's Indian River Inlet Bridge (IRIB), a cable-stayed bridge located in southern Delaware, has a permanent array of instruments that were installed in the form of a structural health monitoring system. Immediately after the IRIB was opened to traffic, a series of diagnostic load tests were conducted to establish the "healthy condition" or baseline behavior of the bridge. Additional diagnostic load tests or "physicals" have been conducted every 2 years to create an evolving "health record" for the bridge. To date, six load tests have been performed. This paper presents the methodology employed to build a comprehensive health record of the IRIB from biennial diagnostic load tests conducted utilizing the bridge's SHM system.

DESCRIPTION OF THE CABLE-STAYED BRIDGE AND THE STRUCTURAL HEALTH MONITORING SYSTEM

The following sections provide both details of the IRIB bridge and of the installed SHM system. More extensive descriptions can be found in Shenton et al. (2017a,b).

Cable-Stayed Bridge Description

The Charles W. Cullen Bridge at the Indian River Inlet, also called the Indian River Inlet Bridge (IRIB), is a 1,749 ft (533 m) long cable-stayed bridge with a 948 ft (289 m) main span and two 397 ft (121) m back spans. The bridge was designed using a combination of precast and cast-in-place reinforced concrete. The bridge is 105 ft (32 m) in width with two lanes of traffic and a shoulder in each direction. A 11 ft 9 ¾ in (3.6 m) wide pedestrian walkway is located on the east side of the bridge. This causes the centerline of the roadway to shift toward the west edge girder. The bridge is fixed at the north pylon but is free to expand at the south pylon and the abutments.

The deck is comprised of two edge girders, transverse floor beams spaced at 11 ft 9 ¾ in (3.6 m) on center, and a cast-in-place deck. The continuous cast-in-place edge girders are roughly rectangular in shape with dimensions of 5 ft 7/8 in (1.8 m deep) and 4 ft 11 in (1.5 m wide). The 8 ½ in (21.6 cm) thick cast-in-place deck has 1 5/8 in (4.13 cm) of latex modified concrete as a wearing surface. The bridge has two twin pylons that reach a height of 248 ft (75.6 m) above the ground. The pylons have a hollow box cross-section that is uniform below the deck level and above deck level tapers to the top of the pylon. There is a total of 152 stays, 38 per pylon. Nineteen stays emanate from each side of the pylons and are anchored to the edge girder on 24 ft (7.3 m) centers. The stay cables consist of seven wire strands in bundles of 19–61. The strands are waxed and encapsulated in high-density polyethylene sheathing. The stays are enclosed in a helical high-density polythene pipe with a raised helical strake to minimize the potential for wind-rain induced vibrations.

Construction of the bridge started in 2009 with the driving of the piles for the pylons. The bridge was opened to limited traffic in the winter of 2012 and was completed and opened

FIGURE 1 | Layout of sensors in the SHM system.

to full traffic in May of 2012. Additional details of the bridge design and construction can be found in Delaware Department of Transportation (2019) and Nelson (2011).

Structural Health Monitoring System

The IRIB bridge was built with a fiber-optic SHM system installed throughout the full length of the bridge to monitor a variety of types of structural response. The system includes seven different types of sensors, with a total of 144 individual sensors installed on the bridge (**Figure 1**). The different sensors are designed to measure the structural response of the bridge under various environmental loads and live load conditions. They include:

- 70 strain sensors, located in the edge girders, pylons, and deck
- 44 accelerometers, mounted to the deck, pylons, and stay cables
- 9 tiltmeters mounted along the east edge girder
- 3 displacement sensors, one at each of the bridge expansion bearings (the two abutments and the south east pylon)
- 2 anemometers that measure wind speed and direction, one at deck level and one at the top of one pylon
- 16 chloride sensors in the deck in 10 locations

All of the sensors are optical sensors, with the exception of the anemometers and 10 of the chloride sensors, which are conventional analog devices (Shenton et al., 2017a).

The SHM system operates 24/7. During operation two basic types of data are collected: "monitor" data and "event" data. Monitor data is collected continuously at both low and high frequency. For low frequency data, a single average sensor reading, computed from data taken at 125 Hz over a 10-min period, is recorded. For high frequency data, the data is continuously recorded at 25 Hz. The monitor data is used to quantify the response due to ambient live loads and well as to monitor long-term, gradual variations in bridge behavior. These long-term variations might be due to daily or seasonal thermal variations or slow degradation due to environmental

effects or sustained load. In particular, ongoing data from SHM system is being used to evaluate long-term effects including cable forces (using cable vibrations), bearing condition (using bearing displacements), bridge ratings (using strain gauges), bridge deflections (using inclinometers), and thermal response (using multiple types of sensors). These applications have been outlined in Chajes et al. (2018).

USING A SERIES OF DIAGNOSTIC TESTS TO MONITOR BRIDGE HEALTH

As mentioned, the SHM system is being used to monitor long-term response of the bridge due to ambient traffic and thermal changes/wind effects. However, none of this response data is due to controlled loads. While it would typically be very expensive to instrument and test a long-span bridge using controlled loads, even one time, by leveraging the existence of the permanent SHM system, it has become possible to conduct an ongoing series of controlled and calibrated diagnostic tests on the IRIB. While the predominant stresses long-span bridges come from dead loads, calibrated live load tests can be effectively used to assess change in bridge response and associated change in condition. In order to accurately and effectively evaluate the response of the bridge over time using the diagnostic load tests, a set of standard test procedures and the determination of the baseline response of the bridge that represents the "healthy" condition must first be determined. Doing this involves; (1) establishing a standard testing protocol, (2) establishing the baseline loading and baseline response, and (3) establishing key response parameters for future comparison.

Establishing Test Protocol

The determination of testing protocols takes place before any testing occurs. It involves, among other lesser details, determining the number of trucks to be used to load the bridge,
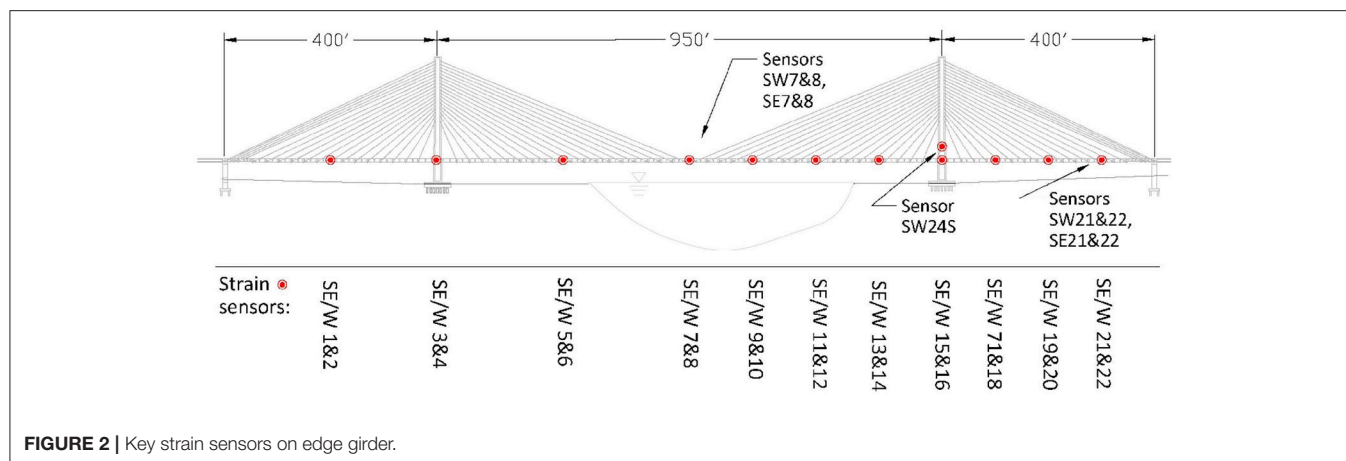
FIGURE 2 | Key strain sensors on edge girder.

their weight, the configurations (or passes) to be used to load the bridge, the number of passes, the timing of the test, and the required traffic control. Also included is whether the load passes will be static (stationary trucks or applied loads), pseudo-static (trucks moving at a slow crawl), or dynamic (trucks moving at full-speed).

Establishing Baseline Loading and Baseline Response

To establish the baseline loading and baseline response, a series of diagnostic load tests should be conducted a few months apart over the first year of service of the bridge. The first test should be conducted as close to the completion of bridge construction as possible. The remaining tests should be conducted when time dependent effects, such the increase in strength and stiffness of the concrete, concrete creep and shrinkage and associated pre-stressed losses, and any other ongoing changes that will affect bridge response, are believed to have stabilized. For some bridges this might take 6 months to a year after the bridge construction is completed. When comparing the response from these preliminary tests, one can look at both the nature of the time-history response due to the slowly moving truck loading or the magnitude of sensor data. While one should not expect perfect correlation, if the comparison of results from these initial tests are consistent and within an established variability of the data, the baseline test can be selected. The earliest test during which the bridge response is deemed to have stabilized will be selected as the baseline. While initial baseline tests may utilize a wide variety of load passes, based on evaluating the results from each pass, a baseline set of load passes should be determined. This baseline set of load passes should be the minimum number of passes that will yield comprehensive response results, and is called the "baseline loading." The response resulting from the baseline loading is called the "baseline response." The test for which these baseline results come is called the "baseline test."

Establishing Key Parameters for Future Evaluation

While a large number and wide distribution of sensors may be needed to ensure that a comprehensive record of bridge response

is captured, to simplify comparisons of future response to the baseline response, it is useful to identify a smaller number of key sensors for use in initial comparisons. If the comparisons indicate changes in response has occurred, the use of a more extensive set of sensors can then be employed. The key sensors will typically be those located at regions associated with maximum load effects. The key locations can be defined based on analytical results from the design process (such as locations that govern the load rating), as well as from the recorded response data from the initial load tests. At the key locations, both time histories and peak response resulting from various load passes can be used to make the initial evaluation of response compared to the baseline. For the IRIB bridge, the key sensors (see **Figure 2**) will be the strain gauges located on the west and east edge girder at midpsan (S-W7/8 and S-E7/8), at the controlling location (S-W21/22 and S-E21/22), as well as the strain gauge located in pylon 6 west just above the deck level (S-W24S). The controlling location is the longitudinal location along the edge girder that governs the bridge load rating. This happens to be at the quarter point of the backspan, and is within a few meters of strain gauges S-W21/22 and S-E21/22 (see **Figure 2**). The governing computed load rating is 1.17 (Al-Khateeb, 2016).

Other parameters that can be used to evaluate structural response are computed parameters such as the summation of girder strains across the bridge cross-section, load distribution factors, or girder neutral axis location. Which particular response parameters to use will depend on the specific bridge being evaluated.

DIAGNOSTIC LOAD TESTS CONDUCTED ON THE IRIB

The following sections describe the series of six diagnostic load tests that were conducted over the first 6 years of operation of the IRIB and used to both establish the baseline response and track the condition of the bridge over time.

Testing Protocol

A final testing protocol for how the load tests should be conducted and what passes should be included was determined

TABLE 1 | Baseline loading.

Pass	Identifier	Description	Direction of travel
ONE TRUCK			
1, 7	1e	Southbound shoulder	Northbound (NB)
2, 8	1a	Southbound slow-lane	
3, 9	1b	Southbound fast-lane	
6, 12	1f	Northbound shoulder	
5, 11	1d	Northbound slow-lane	
4, 10	1c	Northbound fast-lane	
FOUR TRUCKS			
13, 14	4a	Side by side, one in each travel lane	NB
SIX TRUCKS			
15, 16	6a	Side by side, one in each lane and shoulder	NB

FIGURE 3 | Truck configurations for baseline load passes.

after the initial three load tests were completed and evaluated. The final protocol included the minimum number of passes that should be conducted during each load test in order to assess bridge's condition. During several of the tests, extra passes were conducted to examine specific phenomena, however will not be discussed here as they were for independent focused research studies.

The final test protocol is comprised of 16 slow crawl passes. The first 12 passes involve single trucks traveling in one of the four travel lanes or one of the two shoulders. Next, two four truck passes involve trucks in a side-by-side formation traveling in the four travel lanes. Finally, two six truck passes involve trucks in a side-by-side formation across all six lanes (travel and shoulders). The pass number, pass identifier, truck formations, and direction of travel are given in **Table 1** and pass configurations are shown in **Figure 3**. During the load tests, live loads are applied using up to six test trucks with a maximum combined weight of roughly 380 kips (1,690 kN). To minimize thermal effects during the testing period, all tests have been conducted at night, generally starting no earlier than 10 pm. This also minimizes traffic disruption. A complete load test report is submitted to DelDOT following each test.

Load Tests Conducted

Six diagnostic load tests have been conducted on the IRIB bridge since it was built. The initial test coincided with the opening of the bridge to full traffic. The next two tests were performed after 6 months of service and after 1 year of service (these three were used to establish the baseline). Following the initial three tests, ongoing tests have been conducted to provide response data at 2-year intervals. Thus, far, the 2, 4, and 6-years tests have been completed. DelDOT's plan is to continue conducting these biennial diagnostic tests as they will become increasingly valuable as the bridge ages. One important question that should be asked is whether the SHM system is robust enough to last years into the future when changes in bridge condition is much more likely to be seen. This is a very valid concern. To address this concern fiber optic sensors were selected as they are known for their excellent durability. Furthermore, the strain sensors are
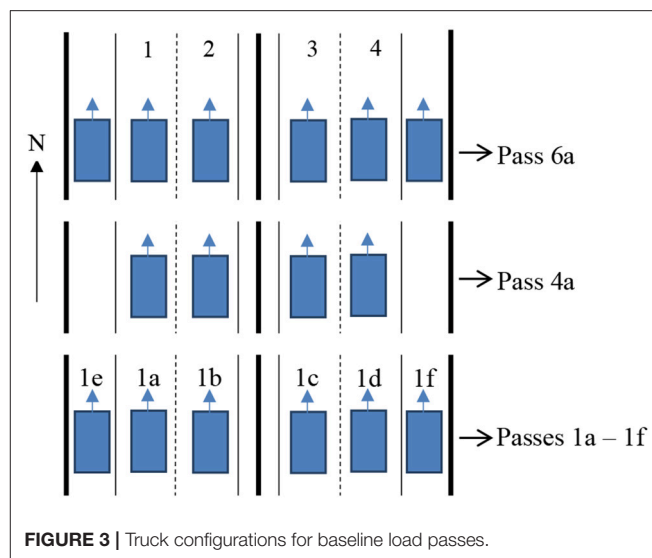
embedded in the concrete and this should increase the chances of their survival. Redundancy of sensor locations has been built into the system, and DelDOT is allocating ongoing funds to actively replaced sensors that have stopped working or don't have reliable measurements. There is also a plan to duplicate the key sensors by installing additional surface mounted sensors. However, until such long-term demonstration projects play out, we cannot know for sure that the systems will remain useable, and only by doing this can we learn how to design and implement SHM systems that will have long service lives.

Baseline Diagnostic Load Tests

As described, the first three load tests were all performed within the first year of service of the bridge and were used to establish the baseline response. Details of these three tests are summarized next.

Load test 1—April 30, 2012

In the first load test, conducted right before the bridge was fully opened to traffic, four trucks were used. The average truck weight was 63.5 kips (282 kN). A total of 17 passes were made in this first load test, 15 slow crawl passes and two dynamic passes. The first four passes were single truck passes and were all conducted using the same truck in each of the four travel lanes. Next, six passes were made with two trucks in specified formations. Finally, five passes were made in which all four trucks were placed in different formations. The dynamic, or high-speed, tests were conducted with all four trucks traveling at ~55 mph (88.5 km/h) with approximately a 100 ft. (30.5 m) interval between each truck.

Load test 2—November 28, 2012

After analyzing the results of the first load test, and reviewing the test procedures, a decision was made to add two more trucks in load test 2. By doing this all four travel lanes and both shoulders could be loaded simultaneously, thereby creating the maximum possible loading across the width of the bridge. The average truck weight for this test was 62.4 kips (282 kN).

A total of 25 passes were made in the second load test, 23 slow crawl passes and two dynamic passes. The first six passes were single truck passes in each of the four lanes and two shoulders. Next, eight two-truck passes were made in different formations and alignments. This was followed by two, three-truck passes, and then five four-truck passes. Finally, six trucks were used to make two passes in a side-by-side formation. The dynamic, or high-speed, tests were conducted with all four trucks traveling at ~55 mph (88.5 km/h) with approximately a 100 ft. (30.5 m) interval between each truck.

Load test 3—May 9, 2013
In the third load test, conducted 1 year after the bridge was fully opened to traffic, six trucks were used, with an average truck weight of 60.2 kips (268 kN). During this test, nine distinct pass configurations were used, and each pass configuration was repeated (repeatability of data is an important step in data validation). A total of 18 passes were made in the third load test, 16 slow crawl passes and two dynamic passes. The first 12 passes were single truck passes in each of the four lanes and two shoulders. Next, two four truck passes were made with the trucks in a side-by-side formation and two six-truck passes were made with the trucks in a side-by-side formation. Finally, the dynamic, or high-speed tests, were conducted with a single truck traveling at approximately 55 mph (88.5 km/h) in southbound slow lane.

Diagnostic Load Tests Used to Monitor the Bridge's Health
As described earlier, the next three load tests were performed at 2-year intervals. Details of these three tests are summarized next.

Load test 4—May 7, 2014
The fourth load test, conducted 2 years after the bridge was fully opened to traffic, was conducted following the standard test protocol with an average truck weight of 63.4 kips (282 kN). This test included additional passes with specific research objectives. In addition to the standard 16 slow crawl passes described in the protocol, there were also two dynamic, or high-speed, tests conducted with a single truck traveling at ~55 mph (88.5 km/h) in southbound slow lane. In addition, a couple of passes were conducted multiple times (six times) to assist in the quantification of measurement variability. Finally, at one point during the testing, the bridge was closed to traffic for 5 min and ambient measurements were taken to further assist in quantifying low-level sensor "noise."

Load test 5—May 18, 2016
The fourth load test, conducted 4 years after the bridge was fully opened to traffic, was conducted following the standard test protocol with an average truck weight of 63.1 kips (281 kN). This test included additional passes with specific research objectives. In addition to the standard 16 slow crawl passes described in the protocol, this test included 10 additional passes. A total of 26 passes were conducted, 20 slow crawl passes and 6 dynamic passes. The first 18 passes were identical to the 16 included in protocol. To better assess the effect of the high-speed passes, dynamic passes were made of a single

truck in the southbound shoulder, in the southbound fast-lane, in the northbound fast-lane, and in the northbound slow lane. Theses dynamic, or high-speed tests, were conducted with trucks traveling at approximately 55 mph (88.5 km/h). Finally, to simulate long trucks and their effect, additional passes were made using a two-truck train in the southbound slow-lane (twice), a three-truck train in the southbound slow-lane, and a four-truck train in the southbound slow-lane (all of these passes were conducted with the truck trains moving at a crawl speed).

Load test 6—June 6, 2018
Finally, the sixth load test, conducted 6 years after the bridge was fully opened to traffic, was identical to third load test (the standard 16 slow crawl passes described in the protocol plus two dynamic passes) with an average truck weight of 62.1 kips (276 kN).

RESULTS

The following sections contain (1) a review the baseline response and associated response parameters that were established based on the first three load tests, (2) an evaluation as to how the response during the ensuing three load tests (years 2, 4, and 6) compares to the baseline response, and (3) a qualitative assessment as to how the response of the bridge has varied over time. Ongoing work is being conducted to determine at what level do individual changes in response, or a changing trend in response represent changes in bridge behavior. This work is aimed at establishing how severe a change in condition must be before the response parameters are "significantly" affected. Having data from this series of six tests has been very useful for the ongoing sensitivity evaluation.

Baseline Response
The baseline response was found from the three tests conducted within the first year of service of the bridge. From the second test (6 months) on, it was found that the bridge response stabilized. As such, the second load test was deemed to be the baseline test, and results from that test have been defined as the baseline results. The following will serve as a summary of those results.

Post-processing and Interpreting Data
Before looking at individual load test results, it is important to note that the same procedure was used to post-process test results from each test. For each sensor, the time-history record was first "zeroed" by taking the average of the first 25 data points and subtracting that value from the entire time history. In this way any initial offset in the record was eliminated. Next a moving average was computed using a window of 1.6 s (25 data points for data recorded at 15.6 Hz). This smoothing was performed to eliminate the inherent low-level noise in the sensor data. Finally, the maximum and minimum (i.e., peak) values of the record were determined.

When interpreting the results, it is important to note that strains, and associated stresses, with a positive value indicates

TABLE 2 | Baseline response peak strain.

Sensor	Single truck		Four trucks		Six trucks	
	Max. strain (με)	Min. strain (με)	Max. strain (με)	Min. strain (με)	Max. strain (με)	Min. strain (με)
S-W7	–	−14 (1e)	–	−26 (4a)	–	−41 (6a)
S-E7	–	−13 (1f)	–	−21 (4a)	–	−31 (6a)
S-W8	36 (1e)	–	91 (4a)	–	138 (6a)	–
S-E8	32 (1f)	–	78 (4a)	–	119 (6a)	–
S-W21	–	−18 (1e)	–	−40 (4a)	–	−59 (6a)
S-E21	–	−16 (1f)	–	−31 (4a)	–	−48 (6a)
S-W22	33 (1e)	–	91 (4a)	–	151 (6a)	–
S-E22	30 (1f)	–	80 (4a)	–	131 (6a)	–
S-W24S	9 (1e)	−11 (1e)	25 (4a)	−26 (4a)	36 (6a)	−42 (6a)

tension. That means that maximum positive strains indicate the largest live-load tensile strain recorded and maximum negative strains indicate the largest live-load compression strain recorded. One should further note that having a live-load tensile strain/stress during the test does not necessarily mean that the element is in a state of net tension, as there can be a large initial compression component due to pre-stressing or post-tensioning that keeps the element in net compression. Where live load stress is reported, it is obtained by multiplying strain by Young's modulus of 29,000 ksi (200 GPa) for steel and 5,164 ksi (35.6 GPa) for concrete. For the concrete, the Young's modulus is based on an average compressive strength of 8,240 psi (56.8 MPa) determined from the tests of cylinders made during the concrete pours.

Baseline Peak Values

Table 2 shows the baseline peak strains for the key sensors for single, four, and six truck passes. For girder sensors, odd numbers indicate top sensors, where we will focus on peak negative values and even numbers indicate bottom sensors where we will focus on peak positive values. In the table, the peak positive values for the top sensors, and peak negative values for the bottom sensors are not shown as they are not significant compared to the other peaks. Gauge S-W24S is a pylon sensor and both positive (tension) and negative (compression) peaks are of similar magnitude and are both shown. The pass identifier for each peak value is given in parentheses.

One can see that the west girder experiences larger strains than the east girder. This is because traffic is skewed toward that side of the bridge due to a wide pedestrian sidewalk on the east side of the bridge. This causes the centroid of the traffic lanes to be closer to the west girder. For the single truck passes, pass identifier (1e) produces the largest strains because that pass consists of a truck in the shoulder closest to the west girder.

In terms of the magnitude of peak strains, the very largest occurred during six side-by-side truck passes. The largest tension strain recorded during any of the load passes was 151 με at gauge S-W22. This gauge is located at the bottom of the western edge

girder between pylon 6W and pier 7 (very close to the controlling location for load rating). The strain of 151 με corresponds to a live-load tensile stress in steel of 4.38 ksi (30.2 MPa) and a live-load tensile stress in concrete of 780 psi (5.38 MPa). The largest compression strain recorded during any of the load passes was −59 με at gauge S-W21. This gauge is located at the same location as gauge S-W22 (the controlling location), but is in the top face of the western edge girder. This strain corresponds to a live-load compression stress of 1.71 ksi (11.8 MPa) in steel and a live-load compression stress in concrete of 305 psi (2.10 MPa). The maximum tension and compression strains in the pylon recorded during any of the load passes were 36 με and −42 με, respectively. The strain of 36 με corresponds to a live-load tensile stress in steel of 1.04 ksi (7.17 MPa) and a live-load tensile stress in concrete of 184 psi (1.27 MPa). The strain of −42 με corresponds to a live-load compression stress of 1.21 ksi (8.34 MPa) in steel and a live-load compression stress in concrete of 215 psi (1.48 MPa). These pylon strains were recorded by strain gauge S-W24S (located in pylon 6 west just above the deck level).

Baseline Time Histories

Figure 4 shows the baseline time histories for the key strain gauges (S-W7 & SW-8, S-W21 & S-W22, and S-W24S) due to the six side-by-side truck pass. These time histories will be used later for comparison to load tests 4, 5, and 6. Please note that the plots of the time history are strain vs. time and not strain vs. distance. As such, the length of the plots varies depending on the exact velocity of the truck(s). Also note that the data recording always starts prior to any trucks coming onto the bridge, and so the first portion of the plot essentially measures ambient response and can be shortened as appropriate for plotting the results.

Baseline Distribution Factors and Summation of Edge Girder Strains

Transverse load distribution is an important characteristic of a bridge and can be a useful quantity to track over time. The distribution factors for the IRIB were computed at midspan and at the controlling location based on one, four, and six loaded lanes. **Table 3** shows the distribution factors that were computed at midspan and the controlling location.

To further improve the quantitative comparison, we can also look at the sum of the peak edge girder strains (top and bottom) at midspan (S-W7 + S-E7, S-W8 + S-E8) and at the controlling location (S-W21 + S-E21, S-W22 + S-E22). By using the sum of the two strains, some of the variability due to differences in transverse truck location can be eliminated. In a way, the sum of the peak strains is closely correlated to the total moment across the section at the two locations. **Table 4** shows the summation of the girder strains at midspan and the controlling location.

It should be noted that we are not tracking distribution factors for the floor system as those members are not instrumented. It is believed that the very basic distribution between the two edge girders can be an indicator of change in behavior, perhaps due to changes in cable forces which are being monitored using cable vibrations as part of the SHM long-term monitoring effort.

FIGURE 4 | Baseline strain time histories for six truck pass: **(A)** midspan; **(B)** controlling location; **(C)** pylon.
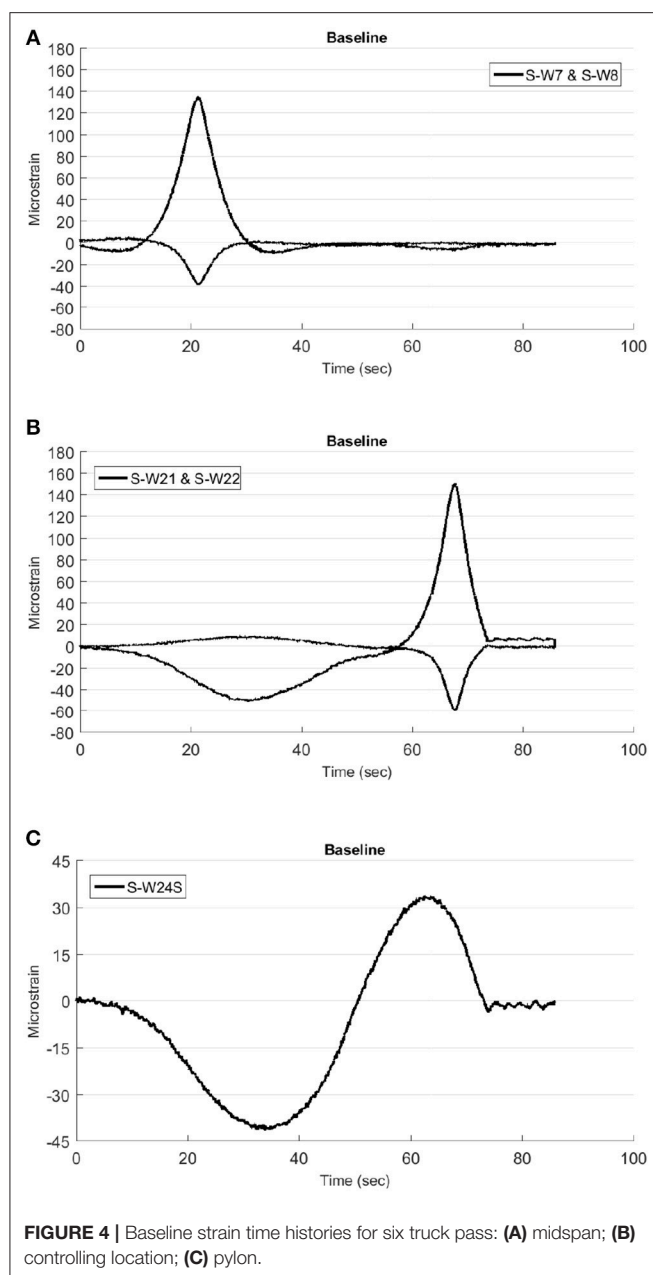
Sensor Variability

In comparing results of "duplicate" passes, it is important to quantify the variability in the sensor readings that can come from (1) variations in truck location for duplicate passes, (2) bridge vibrations even in relatively low winds, and (3) general sensor noise related to sensor resolution. To establish this, (1) data can be collected for several minutes while no traffic is on the bridge and the wind is calm, and (2) several replicates of specific truck passes can be conducted. To accomplish this for the IRIB, traffic was stopped for 5 min and no cars or trucks were permitted to cross the bridge while data was recorded at 125 Hz (the test was conducted at night in calm wind conditions). In addition, six

TABLE 3 | Baseline response live load distribution factors.

Lanes loaded	DF at midspan	DF at controlling location
1	0.85	0.63
4	2.1	1.9
6	3.2	3.2

TABLE 4 | Baseline response summation of girder strains.

Sensor	Summation of strains ($\mu\varepsilon$)
S_W7 + S_E7	−72
S_W8 + S_E8	257
S_W21 + S_E21	−107
S_W22 + S_E22	282

replicates of both a single truck pass (Pass 1e) and six side-by-side truck passes (Pass 6a) were conducted. By analyzing the results from these two series of tests, the threshold for a meaningful difference between measured strain values from different tests but from similar passes was found to be ± 4 $\mu\varepsilon$. This value can be used when evaluating the results from successive diagnostic load tests. Additional details regarding its determination can be found in Aloupis et al. (2019).

Bridge Response Compared to Baseline

In the following sections, the recorded response of the IRIB bridge during tests conducted at 2 years (load test 4), 4 years (load test 5), and 6 years (load test 6) after the bridge was opened to traffic are evaluated by comparing them to the baseline response. While it would not be expected that significant changes in condition and associated response would be noticed this early in the life of the structure, these test results represent the beginning of the "medical file" for the bridge (as if the bridge were a person undergoing biennial physicals). In fact, the bridge remains in excellent "health" as evidenced by the data about to be shown, and also as evidenced by the biennial inspection reports on the bridge. As noted in section Sensor Variability, variability between tests and due to sensor accuracy should lead to a strain variability of ±4 $\mu\varepsilon$. A very valid question is what level of change in strain is needed to signal a change in condition? This is an active area of ongoing research by the research team both for strain data due to diagnostic tests as well as all sensor data due to long-term ambient monitoring. Clearly the nature and location of the change in condition will how much the measured strain will change. By repeating the test every 2 years, both one-time changes and trending changes can be captured. It is anticipated that changes that follow a trend will be the best signals of bridge condition change. Finally, it is important to note that for all results presented, the response has been normalized to the loading magnitude of the baseline test.

Comparison of Time Histories

Figure 5 shows a comparison of the time history response of the key strain gauges at midspan (S-W7/8), the controlling
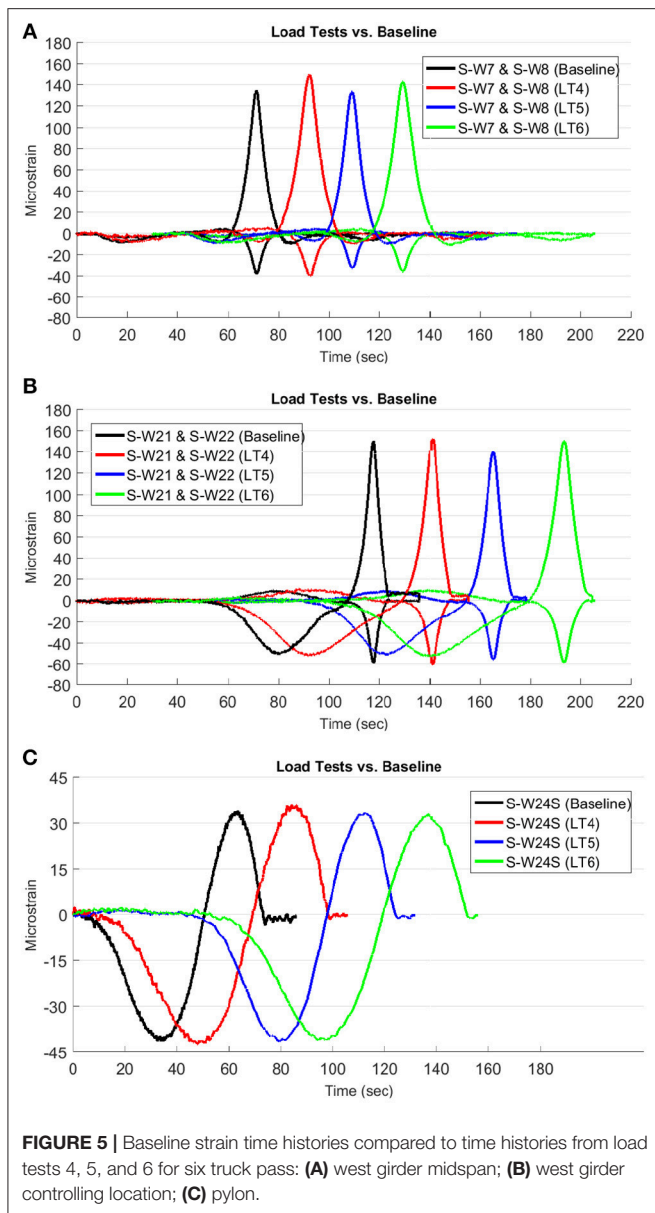
FIGURE 5 | Baseline strain time histories compared to time histories from load tests 4, 5, and 6 for six truck pass: **(A)** west girder midspan; **(B)** west girder controlling location; **(C)** pylon.

TABLE 5 | Comparison of peak baseline strain for key sensors to peak strains for load tests 4, 5, and 6 for six truck passes.

Sensor	Baseline Test	Load Test 4		Load Test 5		Load Test 6	
	Strain ($\mu\varepsilon$)	Strain ($\mu\varepsilon$)	Difference (%)	Strain ($\mu\varepsilon$)	Difference (%)	Strain ($\mu\varepsilon$)	Difference (%)
S_W7	−41	−39	3.8	−33	19.2	−36	13.2
S_E7	−31	−30	3.5	−28	9.0	−29	7.2
S_W8	138	149	−8.1	135	2.4	143	−3.7
S_E8	119	118	1.4	111	6.8	97	19.0
S_W21	−59	−60	−2.6	−53	9.6	−58	1.4
S_E21	−48	−45	6.1	−42	12.4	−43	11.0
S_W22	151	153	−1.6	139	8.3	151	0.1
S_E22	131	125	4.9	116	11.7	119	9.8
S_W24S	36	36	−0.3	33	6.1	33	7.7
S_W24S	−42	−43	−2.2	−41	0.4	−41	1.7
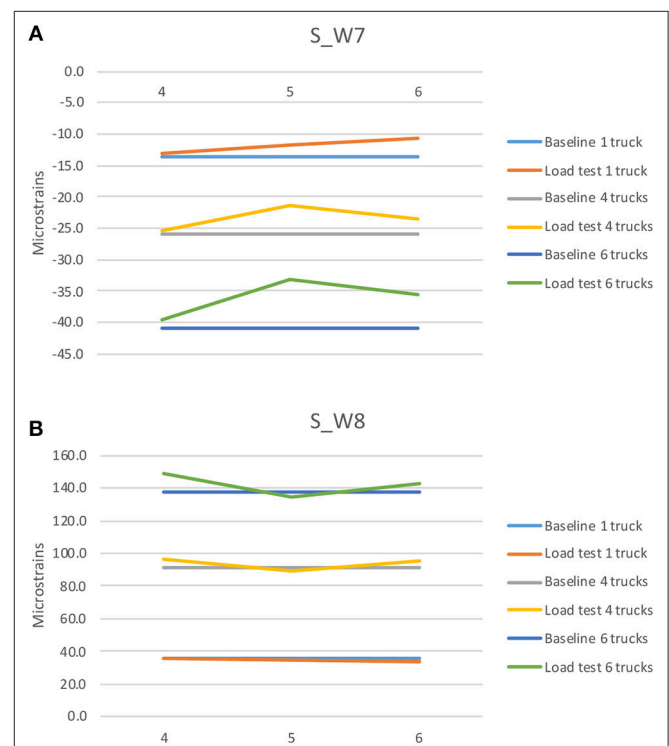
FIGURE 6 | Peak strains at midspan from load tests 4, 5, and 6 compared to the baseline value: **(A)** top of west edge girder; **(B)** bottom of west edge girder.

location (S-W21/22), and in the pylon (S-24S). One can see that qualitatively, the response from test to test is very consistent. The peaks show some variation, but no trend of increasing nor decreasing magnitude is clear. In the next section, the specific values of the peaks will be investigated.

Comparison of Peak Values

Table 5 presents a comparison of the peak strains recorded by key sensors during load tests 4, 5, and 6 to the baseline strains. Of the 30 differences from the baseline that were computed, 24 were <10%. Taking the absolute value of all 30 differences, the average difference is 6.5%. Furthermore, while there is no apparent trend in strain data, if any slight trend exists, it is for the peak strains to be getting smaller over time. Compared to the baseline, only one

of the ten peak strain values during load test 6 was larger than the baseline value. In **Figures 6**, **7**, one can graphically see how the peak strains have varied over time in comparison to the baseline value (the horizontal lines in the plots). This visual representation of the peak values shows that the ongoing response is quite similar to the baseline response, and with no discernable pattern of change.
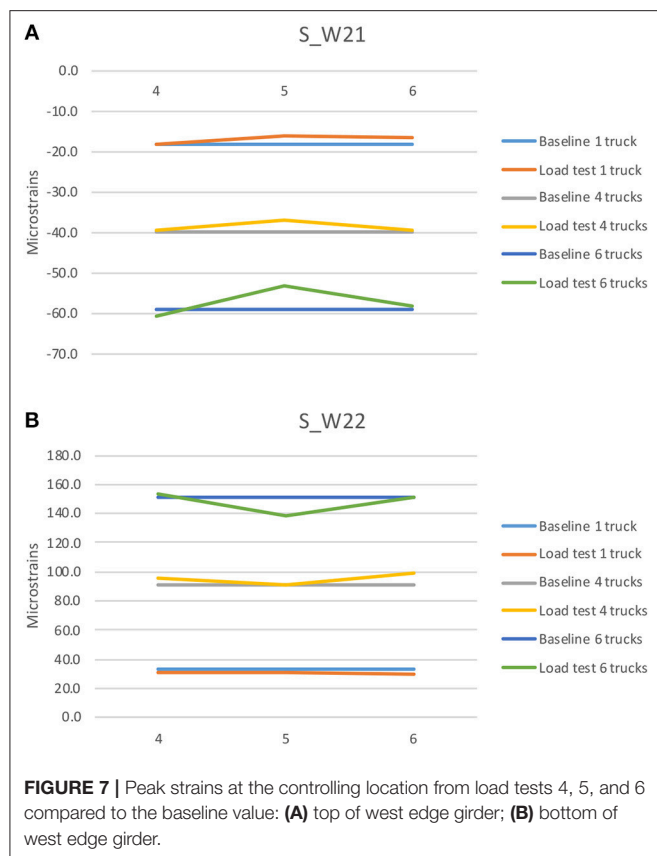
FIGURE 7 | Peak strains at the controlling location from load tests 4, 5, and 6 compared to the baseline value: (A) top of west edge girder; (B) bottom of west edge girder.

TABLE 6 | Baseline distribution factors at midspan and controlling location compared to distribution factors from load tests 4, 5, and 6.

Lanes loaded	Baseline test	Load test 4		Load test 5		Load test 6	
	DF	DF	Difference (%)	DF	Difference (%)	DF	Difference (%)
DISTRIBUTION FACTORS AT MIDSPAN (BOTTOM SENSORS)							
1	0.84	0.83	1.06	0.82	2.74	0.79	6.72
4	2.1	2.2	−6.09	2.1	1.97	2.2	−4.48
6	3.2	3.5	−8.10	3.1	2.39	3.3	−3.70
DISTRIBUTION FACTORS AT CONTROL LOCATION (BOTTOM SENSORS)							
1	0.70	0.67	4.00	0.65	6.53	0.64	8.39
4	1.9	2.0	−5.20	1.9	0.45	2.1	−8.33
6	3.2	3.3	−1.60	2.9	8.31	3.2	0.10

TABLE 7 | Comparison of baseline summation of peak top and bottom girder strains at midspan and the controlling location to summation of peak top and bottom girder strains from load tests 4, 5, and 6 for six truck passes.

Sensors	Baseline Test	Load Test 4		Load Test 5		Load Test 6	
	Strain (με)	Strain (με)	Difference (%)	Strain (με)	Difference (%)	Strain (με)	Difference (%)
S_W7 + S_E7	−72	−70	3.60	−61	14.8	−64	10.6
S_W8 + S_E8	257	267	−3.89	246	4.33	240	6.70
S_W21 + S_E21	−107	−106	0.935	−95	10.8	−101	5.61
S_W22 + S_E22	282	278	1.42	254	9.76	269	4.49

Comparison of Distribution Factors and Summation of Edge Girder Strains

As mentioned earlier, both transverse load distribution factors and summation of top and bottom edge girder strains (east and west) can be useful parameters to track over time.

Table 6 provides a comparison of single, four, and six lane loaded distribution factors from load tests 4, 5, and 6 as compared to the baseline values. Of the 18 differences that were computed (absolute values), 10 were below five percent and all were below 10%. Using the absolute value of all 18 differences, the average difference is 4.5%. Table 7 shows the summation of top and bottom edge girder strain gauges at midspan for load tests 4, 5, and 6 as compared to the baseline value. Of the 12 differences that were computed (absolute values), nine were below ten percent and all were below 15 percent. Using the absolute value of all 12 differences, the average difference is 6.4%. If any minor trend is noted, it is that the summation of strains is getting smaller over time. Figure 8 shows graphically how the summation of strains have varied over time.

Summary of Comparisons

The comparisons of time histories, peak values, and distribution factors all indicate that the bridge condition has remained unchanged during the first 6 years of service. While this is what would be expected, the database of response will be extremely valuable in the years to come. This data does contain variability,

but absent trends in the data, suggest that future variability within the ranges seen here should be of no concern. On the other hand, trends in the data, or variability beyond what has been documented, would be cause for further investigation.

CONCLUSIONS AND FUTURE WORK

This paper has described how SHM systems can be utilized to facilitate ongoing bridge health monitoring using regularly performed diagnostic load tests. The process involves first establishing a baseline response and then comparing future response to that baseline. In essence, the series of tests is analogous to a series of "physical exams" and together they create a "health record" for the bridge. The baseline response represents the "healthy" condition of the structure, and each successive test adds valuable information to record with which the change in condition and associated health of the structure can be assessed.

In the case of the IRIB, three diagnostic load tests were conducted to establish the baseline response of the bridge, and three additional diagnostic load tests (physical exams) have been conducted at 2-year intervals to create a health record for the

FIGURE 8 | Summation of west and east peak strains: **(A)** top of edge girders at midspan and controlling location; **(B)** bottom of edge girders at midspan and controlling location.
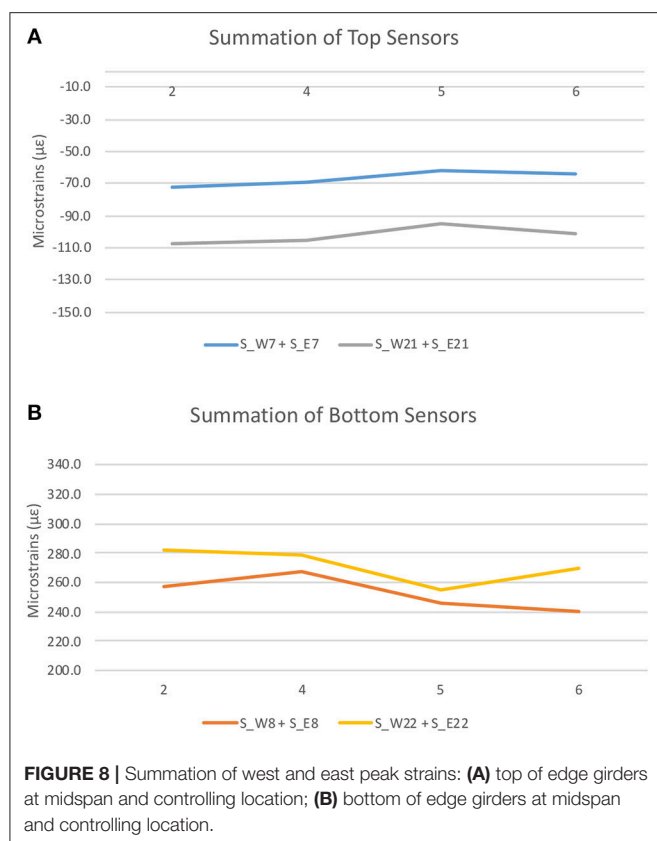
bridge. The results indicate that the bridge is performing as expected. While some variability in response is observed, no defined pattern or trend in the response over time is evident. Future tests will be added to the health record (which also included visual inspection result), thereby enabling the owner to develop a more quantitative measure of the bridge's condition.

Should some event occur or condition arise in the future that raises concern about the health of the bridge, a load test can be quickly and easily conducted, and the results used in conjunction with visual inspection and theoretical analyses to fully assess the condition of the bridge. This becomes just one more tool in the engineer's toolbox for evaluating the bridge in such an instance.

The work presented shows how a bridge SHM system can provide value to a bridge owner. In addition to (ideally) providing automatic early clues to potential problems, a periodic controlled load test can provide confirmation that conditions have not changed.

Future work will focus on developing a more detailed characterization of test-related variability of the response parameters and on determining when changes in response indicates actual structural change and is not simply due to expected test-related variability. The preliminary result of that effort are presented in Aloupis et al. (2019).

AUTHOR CONTRIBUTIONS

HA-K, HS, and MC contributed to the conception and design of the study. HS was in charge of developing the SHM system, and oversaw all of the load tests. HA-K and CA performed the data analysis. HA-K, CA, and MC wrote portions of the first draft of the manuscript. All authors contributed to manuscript revision, and read and approved the submitted version.

FUNDING

ACKNOWLEDGMENTS

REFERENCES

AASHTO (2003). *Manual for Condition Evaluation and Load and Resistance Factor Rating (LRFR) of Highway Bridges*. Washington, DC: American Association of State Highway and Transportation Officials.

Al-Khateeb, H. T. (2016). *Bridge Evaluation Utilizing Structural Health Monitoring Data*. Ph.D. Dissertation, University of Delaware, Newark, DE.

Al-Khateeb, H. T., Shenton, III., H. W., Chajes, M. J., and Wenczel, G. (2018). Computing continuous load rating factors for bridges using structural health monitoring data. *J. Civil Struct. Health Monitor* 8, 721–735. doi: 10.1007/s13349-018-0313-4

Aloupis, C., Chajes, M. J., Shenton, H. W. (2019). "Quantification of uncertainties in diagnostic load test data," in *Proceedings of the Bridge Engineering Institute Conference* (Honolulu, HI).

Bayraktar, A., Turker, T., Tadla, J., Kursun, A., and Erdis, A. (2017). Static and dynamic field load testing of the long span nissibi cable-stayed bridge. *Soil Dyn. Earthq. Eng.* 94, 136–157. doi: 10.1016/j.soildyn.2017.01.019

Carden, E. P., and Fanning, P. (2004). Vibration based condition monitoring: a review. *Struct. Health Monitor* 3, 355–377. doi: 10.1177/1475921704047500

Chajes, M. J., Mertz, D. R., and Commander, B. (1997). Experimental load rating of a posted girder–and–slab bridge. *J. Bridge Eng.* 2, 1–10. doi: 10.1061/(ASCE)1084-0702(1997)2:1(1)

Chajes, M. J., and Shenton, H. W. (2006). Using diagnostic load tests for accurate load rating of typical bridges. *J. Bridge Struct.* 2, 13–23. doi: 10.1080/15732480600730805

Chajes, M. J., Shenton, H. W., Al-Khateeb, H. T., Wenczel, G., Natalicchio, C., Chen, J., et al. (2018). "*Structural Health Monitoring of Delaware's Indian River Inlet Bridge*," in *Proceedings of the International Bridge Conference* (Washington, DC).

Chajes, M. J., Shenton, H. W. III, and O'Shea, D. (2000). Bridge condition assessment and load rating using nondestructive evaluation methods. *J. Transport. Res. Rec.* 1696, 83–91. doi: 10.3141/1696-48

Chajes, M. J., Shenton, III., H. W., and O'Shea, D. (1999). "Use of field testing in delaware's bridge management program," in *Proceeding of the 8th International Bridge Management Conference, TRB, National Research Council* (Denver, CO).

Das, S., Saha, P., and Patro, S. K., (2016). Vibration-based damage detection techniques used for health monitoring of structures: a review. *J. Civil Struct. Health Monitor* 6, 447–507. doi: 10.1007/s13349-016-0168-5

Delaware Department of Transportation (2019). *Indian River Inlet Bridge.* Available online at: https://www.deldot.gov/information/projects/indian_river_bridge/ (accessed January 1, 2019).

Doebling, S. W., Farrar, C. R., Prime, M. B., and Shevitz, D. W. (1996). *Damage Identification and Health Monitoring of Structural and Mechanical Systems from Changes in Their Vibration Characteristics: A Literature Review.* Los Alamos National Laboratory Report. LA-13070-MS, Los Alamos, NM.

Fu, G., Pezze, F., and Alampalli, S. (1997). Diagnostic load testing for bridge load rating. *J. Transport. Res. Rec.* 1594, 125–133. doi: 10.3141/1594-13

Fu, G., and Tang, J. (1992). *Proof Load Formula for Highway Bridge Rating.* Transport Research Record, 1371, Washington, DC.

Hosteng, T., and Phares, B. (2013). "Demonstration of load rating capabilities through physical load testing: ida county bridge case study," in *Part of InTrans Project 12-444, Bridge Engineering Center.* (Ames, IA: Iowa State University).

Jeffrey, A., Breña, S. F., and Civjay, S. (2009). *Evaluation of Bridge Performance and Rating through Nondestructive Load Testing.* Amherst, MA: University of Massachusetts.

Li, H., and Ou, J. P. (2016). The state of the art in structural health monitoring of cable-stayed bridges. *J. Civil Struct. Health Monitor.* 6, 43–67. doi: 10.1007/s13349-015-0115-x

Lichtenstein, A. G. (1995). *Bridge Rating Through Nondestructive Load Testing.* Final Report, NCHRP Project 12-28A, Washington, DC.

Mesquita, E., Antunes, P., Coelho, F., Andre, P., Andre, A., and Varum, H., (2016). Global overview on advances in structural health monitoring platforms. *J. Civil Struct. Health Monitor.* 6, 461–475. doi: 10.1007/s13349-016-0184-5

Moses, F., Lebet, J. P., and Bez, R. (1994). Applications of field testing to bridge evaluation. *J. Struct. Eng. ASCE* 120, 1745–1762. doi: 10.1061/(ASCE)0733-9445(1994)120:6(1745)

NCHRP (1998). *Manual for Bridge Rating Through Load Testing.* NCHRP Project l2-28 A, Transportation Research Board, Washington, DC.

Nelson, E. T. (2011) *Indian River Inlet Bridge – Surviving the Storms.* Chicago, IL: Aspire the Concrete Bridge Magazine, Precast/Prestressed Institute.

Nowak, A. S., and Saraf, V. K. (1996). *Load Testing of Bridges, Research Report UMCEE 96-10.* Ann Arbor, MI: University of Michigan.

Olaszek, P., Lagoda, M., and Casas, J. R, (2014). Diagnostic load testing and assessment of existing bridges: examples of application. *Struct. Infrastruct. Eng. Mainten. Manag. Life-Cycle Design Perform.* 10, 834–842. doi: 10.1080/15732479.2013.772212

Peiris, A., and Harik, I. (2016). "Load testing of bridges for load rating," in *7th International Conference on Sustainable Built Environment* (Kandy).

Pinjarkar, S. G., Guedelhoefer, O. C., Smith, B. J., and Kritzler, R. W. (1990). *Nondestructive Load Testing for Evaluation and Rating.* NCHRP Project 12-28 Final Report.

Schiff, S. D., Piccirilli, J. J., Iser, C. M., and Anderson, K. J. (2006) *Load Testing for Assessment and Rating of Highway Bridges.* Research Project No. 655, Clemson University, Clemson, SC.

Seo, J., Hu, J. W., and Lee, J. (2016). Summary review of structural health monitoring applications for highway bridges. *J. Perform Construct. Facilities* 30:04015072. doi: 10.1061/(ASCE)CF.1943-5509.0000824

Shenton, H. W. III, Al-Khateeb, H. T., Chajes, M. J., and Wenczel, G. (2017a) Indian river inlet bridge (Part A): description of the bridge and the structural health monitoring system. *Bridge Struct.* 13, 3–13. doi: 10.3233/BRS-170111

Shenton, H. W. III, Al-Khateeb, H. T., Chajes, M. J., Wenczel, G., Arndt, J., and Stevens, C. (2017b) Indian river inlet bridge (Part B): lessons learned from the design, installation and operation of the structural health monitoring system. *Bridge Struct.* 13, 15–24. doi: 10.3233/BRS-170112

Sohn, H., Farrar, C. R., Hemez, F. M., Shunk, D. D., Stimemates, D. W., and Nadler, B. R. (2003). *A Review of Structural Health Monitoring Literature: 1996–2001.* Los Alamos National Laboratory Report, LA-13976-MS, Los Alamos, NM.

The Institution of Civil Engineers (1998). *Guidelines for the Supplementary Load Testing of Bridges, The Institution of Civil Engineers, National Steering Committee for the Load Testing of Bridges.* London: Thomas Telford Publications.

Conflict of Interest Statement: HA-K was employed by the company Jacobs Engineering

The remaining authors declare that the research was conducted in the absence of any commercial or financial relationships that could be construed as a potential conflict of interest.

Stop Criteria for Flexure for Proof Load Testing of Reinforced Concrete Structures

Eva O. L. Lantsoght [1,2*], Yuguang Yang [2], Cor van der Veen [2], Dick A. Hordijk [2] and Ane de Boer [3]

[1] Politécnico, Universidad San Francisco de Quito, Quito, Ecuador, [2] Concrete Structures, Department of Engineering Structures, Civil Engineering and Geosciences, Delft University of Technology, Delft, Netherlands, [3] Ane de Boer Consultancy, Arnhem, Netherlands

Existing bridges with large uncertainties can be assessed with a proof load test. In a proof load test, a load representative of the factored live load is applied to the bridge at the critical position. If the bridge can carry this load without distress, the proof load test shows experimentally that the bridge fulfills the requirements of the code. Because large loads are applied during proof load tests, the structure or element that is tested needs to be carefully monitored during the test. The monitored structural responses are interpreted in terms of stop criteria. Existing stop criteria for flexure in reinforced concrete can be extended with theoretical considerations. These proposed stop criteria are then verified with experimental results: reinforced concrete beams failing in flexure and tested in the laboratory, a collapse test on an existing reinforced concrete slab bridge that reached flexural distress, and the pilot proof load tests that were carried out in the Netherlands and in which no distress was observed. The tests in which failure was obtained are used to evaluate the margin of safety provided by the proposed stop criteria. The available pilot proof load tests are analyzed to see if the proposed stop criteria are not overly conservative. The result of this comparison is that the stop criteria are never exceeded. Therefore, the proposed stop criteria can be used for proof load tests for the failure mode of bending moment in reinforced concrete structures.

Keywords: assessment, bending moment capacity, crack width, field test, proof load test, reinforced concrete, reinforced concrete bridge, strain

INTRODUCTION

Proof load testing is a method of assessment that can be particularly interesting for structures with large uncertainties (Lantsoght et al., 2017g). These uncertainties can be related to the (lack of) information available about the structure (Aguilar et al., 2015), to the effect of deterioration on the structural capacity (Lantsoght et al., 2017b), and to the overall structural behavior at load levels beyond the serviceability state (Faber et al., 2000). In a proof load test, a load representative of the factored live load, the so-called target proof load, is applied to the bridge at the critical position. For the target proof load to be equivalent to the factored live load or the considered factored load combination, the target load is determined for which the sectional moment or shear is the same as for the factored live load or the considered factored load combination (Halicka et al., 2018). The proof load should be applied at the critical position, which currently is assumed to be the position that results in the largest load effect (Chen et al., 2018).
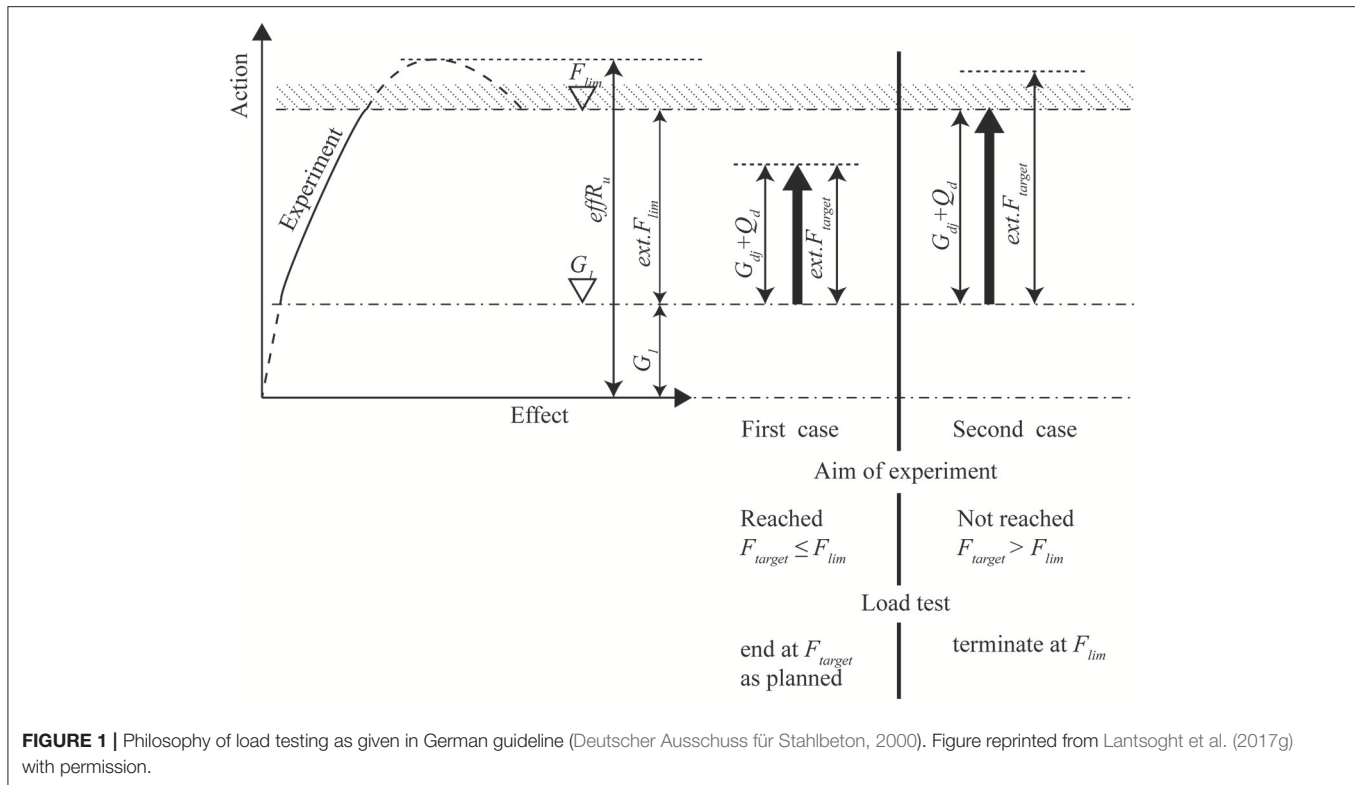
FIGURE 1 | Philosophy of load testing as given in German guideline (Deutscher Ausschuss für Stahlbeton, 2000). Figure reprinted from Lantsoght et al. (2017g) with permission.

For bridges with a variable height or changing reinforcement layout, the position with the largest Unity Check (factored load effect divided by factored capacity) can be different from the position that results in the largest load effect. In some cases, however the reinforcement layout is not known, which complicates using the Unity Check for determining the critical position. If the bridge can carry the target load without distress, the proof load test is successful. The test then shows experimentally that the bridge fulfills the requirements of the code with regard to strength. If distress occurs prior to reaching the target proof load, the proof load test must be terminated and further loading is not permitted. In this case, the structure may still be used for lower load levels, depending on the largest load the structure could carry without signs of distress. In some cases, the load is increased further after reaching the target proof load to study the load at which non-linearity and distress occur. This application is not part of standard proof load testing protocols but may be interesting for research applications or to study the behavior of certain bridge types (Schmidt et al., 2018).

Because proof load tests require large loads, the structure or element that is tested needs to be carefully monitored during the test. Monitoring the structural responses is important for the safety of the executing personnel and, for bridges, for the traveling public in the vicinity of the tested bridge. The monitored structural responses are interpreted in terms of stop criteria. If a stop criterion is exceeded, an indication is given that further loading can result in irreversible damage or failure. If a stop criterion is exceeded before reaching the target proof load, no further loading is permitted and the conclusion is that the

structure does not fulfill the code requirements for the factored load combination that corresponds to the target proof load. **Figure 1** shows this approach and the safety philosophy for proof load testing: the target load is F_{target}, and the load that needs to be applied in addition to the available permanent load G_1 is ext.F_{target}. The load ext.F_{target} should be representative of the additional permanent loads not present at the time of load testing, G_{dj}, and the live loads Q_d. The load at which a stop criterion is reached is F_{lim} and this load relative to the present permanent loads is ext.F_{lim}, with $F_{lim}-G_1 = $ ext.F_{lim}. The load level at which the sectional capacity of the structure is reached is effR_u. There are two possible outcomes of a proof load test, illustrated in **Figure 1**. If ext.F_{target} is smaller than or equal to ext.F_{lim}, then the target proof load can be applied before reaching the onset of non-linear behavior, and the proof load test is considered successful (First case in **Figure 1**). The bridge has then been shown to be able to carry the code-prescribed loads. The second possible outcome is that ext.F_{target} is larger than ext.F_{lim}: the bridge exhibits non-linear behavior before the full target proof load is applied. The full target proof load can then not be applied. Further loading past the onset of non-linearity is not allowed, as it can result in permanent damage or collapse. Depending on the largest load level that was reached during such a proof load test, the conclusion may still be that the bridge fulfills the code requirements for reduced live load, that a traffic restriction should be imposed, or that load posting should be installed.

Proof load testing can be used for new bridges and for the assessment of existing bridges. For new bridges, proof load testing was more common in the past, when a proof load test demonstrated to the traveling public that a new bridge was safe

for use. Nowadays, with better analytical tools for the design of bridges, there is less of a need for such demonstrations. Where load tests are required prior to opening a new bridge, diagnostic load tests are often sufficient (Bonifaz et al., 2018). For existing bridges, proof load tests are a valuable method for the assessment when analytical methods cannot be used or are insufficient (Lantsoght et al., 2017a).

Since proof load tests involve the use of high load levels, monitoring the structural response is important to guarantee the structural safety as well as the safety of personnel on site and the traveling public. This paper focuses on stop criteria for flexure. Such stop criteria exist, but we show that improvements based on the cross-sectional analysis and principles of concrete cracking can be proposed to have a more solid basis. The proposed theoretically-derived stop criteria are then compared to results from laboratory tests to check the margin of safety, and to results from field tests to check if the proposed criteria are not overly conservative.

STOP CRITERIA IN EXISTING CODES AND GUIDELINES

German Guideline

In Germany, guidelines for load testing of concrete structures (Deutscher Ausschuss für Stahlbeton, 2000), mostly aimed at buildings, are available to ensure a safe execution of such tests. The scope of the guidelines is plain and reinforced concrete structures, and the guideline only considers the ductile failure mode of flexure. Testing for shear is not allowed. The German guideline describes detailed stop criteria. The first stop criterion limits the measured concrete strain ε_c:

$$\varepsilon_c < \varepsilon_{c,lim} - \varepsilon_{c0} \qquad (1)$$

The limit is the difference between $\varepsilon_{c,lim}$ (600 με or maximum 800 με for concrete with a compressive strength larger than 25 MPa) and ε_{c0}, the analytically determined short-term strain in the concrete caused by the permanent loads that are acting on the structure before the application of the proof load. The second stop criterion limits the measured strain in the reinforcement steel ε_{s2}:

$$\varepsilon_{s2} < 0.7 \frac{f_{ym}}{E_s} - \varepsilon_{s02} \qquad (2)$$

The limit is the difference of 70% of the yield strain of the tension steel, determined by dividing the average yield strength f_{ym} of the steel reinforcement on the tension side of the cross-section by the modulus of elasticity of the tension steel E_s and the strain ε_{s02}, the analytically determined strain in the reinforcement steel caused by the permanent loads acting on the structure before the application of the proof load, assuming that the concrete cross-section is cracked. When the full stress-strain diagram of the steel is known, Equation (2) can be replaced by:

$$\varepsilon_{s2} < 0.9 \frac{f_{0.01m}}{E_s} - \varepsilon_{s02} \qquad (3)$$

TABLE 1 | Requirements for crack width for newly developing cracks w and increase in crack width for existing cracks Δw (Deutscher Ausschuss für Stahlbeton, 2000).

	During proof loading	After proof loading
New cracks	$w \leq 0.5$ mm	$\leq 0.3\ w$
Existing cracks	$\Delta w \leq 0.3$ mm	$\leq 0.2\ \Delta w$

in which $f_{0.01m}$ is the average value of the stress in the reinforcement steel at a strain of 0.01%, which marks the end of the elastic range of the steel. The reader should note that this stop criterion requires measuring the strains in the reinforcement steel, which practically means removing the concrete cover to instrument the rebar. Most owners will not allow such damage to their structure, so that in practice this stop criterion can seldom be evaluated for bridges.

The third stop criterion limits the crack width w for new cracks, and the increase in crack width Δw for existing cracks. The guideline limits the maximum crack width or increase in crack width during proof loading, as well as the residual crack width after removal of the proof load, see **Table 1**.

The fourth stop criterion limits the deflections as monitored with the load-deflection diagram in real-time during the test. In the cracked state, the stop criterion for deflection is either a clear non-linear increase in the deflection or a residual deflection of 10% after removal of the load.

The last stop criteria on limits the strains in the shear span of beams with shear reinforcement. The limiting concrete strain is then 60% of the limit from Equation (1) and the limiting steel strain in the shear reinforcement is then 50% of the limit from Equations (2) or (3), depending on the available material properties.

Czech and Slovak Codes

In the Czech Republic (Ceský normalizační institut, 1996) and Slovakia (Slovak Standardization Institute, 1979), a code is available for diagnostic (static and dynamic) and proof load testing of bridges (Frýba and Pirner, 2001; Kopácik, 2003). These bridges can be reinforced concrete, pre-stressed concrete, or steel. Note that our current work only deals with reinforced concrete, but the provisions from these codes for other building materials have been included to show the more complete scope of these codes. The code describes acceptance criteria, which are verified after a load test to check if the performance was adequate. These criteria do not have as their goal to warn before possible failure or irreversible damage. The first acceptance criterion prescribes the bounds for the ratio of the elastic deformation S_e to the calculated value S_{cal}:

$$\beta < \frac{S_e}{S_{cal}} \leq \alpha \qquad (4)$$

Table 2 gives the values for the limits α and β depending on the type of bridge.

Bridge type	α	α_1	α_2	α_3	β
Pre-stressed concrete	1.05	0.2	0.5	0.1	0.7
Reinforced concrete	1.10	0.25	0.5	0.125	0.6
Steel	1.05	0.1	0.3	0.05	0.8

Bridge type	Environmental class	Maximum crack width
Reinforced concrete	1 (dry)	0.4 mm
	2, 3 (humid)	0.3 mm
	4, 5 (aggressive)	0.1 mm
Partially pre-stressed	1 (dry)	0.2 mm
	2, 3 (humid)	0.1 mm for post-tensioning
		0 mm for pre-stressing
	4, 5	0 mm
Fully pre-stressed	any	0 mm

The second acceptance criterion evaluates the ratio of the permanent deformation S_r to the total deformation $S_{tot} = S_r + S_e$:

$$\frac{S_r}{S_{tot}} \leq \alpha_1 \qquad (5)$$

Table 2 gives the value of α_1 as a function of the bridge type. For new bridges, repeated testing can be necessary to meet the acceptance criteria. Equation (5) can then be replaced with

$$\frac{S_r}{S_{tot}} < \alpha_3 \qquad (6)$$

provided that the measured deformations during the first loading fulfill:

$$\alpha_1 < \frac{S_r}{S_{tot}} < \alpha_2 \qquad (7)$$

Table 2 gives the values of α_1, α_2, and α_3 as a function of the bridge type. If the measurements of the retest do not satisfy (Equation 6), a third test may be necessary, for which the deformation should fulfill:

$$\frac{S_r}{S_{tot}} \leq \frac{\alpha_1}{6} \qquad (8)$$

Table 3 summarizes the limits to the crack width as a function of the environmental class, which form the third acceptance criterion. If the measurements do not fit within the bounds of the acceptance criteria, the Czech and Slovak codes require a special investigation, long-term monitoring, and/or dynamic testing of the bridge.

Spanish Guidelines

In Spain (Ministerio de Fomento - Direccion General de Carreteras, 1999; Ministerio de Fomento, 2009, 2010), load testing of new bridges prior to opening is required. The stop criteria are based on the remanence, α_{rem}:

$$\alpha_{rem} = 100 \frac{f_r}{f} \qquad (9)$$

with f_r the remaining measurement and f the total measurement. The stop criterion is related to the maximum remanence α_{lim}, which is 20% for reinforced concrete bridges, 15% for pre-stressed bridges or composite bridges, and 10% for steel bridges. When $\alpha_{rem} \leq \alpha_{lim}$ the stop criterion is fulfilled. When $\alpha_{lim} < \alpha_{rem} \leq 2\alpha_{lim}$, the bridge has to be loaded to the same load level again. If $\alpha > 2\alpha_{lim}$ the stop criterion is exceeded and further loading is not permitted. When a second load cycle is used, the remanence in the second cycle is α_{rem}^*. The stop criterion then is $\alpha_{rem}^* \leq \alpha_{rem}/3$.

The performance of a new bridge is considered adequate when it fulfills the acceptance criteria. The Spanish guidelines give four acceptance criteria. The first acceptance criterion is that the maximum measured deflection should not be more than a certain percentage of the analytically determined deflection. For pre-stressed and steel bridges, this percentage is 10%, and for composite and reinforced concrete bridges, it is 15%. If the maximum measured deflection is <60% of the analytically determined deflection, the reason for this difference should be found. The second acceptance criterion states that for continuous bridges a simplified test can be used if the results of the simplified test do not differ more than 10% with the full load test. The third acceptance criterion states that the crack widths should not exceed the limits for the serviceability limit state. The last acceptance criterion allows no signs of distress or exhaustion of the structural capacity.

Other Existing Codes and Guidelines

The following codes and guidelines are available that give information about load testing of bridges and that give some guidance in terms of stop or acceptance criteria: the Manual for Bridge Evaluation (AASHTO, 2016), the Swiss code (SIA, 2011), the Polish code (Research Institute of Roads and Bridges, 2008), and the Spanish code for acceptance testing of new bridges prior to opening (Ministerio de Fomento - Direccion General de Carreteras, 1999). The Manual for Bridge Evaluation (AASHTO, 2016) does not contain quantitative stop criteria, but mentions that no non-linear behavior should occur during the test. The Swiss code (SIA, 2011) prescribes that the behavior during the test should be linear, that the residual displacements should be zero, and that the crack width should be "within acceptable limits." The Polish code (Research Institute of Roads and Bridges, 2008; Filar et al., 2017; Halicka et al., 2018) gives the requirements for load tests on concrete bridges. Two stop criteria are given. The first criterion is that no non-linear behavior can occur. The second criterion limits the residual deformation to maximum 20% for reinforced concrete bridges and to maximum 10% for pre-stressed concrete bridges.

Type of structure	Ratio of residual and total deformation (in %)	
	Testing for acceptable condition	Testing for adequate condition
Riveted steel structure	15	20
Welded steel structure	12	15
Steel with bolted connections	20 (25)	25 (30)
Pre-stressed concrete	20	25
Reinforced concrete	25 (30)	30 (35)
Steel-concrete composite	20	25
Timber structure	30	40

*The values between brackets are valid for γ < 0.5 with γ the ratio of permanent loads to
the sum of permanent and proof loads.*

For buildings, procedures for load testing and stop or
acceptance criteria are given in the ACI 437.2M-13 (ACI
Committee 437, 2013) code and in the Hungarian guidelines
(Hungarian Chamber of Engineers, 2013). The acceptance
criteria in ACI 437.2M-13 for load testing of existing buildings
are a maximum deflection of 1/180 of the span length, a
maximum residual deflection of 25% of the maximum deflection,
a limiting deviation from linearity index, and a limiting
permanency ratio. The latter two acceptance criteria are strongly
related to the loading protocol from ACI 437.2M-13, which
is not directly applicable to bridges (Lantsoght et al., 2017i).
The Hungarian guidelines (Hungarian Chamber of Engineers,
2013) give stop criteria and acceptance criteria for buildings.
The stop criteria are the following: fracture, rupture, yielding,
damage of concrete under compression, buckling, deflections
larger than 1/50 between points of contraflexure, cracks in
concrete larger than 1 mm, cracks in steel, excessive deformations
of the cross-section, extensive shell-buckling, and masonry cracks
larger than 1 mm. Moreover, the Hungarian guidelines give
three acceptance criteria. The first acceptance criterion limits the
residual deformation to a certain percentage of the maximum
deformation depending on the structure type, see **Table 4**. This
table includes all structure types covered by the Hungarian
guidelines. The reader should be aware that the focus of our
current work is limited to reinforced concrete bridges. The
second acceptance criterion limits the deflection under the
characteristic proof load to the maximum deflection for the
serviceability limit state. The third acceptance criterion is only
relevant for concrete structures and limits the crack width under
the characteristic proof load to the limits for the serviceability
limit state.

The limitations of the currently available stop criteria are as
follows. The stop criteria from the German guideline are not
applicable to structures with existing cracking, which is often
the case for existing bridges. The stop criterion based on the
steel strain requires removal of the concrete cover, and is thus
not often used in practice. The Czech and Slovak codes provide
acceptance criteria, which serve a different purpose than stop
criteria, and can thus not be used for monitoring structural safety
during a proof load test. The stop criteria from the Spanish

guidelines are developed for diagnostic load tests for new bridges
prior to opening. As such, they are not suitable for proof load
testing of existing structures. Similar limitations are found in the
other existing codes and guidelines mentioned before.

PROPOSED STOP CRITERIA FOR FLEXURE

Performance Requirements for Stop Criteria

The existing codes and guidelines contain stop criteria for flexure
since flexure is a ductile failure mode. The first and foremost
requirement for a stop criterion is that it should perform well: it
should warn with sufficient anticipation for irreversible damage
or failure. This requirement for a stop criterion is based on the
basic definition of a stop criterion; if this requirement is not
fulfilled, the stop criterion loses its meaning. At the same time,
the stop criterion should not be so conservative that it causes
a load test to be stopped prematurely. For this purpose, one
should compare the stop criterion to the structural responses
obtained with failure tests and with proof load tests. Comparing
to failure tests gives insight in the margin of safety provided
by the stop criterion. Comparing to proof load tests in which
the bridge is instrumented extensively gives an idea about the
performance of the stop criterion in terms of prematurely ending
proof load tests. A third requirement for a good stop criterion
is that theoretical principles should lie at its basis. The current
codes and guidelines use arbitrary limits or limits related to the
performance at the serviceability limit state. The latter element is
suitable for acceptance criteria after a test to ensure the durability
of the structure after the test, but do not give us insight in whether
irreversible damage or failure is near or not. A final requirement
for stop criteria for proof load testing of bridges is that the
criterion should be based on a structural response that can be
measured easily and with a robust measurement technique. The
stop criterion should also be in line with the evolution toward
non-contact measurements (Kohut et al., 2012).

The stop criteria developed in this paper are based on flexural
theory. As such, they fulfill the third requirement for stop
criteria. The proposed stop criteria use measurable quantities:
strains, crack widths, and deflections; and as such fulfill the first
requirement. With the information from available failure tests
and proof load tests, we then check if the proposed stop criteria
fulfill the first two requirements for stop criteria.

Theoretical Derivation
Limiting Strain in the Concrete

To find a limiting strain in the concrete, the stress in the
tension steel is limited to 65% of the mean yield stress f_{ym}. This
criterion avoids stresses in the steel to reach the yield stress
with a considerable margin of safety, so that larger deformations
in the structure are avoided. Based on the limiting stress in
the tension steel, we can derive the stresses and strains in the
cross-section. For a singly reinforced rectangular concrete beam,
Figure 2 shows the section, strains, stresses, and resultant forces.
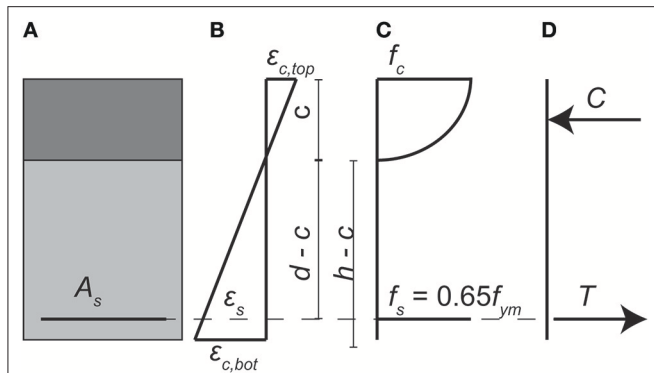
FIGURE 2 | Singly reinforced rectangular concrete beam at moment of achieving stop criterion for concrete strain based on flexural theory: **(A)** cross-section of beam; **(B)** strains; **(C)** stresses; **(D)** resultant forces. Modified from (Lantsoght et al., 2018).

FIGURE 3 | Stress-strain parabola of concrete, with f_{cm} in MPa. Modified from (Lantsoght et al., 2018).

The strain at the bottom of the cross-section $\varepsilon_{c,bot}$ corresponds to the stress state of 65% of the yield stress in the tension steel, assuming that the strains are linear over the height of the cross-section. For the case with tension on the bottom of the cross-section, the strain in the concrete $\varepsilon_{c,bot}$ is related to the strain in the steel ε_s following equivalent triangles:

$$\varepsilon_{c,bot} = \frac{h-c}{d-c}\varepsilon_s \qquad (10)$$

The geometry in Equation (10) considers the height h, the effective depth d, and the compression zone c. For the limit on the steel stress of 65% of the yield strength, Equation (10) can be rewritten as a function of the limiting steel stress, resulting in the maximum stress $\varepsilon_{c,bot,max}$:

$$\varepsilon_{c,bot,max} = \frac{h-c}{d-c} \times \frac{0.65 f_{ym}}{E_s} \qquad (11)$$

with f_{ym} the mean yield stress of the steel, and E_s the Young's modulus of the steel. To find the height of the compression zone, the stress-strain relation for concrete can be expressed with Thorenfeldt's parabola, see **Figure 3**. The expressions of the parabola are a function of the maximum strain in the concrete under compression $\varepsilon_{c,comp}$, which for the case in **Figure 2** with tension on the bottom corresponds to $\varepsilon_{c,top}$. The following material parameters are required for defining the parabola:

$$n_{th} = 0.8 + \frac{f_{cm}}{17.24} \text{ with } f_{cm} \text{ in MPa} \qquad (12)$$

$$\varepsilon_0 = \frac{f_{cm}}{E_c}\left(\frac{n_{th}}{n_{th}-1}\right) \qquad (13)$$

To describe both pre- and post-peak behavior in the stress-strain relationship, the factor k_{th} is introduced. The following expressions then describe the parabolic relation between stresses and strains in the concrete:

$$k_{th} = \begin{cases} 1 \text{ if } \frac{\varepsilon_{c,comp}}{\varepsilon_0} \le 1 \\ 0.67 + \frac{f_{cm}}{62.07} \text{ if } \frac{\varepsilon_{c,comp}}{\varepsilon_0} > 1 \end{cases} \text{ with } f_{cm} \text{ in MPa} \qquad (14)$$

$$f_{c,th} = \frac{0.9 f_{cm} \times n_{th} \times \frac{\varepsilon_{c,comp}}{\varepsilon_0}}{n_{th}-1+\left(\frac{\varepsilon_{c,comp}}{\varepsilon_0}\right)^{n_{th}k_{th}}} \qquad (15)$$

The factor β_{th} converts the concrete stress from the maximum stress $f_{c,th}$ to the average stress $\beta_{th} \times f_{c,th}$:

$$\beta_{th} = \frac{\ln\left(1+\left(\frac{\varepsilon_{c,comp}}{\varepsilon_0}\right)^2\right)}{\frac{\varepsilon_{c,comp}}{\varepsilon_0}} \qquad (16)$$

To fulfill horizontal equilibrium, the resultant under compression C and the resultant under tension T should be equal. The value of the height of the compression zone c should be calculated (analytically or iteratively) so that the equilibrium condition is fulfilled. The expressions for the force resultants are:

$$C = \beta_{th} \times f_{c,th} \times b \times c \qquad (17)$$

$$T = A_s \times 0.65 \times f_{ym} \qquad (18)$$

Once $\varepsilon_{c,bot,max}$ is calculated for the value of the height of the compression zone c which corresponds to the limit of 65% of the yield stress in the steel, a stop criterion for the strains ε_{stop} can be defined based on this limiting strain and taking into account the strain ε_{c0} caused by the permanent loads:

$$\varepsilon_c \le \varepsilon_{c,bot,max} - \varepsilon_{c0} = \varepsilon_{stop} \qquad (19)$$

Since the tensile strain in the concrete is highly non-uniform, the proposed stop criterion refers to an averaged tensile strain over a length that includes at least one crack. The contribution of this crack is then smeared over this length. We recommend the use of a horizontally placed LVDT, measuring over 1 m length for the evaluation of this stop criterion.

Limiting Crack Width

The limiting crack width w_{stop} results from the theoretical model for crack width in reinforced concrete members subjected to bending of Frosch (1999). The advantage of the model by Frosch is that the resulting crack width is suitable for larger concrete covers, as present in real structures. The limiting stress in the reinforcement steel is again $0.65f_{ym}$, as used for the stop criterion for the strains. According to Frosch, the maximum crack width w_c in a reinforced concrete member subjected to bending is:

$$w_c = 2\frac{f_s}{E_s}\beta_{fr}\sqrt{d_c^2 + \left(\frac{s}{2}\right)^2} \qquad (20)$$

with f_s the stress in the steel, E_s the Young's modulus of the reinforcement steel, d_c the concrete cover to the centroid of the tension steel, s the reinforcement spacing, and β_{fr} the strain gradient term, given as:

$$\beta_{fr} = \frac{h - c}{d - c} \qquad (21)$$

The value of β_{fr} can be approximated as:

$$\beta_{fr} = 1 + 3.15 \times 10^{-3}d_c \qquad (22)$$

with d_c in mm To derive a suitable stop criterion, the effect of the permanent loads needs to be taken into account, and the limiting steel stress needs to be implemented in Equation (20). The resulting limiting crack width w_{stop} is:

$$w_{stop} = 2\frac{0.65f_{ym} - f_{perm}}{E_s}\beta_{fr}\sqrt{d_c^2 + \left(\frac{s}{2}\right)^2} \qquad (23)$$

with the stress caused by the permanent loads f_{perm}:

$$f_{perm} = \frac{d - c}{h - c}\varepsilon_{c0}E_s \qquad (24)$$

with c in Equations (24) and (21) the height of the compression zone that corresponds with $0.65f_{ym}$ as a stress in the reinforcement steel.

Proposal

Figure 4 gives an overview of the proposed stop criteria for flexure. Preliminary tests (Lantsoght et al., 2017i) showed that the behavior of beams previously cracked in bending is different from beams not cracked in bending, and therefore the proposal separates both cases. For the proposed stop criteria, the only difference between the case of a beam previously cracked in bending and a beam not previously cracked in bending lies in the limit to the residual crack width w_{res}. Note that for a beam previously cracked in bending the crack width w, the maximum crack width w_{max}, and residual crack width w_{res} can be the width
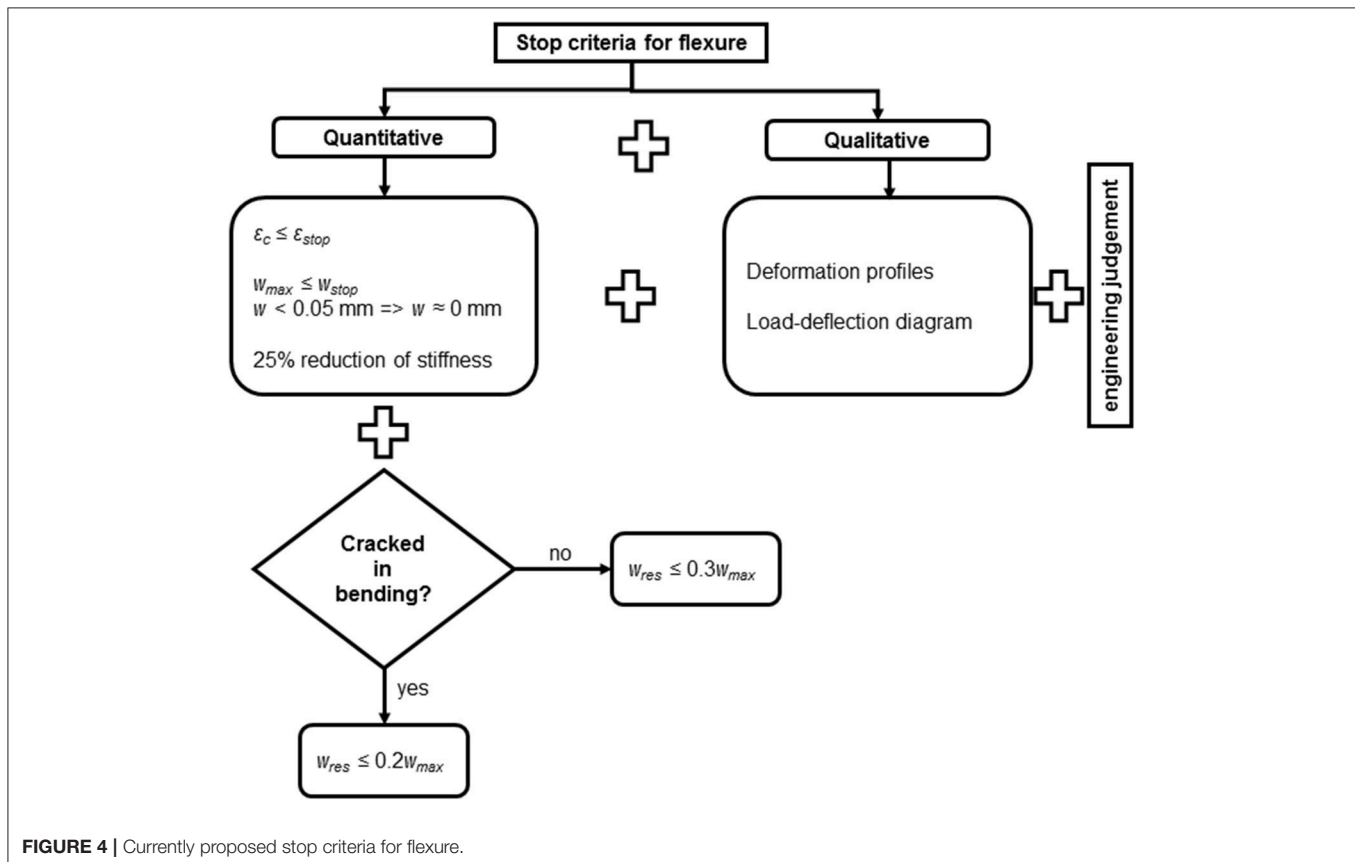
FIGURE 4 | Currently proposed stop criteria for flexure.

of a newly developed crack or the increase in width of an existing crack.

Figure 4 gives the two theoretically derived stop criteria from Equation (19) for strain and Equation (23) for the maximum crack width. In addition to these stop criteria, **Figure 4** proposes to neglect all cracks that are smaller than 0.05 mm. The limit for the residual crack width w_{res} as a function of the maximum crack width w_{max} is taken from the German guideline, see **Table 1**. To limit non-linearity, we propose to limit the reduction of the stiffness determined in the load-deflection diagram to maximum 25%.

In addition to these quantitative stop criteria, **Figure 4** contains qualitative stop criteria. The test engineer should follow the overall structural behavior during the load test based on the load-deflection diagram and deformation profiles. After the test, the behavior of the load-deflection diagram is evaluated with the reduction in stiffness. Examples of deformation profiles include lines of deflections in the longitudinal direction and transverse direction, resulting in plots that give insight in the overall structural behavior during the load test. Changes in these profiles indicate changes in the load distribution behavior. During the load test, the test engineer should interpret such changes.

VERIFICATION OF PROPOSED STOP CRITERIA

Available Experiments

Laboratory Tests

Two series of experiments serve for the comparison between the proposed stop criteria and the results obtained in the laboratory. The beams in these experiments are subjected to a loading protocol that is similar to the cyclic loading protocol recommended for proof load testing. As such, these experiments are suitable for comparison to the stop criteria that are proposed for use in the field. Since these beams were tested to failure, the measured structural responses give an indication of the margin of safety to collapse when these are compared to the stop criteria.

The first series, the P series, consists of two beams with plain bars cast in the laboratory (Lantsoght et al., 2017h). Four experiments were carried out, two of which resulted in a flexural failure. The second series, the RSB series, consists of beams sawn from the slab of the Ruytenschildt Bridge (Lantsoght et al., 2016b). This series consisted of five tests on three beams. The four tests that resulted in a flexural failure are included in this study. **Table 5** gives an overview of the properties of the tested beams and the maximum applied load P_{max}. For the RSB beams, the given area of the cross-section A_c is the area of the cross-section of the beam sawn from the bridge. Since sawing does not lead to a rectangular cross-section, the value of A_c is the area of the actual section, not the product of the height and the average width b. All experiments summarized in **Table 5** are three-point bending tests on beams with a span length l_{span} and a center-to-center shear span a.

Field Tests

Two types of field tests are available: proof load tests and failure tests (collapse tests). The available results from proof load tests are part of the series of pilot proof load tests from

TABLE 5 | Overview of properties of beams tested in the laboratory failing in flexure.

Test	d (mm)	b (mm)	A_c (m^2)	ρ_l (%)	l_{span} (m)	a (m)	f_{cm} (MPa)	f_{ym} (MPa)	P_{max} (kN)
RSB01F	503	576	0.290	0.91	5	2.50	52.2	282	276
RSB02A	516	576	0.297	0.89	5	1.25	52.2	282	369
RSB02B	520	589	0.307	0.96	5	1.25	52.2	282	416
RSB03F	521	1062	0.596	0.95	5	2.50	52.2	282	607
P804A1	755	300	0.240	0.83	8	3.00	63.5	297	207
P502A2	465	300	0.150	0.63	5	1.00	71.5	297	150

TABLE 6 | Overview of properties of pilot proof load tests for flexure.

Test	l_{span} (m)	b (m)	d (mm)	ρ (%)	P_{target} (kN)	Conclusion
Vlijmen-Oost	14.07	12.20	612	1.01	900	Assessment with combination of proof load test and finite element modeling
Halvemaans Bridge	8.20	7.50	406	1.60	900	Successful proof load test for flexure
Zijlweg	10.32	6.60	550	0.75	1,368	Successful proof load test for flexure
De Beek	10.81	9.94	462	1.14	1,751	Successful proof load test for flexure for first span, but second span critical

the Netherlands (Lantsoght et al., 2017e). Four bridges and viaducts were proof loaded to evaluate the failure mode of flexure: the viaduct Vlijmen Oost (Fennis et al., 2014), the Halvemaans Bridge (Fennis and Hordijk, 2014), the viaduct Zijlweg (Lantsoght et al., 2017b), and the viaduct De Beek (Lantsoght et al., 2017c,f), see **Table 6**. Vlijmen Oost carries three lanes, De Beek originally carried two lanes but is restricted to one lane, and the Halvemaans Bridge and Zijlweg carry a single lane. Vlijmen Oost was tested with a loading truck (Steffens et al., 2001) whereas the other bridges were loaded with a system of a steel spreader beam, counterweights, and hydraulic jacks. The proof load tests on the Halvemaans Bridge and viaduct Zijlweg directly showed that these structures fulfill the code requirements. The proof load test on Vlijmen Oost required a combination with finite element models to assess the bridge, since the applied load was small as compared to the code-prescribed load for a viaduct with three lanes. On viaduct De Beek, the test was limited for safety reasons to the first span, which does not cross the highway. However, the second span is critical and thus other assessment methods are required to evaluate viaduct De Beek and to evaluate if the bridge can be opened again for two lanes of traffic.

The sensors plan of these pilot tests was very extensive, so that the structural behavior could be followed in detail. The conclusion from the analysis of the behavior was that the proof load test did not result in irreversible damage to the structure. For the stop criterion to fulfill its aim, it should thus not be exceeded in these experiments when we reanalyze the measured structural responses. When the stop criterion performs adequately, future proof load tests can be done with less instrumentation (thus

being more economic and taking less time). The sensor plan then only consists of the instrumentation required to evaluate the stop criteria.

Besides the pilot proof load tests, a failure test on slab bridge, the Ruytenschildt Bridge (Lantsoght et al., 2016a,b,c,d, 2017d), was carried out. The Ruytenschildt Bridge was a bridge with five spans of 9 m long and a width of 12 m. For testing and staged demolition, a saw cut was introduced, leaving a structure with a width of 7.365 m for testing. The bridge was tested in two spans at a shear-critical position. In the first span, the maximum applied load was 3,049 kN and the load was limited by the available counterweight. Failure did not occur, but flexural distress was observed. In the second span, the maximum applied load was 3,991 kN. The failure mode was a combination of settlement of the support and yielding of the reinforcement in the sagging moment region, resulting in large cracking. The deck did not collapse. Whereas these tests were intended to be shear tests, shear failure did not occur and we can use the results of these experiments to analyze the available margin of safety for the proposed stop criteria for bending.

Comparison Between Experiments and Stop Criteria
Comparison With Failure Tests

The tests in which failure was reached are used to evaluate the margin of safety provided by the proposed stop criteria for

flexure. These tests are the laboratory tests and the failure tests on the Ruytenschildt Bridge. For the first span of the Ruytenschildt Bridge, the value of $\varepsilon_{c,bot,max} = 1,061\ \mu\varepsilon$, which gives a stop criterion for the strain of $\varepsilon_{stop} = 1,022\ \mu\varepsilon$. For the second span, $\varepsilon_{c,bot,max} = 1,060\ \mu\varepsilon$ so that $\varepsilon_{stop} = 1,051\ \mu\varepsilon$. For the first span, the stop criterion for the crack width is calculated as $w_{stop} = 0.19$ mm and for the second span the value is also $w_{stop} = 0.19$ mm. **Table 7** gives an overview for the loads at which each stop criterion is exceeded. The stop criteria for the case of a structure already cracked in bending are considered. In the first span, the stop criterion for the crack width is not exceeded, since the monitored crack was not activated during the test. This observation shows that punctual monitoring of crack widths during tests should be replaced with non-contact methods that can monitor all cracks in the region of interest. The stop criterion for the concrete strain is not exceeded in the first span, which can be explained by the fact that the experiment was not continued until failure was achieved but until the maximum available load was applied.

For both spans, the stop criterion that is exceeded first is the criterion related to the deformation profiles in longitudinal and transverse direction. This criterion is exceeded at 62% of the maximum applied load in span 1 and at 65% of the failure load in span 2, see **Table 7**. Note that the results for the evaluation of the load-displacement diagram are not included in **Table 7**, since this criterion is observed qualitatively in real-time during the test, and after the test it is converted in a quantitative measure of the reduction of the stiffness; both criteria serve the same purpose.

Table 8 gives an overview of the loads F_{lim} for which the proposed stop criteria were exceeded, and the margin of safety F_{lim}/P_{max} for the governing stop criterion (or criteria). The stop criteria for a structure uncracked in bending are considered for the RSB beams and P804A1, since the RSB beams are taken out of their original structural system, whereas P804A1 is newly cast. Only P502A2 is considered previously cracked in bending, since it is a repeat test on the beam P502. For P502A2, no unloading branches were included in the loading protocol, so that the residual crack cannot be determined and the associated stop criterion cannot be evaluated. For the RSB experiments, the measurements of two lasers on each side of the beam

TABLE 7 | Load F_{lim} for which proposed stop criteria are exceeded and resulting margin of safety during failure tests on Ruytenschildt Bridge.

Criterion	Span 1		Span 2	
	F_{lim} (kN)	F_{lim}/P_{max} (%)	F_{lim} (kN)	F_{lim}/P_{max} (%)
Concrete strain	>P_{max}	>100	3,377	85
Maximum crack width	>P_{max}	>100	3,702	93
Residual crack width	>P_{max}	>100	>P_{max}	>100
Stiffness reduction	1,923	63	3,159	79
Deformation profiles—longitudinal	1,900	62	2,600	65
Deformation profiles—transverse	1,900	62	2,600	65

TABLE 8 | Limits from proposed stop criteria, load F_{lim} for which proposed stop criteria are exceeded and resulting margin of safety during laboratory tests on beams.

Criterion	F_{lim} (kN)					
	RSB01F	RSB02A	RSB02B	RSB03F	P804A1	P502A2
Concrete strain	145	170	257	366	107	121
Maximum crack width	147	195	267	379	115	78
Residual crack width	150	226	416	P_{max}	140	–
Stiffness reduction	77–274	>P_{max}	175-P_{max}	244	120	P_{max}
Deformation profiles—horizontal	150	175	225	342	120	125
Deformation profiles—vertical	150	175	225	342	160	125
F_{lim}/P_{max} (%)	53	46	54	58	52	52
Concrete strain ($\mu\varepsilon$)	1,008	1,011	1,011	1,007	1,018	1,074
Max. crack width (mm)	0.16	0.16	0.16	0.16	0.13	0.15

TABLE 9 | Comparison between proposed stop criteria and measurements obtained from pilot proof load tests for flexure.

Test	$\varepsilon_c(\mu\varepsilon)$	$\varepsilon_{stop}(\mu\varepsilon)$	w_{max}(mm)	w_{stop}(mm)	w_{res}(mm)	$w_{res,lim}$(mm)	ΔEI_{meas}(%)	LD	TD
Vlijmen Oost	80	869	0	0.15	0	0.05	3.7	$>F_{target}$	NA
Halvemaans Bridge	150	729	0	0.11	0	0.04	+-0	F_{target}	$>F_{target}$
Zijlweg	240	842	0	0.17	0	0.07	4	$>F_{target}$	$>F_{target}$
De Beek	887	919	0.12	0.13	0	0.02	18	$>F_{target}$	$>F_{target}$

give rather different results for the reduction in the stiffness. Therefore, the two values of these results are given in **Table 8**. However, the variability in the results stems from the fact that the beams are not straight since they were sawn from the bridge. Therefore, for this particular case, the stiffness reduction is not considered a reliable stop criterion, and the results are indicated in italic in **Table 8**. **Table 8** also gives the calculated values for the maximum crack width and the maximum strain for direct comparison to the values recommended by the German guideline (Deutscher Ausschuss für Stahlbeton, 2000). The results show that the limiting strain from the proposed stop criteria is higher than the strain limit from the German guideline, whereas the limiting crack width is smaller than the limit from the German guideline.

The results in **Table 8** show that there is not a single stop criterion that is governing for each beam experiment, but that all stop criteria should be evaluated. The stop criteria are exceeded with a margin of safety between 42 and 61% and are thus conservative for use in practice. The results also show that the load for which the stop criterion for the limiting strain is exceeded is similar to the load for which the stop criterion for the limiting crack width is exceeded. This observation is expected, since both stop criteria are related to a maximum stress in the reinforcement steel of 65% of the yield stress.

Comparing the results from **Table 8** to the results from **Table 7** shows that a similar, yet slightly smaller margin of safety is found for the failure tests on an existing bridge. The margin of safety on the Ruytenschildt Bridge is slightly smaller, since in the first span, loading was not continued until collapse, whereas in the second span, perhaps more load could have been carried if the substructure would not have failed. The resulting margin of safety is sufficiently conservative to recommend these stop criteria for the application to proof load tests on reinforced concrete structures that are flexure-critical and are expected to fail in a ductile manner.

Comparison With Pilot Proof Load Tests

In this part, the available pilot proof load tests are analyzed to see if the proposed stop criteria are not overly conservative and would have resulted in a premature termination of these tests. **Table 9** gives an overview of the proposed stop criteria for the pilot proof load test for bending. For the Halvemaans Bridge, the strain due to the permanent loads ε_{c0} is estimated with a conservative hand calculation, whereas for Zijlweg and De Beek this value is taken from the finite element model used to prepare the test. For Vlijmen Oost, this value is derived from the bending moment caused by the permanent loads

from the finite element model used to assess the viaduct. For all cases, crack widths smaller than 0.05 mm are taken as equal to 0 mm. Therefore, for all experiments, the maximum residual crack width is negligible. The results for $w_{res,lim}$ also show that for many cases the resulting limit is negligible. The reduction in stiffness for the Halvemaans Bridge is given as "+-0," since the value of the stiffness slightly increased over the load cycles. The longitudinal deflection profiles "LD" and transverse deflection profiles "TD" are qualitatively studied. If there are no observations during the entire proof load test, the stop criterion is never exceeded and ">F_{target}" is added to **Table 9**. For Vlijmen Oost, no measurements for the deflection in the transverse direction are available, so that "NA" is shown in **Table 9** for this stop criterion. For the Halvemaans Bridge, in the last load step the deflections increased larger than expected, so that the stop criterion for the longitudinal deflection profiles is reached in the last load step. For none of the pilot proof load tests, a stop criterion was exceeded during the test. This conclusion corresponds with the conclusions from each of the proof load tests, where an analysis of the structural responses measured with the extensive instrumentation plans showed that no irreversible damage occurred during the proof load tests.

DISCUSSION AND FUTURE RESEARCH

The proposed stop criteria for flexure are evaluated in two ways. First, we checked if the margin of safety on the proposed stop criteria is sufficient when compared to failure tests. Since the margin of safety ranges from 42 to 65%, the stop criteria provide sufficient conservatism. Secondly, we checked if the proposed stop criteria are not overly conservative. The requirement for this evaluation parameter is that in the heavily instrumented pilot proof load tests, the measured structure responses should never exceed the proposed stop criteria. **Table 9** shows that the proposed stop criteria fulfill this requirement.

The proposed stop criteria for flexure are an improvement of the state of the art. The existing codes and guidelines contain stop criteria for flexure, but the limits on strains and crack widths that are provided are arbitrary or related to serviceability requirements. To function as a stop criterion, the limit should be linked to the onset of non-linear behavior and have a theoretical background. The proposed stop criteria fulfill this requirement, since they are related to reaching 65% of the yielding stress in the reinforcement steel. These stop criteria can be easily programmed in a spreadsheet, and the limiting values can be read off from

this spreadsheet during the preparation stage of a proof load test. The limits related to serviceability requirements can be used for acceptance criteria, but do not serve the purpose of stop criteria.

The proposed stop criteria do not include limits to the largest deflection and residual deflection, as most existing codes and guidelines. The reason why deflection and residual deflection are not included is that beam experiments (Lantsoght et al., 2016d, 2017i) indicated that a stop criterion based on a maximum and residual deflection is not reliable. The German guidelines (Deutscher Ausschuss für Stahlbeton, 2000) contain a limiting strain in the steel reinforcement. A similar stop criterion is not included in the proposal, since measuring the steel strain requires the removal of the concrete cover. Most bridge owners are not keen on inflicting such damage to a bridge.

All pilot proof load tests had a flexure-critical section in the sagging moment region. This situation is common for reinforced concrete slab bridges. Typically, higher reinforcement ratios, and sometimes larger cross-sections are used in the hogging moment region. If, however, the engineer needs to assess a bridge where the flexure-critical section lies in the hogging moment region, the practical application of the proposed stop criteria may be more complicated. The presence of an asphalt layer may make instrumenting the tension side of the cross-section more complicated. For those cases, load application and instrumentation occur on the same side of the cross-section, which may complicate execution, wiring, and positioning details of the load and the sensors. Future work based on case studies of bridges that are flexure-critical in the hogging moment region should address these issues.

One limitation in terms of instrumentation in the pilot proof load tests is the use of contact sensors. To measure the crack widths, we selected one or more existing cracks to monitor during the test. The selected crack(s) may or may not have been the governing crack during the test. Similarly, we measured the strain at one position only. To avoid this limitation, non-contact measurements should be used and this instrumentation should monitor the entire region of interest. Possible options are the use of photogrammetry measurements to monitor the entire region of interest, or the use of fiber optics to check strains over a larger length or surface. To improve the current practice of proof load testing, the application of better measurement techniques should be studied together with the improved stop criteria.

SUMMARY AND CONCLUSIONS

In proof load tests, a load representative of the factored load combination is placed on a structure to show directly that this structure can carry the code-prescribed loads without problems. Since proof load testing involves large loads, it is necessary to evaluate if the test is safe in real-time. Stop criteria are limits to the structural responses that are evaluated in real-time during the test to evaluate the safety. A number of existing codes and guidelines for proof load testing contain stop criteria for flexure, including the German guideline for load testing, the Czech and Slovak codes, and the Spanish guidelines. In

most cases, however, the available stop criteria are arbitrary limits, or related to serviceability requirements. Serviceability requirements should dictate acceptance criteria, not stop criteria, since they give no information about structural safety, but about future durability.

To develop stop criteria that give information about structural safety, the theory of flexure in reinforced concrete beams was used. This theoretical basis results in a stop criterion for the concrete strain. Using the theoretical work on the maximum crack width of reinforced concrete elements in bending resulted in a stop criterion for the crack width. The set of stop criteria is completed with the limit to the residual crack width from the German guideline, a limit to the stiffness reduction, and a qualitative evaluation of deflection or deformation profiles and the load-deflection profile.

The evaluation of the stop criteria uses two requirements. The first requirement is that the comparison to failure tests should show sufficient margin of safety. For this purpose, the proposed stop criteria are compared with the results of two series of beam experiments from the laboratory and the failure tests on the Ruytenschildt Bridge. The margin of safety lies between 42 and 65% for the proposed stop criteria and thus fulfills this requirement. The second requirement is that the stop criteria should not be overly conservative. We evaluated this requirement by comparing the proposed stop criteria to the measured structural responses from a series of pilot proof load tests. These bridges were heavily instrumented, and the conclusion from these proof load tests was that the test did not lead to irreversible damage. The analysis of the stop criteria, which use fewer sensors, leads to the same conclusion. The proposed stop criteria thus fulfill the two requirements and can be proposed for proof load tests on reinforced concrete structures that are flexure-critical.

AUTHOR CONTRIBUTIONS

EL: theoretical work, experiments, and manuscript writing. YY: discussions of proposed stop criteria and experiments. CvdV: supervision of experiments and modifications to manuscript. DH: coordination of load testing research. AdB: practical perspective of proposal.

FUNDING

ACKNOWLEDGMENTS

REFERENCES

AASHTO (2016). *The Manual for Bridge Evaluation With 2016 Interim Revisions.* Washington, DC: American Association of State Highway and Transportation Officials.

ACI Committee 437 (2013). *Code Requirements for Load Testing of Existing Concrete Structures (ACI 437.2M-13) and Commentary.* Farmington Hills, MI: ACI Committee 437.

Aguilar, C. V., Jáuregui, D. V., Newtson, C. M., Weldon, B. D., and Cortez, T. M. (2015). "Load rating a prestressed concrete double-tee beam bridge without plans by proof testing," in *Transportation Research Board Annual Compendium of Papers* (Washington, DC).

Bonifaz, J., Zaruma, S., Robalino, A., and Sanchez, T. A. (2018). "Bridge diagnostic load testing in ecuador – case studies," in: *IALCCE 2018* (Ghent).

Ceský normalizační institut (1996). *CSN 73 6209 (736209) Loading Tests of Bridges (Zatěžovací zkoušky mostu)* (Prague).

Chen, X., Yang, Y., Evangeliou, P., and van der Ham, H. (2018). "Critical proof load for proof load testing of concrete bridges based on scripted fem analysis," in *IALCCE 2018* (Ghent).

Deutscher Ausschuss für Stahlbeton (2000). *DAfStb-Guideline: Load Tests on Concrete Structures (in German) (DAfStb-Richtlinie: Belastungsversuche an Betonbauwerken).* Berlin: Deutscher Ausschuss fur Stahlbeton.

Faber, M. H., Val, D. V., and Stewart, M. G. (2000). Proof load testing for bridge assessment and upgrading. *Eng. Struct.* 22, 1677–1689. doi: 10.1016/S0141-0296(99)00111-X

Fennis, S. A. A. M., and Hordijk, D. A. (2014). *Proof Loading Halvemaans Bridge Alkmaar (in Dutch).* Delft: Delft University of Technology.

Fennis, S. A. A. M., van Hemert, P., Hordijk, D., and de Boer, A. (2014). Proof loading Vlijmen-Oost; research on assessment method for existing structures (in Dutch). *Cement* 5, 40–45. Available online at: https://www.cementonline.nl/artikel/proefbelasting-viaduct-vlijmen-oost

Filar, Ł., Kałuza, J., and Wazowski, M. (2017). Bridge load tests in Poland today and tomorrow – the standard and the new ways in measuring and research to ensure transport safety. *Proc. Eng.* 192, 183–188. doi: 10.1016/j.proeng.2017.06.032

Frosch, R. J. (1999). Another look at cracking and crack control in reinforced concrete. *ACI Struct. J.* 96, 437–442.

Frýba, L., and Pirner, M. (2001). Load tests and modal analysis of bridges. *Eng. Struct.* 23, 102–109. doi: 10.1016/S0141-0296(00)00026-2

Halicka, A., Hordijk, D. A., and Lantsoght, E. O. L. (2018). "Rating of concrete road bridges with proof loads," in *ACI SP 323 Evaluation of Concrete Bridge Behavior Through Load Testing - International Perspectives,* (Farmington Hills, MA), 16.

Hungarian Chamber of Engineers (2013). *Guidelines for Interventions in Hungary (in Hungarian).* Budapes: Hungarian Chamber of Engineers.

Kohut, P., Holak, K., Uhl, T., Krupinski, K., Owerko, T., and Kura,ś, P. (2012). Structure's condition monitoring based on optical measurements. *Key Eng. Mater.* 518, 338–349. doi: 10.4028/www.scientific.net/KEM.518.338

Kopácik, A. (2003). "Loading tests of highway bridges in Slovakia," in *11th FIG Symposium on Deformation Measurements* (Santorini).

Lantsoght, E.O.L., van der Veen, C., and de Boer, A. (2016a). "Shear and moment capacity of the Ruytenschildt bridge," in *IABMAS 2016* (Foz de Iguacu).

Lantsoght, E.O. L., Van der Veen, C., and Hordijk, D. A. (2018). "Monitoring crack width and strain during proof load testing," in *IABMAS 2018* (Melbourne, VIC).

Lantsoght, E. O. L., De Boer, A., and Van der Veen, C. (2017a). Levels of approximation for the shear assessment of reinforced concrete slab bridges. *Struct. Concrete* 18, 143–152. doi: 10.1002/suco.201600012

Lantsoght, E. O. L., Koekkoek, R. T., Hordijk, D. A., and De Boer, A. (2017b). Towards standardization of proof load testing: pilot test on viaduct Zijlweg. *Struct. Infrastruct. Eng.* 16, 365–380. doi: 10.1080/15732479.2017.1354032

Lantsoght, E. O. L., Koekkoek, R. T., van der Veen, C., Hordijk, D. A., Boer, A. (2017c). Pilot proof-load test on Viaduct De Beek: case study. *J. Bridge Eng.* 22:05017014. doi: 10.1061/(ASCE)BE.1943-5592.0001131

Lantsoght, E. O. L., van der Veen, C., de Boer, A., and Hordijk, D. A. (2016c). Probabilistic prediction of the failure mode of the Ruytenschildt Bridge. *Eng. Struct.* 127, 549–558. doi: 10.1016/j.engstruct.2016.08.054

Lantsoght, E. O. L., Van der Veen, C., De Boer, A., and Hordijk, D. A. (2017d). Collapse test and moment capacity of the ruytenschildt reinforced concrete slab bridge. *Struct. Infrastruct. Eng.* 13, 1130–1145. doi: 10.1080/15732479.2016.1244212

Lantsoght, E. O. L., van der Veen, C., De Boer, A., and Hordijk, D. A. (2017e). Proof load testing of reinforced concrete slab bridges in the Netherlands. *Struct. Concrete* 18, 597–606. doi: 10.1002/suco.201600171

Lantsoght, E. O. L., van der Veen, C., de Boer, A., and Hordijk, D. A. (2017f). Required proof load magnitude for probabilistic field assessment of viaduct De Beek *Eng. Struct.* 148, 767–779. doi: 10.1016/j.engstruct.2017.07.010

Lantsoght, E. O. L., van der Veen, C., Hordijk, D. A., and de Boer, A. (2017g). State-of-the-art on load testing of concrete bridges. *Eng. Struct.* 150, 231–241. doi: 10.1016/j.engstruct.2017.07.050

Lantsoght, E. O. L., Yang, Y., Tersteeg, R. H. D., van der Veen, C., and de Boer, A. (2016d). "Development of Stop Criteria for Proof Loading," in *IALCCE 2016* (Delft).

Lantsoght, E. O. L., Yang, Y., van der Veen, C., de Boer, A., and Hordijk, D. (2016b). Ruytenschildt bridge: field and laboratory testing. *Eng. Struct.* 128, 111–123. doi: 10.1016/j.engstruct.2016.09.029

Lantsoght, E. O. L., Yang, Y., van der Veen, C., de Boer, A., and Hordijk, D. A. (2017i). Beam experiments on acceptance criteria for bridge load tests. *ACI Struct. J.* 114, 1031–1041. doi: 10.14359/51689786

Lantsoght, E. O. L., Yang, Y.,Van der Veen, C., De Boer, A., and Hordijk, D. A. (2017h). "Determination of loading protocol and stop criteria for proof loading with beam tests," in *fib Symposium 2017.* (Maastricht).

Ministerio de Fomento - Direccion General de Carreteras (1999). *Recomendaciones Para la Realizacion de Pruebas de Carga de Recepcion en Puentes de Carretera.* Madrid: Ministerio de Fomento - Direccion General de Carreteras.

Ministerio de Fomento (2009). *Instrucciones Para la Puesta en Carga de Estructuras (Pruebas de Carga Provisionales).* Ministerio de Fomento.

Ministerio de Fomento (2010). *Instrucción de Acciones a Considerar en Puentes de Ferrocarril (IAPF).* Ministerio de Fomento.

Research Institute of Roads and Bridges (2008). *The Rules for Road Bridges Proof Loadings (in Polish) (Zalecenia Dotyczace Wykonywania Badan pod Próbnym Obciazeniem Drogowych Obiektów Mostowych).* Warsaw: Research Institute of Roads and Bridges.

Schmidt, J. W., Halding, P. S., Jensen, T. W., and Engelund, S. (2018). "High magnitude loading of concrete bridges," in *ACI SP 323 Evaluation of Concrete Bridge Behavior Through Load Testing - International Perspectives,* (Farmington Hills, MA).

SIA (2011). *Existing Structures – Bases for Examination and Interventions.* SIA.

Slovak Standardization Institute (1979). *STN 73 6209 (736209) Loading Tests of Bridges (ZataŽovacie Skúšky Mostov).* Bratislava: Slovak Standardization Institute.

Steffens, K., Opitz, H., Quade, J., and Schwesinger, P. (2001). The loading truck BELFA for loading tests on concrete bridges and sewers (in German). *Bautechnik* 78, 391–397. doi: 10.1002/bate.200102600

NOTATION LIST

a	shear span
b	width of structural member
c	height of the compression zone
c_{cover}	concrete cover
d	effective depth
d_c	cover to the centroid of the tension reinforcement
$effR_u$	capacity of the structure
$ext.F_{lim}$	additional load that can be applied to reach the onset of non-linear behavior
$ext.F_{target}$	additional load to achieve the target proof load
f	total measurement
f_c	stress in the concrete in compression
f_{cm}	average concrete compressive strength
$f_{c,th}$	maximum stress in the concrete in the compression zone resulting from the stress-strain parabola by Thorenfeldt
f_{ctm}	average tensile strength of the concrete
f_{perm}	stress in the steel caused by the permanent loads
f_r	remaining measurement
f_s	stress in the steel
f_{ym}	the average yield strength of the tension reinforcement steel
$f_{0.01m}$	average value of the stress in the reinforcement steel at a strain of 0.01%, which marks the end of the elastic range of the steel
h	height of cross-section
h_{eff}	effective height, height of the fictitious tension tie in the tension zone of the concrete member subjected to bending
$l_{s,max}$	length over which slip between steel and concrete occurs
l_{span}	span length
n_{th}	material parameter in Thorenfeldt's parabola, function of the concrete compressive strength
s	reinforcement spacing
w	crack width
w_c	maximum crack width according to the method of Frosch
w_{max}	maximum crack width
w_{res}	residual crack width after unloading
$w_{res,lim}$	stop criterion for residual crack width after unloading
w_{stop}	limiting crack width
A_c	area of concrete cross-section
A_s	area of tension reinforcement
C	resultant of compression
E_c	instantaneous modulus of elasticity of concrete
E_s	modulus of elasticity of reinforcing bars
F_{lim}	load at which the onset of non-linear behavior occurs
F_{target}	target proof load
G_1	permanent loads
G_{dj}	permanent loads not acting on the structure at the moment of testing
P_{max}	maximum load in failure test
Q_d	live loads
S_{cal}	calculated value of the elastic deformation
S_e	measured value of the elastic deformation

(Continued)

S_r	permanent deformation
S_{tot}	total deformation, sum of elastic and permanent deformation
T	resultant of tension
α	limit to the elastic deformation
α_1	limit to the total deformation
α_2	limit to the deformation for a repeat load test on a new bridge
α_3	limit to the permanent deformation after a repeat load test on a new bridge
α_e	ratio of modulus of elasticity of steel to modulus of elasticity of concrete
α_{lim}	limit to the remanence
α_{rem}	remanence
α^*_{rem}	remanence in a repeat load cycle
β	limit to the elastic deformation
β_{fr}	strain gradient factor used in the method of Frosch
β_{th}	factor to go from maximum value in a parabola to average value
β_{cr}	coefficient that depends on type and duration of loading
γ	the ratio of the permanent loads to the sum of permanent and proof loads
Δw	increase in crack width
ΔEI_{meas}	stiffness reduction in experiment
ε_0	strain that corresponds to the maximum stress in a parabolic stress-strain diagram
ε_c	measured strain in the concrete
$\varepsilon_{c,bot}$	concrete strain at bottom of cross-section
$\varepsilon_{c,bot,max}$	concrete strain at the bottom of cross-section that corresponds to a yield stress in the steel of 90% of the yield strength
$\varepsilon_{c,comp}$	maximum strain in the concrete under compression
$\varepsilon_{c,top}$	concrete strain at top of cross-section
ε_{c0}	analytically determined short-term strain in the concrete caused by the permanent loads acting on the structure before the application of the proof load
$\varepsilon_{c,lim}$	limiting strain, $600\mu\varepsilon$ which can be increased to $800\mu\varepsilon$ for concrete with a compressive strength larger than 25 MPa
ε_{cm}	average concrete strain within $l_{s,max}$
ε_{cs}	shrinkage or swelling strain
ε_s	strain in tension reinforcement
ε_{s2}	measured strain in the reinforcement steel
ε_{s02}	analytically determined strain in the reinforcement steel caused by the permanent loads acting on the structure before the application of the proof load, assuming that the concrete is cracked
ε_{sm}	mean steel strain
ε_{stop}	stop criterion for strain at the bottom of a flexure-critical reinforced concrete member subjected to sagging moment
η_r	coefficient that depends on type and duration of loading
ρ	longitudinal reinforcement ratio
$\rho_{s,eff}$	reinforcement ratio over the effective height
σ_s	steel stress
σ_{sr}	steel stress at cracking
τ_b	bond stress
φ_s	bar diamete

Experimental Determination of the Longitudinal Pier Stiffness of a Long Railway Viaduct

Marc Wenner[1], Thomas Meier[2], Frederik Wedel[1], Gregor Schacht[1*] and Steffen Marx[3]

[1] Marx Krontal Partner, Hanover, Germany, [2] Baugrund Dresden Ingenieurgesellschaft mbH, Dresden, Germany, [3] Institute of Concrete Construction, Leibniz University Hannover, Hanover, Germany

Track–bridge interaction plays a decisive role in the design of long railway bridges due to the high braking and acceleration forces that occur and the fact that the continuous rail is attached to the superstructure. A fundamental parameter for the calculation of the effects of track–bridge interaction is the equivalent longitudinal stiffness of piers and abutments with fixed bearings. The equivalent horizontal stiffness is commonly calculated using a pile group model. The static and "dynamic" stiffnesses of the Itz valley railway viaduct were determined experimentally by using a static diagnostic load test and a braking test, which allowed for the verification of the additional rail stresses and the bearing forces with realistic input parameters. Furthermore, numerical 3D FE analyses of the deep foundation system were carried out to provide class-A predictions of the experimental results. In this article, the experimental setup and the execution and evaluation of the two tests are presented. A comparison of the experimental results and the numerical predictions is also carried out.

Keywords: experiment, diagnostic load test, braking test, railway viaduct, pier stiffness, track–bridge interaction

INTRODUCTION AND OBJECTIVE

In the design of railway bridges, the higher traffic loads, greater braking, and acceleration forces than those in road bridges, and the small allowable deflections play a decisive role. The bridge dynamics and track–structure interaction represent governing criteria in the design process of railway bridges (Marx and Geißler, 2010; Marx and Seidl, 2011; Marx and Schneider, 2014; Wenner et al., 2018, 2019). The ballasted or non-ballasted track provides the connection between the track and the structure. When thermal deformations occur in the bridge or longitudinal displacements take place in the superstructure due to vehicles braking or accelerating, the track and structure interact and jointly contribute to transferring the longitudinal loads (Wenner et al., 2016a,b). This leads to additional rail stresses and bearing forces, as well as deformations, which have to be determined analytically and compared with the limit values stipulated in the relevant standard.

To ensure compatibility between the rails and the bridge structure and to limit the magnitude of the rail stresses, several parameters can be varied during the design. The design of the track superstructure (type of track superstructure, properties of the components, presence of rail expansion joints), the superstructure length, and the equivalent horizontal spring stiffness in the longitudinal direction of the substructures (which consist of piers and pile caps, bored piles, and the surrounding soil) are the biggest influencing factors. This equivalent horizontal spring stiffness will henceforth be referred to as "substructure stiffness."

FIGURE 1 | Itz valley railway viaduct. The motorway viaduct of the A 73 runs parallel to the railway viaduct (in the background). Reproduced from Wenner et al. (2019) with permission from [Ludolf Krontal].

Stiff substructures generally reduce the stress experienced by the track superstructure and are therefore desirable. Even though the rail stresses caused by the thermal deformations of the bridge can increase due to stiff substructures, such substructures attract the braking and acceleration forces, thereby reducing rail stresses and allowing for low-deformation longitudinal load transfer. However, the effective substructure stiffness is often underestimated in structural analysis. In order to develop a more economic design or assess the state of an existing structure, it may be necessary to carry out a more detailed investigation of the substructure stiffness and a more precise calculation of the stresses in the rails and structure.

During the detailed design of the non-ballasted track of the Itz valley railway viaduct (**Figure 1**) it was discovered that the rail stresses exceed the allowable stresses by a large margin. As the values of the analytically determined rail stresses react very sensitively to the assumed longitudinal substructure stiffness and a greater stiffness would reduce the magnitude of the rail stresses, it was decided to determine the actual longitudinal stiffness of the substructures experimentally. It is known that the soil reacts a great deal more stiffly under short-term than quasi-static loading [see also Ril 804.3401, section 6(2)]. For this reason, both static tests (see section Static Diagnostic Load Test) and braking tests (see section Braking Test) were carried out and accompanied by detailed numerical analyses.

ITZ VALLEY RAILWAY VIADUCT

The Itz valley railway viaduct is part of the new high-speed rail line between Ebensfeld (Bavaria) and Erfurt (Thuringia); see **Figure 1**. The 868-m structure spans across the Itz valley, the Coburg–Sonneberg rail line, and several roads near Rödental (Bavaria) at a height of ∼25 m.

The structure has 15 spans, each 57 m long, and consists of six 2-span and one 3-span superstructure segments; see **Figure 2**. The railway bridge, which was erected in 2005, is a steel–concrete composite structure, in which two steel trusses at a mutual

distance of 6.20 m support the reinforced concrete deck. The track superstructure was executed as non-ballasted track. The structure was intended to have continuous tracks along its entire length, without any expansion joints.

The piers in the middle of the two-span superstructure segments serve as longitudinally fixed points for these segments. The three-span superstructure segment has two longitudinally fixed points (at axes 100 and 110) and is therefore statically indeterminate. The reinforced concrete piers have a box cross section. They are founded on inclined large bored piles with pile caps; see **Figure 3**.

The bridge site is located in the main block of southern Germany (*Süddeutsche Großscholle*), which consists of Mesozoic rock. The deeper region of the subsoil consists of various types of the slightly weathered clay- and siltstone of the *Lehrbergschichten*, and is covered by cover and riverine loam, as well as by river and bench gravel. The piles of the deep foundation extend into load-bearing material, either rock or slightly weathered clay- and siltstone, which, depending on the axis, is found at depths from 14 to 29 m. The subsoil layers at axis 60 are shown in **Figure 3** as an example.

STATIC DIAGNOSTIC LOAD TEST
Conceptual Development and Preparation of the Test

The goal of the test was to determine the stiffness of the substructure (piles and foundation) in the longitudinal direction of the bridge for all fixed points in order to obtain the most realistic parameters possible for verifying that the rail stresses do not exceed the allowable values. The measurement concept was designed to generate horizontal forces in the piles and measure the resulting pile deformations, so that the load–deformation behavior could be used to calculate the equivalent global spring stiffnesses of the deep foundation systems and piles (referred to as "substructure stiffness" in this paper).

The longitudinal forces in the bridge superstructure were generated by two hydraulic presses positioned in the gaps between the bottom flanges of two neighboring superstructure segments. The applied forces were recorded with load cells; see **Figure 4B**. The presses were used to introduce forces of equal magnitude in the two superstructures. The forces were transferred through the superstructure segments and generated stresses in the adjacent, longitudinally fixed piers.

The pier head displacement required to determine the substructure stiffness is comprised of several components (see also **Figure 4A**)

- Tilt of the foundation w_{ϕ}.
- Displacement of the foundation w_h.
- Bending of the pier w_{EI}.

To evaluate the results and compare the analytical and measurement results, the displacement of the pier head needs to be recorded and a separation of the displacement components must be carried out. To measure the deformations and displacements, the following measures were taken (**Figure 4B**):
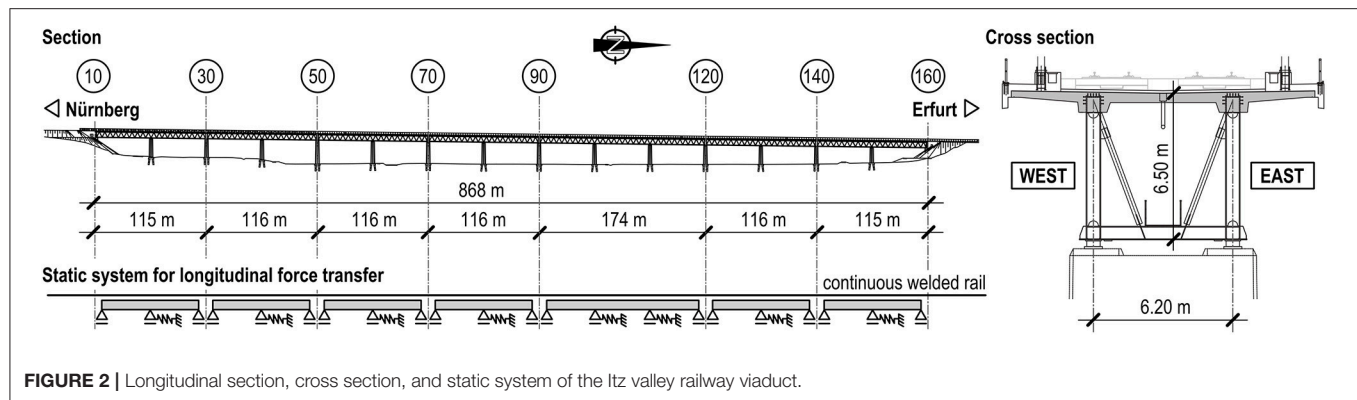
FIGURE 2 | Longitudinal section, cross section, and static system of the Itz valley railway viaduct.
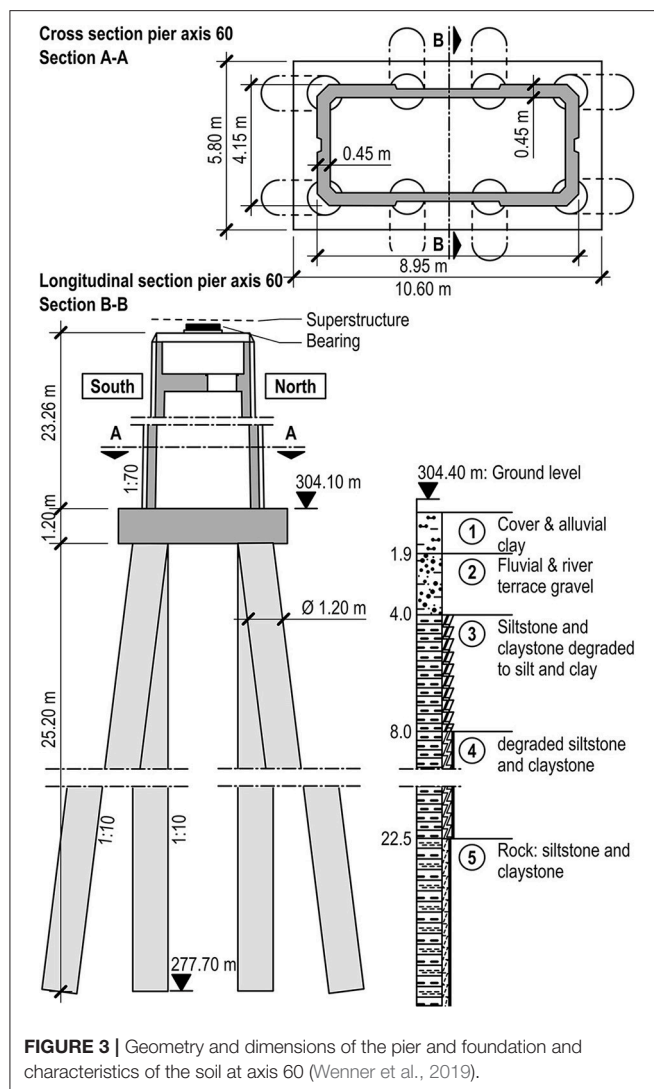
FIGURE 3 | Geometry and dimensions of the pier and foundation and characteristics of the soil at axis 60 (Wenner et al., 2019).

- Measurement of the relative longitudinal displacements and rotations of the structure, using six displacement sensors in each of the eight joints of the superstructure.
- Determination of the absolute pier head displacement through geodetic measurements, using a tachymeter and prisms.

- Measurement of the bearing play of the fixed bearings at the fixed points.
- Measurement of the tilt of the pier at its bottom, using an inclination sensor just above ground level.
- Measurement of the displacement of the pier at its bottom by using a laser distance sensor positioned at a distance of about 10 m from the pier and outside the zone affected by subsoil movements.

To avoid overloading the structure during the test, the longitudinal force to be introduced was limited to 80% of the characteristic bearing loads assumed in the design of the structure (2 · 1.25 MN).

In preparation for the monitoring of the tests, FE analyses of the various subtests were carried out and expected values for loads and deformations were extracted. The exceeding of the expected values, disproportionate changes in forces or displacements during load application, and a larger-than-expected difference in the forces of the two hydraulic presses were defined as abort criteria.

This kind of real-scale test is very rarely executed. A similar test, carried out on the Sinntalbrücke Schaippach bridge on the Hanover–Würzburg rail line (Kempfert and Schwarz, 1984), has been reported in the literature. These tests were executed during the construction stage—the superstructure had not yet been built and the piers were thus not loaded.

Execution

A special load application construction was used to uniformly introduce the longitudinal forces, which reached magnitudes up to 1.25 MN, into the protruding web plates of the box-section bottom chords; see **Figure 5A**.

Six subtests were carried out to investigate the forces on the longitudinally fixed piers. To do this, load was applied to the longitudinally fixed pier closest to the press, so that the substructure stiffness for this pier could be determined. After each subtest the presses were removed, transported along the maintenance gantry to their next location between superstructure segments and installed.

The superstructure segments are linked longitudinally by the rails. To avoid the rails transferring an unknown part of the forces introduced into the superstructure, the rail joints above the location of the press and at the joints of the neighboring

FIGURE 4 | (A) Components of the pier head deformation. (B) Schematic of the test setup at axis 30.

FIGURE 5 | (A) Hydraulic press, load cell, and load application construction. Source: Marc Wenner. (B) Rails close to the bridge joint were released to decouple the neighboring superstructure segments. Reproduced from Wenner et al. (2019) with permission from [Marc Wenner].
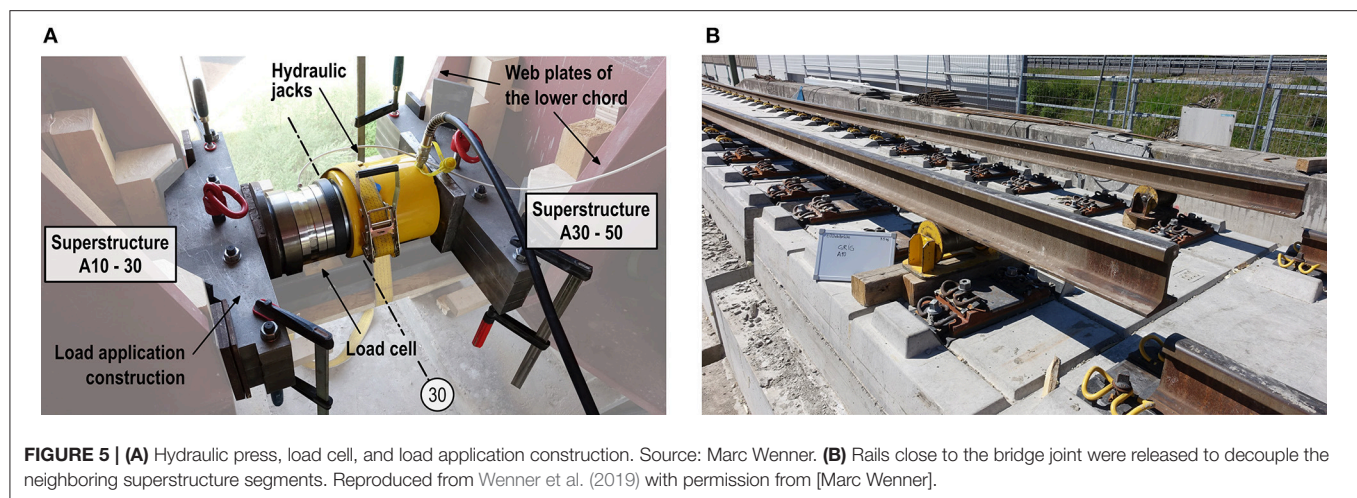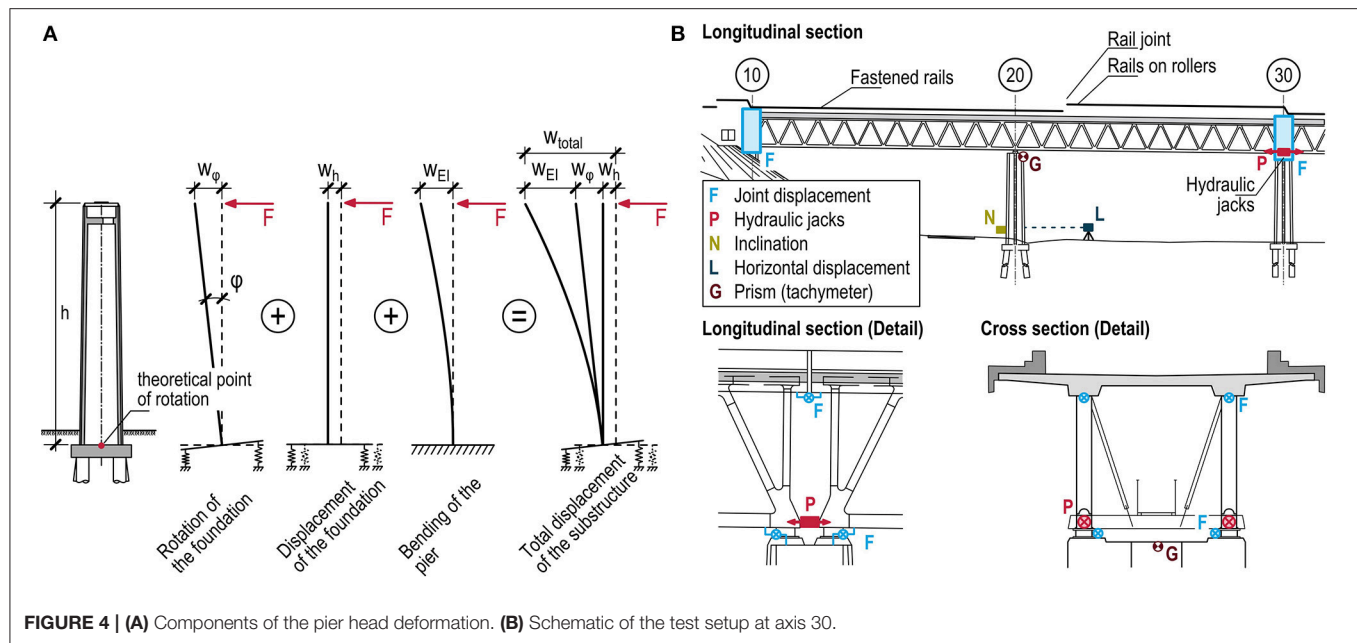
superstructure segments were opened during the tests. This ensured that the longitudinal force was transferred exclusively by the structure (see also **Figure 5A**). As the track superstructure was still under construction at the time of testing and not all rail segments had yet been welded together, the rail fasteners of the four rails in between the three relevant axes and up to the closest rail gap/fishplates were released in each subtest, and the rails were placed on rollers (**Figure 5B**).

Each subtest consisted of various load cycles (LZ), as shown in **Figure 6A**. During the first load cycle, the target load was carefully approached in several steps. At each step, the plausibility of the measurements was checked and the behavior was compared with the expected values. In load cycles two and three the same target load was applied, however using fewer load steps in order to generate a statistically sound basis. In the fourth, and last, load cycle, the load application rate was

increased significantly. The force was applied with the full power of the hydraulic press, and for unloading the hydraulic pipes were opened rapidly. The unloading process lasted ∼5 s and was intended to represent the quasi-dynamic load case. The measurement data was acquired with a sample rate of 1 Hz. The geodetic measurements were carried out during each load break, as shown in **Figure 6A**.

To monitor and control the test, the governing control parameters (press force, expansion joint, and pier deformations) were visualized on two screens in real time. It was thus possible to compare the measurement results with the independent geodetic measurements and the expected values while the test was being executed, so that the test could be aborted if unusual behavior was observed or one of the abort criteria defined in section Modeling of the Foundation to Predict the Substructure Stiffness was fulfilled.
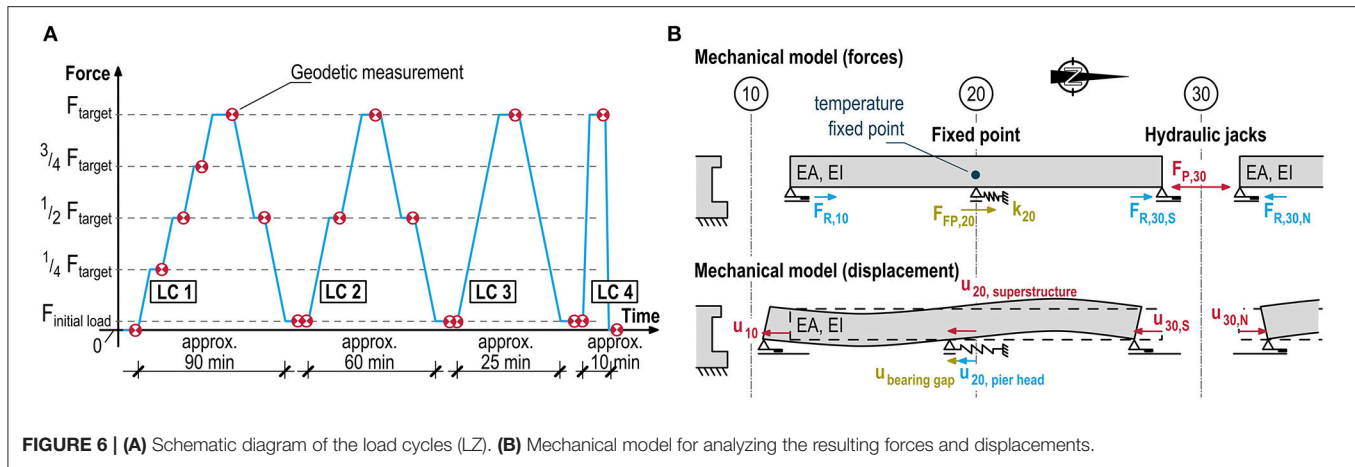
FIGURE 6 | **(A)** Schematic diagram of the load cycles (LZ). **(B)** Mechanical model for analyzing the resulting forces and displacements.
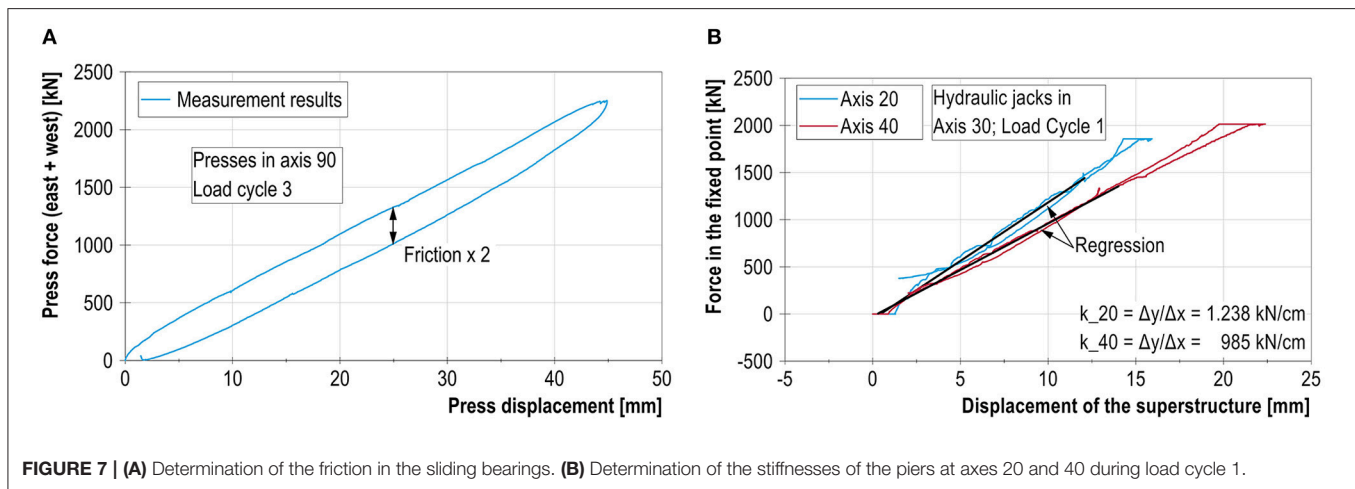
FIGURE 7 | **(A)** Determination of the friction in the sliding bearings. **(B)** Determination of the stiffnesses of the piers at axes 20 and 40 during load cycle 1.

Evaluation and Results

The stiffness with respect to the bottom edge of the superstructure is an important parameter for the calculation of the track–structure interaction. This stiffness differs from the stiffness with respect to the pier head by the active bearing displacement (bearing play and elastic deformation), which was also measured.

It was not possible to directly measure the fixed point displacements and forces which were required for the calculation of the substructure stiffnesses. Therefore, these parameters were determined using a mechanical model as shown in **Figure 6B**, using the executed measurements and reasonable assumptions for the superstructure deformations.

Using the subtest with the presses located at axis 30 as an example, the model and approach are presented. The following forces act at axis 30: the press forces ($F_{P,30}$), which push apart the bottom chords of the two neighboring superstructure segments, and the friction forces ($F_{R,30}$), which are activated due to the displacement of the superstructure on the sliding bearings and act in the opposite direction of the press force. Identical friction forces occur in the sliding bearings at axis 10 ($F_{R,10}$) and axis 50 ($F_{R,50}$). These were determined from the hysteresis loop in the

load–deformation diagram shown in **Figure 7A**. The fixed point forces in axes 20 and 40 ($F_{FP,20}$ and $F_{FP,40}$) can be obtained from the appropriate force equilibria of the respective partial systems.

The fixed point displacements at the level of the bottom chord are calculated from the displacements of the superstructure joints (measured inside the joints). The measurements contain other displacement and deformation components which must be taken into account. Due to the flexural and tensile stiffness of the bridge girders and the localized and eccentric load introduction into the bottom chords of the superstructure segments, a shortening of the superstructure and twisting of the cross sections occur, as shown schematically in **Figure 6B**. To determine these components, a numerical analysis simulating the press force load case is carried out, which allows a combined evaluation of the measurement and calculation data. Thermal deformations, occurring because of the long duration of the tests and the temperature load on the steel bottom chords due to solar radiation, must also be taken into account. The results of the geodetic measurements were used for plausibilization purposes. The calculated and measured displacement agree very well with each other (see, for example, **Figure 8**), thereby confirming the suitability of the applied methodology.

FIGURE 8 | Components of the pier head deformation at axis 20 (hydraulic presses located at axis 30).
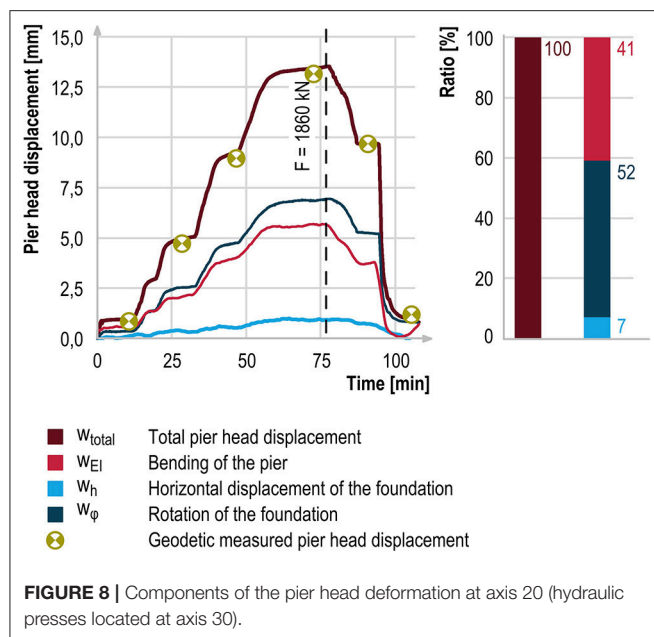
Using the measured force acting at the fixed point and the corresponding deformation of the superstructure at the same location (above the fixed point), the substructure stiffnesses for each individual fixed pier can be determined (shown in **Figure 7B** for axes 20 and 40). The curve is nearly linear, and the stiffness is higher for small displacements (up to 2 mm). A higher stiffness was also observed at the beginning of the unloading process in load cycle 4, in which the force decreased very rapidly.

The results are presented in section Comparison of the Experimental and Analytical Results and compared with the results of the three-dimensional finite element analyses.

A further goal of the test was the separation of the deformation components of the pier head displacements (see also **Figure 4A**) in order to assess the causes of possible differences with respect to the 3D FE model.

During the tests, the tilt and displacement of each foundation was measured directly with an inclination sensor or a laser distance sensor. It should be noted that due to the presence of backfill both the laser distance sensor and the inclination sensor were located above the top edge of the foundation and the analytical pivot point; see **Figure 4A**. The measurement results had to be adjusted to exclude the components due to bending and twisting and converted to refer to the top edge of the foundation. The component due to bending of the pier w_{EI} was determined from the remaining amount ($w_{total} - w_\phi - w_h$). The plausibility and quality of the evaluation process are confirmed by the good agreement between w_{EI} and the analytical deformation of the cantilever beam. As an example, the separated components for pier axis 20 (which was used to illustrate the approach for determining the stiffnesses) are shown in **Figure 8**. The pier head displacement is 13.5 mm; the corresponding fixed point force is 1,860 kN. The smallest contribution (7%) is made by the direct horizontal displacement of the pier. The bending of the pier

accounts for 41% of the total deformation, and the tilting of the foundation has the largest influence on the deformation (52%).

Modeling of the Foundation to Predict the Substructure Stiffness

In geotechnical practice, two different approaches are generally used to analytically determine the equivalent spring stiffnesses of pile foundation systems (**Figure 9**).

One approach uses FE programs to analyse pile groups modeled as frameworks, in which the subsoil in the vicinity of the piles and underneath the pile group cap (if applicable) is taken into account by using elastic foundation approaches based on empirical values (method 1). The elastic foundation approaches for piles generally assume that the foundation stiffness varies with the depth, while a constant foundation stiffness is assumed underneath the foundation. It is well known that the subsoil reaction depends on the occurring displacement if the subsoil is subjected to loads generated by piles or pile caps. This can be accounted for by iteratively adjusting the foundation approaches. Information on this topic can be found in the publication *EA Pfähle* (Deutsche Gesellschaft für Geotechnik [Hrsg.], 2012), for example.

Alternatively, when using the finite element method (FEM) or the finite difference method (FDM) in the area of foundation engineering, the subsoil is modeled with continuum elements. Combined with a suitable material model and contact formulations for the interfaces between the subsoil and reinforced concrete structural elements, their interaction under load can be modeled realistically (method 2). To achieve this, the material model should reflect at least the fundamental soil-physical properties of stress dependence, history dependence, and deformation dependence ("small strain stiffness") of the Young's and shear moduli.

The calculation results obtained with this method also include the load- and displacement-dependent elastic foundation stiffnesses of the piles and pile group cap. If, for example, the deep foundation of bridge piles in uneven/inclined terrain is to be investigated, a realistic consideration of this influence is only possible with method 2.

Comparison of the Experimental and Analytical Results

In this investigation, both approaches were used to provide class-A predictions, i.e., the analytical load–deformation predictions were determined prior to the execution of the diagnostic load tests. For method 1, a pile group program was used to carry out the static analysis of the existing structure. The calculations according to method 2 were executed with the software Plaxis® 3D.

The analytical results for the tilting and displacement and the results of the diagnostic load test are illustrated in **Figure 10** for pier axis 40. Furthermore, a comparison of the resulting global stiffnesses at the level of the bottom edge of the substructure is shown in **Table 1**.

The conclusions drawn from the comparison of the analytical and experimental results are as follows:

FIGURE 9 | Comparison of the two methods for the calculation of the deep foundation stiffness.
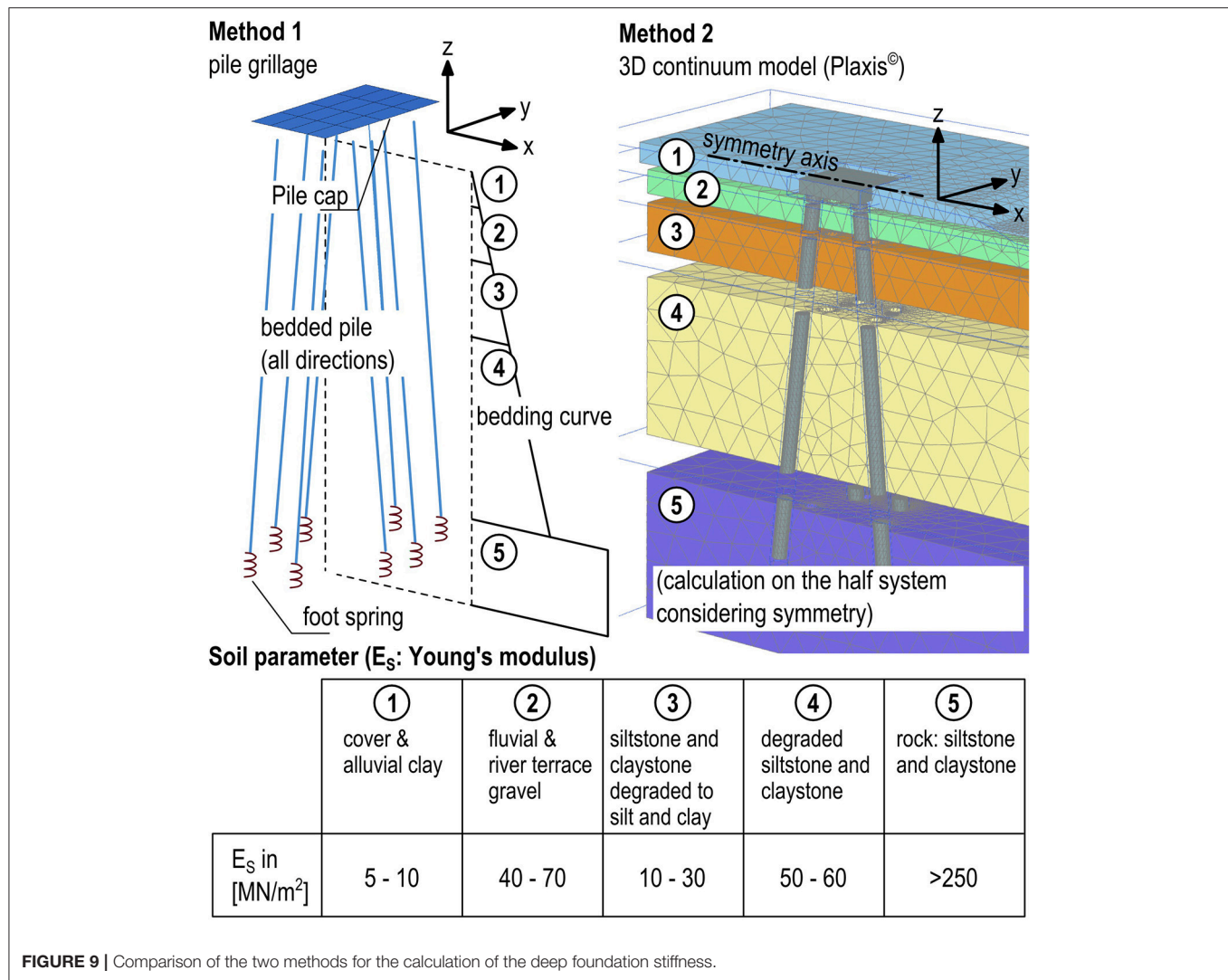
- The pile group method (method 1) with piles on a horizontal elastic foundation yields significantly lower stiffnesses than the *in-situ* tests and the FE analyses of method 2. The experimentally determined stiffnesses of the shorter piles in axes 20 and 150 are 250 and 310% higher, respectively, than the stiffnesses obtained with method 1. The stiffnesses of the longer piles are underestimated by about 170 to 200%. Whether these results can be considered to be conservative depends on the type of verification to be carried out. A lower stiffness leads to an overestimation of the rail stresses due to braking and an underestimation of the bearing forces.
- The calculations according to method 2 yield a load- (and hence deformation-) dependent, nonlinear, and slightly direction-dependent behavior of the resulting equivalent horizontal spring stiffnesses. As expected, the stiffnesses for smaller displacements are larger than those for larger displacements. The direction-dependency (see **Figure 11**) is due to the topology of the terrain. In the test, however, this strong nonlinearity was not observed (see **Figure 10**).

- The results of the 3D FE analysis according to method 2, in which characteristic values based on the information from the geotechnical report (upper limit) were used, agree with the evaluation results of the static diagnostic load tests of the three analytically investigated pier axes (20, 40, and 60). In the tests, the foundation reacted more stiffly to higher fixed point forces than predicted with method 2.
- The good agreement between the numerical results of method 2 and the evaluation results of the static *in-situ* diagnostic load tests can be considered as a validation of this approach for the analytical determination of equivalent spring stiffnesses. Even so, the quality of the results still depends on the quality of the geotechnical survey and its interpretation for deriving the soil-mechanical parameters.
- When the maximum press force was kept constant during 30 min of the static *in-situ* diagnostic load tests, additional displacements of up to ~1 mm were measured. Due to the project-specific boundary conditions

FIGURE 10 | (A) Comparison between measured and calculated displacements and rotation of the foundation at axis 40. **(B)**. Comparison between the measured and calculated stiffness of the substructure at axis 40.
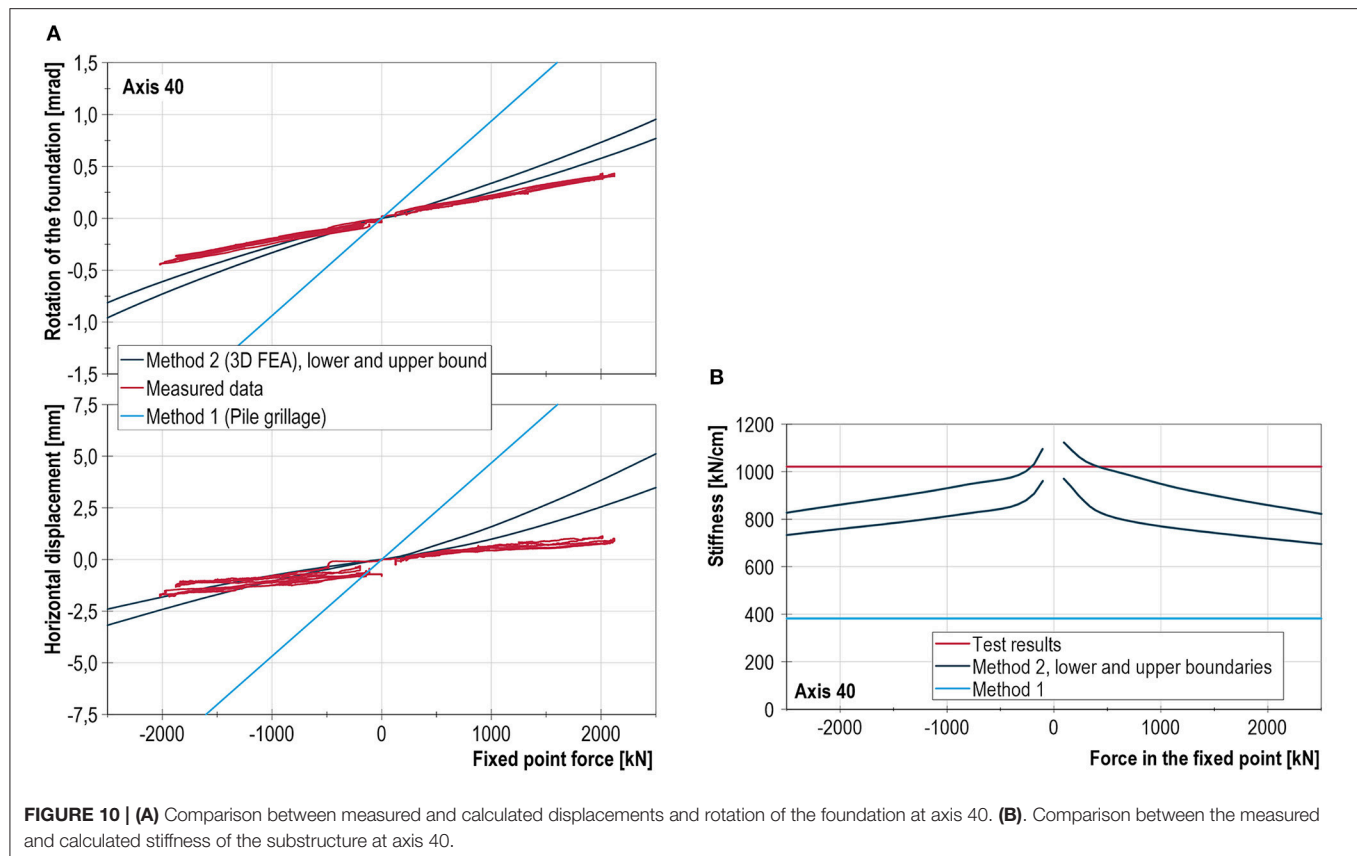
and time constraints it was not possible to maintain the load at this level until the displacements became negligibly small.

- Deep foundations located in saturated fine-grained soil, such as those of the presented bridge, and subjected to long-term unidirectional load, can experience additional horizontal fixed point displacements due to the consolidation and creep of the subsoil. This results in a decrease in bearing stiffness over time, which has not been considered in the experimental and analytical investigations carried out to date. With method 2 it is possible, in principle, to consider deformations due to consolidation and creep effects in the analysis. To take into account creep effects, however, more detailed material models and appropriate expertise for determining the model parameters are required.

BRAKING TEST

Concept

The primary goal of the braking tests executed on the Itz valley railway viaduct was the determination of the actual rail stresses due to braking events and their comparison with analytically determined expected values. Similar tests have been documented in the literature (Bernhard, 1936; Office de recherche et d'essais (ORE), 1967; Geißler et al., 2002; Stein and Quoos, 2005; Seidl, 2013; Marx et al., 2018; Schacht et al., 2018). A further, less

TABLE 1 | Comparison of the stiffnesses.

	Analytical stiffness | method 1 [kN/cm]	Analytical stiffness | method 2 [kN/cm]	Test [kN/cm]
Axis 20	305	936…1,031	1,262
Axis 40	382	738…858	1,021
Axis 60	219	531…583	660
Axis 80	264	-	806
Axis 100	379	-	1,043
Axis 110	369	-	1,069
Axis 130	344	-	1,009
Axis 150	463	-	1,622

The results for method 2 are given for the upper and lower limits of the soil parameters and a force of 2,000 kN. The test results are the average values of all the load cycles.

important goal of the test was the estimation of the "dynamic stiffness" activated during the braking process.

To achieve these goals, the structural reactions of the bridge and rails (resistance) and the applied braking force (action) was measured. The resistance was measured as follows (only the decisive measures are shown):

- Measurement of the relative longitudinal displacements of the structure at each of the eight bridge joints (see **Figure 4A**).
- Measurement of the longitudinal strains of the rails at the level of the neutral axis of the rails at each of the eight bridge joints.
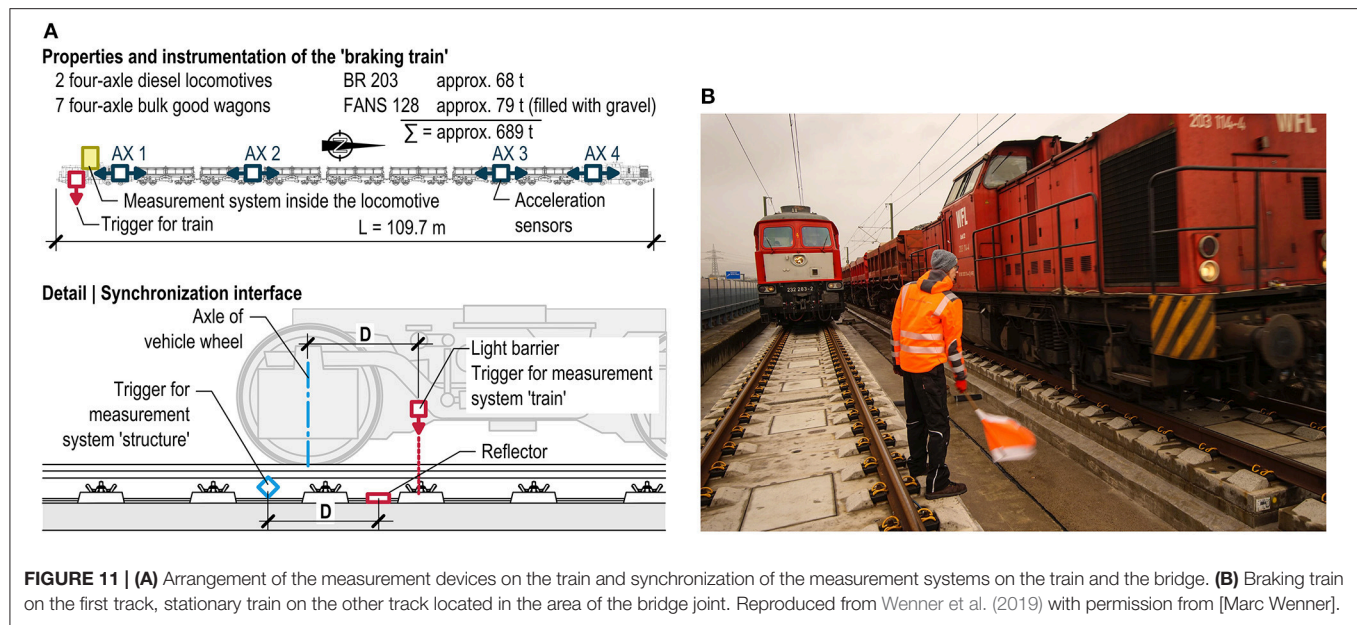
FIGURE 11 | (A) Arrangement of the measurement devices on the train and synchronization of the measurement systems on the train and the bridge. **(B)** Braking train on the first track, stationary train on the other track located in the area of the bridge joint. Reproduced from Wenner et al. (2019) with permission from [Marc Wenner].

This measurement was executed with strain gauges located on one rail per track.

To determine the braking force, the horizontal accelerations of the vehicle were measured at four locations along the train length (**Figure 11A**). Using the mass of the railway wagons, which were weighed prior to the test, the braking force was determined.

The measurements were carried out by two separate and independent measurement systems attached to the train and the structure. The evaluation of the measurement results, however, requires the chronologically synchronous acquisition of the signals by both measurement systems. If a synchronized trigger in both systems is released when the vehicle passes over a specific location on the rail (see **Figure 11A**), a precise synchronization of the signals during data evaluation can be achieved.

Execution

Two trains were used to carry out the braking test. The instrumented "braking train" was used to generate the braking force, while the second train served solely as superimposed vertical load destined to induce a local increase of the resistance to longitudinal displacements on the neighboring track during selected braking processes (**Figure 11B**). Some reference trips were carried out at the beginning of the test series so as to determine the influence of the vertical load of each train individually (in the form of influence lines). Subsequently, the actual braking tests were carried out. The braking was executed as emergency braking in brake position P. This combination ensures the rapid and complete venting of the main brake pipe of the train, and thus the full braking effect is achieved in the shortest time possible. The selected configuration of the train is chosen to ensure that the entire train is located on the substructure when the brake is activated.

The sequence of the test was designed to ensure that the "braking train" comes to a halt on each superstructure segment,

in each direction once. For the statistical validation of the results, three successful braking events should be achieved in each target stopping position—a brake event was considered to be successful if the vehicle stopped within 2 m of the target stopping position, which was located at a distance of 5 m from the bridge joint. The brake events occurred with an initial speed of 20 km/h (shunt track) and were initiated with a flag signal (**Figure 11B**), given at a distance of the braking length from the target stopping position. The braking distance was ∼20 m in dry weather and was reliably reproducible (scatter ∼±1.5 m), so that generally no more than three tests had to be carried out. On the second day of testing it rained and therefore only service braking was executed, which negatively affected both the magnitude of the braking force and the precision of the stopping position of the vehicle (scatter of ∼±10 m).

Evaluation and Results

The braking acceleration measurements on the train showed that the wagons experience a significantly greater acceleration during the braking jerk than the locomotives (**Figure 12**). Also, the front wagons of the train come to a halt later than the back wagons (by ∼0.02 s), which can be attributed to the collision of the back wagons with the front wagons; refer also to Bundesbahn-Zentralamt München (1979). On the first day of testing, a braking acceleration of up to a = 2.2 m/s^2 (during the braking jerk) was achieved by carrying out emergency braking under dry track conditions. This corresponds to a coefficient of friction of μ = a/g = 0.22 and a braking force of up to 1,470 kN for a train with a weight of 689 t. On the second day of testing, only 50% of this force could be reached, because only service braking could be executed on the wet tracks.

To analyse the behavior of the system, the force sustained by the bearings and the corresponding longitudinal displacement had to be determined. To do this, geometric and static

FIGURE 12 | Braking acceleration measured by the four sensors installed along the train.
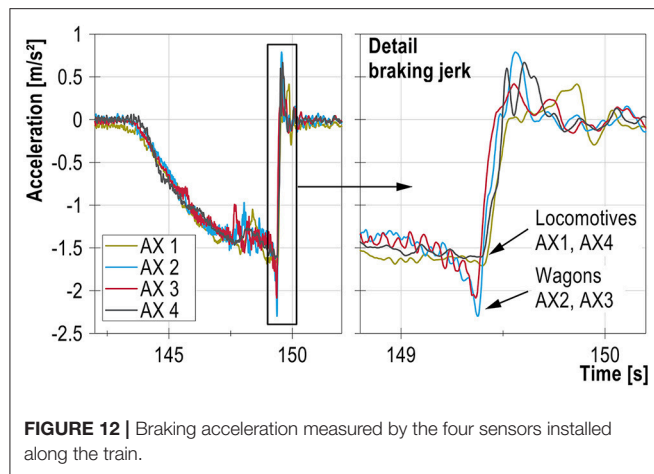
assumptions were made (**Figure 13**), and a static equilibrium was assumed. As the superstructure experiences vibration during and after braking (**Figure 14**), the developed equations are only valid under certain conditions. Up to the braking jerk, the acceleration of the superstructure is small, and thus the equations can be used to yield approximate results for this time span. As soon as the superstructure starts to vibrate, however, inertia forces are activated which are not taken into account in the developed equations.

In a second step, the behavior of the structure and track superstructure was analyzed. A typical structural reaction is shown in **Figure 14**, using the example of the braking process executed on superstructure segment A10–A30 in the direction of axis 10. The joint at axis 10 closes, while all other joints open. An elongation occurs in the structure between axes 30 and 160. Owing to the inertia of the superstructure segments, the reactions of the individual segments occur with time delays—~0.5 s between axes 10 and 160. The amplitudes of the deformations are 1.6 mm at the most and increase with increasing distance to the target stopping position (**Figure 14**). As expected, the development of the rail stresses over time corresponds with that of the deformations of the bridge structure. The maximum tensile and compressive stresses during the braking jerk are ~+10 N/mm^2 (axis 30) and − 20 N/mm^2 (axis 10). Depending on the superstructure segment, ~35–45% of the braking force is transferred to the substructure of this segment; the remaining force is transferred to neighboring superstructure segments by the rails.

After the deformation due to the braking jerk, the bridge structure, which has a significant mass, undergoes deformation recovery at great speed, followed by the attenuation of the vibration over several periods. This leads to displacements and stresses with opposite signs to those recorded during the braking jerk. During the first downswing and the upswing of the second period, the stresses at nearly all the axes are higher than those recorded during the actual braking jerk, with the exception of the directly affected bridge joints (see also Stein and Quoos, 2005). The dynamic response of the multi-mass oscillator that is the bridge structure strongly influences the behavior of the

system and the magnitude of the rail stresses during braking. Due to the phase-delayed vibration of the individual superstructure segments following the braking jerk, the static model used for calculating the response of the bridge and track superstructure cannot model the occurring effects. It was observed, however, that by modeling multiple load cases and vehicle configurations on the structure and using more conservative model assumptions (such as a higher resistance to longitudinal displacement) the occurring maximum rail stresses during braking are estimated by the model with sufficient accuracy.

Finally, the force transfer to the substructure was analyzed. To do this, the sum of the longitudinal force transferred to the substructure (determined according to **Figure 13**) as a function of the calculated superstructure displacement was drawn for each braking event. As explained above, this could only be done for the time period leading up to the braking jerk (the time period between 143.5 and 149.5 s for braking event 2.1.3, for example). As an example, the result for axis 20 for a "braking drive" on superstructure segments A10–A30 is shown in **Figure 14B**.

A definite distribution of the forces between the various pier axes ($F_{R,10}$, $F_{A,20}$, and $F_{R,30,S}$ in the example shown) and subsequent determination of the "dynamic stiffness" of the longitudinally fixed axis is not possible due to the following reasons:

- The forces acting at the level of the pier heads were not measured directly. It was not possible to quantify exactly the magnitude of the friction forces and the influence of the bearing play and the inertia forces; only the sum of the superstructure forces can be determined.
- The deformations of the pile heads were not measured directly, but rather calculated from the measured relative displacements and assumed deformations of the bridge structure. As the displacements are relatively small, the results exhibit some uncertainty due to the utilized methodology.

The friction forces were determined during the static diagnostic load test (section Static Diagnostic Load Test). These range from 30 to 70 kN, depending on the bearing, which corresponds to a friction force of up to 280 kN for an individual superstructure segment. Higher friction forces can be expected to occur due to dynamic actions under vertical train loads. The results obtained under corresponding assumptions show that the substructure stiffness of the longitudinally fixed piers during braking tends to be approximately twice as high as that determined in the static test (section Braking Test). This stiffening effect was taken into account in subsequent calculations. For comparison's sake, this "stiffness factor" was calculated for tests published in Kempfert and Schwarz (1984) taking into account the reported boundary conditions: it ranged between 2.1 and 4.5. It must be noted, however, that these tests were executed on a free-standing, unloaded pier by abruptly releasing a tensioned cable.

Evaluation and Results

Because of the dynamic nature of the braking and the additional weight of the train, an activation of the resistance of the piers at the joints of the superstructure segments occurs due to the
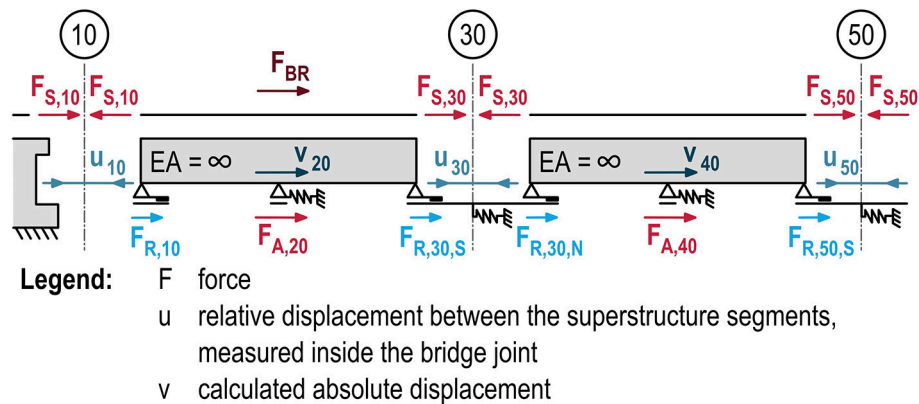
FIGURE 13 | Detail of the equivalent static and geometric system for a braking event on superstructure segment A10–30.
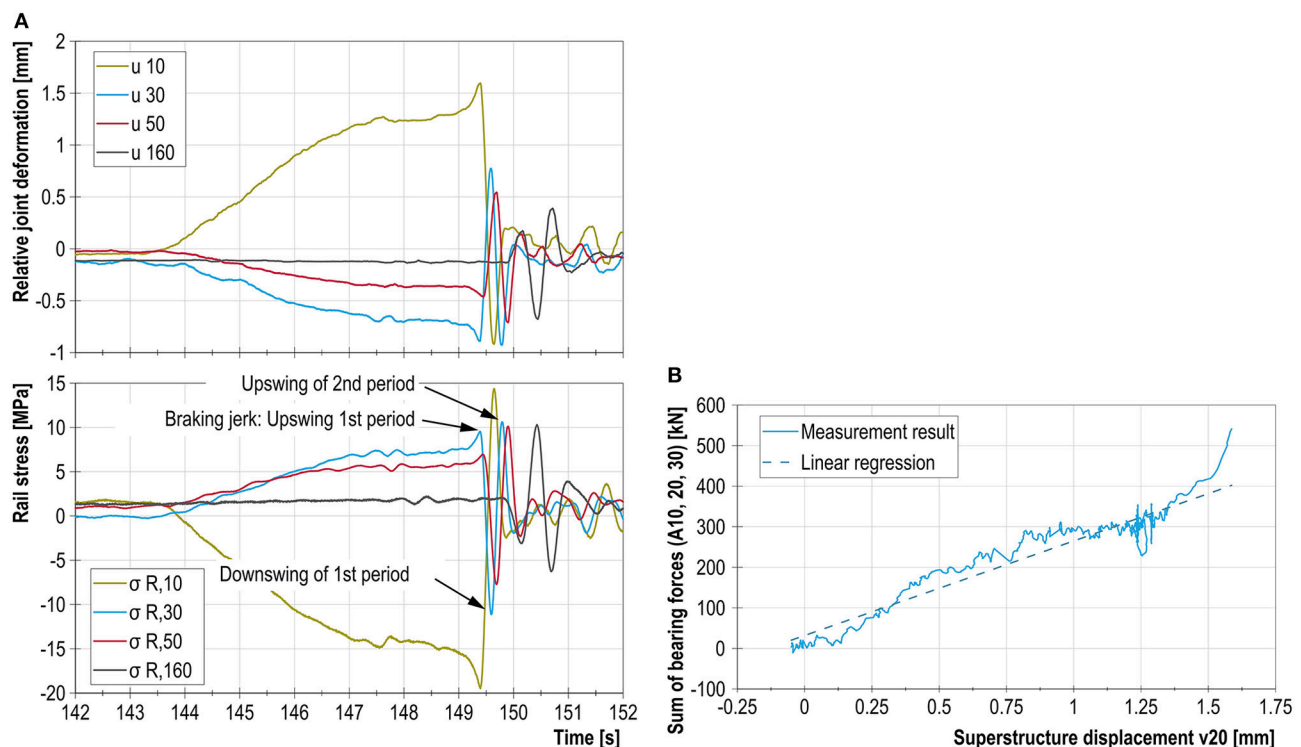
FIGURE 14 | (A) Development of the longitudinal deformation of the bridge and the rail stresses at the joints over time. **(B)** Sum of the horizontal forces in the substructure of superstructure segment A10–30 vs. horizontal deformation of the substructure.

friction in the sliding bearings. This has a positive impact on the rail stresses and the longitudinally fixed bearings. The tendency of the substructure to react more stiffly during braking than under static loads can be explained by both the stiffening of the pier itself (dynamic Young's modulus) and the stiffening of the soil when subjected to small and rapid movements.

From a soil mechanics point of view, a stiffening of the soil during braking can be attributed to various effects. Besides depending on the type of the reinforced concrete elements (piles,

pile group cap), the horizontal equivalent spring stiffnesses of deep foundations also depend strongly on the shear stiffness of the subsoil. The shear stiffness of soil materials is a function of the stress state, density, recent deformation history (see Meier, 2009, for example), magnitude of the occurring shear strains, and, in the case of fine-grained soils, also of the load rate [viscous effects (Niemunis, 2003)] as well as, to a lesser extent, the number of alternating load cycles (Studer and Koller, 1997).

FIGURE 15 | Ratio of "dynamic" to static stiffness (copied from Wichtmann and Triantafyllidis, 2009).
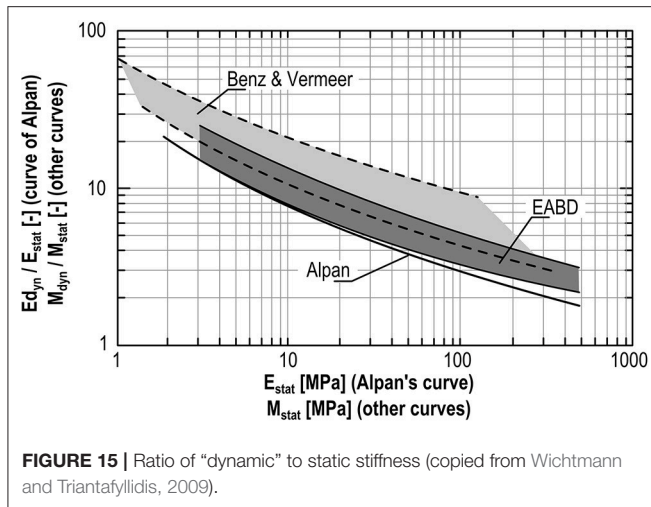
The dependence of the shear stiffness on the magnitude of the shear stress is indirectly shown in **Figure 15**. At very low shear stresses ($\approx 10^{-6}$), this stiffness is referred to as the "dynamic stiffness," and at significantly higher shear stresses ($\approx 10^{-3}$) it is called the "static stiffness." Their ratio as a function of the "static stiffness" has been investigated and described by Alpan (1970), among others.

The experimentally determined difference in stiffness can be explained fundamentally and qualitatively using the aforementioned properties of soils and concrete and is therefore deemed to be plausible.

SUMMARY

To allow for analyses of the additional rail stresses occurring on and near the Itz valley railway bridge to be carried out using realistic substructure stiffnesses, both static and dynamic test were carried out to determine these parameters.

During the static test, loads of up to 2.5 MN were introduced into the piers in order to characterize the deformation behavior of the substructure in the longitudinal direction of the bridge. The utilized measurement concept allowed for the determination of not only the global equivalent spring stiffness but also the various

deformation components (due to the tilting and displacement of the foundation and the deflection of the pier). By executing numerical analyses of the subsoil it was shown that the traditional pile group method significantly underestimates the measured stiffnesses (by a factor between 3 and 5). In contrast, very good agreement with the experimental results was achieved by using 3D FE models to take into account the interaction between the subsoil and the structural elements. Based on the insights gained from the test, it is therefore recommended that for larger railway bridges, in which the static verifications of the rail stresses and bearings react sensitively to the substructure stiffness, this stiffness be determined with more precise models of the foundation system (method 2). These models can be refined further by incorporating the results of diagnostic load tests of piles.

The "dynamic stiffness" was determined with braking tests. However, it is much more difficult to derive accurate and reliable stiffness values from these tests than from the static tests for the following reasons: (1) the forces introduced into the substructure and the occurring deformations are smaller than those observed in the static tests and were not measured directly, (2) friction forces in the sliding bearings are activated, but they cannot be separated from the measured longitudinal force occurring in the substructure, and (3) inertia forces that are difficult to quantify are activated due to the dynamic excitation of the bridge structure. The results show that, compared to the static substructure stiffness, for dynamic processes the stiffness tends to be higher by a factor of two. It is therefore recommended to include in the analysis an investigation of the effects of a higher dynamic stiffness (in particular on the bearing forces). Furthermore, the analysis of the measurement results of the braking test shows that the activation of the friction forces mobilizes significant structural reserves in the system and leads to lower stresses in both the rails and the longitudinally fixed bearings. It is difficult, however, to determine these reserves by way of calculations.

AUTHOR CONTRIBUTIONS

All authors listed have made a substantial, direct and intellectual contribution to the work, and approved it for publication.

REFERENCES

Alpan, I. (1970). The geotechnical properties of soils. *Earth Sci. Rev.* 6, 5–49. doi: 10.1016/0012-8252(70)90001-2

Bernhard, R. (1936). Über die Verteilung der Bremskräfte auf stählernen Eisenbahnbrücken. *Der Stahlbau* 9, 36–39, 53–56.

Bundesbahn-Zentralamt München (1979). *Bericht zu den Bremsversuchen mit einer etwa 690 m langen Güterzug.* Report Number 14.1412 Ibvm 682

Deutsche Gesellschaft für Geotechnik [Hrsg.] (2012). *EA-Pfähle, Empfehlungen des Arbeitskreises "Pfähle", 2nd edn-January 2012.* Berlin: Ernst & Sohn.

Geißler, K., Graße, W., Schmachtenberg, R., and Stein, R. (2002). Zur messwertgestützten Ermittlung der Verteilung der Brems- und Anfahrkräfte an der Eisenbahnhochbrücke Rendsburg. *Stahlbau* 71, 735–747. doi: 10.1002/stab.200202480

Kempfert, H.-H., and Schwarz, P. (1984). *In situ-Versuche zur Ermittlung der Unterbausteifigkeit an zwei Pfeilern der Sinntalbrücke Schaippach.* issue 3, Schriftenreihe des Lehrstuhls und Prüfamt für Grundbau, Bodenmechanik und Felsmechanik der Technischen Universität München.

Marx, S., and Geißler, K. (2010). Erfahrungen zur Modellierung und Bewertung von Eisenbahnbrücken mit Resonanzrisiko. *Stahlbau* 79, 188–198. doi: 10.1002/stab.201001295

Marx, S., and Schneider, S. (2014). Entwerfen von Eisenbahnbrücken für dynamische Einwirkungen aus dem Hochgeschwindigkeitsverkehr. *Bautechnik* 91, 75–90. doi: 10.1002/bate.201300097

Marx, S., and Seidl, G. (2011). Integral Railway Bridges in Germany. *Struct. Eng. Int.* 21, 332–340. doi: 10.2749/101686611X1299496 1034534

Marx, S., Wenner, M., Käding, M., and Wedel, F. (2018). "Vom Rechnen und Wissen – Monitoring an den Talbrücken der Neubaustrecke Erfurt-Leipzig/Halle," in *(Hrsg.): Tagungsband des 28. Dresdner Brückenbausymposiums, Vol.* 13. ed M. Curbach, Technische Universität Dresden, Dresden, 41–56.

Meier, T. (2009). *Application of Hypoplastic and Viscohypoplastic Constitutive Models for Geotechnical Problems*. dissertation, Veröffentlichung des Instituts für Bodenmechanik und Felsmechanik/Universität Karlsruhe.

Niemunis, A. (2003). *Extended Hypoplastic Models for Soils, Vol.* 34. Monografia Nr. Politechnika Gdanska.

Office de recherche et d'essais (ORE) (1967). Frage D101: Brems- und Anfahrkräfte auf Brücken und Wechselwirkung zwischen Gleisen und Brücken (Report 1 to 28).

Schacht, G., Wedel, F., and Marx, S. (2018). Bridge load testing in Germany. ACI Special Publication 323 (accepted to be published).

Seidl, G. (2013). *Bericht ÖBB Strecke Linz – Selzthal km 88,488 Trattenbachbrücke Auswertung Monitoring* (unpublished).

Stein, R., and Quoos, V. (2005). "Bremsversuch auf der Eisenbahnhochbrücke Hochdonn," in *(Hrsg.): Tagungsband des 3. Symposiums Experimentelle Untersuchungen von Baukonstruktionen, Vol.* 9. ed M. Curbach. Technische Universität Dresden, Dresden, 1–20.

Studer, J. A., and Koller, M. G. (1997). *Bodendynamik, 2nd* Auflage. Berlin/Heidelberg: Springer-Verlag. doi: 10.1007/978-3-662-06123-7

Wenner, M., Lippert, P., Plica, S., and Marx, S. (2016a). Längskraftabtragung auf Eisenbahnbrücken, Teil 1: Geschichtliche Entwicklung und ModellFigureung. *Bautechnik* 93, 59–67. doi: 10.1002/bate.201500107

Wenner, M., Lippert, P., Plica, S., and Marx, S. (2016b). Längskraftabtragung auf Eisenbahnbrücken, Teil 2: Hintergründe des Nachweises. *Bautechnik* 93, 470–481. doi: 10.1002/bate.201600034

Wenner, M., Meier, T., Wedel, F., and Marx, S. (2019). Versuchsgestützte Ermittlung der Unterbausteifigkeit einer großen Eisenbahnbrücke. *Bautechnik* 96, 99–111. doi: 10.1002/bate.201800019

Wenner, M., Wedel, F., Meier, T., and Marx, S. (2018). "Load testing on a high railway bridge to determine the longitudinal stiffness of the substructure," in *IALCCE 2018, The Sixth International Symposium on Life-Cycle Civil Engineering*. eds R. Caspeele, L. Taerwe, and D. Frangopol. (Ghent). (Accessed October 28–31, 2018).

Wichtmann, T., and Triantafyllidis, T. (2009). On the correlation of "static" and "dynamic" stiffness moduli of non-cohesive soils. *Bautechnik* 86, 28–39. doi: 10.1002/bate.200910039

frontiers
in Built Environment

Evolution of Bridge Diagnostic Load Testing in the USA

Brett Commander*

Bridge Diagnostics, Inc., Louisville, CO, United States

Driven by advancements in technology, along with the ever-growing demands of our aging infrastructure, structural evaluation through testing has progressed from a number of research endeavors to a full-fledged industry. Guidelines for Non-Destructive Evaluation (NDE) methods, diagnostic load testing, and proof load testing were published by the American Association of State Highway and Transportation Officials (AASHTO) in 2003 and were largely shaped by the technologies that were available in the 1990s. While specifications in subsequent AASHTO bridge evaluation manuals have remained relatively constant over the last 15 years, commercial applications have sprung forth in all areas of field-based bridge assessment. Much of the development has revolved around inexpensive high-speed data acquisition, high-speed wireless communications, and the surge of cloud-based data management. The market of equipment and services has developed around three main camps; NDE, Controlled Load Testing, and Structural Health Monitoring (SHM), with each field having a variety of subcategories. For example, Diagnostic Load Tests and Proof Load Tests are the two primary forms of controlled load testing. Selection of the appropriate tools and methods to solve any bridge assessment is a function of what information is available and the required functional serviceability of the structure. In many cases, a combination of methods must be employed to achieve a complete assessment. As such, the lines between NDE, Load Testing, and SHM have blurred and have become increasingly integral gears of a larger machine. This article provides a history of the primary field bridge evaluation techniques and includes the driving forces in commercial development. Focus is placed primarily on diagnostic load test methodology; however, a variety of testing methods are outlined to illustrate the best tool for the job, along with the several pros and cons of various testing and monitoring methods. Finally, a glimpse into the future of bridge evaluation is provided based on current trends and emerging technologies.

Keywords: diagnostic load test, proof load test, non-destructive evaluation, load rating, structural health monitoring

INTRODUCTION

The history of bridge testing specifically and bridge evaluation in general is one of failure. Bridges have been the linchpin to human mobility for thousands of years and today are scattered throughout our vast infrastructure, ranging from grand sculptures crossing major rivers to culverts that go unnoticed by the drivers who cross them daily. While everybody appreciates the ability to quickly cross the various obstacles between here and there, very few people appreciate the efforts

required in bridge design, assessment, or maintenance. That is until an epic bridge failure occurs, and people are injured and killed, at which point bridge condition is on everybody's mind and things change. The most infamous failure in US history was the collapse of the Silver Bridge over the Ohio River in 1967, killing 46 people. This tragedy spawned the National Bridge Inspection Program as part of the "Federal Highway Act of 1968" and the National Bridge Inspection Standards (NBIS) were established in 1971. This established inspection procedures, inspection frequencies, personnel qualifications, and reporting methods at a federal level and also required that states had to maintain bridge inventories.

A wide range of failures have occurred over the decades, which continue to shape inspection and evaluation techniques, and in turn provide the impetus for bridge research. The Manual for Inspection of Fracture Critical Bridge Members was the result of Connecticut's Mianus River Bridge collapse in 1983. The collapse of New York's Schoharie Creek Bridge in 1987 turned the attention to underwater inspection and scour. While the failures of large structures catch national attention and result in significant code and policy changes, a big concern for bridge owners has been the sheer volume of deteriorating inventory and limited funds for maintenance, repair, or replacement. The failure to plan by the communities and their transportation officials means a lot of bridges must remain in service, or roads must be closed if they cannot remain in service. Closed routes have a significant economic impact on commercial and public transport, which can very quickly escalate into a political issue, so even the small fails can create motivation for progress. As a result, the Federal Highway Administration (FHWA) funded numerous research projects through various funding mechanisms in attempt to more accurately evaluate bridges using field test activities. Three core physical evaluation methods emerged from the efforts which are outlined in the current AASHTO Manual for Bridge Evaluation (MBE): NDE; Load Testing; and SHM.

Public and political interests in bridge evaluation increase with each disaster and the continual decay of our infrastructure. At the same time, the structural instrumentation and testing market is being driven by implementation of new technology. Technologies from other business sectors, such as aerospace, medical, oil and gas, and the explosion of the Internet-of-Things (IOT), are being utilized by clever engineers for a wide range of condition and load response assessment. With every successful research activity, additional fuel is thrown into the emerging market by bringing in new investors and commercial products to the table. Combined public, political, and commercial pressure is finally pushing physical bridge evaluation methods out of research and into an actual industry. This is evident by the flow of money from government agencies for load testing, structural monitoring, and a variety of NDE projects that are geared toward emergency assessment, predictive maintenance, and asset management, rather than purely university research. Also evident is the change of players in the game; the big engineering firms are now tooling up with the latest gadgets and testing personnel and competing for statewide testing and monitoring contracts.

This article provides a brief history of the bridge testing market and outlines the primary testing methods utilized today. A glimpse into the future is also provided based on the research activities currently being performed and the new tech that researchers are playing with.

HISTORICAL METHODS OF BRIDGE EXAMINATION

The concept of load rating bridges goes as far back as 1941, where the Standard Specification for Highway Bridges (AASHTO, 1941) included provisions for evaluating existing structures. Load rating was a method to compute safe load limits for a specific vehicle and was a simple rework of the standard design equation (Equation 1). Whereas, for a safe design, a bridge component's capacity must be greater than all applied dead-load and live-load effects on that component, a Rating Factor (*RF*) for a component was computed as the ratio of the capacity available for live-load and the applied live load (Equation 2). This ratio was essentially the scale factor for a particular load that would be considered allowable to cross the bridge within design tolerances. A load Rating Factor >1.0 indicated the vehicle could cross the bridge without restriction and vehicles with rating factors <1.0 should not cross. This equation is still in use today with additional load and resistance factors to be consistent with current Load and Resistance Factor Design (LRFD) principles (Equation 3).

$$\text{Design Equation}: \Phi C \geq A_1 D + A_2 LL(1+I) \qquad (1)$$

Where:

Φ Capacity reduction factor (Design code or additional condition reduction)
C Component Capacity (i.e., Axial force, moment, shear, etc.)
A_1 Load Factor applied to dead load
D Dead load effect
A_2 Load Factor applied to live-load
LL Live-load effect
I Impact or dynamic effect

General Load Rating Equation: $\mathbf{RF} = \Phi C - A_1 D/(A_2 L(1+I))$ (2)

RF Rating Factor (vehicle weight multiplier that can satisfy design equation)

LRFD Load Rating Equation: $\mathbf{RF} = (C - \gamma_{DC} DC - \gamma_{DW} DW)/(\gamma_{LL} LL(1+IM))$ (3)

Where:

C Component Capacity (i.e., Axial force, moment, shear, etc) = $\phi_c \phi_s \phi R_n$
ϕ_c Condition factor; ϕ_s System factor; ϕ design resistance factor
Rn Nominal resistance as inspected
γ_{DC} Load Factor applied to structural component dead load effects

DC	Dead load effect due to structural components
γ_{DW}	Load Factor applied to wearing surface dead load effects
DW	Dead load effect due to wearing surface
γ_{LL}	Load factor applied to live-load effects
IM	Impact or dynamic effect.

While the principles are sound, inaccuracies of load rating calculations can occur with existing bridges for a variety of reasons. Primary issues include the inability to determine component capacities due to unknown material specifications, unknown component conditions, and/or inaccurate calculation of load effects due to unrealistic structural analyses.

Bridge load capacity is typically estimated by some level of structural analysis, design code provisions, and the material specifications. However, when dealing with older structures, design calculations, and material specifications are often lost or no longer applicable due to deterioration. Furthermore, design calculations for nearly all bridges built prior to 2,000 were based on simplified analysis methods that were intentionally conservative and often have little resemblance to a structure's actual load response behavior. For example, the AASHTO Bridge Design code has always proposed that a bridge girder can be analyzed as a single beamline with a distribution factor (DF), which accounts for the portion of truck or lane-load carried by the individual beam. DFs are generally a function of beam spacing and type of bridge deck and are intended to be a simple design tool that produces conservative results for a wide range of construction methods. While a handy and inexpensive design method, DFs are often not a realistic analysis method to evaluate actual load paths of an existing bridge. As highway loads increased over the years, bridges were often posted or load restricted based on original design loads at the time of construction and a potential reduction to account for visual condition without any further analyses. Due to the economic cost of restricting traffic and frequent discrepancies between apparent condition and allowable load limits, the need for more accurate assessment became a high priority. This need for improved load rating accuracy has led to the practice of load testing bridges to determine realistic load capacities.

Controlled Load Tests

Several notable load testing programs were carried out in the late 1980s. Two of them were completed at the University of Colorado: "Simple Load Capacity Tests for Bridges to Determine Safe Posting Levels" sponsored by FHWA and the Pennsylvania Department of Transportation (Goble et al., 1990), and "Load Prediction and Structural Response" sponsored by FHWA (Goble et al., 1992). These projects incorporated controlled load tests and response measurements to provide field verified analytical models. The process was considered Diagnostic Load Testing as the goal was to diagnose bridge performance during the application of normal service loads and validate the accuracy of the analyses. During roughly the same period, a number of research projects were completed where bridges were loaded to failure (Burdette and Goodpasture, 1988; Bakht and Jager, 1992). This data provided the basis for defining appropriate

Proof Load Tests procedures and specifications. Much of this work was then summarized by A. G. Lichtenstein in the National Cooperative Highway Research Program (NCHRP) Project, "Bridge Rating Through Non-destructive Load Testing" (Lichtenstein, 1998). This work produced the "Manual for Bridge Rating Through Load Testing" which became a significant portion of the AASHTO Manual for Condition Evaluation of Bridges in 1994. Two and half decades later, procedures for the two primary load test methods, diagnostic and proof load, are still presented with minimal updates in the current AASHTO (2018).

Regardless of the testing method, the primary objective of any load test is to obtain a more accurate load capacity assessment. Improved load rating accuracy is usually beneficial to the bridge owner and bridge users because it will, in most cases, yield greater capacity than simplified analyses based on conservative assumptions. **Figures 1**, **2** illustrate a typical load test and instrumentation procedures on a small access road. While simple calculations indicate the bridge had deficient load capacity and required posting, the bridge was in good visual condition. The purpose of the test was to measure the actual bridge performance, validate a more accurate structural analysis from which to generate load rating, and determine if the load posting could be removed.

Diagnostic Load Testing

Diagnostic Load Tests are described in the AASHTO MBE as a means to determine specific response characteristics of the bridge such as lateral load distribution and secondary stiffening effects and to validate the load rating analytical models. This type of test is generally performed with controlled load situations and a variety of sensors for measuring response performance, such as strain gages, accelerometers, displacement sensors, and highly sensitive rotation devices. Load applications are typically at legal loads or load levels known to be safe for a particular structure based on its observed history. The goal of a diagnostic test is not to test the load capacity directly, but to measure structural deformations for a set of applied load conditions. These measured responses are then compared with theoretical responses for the same applied load conditions. The data comparison is the basis for validating the theoretical model and defining how accurately the model simulates actual load paths.

A simple procedure is provided in the MBE to correlate diagnostic load test results with analytical results and thereby improve load rating results. This simplified method is commonly referred as the "K Factor" approach as it is based on an adjustment factor "K." This factor is a function of the difference between measured and analytically predicted results. There are considerations for the magnitude of difference and the probable causes for the difference and to what extent those effects may be considered. While simple to apply, the approach is highly subjective and there are no real guidelines for verifying the cause for discrepancies between measured and calculated results. A major shortfall of this approach is that rating results are heavily skewed by how poorly the analysis represents the actual structure.

FIGURE 1 | Controlled load test on a posted local access bridge.

Strain transducer to measure flexural bending

Instrumentation across midspan slab bridge

Rotation sensor near abutment
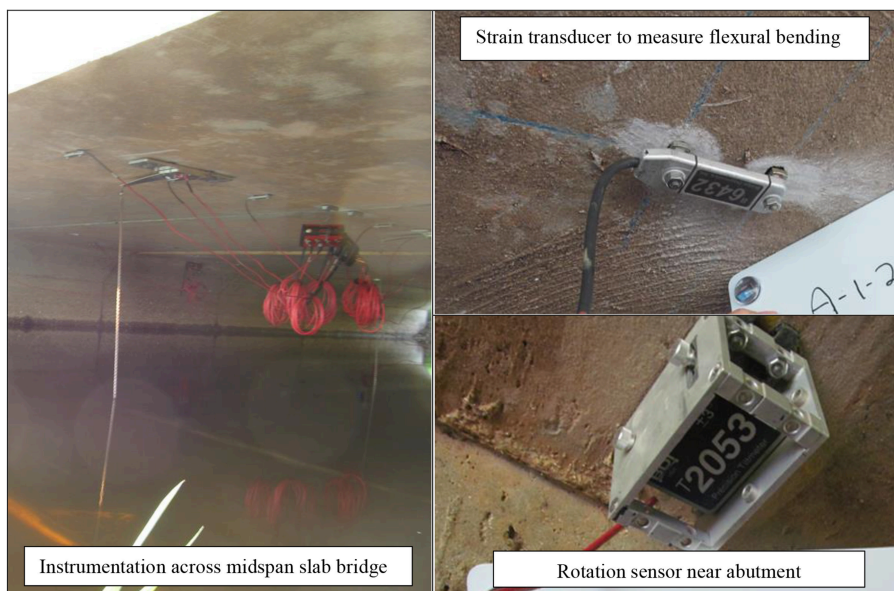
FIGURE 2 | Instrumentation to capture displacement, rotation, and flexural strain.

Integrated Approach

A more thorough diagnostic testing approach has been adopted by numerous agencies, researchers, and practitioners known as the Integrated Approach (Halfawy et al., 2002; Wipf et al., 2003). In this approach, the principal of diagnostic testing is the same in that the goal is to measure physical responses, compare responses with calculated values, and validate the analytical model. However, additional steps are taken to generate a realistic model through model calibration methods. The benefit of the Integrated Approach comes from the model calibration process, where the cause of the differences between measured and theory are identified and often quantified. For example, it may be observed that midspan moments are reduced by 30% due to the method of casting beam-ends into a concrete abutment. The rotational resistance of the beam end-conditions would be a parameter that is extracted from the structural identification. The

engineer who must perform the load rating can then decide based on construction details and condition, if that end-condition should be utilized for load rating and to what extent it can be applied. As another example, load test and model calibration results may also show that steel guard rails attached to the edge of the bridge deck significantly influence lateral load distribution during the application of a relatively light test truck. Knowing that the influence of the guard rails could diminish with minor damage to the rails or that the rails could simply buckle with heavier load applications, the load rating engineer can simply choose to eliminate the effect within the model when load rating calculations are performed. Compared to the "K Factor," the Integrated Approach gives the engineer additional information about the load response performance of the bridge and full control on how to apply load test results.

The ability to calibrate a structural model is the primary concept behind the Integrated Approach and this process is commonly referred to as Structural Identification (Yun et al., 2012). The goal is to obtain an accurate structure model that can be used to further evaluate the structure for a wide range of load conditions. The basis of comparison can be static and/or dynamic structural responses generated by a known loading condition. Static measurements are often global responses such as midspan displacement and girder rotation at an abutment or local member cross-section responses such as axial or flexural deformation obtained from strain measurements. Dynamic measurements usually consist of acceleration, which are further processed to generate structural mode shapes and natural frequencies.

Regardless of the method, the goal of structural identification is to solve numerous unknown structural parameters (variables) within a model until an acceptable match is obtained between the measured and model generated data sets. From the bridge engineer's perspective, the model parameters to be solved are those that influence transverse load distribution, longitudinal stiffness, and resistance of support conditions. However, the problem to be solved is usually one of uniqueness rather than simply accuracy. For example, if only a single displacement measurement were made at midspan of a bridge for a single load condition, it would be very easy to get an exact match from the model. The problem would be that an accurate match could be obtained from numerous combinations of model parameters. Modifications could be made to the beam stiffness, rotational resistance at the abutments, contribution of edge stiffening from parapets, or lateral load distribution from the deck. Any, or all of the parameters could be adjusted to the point of achieving the correct midspan displacement, hence the problem does not have a unique solution. In a perfect world of linear-algebra, the best-case scenario would be to have the same number of data comparison points as the number of optimization variables, then a unique solution would exist. With that concept in mind, instrumentation plans should be developed so that sensors are placed to specifically address every possible unknown structural stiffness parameter. However, everything involved in a structural load test has some level of uncertainty and error; the weight of the truck, the location of the truck, dimensions of the structure, and the precision of each measurement. Therefore, statistical measures must be employed rather than pure linear-algebra.

The key to successful diagnostic load tests is to generate large data sets having a high-degree of relevance. The problem to be solved will therefore be an over determined set of equations, meaning there are more equations than unknowns. An exact solution is generally not possible, so advanced numeric methods are required to achieve a best fit. Much research has gone into this type of problem solving and there is a plethora of error-minimization tools available from numerous math libraries that can be applied to achieve best possible matches (Necati et al., 2013). Regardless if parameter adjustment is based on linear relationships, such as least squares, random selection through Monte Carlo simulations, or highly advanced machine learning algorithms, numerous analysis iterations will be required to achieve a model that accurately represents a real structure.

With the computational methods and processing horsepower readily available today, the method of solving structural identification parameters has become somewhat academic. The primary difficulty is generating a well-defined mathematical problem to start with. While generating a comparison or error minimization function, there are numerous modeling considerations including the need for realistic structure geometry, accurate load application (geometry, magnitude, and placement), realistic boundary conditions, and correct alignment between measurements and model response simulations. In addition, care must be taken with the selection of structural variables to identify. The variables must be relevant to the error function and multiple variables having identical influence cannot be assigned at the same time (Ziehl and Caicedo, 2012). As a simple example, solving for a beams material stiffness (E) and cross-sectional stiffness (I) would cause an error minimization routine to fail as the two variables have identical effects on the calculated results. An important limitation is that the analysis process must represent the actual responses. Only linear-elastic responses can be simulated by a linear-elastic model. In cases with one-directional supports or friction type resistance some level of error can be expected with a linear analysis method.

There are many different types of bridges with a wide range of construction techniques, so it is impossible to define set rules for instrumentation and diagnostic test procedures that cover all situations. Furthermore, the purpose of a load test can vary with each situation. A load test might be performed to evaluate whether a damaged section is still carrying load or to determine the performance of a repair. In most cases however, the goal is to obtain an accurate assessment of load transfer throughout the structure for the purpose of an accurate load rating. In these cases, it is important to first define whether a load test would likely be beneficial at all. For example, load testing a twin-girder bridge to assess the girder load rating would generally be of little benefit since very little is unknown about the load paths. Simple analysis of the girder loads should in most cases produce accurate results. The benefit of diagnostic load testing generally increases with the complexity of the structure geometry and the degree of static indeterminacy. The more load paths that exist, the more complex the analyses, and the more potential for a simple analysis to produce incorrect results. Bridges with many beam lines and substantial curbs have complex lateral load distribution and therefore often benefit from a load test. Even though simple

reinforced concrete slabs are considered simple structures, load paths in a slab can be very complex so a load test and a refined analysis often result in significantly improved load ratings.

Complex support conditions, such as beam-ends embedded into a concrete abutment wall, present a case where load tests can be beneficial. The degree of end-restraint on a beam can have a dramatic influence on the midspan moment, therefore accurate assessment of the beam bearing conditions through a load test can significantly influence a bridge's load rating. A caveat to this, is whether any significant end-restraint can be considered from a load rating perspective. For example, if a beam's roller bearing is locked due to corrosion and debris, a load test may reveal a significant reduction in the beam's midspan moment due to the unintended end-restraint. However, this occurrence should be eliminated from any load rating analysis as it would not be considered a reliable or consistent resistance.

Span length is another consideration with regards to the load test benefit. In the case of load rating, diagnostic load tests are most applicable to short and medium span bridges where the weight of a single vehicle can have a significant influence on the structure. With exception to floor-system components such as stringers and floor-beams, load tests would be very impractical, and expensive to perform on a long-span bridge. Furthermore, there would be little gain as load ratings of long-span structures are generally not vehicle specific. Controlling live-load configurations for a long-span bridge are nearly always distributed lane-loads.

General procedures have been developed to define test specifications for a given bridge type and ensure accurate results. The first step is to identify the general load paths and unknown parameters associated with those paths. Load test plans are then developed with the intent to provide enough instrumentation to capture load distribution associated with those various parameters. This means it is necessary to examine all information available and determine what is known and what is not accurately known with regards to structural performance prior to defining instrumentation plans. For a typical slab on girder bridge composed of several beam-lines, the primary load rating concern is often flexural moment of the longitudinal girders near midspan. Following is a general description of the minimum instrumentation requirements to achieve an accurate and unique model using parameter identification techniques. This is further illustrated by the instrumentation plan in **Figure 3** which depicts the plan and cross-section views of a reinforced concrete T-beam bridge with numerous beam lines and beam bearings embedded into the abutment wall.

- A pair of strain gages near midspan—Strain gages should be at different heights within the girder cross-section to measure flexure and locate the position of the neutral axis.
- Measure flexure from all girders—measurements should be made on all girders near the midspan cross-section to capture load distribution of the bridge deck.
- Flexure should be measured at two additional cross-sections along the span length. The other locations do not need to

be at high moment regions, their purpose is to capture the flexural shape of the girder, or essentially the shape of the moment diagram.
- Rotation measurements are also very helpful in identifying the degree of continuity over a pier or the rotational resistance of a girder bearing.
- Global measurements such as midspan deflection are also useful when they can be feasibly obtained.

Another way to improve data relevance is to provide measurements at each sensor for a wide range of applied load conditions. When responses are generated through multiple load paths, they help identify stiffness parameters of components between the sensor location and the applied load. The easiest way to obtain data for numerous load conditions is by measuring structure responses with moving loads rather than static truck positions. In addition, several different vehicle paths should be applied. Performing load tests with moving loads can be very efficient and minimize impact on traffic, but it requires that truck position be monitored and recorded along with all the structural responses. A very important concept of the Integrated Approach is an apples-to-apples comparison of data. Therefore, a convenient method for extracting field data for specific truck positions corresponding to the simulated load cases from the model must be available. The point of the load test is to provide direct comparison of responses for many sensor locations and many different load cases.

The result of the load test is a series of response histories that can be presented as a function of load position as shown in **Figure 4**. In the data plots the solid lines represent the measured data and the markers show the computed data resulting from discrete analyzed truck positions. Here measured and computed strain histories are shown from three locations on a single beam resulting from a single truck crossing. Through examination of the plot, it is easy to see the flexural relationship between the three locations and it is obvious that when maximum midspan moment is obtained, significant negative moment was generated at the beam ends. It is important for the engineer to use visual references to validate response comparisons and model calibration results. However, a best fit model can only be obtained when a computer can perform several thousand of these comparisons with numerous truck positions and numerous relevant instrumentation locations. This example is based on quasi-static data, a similar approach is often done by comparing mode shapes and frequency responses throughout the structure.

While the concept of diagnostic load tests is simple, implementation can be a relatively complex process requiring specialized components and detailed procedures. Installation of numerous sensors on the bridge requires skilled technicians and engineers with proper safety training who can operate lifts or hang from ropes. The sensors and data acquisition must be rugged, completely weatherproof, and be easy to use in the field. Fast deployment of test equipment often requires wireless transmission in cases of moveable structures or difficult access. Beyond the field work, significant computer and software resources are required to perform the structural analysis and model calibration. Realistic modeling tools are required and
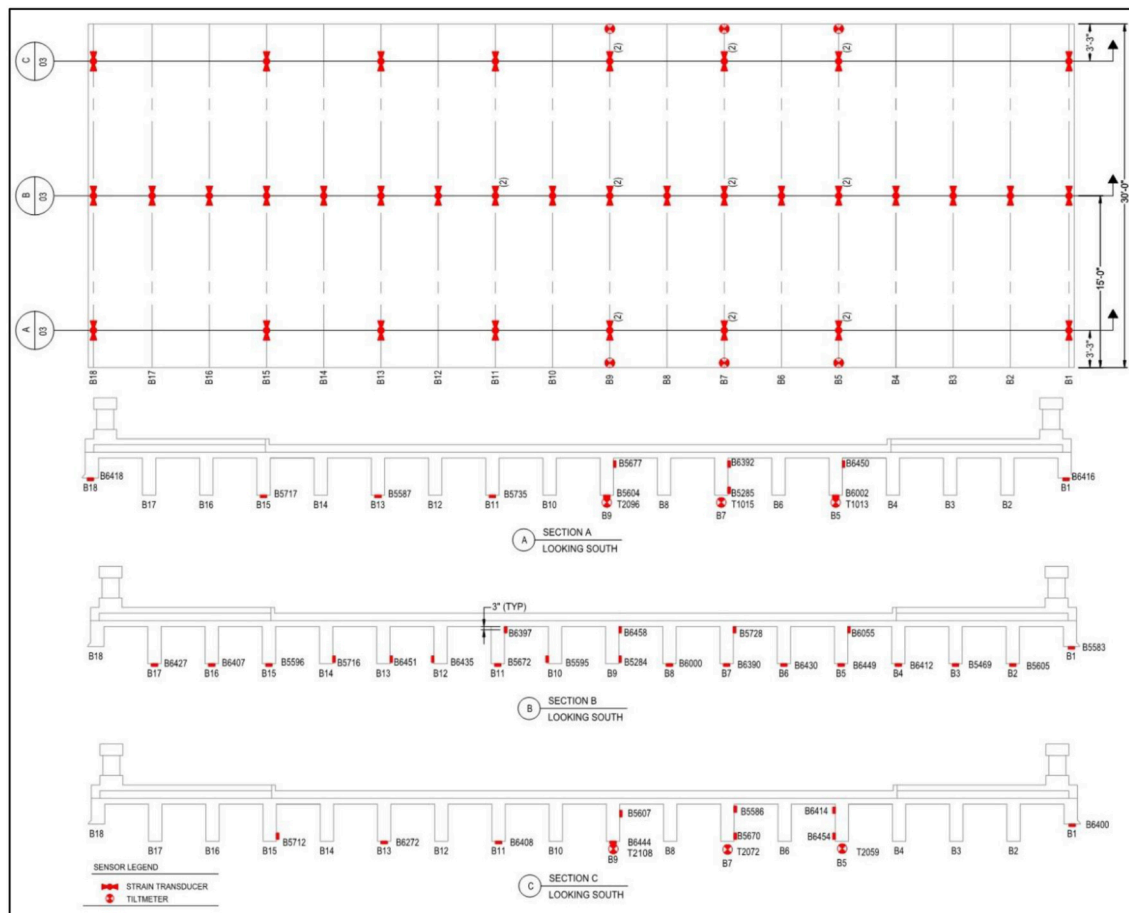
FIGURE 3 | Instrumentation plan for a multi-beam RC T-Beam bridge.

there is an enormous amount of bookkeeping to correlate the vast amount of measured and computed data. In a properly defined optimization procedure, there are thousands of data points to be compared for each analysis run. The number of data points used in the apples-to-apples comparison can generally be considered as the number of sensors multiplied by the number of analytical truck positions (load cases). Computer run times can be significant because parameter optimization methods are an iterative process associated with each variable, so the number of analysis cycles can run into the hundreds or thousands depending on the number of variables to solve.

Beyond the load test and structural identification, the final step of the Integrated Approach is to transform results into a load rating. Prior to performing load rating analyses, the model calibration must be checked and validated against realistic values. Therefore, it is important to understand reasonable or allowable limits that a parameter could have. For example, it would not be reasonable to allow the elastic modulus of a concrete member to increase above a realistic value. In cases where best fit matches are obtained with unrealistic structural properties, it generally means additional parameters need to be accounted for in the model, or a modeling error needs to be eliminated. Knowledge of structural design, a high level of structural analysis expertise,

and experience with load test data are therefore required along with a good selection of instrumentation tools.

The field portion of diagnostic load tests are relatively inexpensive to perform because they can be done quickly, with minimal impact on traffic, and with readily available vehicles. A legally loaded dump-truck is typically used as the test vehicle, and instrumentation is installed in temporary fashion which can usually be installed in a day with a small crew. Actual tests occur with brief road closures or moving blockades to minimize conflicts with the traveling public. Roughly half the cost of diagnostic load tests is in the engineering associated with the detailed FEA analyses and load rating calculations.

The primary limitation of a diagnostic load test is that it does not completely address all parameters of the aforementioned load rating equation. In general, diagnostic load tests provide the information to ensure a model realistically captures the live-load (LL) demand and in some cases dynamic studies can be performed to define impact (I). Dead-load (DL) effects must be calculated and the engineer must understand how the structural behavior may be different for resisting dead-load and live-load applications. The potential deficiency is that diagnostic load tests cannot directly deal with the component capacities (C). Typically, the capacity side of the equation is addressed through
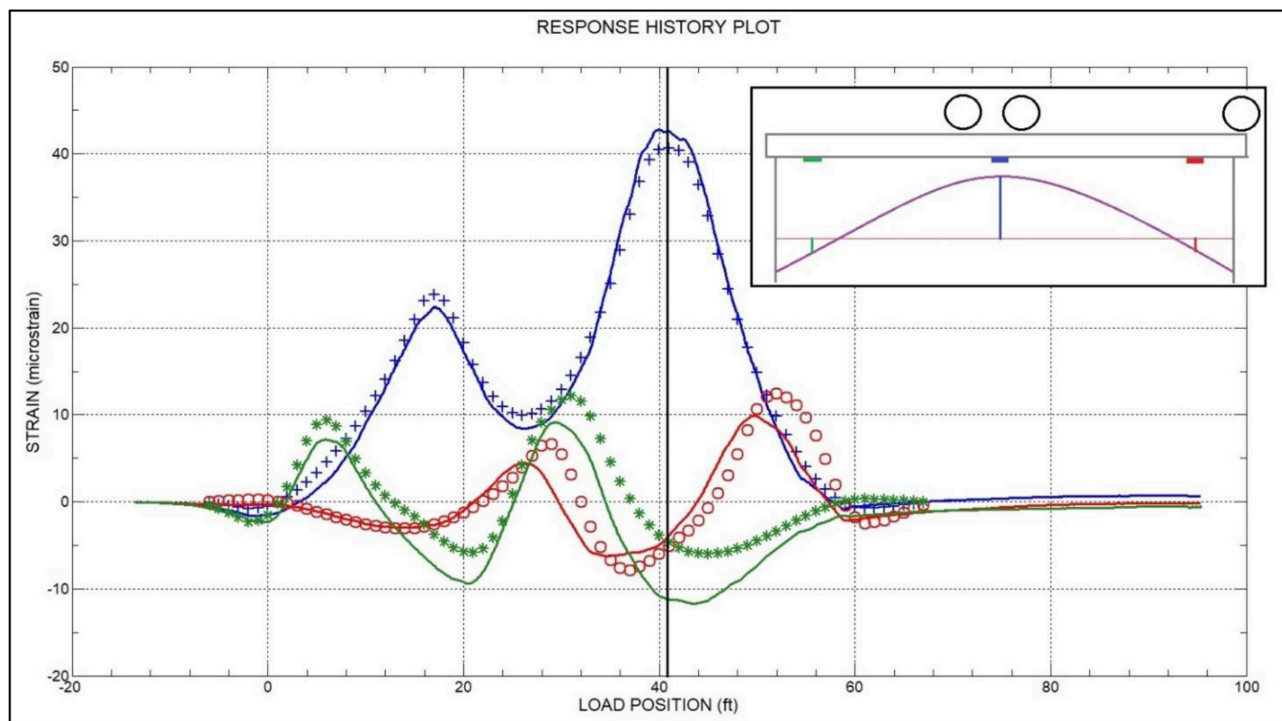
FIGURE 4 | Measured and computed strain histories at three locations on a single beam-line.

information in the design drawings, the material specifications, and the standard code provisions. However, this requires that the design or as-built structural and material details must be available, which is sometimes not the case with older bridges. Hence, while diagnostic load tests usually result in accurate structure models, it is only applicable to the end-goal of load rating when component capacity information is available.

Comparison With Proof Load Testing

Proof Load Testing is also outlined in the AASHTO MBE and is described as a test method for determining the maximum safe load capacity of a bridge. As the name implies, the load capacity is proved, or disproved by the physical test. The primary concept is based on incrementally increasing load on a structure until a target load is reached, or some form of distress or non-linear behavior is observed. Target loads are based on a desired allowable load limit and a required minimum factor of safety, which is a function of structure type, redundancy, condition, level of inspection and traffic volume. Other considerations are if the load test is to validate a permit load or determine posting limits.

Instrumentation and data acquisition equipment are similar to those used for diagnostic testing; however, placement of sensors is typically focused on points of maximum response or points of potential failure (Moussa and Shahawy, 1993). The goal is not to characterize the responses throughout the structure but determine if responses at controlling locations reach maximum limits or verify that they remain linear with respect to load magnitude.

A primary difference from diagnostic tests is the magnitude and application of loads. Load magnitudes are applied incrementally so that linear response behavior can be checked throughout the test procedure. By nature of the incremental loading, proof load tests are generally applied statically so that response stability can be observed during each phase of load. In addition, the final load conditions are generally well-above what a normal vehicle can carry. Load magnitudes are often more than 50 percent greater than design or legal loads because the target load must include a desired factor of safety and the effects of dynamic amplification. In some cases, test loads are applied with blocks, sandbags, water-bags, special loading vehicles, or custom load frames (Lantsoght et al., 2017).

Proof load tests have one significant benefit over diagnostic load testing in that a maximum load limit can be determined directly from the tests. A detailed analysis is not required, although they may be performed to provide estimated responses at each load stage. Capacity calculations are generally not performed either, as the reason for a proof load test is usually that capacity calculations cannot be completed due to lack of design, or as-built information.

Cost of proof load tests may be significant due the transportation and application of the test loads. However, since detailed analyses are not required, the overall cost may not be significantly more than a diagnostic test. Impact on traffic however will be considerably greater with a proof load test because the bridge will be closed for the duration of the test procedure and if the bridge crosses another road, the road below would also have to be closed.

Another consideration is the potential for damage and reduction of service life when performing proof load tests. Since the applied loads will very likely be much greater than

the bridge has previously experienced, new cracks in concrete components are likely to occur and existing cracks will open wider. Termination of a proof test occurs when the target load has been reached or signs of distress or measurable non-linear behavior are observed. The very concept implies that the test may reach the non-linear range of the bridge and induce some level of distress. Observation of non-linear responses can only occur after the fact and it is not always easy to detect the early onset. Therefore, a higher risk is associated with proof tests compared to diagnostic load tests. For this reason, proof tests in the United States are usually performed by or supervised directly by the agency responsible for the bridge.

Related Services—Non-destructive Evaluation Methods and Structural Health Monitoring

While not the focus of this article, NDE techniques are another key component in bridge testing. A wide range of NDE technology is available to evaluate component and material conditions and are outlined in the NBI Bridge Inspection Manual (2012). As of 1971, visual and hands-on inspections have been the primary methods for bridge condition evaluation. This will continue to be the case for generations to come, however additional tools have emerged in bridge inspection to address what cannot be seen. A variety of energy wave or chemical based non-destructive evaluation tools are utilized to provide images of what is beyond the exterior surface of a material.

In general, the goals of most NDE procedures are to identify the material properties and condition so that component durability and capacity can be realistically defined. This is necessary for the cases where design information is not available, or the condition of the material has likely altered the material properties so that the design values are no longer valid. In the case of concrete structures, Ground Penetrating Radar (GPR) is frequently used to detect invisible defects such as voids and delaminations as well as to measure the location of reinforcing steel. Rebound hammers, impact echo devices, and pullout testing methods are geared toward providing reasonable estimates of, or at least consistency of, concrete strength. Identifying reinforcing details and concrete strength are vital to the computation of concrete member capacities. The majority of steel NDE methods are geared toward detection and measurement of cracks and thereby can have a significant impact on component strength and conditions factors. NDE results are paramount in identifying future repair and maintenance needs and solving for one of the key factors in the load rating equation. Inspection and NDE techniques often provide the information required to solve for component capacity (**C**) but they do not address structural response issues. Therefore, NDE procedures are often performed alongside diagnostic load testing applications to obtain information required to fully address all aspects of an accurate load rating.

Another onsite service that is closely related to load testing is SHM. As with NDE, SHM is not the focus of this paper but is mentioned here because there has been significant growth in the monitoring market, and it has driven much of the new technology implementation. While there are a wide range of monitoring methods and monitoring goals, the instrumentation

and data acquisition equipment used for SHM is generally similar in concept to load test equipment. Both activities require measuring and capturing various forms of structural deformation. However, testing and monitoring are generally considered different activities. A primary difference is that load testing is usually based on controlled load application whereas SHM is designed to capture responses due to cyclic and random load events. The more significant difference is the duration SHM equipment is typically installed on a structure and the cost ramifications associated with long-term monitoring. Due to the need for permanent power, conduit for wiring, remote communications, and protection for sensors SHM projects tend to be many times more expensive than short-term load tests. Because of the cost factors, greater reliability requirements, and the need for more intelligent data collection, a lot of research and development has gone in to sensors and data acquisition for the SHM market. The result is an influx of durable and power efficient sensors as well as data logging equipment that work well as monitoring tools as well as load test equipment.

Even though SHM and load testing are considered different activities with significantly different goals and budgets, the lines between the two activities have blurred due to the similarities in measurement equipment. With improvements in electronic efficiency and intelligent data acquisition, load test equipment can now be left onsite for several weeks after a controlled test and collect data due to live traffic or other random dynamic events during that period. With this type of system, the best of both worlds can be achieved through short-duration monitoring without the cost associated with permanent installation. Depending on the monitoring goals, a few weeks may be enough time to address the questions at hand such as frequency responses or stress cycle counting for fatigue analyses.

NEW TECHNOLOGIES

New technologies have emerged in all areas of evaluation and testing methods including controlled testing, monitoring, and NDE. Improvements in the NDE arena are largely due to faster sampling and processing along with better sensing elements. Most NDE tools are based on the measurement of some form of energy moving through and reflecting within a material. Accuracy of time-based measurements continue to get better and the ability to translate return signals into images will continue to produce more clear and detailed pictures. Likewise, load testing and monitoring equipment is improving along the same lines with improved performance at a lower cost.

One emerging technology that is having a significant impact on instrumentation is digital imaging and it is likely that digital image correlation (DIC) equipment will be among the biggest game changers with regards to future instrumentation for controlled testing, long-term monitoring, and condition assessment. Improvements in camera resolution, frame speed, and the ability to process images faster will make DIC a serious competitor to nearly all discrete measurement devices. It has already become a major player in capturing large scale movements such as pier rotation, span deflection, and monitoring of crack movement and crack growth (Khatereh et al., 2012). At the smaller scale, technology already exists such that DIC can be used to capture deformation at the micro-strain level,

however at this time it is relatively expensive compared to strain gages and the frequency response rate is limited.

Cameras will continue to get better and more affordable, but the greatest potential improvement of DIC is in software and ease of use. Digital imaging has the potential to replace numerous discrete sensors because it is possible to detect changes in rotation, displacement, and relative movement between points. But the ability to retrieve that information is currently very custom and requires a programmer with advanced knowledge of the DIC software and monitoring equipment software. As this software becomes more flexible and easier to use, power of image-based measurements will be in the hands of the user rather than the developer. This will greatly expand the ability to integrate digital image results with other monitoring data. As more people can utilize digital imaging technology, the DIC monitoring market share will greatly expand in the instrumentation world.

A GLIMPSE INTO FUTURE BRIDGE TESTING

Electronics, sensor technology, and software will continue to improve which will make various aspects of each bridge evaluation method easier, less expensive, and generally better. While arguments will continue as to which evaluation method is best for a certain set of conditions, the greatest benefit to overall bridge assessment will be the integration of multiple technologies. Combining features of NDE, diagnostic load testing, and proof load testing could potentially provide the best load capacity evaluation for a wide range of bridges. Take for example, a post-tensioned concrete box girder bridge where as-built plans are missing or there is concern the bridge was not built according to specification. While this seems to be an isolated case, it is relatively common in regions that have experienced severe flooding, agencies that have been victims of computer hacking, or regions that have been influenced by war and regime change. Even in the modern era, records get lost and things don't get built according to specifications. For this situation, realistic structural evaluation would rely on determination of structure condition, component strength, and accurate assessment of load distribution.

With missing or uncertain information regarding reinforcement and post-tension stressing details, there is no method to compute girder strength limits from which to derive truck weight limits. What could be reasonably determined however, are serviceability limits of the structure; essentially what loads can be applied to the structure without inducing damage or non-linear responses. Obtaining these limits would be beneficial because serviceability is defined by AASHTO as a valid limit state and in many cases a conservative estimate of strength capacity can be extrapolated once service limits are known. For pre-stressed and post-tension concrete bridges, serviceability-based load limits are defined so that the allowable truck loads would not induce cracks in the pre-stressed concrete members. Neither diagnostic or proof load tests would be suitable to determine the load limits for this situation. Conventional proof load testing would certainly induce cracks into the PS/C girders which would usually be considered an unacceptable method by the bridge owner. Diagnostic load testing would measure performance at the applied test loads but not provide any indication as to how the bridge would perform at higher loads or what the effective factor of safety would be for legal traffic loads. NDE procedures alone would also be inadequate to address load rating, as it is generally impossible to determine the amount of post-tension steel, or existing post-tension force. In general, NDE procedures do not address performance issues. However, using all of the technologies together could be utilized to obtain a realistic load capacity.

The futuristic solution would be a combination of diagnostic and proof testing procedures to load a bridge up to its serviceability limit without inducing any damage to the structure or cause any reduction to service life. New NDE techniques would also be employed prior to and during the load tests to estimate a serviceability limit and identify when the serviceability limit was being approached. To achieve this outcome, relatively minor improvements of NDE methods or improved utilization of existing techniques could be employed. One potential method would be to measure *in-situ* concrete stress at controlling locations. In the case of a PS/C box girder, the measured *in-situ* stress would include the initial post-tension stress, dead-load stress, and all elastic and inelastic losses in post-tension stress resulting from creep and shrinkage. If an *in-situ* stress could be accurately measured, this would provide a direct calculation of the serviceability stress-limit available for live-load. While a number of research projects have made headway on this concept (Ruan and Zhang, 2015; Michael and Pessiki, 2016), the effort has not been sufficient to generate standards such that the approach can be used on a routine basis with a quantifiable level of certainty. Thus, an area for further research and future standardization.

In addition to identifying *in-situ* stress, additional measurement techniques could be employed to determine when a serviceability limit was reached as the applied live-load was incrementally increased. The goal here would be to identify the onset of micro-cracking which would indicate the live-load stresses have overcome compression stresses due to post-tensioning and the concrete has approached its tensile stress limit. Theoretically, the onset of micro-cracking can be identified through a number of procedures. A few of the possible methods are acoustic emissions; high-resolution imaging; and measurable shifts in wave transmission speed. Micro-crack detection methods would be applied during the course of controlled load applications and conventional instrumentation procedures commonly used in diagnostic and proof load tests. The end goal of the procedure would be to obtain a realistic model of the bridge and determine the loading and component stress changes associated with a serviceability limit. The use of incremental load increases is a concept taken from proof load testing, while instrumentation throughout the bridge would be required for model calibration as is the basis of diagnostic load testing. The integration of NDE techniques to identify serviceability limit states during the test procedures would allow for a complete load rating solution without inducing damage to the structure.

While the above scenario would provide acceptable load limits, there would still be a lack of as-built plans and some level of uncertainty for long-term performance. Therefore, continued SHM may be warranted to examine performance over time.

Parameters to track would typically be changes in stress in critical regions, changes in deflection, identification of crack activity, and identification of corrosion and steel strand breaks. Future technologies will increase the ability to perform these tasks at an acceptable price.

CONCLUSIONS

The primary point of this paper is that capabilities in instrumentation, electronics, and computing technology have improved exponentially in the last 30 years while the load testing specifications and largely the thought processes behind testing have remained unchanged. It is time to recognize that many of the codified procedures were based on the technologies available at the time and that there may be better ways to solve the problems at hand. The overall questions to be answered are still the same, "What is the load capacity of this bridge?" What has changed are the tools and methods for addressing the unknowns that make the question difficult to answer. Given that technology will continue to advance, attempting to update the MBE to today's technology, codify specific test methods, and analysis procedures would be a futile effort. Rather the code should provide a range of recommended options for a range of load rating issues along with defining required standards for qualifications, certifications, record keeping, and reporting. Results of any load tests must

ultimately be certified by the Responsible Engineer which implies a sufficient level of care will be taken, however it does not mean that level of care will be consistent. While exact procedures will be specific to the load test and cannot be codified, minimum standards can be defined for processes and documentation. This exercise will fall upon the researchers and practitioners to work in the appropriate committees within the Transportation Research Board and other agencies to provide a workable document.

Another concept addressed is that a single technology, or testing process is often not sufficient to address the entire problem at hand. Combinations of load test methods, NDE, and monitoring may be required to characterize structural performance, define component capacities, and evaluate the long-term reliability of the assessment. Therefore, testing methods should not reside in isolated camps when all test methods are essentially part of the same industry. This again will require collaboration between the industry researchers and practitioners to provide manuals and instructions on how best to solve common bridge assessment problems.

AUTHOR CONTRIBUTIONS

This manuscript was written entirely by BC and is based on his 30 years of load testing experience and his vision of the future load testing market.

REFERENCES

AASHTO (1941). *Standard Specification for Highway Bridges–Revision 3*, AASHTO.

AASHTO (2018). *The Manual for Bridge Evaluation, 3rd Edn.,* American Association of State Transportation Officials.

Bakht, B., and Jager, L. G. (1992). Ultimate load test of slab-on-girder bridge. *ASCE J. Struct. Eng.* 118, 1608–1624.

Burdette, E. G., and Goodpasture, D. W. (1988). *Correlation of Bridge Load Capacity Estimates with Test Data.* NCHRP Report.

Goble, G. G., Schulz, J. X., and Commander, B. C. (1990). *Simple Load Capacity Tests for Bridges to Determine Safe Posting Levels.* Report to Pennsylvania Department of Transportation and Federal Highway Association, University of Colorado.

Goble, G. G., Schulz, J. X., and Commander, B. C. (1992). *Load Prediction and Structural Response.* Final Report, University of Colorado and Federal Highway Administration.

Halfawy, M., Wipf, T., Wood, D., Ahmad, A.-H., Phares, B. (2002). "Bridge load rating using an integrated load testing and finite element analysis approach: a case study." in *4th Structural Specialty Conference of the Canadian Society for Civil Engineering* (Montréal, QC).

Khatereh, V., Oats, R. C., Harris, D. K., Ahlborn, T. M., Brooks, C. N., Endsley, K. A., et al. (2012). Evaluation of commercially available remote sensors for highway bridge condition assessment. *J. Bridge Eng.* 17, 886–895. doi: 10.1061/(ASCE)BE.1943-5592.0000303

Lantsoght, E., Cor, V., Ane, B., and Dick, A. H. (2017). State-of-the-art on load testing of concrete bridges. *Eng. Struct.* 150, 231–241. doi: 10.1016/j.engstruct.2017.07.050.

Lichtenstein, A. G. (1998). *Bridge Rating Through Non-destructive Load Testing.* National Cooperative Highway Research Program (NCHRP) Project 12-28(13)A.

Michael, J. M., and Pessiki, S. (2016). Experimental study of the core-drilling method for evaluating *in situ* stresses in concrete structures. *J. Mater. Civil Eng.* 28:2. doi: 10.1061/(ASCE)MT.1943-5533.0001294

Moussa, A. I., and Shahawy, M. A. (1993). *Dynamic and static tests of prestressed concrete girder bridges in Florida.* Technical Report. Structural Research

Center at the Florida Department of Transportation. Tallahassee, FL. Available online at: https://fdotwww.blob.core.windows.net/sitefinity/docs/default-source/content/structures/structuresresearchcenter/final-reports/dynamic-and-static-tests-prestressed-concrete-girder-bridges-in-florida.pdf?sfvrsn=35489a35_0

NBI Bridge Inspection Manual (2012). "NBI Bridge Inspector's Reference Manual," in *U.S. Department of Transportation - Federal Highway Administration, Publication No. FHWA NHI 12-049.*

Necati, Ç., Kijewski-Correa, T., and Aktan, A. E. (2013). *Structural Identification of Constructed Systems: Approaches, Methods, and Technologies for Effective Practice of St-Id.* American Society of Civil Engineers

Ruan, X., and Zhang, Y. (2015). *In-situ* stress identification of bridge concrete components using core-drilling method. *Struct. Infrastruct. Eng.* 11, 210–222. doi: 10.1080/15732479.2013.862729

Wipf, T. J., Phares, B. M., Klaiber, F. W., Wood, D. L., Mellingen, E., and Samuelson, A. (2003). *Development of Bridge Load Testing Process for Load Evaluation, Iowa State University Final Report.* Iowa DOT Project TR-445, CTRE Project 00–65.

Yun, Z., Prader, J., Weidner, J., Dubbs, N., Moon, F., and Aktan, A. E. (2012). Structural Identification of a deteriorated reinforced concrete bridge. *J. Bridge Eng.* 17, 774–787. doi: 10.1061/(ASCE)BE.1943-5592.0000309

Ziehl, P., and Caicedo, J. (eds.). (2012). "Chapter 9: Inspection, testing, and monitoring of buildings and bridges," *The National Council of Structural Engineers Associations* (Boulder, CO: International Code Council), 127–156.

Check for updates

Diagnostic Testing of a Vertical Lift Truss Bridge for Model Verification and Decision-Making Support

Vahid Shahsavari, Maryam Mashayekhi, Milad Mehrkash and Erin Santini-Bell*

Department of Civil and Environmental Engineering, University of New Hampshire, Durham, NH, United States

A practical long term structural health monitoring program must be based on reasonable field capabilities, the needs of the bridge owner, and the anticipated structural behavior unique to the structure. Each sensor installed as part of the monitoring program should provide information directly in response to operational needs related to the structure's short term and long term performance. A thoughtfully considered instrumentation plan developed in cooperation with the bridge designer, bridge manager, bridge maintenance operator and academic researchers will provide data to enhance both the state of the practice and state of the art for the bridge structural design, management and maintenance. Monitoring a bridge's structural response has the potential to (a) detect the presence of structural changes for condition assessment, (b) inform the bridge manger to assist in daily operational decision-making and (c) validate the structural design assumptions and (d) refine a structural model of the bridge to be used for performance prediction. The excitation for these responses typically comes from traffic or environmental demands. Vertical lift bridges provide a unique opportunity for structural health monitoring based on the dynamic response due to the frequent and repeated impact imparted on the structure each time the lift span opens and closes. In this paper, a structural health monitoring system designed to provide valuable information for design verification, structural model calibration, fatigue monitoring, and operational decision-making support for the reconstructed Memorial Bridge carrying US Route 1 between Portsmouth, New Hampshire and Kittery, Maine. This paper will detail the development of the sensor layout including input from stakeholders, accessibility issues and complementary and contradicting objectives. A set of structural models with varying degrees on complexity were created based on the structural performance objectives. The data collected during a pseudo-static truck load test was used to calibrate the structural models of the bridge and to select the appropriate model for each post-processing and decision-making tools related to structural performance.

Keywords: structural health monitoring, load testing, structural model calibration, vertical lift bridge, structural condition assessment

INTRODUCTION

Restoring and improving the urban infrastructure of the United States is one of the National Academy of Engineering Grand Challenges highlighting the need for data-driven, effective and efficient bridge management (NAE, 2017). Critical components of the US transportation infrastructure are bridge structures, which elevates the importance of the design and maintenance of bridge structures for bridge designers, owners and the general public. According to a 2015 accounting of the United States' bridges, 144,621 of the nation's 608,445 bridges (23.8%) are considered structurally deficient or functionally obsolete by the Federal Highway Association (Ingraham, 2015). As these bridges are repaired and replaced, engineers look to incorporate innovation to increase the service life of the structure (AASHTO, 2008). The idea of continuously monitoring these structures, which results in more efficient maintenance and inspections management, is not feasible for every bridge. However, signature bridges that push the design envelope and are operationally critical to an infrastructure network are ideal candidates for structural health monitoring. This selective application of sensors can contribute to the goal of managing an aging bridge inventory with high maintenance and replacement costs. Structural Health Monitoring (SHM) systems, which have recently expanded in application with respect to infrastructure management, include not only sensors but controlled non-destructive load tests and post-processing algorithms for condition assessment and decision-making framework for short term and long term operational resource allocation.

Within the nation's bridge inventory, movable bridges play an integral role in modern transportation infrastructure systems. As means of passage for both vehicular and naval traffic at a single location, their reliable performance is a matter of concern since they must work in harmony to minimize the down time both for vessel and vehicle traffic. For instance, the maintenance of movable bridges like vertical lift bridges is of high importance given the frequency of lift operation to allow for marine traffic. However, with the hundreds of movable bridges in the US, which are typically located in coastal environments that are typically highly susceptible to extreme weather events, there are few long term monitoring programs for these bridges subjected to vertical operations in addition to traffic and environmental loads (Catbas et al., 2014).

LITERATURE SURVEY

The importance of structural health monitoring to detect structural damage in a global sense has been demonstrated in recent works (Doebling et al., 1998). In the context of civil SHM, the term structural damage often refers to any deficiency presented in the structural system during the design or construction as well as any deterioration during the lifetime of the structure (Yao, 1985). SHM and control systems cover a broad range of techniques to effectively monitor the behavior of structures and provide in-service information with respect to their actual conditions. Various techniques ranging from statistical approaches (Shahsavari et al., 2017a,b) and machine

learning algorithms (Vafaei et al., 2018) to system identification methods including both time-domain and frequency-domain techniques (García-Palencia and Santini-Bell, 2014; Shahsavari et al., 2018a,b) can be a means to derive meaningful structural performance information from the collected data. As bridges age and deteriorate over time, the idea of proactively monitoring their behavior and the ability to predict the impact of structural changes on the structural performance is becoming a leading area of research to increase the service life of the structure. In recent years, with an ever-increasing number of instrumented bridges, there is strong and growing interest among engineers, researchers, and bridge owners to ensure efficient resource allocation via a cost-effective and optimized instrumentation strategy for which the SHM sensors are mainly dedicated to capturing the response of critical members. The more sensors spatially dispersed throughout the structure, the more meaningful the information collected from the bridge, which can ultimately lead to a more reliable structural condition assessment. The complex mechanism of damage within the structural components as well as the uncertainties associated with the structural behavior at different locations are factors that impose challenges to confidently determine the condition and impact of members that are critical to maintaining the bridge performance. Hence, in operationally critical bridges having a sophisticated design and geometry, such as movable bridges, the main difficulty in sketching the preliminary concepts of the instrumentation plan is the identification of the members whose damage would considerably affect the load carrying capacity of the bridge.

Since the structural performance and load carrying capacity of bridges would be altered due to likely damage scenarios imposed on critical components, the ability to confidently predict the remaining service life and load rating reduction is one of the major concerns for bridge engineers. Structural model calibration is a well-documented tool that can be used for structural condition assessment and performance prediction (Cardini and DeWolfe, 2009; Santini-Bell et al., 2013). A global structural model of the bridge system will aid in both the design of the instrumentation plan, as well as serve as a tool for performance assessment, and prediction of the structural behavior once the model is calibrated using the collected structural response data. As steel bridges are subjected to cyclic (fatigue) loading, mainly due to high traffic volumes, a verification of bridge structural components becomes crucial in terms of fatigue life. Fatigue damage in steel bridges is a local phenomenon which can progress continuously and threaten the healthy performance of the structure. Fatigue cracks may initiate at the vicinity of the possible defects, material degradations and the concentrated high-stressed areas which can progressively propagate leading to failure of the component.

Fatigue is often a decisive degradation phenomenon for steel bridges that, at the same time, is afflicted with large uncertainties on the resistance side as well as on the action effect side (Leander et al., 2018). An efficient SHM program can provide valuable information regarding the actual performance and live-load induced stresses at the critical instrumented areas of the structure. However, development of stress range spectra for the

evaluation of fatigue life of structural details in bridges is a challenging task as they are strongly site-specific depending upon various factors such as vehicle types, the range of vehicle speeds, road roughness conditions, ambient environment and bridge type (Laman and Nowak, 1996). While field measurements can be used to account for some of these uncertainties, *in situ* monitoring of all the fatigue-prone regions of a bridge is not feasible in practice (Kwad et al., 2017). Nevertheless, fatigue life prediction of bridges has been accomplished by a number of researchers through field measurements and experimental testing. García et al. (2018) performed a fatigue analysis study on experimental specimens obtained with the same steel grades as those used in a welded joints of a suspension bridge and with the same welding procedures as those practiced in the structure. Mohammadi et al. (1998) reported an application of field measurements for fatigue evaluation of highway bridges. Kashefi et al. (2010) presented the procedures used for assessment of remaining fatigue life of an aging steel deck bridge using strain field measurements carried out on critical fatigue details as well as laboratory tests on limited samples. Liu et al. (2017) performed a fatigue life evaluation for critical connections of a suspension bridge under the passing fatigue truck load. Leander et al. (2018) presented a case study of a steel railway bridge subjected to fatigue deterioration with an overall aim to support rational decisions on how to evaluate and procure different assessment actions to improve the accuracy of the predicted service life of existing bridges. Aygül et al. (2013) discussed the accuracy and benefits of different fatigue failure assessment methods for commonly welded details in steel bridges to conclude how well each method describes the fatigue strength of each welded detail. The authors performed statistical investigations on the results of finite element analyses obtained from solid element based finite element models for welded bridge details and the fatigue test data collected from the literature. The present case study reviews the results of a comprehensive research comparing the applicability of the nominal stress and hot-spot stress methods for fatigue assessment of a bridge connection. While the nominal stress approach is a non-local fatigue assessment method the hot-spot stress method considers a fictitious stress at a fatigue-critical point, the so-called hot-spot point, where the stress is considered representative of the component.

Besides fatigue, bridges are also subjected to other types of damage such as corrosion, vehicular collision, vessel impact, fire, etc. Therefore, the ability to confidently evaluate the decreased load carrying capacity of the damaged bridge with respect to its performance is essential for effective and efficient bridge management. The Hercílio Luz Bridge (HLB), which is an eye-bar chain suspension bridge located between the Santa Catarina Island and the mainland of Brazil, was completely closed to traffic in 1991 due to high corrosion levels and deterioration of its critical members (Carvalho et al., 2017). Truck accident is the third leading cause of bridge failure or collapse in the United States. Although current AASHTO guide specifications recommend static load to improve the impact resistance of bridge piers against truck impacts, recent investigations have revealed that the dynamic loads due to truck impacts may be significantly higher than that prescribed by

AASHTO (Agrawal et al., 2013). The collapse of the I-5 Skagit River Bridge, located in Washington, is one of the most recent bridge collapse disasters due to collision of an over-height truck to the over-head braces of the through-truss bridge on May 23, 2013. This incident caused a 49-m (160-ft) simple-span section of the 339-m (1,112-ft) bridge collapsing into the river while, at the same time, two passenger vehicles fell into the river (Stark et al., 2016). Among bridges, the movable bridges are highly susceptible to impact damage by marine vessels for which even minor impact on the substructure or superstructure can disrupt the bridge operations causing the closure of the bridge until repairs are made. In 2013, a 144 m (473 ft) cargo ship broke loose from its moorings and impacted the south span of the Sarah Mildred Long Bridge in New Hampshire, thereby causing damage to a diagonal member, a vertical member, and the lower chord of the bridge. As a result of this incident and because of unclear understanding of the bridge structural response under operating conditions, the bridge owners shut down the bridge to all traffic for 6 weeks while the damaged members were repaired (Fu et al., 2015).

Post-event evaluation of bridge condition and through understanding its capacity is a critical component in any bridge management and maintenance system. Although the requirements of the Guide Specifications for vessel-collision of highway bridges were developed to give designers specific guidelines in protecting these structures (Knott and Damgaard, 1990), there is lack of effective warning systems to support the development of real-time operational decision-making protocols in the event of an impact damage. Long term SHM data can be integrated into a bridge management protocol to better assess the actual condition of the bridge and improve the level of service that bridge owners can provide to the traveling public. In recent years, considerable efforts have been made to explore the features that represent the highest sensitivity to structural deficiency in bridges and that can be used as a prime candidate for real-time assessment of the system response (Santini-Bell et al., 2013). The implementation of an effective pattern recognition algorithm such as the X-bar control chart analysis into the wavelet packets extracted from post-processing of the SHM data has been found promising to reliably distinguish between two different states (damaged, undamaged) of the structure. The wavelet packet transform (WPT) is indeed a robust signal processing tool that has been recently favored over traditional methods to extract more detailed information from vibration data. To extend the application of wavelets for damage assessment of bridge structures, Sun and Chang (2002) used the wavelet packet component energies obtained from a three-span continuous bridge as inputs into neural networks. Shahsavari et al. (2018a) reported a combined application of the WPT and statistical control chart analysis to quantify the change in a bridge system response based on the average normalized energy stored in the wavelet packets. This case study presents an operational decision-making criterion based on the procedure of Shahsavari et al. (2018a) to enhance the discrimination of wavelet features between two different states of a bridge. The wavelet indices extracted from a calibrated model of an instrumented bridge are used to study the applicability of the proposed

approach to damage detection problem studies under progressive damage scenarios.

A series of controlled load tests (pseudo-static and dynamic) are conducted to calibrate the analytical models used for fatigue performance prediction, load rating degradation, and real-time condition assessment for decision support described in Chapter 6. Diagnostic load tests are generally performed to compare the resulting structural response of a bridge with its analytical models, estimate the load carrying capacity of an in-service bridge and/or determine the safety and serviceability of a newly built bridge before putting into service (Sanayei et al., 1997; Olaszek et al., 2014). This paper highlights the advantage of structural health monitoring, diagnostic testing and structural modeling to provide three means of using the collected structural response information into a decision-making approach related to bridge management. The efficiency of the proposed case study is defined via a cost-effective strategy integrating the collected field data from structural health monitoring with current engineering practices, according to the AASHTO Manual for Bridge Evaluation provisions, and model-predicted structural response information to meet the paper objectives for "local" and "global" performance-based assessment of an in-service bridge. A method for fatigue assessment and load rating reduction prediction will directly use the field responses as well as the bridge predicted response from a calibrated structural model, while a real-time condition assessment using wavelet packets is presented that only requires the use of the collected structural responses. A long term SHM program is developed based on a short term monitoring program to design an efficient and cost-effective layout for collection of data at locations where the bridge components are highly susceptible to fatigue, impact damage and excessive dynamic movements.

CASE STUDY: MEMORIAL BRIDGE

Memorial Bridge carries US Route 1 across the Piscataqua River connecting Portsmouth, NH with Kittery, ME. The bridge is also the only pedestrian link between the two communities, who value this bridge as much for its function as a transportation link as for its beauty and the access to the water views. The original Memorial Bridge, constructed in 1923, was a through truss vertical lift bridge. The bridge was closed to vehicular traffic in 2012 due to structural concerns. The new Memorial Bridge, partially funded by the Transportation Investment Generating Economic Recovery (TIGER) program at the Federal Highway Administration (FHWA), was opened to traffic in July 2013. The new Memorial Bridge includes an innovative "gusset-less" truss connection and a metalized corrosion protective coating (see **Figure 1**). The gusset-less truss connection is unique to this bridge and is the only connection of its kind in a vehicular bridge, which makes the verification of the design procedure vital for future applications of this connection type (Nash, 2016). This paper will detail the development of the instrumentation layout to support a long term structural health monitoring program with short term applications. The planning process to create the long

term monitoring program includes structural modeling and data analysis as well as the preliminary model and short term data collections that were used to assist in designing the monitoring system.

For this case study, the instrumentation plan is focused only on the Portsmouth-side span with a 297 ft length as well as the Portsmouth-side vertical lift tower with a 158 feet height. The truss elements consist of W14 section diagonals ranging in size from a W14x90 to a W14x211 depending on location along the span and built-up chord elements with an integral knuckle connection. The chord elements are constructed with 1-inch and 1-1/4-inch thick web plates. The top chord web plates are 24 inches tall and the bottom chord web plates are 36 inches tall. The flange plates range in thickness from 1–1/4-inch to 2–3/4 inches and are 26 inches to 36 inches wide. The web-flange connection is a 5/8-inch (1.6 cm) weld (Adams et al., 2017).

DESIGN OF STRUCTURAL HEALTH MONITORING SYSTEM

In order to make an efficient and cost-effective plan for structural health monitoring, several components must be considered. The main goals for monitoring, the type of the structure, the region and its environmental condition, the volume and type of traffic, as well as the bridge owners' particular demands are key factors for successful strategic planning. Likewise, the accessibility for installation and maintenance of the sensor networks as well as the power and communication infrastructure available at the bridge can significantly increase the cost of a monitoring plan if they are not included in the design process. These factors should be considered during the SHM design process, especially for post-construction sensor installation.

In this case study, the proposed monitoring program was designed based on short term and long term design strategies to effectively capture the structural response at critical locations that are prone to fatigue, impact damage based on bridge operation and significant dynamic movements. These objectives were developed through collaboration with the bridge owners and the bridge designer. The short term approach mainly aimed to provide bridge operators with information related to environmental conditions, specifically wind speed, and their impact on the vertical lift operation. The long term goals for this SHM system are (1) monitoring the dynamic performance of both the horizontal span and the lift tower of the instrumented portion of the Memorial Bridge (see **Figure 1**), (2) the strain distribution through the gusset-less connection for design verification and fatigue performance assessment, including the fracture-critical radiused weld connecting the web and flange on the bottom chord and (3) monitoring of the impact of corrosion overtime on load-carrying capacity given the harsh coastal environment and that the structural deficiency due to material loss caused the closure of the original Memorial Bridge in 2012 (Mashayekhi et al., 2018).

The long term monitoring program was focused to approximate an optimum number of different types of sensors at sparse locations through which the actual performance of

FIGURE 1 | The new Memorial Bridge connecting Portsmouth, NH to Kittery ME, highlighting the bridge gusset-less truss connection and the fixed truss span cross-section.
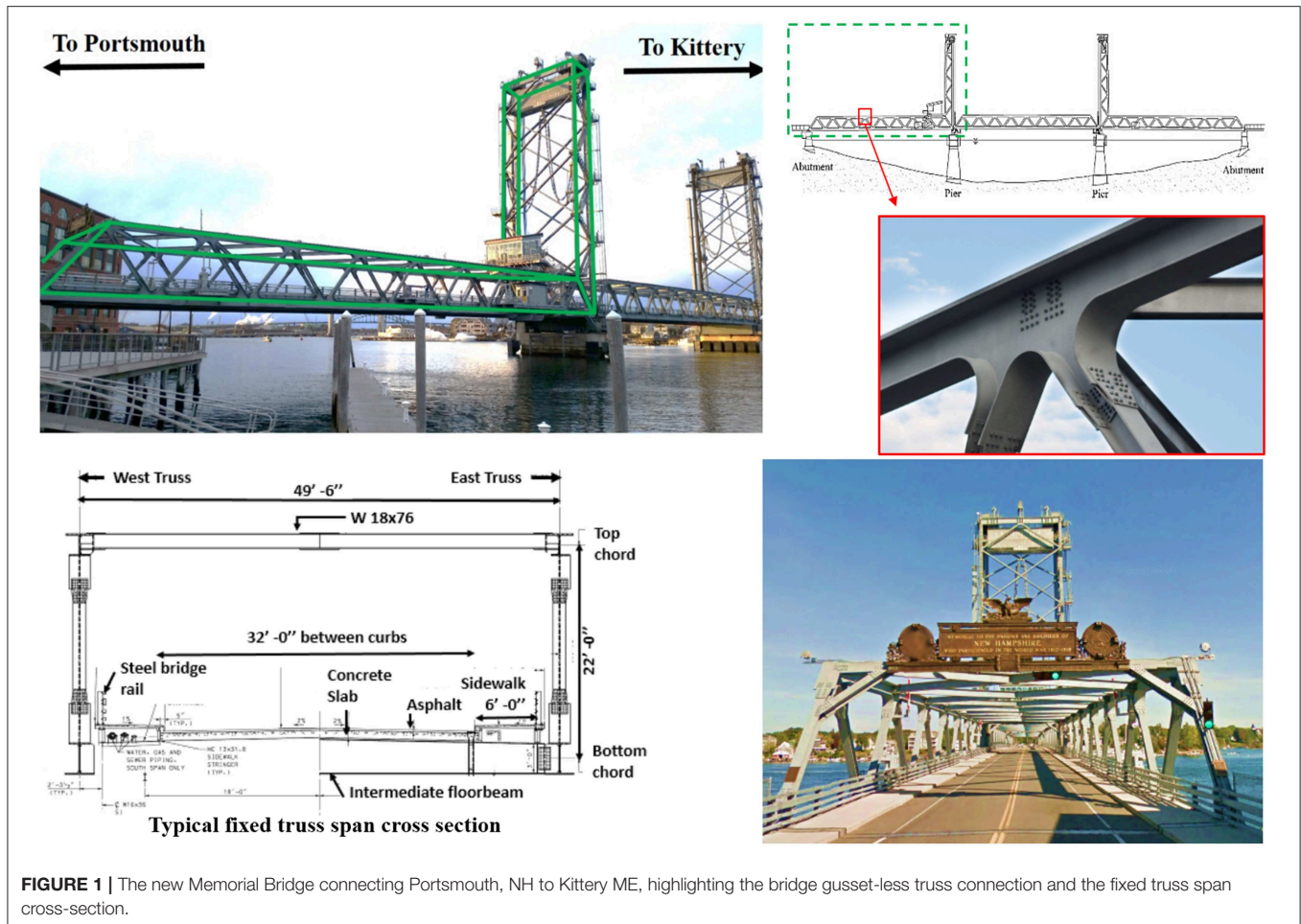
the bridge can be evaluated. In addition, the limited access for sensor installation and maintenance as well as the electrical conduit configuration and communications capabilities were other factors considered during the development of a cost-effective and efficient monitoring program. The complexity of the structural elements particularly the gusset-less connections of the Memorial Bridge necessitates a detailed Finite Element (FE) model, which requires a significant resource investment for creation and analysis. Therefore, prior to embarking on a lengthy multi-purpose modeling program, a preliminary analysis was performed by creating a three-dimensional wire-frame structural model of the Portsmouth-side horizontal span and lift tower in SAP2000® (see **Figure 2**). The model was created to get an overview of the behavior of the bridge and verify the modeling procedures through comparison with collected acceleration data from short term initial monitoring. It should be noted that the monitoring program includes the Portsmouth-side of the bridge; therefore, only the Portsmouth-side of the bridge is included in this work. Given the output obtained from the structural modeling in SAP2000®, three areas were determined over the bridge as temporary locations for sensor installation and short term response collection. These areas are marked in **Figure 3**.

FIGURE 2 | Structural model of the south span of the Memorial Bridge in SAP2000®.
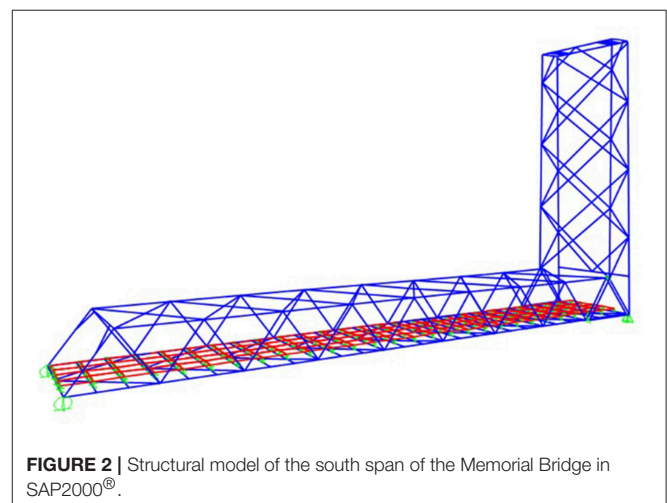
Preliminary Short Term Monitoring

Prior to the long term monitoring program design, it is beneficial to get an overview of the bridge's behavior thorough some short term monitoring. With these goals in mind, accelerometers and

strains transducers were temporarily deployed at three strategic locations during six short term SHM sensor deployments (4–6 h each) and data collections in 2015 (Adams et al., 2017). The sensors for this monitoring were clamped in place in three areas of the bridge, the south span at midspan (Area 1), the base of the south tower (Area 2), and the top of the south tower (Area 3), as shown in **Figure 3**. The sensors used at Area 1 included uniaxial strain gages on the top chord and diagonals as well as uniaxial accelerometers on the top chord and deck. Uniaxial strain gages were used at Area 2 to capture the maximum strains in the tower trusses during lift events and truck passages. Uniaxial and triaxial accelerometers were placed in Area 3 to measure the vibration of the top of the tower during lift events and truck passages.

While **Figure 4A** shows the data from the strain response (blue line) and the acceleration response (red line) from Area 1 due to a truck crossing the bridge, the time-history shown in **Figure 4B** corresponds to the acceleration response collected at Area 1 during a vertical lift of the center span. This data clearly shows the traffic stopping when the gates close for the lift, the lifting operation, the span in the up position, the lowering operation and the impact of the lift span as it locks in place. The vertical lift operation provides a consistent excitation for dynamic data collection. The correlation between the traffic monitoring image and the structural response data was instrumental in discussion with the bridge owners as it clearly demonstrated the ability of the sensors to clearly capture the difference in response between a truck and car passage.
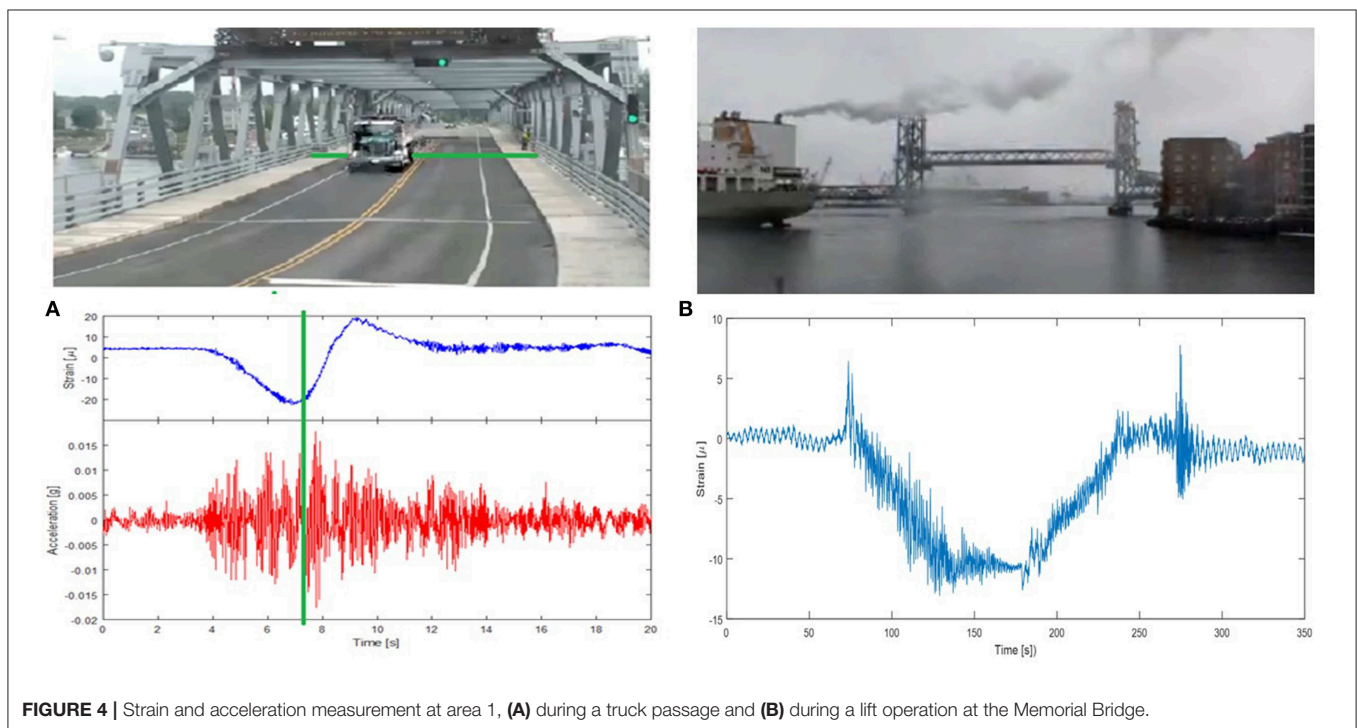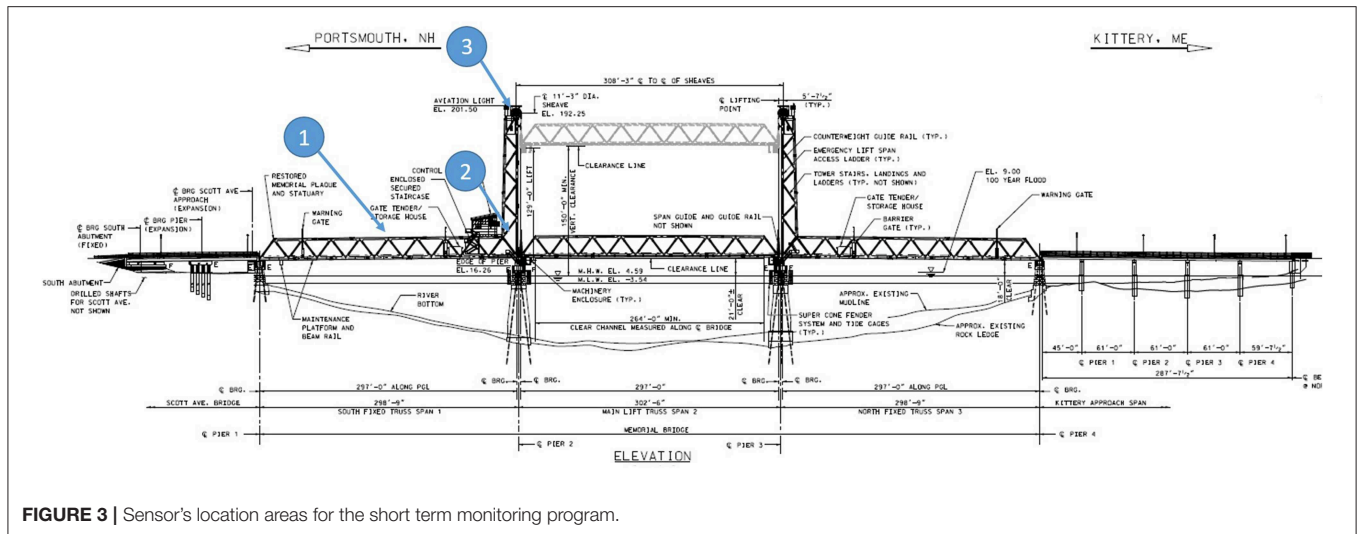
Long Term Monitoring Program and Associated Structural Models

The results from the temporary data collections, together with the response predicted by the structural model and the special considerations for the bridge, detailed in the previous section, informed the development of a long term structural monitoring plan installed at the Memorial Bridge, shown in **Figure 5** (Mashayekhizadeh et al., 2017). The bridge is instrumented by a series of SHM sensors including accelerometers, uniaxial strain gauges, strain rosettes, and tiltmeters. A total number of twelve uniaxial accelerometers are deployed for monitoring the bridge vibration response along the length of the horizontal span and height of the tower. The instrumentation system includes a set of six accelerometers along the top and bottom chords of the span on the downstream (east) truss as well as two additional accelerometers deployed on the upstream (west) truss, allowing the comparison of both east and west sides vibration modes. There are also four additional accelerometers on the south facing lift tower, where the two accelerometers installed at the base of the lift tower on both east and west sides able one to identify torsional motion in the tower. In addition to accelerometers, there are clusters of five strain rosettes at two gusset-less connections on the span, and six strain rosettes at three joints on the tower which allow for investigation of force path through the webs of the gusset-less connections shown in **Figure 5**. Uniaxial strain gauges are mounted on a diagonal member connecting the instrumented connections on both east and west faces of the bridge. This is done to assess the symmetric behavior of the

bridge. There are also two bi-axial tiltmeters at the top and bottom of the tower to study the movement of the tower due to the wind load, bridge lifts, and combinations of the two. The long term monitoring system was installed and operational in March 2017.

A set of more detailed FE models were simultaneously created in Lusas® to assess the data given the complexity to the gusset-less connection (see **Figure 6**). The structural responses predicted by these models, once calibrated, were used to determine the performance of the structure with respect to the design expectations. In creating the global models in Lusas®, as-built drawings of the bridge, provided by the bridge owner, were used. The element used for the shell element model (see **Figure 6A**), is a four-noded quadrilateral element, QTS4, to represent thick shell behavior due to the sizable thickness of the members. The use of thick shell elements also provides stress results throughout the thickness of the element. The size and shape of the elements vary due to the geometry of each part from irregular dimension element for the gusset-less connections to the biggest elements for beams and cross braces to minimize the analysis time. Given the complex geometry of the gusset-less connection, a well-detailed FE model of the bridge is required to provide response predictions for both the local and global assessment of the structural performance. However, a global FE model developed with higher dimensional elements may not provide additional valuable performance information with respect to project objectives and will result in a time-consuming analysis, thereby limiting the application of the model for complex analyses. In this study, a multi-scale modeling approach was applied to achieve the desired global FE model to accurately represent the local performance of the connection with efficient computational efforts. In order to create the multi-scale models (see **Figures 6B,C**), different dimensions of elements were connected by defining the appropriate constraint equations at the interface point to ensure the uniformity of the stress distributions and displacements (Mashayekhi and Santini-Bell, 2019). In the application of the multi-scale approach for a global model, the interface point showing the ratio of the higher to lower dimensions of elements plays a dominant role in the global stiffness of the structure. In addition, the interface points surrounding the higher scale element determine the local stiffness of the component which is required to be positioned in optimum locations to provide a harmonic balance for the components.

A well-detailed global model of the case study bridge (see **Figure 6A**), at which all members were modeled with higher-scale elements (shell element), was initially developed and used as a baseline for the development of efficient multi-scale models (Mashayekhi et al., 2018). The shell element model was considered as the baseline to understand the structural performance of the members which can be conveniently modeled with lower scale beam elements without a significant decrease in accuracy. The shell elements are indeed three-dimensional 4-noded thick shell elements having 6-nodal degrees of freedom (DOF) each. In particular, this model was developed to study the continuous stress variations between the gusset-less connection and the other connecting members to the connection.

FIGURE 3 | Sensor's location areas for the short term monitoring program.

FIGURE 4 | Strain and acceleration measurement at area 1, **(A)** during a truck passage and **(B)** during a lift operation at the Memorial Bridge.

The second model is the detailed multi-scale model (see **Figure 6B**), that considers both the beam and shell elements in the model. The beam elements are three-dimensional thick beam elements that have 6-nodal DOFs. This model was developed for simulating the lifting action of the bridge. The east and west truss of the bridge, as well as the deck of the bridge were modeled with shell elements. The long members that are in the out-of-plane direction of the trusses were modeled with beam elements. These long members include the braces in the tower and the top of the south span, the floor beams and the skewed floor beams. The selection of these members was based on the beam-like performance of the members, observed in the shell element model. The reduction in the dimension of the selected members can significantly increase the efficiency of the model by reducing the computation time. The development of the detailed multi-scale model was performed through a step-wise procedure by replacing the groups of similar members initially modeled with shell elements with a single beam element and application of the appropriate constraint equations. After each step of a scale-reduction, the optimum location of the interface point was determined by minimizing the difference between the structural responses of the two models.
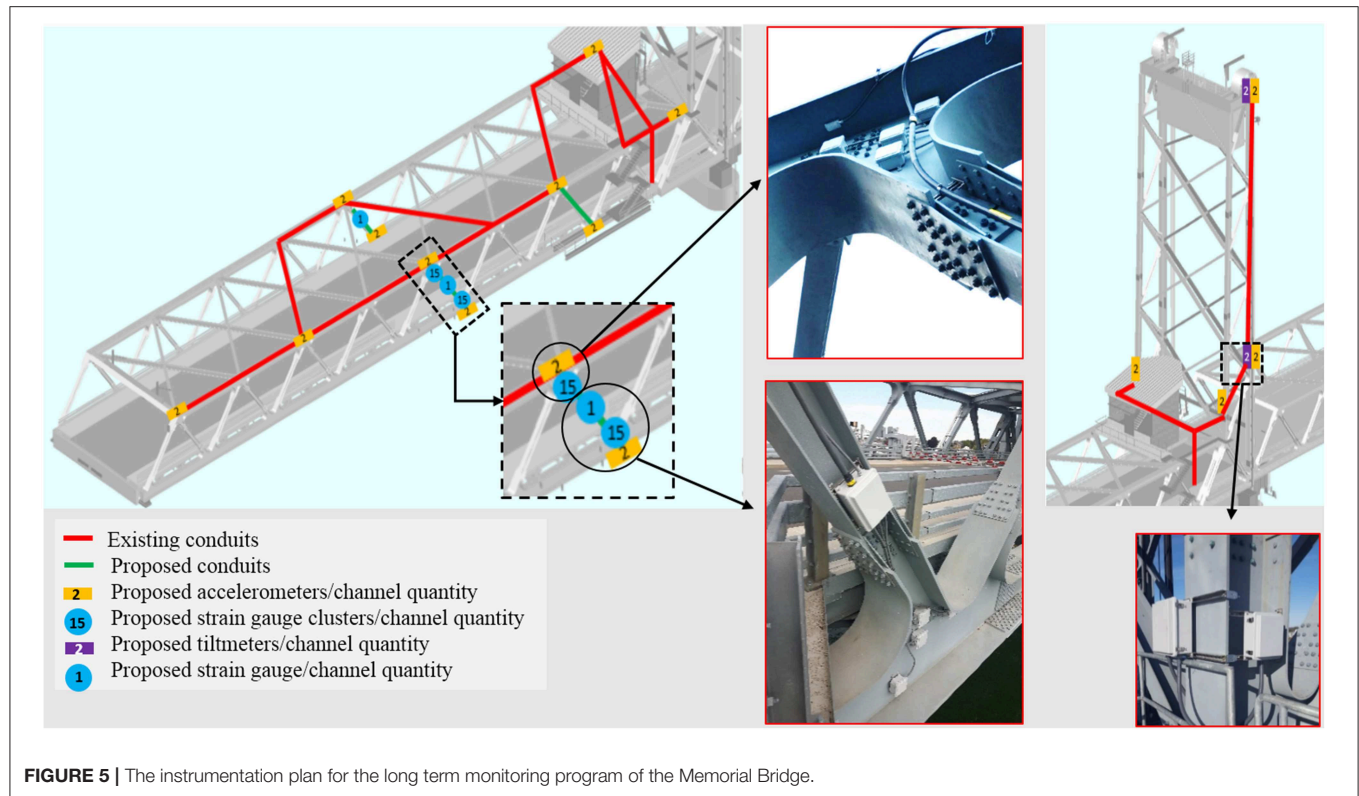
FIGURE 5 | The instrumentation plan for the long term monitoring program of the Memorial Bridge.
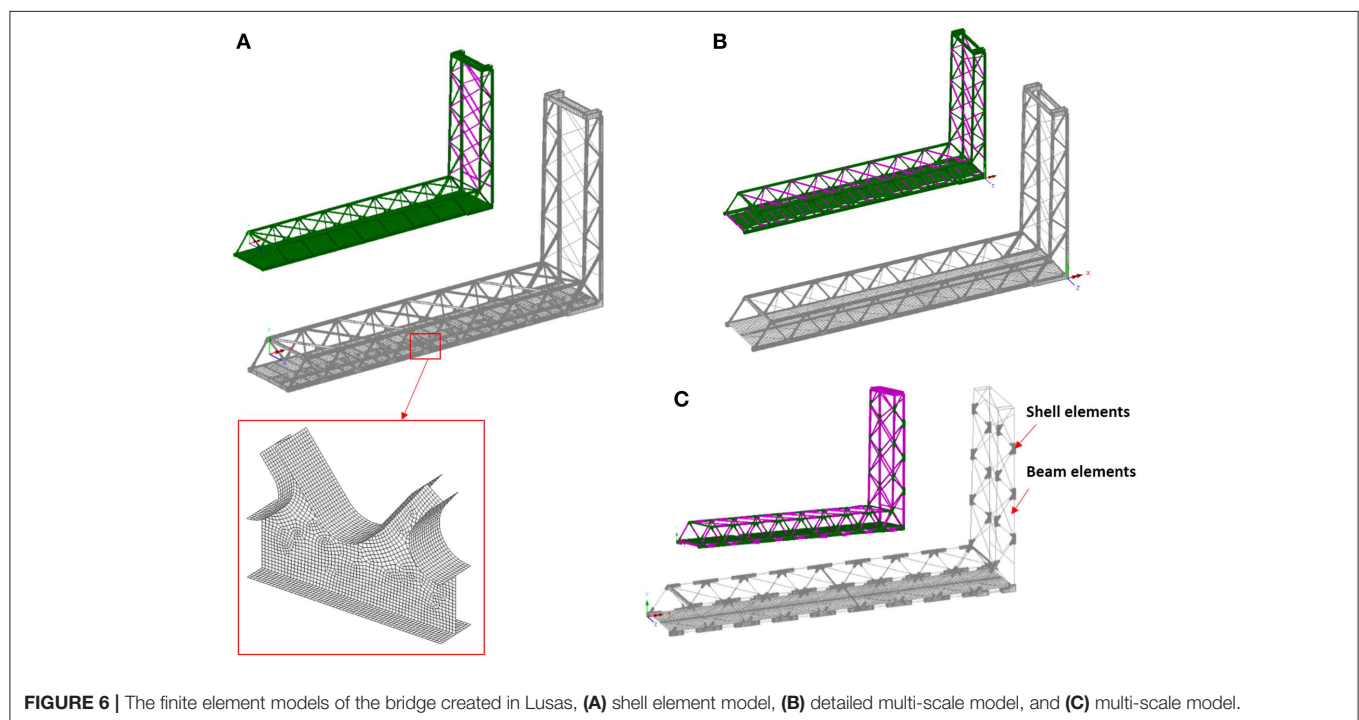
FIGURE 6 | The finite element models of the bridge created in Lusas, **(A)** shell element model, **(B)** detailed multi-scale model, and **(C)** multi-scale model.

The third model is the multi-scale model (see **Figure 6C**), at which the gusset-less connections and the deck of the bridge were modeled with beam elements. This model was developed for an efficient performance assessment of the

gusset-less connections under the traffic loads, which is applied for fatigue assessment of the connection. In the detailed multi-scale model, the remaining long members having less-complex geometric properties including the floor beams and braces were

modeled by beam elements while the gusset-less connections and chord members by modeled with shell elements. Similar beam and shell elements as those used in aforementioned models were applied in this model. The coupling between two different dimensions of the elements at the interface point of the beam and shell elements were provided using the multi-point constraint equations (McCune et al., 2000; Mashayekhi et al., 2018).

The multi-scale models were developed with an overall aim to create an efficient representative model by reducing the computational time and limiting the element complexity, which leads to a major increase in the number of degrees of freedom. To do so, a mesh sensitivity analysis was performed to acquire the optimum size of the mesh for the beam and thick shell elements. For the multi-scale model, shown in **Figure 6C**, the top chords, bottom chords and diagonals were also modeled by the beam elements while the same interface coupling was applied. The run time for modal analysis varies from 40 min for the shell model to 14 min for the detailed multi-scale model. Lastly, the multi-scale model was determined to adequately represent both the global and local performance of the bridge based on a comparison with structural response data collected during a diagnostic truck load test, as detailed in section the next section.

DIAGNOSTIC TESTING FOR MODEL VERIFICATION OF THE MEMORIAL BRIDGE

Load testing is a common practice among bridge engineers for the assessment of bridge safety and serviceability. Diagnostic load testing is one type of load test methods that helps establish a comparison between the resulting structural response of a bridge and its analytical predictions. This method can be used either as a means for estimating the load carrying capacity of an in-service bridge or as an acceptance test before the bridge is put into service (Olaszek et al., 2014). Given a controlled load test, the calibrated models would be beneficial to be used for operational decisions such as those relating to maintenance scheduling and overweight vehicle permitting. Creating a calibrated structural model that can predict the impact of operational and environmental variations on the lift operation and bridge performance will allow for the creation of a data-driven decision-making matrix for fatigue performance prediction, load rating deterioration and real-time condition assessment.

Description of the Design and Implementation of the Load Test for the Memorial Bridge

A series of controlled pseudo-static and dynamic load tests were designed and conducted on the Portsmouth span of the bridge using a tri-axial NHDOT dump truck. The gross weight of the truck was measured at 39 kips, including rear and front axles weighing 22 and 15 kips, respectively (see **Figure 7A**). Each run of the load test included a series of individual truck passes to ensure collection of high-quality data with the least
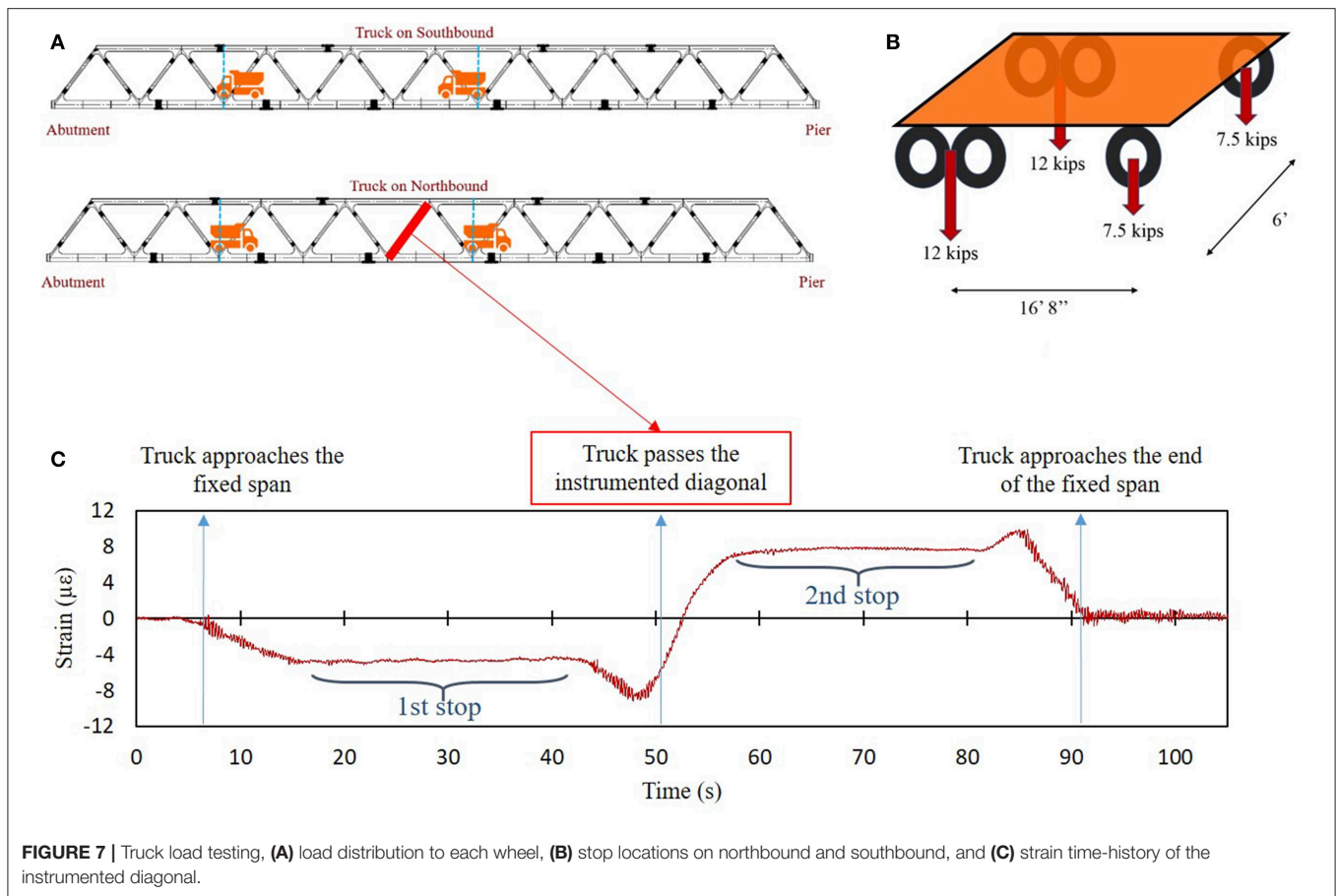
measurement errors due to uncertainty and variability in the field testing. The dynamic truck tests were conducted with the approximate speed of 30 miles/h, the maximum speed which could be safely attained within the limits of each lane on the bridge. The static tests were designed for two stopping positions on both northbound and southbound of the bridge. **Figure 7B** shows the stop locations and the distribution of the loads to each truck wheel.

With the bridge temporary closed to traffic, the collection of data was performed using a sampling frequency of 100 Hz for all sensors deployed over the span and tower of the bridge. The sensors were connected to a digital data acquisition system, provided by Bridge Diagnostic Inc., collecting the monitoring data during the test. To minimize the adverse effects of environmental conditions on data reading, namely temperature, for each run of the test, all sensors were zeroed prior to each truck passage. The loaded truck was heavy enough to develop substantial stresses in the structural members while maintaining a linear elastic structural response. The average zero mean value of strains, at both extremities of the recorded time-history, developed in the instrumented diagonal shown in **Figure 7C** implies the linear elastic behavior of the bridge during the load test. In this instance, the truck was positioned on the northbound lane of the bridge. The negative and positive signs of strain correspond to compressive and tensile strains developed in the instrumented diagonal, respectively. It is also noticed that the sign of the strain changes when the truck passes the instrumented diagonal member.

To approximate reliably the bridge structural behavior and calibrate the finite element models created in this project, the live load strains developed in instrumented members in addition to bridge natural frequencies predicted by the analytical models were compared with the bridge structural response. In this study, the calibration of the FE models was performed based on the pseudo-static truck load test to verify the analytical models with respect to the bridge's structural performance. The following sections demonstrate the application of the proposed diagnostic load testing for two different approaches, including the static model calibration of the FE models developed in Lusas® and structural system identification of the numerical model in SAP2000®. While the former approach has been mainly considered to accurately reflect the fatigue behavior of gusset-less joints and critical regions via the multi-scale models, the latter approach has been used finite element model updating and global structural condition assessment of the bridge.

Static Model Calibration

The static calibration of the FE model using the field data is essential to reduce possible errors induced by simplifications or inaccurate assumptions made in model development (Sanayei et al., 1997). Wrong assumptions are mostly caused by insufficient knowledge about structural details, materials properties, inevitable simplifications of the details or ignorance of the non-structural components, and boundary conditions. In the model calibration procedure, prior to refining the wrong assumptions made in the model developments, it is essential to

FIGURE 7 | Truck load testing, **(A)** load distribution to each wheel, **(B)** stop locations on northbound and southbound, and **(C)** strain time-history of the instrumented diagonal.

determine the important parameters causing a deviant response in the model. The refinement attempts are required to change the recognized influential parameters and minimize the errors until the desired accuracy is achieved (Catbas et al., 2007). The strain response of the bridge at the location of the strain rosettes has a more local property compared to the modal response. The comparison between the strain response of the field data and analytical model at a single node becomes difficult as the analytical responses will be mesh-sensitive and therefore, less considered in model calibration studies (Aktan et al., 1998).

In this case study, the strain time-history response of the strain rosettes recorded during the quasi-static load test provides sufficient information for static model calibration of the multi-scale models in Lusas®. The deck of the models at both the northbound and southbound stop locations during the load test was re-meshed to consider an accurate path to account for the truck applying loads. In the initial evaluation of FE models, it was understood that the strain response is more sensitive to the defined boundary conditions, loading conditions and the interface point for the multi-scale model. The refined boundary conditions tuned with the modal response, which expressed in the previous section, was considered as finalized and thus did not change in this part of static model calibration. In the static analysis of the FE models, it was realized that the strain response of the models under the applied truck load simulated as

a distributed load and the discrete load is not effectively different. However, more diversity in the strain responses was observed through the change in the distance of the applied load from the truss axles, which indicates that accurate load location has significant impact on the model calibration effort.

In the multi-scale model, it was found that the local stiffness of the gusset-less connection and the induced strain response can be conveniently refined through a minor change in the interface point location. However, in the single scale, the calibration of the shell element model as compared to the multi-scale model using strain response was more restricted. The contours for the principal strain response of the developed FE models in addition to the locations of stress concentration (nominal and hot-spot locations for fatigue assessment) are shown in **Figure 8**. The numerical results obtained from the FE models were used to be compared to the equivalent field strain response during the load test. The shell model, **Figure 8A**, shows the most uniform stress distribution at the gusset-less connection. The minor stress concentration areas are observed in the multi-scale models, **Figures 8B,C**, at the location of the floor beam's connection to the gusset-less connection. The concentrated strain areas indicate that the interface point location must be located as a greater distance from the web of the gusset-less connection. However, since the main objective of developing the multi-scale models is to obtain a cost-efficient model by reducing

the degree of freedoms, the current models were accepted and applied for further condition assessment purposes. **Table 1** shows the comparison results between the strain responses acquired through the structural analysis of the developed FE models with those calculated from the field data. The representing analytical responses belong to the horizontal strain gauges (Ex) for the bottom connection under the truck load corresponding to the second stop during the load test. The structural response data in **Table 1** illustrates that the detailed multi-scale model produces lower strain responses indicating a stiffer connection, as expected with more beam elements, when compared to the multi-scale and shell element models. Consequently, the detailed multi-scale model shows a better agreement to the field data compared to other models.

The verification and calibration of the FE models were also performed through the application of a dynamic moving load on the models to compare with the dynamic load test results. Model calibration under the dynamic load provides more realistic information on the performance of the structure. This was performed through the application of the moving dynamic load on the model considering the truck configurations and speed information while neglecting the influence of the vehicle dynamic impact in the model. **Figure 9** shows the comparison between the resulting strain time-history response of the detailed multi-scale model, as shown in **Figure 6B**, in the horizontal direction (Ex) and the strain response of the bridge recorded by a strain rosette in the same direction.

Structural System Identification

The structural beam model of the bridge developed in SAP2000® was updated to reflect field observed structural behavior better. The updating of the model was performed based on a parameter estimation procedure that changes the stiffness values of the structural members so that the error between the analytical model and the in-service bridge is minimized. For the Memorial Bridge, in particular, the stiffness of the gusset-less connections is a critical concern and the mechanical behavior of this innovative type of connection is not well-known (Mehrkash and Santini-Bell, 2018). There are numerous techniques for finite element model updating and structural condition assessment for which many of these methods require the modal properties of the structure, i.e., natural frequencies and mode shapes obtained by processing the monitoring data (Sanayei et al., 1999).

The diagnostic load test data was not used for model system identification, as the lift response data provided a larger dynamic response and would be more informative for this operation. With a total number of twelve accelerometers deployed on the Portsmouth-side span and lift tower of the bridge, the accelerometers have been capturing the bridge dynamic acceleration response continuously. However, since the excitation source of the bridge is not known clearly, the bridge excitation was categorized as ambient vibrations to pursue structural modal analysis in this work. In the output-only modal identification methods, the frequency domain decomposition is an efficient approach for the modal extraction. For the ambient vibration, the input can be assumed as a zero-mean Gaussian white noise, so the power spectral density of the input is a constant matrix. Therefore, we can write (Brincker et al., 2001):

$$G_{yy}(\omega) = \sum_{k \in Sub(\omega)} \frac{d_k \phi_k \phi_k^T}{\omega - \lambda_k} + \frac{\bar{d}_k \bar{\phi}_k \bar{\phi}_k^T}{\omega - \bar{\lambda}_k} \tag{1}$$

where ω is the frequency, $G_{yy}(\omega)$ is the power spectral density matrix of the responses, d_k is a scalar constant, ϕ_k is the mode shape, λ_k is the pole and "‾" and T indicate complex conjugate and transpose, respectively.

To perform the frequency domain decomposition, using the singular value decomposition, the output power spectral density is decomposed as follows:

$$\hat{G}_{yy}(\omega) = U_i S_i U_i^H \tag{2}$$

where $\hat{G}_{yy}(\omega)$ is the estimate of the output power spectral density, the matrix $U_i = [u_{i1}, u_{i2}, \dots, u_{im}]$ is a unitary matrix including

TABLE 1 | Verification of the strain of the developed FE models in Lusas® with the field data.

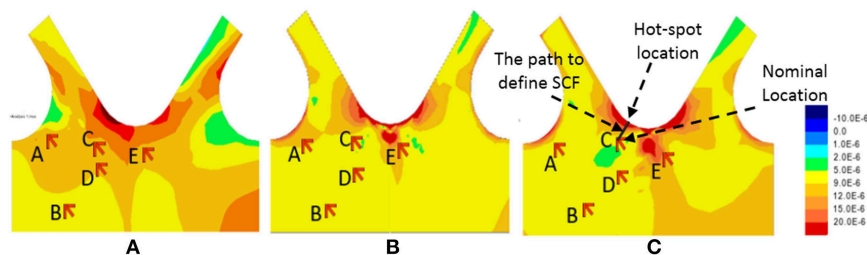| Strain gauge (location)	Shell element model (με)	Detailed Multi-scale model (με)	Multi-scale model (με)	Field data (με)
A	8.03	7.99	7.86	7.50
B	6.22	6.15	7.79	8.21
C	7.98	7.85	7.93	8.00
D	7.66	6.40	6.52	7.62
E	10.82	10.66	11.03	10.03

FIGURE 8 | The principal strain contours of the Lusas® FE model, **(A)** shell element model, **(B)** detailed multi-scale model, and **(C)** multi-scale model.
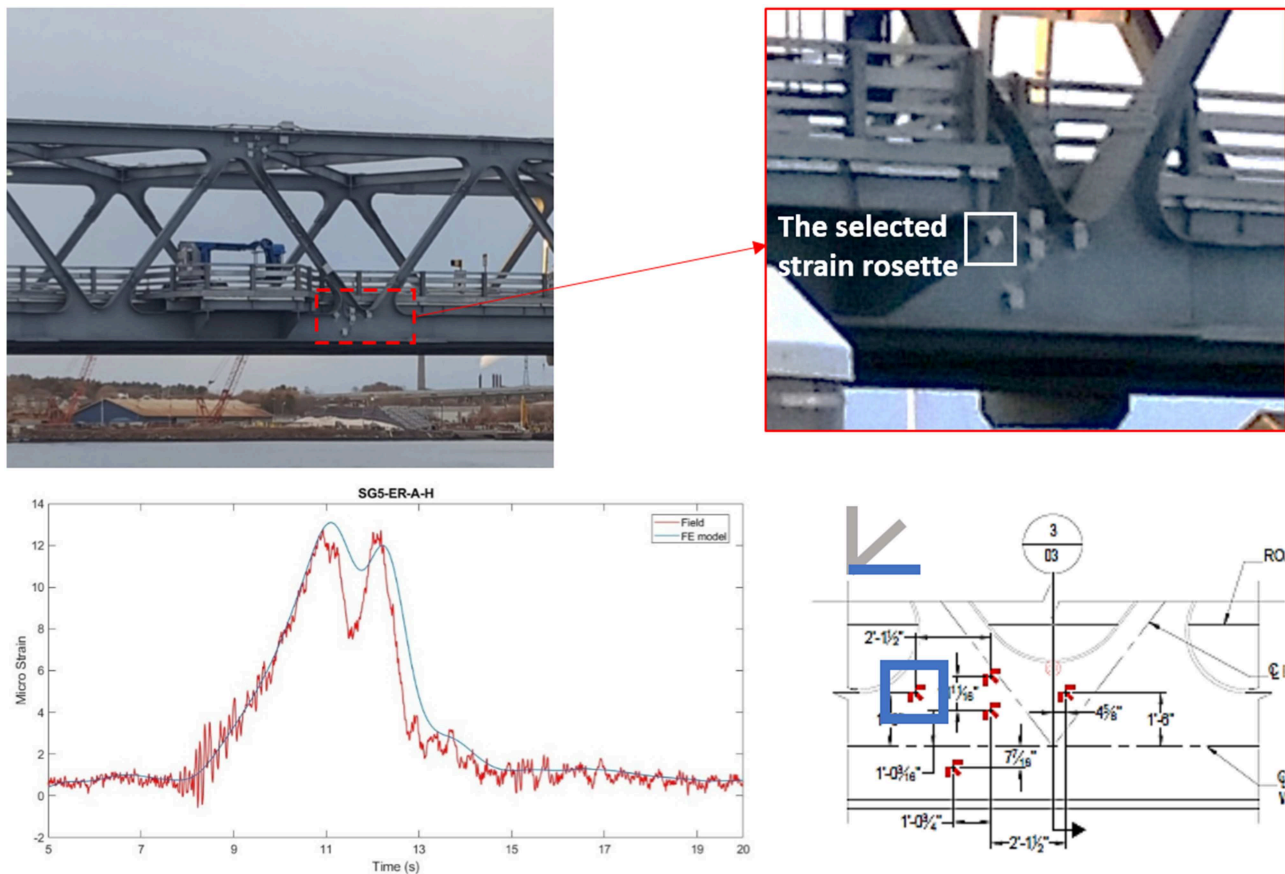
FIGURE 9 | Analytical vs. field time-history response at the strain gage location under the moving truck load.

vectors u_{ij}, S_i is a diagonal matrix holding the singular vectors and superscript H denotes conjugate response. While the peaks of the output spectrum show the natural frequencies of the system, the first singular vector estimates the corresponding mode shape. **Figure 10A** shows the acceleration time history captured by an accelerometer located on the top chord during a lift event.

By a sampling rate of 50 Hz and using a Hanning window with 60% overlap, while a bandpass Butterworth IIR filter of 4th order with the lower cutoff frequency of 1 Hz and higher cutoff frequency of 5 Hz were applied, the singular values and their corresponding singular vectors were identified. **Figure 10B** shows the output spectrum in which the peaks represent the first three natural frequencies of the bridge. For this case, the accelerometers on the tower of the bridge were not considered. To make sure there is not any periodicity in the signal, only the part of the signal between the lowering of the lift span at the end of a lift operation and resuming of vehicular traffic was used for the frequency domain decomposition. While **Figure 10C** shows the mode shapes corresponding to the first three vibration modes of the bridge from the SAP2000® model. **Table 2** compares the resulting natural frequencies of both SAP2000® and Lusas® FE models with monitoring data.

DECISION SUPPORT USING THE VERIFIED MODEL

Management decision related to in-service bridges must consider resource constraints and the need to maintain the structural health of the bridge components and the infrastructure network. A verified structural model of a complex high-value bridge can benefit management and operational decision-making. The verified models of the Memorial Bridges were used to predict fatigue damage, reduction in load carrying capacity, real-time condition assessment and member vulnerability with respect to likely damage scenarios.

Fatigue Damage Prediction

The radiused filet welds at the gusset-less connection of the Memorial Bridge connecting the cold bent flanges to the web of the connection (as shown in **Figure 8**) can make the weld toe of the connection a hot-spot location. The geometric complexities and discontinuities induce the hot-spot stresses at the toe of the welded connections. Due to the limitations in existing sensor installation location, the installed strain gages at the gusset-less connection are 2-inches away from the weld toe, as shown in **Figure 5**, and therefore; these sensors are able
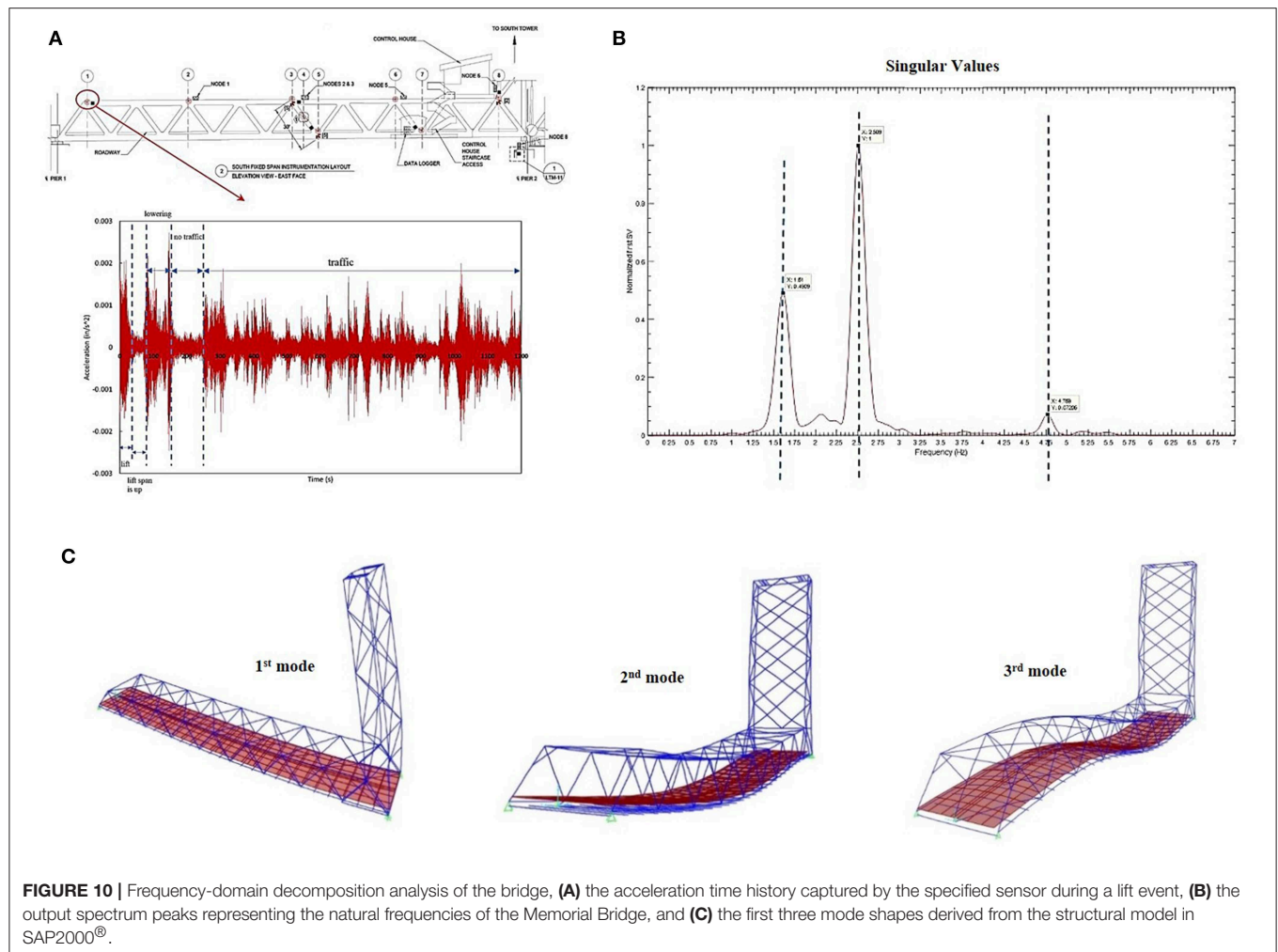
FIGURE 10 | Frequency-domain decomposition analysis of the bridge, **(A)** the acceleration time history captured by the specified sensor during a lift event, **(B)** the output spectrum peaks representing the natural frequencies of the Memorial Bridge, and **(C)** the first three mode shapes derived from the structural model in SAP2000®.

TABLE 2 | Verification of the bridge natural frequencies for both SAP2000® and Lusas® FE models with monitoring data.

Mode number	Natural frequencies (Hz)				
	SAP2000® beam model	Lusas® shell element model	Lusas® detailed multi-scale model	Lusas® multi-scale model	Monitoring data (FDD)
1	1.23	1.49	1.50	1.56	1.61
2	2.04	2.41	2.45	2.51	2.51
3	4.17	4.04	4.03	4.07	4.77

to record the nominal strains (stress) of the connection. In consequence, the application of the field collected nominal strains recorded through the strain gauges for fatigue assessment of the connection may not properly inform on fatigue status of the component. Consequently, the acquired fatigue damage response may lead to overestimating the remaining life of the component.

The captured strains by the sensors at the bridge are the nominal strains which can be less critical for fatigue damage assessment. In this study, considerable efforts were made to determine the hot-spot locations using the calibrated FE model developed in Lusas®. To measure the fatigue damage of the gusset-less component, it is essential to determine the stress ranges and stress cycles under the live loads experienced by the structure. The measured nominal stress range, S_{nom}, is represented as the difference between the maximum stress, σ_{max}, and the minimum stress, σ_{min}, measured in one stress cycle expressed in Equation (3) (Ni et al., 2010). The hot-spot stress range can be calculated using the Stress Concentration Factor (SCF) through the Equation (4):

$$S_{nom} = \sigma_{max} - \sigma_{min} \qquad (3)$$

$$S_{hot} = (\sigma_{max} - - \sigma_{min}) \times SCF \qquad (4)$$

The SCFs for the standard welded connections are well-documented in the previous studies and available codes for welding (IIW, 2000; Niemi et al., 2006). The SCF factors for the complex components which are not documented on the codes, can be measured through a validated FE model by dividing the

hot-spot stress, σ_{hot}, by the nominal stress, σ_{nom}, expressed in Equation (5):

$$SCF = \sigma_{hot}/\sigma_{nom} \qquad (5)$$

To determine the appropriate SCF, the numerical strain response at the toe of the weld and the nominal strain response at the location of the strain rosette are applied. The numerical nominal and hot-spot stress range are computed from Equation (5) using the time-history responses of the model, as expressed in **Figure 9**. The SCF for the location of the strain rosette C is

computed using a perpendicular path starting from the strain rosette location to the weld toe, as shown in **Figure 8C**. Through the FE analysis, the SCF was acquired 1.38. The resulting SCF is applied to be multiplied by the field collected stress ranges from the investigating strain rosettes.

The field collected stress responses, induced by the traffic loads have a variable amplitude property. To measure the variable amplitude stress ranges the rain-flow cycle counting algorithm (Downing and Socie, 1982) was applied to extract the stress range and the stress cycles through the field time-history strain responses. The nominal stress ranges are multiplied by the
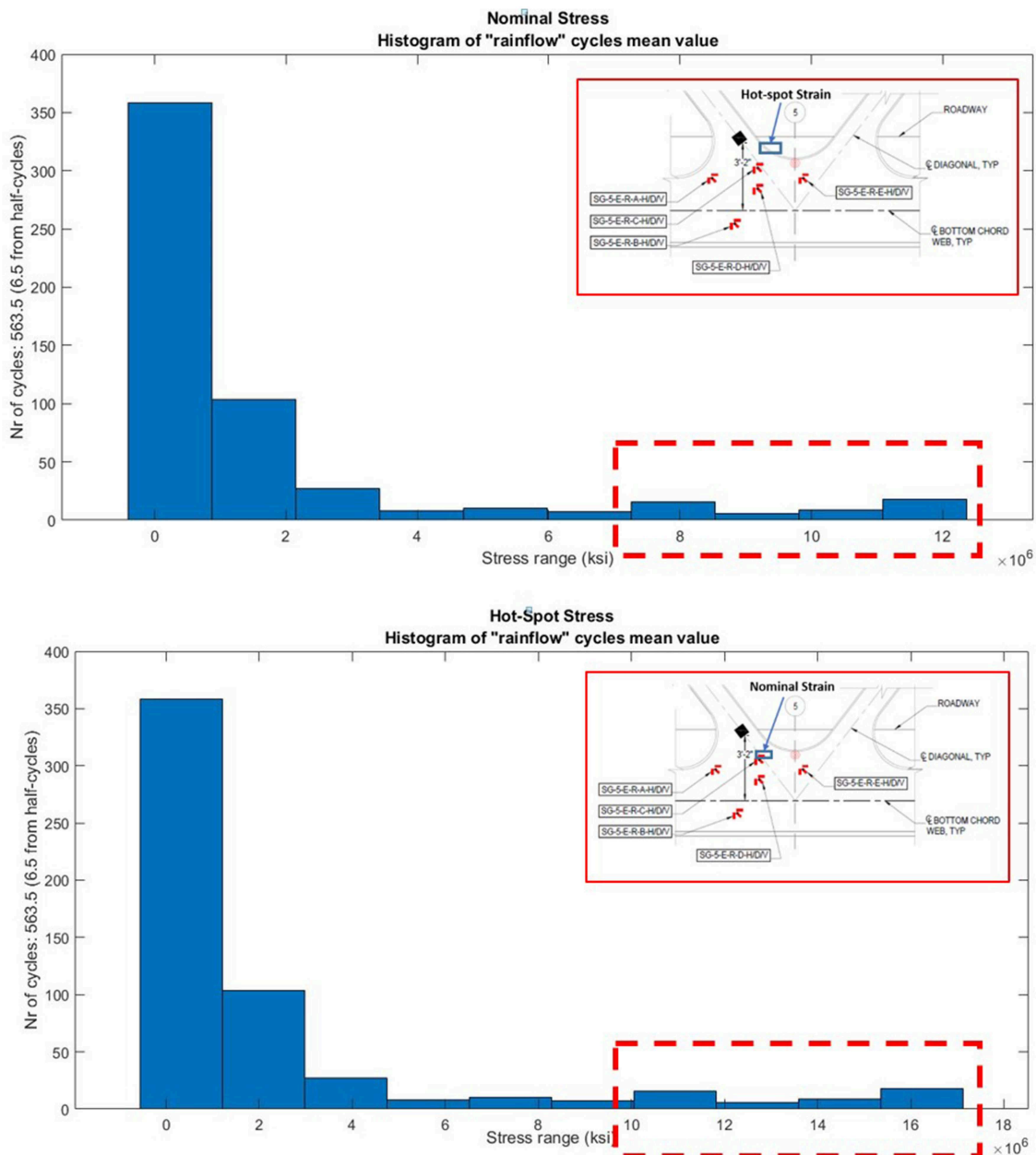

FIGURE 11 | Nominal stress vs. hot-spot mean stress range.

measured SCF to achieve the hot-spot stress ranges. The acquired stress cycles are applied to measure the fatigue damage index using the S-N curve and Miner's rule given by Equation (6) (Miner, 1945):

$$D = \sum_i \frac{n_i}{N_i} \qquad (6)$$

where n_i denotes the number of the cycles for the stress range, S_i and N_i is the number of cycles to failure at the stress range of S_i. In applying the S-N curve for the fatigue damage measurement, the novel gusset-less connection is not categorized among the recognized components existing in American Association of State and Highway Transportation Officials (AASHTO) fatigue categories. However, the Category C is considered for component investigating at the toe of the weld based on the designer's assumptions and the AASHTO categorized specifications considered for the filet welds (AASHTO, 1995). Also, category B is considered for the nominal stress ranges. **Figure 11** illustrates the results of the mean stress histograms at the hot-spot location of the weld toe and the nominal stress at the instrumented locations of the gusset-less connections. The results of the nominal and hot-spot stress ranges as well as the associated fatigue responses are expressed in **Table 3**. The resulting fatigue responses due to the limited number of cycles are still representing infinite fatigue life. However, it can be observed for the considering period, the hot-spot fatigue response is about four times of the nominal fatigue response. In the longer periods of data collection, higher number of cycles of stress ranges are achieved. With the higher recorded cycles of stress ranges (considerable for fatigue assessment), the difference between the nominal and hot-spot fatigue responses can be infinite and finite reports of the remaining life of the component. Consequently, it is essential to measure the nominal and hot-spot fatigue responses in evaluating the health status of the fracture critical structural components.

Load Rating Degradation Due to Damage Scenarios

The calibrated structural model created in SAP2000® was used for reliable assessment of the bridge actual condition subjected to likely damage scenarios. In particular, such models can be used to verify how the damage of one or more particular member(s) may degrade the load carrying capacity or load rating of the bridge. The load rating of a bridge is defined as (AASHTO, 2011):

$$RF = \frac{C - (\gamma_{DC})(DC) - (\gamma_{DW})(DW)}{(\gamma_{LL})(LL + IM)} \qquad (7)$$

where RF is the rating factor, C is the capacity of one member, DC, DW and LL are Dead load effect due to structural components and attachments, Dead load effect due to wearing surface and utilities and Live load effect, respectively. Also γ_{DC}, γ_{DW} and γ_{LL} are LRFD load factor for structural components and attachments, LRFD load factor for wearing surfaces and

TABLE 3 | The results of the nominal and hot-spot stress ranges as well as the associated fatigue responses for the Lusas® FE model.

Nominal stress range (ksi)	Hot-spot stress range (ksi)	Number of cycles	Number of considered cycles in a period	Nominal fatigue response	Hot-spot fatigue response
8.20	11.31	12	500	5.51E-7	3.95E-6
9.11	12.57	9	500	5.67E-7	4.06E-6
10.03	13.84	5	500	4.60E-7	3.01E-6
				2.69E-6	11.02E-6

utilities, and live load factor, respectively and IM is the dynamic load allowance.

For instance, if a bottom chord of the bridge in the middle of the fixed-span and its neighboring diagonal is hit by a vessel collision, the load rating capacity of the bridge is diminished. Based on the intensity of the ship collision, one may consider various percentages of damage. If the damage intensity is simulated by reduction of property modifiers of the damaged members in the analytical model and the capacity of the damaged member is diminished by corresponding reduction factors, the degradation of load rating of the bridge can be obtained. The calibrated model of the bridge was used for understanding the bridge capacity due to likely damage scenarios. **Figure 12A** shows a typical example of the load rating degradation of the bridge based on the bending capacity of the damaged bottom chord and its neighboring diagonal as shown in **Figure 12B**. The redundancy of the structural system allows for load redistribution to surrounding health members. This analysis indicates that these members do not need to be repaired but it does demonstrate the design system redundancy and safety factor.

Real-Time Condition Assessment for Operational Decision-Making Protocol

When a bridge experiences an unexpected occurrence of accidental events, such as the vessel collision as expressed in the previous section, a major concern for bridge managers is effective and informed operational decision-making with respect to the remaining capacity of the bridge. This protocol could be functional via the monitoring data collected through a long term SHM system to predict the bridge structural behavior in the presence of damage. Since the Memorial Bridge is a relatively new bridge suffering no damage so far, in a parallel study, considerable efforts were performed to take advantage of the frequent and repeated lift operations that impart a significant impact load on the bridge. The simulated lift impact vibrates the fixed-span of the verified SAP2000® model so that the resulting accelerations can be collected under varying health and damage scenarios. The principal concept behind the excitation technique is explained in detail by Shahsavari et al. (2018a).

Given the load rating reduction estimated by the bridge analytical model, an integrated decision-making protocol combining different approaches will be beneficial to bridge
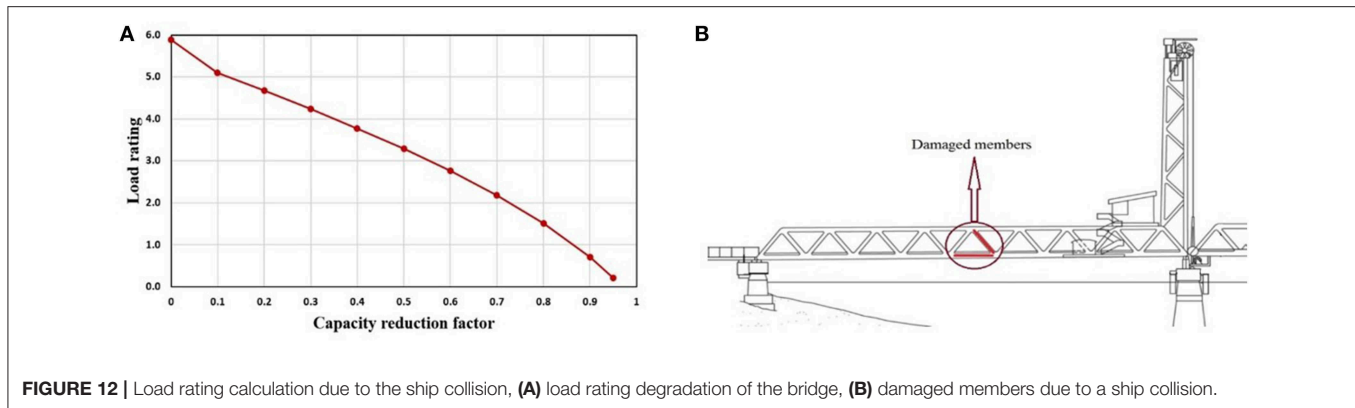
FIGURE 12 | Load rating calculation due to the ship collision, **(A)** load rating degradation of the bridge, **(B)** damaged members due to a ship collision.

managers for making decisions on the damaged (pre-repair) state of the structure with respect to different damage scenarios. Therefore, in this case study, the verified structural model was used as a baseline to (a) determine the structural system response for damage detection using the combined application of signal processing and statistical pattern recognition techniques and (b) investigate the bridge decreased load carrying capacity according to the AASHTO Manual for Bridge Evaluation (AASHTO, 2011). Various damage scenarios were modeled near the mid-length of the fixed-span to simulate damage caused by truck accident, vessel collision, fatigue damage in the gusset-less connection, and loose bolts. These case scenarios were simulated to be reflective of likely damage scenarios jeopardizing the structural safety and serviceability of the bridge under operating conditions.

A damage detection criterion relying on the wavelet energy rate index of acceleration signals was proposed to continuously post-process the bridge collected dynamic data as a means for real-time condition assessment. The damage detection procedure of Shahsavari et al. (2018a) was employed to discriminate between two different states of the structure using the collected acceleration data obtained from the SAP2000® model at pseudo-sensor (accelerometer) locations throughout the bridge model. For each structural condition, the bridge was subjected to multiple random excitations to simulate the frequent and dynamic impacts of the bridge movable (lift) span on the fixed-span and tower. The Wavelet Packet Component (WPT) was used to determine how the bridge system response will be affected by damaged-induced change in dynamic properties. By definition, the wavelet packet function is expressed by:

$$\psi_{j,k}^i(t) = 2^{j/2}\psi^i\left(2^j t - k\right), \; i = 1,2,3,... \tag{8}$$

where i, j, and k denote the modulation, scale, and translation parameters, respectively. The wavelet packet component $f_j^i(t)$ is given by:

$$f_j^i(t) = \sum_{k=-\infty}^{\infty} c_{j,k}^i(t)\,\psi_{j,k}^i(t) \tag{9}$$

where $c_{j,k}^i(t)$ is the wavelet coefficient at time instant (t). In theory, the wavelet coefficient is used as a scalar value specifying

the degree of correlation between the wavelet function and the analyzed portion of the signal at an instant of time. The WPT is based on a binary decomposition algorithm in which each level of decomposition (j) offers 2^j number of wavelet packet components (i) in total. The energy distribution (E) of the wavelet packet component $f_j^i(t)$ is computed by:

$$E_{f_j^i(t)} = \int_{-\infty}^{\infty}\left(c_{j,k}^i(t)\right)^2 dt \tag{10}$$

Given that the energy rate index corresponding to acceleration time-series are highly correlated to structural dynamic characteristics, the average energy rate index investigated from the energy distribution of all accelerometers was used as representative of the bridge dynamic response for different structural conditions. The proposed damage detection criterion is based on performing a control chart analysis on the wavelet packet averaged data for feature classification between different states. The core of the control chart analysis is to enclose the inherent variations of the wavelet-based vibration features, measured in the healthy state of the structure, within two threshold lines (upper and lower control limits). Given the statistical enclosure, an exceedance of sample mean μ corresponding to alternate (damaged) models beyond the control limits can be attributed to the presence of unusual sources of variability with high confidence.

For this case study, the statistical baseline was constructed by enclosing the reference data within plus and minus three standard deviations σ from the sample mean μ for the undamaged state of the bridge, resulting in a 99.7% confidence interval. **Figure 13** represents the control chart analysis of sample (wavelet) data due to damage induced to the bridge members by the vessel collision shown in **Figure 12B**. In this instance, various levels of damage, ranging from 10 to 90% reduction in cross sectional properties of the damaged members, were simulated to account for the intensity of the potential ship impact. As shown in the graph, as the damage level increases the average normalized energy of signals increases which in turn may cause sample data to exceed the threshold lines based on the observations measured in the reference (undamaged) state of the bridge. The proposed approach was mainly developed to make the bridge owners aware
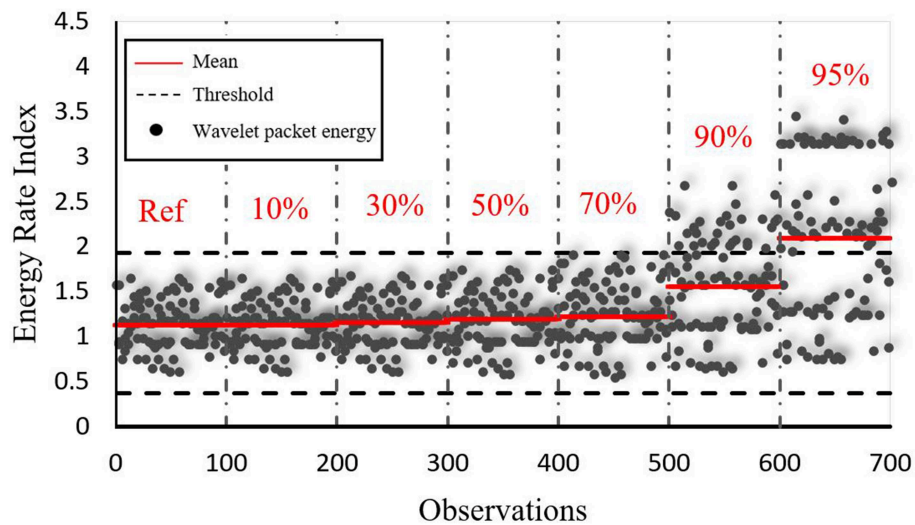
FIGURE 13 | Control chart analysis for incremental levels of damage due to the ship collision.

of a significant change in the system performance due to likely damage to determine the need for more costly actions, either through a targeted visual inspection for areas of potential damage or model updating and parameter estimation depending on the available data (Santini-Bell et al., 2007; Sanayei et al., 2011).

In general, the wavelet-based decision-making methodology consists of different steps sequentially come after each other. Once the source of damage is identified, the next step is to assess the damage impact on the load carrying capacity of the bridge, which is quantified by load rating concept using the AASHTO design code provisions, Equation 7, to better prioritize management strategies for a deteriorated bridge. The proposed protocol was developed to demonstrate how the use of sensor technology and structural modeling combined with enhanced methodologies and engineering practices can yield reliable bridge condition assessment and proactive visual inspection and subsequent load rating evaluation on demand basis. This approach not only provides bridge owners with additional time and flexibility for maintenance and rehabilitation of deteriorated bridges, but it also can facilitate a better resource allocation to repair or replace damaged components.

CONCLUSION

This paper presents a case study to better prioritize the management strategies for smart and in-service bridges instrumented by structural health monitoring sensors. The paper is structured in a manner that provides three means of using the collected structural response information, diagnostic testing and structural modeling into a decision-making approach. The Memorial Bridge, owned by New Hampshire and Maine Departments of Transportation, is outfitted with a number of monitoring sensors to continuously monitor the bridge response from structural performance to fatigue assessment and load rating reduction prediction using the bridge calibrated analytical

models developed in Lusas® and SAP2000®. These models are developed based on local and global performance assessment goals. The main finding is that the multi-scale modeling approach developed in Lusas® is promising to accurately represent the local performance of the bridge gusset-less connections for fatigue evaluation whereas the SAP2000® wired-based model has a high potential to predict the system response and load rating degradation due to likely damage scenarios or excessive change in dynamic characteristics.

The fatigue assessment results represent infinite fatigue life for the bridge gusset-less connection, the measured fatigue damage response at the hot-spot region is about four times of the estimated fatigue response for the nominal stress location. Based on this observation, both the nominal and hot-spot fatigue responses are essential for evaluating the health status of the fracture critical complex structural components.

This paper also presents the application of a wavelet-based method based on the real-time data collected from the SHM sensors to quantify the change in the bridge system response in the presence of likely damage scenarios. The proposed approach demonstrates how the SHM data collected from an instrumented bridge can be integrated into an objective decision-making protocol with the aim to reliability assess the actual condition of deteriorated bridges on demand basis and facilitate a better resource allocation for bridge maintenance. The vessel impact is assessed using the wavelet-based damage detection criterion. For the case scenario at which the damage has reached its critical level, the results indicate that there is statistically significant evidence to detect a noticeable change in the bridge performance. If the bridge experiences a vessel collision causing a significant reduction in the overall capacity of the target members as modeled in this work, ≥90% of the member capacity, deliberate actions should be taken immediately to reduce demand or replace the damaged members. Potential actions include setting management strategies such as closing the bridge, posting load

limits, and performing analytical investigations to repair or replace the damaged members.

This practice demonstrates the need for establishment of performance-based warning systems to proactively keep informed the bridge managers and maintenance engineers of any appreciable change in global response of important transportation infrastructure. Further studies are underway presenting a more reliable methodology to better support operational decision-making protocols for structural condition assessment using the AASHTO LRFD Bridge Design Specifications.

AUTHOR CONTRIBUTIONS

VS coordinated the contributions from all authors, provided editorial support and conducted and drafted the real-time condition assessment using wavelet packets section of this manuscript. MMa created the multi-scale finite element models, performed the static model calibration, and conducted the fatigue assessment included in this manuscript. MMe created the beam structural model, performed the modal model calibration, and conducted load rating degradation study included in this manuscript. ES-B led the design and deployment of the instrumentation plan, load test, model creation, data post-processing efforts, and developed the architecture for this manuscript.

FUNDING

ACKNOWLEDGMENTS

REFERENCES

AASHTO (1995). *Guide Specifications for Fatigue Evaluation of Existing Steel Bridges*. American Association of State Highway and Transportation Officials.

AASHTO (2008). *Bridging the Gap-restoring and Rebuilding the Nation's Bridges*. American Association of State Highway and Transportation Officials.

AASHTO (2011). *Manual for Bridge Evaluation, 2nd Edn*. Farmington Hills, MI: American Association of State Highway and Transportation Officials.

Adams, T., Mashayekhizadeh, M., Santini-Bell, E., Wosnik, M., Baldwin, K., and Fu, T. (2017). *Structural Response Monitoring of a Vertical Lift Truss Bridge*. Transportation Research Board. No. 17-06353. Washington, DC.

Agrawal, A. K., Liu, G. Y., and Alampalli, S. (2013). "Effects of truck impacts on bridge piers," in *Advanced Materials Research, Vol. 639*, eds X. Zhou, G. He, Y. Fan, Y. Xiao, S. K. Kunnath, and G. Monti (Trans Tech Publications), 13–25.

Aktan, E., Catbas, N., Turer, A., and Zhang, Z. (1998). Structural identification: analytical aspects. *Struct. Eng.* 124, 817–829. doi: 10.1061/(ASCE)0733-9445(1998)124:7(817)

Aygül, M., Bokesjö, M., Heshmati, M., and Al-Emrani, M. (2013). A comparative study of different fatigue failure assessments of welded bridge details. *Int. J. Fatigue* 49, 62–72. doi: 10.1016/j.ijfatigue.2012.12.010

Brincker, R., Zhang, L., and Andersen, P. (2001). Modal identification of output-only systems using frequency domain decomposition. *Smart Mater. Struct.* 10, 441–445. doi: 10.1088/0964-1726/10/3/303

Cardini, A. J., and DeWolfe, J. T. (2009). Implementation of a long-term bridge weigh-in-motion system for a steel girder bridge in the interstate highway system. *Bridge Eng.* 14, 418–423. doi: 10.1061/(ASCE)1084-0702(2009)14:6(418)

Carvalho, H., Fakury, R. H., and Vilela, P. M. L. (2017). The challenges of rehabilitating the Hercilio Luz suspension bridge. *Latin Am. J. Solids Struct.* 14, 700–713. doi: 10.1590/1679-78253401

Catbas, F. N., Ciloglu, S. K., Hasancebi, O., Grimmelsman, K., and Aktan, A. E. (2007). Limitations in structural identification of large constructed structures. *Struct. Eng.* 133, 1051–1066. doi: 10.1061/(ASCE)0733-9445(2007)133:8(1051)

Catbas, F. N., Gul, M., Gokce, H. B., Zaurin, R., Frangopol, D. M., and Grimmelsman, K. A. (2014). Critical issues, condition assessment and monitoring of heavy movable structures: emphasis on movable bridges. *Struct. Infrastruct. Eng.* 10, 261–276. doi: 10.1080/15732479.2012.744060

Doebling, S. W., Farrar, C. R., Prime, M. B., and Shevitz, D. W. (1998). A review of damage identification methods that examine changes in dynamic properties. *Shock Vibrat. Digest*. 30, 91–105. doi: 10.1177/058310249803000201

Downing, S. D., and Socie, D. F. (1982). Simple rainflow counting algorithms. *Int. J. Fatigue* 4, 31–40. doi: 10.1016/0142-1123(82)90018-4

Fu, T. S., Garcia-Palencia, A. J., Bell, E. S., Adams, T., Wells, A., and Zhang, R. (2015). Analyzing Prerepair and Postrepair vibration data from the Sarah Mildred Long Bridge after Ship Collision. *Bridge Eng.* 21:05015002. doi: 10.1061/(ASCE)BE.1943-5592.0000856

García, M. D., Cicero, S., and Gutiérrez, O. R. (2018). Structural integrity assessment of the welded joints of the constitution of 1812 bridge (Cádiz, Spain). *Eng. Failure Anal.* 90, 518–533. doi: 10.1016/j.engfailanal.2018.04.012

García-Palencia, A. J., and Santini-Bell, E. (2014). Structural model updating using dynamic data. *Civil Struct. Health Monitor.* 4, 177–194. doi: 10.1007/s13349-014-0073-8

IIW (2000). *Fatigue Design Procedures for Welded Hollow Section Joints*. IIW Doc. XIII-1804-99/XV-1035-99. Recommendations for IIW subcommision XV-E. International Institute of Welding.

Ingraham, C. (2015). *Mapping America's Most Dangerous Bridges*. Available online at: http://www.washingtonpost.com/blogs/wonkblog/wp/2015/02/04/mapping-americas-most-dangerous-bridges/

Kashefi, K., Zandi, A. P., and Zeinoddini, M. (2010). Fatigue life evaluation through field measurements and laboratory tests. *Procedia Eng.* 2, 573–582. doi: 10.1016/j.proeng.2010.03.062

Knott, M. A., and Damgaard, L. O. (1990). *Guide Specification and Commentary for Vessel Collision Design of Highway Bridges*. US Department of Transportation, Federal Highway Adminstration, Publ. No. FHWA-RD-91-006.

Kwad, J., Alencar, G., Correia, J., Jesus, A., Calçada, R., and Kripakaran, P. (2017). Fatigue assessment of an existing steel bridge by finite element modelling and field measurements. *J. Phys.* 843:012038. doi: 10.1088/1742-6596/843/1/012038

Laman, J. A., and Nowak, A. S. (1996). Fatigue-load models for girder bridges. *Struct. Eng.* 122, 726–733. doi: 10.1061/(ASCE)0733-9445(1996)122:7(726)

Leander, J., Honfi, D., Ivanov, O. L., and Björnsson, Í. (2018). A decision support framework for fatigue assessment of steel bridges. *Eng. Failure Anal.* 91, 306–314. doi: 10.1016/j.engfailanal.2018.04.033

Liu, Z., Hebdon, M. H., Correia, J. A. F. O., Carvalho, H., Vilela, P., De Jesus, A. M. P., et al. (2017). Fatigue life evaluation of critical details of

the Hercílio Luz Suspension Bridge. *Procedia Struct. Integr.* 5, 1027–1034. doi: 10.1016/j.prostr.2017.07.063

Mashayekhi, M., Mehrkash, M., Shahsavari, V., and Santini-Bell, E. (2018). *Multiscale Finite Element Model Development for Long-term Condition Assessment of a Vertical Lift Bridge*. Fort Worth, TX: ASCE Structure Congress.

Mashayekhi, M., and Santini-Bell, E. (2019). Three dimensional multiscale finite element models for in-service performance assessment of bridge. *Comput. Aided Civ. Inf. Eng.* 34, 385–401. doi: 10.1111/mice.12424

Mashayekhizadeh, M., Santini-Bell, E., and Adams, A. (2017). "Instrumentation and structural health monitoring of a vertical lift bridge," in *Proceedings of the ASNT 26th Research Symposium* (Jacksonville, FL).

McCune, R. W., Armstrong, C. G., and Robinson, D. J. (2000). Mixed dinetional coupling in finite element models. *Numerical Methods Eng.* 49, 725–750. doi: 10.1002/1097-0207(20001030)49:6<725::AID-NME967>3.0.CO;2-W

Mehrkash, M., and Santini-Bell, E. (2018). "Modeling and characterization of complicated connections in structural and mechanical systems as applied to a gusset-less truss connection," in *97th Annual Meeting of Transportation Research Board* (Washington, DC).

Miner, M. A. (1945). Cumulative damage in fatigue. *Appl. Mech.* 12, A159–A164.

Mohammadi, J., Guralnick, S. A., and Polepeddi, R. (1998). Bridge fatigue life estimation from field data. *Pract. Period. Struct. Des. Const.* 3, 128–133. doi: 10.1061/(ASCE)1084-0680(1998)3:3(128)

NAE (2017). *NAE Grand Challenges for Engineering*. National Academy of Engineering. Available online at: http://www.engineeringchallenges.org/challenges/infrastructure.aspx

Nash, T. P. (2016). *An objective protocol for movable bridge operation in high-wind events based on hybrid analyses by European and American design code* (Master's Thesis). University of New Hampshire, Durham, NC, USA.

Ni, Y. Q., Ye, X. W., and Ko, J. M. (2010). Monitoring-based fatigue reliability assessment of steel bridges: analytical model and application. *Struct. Eng.* 136, 1563–1573. doi: 10.1061/(ASCE)ST.1943-541X.0000250

Niemi, E., Fricke, W., and Maddox, S. J. (2006). *Fatigue Analysis of Welded Components: Designer's Guide to the Structural Hot-Spot Stress Approach*. Cambridge: Woodhead Publishing.

Olaszek, P., and Łagoda, M., Casas, J. R. (2014). Diagnostic load testing and assessment of existing bridges: examples of application. *Struct. Infrastruct. Eng.* 10, 834–842. doi: 10.1080/15732479.2013.772212

Sanayei, M., Imbare, G. R., McClain, J. A. S., and Brown, L. C. (1997). Structural model updating. *Struct. Eng.* 123, 792–798. doi: 10.1061/(ASCE)0733-9445(1997)123:6(792)

Sanayei, M., McClain, J. A., Wadia-Fascetti, S., and Santini, E. M. (1999). Parameter estimation incorporating modal data and boundary conditions. *Struct. Eng.* 125, 1048–1055. doi: 10.1061/(ASCE)0733-9445(1999)125:9(1048)

Sanayei, M., Phelps, J. E., Sipple, J. D., Santini-Bell, E., and Brenner, B. R. (2011). Instrumentation, nondestructive testing, and finite-element model updating for bridge evaluation using strain measurements. *Bridge Eng.* 17, 130–138. doi: 10.1061/(ASCE)BE.1943-5592.0000228

Santini-Bell, E., Lefebvre, P. J., Sanayei, M., Brenner, B., Sipple, J. D., and Peddle, J. (2013). Objective load rating of a steel-girder bridge using structural modeling and health monitoring. *Struct. Eng.* 139, 1771–1779. doi: 10.1061/(ASCE)ST.1943-541X.0000599

Santini-Bell, E., Sanayei, M., Javdekar, C. N., and Slavsky, E. (2007). Multiresponse parameter estimation for finite-element model updating using nondestructive test data. *Struct. Eng.* 133, 1067–1079. doi: 10.1061/(ASCE)0733-9445(2007)133:8(1067)

Shahsavari, V., Bastien, J., Chouinard, L., and Clément, A. (2017b). Likelihood-based testing of wavelet coefficients for damage detection in beam structures. *Civil Struct. Health Monitor.* 7, 79–98. doi: 10.1007/s13349-017-0212-0

Shahsavari, V., Chouinard, L., and Bastien, J. (2017a). Wavelet-based analysis of mode shapes for statistical detection and localization of damage in beams using likelihood ratio test. *Eng. Struct.* 132, 494–507. doi: 10.1016/j.engstruct.2016.11.056

Shahsavari, V., Chouinard, L., and Bastien, J. (2018b). "Detection of structural damage under varying environmental conditions," in *Proceedings of the 10th International Conference on Short and Medium Span Bridges (SMSB)* (Quebec, QC: Canadian Society for Civil Engineering (CSCE)).

Shahsavari, V., Mehrkash, M., and Santini-Bell, E. (2018a). "Structural health monitoring of a vertical lift bridge using vibration data," in *Proceedings of the ASNT 27th Research Symposium* (Orlando, FL).

Stark, T. D., Benekohal, R., Fahnestock, L. A., LaFave, J. M., He, J., and Wittenkeller, C. (2016). I-5 Skagit river bridge collapse review. *J. Performance Construct. Facilities* 30:04016061. doi: 10.1061/(ASCE)CF.1943-5509.0000913

Sun, Z., and Chang, C. C. (2002). Structural damage assessment based on wavelet packet transform. *J. Struct. Eng.* 128, 1354–1361. doi: 10.1061/(ASCE)0733-9445(2002)128:10(1354)

Vafaei, M., Alih, S. C., Shad, H., Falah, A., and Halim, N. H. F. A. (2018). Prediction of strain values in reinforcements and concrete of a RC frame using neural networks. *Adv. Struct. Eng.* 10, 29–35. doi: 10.1007/s40091-018-0178-0

Yao, J. T. (1985). *Safety and Reliability of Existing Structures, Vol. 2*. Boston, MA: Pitman Advanced Publishing, Inc.

Load Distribution of a Prestressed Self-Consolidating Concrete Bridge

Eli S. Hernandez and John J. Myers*

Department of Civil, Architectural and Environmental Engineering, Missouri University of Science and Technology, Rolla, MO, United States

Bridge A7957 is the first Missouri Department of Transportation (MoDOT) large-scale project using self-consolidating concrete (SCC) and high-strength self-consolidating concrete (HS-SCC). The objective of this research was to monitor the initial in-service behavior of the precast-prestressed concrete primary elements of Bridge A7957 and to obtain the load distribution of the bridge using field and finite element models (FEM) data. An initial series of diagnostic load tests was conducted on the bridge superstructure. Embedded sensors recorded strain variations at different section of the instrumented girders for different load configurations. An automated total station (ATS) collected the vertical deflection of the girders at several locations during the application of different test loads. The load distribution for moment was obtained experimentally (using deflection and strain data), FEMs, and using the AASHTO LRFD Bridge Design Specifications. The distribution factors for moment estimated with the AASHTO LRFD equations resulted in larger values compared to field test and FEM results. No difference was observed between the response of the SCC and conventional concrete members during the first series of field load tests.

Keywords: girder distribution factors, lateral load distribution, load distribution factors, diagnostic load test, SCC prestressed concrete girders

INTRODUCTION

During the last two decades, self-consolidating concrete (SCC) and high-strength self-consolidating consolidating concrete (HS-SCC) have been successfully implemented in infrastructure projects due to its effective characteristics (Ouchi et al., 2003; McSaveney et al., 2011; Keske et al., 2014; Hernandez and Myers, 2015b). The flowable feature of SCC comes with a better consolidation and placement that result in fewer voids and honeycombing structures. The more condensed microstructure increases the durability properties of concrete, leading to a longer service life of the structure. This, combined with reductions in labor and equipment costs and decreased maintenance costs, lessens the overall initial investment of the project. In addition, HS-SCC brings an enhanced flexural performance to conventional SCC because of its greater compressive strength. This stronger flexural characteristic brings the possibility to reduce the number of main carrying members and interior supports of bridge structures. Despite the benefits that come with using SCC and HS-SCC, there are some concerns related to its structural and service behavior due to its constituent materials and proportions. The effect of the larger paste content and the smaller coarse aggregate size utilized in the mixture is of particular interest (Myers et al., 2012). Therefore, it is essential to monitor the in-service response of full-scale highway infrastructure utilizing self-consolidating and high-strength self-consolidating precast-prestressed concrete members.

An alternative for effectively evaluating the in-service performance of a bridge structure and its live load-carrying capacity is provided by field load tests. In general, the AASHTO Manual for Bridge Evaluation (MBE) defines two different test options: proof load tests and diagnostic load tests (American Association of State Highway Transportation Officials, 2015). Proof load tests are employed to obtain the maximum safe live load a bridge can withstand without undergoing inelastic deformations, while diagnostic load tests are used to better understand the in-service behavior of a bridge. Diagnostic tests are used to validate design assumptions and to verify the performance of a structure. Most of the times, a bridge load rating is improved after a diagnostic load test because this type of tests implicitly consider *in situ* parameters that are beneficial to the response of a bridge superstructure (Cai and Shahawy, 2003). The aim of this research was to obtain the bridge's experimental and FEM lateral load distribution for moment. A diagnostic test plan was proposed and conducted on Bridge A7957 to accomplish this goal.

Load rating consists of estimating the live load carrying capacity a bridge structure can withstand without suffering damage or undergoing collapse. One of the parameters used to obtain the rating factor of a bridge structure is the lateral load distribution. The AASHTO LRFD Bridge Design Specifications (American Association of State Highway Transportation Officials, 2017) presented a methodology for estimating the lateral load distribution factors that quantify the percentage of the live load applied to a bridge that is carried by a primary supporting member. This approach permits to simplify a three-dimensional (3D) structural analysis into a one-dimensional (1D) problem that is easier for design engineers to handle (Barker and Pucket, 2013). Live load effects, such as bending moments and shear forces, are multiplied by these factors to obtain a design effect that is applied to the 1D member instead of the whole 3D system. It is worth noting that the AASHTO LRFD does not present an approach that evaluates how live loads are distributed among the girders for in-service assessments of bridge structures. Instead, the AASHTO approach proposes a methodology that can be applied to bridges with a wide range of span lengths, girder spacings and stiffness to conservatively estimate distribution factors for bridge design (Harris et al., 2010).

The current AASHTO LRFD Bridge Design Specifications do not differentiate the design process for primary and secondary bridge structures. However, the Manual for Bridge Evaluation clearly defines two levels of bridge performance that are independent of the bridge importance. The first performance level is the inventory level that is compared to the capacity of new structures. The second level of performance is the operating level that is used to evaluate existing bridges that were designed for lighter loads than the ones adopted by the current AASHTO LRFD or for bridges that possess a reduced structural capacity due to deterioration. This level generally describes the maximum permissible live load that the structure may carry (Zhao and Tonias, 2012). The inventory and operating performance levels are differentiated by the load and resistance factors employed to obtain the live load effect at the respective level. Gheitasi and Harris (2015) evaluated the
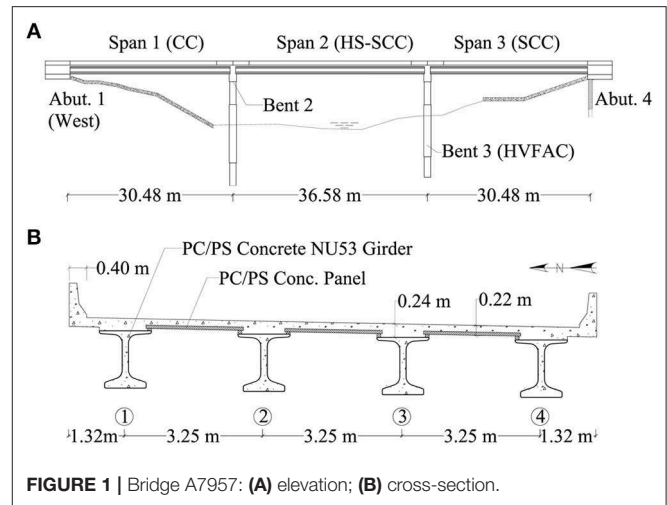
FIGURE 1 | Bridge A7957: **(A)** elevation; **(B)** cross-section.

inelastic distribution behavior of two steel bridges subjected to varying loads and support conditions. Results emphasized the conservativeness of the girder distribution factors for moment as proposed by the AASHTO LRFD approach (both operational and inventory levels) since the applied load corresponding to the critical stage (ultimate capacity) was much larger than the service load. This study focused on using field data to obtain the *in situ* flexural lateral distribution factors of the bridge assuming the global response of the superstructure remains within the elastic range.

In the following sections, the instrumentation, field test program and a comparison between the PC/PS conventional concrete (CC) and SCC members' initial in-service response is presented. In addition, comparisons between the flexural load distribution factors obtained from field measurements, FEM, and the AASHTO LRFD approach are presented to estimate the differences that arise when these three alternative approaches are employed to assess the in-service response of a prestressed concrete bridge.

BRIDGE A7957 DESCRIPTION

Bridge A7957, located along Highway 50 in Osage County, Missouri, is a three-span, continuous, PC/PS concrete bridge with a skew angle of 30 degrees (**Figure 1**). Each span employs PC/PS concrete Nebraska University (NU) 53 girders fabricated with different concrete mixtures. Girders in the first span are 30.48 m long and made of conventional concrete (MoDOT Class A mixture) with a target strength of 55.2 MPa. The girders of the second span measure 36.58 m and were fabricated with an HS-SCC mixture of 68.9 MPa. Girders in the third span are 30.48 m long and employ SCC with a nominal compressive strength of 55.2 MPa (Hernandez et al., 2014b; Hernandez and Myers, 2016c).

PC/PS concrete panels, with a target compressive strength of 55.2 MPa, span between the girders' top flange underneath the cast-in-place (CIP) reinforced concrete (RC) slab deck in the transverse direction (**Figure 1B**). The CIP deck was cast with a 25% fly ash replacement of a portland cement
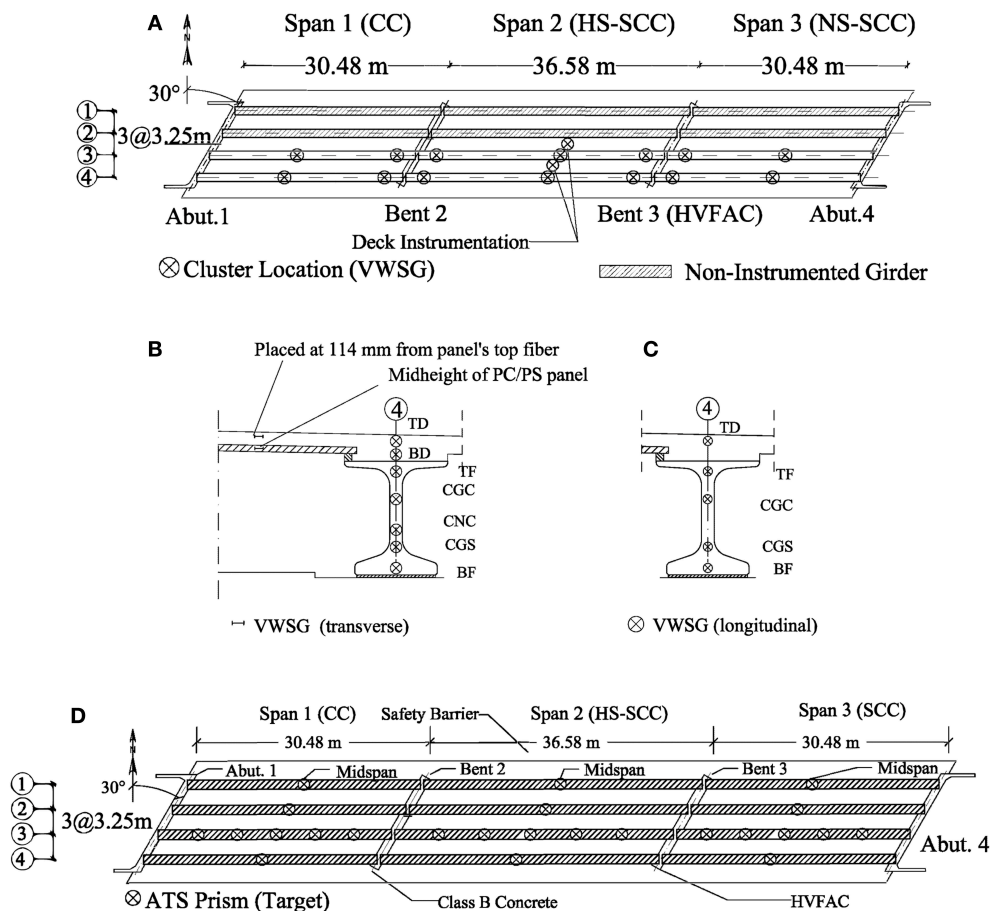
FIGURE 2 | Bridge instrumentation details. (A) VWSG installation layout; (B) midspan cluster location; (C) near-end cluster location; (D) prism layout.

mixture with design strength of 27.6 MPa. The bridge superstructure is supported by two abutments and two intermediate bents (**Figure 1A**). The second intermediate bent and abutments were cast with a concrete mixture that had a 20% fly ash replacement of portland cement and a nominal compressive strength of 20.7 MPa. The third intermediate bent was built using high-volume fly ash concrete (HVFAC) with a 50% fly ash replacement of portland cement and a specified compressive strength of 20.7 MPa. The direction of traffic is along the west-east alienation as shown in **Figures 1**, **2**, **5**.

FIELD DATA ACQUISITION

The structural elements of Bridge A7957 were instrumented during its preconstruction stage. The instrumented elements included: two PC/PS girders per span and two PC/PS panels (**Figure 2A**). The instrumented panels were placed between girder lines 2 and 3 and between girder lines 3 and 4 at midspan of the second span (**Figure 2B**). The type of sensors chosen to be employed and details about their installation are described in the following subsections.

Embedded Sensors

A total of 86 vibrating wire strain gauges (VWSG) with built-in thermistors (type EM-5) were used to monitor temperature changes and stress variations from fabrication through service life (Hernandez et al., 2014a; Hernandez and Myers, 2015b).

Prestressed Concrete Girders

A total of 62 VWSGs were installed in all spans within the PC/PS girders of lines 3 and 4 before casting. The PC/PS girders' cluster locations at which VWSGs were installed are illustrated in **Figure 2**. Within girders of spans 1 and 3, the instrumentation clusters were located at two critical sections: the first at the midspan and the second approximately 0.61 m from the support centerline of bents 2 and 3. The clusters in span 2 were arranged at three different cross-sections: one at the midspan and the other sections approximately 0.61 m from each support centerline. Details on the VWSGs installed at the girders' near-support and midspan sections before the concrete was cast are illustrated in **Figures 2A,C**. The following notation (Hernandez et al., 2014a,b) was used to define the location of the VWSGs within the PC/PS girders:

- TD: 150 mm above the bottom layer of the deck

- BD: 50 mm above the bottom layer of the deck (midspan only)
- TF: 50 mm below the top layer of the girder
- CGC: center of gravity of the composite section
- CNC: center of gravity of the non-composite section (midspan only)
- CGS: center of gravity of prestressed strands
- BF: 50 mm above the bottom layer of the girder.

Cast-in-Place Deck and Prestressed Concrete Panels

VWSGs were installed within the CIP RC deck (**Figure 2C**) in the longitudinal direction (sensors TD and BD). A VWSG was transversely deployed at the mid-height of two selected PC/PS panels (**Figure 2B**). Finally, two VWSGs were in the transverse direction of the bridge, between girder lines 2 and 3 and girder lines 3 and 4. These two sensors were placed directly above the panels' sensors, separated 114 mm from the panels' top fiber (**Figure 2A**).

Remote Non-contact Equipment

An automated total station (ATS), Leica TCA2003 with an accuracy of 1 mm + 1 ppm (distance measurements) and 0.5 arc-seconds (angular measurements), was employed to record the girders' vertical deflection during the live load tests. Twenty-four locations were selected to monitor the superstructure vertical deflection response. During the field test, the ATS continuously read the bar codes on the horizontal and vertical planes by projecting a laser ray to the targets (prisms) mounted on the structure (Hernandez and Myers, 2018a). The accuracy of the ATS has been reported to be ±0.1 mm in vertical deflection measurements (Merkle and Myers, 2004). Fifteen ATS prisms were deployed along the third girder at sections located at 1/6, 1/3, 1/2, 2/3, and 5/6 of the span length. In addition, three prisms were placed at the midspan section of the girders of each span (**Figure 2D**).

FIELD TEST PROGRAM

A monitoring test program, consisting of loading the superstructure during a series of field load tests, was developed to oversee the service response of Bridge A7957. The first series of diagnostic load tests was performed in April and August of 2014. MoDOT dump trucks loaded the bridge superstructure during the tests (Hernandez and Myers, 2016a). A total of thirteen test configurations are reported herein. Six dump trucks were employed during the first part of the first series of load tests (April 2014), and three trucks were used in the second part of the tests (August 2014). The trucks were fully loaded with gravel and sand before the tests were started. **Figure 3** illustrates the different transverse load configurations and the average dimensions of the trucks employed during the test.

Table 1 lists the weight of the axles of the truck (**Figure 3D**) as reported by MoDOT personnel at the beginning of the tests. The weight of the trucks was obtained weighing the front axle alone and the middle and rear axles set at once. For this reason, the weight of the rear and middle axles of a truck was considered as equally distributed between these two axles.
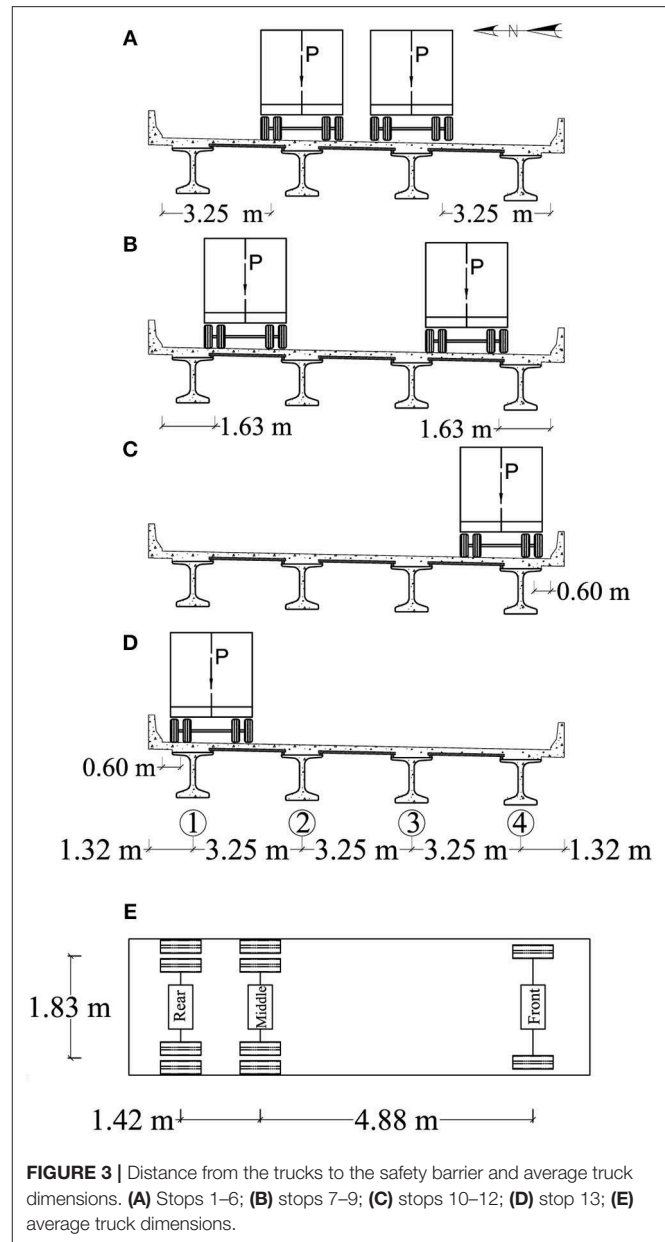
FIGURE 3 | Distance from the trucks to the safety barrier and average truck dimensions. **(A)** Stops 1–6; **(B)** stops 7–9; **(C)** stops 10–12; **(D)** stop 13; **(E)** average truck dimensions.

Figures 3, **4** show the load configurations (stops) used to obtain the maximum response of the bridge when a one or two lanes were loaded. The dimensions shown in **Figure 4** represent the distance measured from the center line of a support (end abutment or pier cap) to a reference line used to locate the exterior wheels (close to safety barrier) of the front axle of trucks 1 and 4 during a test. For the first six load stops, the center of the exterior wheels of each truck was placed 3.25 m from the interior edge of the safety barrier, as shown in **Figure 3A**. In the case of load stops 1–3, two lanes of trucks were driven from east to west and were used to load the central region of spans 3, 2, and 1, respectively, as illustrated in **Figures 4A,C**.

For load stops 4–6, the trucks were driven from west to east and placed at the center of spans 1, 2, and 3, respectively

Test day	Truck	Rear (kN)	Middle (kN)	Front (kN)
1, 2*	1	79.1	79.1	74.0
1, 2*	2	80.8	80.8	57.2
1, 2*	3	75.1	75.1	56.1
1, 2*	4	89.0	89.0	75.3
1, 2*	5	85.1	85.1	77.9
1, 2*	6	83.2	83.2	71.6
3	1	82.3	82.3	61.1
3	2	90.1	90.1	70.9
3	3	84.5	84.5	70.5

Trucks remained loaded with the same weight during days 1 and 2.

(**Figures 4D,F**). For load stops 7–9 (**Figures 4G,I**), the trucks were driven from west to east, and their exterior axles were located 1.63 m from the edge of the safety barrier (**Figure 3B**). It is important to notice that load stops 1–9 represented two-lane loads acting on the superstructure of Bridge A7957. For load stops 10–12 (**Figures 4J,L**), one lane of trucks was moved from west to east, and the trucks were parked on the south side of the bridge, 0.60 m from the edge of the safety barrier (**Figure 3C**). In the case of load stop 13 (**Figure 4M**), the lane of trucks was driven from east to west, and was placed on the north side of the bridge, 0.60 m from the edge of the safety barrier (**Figure 3D**).

TEST RESULTS

Longitudinal Strains

Table 2 reports the longitudinal strain of the bottom flange obtained from experimental data recorded at midspan sections. These values correspond to the two-lane and one-lane load configurations described in the previous section. Larger strains were collected at midspan of the exterior and interior girders close to the area on which loads were applied. The measured strain values, obtained from two-lane load stop configurations acting on spans 1 and 3 (i.e., stop 1 vs. stop 3, stop 4 vs. stop 6, and stop 7 vs. stop 9), were compared. The maximum difference corresponded to a value close to 2%. No significant difference was observed in the in-service exterior and the behavior of the interior girders of spans 1 and 3.

For load stops 7 and 9 (two-lane load cases), the difference in the reported strain values for the interior and exterior girders was close to 10 percent. This difference can be attributed to two possible causes. First, the axles of the truck that loaded the superstructure during these stops might have been placed at locations that did not correspond to the originally planned stop configurations (central region of the spans) shown in **Figures 4G,I**. Second, for the test stops 7–9, the vertical deflection was recorded only at the center line of the girders (midspan locations) due to time restrictions. The necessary time to record the bridge response during tests 7–9 was half the time employed to record the response of the bridge during stops 1–6 (12 vs. 24 min.). This reduction of the duration of the tests might have not allowed the bridge to undergo the total expected flexural response. Both possible sources of poor correlation need to be
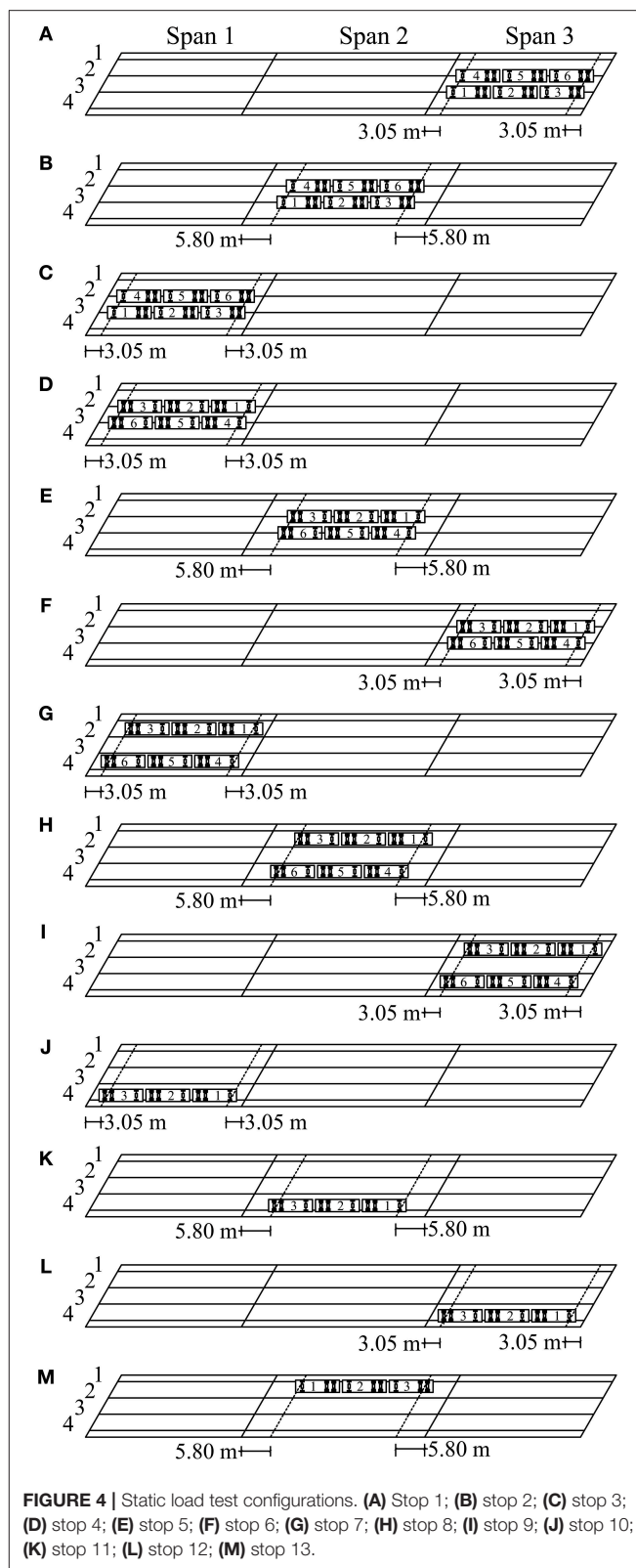
FIGURE 4 | Static load test configurations. **(A)** Stop 1; **(B)** stop 2; **(C)** stop 3; **(D)** stop 4; **(E)** stop 5; **(F)** stop 6; **(G)** stop 7; **(H)** stop 8; **(I)** stop 9; **(J)** stop 10; **(K)** stop 11; **(L)** stop 12; **(M)** stop 13.

investigated in future series of load tests. However, the data collected for the two-lane load configurations in spans 1 (CC girders) and span 3 (SCC girders) were close. These results

TABLE 2 | Experimental strains and vertical deflections.

Stop	Span	ε_{G1} ($\mu\varepsilon$)	ε_{G2} ($\mu\varepsilon$)	ε_{G3} ($\mu\varepsilon$)	ε_{G4} ($\mu\varepsilon$)	Δ_{G1} (mm)	Δ_{G2} (mm)	Δ_{G3} (mm)	Δ_{G4} (mm)
TWO LANES LOADED									
1	3	45*	83*	89	48	4.2	7.1	6.9	4.6
2	2	55*	95*	92	54	6.3	9.7	9.5	6.2
3	1	46*	84*	87	49	5.1	6.9	6.7	4.9
4	1	49*	87*	84	46	4.2	6.7	6.9	4.4
5	2	54*	92*	95	55	6.4	9.8	10.1	6.4
6	3	48*	89*	83	45	4.9	8.4	7.8	5.2
7	1	–	–	73	65	4.9	5.1	5.5	5.7
8	2	–	–	80	75	7.3	7.8	8.1	7.6
9	3	–	–	67	58	4.4	5.5	5.9	5.9
ONE LANE LOADED									
10	1	–	–	44	64	0.1	1.3	3.5	5.0
11	2	4*	17*	51	78	0.8	2.0	4.9	7.7
12	3	–	–	43	65	1.2	2.1	3.5	5.4
13	2	78*	51*	17	4	8.6	5.4	2.6	1.0

*Values were obtained indirectly by assuming that mirrored image load configurations could produce a symmetrical response of the interior and exterior girders (lines 3 and 4) during the load test.

FIGURE 5 | Finite element model of Bridge A7957. **(A)** Entire model; **(B)** Detail of girders and secondary elements (Safety barriers and diaphragm).
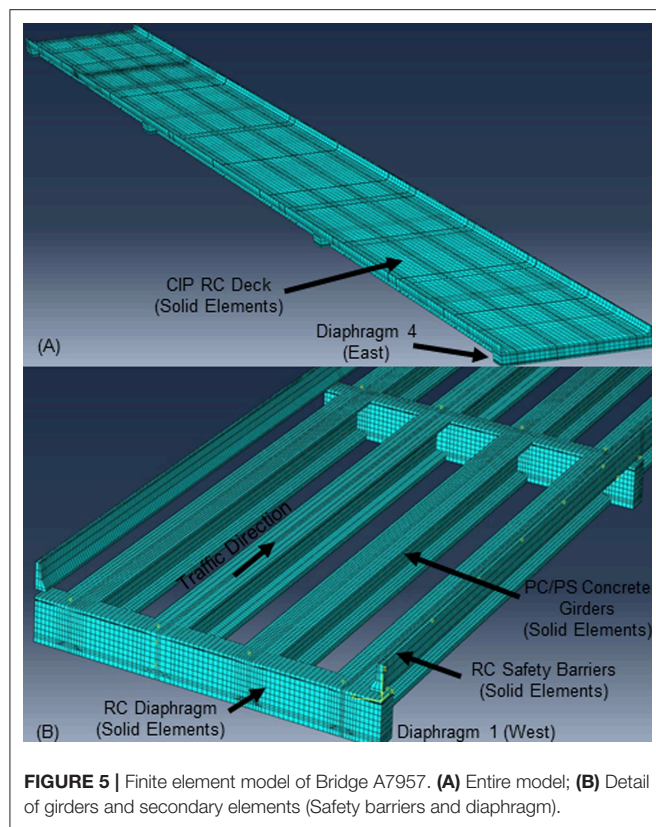
suggest that the flexural response of these spans was independent of the materials employed to fabricate the PC/PS girders.

Vertical Deflections

Table 2 lists the vertical deflections obtained at midspan for the load stops described in the previous section. These deflection values were truncated to the accuracy of the ATS (Hernandez and Myers, 2015a, 2018b). As in the case of the experimental strains, larger deflections were recorded for the girders located close to the region of application of the test loads. Comparable values, corresponding to stops 1 and 3, stops 4 and 6, and stops 7 and 9 (two lanes loaded) were also obtained in spans 1 and 3. For the cases of one-lane loaded (stops 10 and 12), a larger difference ratio (approximately 18% in the case of girder 1) was observed when girders 1 and 2 of spans 1 and 3 were compared (see **Table 2**). This difference can be attributed to the accuracy of the ATS that is close to the measured deflection values. In future load tests, the magnitude of the loads must be planned so that the bridge undergoes vertical deflections larger than the ATS accuracy to minimize the error committed during data collection. It is noted that the behavior of the girders in spans 1 and 3 was within the same order of magnitude. This indicates that the behavior of the span was independent of the type of material employed to fabricate the PC/PS concrete girders.

FINITE ELEMENT MODELS

The commercial finite element analysis (FEA) software ABAQUS (Simulia, 2012) was used to develop 3D, linear, finite-element models (FEMs) of the bridge superstructure for each of the load stop configurations presented in **Figures 3**, **4**. The geometry of the bridge was created from construction documents and was modeled with 20-node solid elements (**Figure 5**). The bridge was modeled considering (1) the primary members (CIP RC deck shown in **Figure 5A** and PC/PS concrete girders shown in **Figure 5B**); (2) the secondary members (RC safety barriers and diaphragms shown in **Figure 5B**). The material of each bridge component was assumed to be linear elastic for the level of load applied during the tests. The modulus of elasticity (MOE) of the different parts was obtained by averaging the results of MOE

Bridge component	Test day 1	Test day 2
Girders (Span 1)	38.80	41.20
Girders (Span 1)	39.30	42.25
Girders (Span 1)	38.70	39.99
Safety barrier	35.51	33.78
CIP deck, diaphragms	31.03	31.03

tests conducted on three companion specimens the same day of the load test. The companion specimens were cast during the fabrication of the PC/PS concrete girders and the construction of the bridge components (CIP RC deck, diaphragms and safety barriers). **Table 3** lists the MOE values of the different bridge components used to create the finite element simulations as reported by Hernandez and Myers (2015b, 2016b). Two different sets of MOE values were used as input of the FEMs, depending whether the load stop was conducted on day 1 (April 2014) or day 2 (August 2014). Experimental deflection values reported by Hernandez and Myers (2016a) were utilized to calibrate and reproduce a finite element model that could predict the response of the bridge with a reasonable level of accuracy. The calibrated FEM may be used to perform "virtual load tests" and predict the response of the bridge subjected to different load configurations (Hernandez and Myers, 2018a).

The position of the trucks over the slab deck and the distances between the axles of the trucks were simulated as recorded for each load configuration. Concentrated forces were applied at the location of the wheels of the trucks to simulate the weight of the axles reported by MoDOT personnel (**Table 1**). **Table 4** reports the longitudinal strains measured at the bottom of the girders (midspan sections) obtained from the FEM simulations. In general, the finite element models predicted the response of the bridge for the different load configurations with a reasonable level of accuracy. The largest difference between the experimental and FEM strains was close to 15% for all the interior and exterior girders during most of the load stops. The exception was observed for the strain value of the exterior girders recorded during stops 11 and 13 that showed a 50% difference. This extreme difference may be attributed to the proximity of the measured strain value to the accuracy of the VWSG sensor.

Table 4 also presents the vertical deflections obtained from FEM simulating the load stops described in the previous section. Larger deflections were observed for the girders located near the truck loads. Comparable values, corresponding to stops 1 and 3, stops 4 and 6, and stops 7 and 9 (two lanes loaded) were obtained in spans 1 and 3. For one-lane loaded cases (stops 10–13), larger difference ratios were observed when the experimental and FEM results were compared. A 500% difference was obtained in the case of stop 10, and a 50% difference in the case of the exterior girders for stops 12 and 13. These differences, as mentioned before, can be attributed to the accuracy of the ATS that is close to the measured deflection values. In general, the response of the girders in spans 1 and 3 was within the same order of magnitude indicating that the response of the spans during the first series

of load tests was independent of the type of material used to fabricate the PC/PS concrete girders (CC and SCC) of spans 1 and 3.

LOAD DISTRIBUTION FOR MOMENT

Lateral distribution factors obtained from field measurements and FEM simulations are defined herein as load distribution factors (LDF). In addition, lateral distribution factors obtained using the AASHTO LRFD approach (American Association of State Highway Transportation Officials, 2017) are referred to as girder distribution factors (GDF) following the nomenclature used by Cai and Shahawy (2003).The LDFs for the exterior and interior girders were computed using strain and deflection values obtained experimentally or using FEM.

The LDFs were estimated using longitudinal strain values in the following manner:

$$LDF_{\varepsilon i} = n \frac{\varepsilon_i}{\sum_i^k \varepsilon_i} \tag{1}$$

where $LDF_{\varepsilon i}$ = lateral distribution factor for moment of the ith girder obtained with longitudinal strains; ε_i = bottom flange longitudinal strain of the ith girder at midspan obtained experimentally or using FEM; n = number of lanes loaded; and k = number of girders). Similarly, the LDFs were estimated using vertical deflection values as follows:

$$LDF_{\delta i} = n \frac{\delta_i}{\sum_i^k \delta_i} \tag{2}$$

where $LDF_{\delta i}$ = lateral distribution factor for moment of the ith girder estimated with vertical deflections; and δ_i = deflection of the ith girder at midspan obtained experimentally or using FEM.

Experimental Load Distribution Factors
Field Longitudinal Strains
The bottom-flange strains of PC/PS girders 1 and 2 were required to compute the LDF. As mentioned above, VWSGs were installed at cluster locations along girder lines 3 and 4 (**Figures 2**, **3**), which allowed direct recording of the strains of girders 3 and 4 for each load stop configuration. The strain values of girders 1 and 2 were indirectly obtained by using the symmetry of the bridge and assuming that mirrored image load configurations could produce a symmetrical response of the interior and exterior girders (lines 3 and 4) during the load test. For two-lane load cases, stops 3 and 4 (span 1), stops 2 and 5 (span 2), and stops 1 and 6 (span 3) were considered as symmetrical (**Figure 4**). Stops 11 and 13 (span 2) were also considered symmetrical load stops for the case of one lane loaded (**Figure 4**). For instance, during stop 2, the strains of girders 3 and 4 were directly measured from the installed sensors (**Table 4**, columns 5–6). The strains for girders 1 and 2, as reported for stop 2 (**Table 4**, columns 3–4), were interpreted from the measurements recorded during stop 5 (collected by sensors installed within girders 3 and 4). The same approach was employed to obtain the strains for girders 1 and 2 for the rest of the load stop configurations. The strain

TABLE 4 | FEM strains and vertical deflections.

Stop	Span	ε_{G1} ($\mu\varepsilon$)	ε_{G2} ($\mu\varepsilon$)	ε_{G3} ($\mu\varepsilon$)	ε_{G4} ($\mu\varepsilon$)	Δ_{G1} (mm)	Δ_{G2} (mm)	Δ_{G3} (mm)	Δ_{G4} (mm)
TWO LANES LOADED									
1	3	46 (−2%)	86 (−4%)	89 (0.0%)	42 (13%)	4.4 (5%)	7.1 (0%)	6.9 (0%)	4.1 (11%)
2	2	55 (0%)	101 (−6%)	102 (−11%)	50 (7%)	5.9 (6%)	10.1 (−4%)	9.9 (−4%)	5.5 (11%)
3	1	44 (4%)	86 (−2%)	84 (−3%)	41 (16%)	4.1 (20%)	6.8 (1%)	6.7 (0%)	3.9 (20%)
4	1	42 (14%)	87 (0%)	89 (−6%)	47 (−2%)	4.1 (2%)	7.0 (−5%)	7.2 (−4%)	4.5 (−2%)
5	2	50 (7%)	101 (−10%)	100 (−5%)	54 (2%)	5.5 (14%)	9.8 (0%)	10.0 (1%)	5.8 (9%)
6	3	44 (8%)	87 (2%)	89 (−7%)	46 (−2%)	4.3 (12%)	7.1 (16%)	7.3 (6%)	4.4 (15%)
7	1	56 (*)	70 (*)	69 (5%)	67 (−3%)	5.0 (−2%)	5.7 (−12%)	6.0 (−9%)	5.6 (2%)
8	2	67 (*)	80 (*)	79 (1%)	74 (1%)	6.8 (7%)	7.7 (1%)	8.0 (1%)	7.5 (1%)
9	3	58 (*)	69 (*)	69 (−3%)	63 (−9%)	5.1 (−16%)	5.7 (−4%)	5.9 (0%)	5.5 (7%)
ONE LANE LOADED									
10	1	4 (*)	16 (*)	41 (7%)	66 (3%)	0.6 (−500%)	1.6 (−23%)	3.6 (−3%)	5.2 (−4%)
11	2	2 (50%)	18 (−6%)	47 (8%)	76 (3%)	0.5 (38%)	2.0 (0%)	4.8 (2%)	7.3 (5%)
12	3	4 (*)	16 (*)	41 (5%)	65 (0%)	0.6 (50%)	1.6 (24%)	3.6 (−3%)	5.1 (6%)
13	2	76 (3%)	46 (10%)	18 (−6%)	2 (50%)	7.3 (15%)	4.8 (11%)	2.0 (23%)	0.5 (50%)

*The values within parentheses represent the percent difference between the values obtained experimentally (reported in **Table 2**) and using FEM simulations (reported herein). The expression [(Exp-FEM)/Exp] was used to compute these ratios. Where Exp = experimental strain or deflection value; and FEM = strain or deflection value obtained from FEM simulations. *Values were not estimated since experimental data was not available.*

values for girders 1 and 2 were not obtained for those load stops without a mirrored load stop image, as was the case of stops 7–10 and 12. **Table 5** presents the LDF values computed using the experimental strain values reported in **Table 2** (columns 3–6). The distribution factor of an interior or exterior girder is defined as the maximum value estimated using the experimental or AASHTO LRFD approach. For the stop configurations used to load the bridge during this first series of load tests, no difference was observed when the LDF of the interior girders 1 and 4 was compared (0.52 vs. 0.52). In the case of the interior girders 2 and 3, the maximum LDF values were 0.654 vs. 0.672, respectively. This difference represents a 1.8% of the absolute live load applied to bridge structure that is distributed to an interior girder. Comparison of the LDF values for the exterior and interior girder of spans 1 and 3 were performed for stops 1 and 3, and 4 and 6 (two-lane load cases). These comparisons are reported in terms of the live load applied to the bridge that was carried by a girder. The maximum difference (1.8%) was noted for the interior girders during stops 1 and 3. This discrepancy might be related to the precision of the sensors and differences in the point of applications of the test load within the central regions of spans 1 and 3.

Field Deflections

Table 6 lists the LDF values estimated with the experimental deflections reported in **Table 2** (columns 7–10). The LDF values reported in **Table 6** are comparable to the experimental LDF values listed in **Table 5** suggesting that both variables can be used to estimate the load distribution for moment using field data. Comparisons of the LDF values for the exterior and interior girders of spans 1 and 3 were performed for stops 1 and 3, 4 and 6, and 7 and 8 (two-lane load cases) in terms of the live load applied to the bridge that was carried by a girder. The maximum difference (6%) was observed for exterior girder 1

during stops 1 and 3. For the interior girders this difference was below 4%. The discrepancy obtained in LDF values was lesser that the one observed in the case of the LDF values estimated with deflection measurements.

FEM Load Distribution Factors
FEM Longitudinal Strains

Table 5 presents the LDF values estimated with the FEM longitudinal strains reported in **Table 4** (columns 3–6). The FEM LDF values are compared to LDFs obtained with experimental strain values. The values within parentheses represent the difference between the experimental and FEM LDF values. This percentages are expressed in terms of the absolute portion of live load applied to the bridge that is carried by a girder.

FEM Deflections

The LDF values, reported in **Table 6**, were determined using the FEM values of the vertical deflections presented in **Table 4** (columns 7–10). These locations were selected as they correspond to maximum deflection and/or positive or negative stress. FEM and experimental LDF values estimated using vertical deflections are reported and compared in this table. The difference is presented within parentheses. As shown in the previous section (FEM Longitudinal Strains), the percentages are expressed in terms of the absolute portion of live load applied to the bridge that is carried by a girder. As in the case of the LDFs estimated with experimental and numerical strain values, it was noted that the experimental and numerical LDFs determined with deflection results were comparable and within the same order of magnitude suggesting that the accuracy of the FEM simulations is acceptable. The FEM models were calibrated using the field data as reported by Hernandez and Myers (2018a). These models may be used to predict the response of the bridge in future load tests if the superstructure is subjected to load configurations different to

TABLE 5 | Experimental and FEM LDFs (estimated with longitudinal strain values).

Stop	Span	LDF_1^E/LDF_1^{FEM}	LDF_2^E/LDF_2^{FEM}	LDF_3^E/LDF_3^{FEM}	LDF_4^E/LDF_4^{FEM}
TWO LANES LOADED					
1	3	0.340/0.350 (−1.0%)	0.626/0.654 (−2.8%)	0.672/0.677 (−0.5%)	0.362/0.319 (4.3%)
2	2	0.372/0.357 (1.5%)	0.642/0.656 (−1.4%)	0.622/0.662 (−4.0%)	0.365/0.325 (4.0%)
3	1	0.346/0.345 (0.1%)	0.632/0.675 (−4.3%)	0.654/0.659 (−0.5%)	0.368/0.322 (4.6%)
4	1	0.368/0.317 (5.1%)	0.654/0.657 (−0.3%)	0.632/0.672 (−4.0%)	0.346/0.355 (−0.9%)
5	2	0.365/0.328 (3.7%)	0.622/0.662 (−4.0%)	0.642/0.656 (−1.4%)	0.372/0.354 (1.8%)
6	3	0.362/0.331 (3.1%)	0.672/0.654 (1.8%)	0.626/0.669 (−4.3%)	0.340/0.346 (−0.6%)
7	1	(*)/0.427 (*)	(*)/0.534 (*)	(*)/0.527 (*)	(*)/0.511 (*)
8	2	(*)/0.447 (*)	(*)/0.533 (*)	(*)/0.527 (*)	(*)/0.493 (*)
9	3	(*)/0.448 (*)	(*)/0.533 (*)	(*)/0.533 (*)	(*)/0.486 (*)
ONE LANE LOADED					
10	1	(*)/0.031 (*)	(*)/0.126 (*)	(*)/0.323 (*)	(*)/0.520 (*)
11	2	0.027/0.014 (1.3%)	0.113/0.126 (1.3%)	0.340/0.329 (1.1%)	0.520/0.531 (−1.1%)
12	3	(*)/0.032 (*)	(*)/0.127 (*)	(*)/ 0.325 (*)	(*)/0.516 (*)
13	2	0.520/0.535 (−1.5%)	0.340/0.324 (1.6%)	0.113/0.127 (−1.4%)	0.027/0.014 (1.3%)

LDF^E, load distribution factor estimated with experimental data; LDF^{FEM}, load distribution factor estimated with FEM results. The values within parentheses represent the difference between the LDF obtained using experimental and FEM data. This percentage is expressed in terms of the absolute portion of live load applied to the bridge that can be carried by a girder. The expression (Exp-FEM) was employed to compute this absolute percent difference between the experimental and FEM LDFs. Where Exp = experimental strain or deflection value; and FEM = strain or deflection value obtained from FEM simulations. *Values were not estimated since experimental data was not available.

TABLE 6 | Experimental and FEM LDFs (estimated with deflection values).

Stop	Span	LDF_1^E/LDF_1^{FEM}	LDF_2^E/LDF_2^{FEM}	LDF_3^E/LDF_3^{FEM}	LDF_4^E/LDF_4^{FEM}
TWO LANES LOADED					
1	3	0.368/0.391 (−2.3%)	0.623/0.631 (−0.8%)	0.605/0.613 (−0.8%)	0.404/0.364 (4.0%)
2	2	0.397/0.376 (2.1%)	0.612/0.643 (−3.1%)	0.599/0.631 (−3.2%)	0.391/0.350 (4.1%)
3	1	0.432/0.381 (5.1%)	0.585/0.633 (−4.8%)	0.568/0.623 (−5.5%)	0.415/0.363 (5.2%)
4	1	0.378/0.360 (1.8%)	0.604/0.614 (−1.0%)	0.622/0.632 (−1.0%)	0.396/0.395 (0.1%)
5	2	0.391/0.354 (3.7%)	0.599/0.630 (−3.1%)	0.618/0.643 (−2.5%)	0.391/0.373 (1.7%)
6	3	0.373/0.372 (0.1%)	0.639/0.615 (2.4%)	0.593/0.632 (−3.9%)	0.395/0.381 (1.4%)
7	1	0.462/0.448 (1.4%)	0.481/0.511 (−3.0%)	0.519/0.538 (−1.9%)	0.538/0.502 (3.6%)
8	2	0.474/0.453 (2.1%)	0.506/0.513 (−0.7%)	0.526/0.533 (−0.7%)	0.494/0.500 (−0.6%)
9	3	0.406/0.459 (−5.3%)	0.507/0.514 (−0.7%)	0.544/0.532 (1.2%)	0.544/0.495 (4.9%)
ONE LANE LOADED					
10	1	0.010/0.055 (−4.5%)	0.131/0.145 (−1.4%)	0.354/0.327 (2.7%)	0.505/0.473 (3.2%)
11	2	0.052/0.034 (1.8%)	0.130/0.137 (−0.7%)	0.318/0.329 (−1.1%)	0.500/0.500 (0.0%)
12	3	0.098/0.055 (4.3%)	0.172/0.147 (2.5%)	0.287/0.330 (−4.3%)	0.443/0.468 (−2.5%)
13	2	0.489/0.500 (−1.1%)	0.307/0.329 (−2.2%)	0.148/0.137 (1.1%)	0.057/0.034 (2.3%)

LDF^E, load distribution factor estimated with experimental data; LDF^{FEM}, load distribution factor estimated with FEM results. The values within parentheses represent the difference between the LDF obtained using experimental and FEM data. This percentage is expressed in terms of the absolute portion of live load applied to the bridge that can be carried by a girder. The expression (Exp-FEM) was employed to compute this absolute percent difference between the experimental and FEM LDFs. Where Exp = experimental strain or deflection value; and FEM = strain or deflection value obtained from FEM simulations.

the ones used during this first series of load tests. In such as a case, if the experimental deflections are larger than the FEM values, it may be an indicator of the incursion of the bridge response within the inelastic range.

AASHTO Girder Distribution Factors

The AASHTO LRFD methodology (American Association of State Highway Transportation Officials, 2017) was used to compute the interior and exterior girder distribution factors (GDFs) for single and multiple loaded lanes. The GDF for an interior girder with two or more (multiple) design lanes loaded was estimated using the following equation (SI units):

$$GDF_{int}^m = 0.075 + \left(\frac{S}{2900}\right)^{0.4} \left(\frac{S}{L}\right)^{0.2} \left(\frac{K_g}{Lt_s^3}\right)^{0.1} \quad (3)$$

where S = girder spacing (mm); L = span length (mm); t_s = deck thickness; K_g = stiffness parameter (mm^4); $K_g = n(I_g + e_g^2 A_g)$; e_g = girder eccentricity (vertical distance from the centroid of the girder to the centroid of the slab); n = modular ratio (E_{girder}/E_{slab}); E = modulus of elasticity of the concrete computed as $57,000(f'_c)^{0.5}$; f'_c = nominal compressive strength of concrete; I_g = moment of inertia of the girder (mm^4); and A_g = area of the cross section of the girder (mm^2). The GDF of an interior girder with a single lane loaded was computed using the following expression (SI units):

$$GDF_{int}^s = 0.06 + \left(\frac{S}{4300}\right)^{0.4} \left(\frac{S}{L}\right)^{0.3} \left(\frac{K_g}{Lt_s^3}\right)^{0.1} \quad (4)$$

The GDF of exterior girders for two or more design lanes loaded was computed with the following expressions (SI units):

$$GDF_{ext}^m = e(GDF_i^m) \quad (5)$$

$$e = 0.77 + \frac{d_e}{2800} \geq 1 \quad (6)$$

where d_e = horizontal distance from centroid of the exterior girder to the inside edge of the barrier or curb (mm). The multiple presence is implicitly considered in the AASHTO LRFD lateral distribution equations following the methodology proposed by Zokaie (2000).

The simple static distribution approach, also known as the lever rule, was employed to estimate the exterior GDF for a single lane loaded. The multiple presence must be considered explicitly when the lever rule method is employed. The following expression was written assuming a hinge develops at an interior support (girder 2 or 3) and by summing moments caused by the acting forces (resultant force P in **Figures 3C,D**) and the exterior girder reaction about the interior girder. Thus:

$$GDF_{ext}^s = m_p \left(\frac{S + d_e - d_R}{S}\right) \quad (7)$$

where m_p = multiple presence factor (equal to 1.2 for a single lane loaded); d_R = horizontal distance from the inside edge of the barrier or curb to the point of application of the force P (resultant force of a truck applied at center of the axle as shown in **Figure 3D**). A skew factor was estimated with the following expressions to modify the AASHTO GDF values.

$$SF = 1 - C_1 (\tan \theta)^{1.5} \quad (8)$$

$$C_1 = 0.25 \left(\frac{K_g}{Lt_s^3}\right)^{0.25} \left(\frac{S}{L}\right)^{0.5} \quad (9)$$

where SF = skew correction factor (if $30° \leq \theta \leq 60°$); and θ = skew angle. **Table 7** summarizes the parameters of the bridge employed to determine the GDF of the exterior and interior girders.

Table 8 lists the GDF values estimated according to AASHTO LRFD approach. The GDF values listed on columns 3 and 5 were corrected using the skew correction factors presented above. The corrected factors are listed in columns 4 and 6.

TABLE 7 | Bridge design parameters.

Variable	Spans 1 and 3	Span 2
A_g (mm^2)	479.9×10^3	479.9×10^3
I_g (mm^4)	1.2383×10^{11}	1.2383×10^{11}
f'_{c_girder} (MPa)	55.2	68.9
E_{girder} (GPa)	35.2	39.3
f'_{c_slab} (MPa)	27.6	27.6
E_{slab} (GPa)	24.9	24.9
n	1.414	1.581
e_g (mm)	880	880
K_g (mm^4)	702.207×10^9	785.936×10^9
d_e (mm)	914	914
S (mm)	3,250	3,250
L (mm)	30,480	36,580
t_s (mm)	216	216
e (mm)	1.096	1.096
θ (°)	30	30
C_1	0.0876	0.0961
SF	0.962	0.961

TABLE 8 | AASHTO LRFD GDFs.

Span	Case (lanes loaded)	GDF_{int}	GDF_{int} (corrected*)	GDF_{ext}	GDF_{ext} (corrected*)
1, 3	≥2	0.819	0.783	0.901	0.861
1, 3	1	0.558	0.533	0.975	0.932
2	≥2	0.788	0.756	0.866	0.832
2	1	0.528	0.507	0.975	0.936

*Skew factors correct the GDF values.

RESULTS AND DISCUSSION

The interior and exterior girder distribution factors for moment are designated as the maximum values of the distribution factor obtained (using field data or the AASHTO LRFD equations) when a single-lane or multiple-lane load cases are evaluated. Several critical load configurations were evaluated to determine the maximum effect acting within the primary carrying members of the bridge. In the case of Bridge A7957, the experimental distribution factor obtained for spans 1 and 3 (**Tables 5, 6**) were comparable showing that this parameter is independent of the type of material employed to fabricate the prestressed concrete girders. The interior load distribution, LDF_{int}, calculated from experimental data and FEM results, corresponded to 0.672 and 0.677, respectively. Furthermore, the exterior load distribution factor, LDF_{ext}, estimated from test and FEM data was 0.520 and 0.535, respectively. The maximum difference observed was close to 4%, suggesting that the calibrated FEM can reproduce the behavior of the bridge with an acceptable level of accuracy for the level of load applied during the load tests. The calibrated FEM can be used to study the response of the bridge for load configurations different to those conducted during the field load test.

The computed AASHTO LRFD interior and exterior girder distribution factors, GDF_{int} and GDF_{ext}, were 0.783 and 0.936, respectively. These values represent approximately 17% and 80% difference for the interior and exterior girder lateral load distribution factors obtained experimentally and using FEM data. In the case of Bridge A7957 and the load configurations used during the first series of diagnostic load tests, these results imply that the AASHTO LRFD GDF values are more conservative than the LDF values obtained from experimental data and FEM simulations.

It should be noted that the AASHTO LRFD methodology is suitable for bridge design. Diagnostic load tests have demonstrated to be more appropriate to assess the load distribution response of existing bridges. Consequently, it is recommended to use more refined methods to estimate the load distribution during the load rating evaluation of existing bridges.

CONCLUSIONS

A first series of diagnostic load tests was conducted to evaluate the initial in-service response and moment load distribution of Bridge A7957. The structural behavior of the main carrying members fabricated with SCC and conventional concrete was compared using the longitudinal strain and vertical deflection values obtained at midspan locations. The results demonstrated that the structural performance of the spans 1 and 3 was independent of the material employed in the fabrication of the prestressed concrete girders (CC and SCC, respectively) and should not hinder the implementation of SCC in future infrastructure projects. Finite element models of the bridge were developed to predict the behavior of the bridge for the different load configurations. The FEM could predict the response of the bridge with an acceptable level of accuracy (about 15% difference for measured strains and deflections). These calibrated models may be used to predict the response of the bridge in future live load tests. LDFs were estimated from field measurements, FEM simulations, and GDFs were obtained using the AASHTO LRFD approach. The AASHTO LRFD distribution factors resulted to be ∼17 and 80% larger than their counterpart experimental values. The difference may be attributed to several causes. The AASHTO LRFD equations are presented to be applied to different types of bridges with a wide range of span lengths, girders spacing, and stiffness. Experimental distribution factors implicitly consider field conditions such as unintended support restraints and contribution of secondary members that improve the service response of the bridge.

In addition, experimental distribution factors consider the actual bridge condition. Consequently, experimental distribution factors are more suitable for conducting a load rating evaluation of an existing bridge. The presence of damage, aging or both in the main carrying members may influence the load distribution response since the main supporting members that exhibit less loss of stiffness are expected to carry larger loads than those members showing larger signals of distress. These two possible scenarios were outside the scope of this study.

AUTHOR CONTRIBUTIONS

FUNDING

ACKNOWLEDGMENTS

REFERENCES

American Association of State Highway and Transportation Officials (2015). *Manual for Bridge Evaluation (2nd Edition) with 2011, 2013, 2014 and 2015 Interim Revisions*. Washington, DC.

American Association of State Highway and Transportation Officials (2017). *Bridge Design Specifications (8th Edition)*. Washington, DC.

Barker, R. M., and Pucket, J. A. (2013). *Design of Highway Bridges: An LRFD Approach*. Hoboken, NJ: John Wiley & Sons.

Cai, C. S., and Shahawy, M. (2003). Understanding capacity rating of bridges from load tests. *Pract. Period. Struct. Des. Constr.* 2003, 209–216. doi: 10.1061/(ASCE)1084-0680(2003)8:4(209)

Gheitasi, A., and Harris, D. K. (2015). Overload flexural distribution behavior of composite steel girder bridges. *J. Bridge Eng.* 20:671. doi: 10.1061/(ASCE)BE.1943-5592.0000671

Harris, D. K., Cousins, T., Sotelino, E. D., and Murray, T. M. (2010). Flexural lateral load distribution characteristics of sandwich plate system bridges: parametric investigation. *J. Bridge Eng.* 15, 684–694. doi: 10.1061/(Asce)Be.1943-5592.0000105

Hernandez, E. S., Griffin, A., and Myers, J. J. (2014a). "Balancing extended service life and sustainable concrete material usage in Missouri Bridge A7957," *in Structural Faults and Repair: European Bridge Conference* (London: SF&R).

Hernandez, E. S., Griffin, A., and Myers, J. J. (2014b). "*Construction and monitoring of sustainable concret* bridge A7957 in Missouri, USA," in *23rd Australasian Conference on the Mechanics of Structures and Materials* (Byron Bay, NSW).

Hernandez, E. S., and Myers, J. J. (2015a). "*In-situ field test and service response of Missouri Bridge A7957,*" in *16th European Bridge Conference (EBC16)* (Edinburgh).

Hernandez, E. S., and Myers, J. J. (2015b). Use of self-consolidating concrete and high volume fly ash concrete in Missouri Bridge A7957. Sustainable performance of concrete bridges and elements subjected to aggressive environments: monitoring, evaluation and rehabilitation. *ACI* 304, 85–100.

Hernandez, E. S., and Myers, J. J. (2016a). "*Field load test and girder distribution factors of Missouri Bridge A7957,*" in *2016 PCI Convention and National Bridge Conference* (Nashville, TN).

Hernandez, E. S., and Myers, J. J. (2016b). "Initial in-service response and lateral load distribution of a prestressed self-consolidating concrete bridge using field load tests," in *The Fifth International Symposium on Life-Cycle Civil Engineering (IALCCE 2016)*, eds J. Bakker, D. M. Frangopol, and K. Van Breugel (Delf: CRC Press), 1072–1079.

Hernandez, E. S., and Myers, J. J. (2016c). "Monitoring the initial structural performance of a prestressed self-consolidating concrete bridge," in *PRO100 - Proceedings of the 8th International RILEM Symposium on Self-Compacting Concrete - SCC 2016*, ed K. H. Khayat (Washington, DC: RILEM Publications SARL 2016), 401–411.

Hernandez, E. S., and Myers, J. J. (2018a). Diagnostic test for load rating of a prestressed SCC bridge. *Spec. Publ.* 323, 11.11–11.16.

Hernandez, E. S., and Myers, J. J. (2018b). "Strength evaluation of prestressed concrete bridges by dynamic load testing," *in Ninth International Conference on Bridge Maintenance, Safety and Management (IABMAS 2018)* (Melbourne, VIC: CRC Press).

Keske, S. D., Miller, D. E., Barnes, R. W., and Schindler, A. K. (2014). Live-load response of in-service bridge constructed with precast, prestressed self-consolidating concrete girders. *PCI J.* 59, 63–76. doi: 10.15554/pcij.09012014.63.76

McSaveney, L., Papworth, F., and Khrapko, M. (2011). Self compacting concrete for superior marine durability and sustainability. *Concr. Aust.* 37, 59–64. Available online at: http://downloads.realviewtechnologies.com/Concrete%20Institute%20Of%20Australia/Concrete%20In%20Australia/June%202011.pdf

Merkle, W. J., and Myers, J. J. (2004). "Use of the total station for load testing of retrofitted bridges with limited access," in *Smart Structures and Materials 2004 - Sensors and Smart Structures Technologies for Civil, Mechanical, and Aerospace Systems*, ed. S. C. Liu (San Diego, CA: Proceedings of SPIE – The International Society for Optical Engineering), 687–694. doi: 10.1117/12.539992

Myers, J. J., Volz, J., Sells, E., Porterfield, K., Looney, T., Tucker, B., et al. (2012). *Self-Consolidating Concrete (SCC) for Infrastructure Elements.* Rolla, MO: Missouri University of Science and Technology.

Ouchi, M., Sada-aki, N., Thomas, O., Hallberg, S. E., and Myint, L. (2003). *Applications of Self-Compacting Concrete in Japan, Europe and the United States.* ISHPC [Online]. Available online at: http://www.fhwa.dot.gov/bridge/scc.pdf (accessed April 15, 2016).

Simulia (2012). *Abaqus Analysis User's Manual. Version 6.12 ed.* Providence, RI: Dassault Systèmes Simulia Corp.

Zhao, J. J., and Tonias, D. E. (2012). *Bridge Engineering: Design, Rehabilitation, and Maintenance of Modern Highway Bridges.* McGraw-Hill.

Zokaie, T. (2000). AASHTO-LRFD Live load distribution specifications. *J. Bridge Eng.* 5, 131–138. doi: 10.1061/(ASCE)1084-0702(2000)5:2(131)

Optimizing Finite Element Models for Concrete Bridge Assessment With Proof Load Testing

Eva O. L. Lantsoght[1,2]*, Ane de Boer[3], Cor van der Veen[2] and Dick A. Hordijk[2]

[1] Politécnico, Universidad San Francisco de Quito, Quito, Ecuador, [2] Concrete Structures, Department of Engineering Structures, Civil Engineering and Geosciences, Delft University of Technology, Delft, Netherlands, [3] Ane de Boer Consultancy, Arnhem, Netherlands

Proof load testing of existing reinforced concrete bridges is becoming increasingly important as the current bridge stock is aging. In a proof load test, a load that corresponds to the factored live load is applied to a bridge structure, to directly demonstrate that a bridge fulfills the code requirements. To optimize the procedures used in proof load tests, it can be interesting to combine field testing and finite element modeling. Finite element models can for example be used to assess a tested structure after the test when the critical position could not be loaded. In this paper, the case of viaduct De Beek, a four-span reinforced concrete slab bridge, is studied. Upon assessment, it was found that the requirements for bending moment are not fulfilled for this structure. This viaduct was proof load tested in the end span. However, the middle spans are the critical spans of this structure. The initial assessment of this viaduct was carried out with increasingly refined linear finite element models. To further study the behavior of this bridge, a non-linear finite element model is used. The data from the field test (measured strains on the bottom of the concrete cross-section, as well as measured deflection profiles) are used to update the non-linear finite element model for the end span, and to improve the modeling and assessment of the critical middle spans of the structure. Similarly, an improved assessment based on a linear finite element model is carried out. The approaches shown for viaduct De Beek should be applied for other case studies before recommendations for practice can be formulated. Eventually, an optimized combination of field testing and finite element modeling will result in an approach that potentially reduces the cost of field testing.

Keywords: assessment, bridge evaluation, concrete bridges, field testing, finite element modeling, load testing, optimization, proof load testing

INTRODUCTION

Proof load testing of existing reinforced concrete bridges is becoming increasingly important as an assessment method for existing bridges, since the current bridge stock in Europe and North America is aging (Lantsoght et al., 2017f). A proof load test serves as a direct verification of the performance of the bridge, and as a demonstration that it can withstand the prescribed loads. As such, this assessment method can be used when analytical models are insufficient. Situations when analytical models are insufficient are: when no structural plans are available (Aguilar et al., 2015),

when there are large uncertainties on the structural capacity as the result of material deterioration or degradation (Lantsoght et al., 2017c), or when the analytical models cannot (fully) consider additional sources of resistance such as transverse load redistribution (Lantsoght et al., 2015) or compressive membrane action (Collings and Sagaseta, 2015).

In a proof load test (Grigoriu and Hall, 1984; Juntunen and Isola, 1995; Saraf et al., 1996; Ransom and Heywood, 1997; Faber et al., 2000; Cai and Shahawy, 2003; Anay et al., 2016), a load that corresponds to the factored live load is applied to the bridge structure, to directly demonstrate that a bridge fulfills the code requirements. The maximum load that needs to be applied to demonstrate that the bridge fulfills the code requirements is called the target proof load. This load is often large, which increases the probability of failure of the bridge during the load test. Therefore, it is important to monitor the structural responses during a proof load test. The measured structural responses are evaluated constantly during the test and are compared to predetermined thresholds that should not be exceeded during the test, the so-called stop criteria (Lantsoght et al., 2018b). When a stop criterion is reached, further loading can result in irreversible damage to the structure or even collapse. The relevant stop criteria can be taken from available codes and guidelines (Ministerio de Fomento - Direccion General de Carreteras, 1999; Deutscher Ausschuss für Stahlbeton, 2000; Frýba and Pirner, 2001; ACI Committee 437, 2013). Where the stop criteria in the available codes and guidelines are insufficient or do not cover the expected governing mode of failure for the structure, thresholds should be carefully selected or derived prior to the load test. When a stop criterion is exceeded in a proof load test before reaching the target proof load, further loading is not permitted. Depending on the highest load level that is achieved during the test, the bridge then may be found to fulfill lower demands or may require posting, a reduction in the number of lanes, strengthening, or demolition and replacement.

To optimize the procedures used in proof load tests, it can be interesting to combine field testing and finite element modeling of the bridge under consideration (Halicka et al., 2018). Typically, finite element models are used during the preparation of a proof load test. During the preparation stage, a linear finite element model can be used to determine the most unfavorable position of the load and the target proof load (Lantsoght et al., 2017e). These models are then usually not used for additional analysis after the proof load test, since the test itself serves as a direct assessment method.

However, finite element modeling is often used together with another type of field tests on bridges: diagnostic load tests (Fu et al., 1997; Velázquez et al., 2000; Chajes et al., 2001; Olaszek et al., 2014; Sanayei et al., 2016; Bonifaz et al., 2018). Diagnostic load tests are carried out at lower load levels than proof load tests. The measurements taken during a diagnostic load test can be used to quantify the difference between the analytical model used for assessment and the actual bridge behavior determined in the field. The analytical model can then be optimized with the measured data, resulting in a field-verified model. Then, a model for rating can be developed that includes the effects of mechanisms that can be reliably counted on at the ultimate

limit state, which leads to an improved assessment. Diagnostic field tests are used to determine (Barker, 2001), amongst others, the actual stiffness of the structure including the non-structural elements such as parapets and barriers, unintended composite action, the influence of frozen bearings, the actual transverse distribution, and the actual lateral live load distribution.

In combination with dynamic load testing, methods have been proposed to update finite element models to capture the behavior under service loads. One method (Duan et al., 2005) proposes a hybrid optimization technique that combines the global searching capability of the chaos-based optimization technique with the high searching efficiency of the trust-region optimization technique. This proposed method was verified with the experimental results of a 14-bay steel frame that was subjected to a dynamic test. A second proposed method consists of a two-phase optimization procedure (Wang et al., 2010): the tower and the bridge are analyzed separately to reduce the number of structural parameters that would require optimization. This proposed method was verified with field test results and ambient vibration measurements of a steel box girder bridge. It should be noted that these existing methods have focused on: (i) steel structures, and (ii) low load levels. For the optimization of finite element models of concrete bridges under proof load levels and high magnitude loads, further research is needed before standardized and automatic procedures can be recommended.

In this paper, the case of viaduct De Beek is studied. During the proof load test on this viaduct, the critical span could not be tested, because the critical span is located over the highway. To test this span, it would be necessary to close the highway to ensure the safety of the traveling public. Since closing the highway would cause large driver delays, the first span, which is not directly above the highway, was tested instead. After the proof load test, a synergy between proof load testing and finite element modeling is sought to improve the assessment of the viaduct and the critical second span with the information obtained during the load test.

DESCRIPTION OF VIADUCT DE BEEK
Geometry
Viaduct De Beek (Koekkoek et al., 2016; Lantsoght et al., 2017a,d), built in 1963, is located in the south of the Netherlands, in the province Noord Brabant. The viaduct lies in the Beekstraat over the highway A67. The viaduct is a four-span reinforced concrete slab bridge, see **Figure 1A**. The length of the end spans is 10.81 m and the length of the mid spans is 15.40 m, see **Figure 2A**. The width of the superstructure is 9.94 m, which gives a carriageway width of 7.44 m. The thickness of the slab at the carriageway varies in the longitudinal direction between 470 mm and 870 mm and follows a parabolic shape, see **Figure 2B**. In the transverse direction, the thickness of the slab at the carriageway varies from 470 mm in the middle to 408 mm at the sides at the end supports, see **Figure 2C**, and similarly it varies from 870 mm in the middle to 808 mm at the sides at the mid supports.

Material Properties
The properties of the concrete and steel were measured by taking material samples. For the concrete compressive and tensile
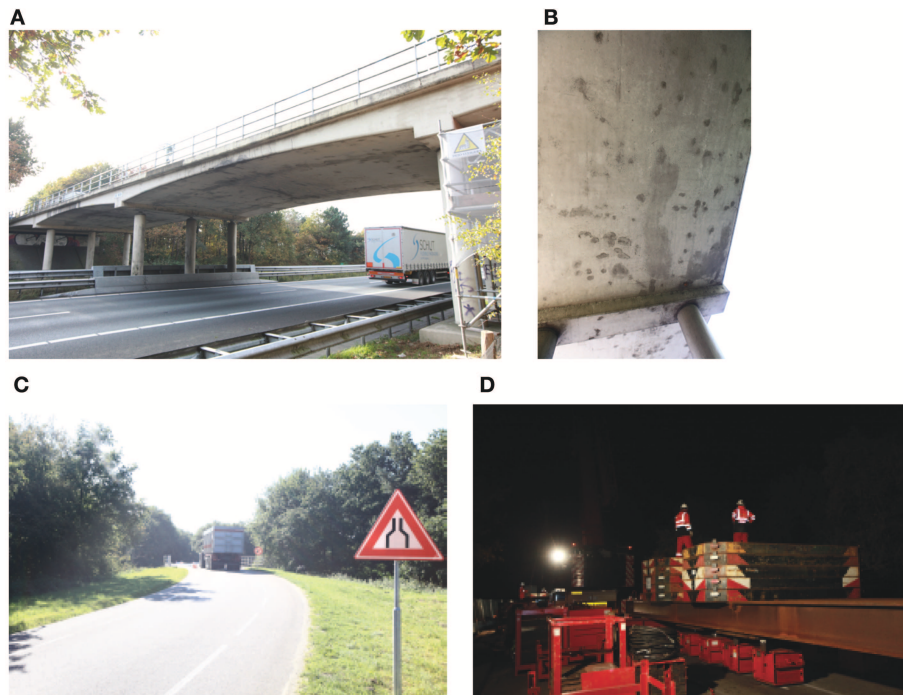
FIGURE 1 | Photographs of viaduct De Beek: **(A)** side view; **(B)** material damage; **(C)** signposting of lane reduction; **(D)** execution of proof load test.
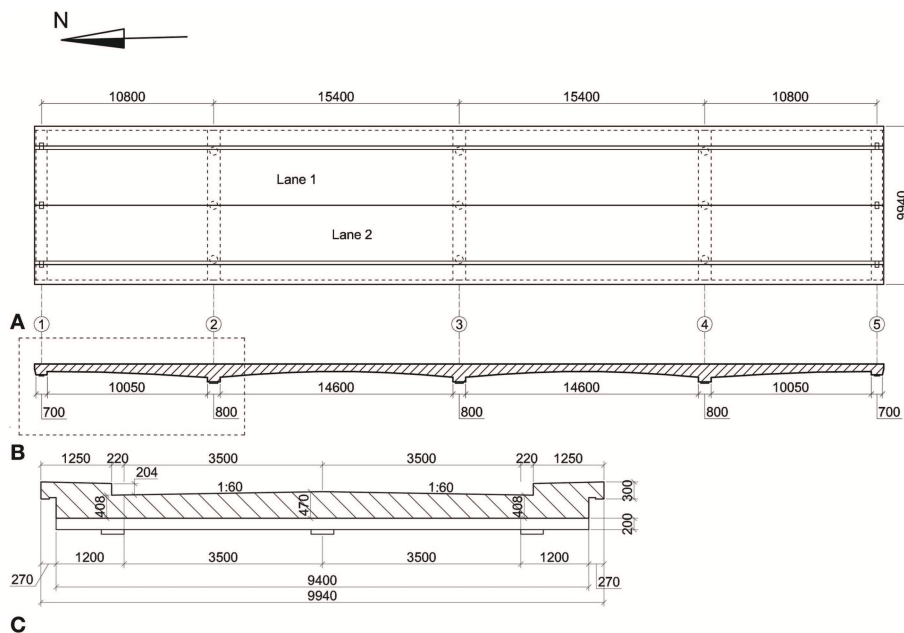

FIGURE 2 | Geometry of viaduct De Beek: **(A)** top view; **(B)** longitudinal view; **(C)** cross-section at end supports. Units: mm.

strength, nine core samples were taken. The characteristic value of the concrete compressive strength is $f_{ck} = 44.5$ MPa and the characteristic value of the splitting tensile strength is $f_{ctk} = 4.4$ MPa. The concrete can thus be categorized as C45/55 according to NEN-EN 1992-1-1:2005 (Comité Européen de Normalisation, 2005), which has a design compressive strength $f_{cd} = 30$ MPa.

Based on three samples of the reinforcement steel, the measured average yield strength is $f_{ym} = 291$ MPa and the

measured average tensile strength is $f_{tm} = 420$ MPa. The reinforcement in the end spans (span 1 and span 4) consists of $\varphi = 25$ mm with a spacing of 93 mm ($A_s = 5,259$ mm^2/m) and the reinforcement in the middle spans (span 2 and span 3) consists of $\varphi = 25$ mm with a spacing of 140 mm ($A_s = 3,506$ mm^2/m).

Inspection and Assessment Results

Upon inspection (Willems et al., 2015), significant cracking was observed at the soffit of the slabs, see **Figure 1B**. This cracking raised concerns with regard to the durability of the bridge. An assessment of the viaduct led to the conclusion that the viaduct does not fulfill the code requirements for bending moment. The bending moment capacity in both the longitudinal and transverse direction was found to be insufficient in all spans. As a result of this assessment, the number of lanes for traffic on the viaduct was reduced from two lanes (one in each direction) to one single lane (Iv-Infra, 2015), see **Figure 1C**.

RESULTS OF PROOF LOAD TESTS

Viaduct De Beek was proof load tested in the end span. The position of the tested span is indicated with a dashed rectangle in **Figure 2A**. The middle spans are the critical spans of this structure, since the assessment of the middle spans resulted in the largest value for the Unity Check (ratio of load effect to capacity). The middle spans could not be tested as they are over the highway and would have required a closing of the highway during the load test, which was not permitted.

In November 2015, viaduct De Beek was subjected to two proof load tests at two positions in span 1. A full description of the preparation, execution, and post-processing of these proof load tests can be found in the report of the test (Koekkoek et al., 2016). The first proof load test studied the failure mode of bending moment, which is the governing failure mode for this span, and the second proof load test studied the failure mode of shear, for research purposes (Lantsoght et al., 2017a,b,d).

The load is applied with a system consisting of a load spreader beam, hydraulic jacks (equipped with load cells for real-time data visualization), and counterweights, see **Figure 1D**. The layout of the load application follows the design tandem of NEN-EN 1991-2:2003 (Comité Européen de Normalisation, 2003). The axle distance is 1.2 m. The center-to-center distance between the wheel prints in the transverse direction is 2 m. The size of the wheel print is 230 × 300 mm, which is the size used for the assessment of joints in the Netherlands, and which is different from the wheel print size of 400 × 400 mm of the Eurocode design tandem.

The critical position of the load depends on the considered failure mode. For bending moment, the critical position is found by moving the Eurocode design tandems in each lane, and finding the position that results in the largest sectional moment. This position is at 3.55 m between the face of the end support and the face of the design tandem. For shear, the critical position for reinforced concrete slabs (Lantsoght et al., 2013) results when the face-to-face distance between the load and the support is 2.5 d_l, with d_l the effective depth to the longitudinal reinforcement. For

span 1, the governing distance is 1.1 m between the face of the end support and the face of the design tandem.

To determine the target proof load, the following procedure was followed:

1. In the linear finite element model of the bridge, the superimposed dead load and the Eurocode live load model are applied, including the load factors. The design tandems are placed at their critical position (depending on the studied failure mode).
2. The resulting sectional moment or sectional shear force (depending on the studied failure mode) is obtained from the output of the finite element model.
3. The Eurocode live load model is replaced by a single design tandem, the proof load tandem, at the critical position in the first lane.
4. The target proof load is the required load on the proof load tandem to get the same sectional moment or sectional shear force (depending on the studied failure mode) as with the total factored live load model.

Using this procedure results in a target proof load of 1,656 kN for the bending moment test and of 1,525 kN for the shear test.

The instrumentation during the proof load tests consisted of 4 laser distance finders, 16 LVDTs (linear variable differential transformers), 6 strain gages, and 7 acoustic emission sensors. The structural responses measured during the proof load tests were: vertical deflections of the slab and at the supports, crack opening, strains in the concrete, strains in the reinforcement steel, and acoustic emissions.

The load was applied in a cyclic manner. After each load cycle, all the measurements were evaluated, stop criteria were checked, and then the decision was made to allow the next load cycle. **Figure 3** shows the loading protocol applied during the proof load test for bending moment. The maximum applied load during the bending moment test, including the self-weight of the jacks and loading plates, was 1,751 kN. For the shear test, the maximum applied load, including the self-weight of the jacks and loading plates, was 1,560 kN. With these applied loads, the end spans were shown to fulfill the code requirements. However, no direct assessment of the critical middle spans could be given based on the proof load test.

DESCRIPTION OF FINITE ELEMENT MODELS

Linear Finite Element Model

The initial assessment of this viaduct was carried out with increasingly refined linear finite element models. These models were developed in the finite element software DIANA FEA version 10.2 (DIANA FEA BV, 2017).

The first linear finite element model was developed for the assessment of the bridge, and to prepare the proof load test. In this first model, the slab is modeled with quadratic shell elements. The elements are 500 × 500 mm with a variable thickness from 470 to 870 mm. The non-structural elements that contribute to the stiffness of the structure (sidewalks and barriers) are not
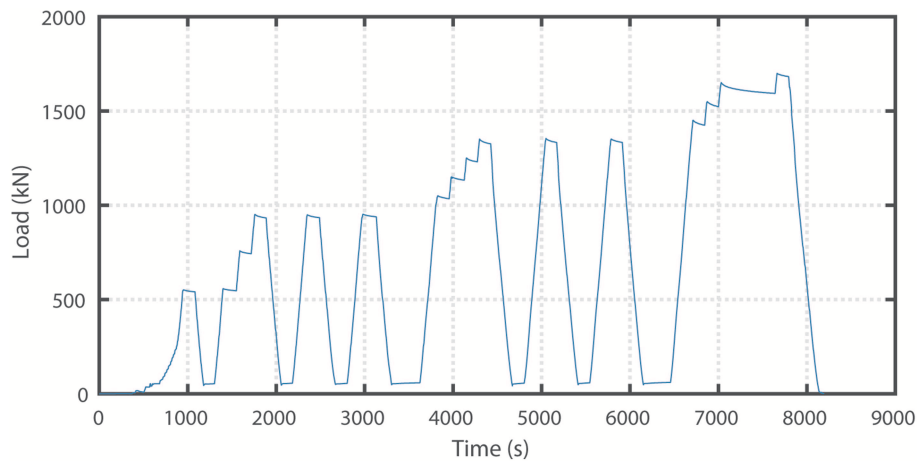
FIGURE 3 | Loading protocol during bending moment test.

modeled in the initial model, but are instead applied as an equivalent permanent load. The supports are modeled as rigid supports and ideal supports. The effect of the cracked concrete on the overall stiffness is taken into account by using orthotropic behavior with a Young's modulus of the concrete of 14 GPa in the cracked direction and of 36 GPa in the uncracked direction. This approach allows for modeling cracking in a linear finite element model (note that this approach differs from the non-linear finite element model, in which the development of cracking in the model will be explicitly taken into account). This model of the slab is subjected to a load combination that consists of the self-weight (and equivalent permanent load of the elements that are not modeled), the wearing surface, and the live load combination Load Model 1 from NEN-EN 1991-2:2003 (Comité Européen de Normalisation, 2003). The wheel print of the design tandem of 400×400 mm was enlarged to take into account vertical load spreading under 45° to the center of the slab.

Non-linear Finite Element Model

To further study the behavior of this bridge and to see if the currently imposed load restriction can be removed, a non-linear finite element model is also used. In the Netherlands, guidelines are available for the use of non-linear finite element models in RTD 1016-1:2017 (Rijkswaterstaat, 2017a) and with a summary validation report in RTD 1016-2:2017 and separate validations for reinforced beams, prestressed beams, and slabs in RTD 1016-3a:2017, RTD 1016-3b:2017, and RTD 1016-3c:2017, respectively (Rijkswaterstaat, 2017b,c,d,e). The scope of these guidelines is reinforced concrete and prestressed concrete, and all bridge types (girder bridges, slab bridges, box girder bridges. . .) as well as tunnels and culverts. The safety format applied in RTD 1016-1:2017 (Rijkswaterstaat, 2017a) is the same as the safety format used in the *fib* Model Code 2010 (fib, 2012). Since these guidelines have been developed in the Netherlands in different (draft) versions over the past decade, quite some practical experience with the use of these guidelines already exists. This experience teaches us that when a non-linear finite element model is used

for the assessment of an existing bridge, an additional capacity of between 10 and 30% can be found as compared to when a combination of a linear finite element model and sectional capacity calculations is used for the assessment.

In a first version of the non-linear finite element model, the situation with one traffic lane (current situation) is studied. The model is developed with DIANA version 10.1 (DIANA FEA BV, 2017). For this case, the loads applied to the slab in the model are one design tandem of 600 kN and a distributed lane load of 9 kN/m². In the non-linear finite element model, the load is applied incrementally by increasing a load factor. For the assessment calculations according to RTD 1016-1:2017 the load factor on the applied live load in the model should increase to 1.6 when non-linear finite element models are used. The value 1.6 is the product of a model factor of 1.06, a factor considering the uncertainties on material properties and the geometry of 1.2, and the live load factor of 1.25 for the Usage level from the Dutch guidelines for the assessment of bridges RBK (Rijkswaterstaat, 2013). Since viaduct De Beek lies in a local road that is subjected to <20,000 trucks per year, a reduction factor for the traffic of 0.9 according to Table NB 4.1 from NEN-EN 1991-2/NA:2011 (Code Committee 351001 2011) can be used. The final load factor that thus has to be achieved for viaduct De Beek is 1.44.

Figure 4 shows the results of the initial non-linear finite element for a load factor of 0.6. At this load level, cracking occurs over the middle support and exceeds the requirements for serviceability (see **Figure 4a** for a top view, **Figure 4b** for a side view, and **Figure 4c** for a detail). The maximum crack width is 0.4 mm. Comparing **Figures 4a,b** shows that the crack over the middle support occurs in the cross-section right next to the transverse support beam. The detail in **Figure 4c** shows the cracking strains at the end support (lower plot) and at the mid support (upper plot), and includes a small part of the bridge deck (cantilevering out from the support beam).

Figure 5 gives an overview of the results of the non-linear finite element model with one traffic lane for the maximum required load factor of 1.44. The maximum strain of 1% occurs
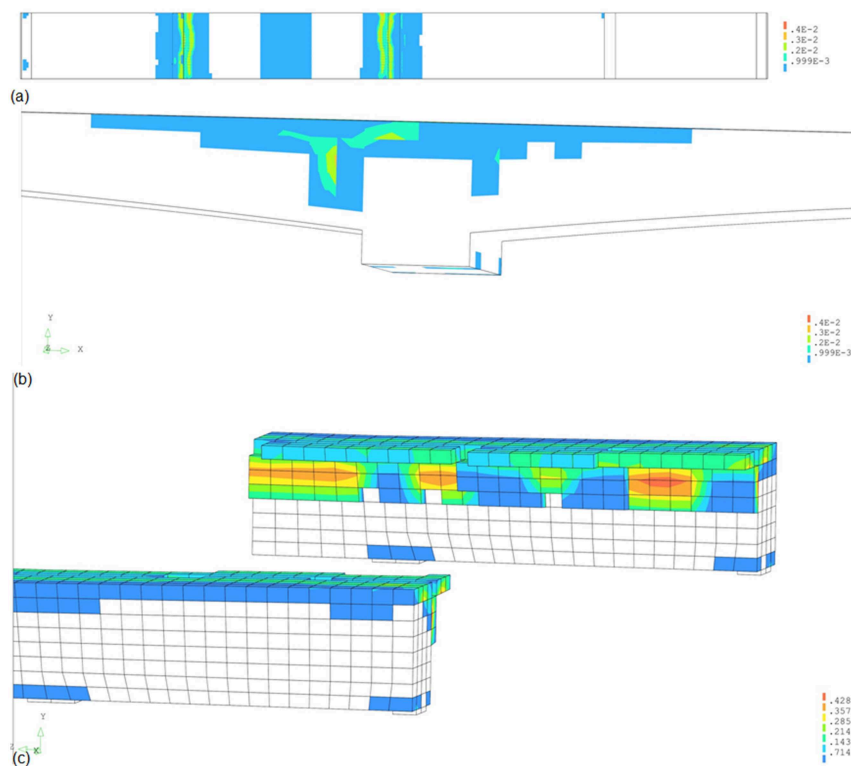
FIGURE 4 | Overview of results of non-linear finite element model for load factor of 0.6: **(a)** top view showing cracking at middle support; **(b)** side view showing cracking at middle support; **(c)** detail of cracking over end support (bottom) and mid support (top), showing support beam.

at support 3 (see **Figures 5A,B** for the general view of the results in span 2, and **Figures 5C,E** for the detailed results at support 3). The associated crack width is 1 mm. **Figure 5D** shows that the tension steel yields at this load level. Failure does not occur at this load level, so the results of the non-linear finite element model show that the bridge fulfills the requirements for one traffic lane.

Since the results in **Figure 5** indicate that the bridge fulfills the requirements for one lane of the traffic (based on the current restriction), in a next step the live loads corresponding to two lanes of traffic (original situation) were applied to the model. **Figure 6** shows the results in terms of the load-deflection diagram for the case with one lane of traffic and for the case with two lanes of traffic. The load is expressed based on the load factor on the live load. The results in **Figure 6** show that the load factor of 1.44 can be achieved for one lane of traffic. For the case with two lanes of traffic, **Figure 6** shows that failure occurs for a maximum load factor of 0.6. As such, the results of the initial non-linear finite element model show that the bridge does not fulfill the code requirements for two lanes of traffic.

ASSESSMENT WITH OPTIMIZED FINITE ELEMENT MODEL

Optimized Linear Finite Element Model
Updating by Refining Modeling of Structure
The initial linear finite element model is used to assess a tested structure after the test, since the proof load test cannot be used

to evaluate the critical middle spans (Lantsoght et al., 2018a). In a first refinement of the initial finite element model, quadratic solid elements are used instead of quadratic shell elements. The solid elements have a size of 100 mm × 140 mm × 73 mm/140 mm. The effect of cracking on the stiffness is again taken into account by using orthotropic properties with a Young's modulus of 14 GPa in the cracked direction and 36 GPa in the uncracked direction. **Figure 7A** gives an overview of the improved finite element model. This figure shows that solid elements are used in spans 1, 2, and half of span 3, and that shell elements are used in the other half of span 3 and in span 4. In other words, the part of the bridge that was tested and is subsequently assessed is modeled in a refined manner by using solid elements (as compared to the model with shell elements that was used for preparation of the test). **Figure 7B** shows a detail of the meshing of the finite element model at the support. **Figure 7C** shows the bottom view of the entire model, and **Figure 7D** shows the top view of the entire model. The applied load on the improved finite element model is the combination of the self-weight (including the equivalent load of the non-structural members), the wearing surface, and live load model 1 from NEN-EN 1991-2:2003 (Comité Européen de Normalisation, 2003). Since solid elements are now used, the actual size of the wheel print of the design tandem (400 × 400 mm) is applied to the model of the slab.

A next improvement of the model included a more realistic modeling of the support conditions. Viaduct De Beek is supported by elastomeric bearings, so in the improved model
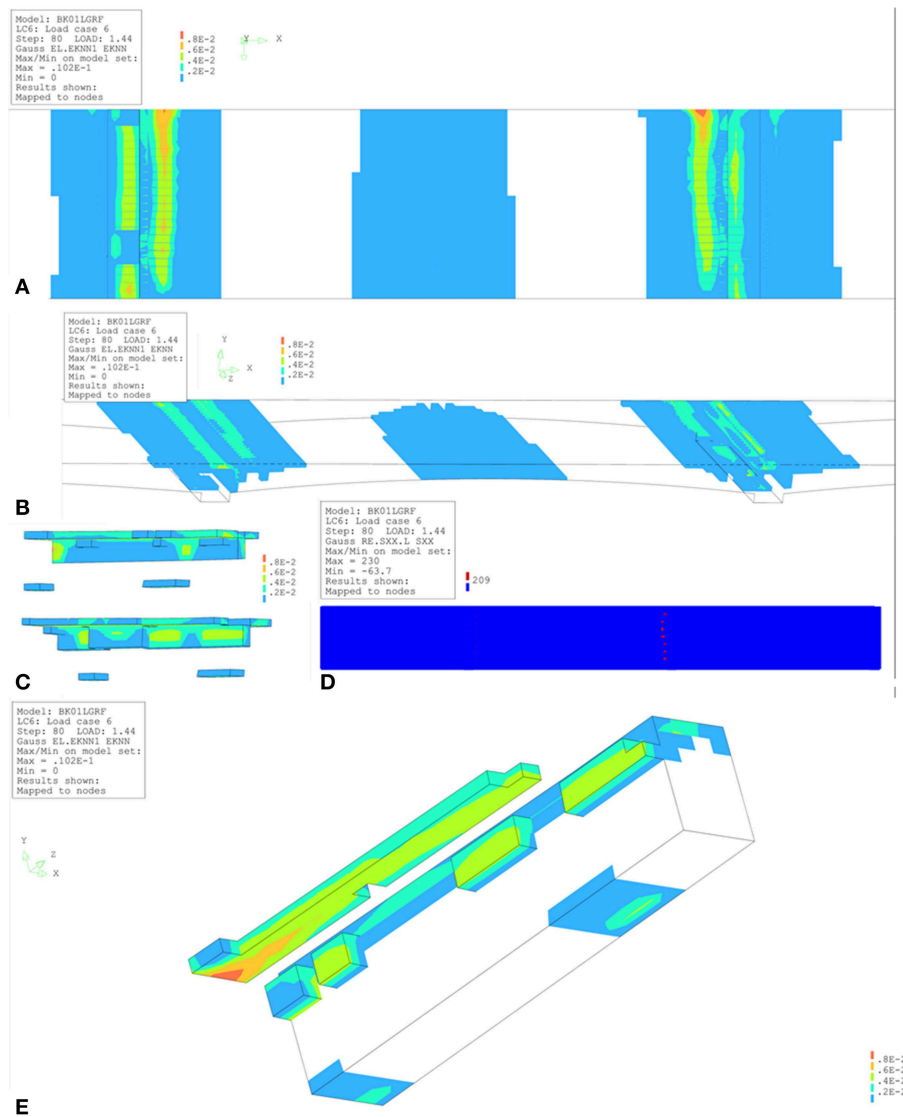
FIGURE 5 | Overview of results from non-linear finite element model with one traffic lane for a load factor of 1.44: **(A)** detailed bottom view; **(B)** detailed top view; **(C)** detail of support 2 (top) and support 3 (bottom); **(D)** steel stresses, where the red dots indicate yielding of the steel; **(E)** results for support 3 where the maximum strain is 0.01 and the crack width equals 1 mm. ε_{knn} is the cracking strain.

the elastic properties in the gravity direction of the bearings were modeled. The second part of **Figure 7** shows the model with elastomeric bearings, with the detail of the end support in **Figure 7E**, the detail of the mid support in **Figure 7F**, the top view showing span 1 and the supports in **Figure 7G**, and the side view showing span 1 and the supports in **Figure 7H**. By using the properties of the bearings, the support beam is subjected to a lower bending moment in the longitudinal direction, and the bending moment at mid span increases.

The next improvement to the linear finite element model is taking into account the non-structural elements. In this case, the curb was modeled, and as such the stiffness of this non-structural element was considered. As a result, the bending moment and shear at the critical cross-section become smaller. However, counting on the full stiffness of the curb may not correspond to

the actual structural behavior. The first reason is that the curb was built later, so phased construction should be considered in the model. Secondly, the reinforcement that connects the slab and the curb is limited (φ 12 mm at 200 mm o.c.), so that full bond and load transfer between the slab and the curb may not be assumed.

A final optimization of the linear finite element model is considering the actual reinforcement layout as shown in **Figure 8**.

Assessment With Optimized Linear Finite Element Model

The optimized linear finite element model is then used to improve the assessment of viaduct De Beek. **Table 1** gives an overview of the results in terms of the bending moment capacity M_{Rd}, the acting bending moment M_{Ed} of the initial and updated model, and the resulting Unity Check UC (M_{Ed}/M_{Rd}) of the

initial and updated model. The results are given for the middle spans (spans 2 and 3), end spans (spans 1 and 4) and the middle support (supports 2 and 4).

The value of the acting bending moment M_{Ed} is not the peak value resulting from the linear finite element but a value averaged over a certain distance in the transverse direction. The transverse distribution width depends on rules of thumb. In the Netherlands, the transverse distribution is either taken as $2d_l$ or 3 m (the notional lane width), and no single codified provision or guideline exists to date. Therefore, for this study, a number of different values were studied for the transverse distribution: 1.46 ($\approx 2d_l$), 1.74, 1.94, 2.24, and 2.42 m. The value of M_{Ed} at the middle support reported in **Table 1** (888 kNm/m in the updated model) is based on a distribution width of 1.94 m. When we use a distribution width of 2.42 m instead, the value of M_{Ed} at the middle support reduces to 841 kNm/m. The justification for using a wider distribution width lies in the measured strains during the proof load test, see **Figure 9**. One can see that the variation in strains in the transverse direction is
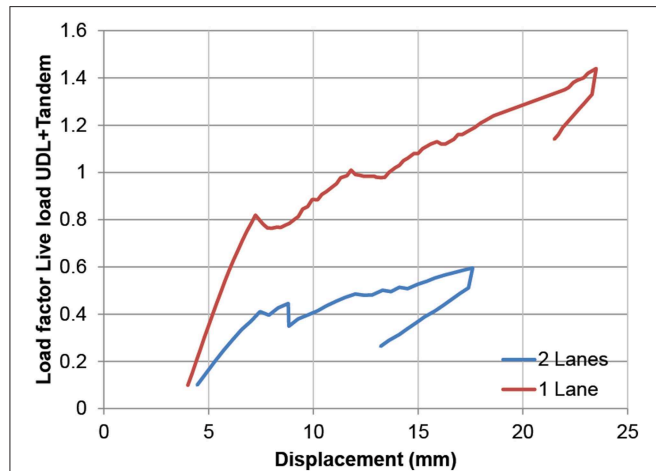

FIGURE 6 | Load-displacement diagram for the situation with one lane and two lanes of traffic.
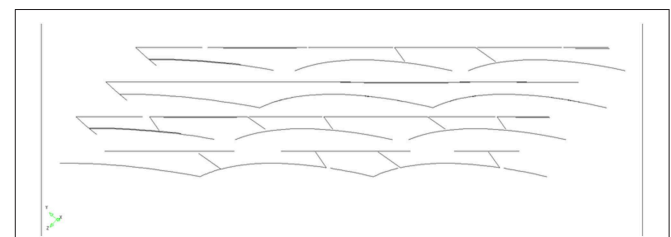

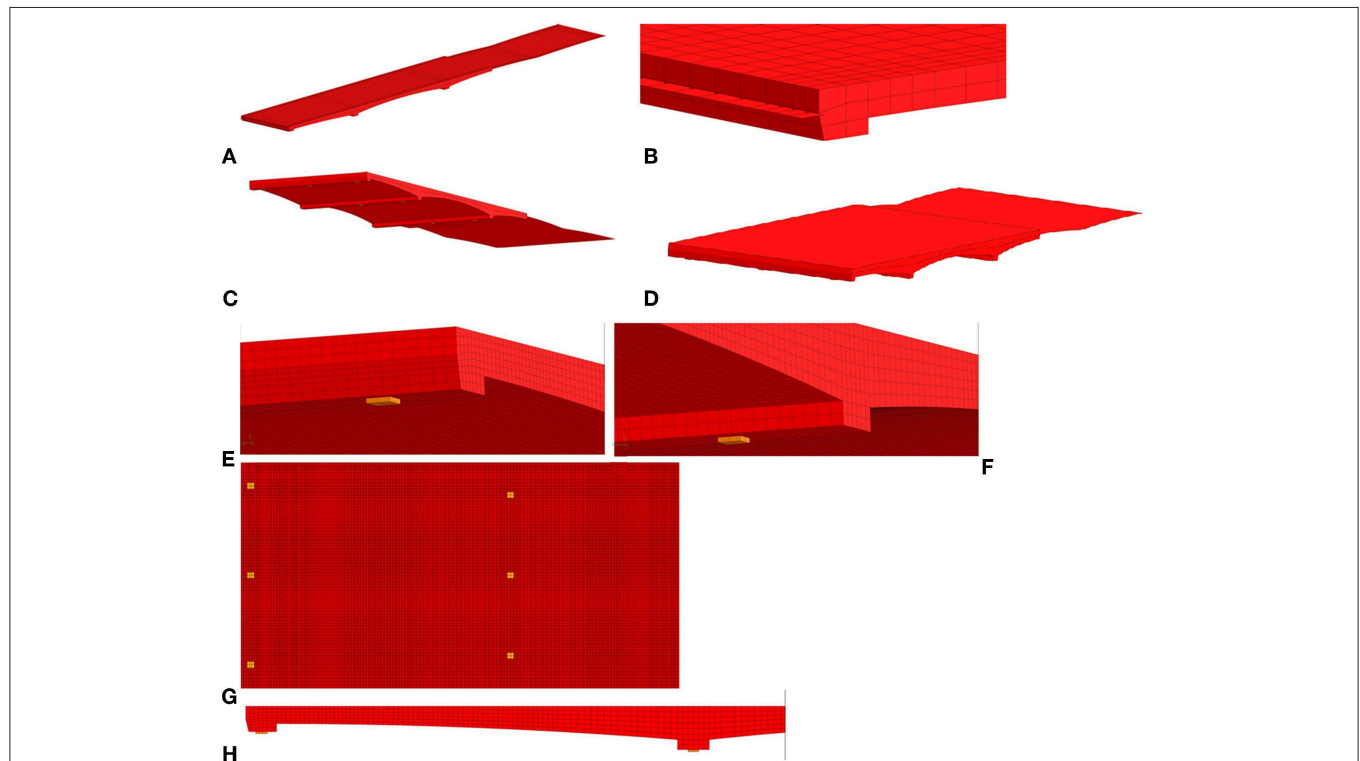**FIGURE 8 |** Layers of reinforcement in optimized model.

FIGURE 7 | Overview of optimized finite element models: **(A)** overview of first model, showing different elements used; **(B)** detail of support in first model; **(C)** bottom view of first model; **(D)** top view of first model; **(E)** detail of elastomeric bearings at end support in second model; **(F)** detail of elastomeric bearings at mid support in second model; **(G)** overview of positions of bearings in span 1 and half of span 2 in second model; **(H)** side view of span 1 in second model.

limited, indicating a larger distribution width in the transverse direction. The distribution width also appears to be a function of the load level: for the lowest load level the distribution width is about 4.5 m and for the highest load level, it is about 2 m.

A section fulfills the code requirements when the Unity Check UC ≤ 1. Based on the results in **Table 1**, we can conclude that with the updated linear finite element model the sections at the end span and middle support fulfill the code requirements, but that the section in the critical spans does not fulfill the code requirements for one lane of traffic based on the presented calculations. The acting bending moment M_{Ed} is the sum of peak values of 96 kNm/m (contribution of the permanent loads) and 291 kNm/m (live loads), which gives a peak value of 387 kNm/m in total. Averaging the peak results in the reported value in **Table 1** of 376 kNm/m. The capacity for live load is 211 kNm/m, or 72.5% of the demand of 291 kNm/m. As such, a maximum design tandem load of 72.5% of 600 kN, i.e., 435 kN should be the maximum allowable load. This load is slightly below the 450 kN design tandem of the VK45 road class in the Netherlands. The next step is then to further refine the calculations and use a non-linear finite element model.

Optimized Non-linear Finite Element Model
Updating With Proof Load Test Results
The data from the field test (measured strains on the bottom of the concrete cross-section and in the steel reinforcement, as well

as measured deflections) can be used to update the non-linear finite element model for the end span. The reader should notice that the non-linear finite element models of the proof load test are based on average material properties and do not use load factors, as the goal of this part of the study is to come to a model that represents the field test as closely as possible. Then, for assessment, characteristic material properties will be used and a load factor for the live loads will need to be achieved. No standardized or automatic optimization procedure was used for this purpose, as we considered engineering judgment and the use of plausible ranges of input parameters very important for this study. The model output that was evaluated for the optimization process were the deflections (magnitudes and profiles in the transverse and longitudinal direction), as well as the strains (magnitudes and profiles).

In the following paragraphs, four iterations of model optimization will be shown: (1) FEA1 considers the support stiffness to match existing cracking patterns, (2) FEA2 is optimized for matching deflections with the proof load test results, (3) FEA3 balances optimizing deflections in longitudinal and transverse deflections as well as strains, and (4) "FEA Final" considers the effect of modeling the contribution of the curb.

A first step in optimizing the model (resulting in "FEA" or "FEA1" in the figures) is to modify the stiffness of the supports to match the existing cracks (**Figure 1B**) in the bridge. Reducing the stiffness of the supports results in a situation in which mostly cracks in spans 2 and 3 were observed. Note that the initial finite element model (**Figure 5**) results in cracking over the supports. The optimization of reducing the stiffness of the support thus matches better the real situation. The results of the comparison between the measured and analytically determined deflection profiles is shown in **Figure 10A** for the longitudinal profiles and in **Figure 10B** for the transverse profiles. These profiles are caused by the maximum proof load applied during the shear test. The actual behavior of the bridge is stiffer than the behavior observed in the non-linear finite element model based on the initial assumptions. The

TABLE 1 | Bending moment capacity M_{Rd}, acting bending moment M_{Ed}, and resulting Unity Check (UC) for initial and updated linear finite element model.

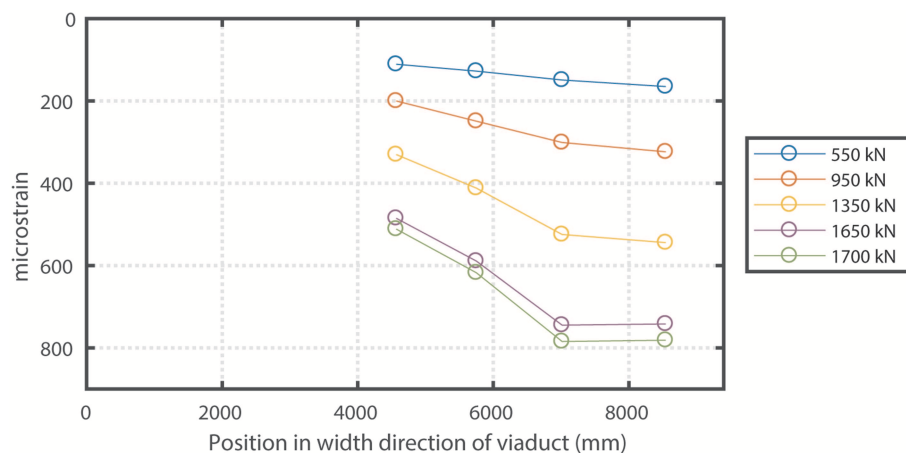| Position	M_{Rd} (kNm/m)	M_{Ed} (kNm/m)		UC	
		Initial	Updated	Initial	Updated
Middle span	307	418	376	1.36	1.22
End span	367	426	335	1.16	0.91
Middle support	896	1,057	888	1.18	0.99

FIGURE 9 | Measured strains at bottom of concrete cross-section during proof load test for bending moment for different load levels.
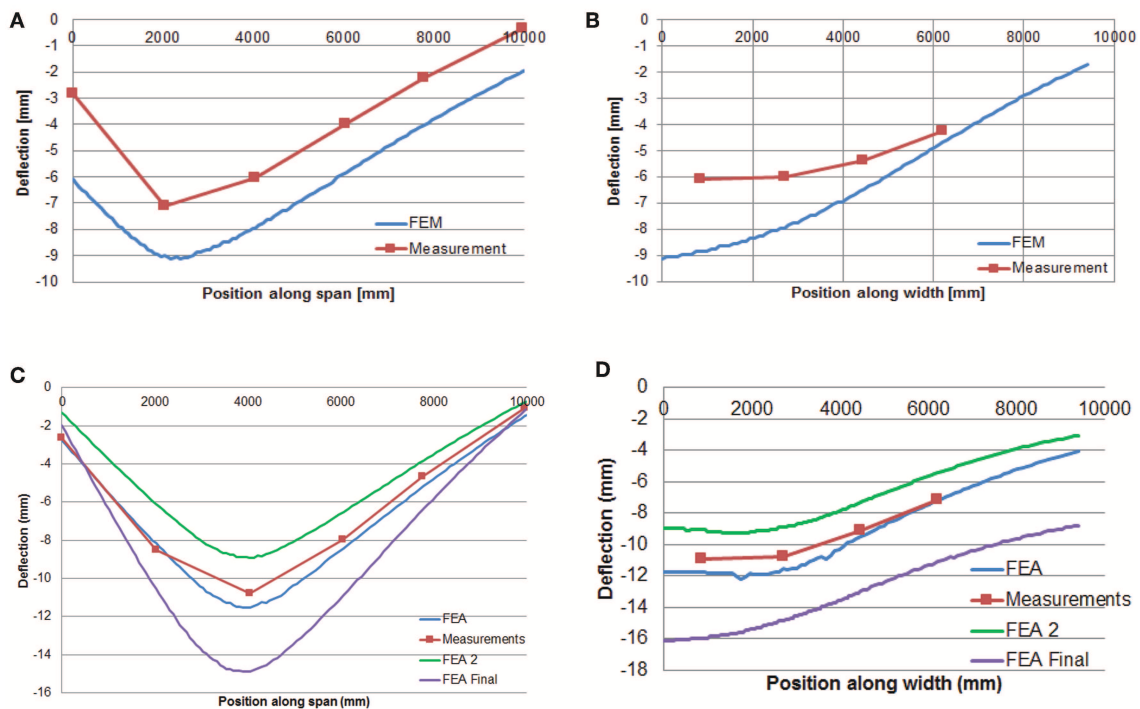
FIGURE 10 | Comparison between measured deflection profile and profile resulting from non-linear finite element model at maximum load during proof load test: **(A)** first updated model, longitudinal deflection profile for shear test; **(B)** first updated model, transverse direction profile for shear test; **(C)** all models, longitudinal deflection profile for bending moment test; **(D)** all models, transverse deflection profile for bending moment test.

deflection at the support is also smaller in reality than in the model. A first step is thus to improve the boundary conditions in the model.

The second optimization step (resulting in FEA2) is based on matching the deflections measured in the field with the deflections in the model. The deflections are optimized to match the longitudinal profile. The results for the maximum load applied during the bending moment test are shown in **Figure 10C** for the longitudinal direction and in **Figure 10D** for the transverse direction.

The third version of the model (resulting in FEA3) is based on optimization to match the deflections in both the longitudinal and transverse direction, as well as by comparing the strains in the non-linear finite element model and the measured strains. The optimization procedure is shown in **Figure 11A** for the bending moment test and in **Figure 11B** for the shear test. For the bending moment test, the strains are the averaged values over the entire last load step. For the shear test, two measured strains are shown: the strains measured at the maximum load (1,509 kN), which was a short peak during the penultimate load step, and the averaged values over the entire last load step. The strains in the plots are corrected for the measurement of the strains caused by temperature and humidity, and are also corrected for the output at a load of 0 kN.

In a last optimization step (indicated with "FEA final" in the figures), the influence of the stiffness of the curb is evaluated. Since the reinforcement that connects the slab and the curb is

limited, it may be that the curb does not contribute to the overall structural behavior. **Figure 12** shows the outcome of the models with and without the curb as compared to the measured load-deflection response. Based on these results, we can conclude that at lower load levels the curb does not contribute to the overall structural behavior. At higher load levels, some contribution of the curb seems to occur. It is however a conservative approach to remove the contribution of the curb.

As can be seen, several models have been developed, and the final selected model ("FEA final") has the most uniform behavior for the deflections and strains, for both the test at the bending moment position and the shear position, and the outcome of the model is on the conservative side. The results show that with the optimized model, the error on the strains at the bending moment position is maximum 12%, whereas for the shear position this error is maximum 61% when the results for the maximum load are considered and 58% when the results for the final load step are considered. The error on the model FEA3 is smaller, but the results are not always on the conservative side. Therefore, it was decided to select the model without the contribution of the curb as the final model.

The shape of the plot of the strains in **Figure 11A** displays a local maximum or minimum value of the strains (for FEA1 and FEA2, respectively) caused by local cracking. This effect is not present anymore in FEA3 and the final finite element model. For both the shear and bending moment test, the final finite element model follows the same overall shape as the profile measured
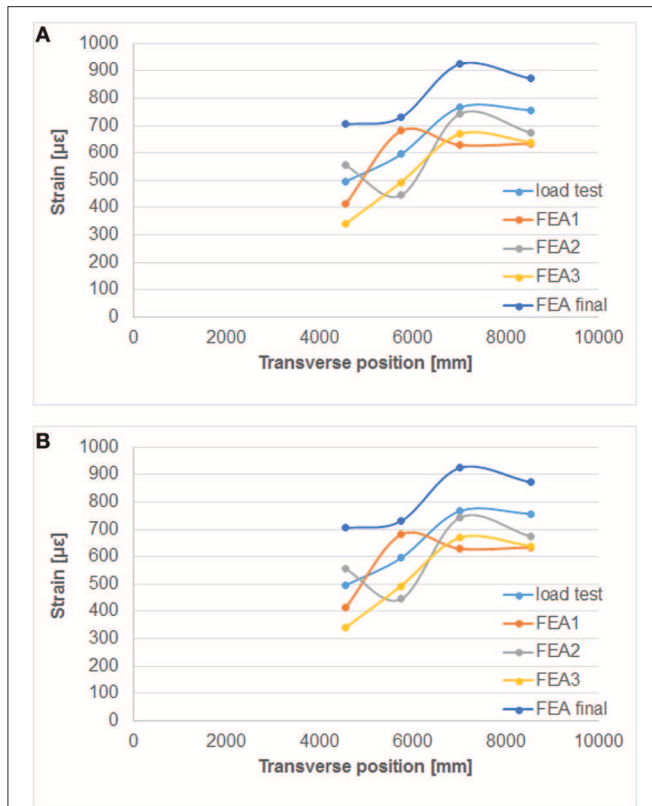
FIGURE 11 | Comparison between measured strains in transverse direction to strains from finite element models, with FEA2 and FEA3 the optimized models and FEA final the final model: **(A)** bending moment test; **(B)** shear test.
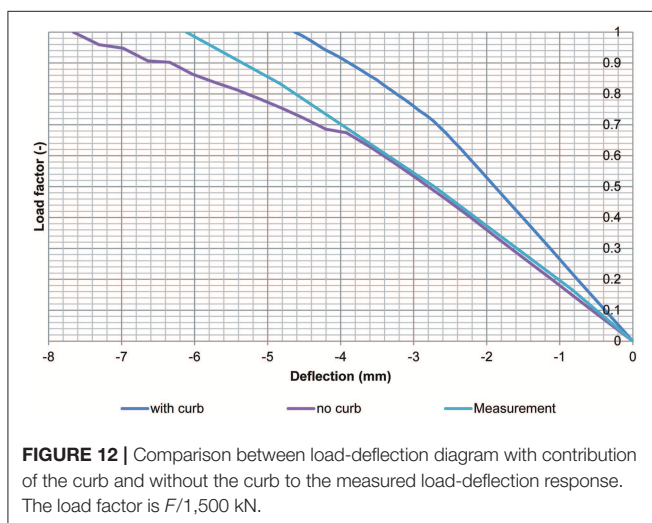

FIGURE 12 | Comparison between load-deflection diagram with contribution of the curb and without the curb to the measured load-deflection response. The load factor is $F/1{,}500$ kN.

during the test, which is an improvement as compared to the other models. The cracking found in the final finite element for the bending moment position can be observed based on the strain plots shown in **Figure 13A** and for the shear position in **Figure 13B**. For the shear position, the maximum cracking strain is $\varepsilon_{knn} = 2{,}044\ \mu\varepsilon$ and the maximum crack width is calculated as 0.205 mm when the element length of 146 mm is considered,

over which an average strain occurs of 1,470 $\mu\varepsilon$. An overview of the development of the principal strains and cracking strains in the shear test at the position where the largest cracking strain is found is given in **Figure 14** as a function of the load factor ($F/1{,}500$ kN).
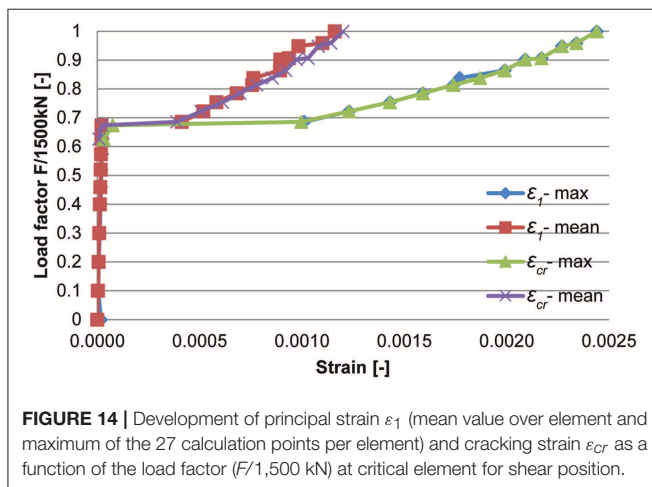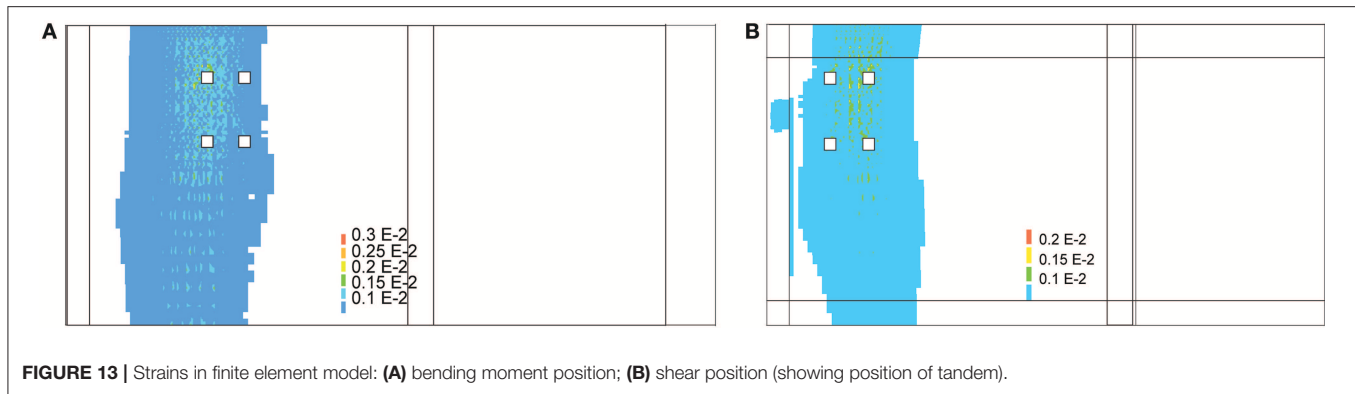
The final finite element model can also be evaluated based on the plots of the deflection. **Figures 10C,D** show the comparison between the output of the final finite element model in the longitudinal and transverse direction, respectively, and the measurements for the bending moment position. In addition, the comparison between the output of the final finite element model in the longitudinal and transverse direction with the measured deflections for the shear position is given in **Figures 15A,B**, respectively. To come to a better representation of the shear test, a possibility would be to change the cracking model from rotating cracking to fixed cracking at a predetermined value of the cracking strain. As compared to the original non-linear finite element model, developed without the knowledge of the field measurements, the current optimized model results in a better correspondence between the measured and analytical deflections, cracking patterns, and strains.

We can see here that selecting the final finite element model requires balancing the performance of the model across the two test positions, and for both strains and deflections. Whereas, an earlier model was fully optimized to fit the deflections in the bending moment test (see **Figures 10C,D**), this model did not result in the best performance overall. Selecting the best model requires engineering judgment, as one can see from the previous discussions.

Assessment With Optimized Non-linear Finite Element Model

The improved model of the proof load test can be used to better estimate the behavior in the spans that were not tested. For the assessment, the characteristic material parameters were used instead of the average (measured) parameters used for the development of the field-verified model. As such, the model with characteristic material properties can be used to come to a more realistic assessment for the critical middle spans of the structure.

The maximum load factor that was found is 1.8 for one lane of traffic, which is larger than the required factor of 1.44. The resulting cracking at the top, bottom, and side in the model are shown in **Figures 16A–C**, respectively. The maximum crack strain is $\varepsilon_{knn} = 9{,}020\ \mu\varepsilon$. To find the maximum crack width, the average strain 7,250 $\mu\varepsilon$ over 150 mm is used, which gives $w_{max} = 1.08$ mm. **Figure 17** shows the load-displacement diagram with the load factor on the y-axis. As the maximum load factor is 1.8, we can conclude that the bridge fulfills the requirements for one lane of traffic. These results can be compared with the results of the initial finite element model in **Figure 6**, where a maximum load factor of 0.6 was found for two lanes of traffic and 1.44 for one lane of traffic. The field-verified model, adjusted for the use of characteristic material parameters, thus shows that the load-carrying capacity of the bridge is larger than determined with the originally developed non-linear finite element model, as expected. The non-linear

FIGURE 13 | Strains in finite element model: **(A)** bending moment position; **(B)** shear position (showing position of tandem).

FIGURE 14 | Development of principal strain ε_1 (mean value over element and maximum of the 27 calculation points per element) and cracking strain ε_{cr} as a function of the load factor ($F/1,500$ kN) at critical element for shear position.

FIGURE 15 | Comparison between deflection as measured during proof load test and as obtained with the final finite element model for the shear position: **(A)** longitudinal direction; **(B)** transverse direction.
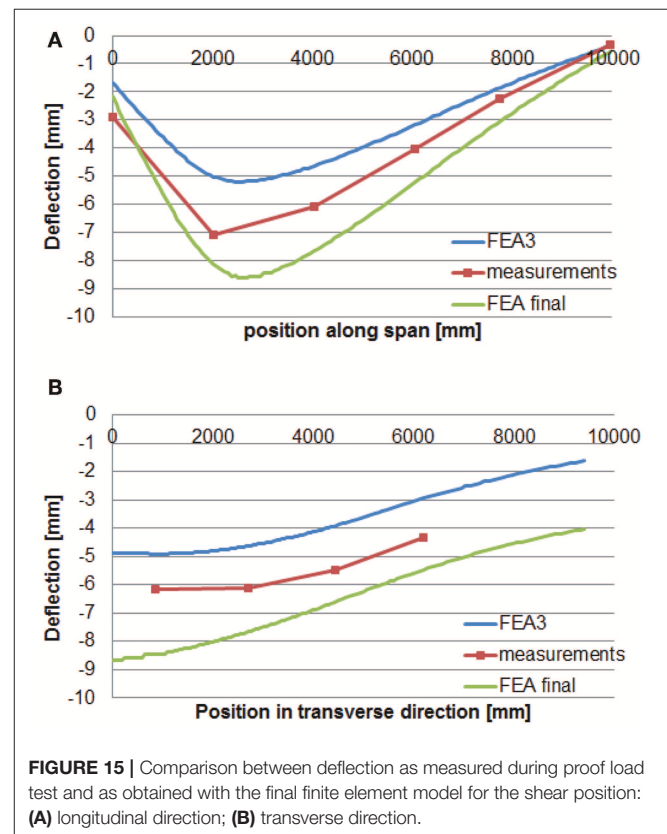
finite element model also gives an improvement when comparing the assessment result based on the linear finite element model (for which load posting was required for one lane of traffic) to the result based on the non-linear finite element model (which shows that the requirements for one lane of traffic are fulfilled).

Since the assessment with the non-linear finite element model shows that viaduct De Beek fulfills the code requirements for one lane of traffic load, the same model is used for evaluating the design situation with two lanes of traffic. **Figure 17** shows the load-displacement diagram for the situation with two lanes of traffic. A maximum load factor of 1.17 is now reached. In other words, the traffic loads should be restricted to 81% of the regular traffic and a load posting should be applied to the bridge when two lanes of traffic are permitted on the bridge. Comparing **Figure 6** (load factor 0.6 for two lanes of traffic) and **Figure 17** (load factor 1.17 for two lanes of traffic) shows the benefit of including the results from a proof load test on a non-linear finite element model.

DISCUSSION

The previous analyses show how field test data as well as details of the structure (reinforcement layout, support conditions, non-structural elements) can be incorporated into the models to improve the assessment of an existing bridge. When the measurements obtained during the proof load test are included, the result is an improved model for the entire structure, which uses the field data of the end span. This improved model then results in an improved Unity Check when linear finite element models are used, or an improved estimation of the maximum load factor (with target value 1.44) when non-linear finite element models are used.

The finite element models are based on the uncracked stiffness of the concrete. This assumption may explain the
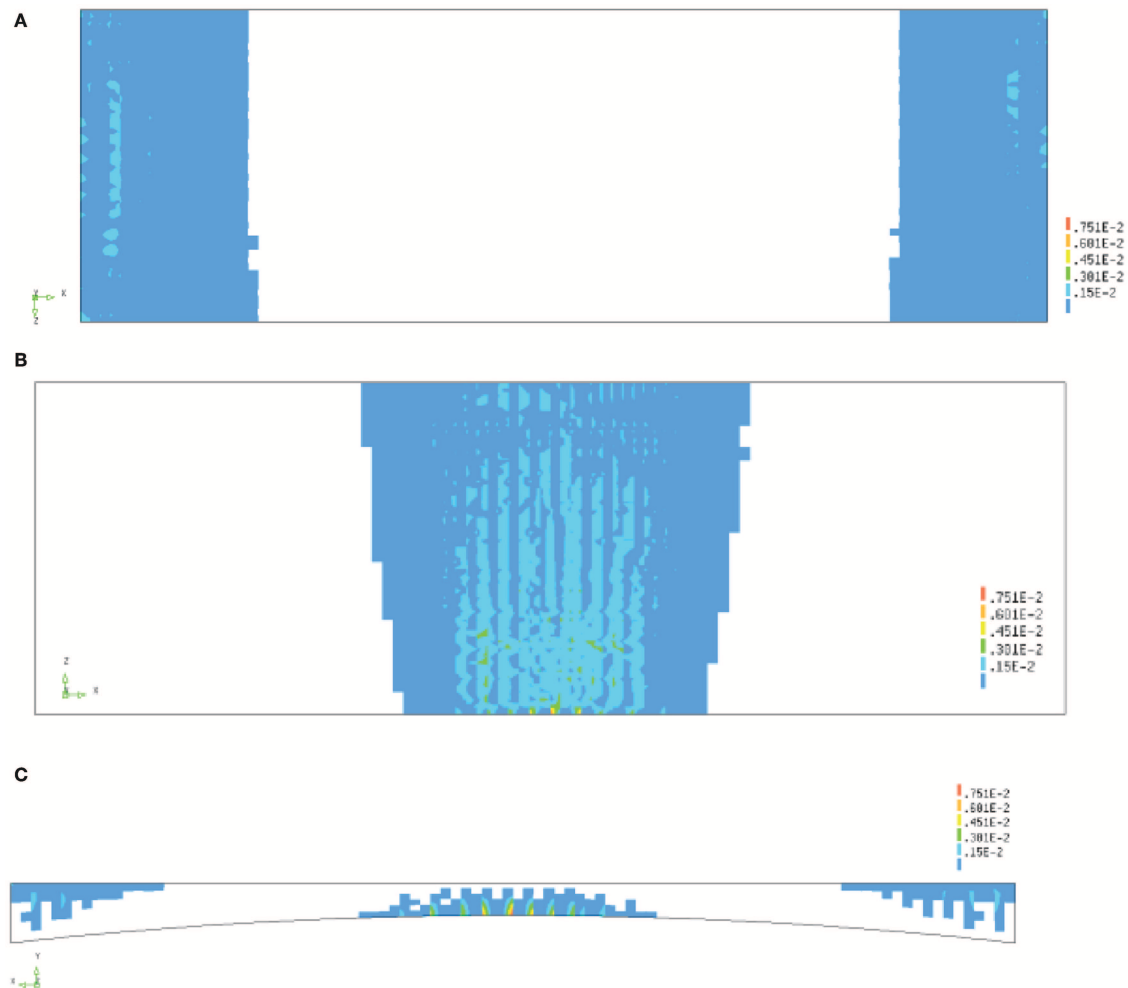
FIGURE 16 | Cracking for load factor of 1.8: **(A)** top view showing cracks over mid supports; **(B)** bottom view for cracks at midspan for span 2; **(C)** side view of cracking over support and at midspan for span 2.
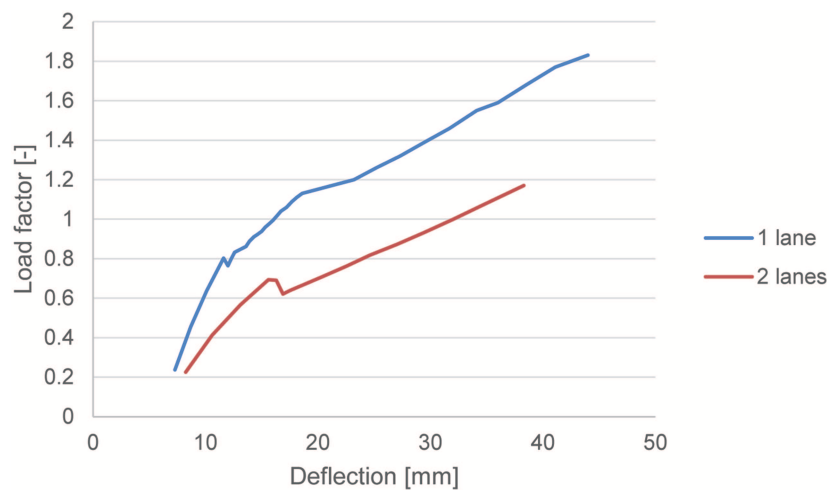

FIGURE 17 | Load-displacement diagram for assessment of span 2, showing the applied live load in terms of a live load factor for one lane of traffic and two lanes of traffic.

differences between the model and the measured deflections and strains. In the non-linear finite element model, cracking occurs as the load increases, but the existing cracks in the bridge were not modeled. Furthermore, recently, diagnostic load tests have been carried out on this bridge: the strains resulting from three vehicle types (six runs per vehicle type) have been measured, which can improve the assumptions regarding the stiffness of the structure. With these data, both the concrete compressive strength (which was determined by taking core samples) and the stiffness can be used as input values for the finite element model. These vehicles can also be placed as preloading on the model, to introduce cracks into the model before applying the proof load on the model, and thus including existing cracks into the model. A preliminary study on the effect of precracking is shown in **Figure 18A** for the bending moment position of the proof load test and in **Figure 18B** for the shear position. Since for loading with the 600 kN vehicle, no cracks occurred in the slab, the effect of precracking was taken into account by lowering the modulus of elasticity of the concrete E_c. When 90% of the original value of E_c is used in a new model, the maximum displacement increases with 0.9 mm and becomes 9.8 mm, see **Figure 18A**. The maximum displacement in the experiment was 10.8 mm. As such, using a reduced value for E_c could provide an additional improvement of the modeling of the non-linear finite element model. Similar observations are drawn from the shear position, as indicated in **Figure 18B**.

When comparing the results of the model without the curb and with the curb in **Figure 18A**, we can observe that the measured structural response lies in between the response with and the response without the curb. Since the reinforcement that ties the curb to the deck is rather limited (φ 12 mm at 200 mm o.c.), it is a conservative approach to leave out the contribution of the curb. However, the experimental results show that the curb has some effect on the overall structural response. A possible step for improvement could thus be to assign a partial contribution to the curb. To find out the contribution of the curb, one could study the response for load factor 1 and find out for which percentage contribution of the curb the measured deflection can be obtained. To model the contribution of the curb, a possible solution is to add interface elements between the curb and the slab. As one can observe in **Figure 18A**, the initial structural response of the measurements corresponds to the model without the curb. Then, as the load increases, redistribution of load to the curb takes place, and the contribution of the curb can be activated. These steps are however outside the scope of the present study.

One possible future application of this approach is the combination between non-linear finite element modeling and non-contact measurement techniques. If we can scan the entire surface of the span that is being tested and can obtain the full surface response of displacements, we can then optimize the non-linear finite element model in such a way that the measured and modeled surface responses are as similar as possible.

The comparison between the initial and final non-linear finite element model shows that, for this case, having a

better understanding of the bridge behavior, based on the field observations and measurements during the proof load test, results in the conclusion that the bridge fulfills the code requirements for one lane of traffic. However, developing the field-verified model based on the proof load test in span 1 turned out to be more difficult than expected initially. Many choices need to be made in this process, and further studies on other bridges seem to be necessary to come up with a general recommendation to couple non-linear finite element models with proof load tests. This paper indicates that the combination of non-linear finite element models with proof load tests can be valuable for cases where access to the site and the most critical position of the viaduct may be limited. However, further research is necessary to specify the way in which the proof load test results should be used to update the original non-linear finite element model, which is not as straight-forward as for linear finite element models. Further research is important, so that this method can be used for an optimal combination of field testing and finite element modeling, in a way that can reduce the costs of field tests. This first case study shows that the first results with this approach are promising.

SUMMARY AND CONCLUSIONS

Proof load testing can be a valuable tool for the assessment of existing bridges when the uncertainties on the capacity are too large to use analytical assessment methods. This paper discusses the case of viaduct De Beek, which was found analytically to not fulfill the code requirements for bending moment in none of its four spans. As a result, traffic is currently only permitted on one lane for this bridge. The most critical spans, with the largest Unity Check, are spans 2 and 3. These spans are directly over the highway. Proof load testing of these spans would require closing of the highway, which was not a feasible option. Therefore, span 1 was subjected to a proof load test at a position resulting in the largest sectional moment and a position resulting in the largest sectional shear. The proof load test demonstrated that span 1 fulfills the code requirements for two lanes of traffic.

To extrapolate the results of the proof load test on span 1 to the critical span 2, two approaches were followed: using linear finite element models, and using non-linear finite element models. The linear finite element model was updated by making the following changes: use of solid elements instead of shell elements, adjusting the stiffness of the supports to represent the actual bearing stiffness, using the reinforcement layout as given on plans, and using a larger distribution width for the peak bending moment. Including these optimizations shows that the bridge does not fulfill the code requirements for one lane of traffic.

The non-linear finite element model was updated by making the following changes: using different assumptions for the material modeling, adjusting the stiffness of the supports to represent the actual bearing stiffness, evaluating the contribution of the curb, and modeling the reinforcement layout completely
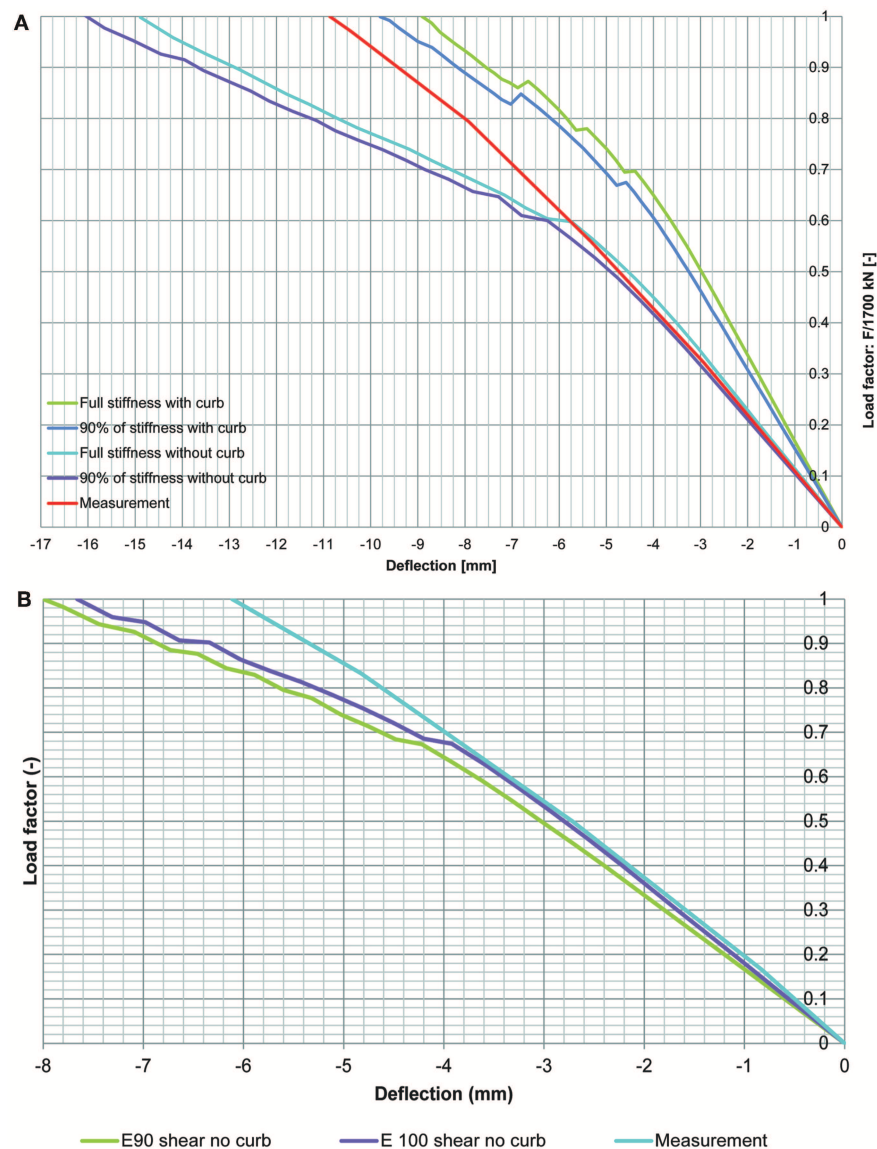
FIGURE 18 | Comparison between load-displacement diagram, for the case with full *E* and 90% of *E*: **(A)** for proof load testing location for bending moment in span 1; **(B)** for proof load testing location for shear in span 1.

as given on the plans. The measured structural responses during the proof load test in span 1 and the responses determined in the non-linear finite element model were compared to evaluate the influence of changing parameters. The responses that were evaluated were strains and deflection profiles in longitudinal and transverse directions, for the bending moment and shear proof load tests. However, this exercise shows that there is no single model that matches each of these outputs completely, and that many choices are left to the engineer. As such, our recommendation at this moment is to apply this approach to more case studies, so that recommendations for the coupling of proof load tests and non-linear finite element modeling can be developed. This first application shows that the updated non-linear finite element model can be used to demonstrate that the bridge fulfills the code requirements for

one lane of traffic, or that two lanes of traffic with posting can be used.

DATA AVAILABILITY

The datasets used for this study are available on request to the corresponding author.

AUTHOR CONTRIBUTIONS

EL: analysis of proof load test results, manuscript writing. AdB: finite element modeling, manuscript review and editing. CvdV: guidance with assessment, modifications to manuscript. DH: coordination of load testing research.

FUNDING

ACKNOWLEDGMENTS

REFERENCES

ACI Committee 437 (2013). *Code Requirements for Load Testing of Existing Concrete Structures (ACI 437.2M-13) and Commentary.* Farmington Hills, MA.

Aguilar, C. V., Jáuregui, D. V., Newtson, C. M., Weldon, B. D., and Cortez, T. M. (2015). "Load rating a prestressed concrete double-tee beam bridge without plans by proof testing," in *Transportation Research Board Annual Compendium of Papers* (Washington, DC). doi: 10.3141/2522-09

Anay, R., Cortez, T. M., Jáuregui, D. V., Elbatanouny, M. K., and Ziehl, P. (2016). On-site acoustic-emission monitoring for assessment of a prestressed concrete double-tee-beam bridge without plans. *J. Perform. Construct. Facilities* 30. doi: 10.1061/(ASCE)CF.1943-5509.0000810

Barker, M. G. (2001). Quantifying field-test behavior for rating steel girder bridges. *J. Bridge Eng.* 6, 254–261. doi: 10.1061/(ASCE)1084-0702(2001)6:4(254)

Bonifaz, J., Zaruma, S., Robalino, A., and Sanchez, T. A. (2018). "Bridge diagnostic load testing in ecuador – case studies," in *IALCCE 2018* (Ghent).

Cai, C. S., and Shahawy, M. (2003). Understanding capacity rating of bridges from load tests. *Pract. Period. Struct. Design Construct.* 8, 209–2016. doi: 10.1061/(ASCE)1084-0680(2003)8:4(209)

Chajes, M. J., Shenton Iii, H. W., and Finch, W. W. (2001). Diagnostic and in-service testing of transit railway bridge. *Transport. Res. Rec.* 1770, 51–57. doi: 10.3141/1770-08

Collings, D., and Sagaseta, J. (2015). A review of arching and compressive membrane action in concrete bridges. *Inst. Civil Eng. Bridge Eng.* 169, 271–284. doi: 10.1680/bren.14.00039

Comité Européen de Normalisation (2003). *Eurocode 1: Actions on Structures - Part 2: Traffic Loads on Bridges.* NEN-EN 1991-2:2003. Comité Européen de Normalisation, Brussels, Belgium.

Comité Européen de Normalisation (2005). *Eurocode 2: Design of Concrete Structures - Part 1-1 General Rules and Rules for Buildings.* NEN-EN 1992-1-1:2005. Comité Européen de Normalisation, Brussels, Belgium.

Deutscher Ausschuss für Stahlbeton (2000). *DAfStb-Guideline: Load Tests on Concrete Structures (in German) (DAfStb-Richtlinie: Belastungsversuche an Betonbauwerken).* Deutscher Ausschuss fur Stahlbeton, Berlin, Germany.

DIANA FEA BV (2017). *Users Manual of DIANA, Release 10.1.* Delft, Netherlands.

Duan, Z., Liu, Y., and Spencer, B. F. (2005). Finite element model updating of structures using a hybrid optimization technique. *Proc. SPIE* 5765, 335–344. doi: 10.1117/12.602009

Faber, M. H., Val, D. V., and Stewart, M. G. (2000). Proof load testing for bridge assessment and upgrading. *Eng. Struct.* 22, 1677–1689. doi: 10.1016/S0141-0296(99)00111-X

fib (2012). *Model Code 2010: Final Draft.* Lausanne: International Federation for Structural Concrete.

Frýba, L., and Pirner, M. (2001). Load tests and modal analysis of bridges. *Eng. Struct.* 23, 102–109. doi: 10.1016/S0141-0296(00)00026-2

Fu, G., Pezze Iii, F. P., and Alampalli, S. (1997). Diagnostic load testing for bridge load rating. *Transport. Res. Rec.* 1594, 125–133. doi: 10.3141/1594-13

Grigoriu, M., and Hall, W. B. (1984). Probabilistic models for proof load testing. *J. Struct. Eng.* 110, 260–274. doi: 10.1061/(ASCE)0733-9445(1984)110:2(260)

Halicka, A., Hordijk, D. A., and Lantsoght, E. O. L. (2018). "Rating of concrete road bridges with proof loads," in *ACI SP 323 Evaluation of Concrete Bridge Behavior Through Load Testing - International Perspectives* (Farmington Hills, MI), 16.

Iv-Infra (2015). *51H-304-01 - De Beek - Recalculation Bridge Deck (in Dutch).* Papendrecht, Netherlands.

Juntunen, D. A., and Isola, M. C. (1995). *Proof Load Test of R01 of 61131 M-37 Over CSX Railroad, South of Bailey, Michigan.* Lansing, MI: Michigan Department of Transportation.

Koekkoek, R. T., Lantsoght, E. O. L., Yang, Y., and Hordijk, D. A. (2016). *Analysis Report for the Assessment of Viaduct De Beek by Proof Loading.* Delft University of Technology, Delft, Netherlands.

Lantsoght, E. O. L., De Boer, A., Van Der Veen, C., and Hordijk, D. A. (2018a). "Modelling of the proof load test on viaduct De Beek", in *Euro-C* (Bad Hofgastein).

Lantsoght, E. O. L., Koekkoek, R., Yang, Y., Van Der Veen, C., Hordijk, D., and De Boer, A. (2017a). "Proof load testing of the viaduct De Beek," in *39th IABSE Symposium - Engineering the Future* (Vancouver, BC).

Lantsoght, E. O. L., Koekkoek, R. T., Hordijk, D. A., and De Boer, A. (2017c). Towards standardization of proof load testing: pilot test on viaduct Zijlweg. *Struct. Infrastruct. Eng.* 16, 365–380. doi: 10.1080/15732479.2017.1354032

Lantsoght, E. O. L., Koekkoek, R. T., Van Der Veen, C., Hordijk, D. A., and De Boer, A. (2017d). Pilot proof-load test on viaduct de beek: case study. *J. Bridge Eng.* 22:05017014. doi: 10.1061/(ASCE)BE.1943-5592.0001131

Lantsoght, E. O. L., Van Der Veen, C., De Boer, A., and Walraven, J. (2015). Transverse load redistribution and effective shear width in reinforced concrete slabS. *Heron* 60, 145–180. Available online at: http://www.heronjournal.nl/60-3/2.html

Lantsoght, E. O. L., Van Der Veen, C., De Boer, A., and Walraven, J. C. (2013). Recommendations for the shear assessment of reinforced concrete slab bridges from experiments. *Struct. Eng. Int.* 23, 418–426. doi: 10.2749/101686613X13627347100239

Lantsoght, E. O. L., Van Der Veen, C., Hordijk, D., and De Boer, A. (2017b). "Recommendations for proof load testing of reinforced concrete slab bridges," in *39th IABSE Symposium - Engineering the Future* (Vancouver, BC).

Lantsoght, E. O. L., Van Der Veen, C., and Hordijk, D. A. (2018b). "Proposed stop criteria for proof load testing of concrete bridges and verification," in *IALCCE 2018.* (Ghent).

Lantsoght, E. O. L., Van Der Veen, C., Hordijk, D. A., and De Boer, A. (2017e). Development of recommendations for proof load testing of reinforced concrete slab bridges. *Eng. Struct.* 152, 202–210. doi: 10.1016/j.engstruct.2017.09.018

Lantsoght, E. O. L., Van Der Veen, C., Hordijk, D. A., and De Boer, A. (2017f). State-of-the-art on load testing of concrete bridges. *Eng. Struct.* 150, 231–241. doi: 10.1016/j.engstruct.2017.07.050

Ministerio de Fomento - Direccion General de Carreteras (1999). *Recomendaciones para la realizacion de pruebas de carga de recepcion en puentes de carretera.* Madrid.

Olaszek, P., Lagoda, M., and Casas, J. R. (2014). Diagnostic load testing and assessment of existing bridges: examples of application. *Struct. Infrastruct. Eng.* 10, 834–842. doi: 10.1080/15732479.2013.772212

Ransom, A. L., and Heywood, R. J. (1997). "Recommendations for Proof Load Testing in Australia," in *Proceedings of the Autostrads 1997 Bridge Conference Bridging the Milenia.* (Sydney).

Rijkswaterstaat (2013). *Guidelines Assessment Bridges - Assessment of Structural Safety of an Existing Bridge at Reconstruction, Usage and Disapproval (in Dutch)*. RTD 1006:2013 1.1, Utrecht, Netherlands.

Rijkswaterstaat (2017a). *Guidelines for Nonlinear Finite Element Analysis of Concrete Structures*. RTD 1016-1:2017, Utrecht, Netherlands.

Rijkswaterstaat (2017b). *Validation of the Guidelines for Nonlinear Finite Element Analysis of Concrete Structures - Part 2: Review of results: RTD 1016-2:2017*. Utrecht, Netherlands.

Rijkswaterstaat (2017c). *Validation of the Guidelines for Nonlinear Finite Element Analysis of Concrete Structures - Part 3A: Reinforced Beams*. RTD 1016-3A:2017, Utrecht, Netherlands.

Rijkswaterstaat (2017d). *Validation of the Guidelines for Nonlinear Finite Element Analysis of Concrete Structures - Part 3B: Pre-stressed Beams*. RTD 1016-3B:2017, Utrecht, Netherlands.

Rijkswaterstaat (2017e). *Validation of the Guidelines for Nonlinear Finite Element Analysis of Concrete Structures - Part 3C: Slabs*. RTD 1016-3C:2017, Utrecht, Netherlands.

Sanayei, M., Reiff, A. J., Brenner, B. R., and Imbaro, G. R. (2016). Load rating of a fully instrumented bridge: comparison of LRFR approaches. *J. Perform. Construct. Facil.* 30. doi: 10.1061/(ASCE)CF.1943-5509.0000752

Saraf, V. K., Nowak, A. S., and Till, R. (1996). "Proof load testing of bridges," in *Probabilistic Mechanics and Structural Reliability: Proceedings of the Seventh Specialty Conference*, eds D. M. Frangopol and M. D. Grigoriu (Worcester, MA). doi: 10.3141/1541-07

Velázquez, B. M., Yura, J. A., Frank, K. H., Kreger, M. E., and Wood, S. L. (2000). *Diagnostic Load Tests of a Reinforced Concrete Pan-Girder Bridge*. Austin, TX: The University of Texas at Austin).

Wang, H., Li, A.-Q., and Li, J. (2010). Progressive finite element model calibration of a long-span suspension bridge based on ambient vibration and static measurements. *Eng. Struct.* 32, 2546–2556. doi: 10.1016/j.engstruct.2010.04.028

Willems, M., Ruiter, P. B. D., and Heystek, A. P. (2015). *Inspection Report Object 51H-304-01 (in Dutch)*. Utrecht.

NOTATION LIST

d_l	Effective depth to the longitudinal reinforcement
f_{cd}	Design concrete compressive strength
f_{ck}	Characteristic concrete compressive strength
f_{ctk}	Characteristic tensile splitting strength of the concrete
f_{tm}	Average tensile strength of the steel
f_{ym}	Average yield strength of the steel
A_s	Area of tension reinforcement
E_c	Modulus of elasticity of the concrete
F	Applied load
M_{Ed}	Acting bending moment
M_{Rd}	Bending moment capacity
UC	Unity check
ε_1	Principal strain
ε_{cr}	Cracking strain in post-processing of results
ε_{knn}	Cracking strain
φ	Diameter of reinforcement bar

Monitoring and Diagnostic Load Testing of a Damaged Railway Bridge

Ivan Duvnjak*, Domagoj Damjanović, Marko Bartolac, Marina Frančić Smrkić and Ana Skender

Structural Testing Laboratory, Department of Engineering Mechanics, Faculty of Civil Engineering, University of Zagreb, Zagreb, Croatia

This study presents a complex experimental research of a damaged steel railway bridge. Before the reconstruction, the elastic behavior of the material was evaluated using the hole-drilling strain gauge method of determining residual stresses at the relevant cross-sections. During the reconstruction project (lifting of the structure), a short-term monitoring system was installed at the critical cross-sections for continuous recording of strain. The aim was to evaluate the quality of the reconstruction intervention and prevent further damages. Following a successful reconstruction, a diagnostic load testing was performed according to Croatian standards. The purpose of the load testing (static and dynamic) was to evaluate the ability of the bridge to carry the design loads and calibrate the finite element models. During static load testing vertical displacement was measured as well as strain. Dynamic load testing of the bridge was performed in order to determine the main dynamic parameters of the structure and to calculate the dynamic factor. In order to select the appropriate measurement parameters and methods used during this experimental research it was necessary to consider the bridge type, materials and reconstruction or strengthening interventions. Especially, since this bridge was an example of insufficient inspection and maintenance during service. A well-designed monitoring and diagnostic load testing needed to be performed in order to obtain useful results for the decision makers involved.

Keywords: monitoring, reconstruction, diagnostic load testing, damaged railway bridge, residual strain, residual stress, static load testing, dynamic load testing

INTRODUCTION

The main purpose of load testing of bridges is to evaluate the performance of existing bridges. This category includes new bridges which are still not open for public, bridges that are already in service and bridges after reconstruction or strengthening. There are two main types of load testing of bridges used in practice, proof and diagnostic load testing. Proof load testing is very useful for the evaluation of bridges when information related to the capacity of the bridge is insufficient. For example, when plans or the results of a structural analysis are not available or when it is difficult to estimate the level of deterioration and material degradation in old bridges (Lantsoght et al., 2017b). The main objective is to check if the bridge can carry a certain load level without damage and fulfill the requirements of the code. The load levels used for the proof load testing are higher than the levels of diagnostic load testing (Lantsoght et al., 2017a). The determination of the target proof load includes multiplying nominal values of the traffic load with proof load factors. Significant efforts are made toward standardization of this type of load testing (Lantsoght et al., 2018).

Diagnostic load testing, on the other hand, is used to verify the assumptions made in analytical models related to the stiffness of the bridge. These models are usually simple linear elastic, three-dimensional finite element (FE) models (Lantsoght et al., 2017a). The differences between calculated and measured values are often due to an inaccurate representation of the geometry, boundary conditions and materials in FE models (Bagge et al., 2018). This type of load testing can also be used to evaluate if the bridge structure is in the elastic range, especially after a reconstruction or strengthening (Olaszek et al., 2014). Diagnostic load testing is usually performed prior to opening to the public as well as after a reconstruction or strengthening of the bridge. It is still a common practice in Croatia and has been so for decades. Existing bridges are tested according to the requirements of the Croatian standard HRN U.M1.046:1984 which is referred to in the Technical regulation for building structures (Official Gazette 17/17). The standard requires static load testing of all road bridges with the length $L \geq 15$ m and for all railway bridges with the length $L \geq 10$ m. The standard also requires dynamic load testing for all bridges. Prior to the actual load testing of the bridge it is necessary to draw up a load testing program which defines the methodology of testing. For that purpose, it is necessary to assess the project documentation and consider the bridge type, materials and reconstruction or strengthening interventions.

In order to meet future demands on the European railway network, i.e., increased loads and higher speeds it is important to collect information and upgrade the existing railway bridges. Developing new monitoring systems and field testing methods of railway bridges is of great importance (Olofsson et al., 2005). In recent years, several steel railway bridges underwent diagnostic load testing after strengthening in Croatia (Damjanović et al., 2016a,b; Marendić et al., 2017).

This paper presents useful methods of assessing the condition of a damaged steel railway bridge before, during and after reconstruction. In order to evaluate the elastic behavior of the material, a method of determining residual stresses by the hole-drilling strain gauge method was implemented (ASTM E837, 2013). Further, a short-term monitoring system was installed at critical cross-sections during the reconstruction of the bridge in order to measure strain. After the reconstruction of the bridge, a diagnostic load testing was performed together with the static and dynamic numerical analysis.

The article is structured as follows. The description of the railway bridge is given in Section Description of the Railway Bridge. The outline of the method of determining the residual stresses is given in Section Method of Determining the Residual Stresses with the results in Section Strain Measurement Results and the Calculation of Stresses. Measurement parameters and the assessment criteria for the diagnostic load testing according to the relevant standard are given in Section Measurement Parameters and Assessment Criteria According to the Standard. The measurement setup and the results are presented in Section Static Load Testing and Results for the static load testing and in Section Dynamic Measurements and Results for the dynamic load testing. Section Conclusions presents the conclusions.

DESCRIPTION OF THE RAILWAY BRIDGE

The double track railway bridge (Sesvete—Velika Gorica) over the river Sava in Zagreb was built in 1968. The length of the three spans over the river is $L = 34.6$ m $+ 65.9$ m $+ 34.6$ m $= 135.1$ m. The riveted steel superstructure of the bridge consists of two main I-section continuous girders spaced 9.1 m apart. The girder web depth is 3.8 m while the width and the thickness of the flanges are 690 and 80 mm, respectively. The cross girders are perpendicular to the axis, spaced 3.95 m apart with the web depth of 1.4 m. There are four 0.62 m high secondary longitudinal girders. The grade of steel is S235. The substructure of the bridge consists of reinforced concrete piers supported by reinforced concrete piles.

In March 2009, one of the piers lost its stability due to scour development during years of exploitation causing a permanent deformation of the bridge and the railway tracks (**Figure 1A**). At the distance of 8 m from the upstream bearing (S6) and 11 m from the downstream bearing (S6), a plasticity zone was developed in the middle span (**Figure 1B**). The upstream main girder deflected 1.6 m and the downstream main girder deflected 0.95 m. Furthermore, under the weight of the structure and the development of a new static system (continuous girder with a plastic hinge), one of the two main girders at the side span was lifted and no longer supported by the pier S4 (Duvnjak et al., 2018). This further increased the bending moment on the support S5 (**Figure 1D**). In addition to the vertical movement, the bridge suffered a horizontal shift and serious damage of the bottom secondary members. Following a detailed analysis and a provisional strengthening of the damaged pier, the reconstruction project of the bridge was developed. The reconstruction project was based on the fact that the plasticity zone was developed near the location where the initial bending moment was close to zero (Mujkanović et al., 2012) (**Figure 1C**). The stages of the reconstruction included the elevation of the bridge superstructure over the provisional piers to the original grade level, reconstruction of the hinge and finally, releasing the superstructure on permanent bearings. Numerical analysis was performed for all stages of the reconstruction and the results can be found in Mujkanović et al. (2012). During the lifting of the superstructure, an experimental research was performed based on strains and stresses at critical cross-sections.

MONITORING OF THE RAILWAY BRIDGE DURING RECONSTRUCTION

Method of Determining the Residual Stresses

The hole-drilling method is used to measure the magnitudes and distributions of principal residual stresses. This method involves attaching strain gauge rosettes to the surface, drilling a hole at the center of the gauges, and measuring residual strains caused by the relaxation of the material surrounding the drill-hole. **Figure 2** shows the stress state near the drilling hole. The hole radius is $2a$, and the stresses are σ_x and σ_y, while σ_1 and σ_2 are the radial and tangential stress caused by the hole drilling. The value α represents an angle between the stress σ_x and the radial stress σ_1.
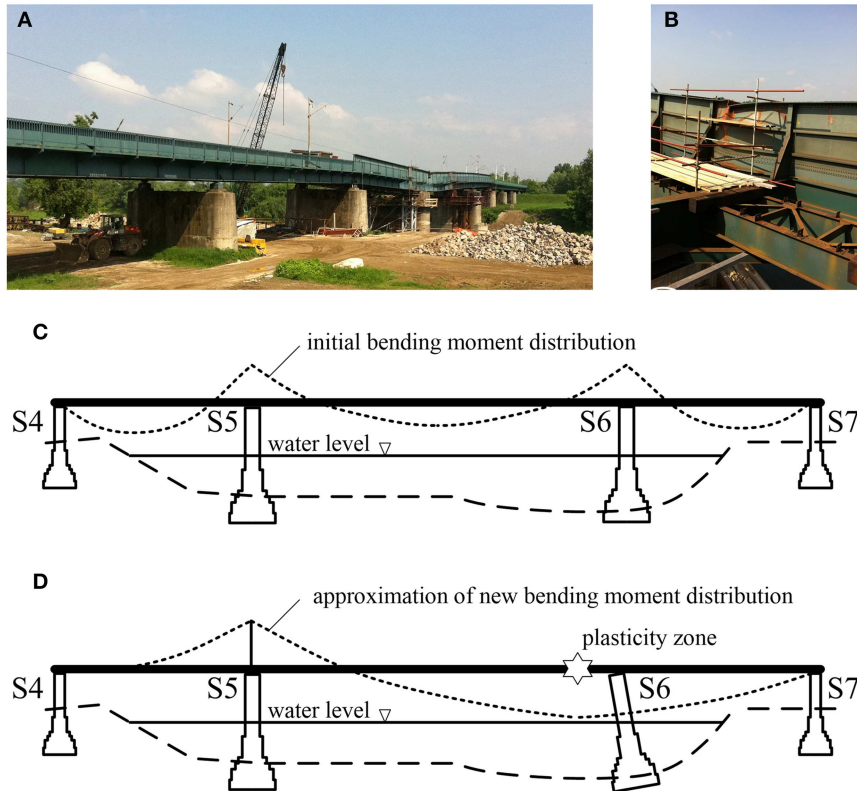
FIGURE 1 | (A) Damaged steel railway bridge; **(B)** plastic hinge on the upstream girder; **(C)** bending moment before damage; **(D)** approximation of bending moment after damage.
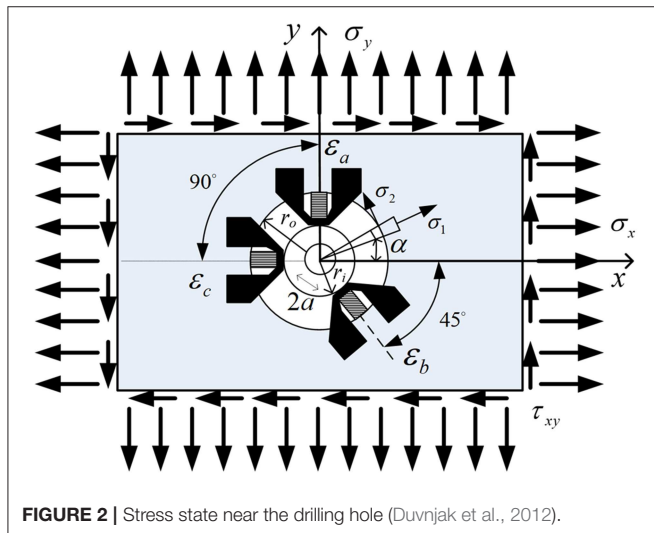

FIGURE 2 | Stress state near the drilling hole (Duvnjak et al., 2012).

The stresses are determined according to the following equations (Hoffman, 1989):

$$\sigma_{1,2} = -\frac{E}{4A}\left(\Delta\varepsilon_a + \Delta\varepsilon_c\right) \pm \frac{E}{4B}\sqrt{\left(\Delta\varepsilon_c - \varepsilon_a\right)^2 + \left(\Delta\varepsilon_a + \Delta\varepsilon_c - 2\varepsilon_b\right)^2} \quad (1)$$

where E is the modulus of elasticity of steel ($E = 2.1\cdot10^5$ MPa) and $\Delta\varepsilon_a$, $\Delta\varepsilon_b$, and $\Delta\varepsilon_c$ are measured residual strains in three different directions related to the initial values of the strain before the drilling.

The constants A and B are as given

$$A = \frac{a^2\left(1+\nu\right)}{2r_o r_i} \quad (2)$$

$$B = \frac{2a^2}{r_o r_i}\left[1 - \frac{a^2\left(1+\nu\right)\left(r_o^2 + r_o r_i + r_i^2\right)}{4r_o^2 r_i^2}\right] \quad (3)$$

where ν is the Poisson's ratio ($\nu = 0.3$), r_o is the outer and r_i is the internal radius of the measurement grid.

The angle α is determined according to the following equation (Ajovalasit et al., 2010):

$$\alpha = \frac{1}{2}\tan^{-1}\left(\frac{\Delta\varepsilon_c + \Delta\varepsilon_a - 2\Delta\varepsilon_b}{\Delta\varepsilon_c - \Delta\varepsilon_a}\right) \quad (4)$$

Strain Measurement Results and the Calculation of Stresses

The measurement of residual strains was performed using the hole-drilling method in order to calculate the residual stresses and evaluate the elastic behavior of the material in two

cross-sections. The critical (relevant) cross-sections were selected at the location of extreme values of the bending moment after damage (**Figure 1D**), i.e., at the location of the fixed bearing at pier S5 and adjacent to the plasticity zone and pier S6 (**Figures 3A,B**). The measurement was performed in order to exclude plastic deformation in relevant cross-sections. Residual strains were measured at the flanges of the upstream main I-section girder (R1 and R2) considering the more significant plastic deformation of that girder. Residual strain measurements recorded during the drilling of the hole and calculated stresses according to Equation (1) are presented in **Figure 4A**. Under the assumption that the neutral axis will occur at the mid-depth of the girder, the estimated stress distribution in the critical cross-section 1-1 derived from the measured values of residual strain is shown in **Figure 4B**.

During the reconstruction, the main girders were gradually lifted with hydraulic jacks over a period of 3 days in steps of 5–10 cm. During that time, strain was measured. The measurement setup (4 measuring points on each girder) for the relevant cross-sections is shown in **Figure 3C** (cross-section 1-1) and **Figure 3D** (cross-section 2-2). Every lift of a main girder caused a "jump" in values of strains and consequently calculated stresses (**Figure 5**). The maximum stresses at all measuring points were below the yield strength of steel.
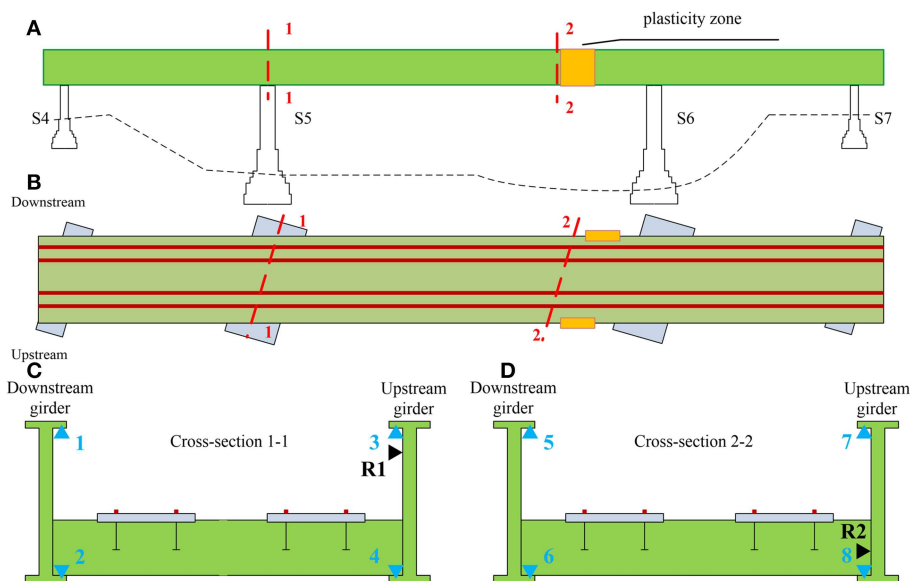

FIGURE 3 | Strain measuring points: **(A)** longitudinal section of the bridge over the river; **(B)** plan view of the bridge; **(C)** cross-section 1-1; **(D)** cross-section 2-2.
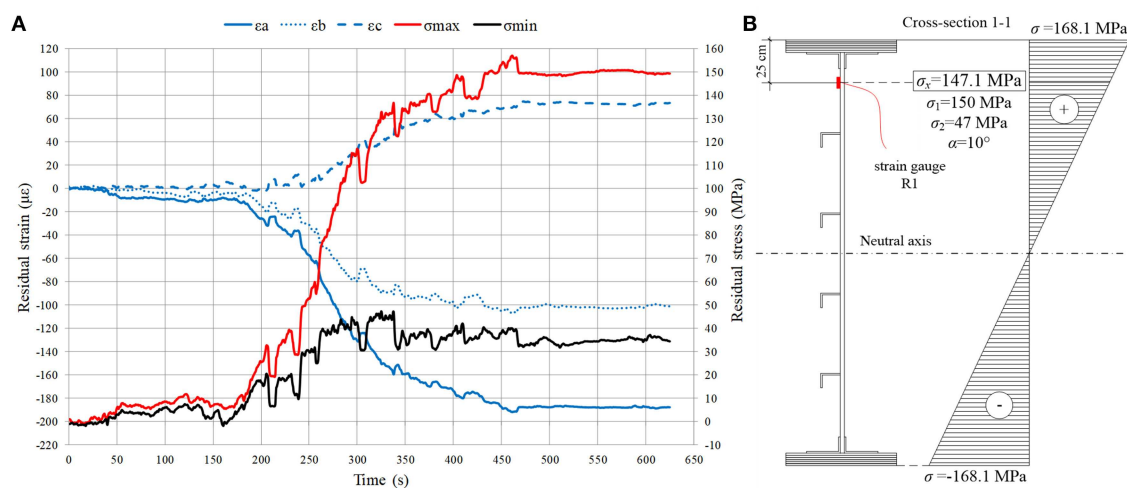

FIGURE 4 | Cross-section 1-1: **(A)** Measured residual strains and calculated stresses; **(B)** Estimated residual stress distribution.
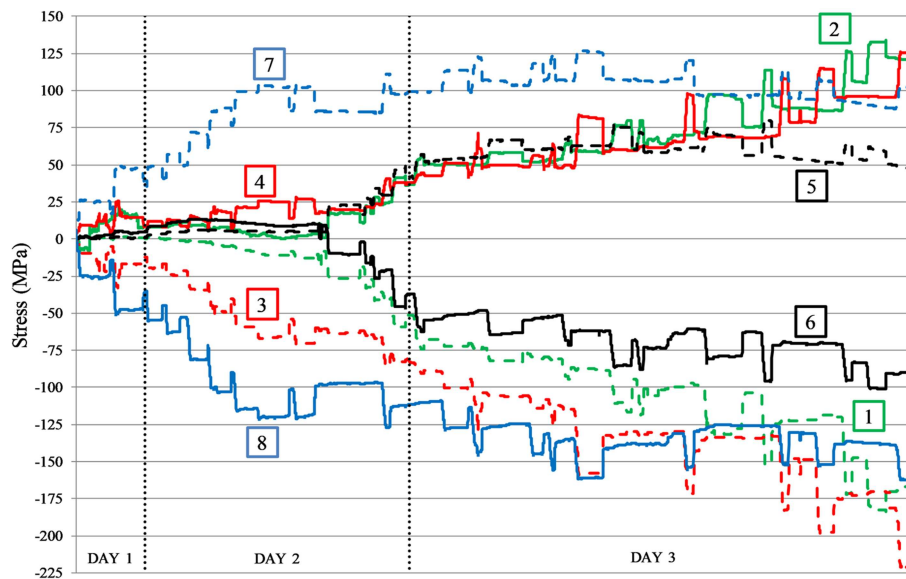
FIGURE 5 | Calculated stresses at all measuring points (reconstruction).

DIAGNOSTIC LOAD TESTING OF THE RAILWAY BRIDGE AFTER RECONSTRUCTION

Following a successful reconstruction of the pier S6 and the bridge superstructure, a diagnostic load testing was performed according to the requirements of the Croatian standard HRN U.M1.046. The standard requires static and dynamic load testing of the bridge in order to calibrate FE models and evaluate the ability of the bridge to carry the design loads without damage. One of the main objectives of this type of load testing is to correctly estimate the traffic load distribution in order to achieve service conditions. Before the actual load testing of the bridge it was necessary to draw up a load testing program which defines the methodology of testing with detailed description of the loading phases and measurement parameters as well as the corresponding measuring points (Rak et al., 2011).

An essential part of the load testing program are the results of the numerical analysis performed with the FE software package SOFiSTiK. The superstructure of the bridge was modeled using beam elements with linear elastic behavior. All connections between the main and cross members were modeled as rigid. The boundary conditions (supports) were modeled as pinned for pier S6 and as a roller in the longitudinal direction of the bridge for the piers S4, S6, and S7. The initial FE model of the bridge was modeled to select the required load of the test locomotive and positions of the locomotives in order to produce the maximum effect on the bridge (displacements and internal forces). The Load Model LM 71 was selected as relevant for normal rail traffic on mainline railways. The selected model comprises of a uniformly distributed load and concentrated load as defined in design codes (HRN EN 1991-2, 2012). The results of the static numerical analysis are shown as internal forces and displacements under test loads V_{stat} and the design traffic loads V_n. These results are used to evaluate the load testing efficiency U given by the following equation (HRN U.M1.046, 1984)

$$U = \frac{V_{stat}}{V_n \cdot \varphi} \tag{5}$$

where φ is the design dynamic factor ($\varphi = 1.0$). In this study, the value of the load testing efficiency was in the range $0.5 \leq U \leq 1.0$ which is considered as acceptable. The results of the dynamic numerical analysis are the main dynamic parameters, i.e., natural frequencies and mode shapes.

The numerical model of a bridge is usually calibrated by changing the material and geometrical properties of the bridge (area, inertia, modulus of elasticity, etc.). The acceptable criterion is to reach the difference between measured (site) deflections and analytical values within ±10% for steel bridges. After site tests, the model is slightly updated by changing an initial modulus of elasticity (from $E = 200$ GPa to $E = 210$ GPa). Afterwards, the diagnostic assessment was carried out by using the updated model.

Measurement Parameters and Assessment Criteria According to the Standard

According to the Croatian standard HRN U.M1.046., the following measurements are performed during the static load testing of railway bridges:

- measurement of the vertical displacement in the middle of each span,
- measurement of the displacement of the supports,
- strain measurement at critical cross-sections,

- measurement of residual displacements and strains after unloading.

The requirement for the measured values of displacements is that they are less or equal to theoretical/numerical values. Measured residual displacements should be <15% of the maximum measured value at the same measuring point for railway bridges.

The following measurements are performed during the dynamic load testing of railway bridges:

- Measurement of the vertical displacement in the middle of selected spans during the crossing of vehicles
- Measurement of dynamic parameters of the structure.

The dynamic behavior of the bridge is considered acceptable if the measured natural frequencies are in accordance with the theoretical/numerical values and if the dynamic factor is in accordance with the design value.

Static Load Testing and Results

Static load testing of the bridge was performed by using 6 electric locomotives in 10 loading and 6 unloading phases. The average mass of the locomotives was 80 t (±1.6 t). The locomotives were positioned symmetrically and asymmetrically in different spans in order to obtain maximum internal forces and displacements of the main carrying structural elements (**Figure 6**). During the static load testing, vertical displacements of the bridge were measured using a method of geometric and trigonometric leveling. Overall, there were 13 measuring points in the middle and at the quarter of each span as well as above the supports along two parallel lines coinciding with the main girders (**Figure 7A**). The maximum measured vertical displacements in the middle of the span during different loading phases are compared to the results of the numerical analysis with actual test loads in **Table 1**. The residual displacements measured during the unloading phases are also shown in **Table 1**. Calculated bending
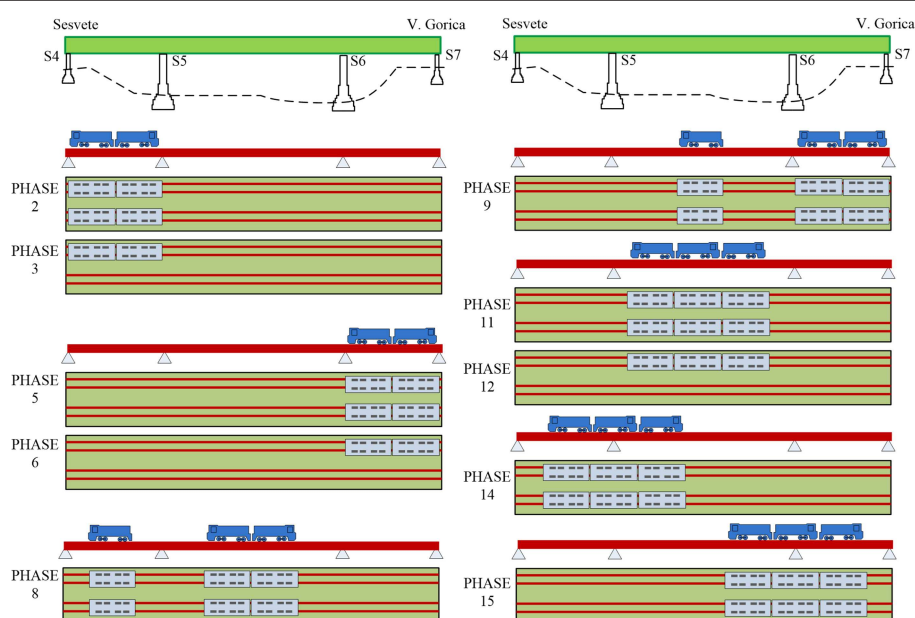
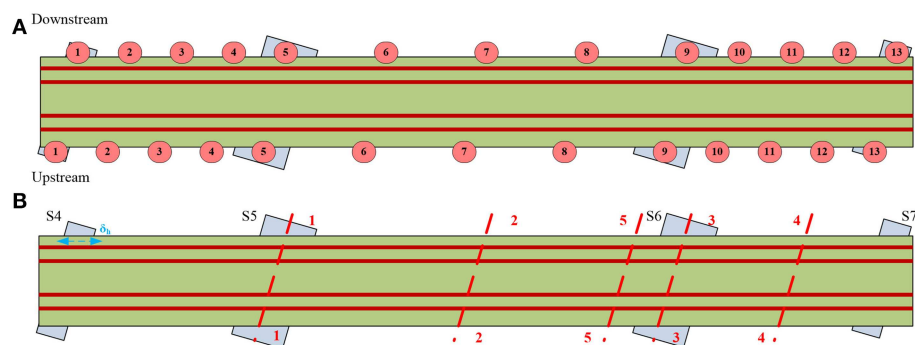

FIGURE 6 | Static load testing phases.

FIGURE 7 | Measuring points: **(A)** vertical displacement; **(B)** strain.

moments and displacements obtained from the loading phase 11, i.e., maximum test load in the central span are shown in **Figure 8**.

Strains were measured with a total of 22 LVDT sensors in five cross-sections and the longitudinal displacement of the main girder was measured with an additional LVDT sensor on pier S4 (**Figure 7B**). The gauge length of the LVDT sensors was 200 mm and a data acquisition system (HBM MGCplus) was used to continually record the data. Four LVDT sensors were located at the flanges of the main girders in the middle of the spans (cross-sections 2-2 and 4-4) and above the piers S5 and S6 (cross-sections 1-1 and 3-3). There were two LVDT sensors on the secondary longitudinal girder near pier S6 and on the cross girder in the middle of the span S5-S6. Strains were also measured on the main girders with the replaced web plates (damaged area) in cross-section 5-5. Strain measurements in the middle

of the central span (cross-section 2-2) are shown in **Figure 9**. During the loading phase 11, at the measuring points 6 and 8 the values of measured strains were 211 με and 228 με, respectively. Calculated stresses at the same measuring points were 44.35 MPa and 47.94 MPa and in accordance with the numerical value of 47 MPa.

Dynamic Measurements and Results

Dynamic measurements during diagnostic load testing of the bridge was performed in two phases. In the first phase, main dynamic parameters of the structure (i.e., natural frequencies, mode shapes, damping ratios) were determined by means of the Operational Mode Analysis (OMA) (Zhang and Brincker, 2005). The measurement was performed during ambient excitation of the bridge which has the characteristics of Gaussian white noise process. Accelerations were measured in 6 measuring points in the vertical direction on both main girders, in the middle and at the quarters of the central span. The measuring points were determined in a way to ensure a quick execution of the measurement and on the other hand to provide enough DOF's for identification of main vertical and torsional mode shapes of the bridge which were used for the calibration of the FE model. High sensitivity accelerometers, 10 000 mV/g, were used during the measurements (B&K 8340 and PCB 393B31) together with data acquisition system B&K 3560-C and appropriate software. The data acquisition was performed using sampling frequency of 400 Hz, over 64 s which resulted in 25,600 captured samples for each accelerometer. Processing of the measured data consists of the Fast Fourier Transform (FFT) of time domain recordings, determination of Power Spectral Density (PSD) and Singular Value Decomposition of PSD matrices. Natural frequencies were determined as resonance peaks from the diagram of singular values of the PSD matrices (**Figure 10A**). Mode shapes were estimated as first singular vectors at the resonance peak and damping ratios were determined using the Inverse Discrete Fourier Transform (IDFT) of the estimated SDOF functions (**Figure 10B**). Measured and numerical values

TABLE 1 | The comparison between maximum measured and numerical vertical displacement.

Loading/unloading phase	Measured vertical displacement (mm)	Numerical vertical displacement (mm)
2	12.5	14.2
3	9.0	8.7
4	0.0	–
5	13.5	14.1
6	9.5	9.0
7	1.0	–
8	36.5	39.0
9	14.0	18.8
10	2.0	–
11	54.0	55.2
12	37.0	38.0
13	2.0	–
14	9.0	10.9
15	9.5	10.9
16	1.0	–
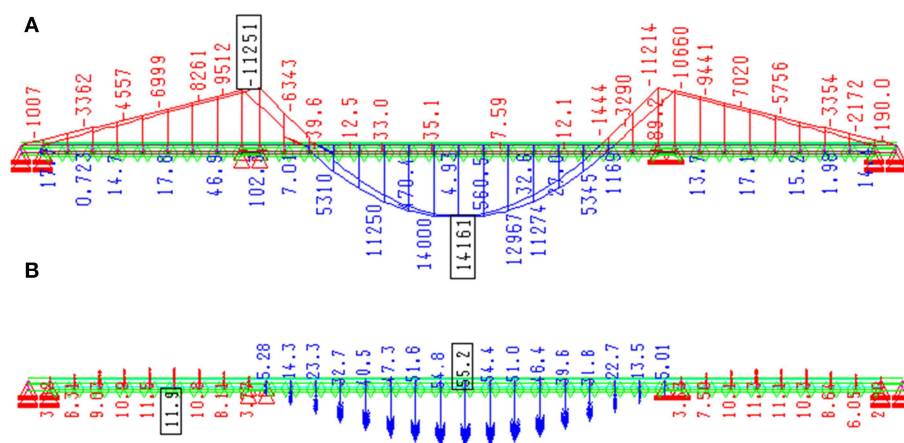
FIGURE 8 | Calculated values—phase 11; **(A)** bending moment; **(B)** vertical displacement.
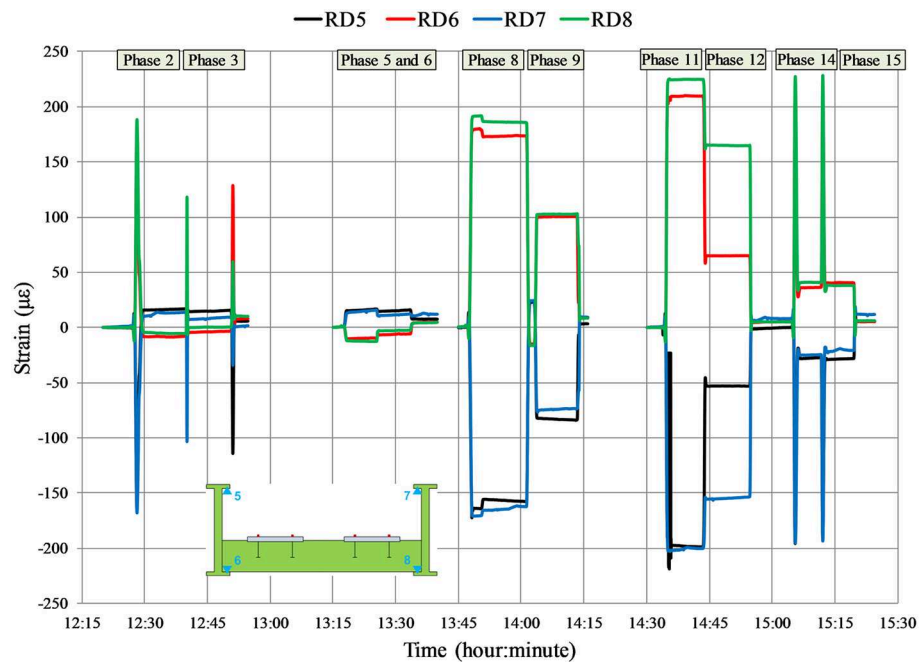
FIGURE 9 | Strain measurements in cross-section 2-2.
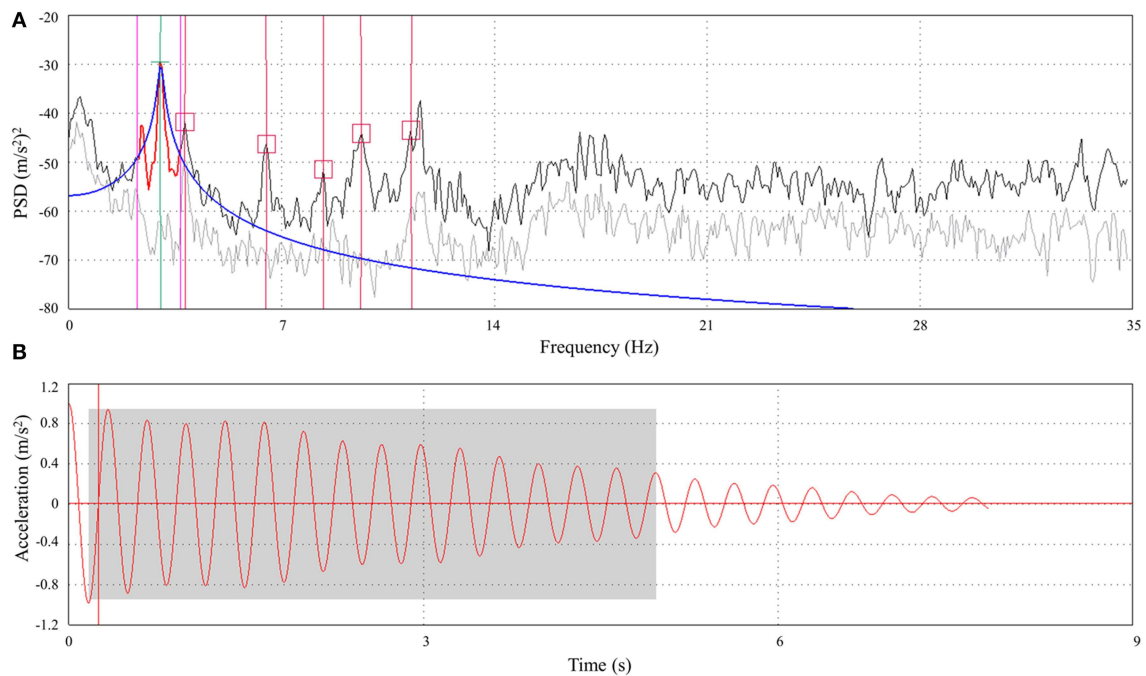
FIGURE 10 | Determination of dynamic parameters: (A) singular values of PSD matrices–1st natural frequency; (B) damping function–1st mode shape (Frančić et al., 2012).

of natural frequencies as well as the measured damping ratios are given in **Table 2**, six modes were determined experimentally. First two mode shapes obtained experimentally are compared to the corresponding numerical mode shapes in **Figure 11**.

During the second phase of the dynamic load testing, the increments of the vertical dynamic displacement caused by locomotives crossing the bridge at different speeds were measured. Based on the dynamic displacement y_{dyn}, the dynamic

factor φ is determined as given

$$\varphi = \frac{y_{dyn} + y_{stat}}{y_{stat}} \qquad (6)$$

where y_{stat} is the numerical vertical displacement under static loads.

The dynamic displacement was measured during the crossing of one or two locomotives over the bridge at different speeds (20, 40 and 60 km/h), but also during braking of the locomotives (one or two) within the central span (∼20–40 km/h). The vibrometer HBM SMU and the digital oscilloscope connected to a personal computer were used to measure the dynamic displacement on both main girders in the middle of the central span (**Figure 12A**). The measured values of the dynamic displacement and the calculated values of the dynamic factor are given in **Table 3**. During the dynamic load testing, strains were measured at the flanges of the main girders in cross-sections 1-1 and 2-2 according to **Figure 7**. Strain measurements during the crossing of two locomotives over the bridge at 60 km/h are shown in **Figure 12B**. The values of strain measured during the dynamic load testing are lower than the values measured during the static load testing.

CONCLUSIONS

This article presents a complex experimental research of a damaged steel railway bridge before, during and after

reconstruction. Both main girders underwent plastic deformation near the damaged pier which represented a challenge. It was necessary to evaluate the state of the material before the reconstruction as well as the quality of the reconstruction intervention. In order to evaluate the elastic behavior of the material, the hole-drilling strain gauge method of determining residual stresses was implemented. Two critical cross-sections were selected at the location of extreme values of the bending moment after damage. Residual strains measured on the more damaged upstream main girder, were used for the calculation of residual stresses. Calculated stresses were below the yield strength of steel. A monitoring system was also installed at the critical cross-sections during the lifting of the bridge over a period of 3 days. Stresses were calculated based on strain measurements and the bridge behaved elastically at the critical cross-sections under reconstruction loading conditions.

After reconstruction, diagnostic load testing was used to verify the assumptions made in FE models by comparing measured and numerical values. Static load testing was performed in 10 loading phases. Values of maximum measured vertical displacements (**Table 1**) were in the expected range and in accordance with numerical values. Normal stresses were calculated at all measuring points based on measured values of strains and the values were in accordance with calculated values. After the unloading of the bridge, the residual vertical displacements and strains were negligible which means that the structure was in the elastic range during static loading. Based on the experimental results of deflections and strains during the load testing it can be evaluated that the load carrying capacity of the bridge after reconstruction is satisfactory. The measured deflections during the significant loading phases are lower than those determined in numerical simulations and the values of stresses in the critical cross sections of the bridge measured during the load testing are not exceeding 50 MPa. Dynamic load testing of the bridge was performed in order to determine the main dynamic parameters of the structure and to calculate the dynamic factor. The measurement was carried out during ambient excitation in order to determine the dynamic parameters and during the crossing of one or two locomotives over the bridge at different speeds in order to determine the dynamic factors. The dynamic response of the superstructure was realistic and as expected.

TABLE 2 | Values of measured and numerical natural frequencies and damping ratios (Damjanović et al., 2011).

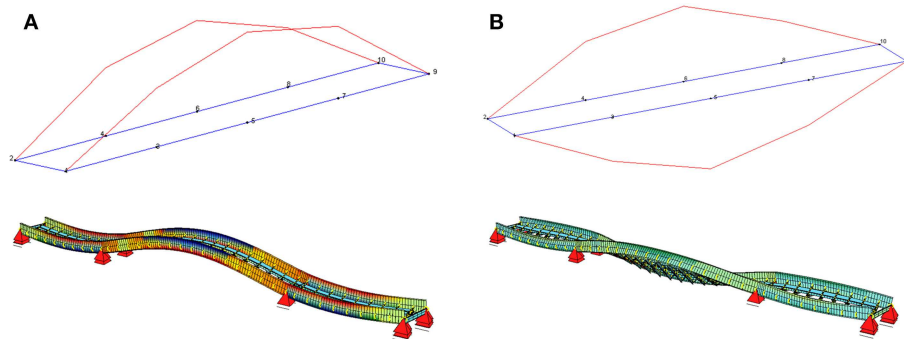| Measured natural frequency (Hz)	Numerical natural frequency (Hz)	Measured damping ratio (%)
3.03	2.84	1.62
3.82	3.69	1.07
6.41	6.52	0.90
8.47	8.34	0.74
9.50	9.38	0.80
11.35	10.82	0.65

FIGURE 11 | Experimental and numerical mode shapes: **(A)** 1st mode shape; **(B)** 2nd mode shape.
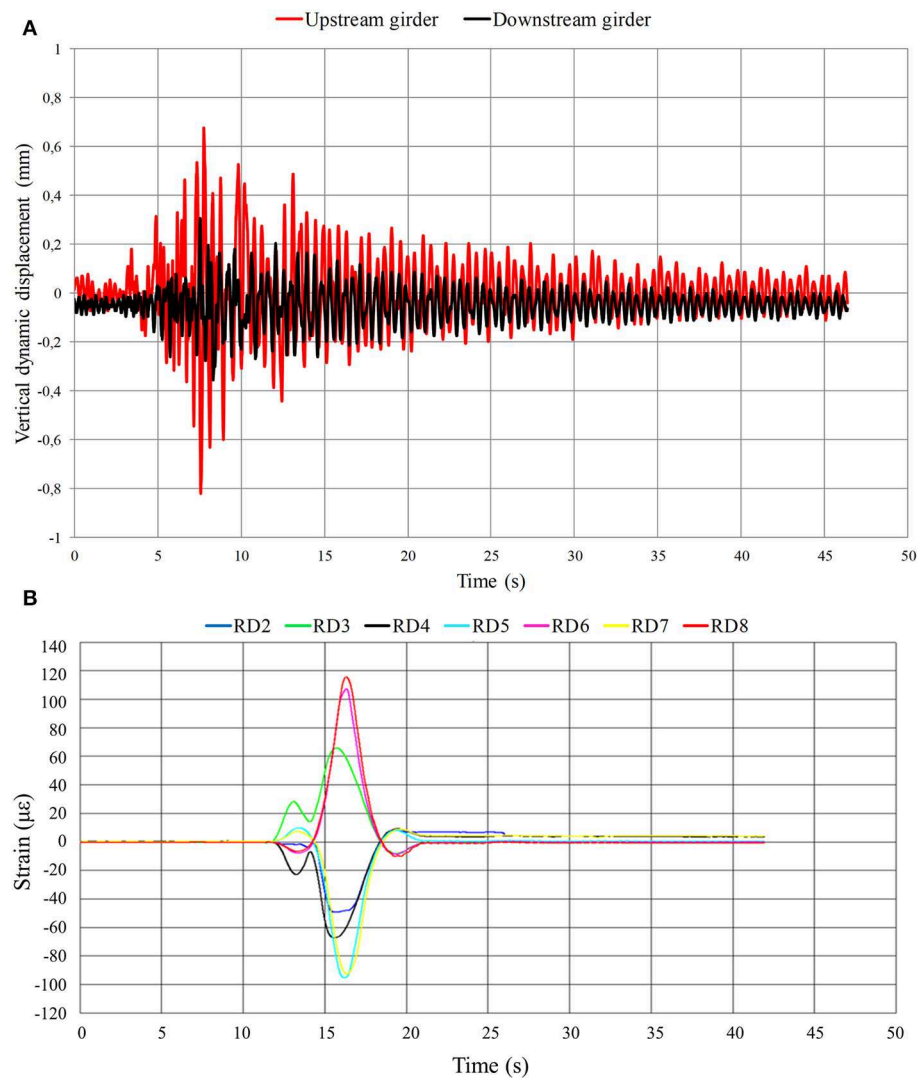
FIGURE 12 | Dynamic load testing (2 locomotives at 60 km/h): **(A)** vertical dynamic displacement in the middle of the central span; **(B)** strain in cross-sections 1-1 and 2-2.

TABLE 3 | Measured dynamic displacements and calculated dynamic factors (Damjanović et al., 2011).

Number of locomotives	Speed (km/h)	Dynamic displacement (mm)	Dynamic factor φ
1	20	0.68	1.042
($y_{stat} = 16.3$ mm)	40	1.08	1.066
	60	1.20	1.073
2	20	0.72	1.029
($y_{stat} = 24.6$ mm)	40	1.07	1.043
	60	1.46	1.059

Measured natural frequencies were in accordance with the calculated values (**Table 2**). Experimental and numerical mode shapes were also in accordance (**Figure 11**). Calculated values of the dynamic factors were in accordance with the design value. After the completion of the diagnostic load testing no damages were detected on the bridge. Based on the load testing results it was concluded that the railway bridge (Sesvete—Velika Gorica) is in accordance with the requirements of the project and the provisions of the Croatian standard HRN U.M1.046.

Monitoring and diagnostic load testing can serve as a method of evaluating the accordance of the structure with the project requirements, the quality of the reconstruction and the ability of the renewed bridge to carry the design loads. It is necessary to consider the bridge type, materials and reconstruction or strengthening interventions. The selection of appropriate measurement parameters and methods for a specific bridge is of great importance, in order to obtain useful results for the decision makers involved.

DATA AVAILABILITY

All datasets generated for this study are included in the manuscript and/or the supplementary files.

AUTHOR CONTRIBUTIONS

All authors have contributed to the contents within this paper. ID prepared the monitoring system and the numerical model as well as analyzed the measurement results. MB prepared the first draft of the paper and analyzed the residual strain results. DD prepared the static load testing and analyzed the measurement results. MF analyzed the dynamic measurement results. The literature review and the final version of the paper was mostly performed by AS. All authors contributed to the manuscript revision as well as read and approved the submitted version.

FUNDING

REFERENCES

Ajovalasit, A., Scafidi, M., Zuccarello, B., Beghini, M., Bertini, L., Santus, C., et al. (2010). "The Hole-drilling strain gauge method for the measurement of uniform or non-uniform residual stresses," in *AIAS Working Group on Residual Stresses.* Florence.

ASTM E837 (2013). *Standard Test Method for Determining Residual Stresses by the Hole-Drilling Strain-Gage Method.* West Conshohocken, PA: ASTM Standards.

Bagge, N., Popescu, C., and Elfgren, L. (2018). Failure tests on concrete bridges: have we learnt the lessons? *Struc. Infrastruc. Eng.* 14, 292–319. doi: 10.1080/15732479.2017.1350985

Damjanović, D., Košćak, J., Bartolac, M., Duvnjak, I., Marendić, A., and Paar, R. (2016a). "Measurements during the testing of steel railway bridges," in *Proceedings of the International Symposiun on Engineering Geodesy - SIG 2016, 113–26.* Varaždin: Croatian Geodetic Society.

Damjanović, D., Košćak, J., Duvnjak, I., and Bartolac, M. (2016b). "Static and Dynamic Testing of Steel Railway Bridge 'Sava.'" in *Road and Rail Infrastructure IV, Proceedings of the Conference CETRA 2016*, ed S. Lakušić, Department of Transportation, Faculty of Civil Engineering, University of Zagreb, (Zagreb).

Damjanović, D., Rak, M., Duvnjak, I., Bartolac, M., and Frančić, M. (2011). *Load Testing Report On Railway Bridge.* Sava Jakuševac: Structural Testing Laboratory, Faculty of Civil Engineering, University of Zagreb.

Duvnjak, I., Bartolac, M., Nilimaa, J., Sas, G., Blanksvard, T., Taljste, B., et al. (2018). "Lessons learnt from full-scale tests of bridges in Croatia and Sweden," in *40th IABSE Symposium: Tomorrow's Megastructures/Cremona, Christian.* Zürich : IABSE. Nantes, France.

Duvnjak, I., Rak, M., Krolo, J., Bartolac, M., and Frančić, M. (2012). "Experimental investigation of the collapsed steel bridge deformation," in *Proceedings of the 29th Danubia-Adria-Symposium on Advances in Experimental Mechanics,* ed Miloslav Ognjanović, Belgrade, Serbia: Serbian Society of Mechanics, Faculty of Mechanical Engineering, University of Belgrade, 26–27.

Frančić, M., Damjanović, D., and Rak, M. (2012). "Testing of the railway bridge 'Sava Jakuševac' after reparation," in *Proceedings of the 29th Danubia-Adria-Symposium on Advances in Experimental Mechanics, edited by Miloslav Ognjanović,* Serbian Society of Mechanics, Faculty of Mechanical Engineering, University of Belgrade (Belgrade), 24–25.

Hoffman, K. (1989). *An Introduction to Measurements Using Strain Gages.* Darmstadt: Hottinger Baldwin Messtechnik GmbH.

HRN EN 1991-2 (2012). *Eurocode 1: Actions on Structures - Part 2: Traffic Loads on Bridges.* Zagreb: Croatian Standards Institute.

HRN U.M1.046 (1984). *Load Testing of Bridges.* Zagreb: Croatian Standards Institute.

Lantsoght, E. O. L., Koekkoek, R. T., Hordijk, D., and de Boer, A. (2018). Towards standardisation of proof load testing: pilot test on viaduct Zijlweg. *Struc. Infrastruc. Eng.* 14, 365–380. doi: 10.1080/15732479.2017.1354032

Lantsoght, E. O. L., Koekkoek, R. T., van der Veen, C., Hordijk, D. A., and de Boer, A. (2017a). Pilot proof-load test on viaduct de beek: case study. *J. Bridge Eng.* 22:05017014. doi: 10.1061/(ASCE)BE.1943-5592.0001131

Lantsoght, E. O. L., van der Veen, C., de Boer, A., and Hordijk, D. A. (2017b). State-of-the-art on load testing of concrete bridges. *Eng. Struc.* 150, 231–41. doi: 10.1016/j.engstruct.2017.07.050

Marendić, A., Paar, R., and Damjanović, D. (2017). Measurement of bridge dynamic displacements and natural frequencies by RTS. *J. Croatian Assoc. Civil Eng.* 69, 281–294. doi: 10.14256/JCE.1804.2016

Mujkanović, N., Vlašić, A., and Šavor, Z. (2012). "Rehabilitation of Railroad Bridge 'Sava Jakuševac.'" in *Construction of Transport Infrastructure,* ed S. Lakušić (Zagreb: Faculty of Civil Engineering, University of Zagreb).

Olaszek, P., Łagoda, M., and Casas, J. R. (2014). Diagnostic load testing and assessment of existing bridges: examples of application. *Structure and Infrastructure Engineering Maintenance, Management, Life-Cycle Design and Performance* 10, 834–842. doi: 10.1080/15732479.2013.772212

Olofsson, I., Elfgren, L., Bell, B., Paulsson, B., Niederleithinger, E., Jensen, J. S., et al. (2005). Assessment of european railway bridges for future traffic demands and longer lives – EC project 'Sustainable Bridges.' *Struc. Infrastruc. Eng.* 1, 93–100. doi: 10.1080/15732470412331289396

Rak, M., Damjanović, D., Duvnjak, I., Bartolac, M., and Frančić, M. (2011). *Load Testing Program On Railway Bridge.* Sava Jakuševac: Structural Testing Laboratory, Faculty of Civil Engineering, University of Zagreb.

Zhang, L., and Brincker, R. (2005). "An overview of operational modal analysis: major development and issues," in *Proceedings of the 1st International Operational Modal Analysis Conference,* Aalborg University (Copenhagen), 179–90.

Field Testing of a Prestressed Concrete Bridge With High Performance and Locally Developed Ultra-High Performance Concrete Girders

Turki S. Alahmari[1]*, Chris S. Kennedy[2], Alain M. Cuaron[1], Brad D. Weldon[1] and David V. Jáuregui[1]

[1] Department of Civil Engineering, College of Engineering, New Mexico State University, Las Cruces, NM, United States,
[2] Stubbs Engineering Incorporated, Las Cruces, NM, United States

Recent research has developed mixture proportions for ultra-high performance concrete (UHPC) using materials primary local to New Mexico, United States of America (USA). In 2017, a two-span bridge was constructed in Anthony, New Mexico, USA consisting of prestressed girders using the locally developed non-proprietary UHPC, for span one, and high performance concrete (HPC), for the second span. Field tests were conducted on the bridge ~9 months apart to investigate the performance and behavior of the UHPC and provide baseline data for future studies and condition evaluation of the bridge. The load tests consisted of various load configurations utilizing up to four trucks weighing 267 kN on average. The load paths were designed to maximize strains along the length of the bridge and investigate transverse load distributions between girders. The measured results provide a comparison of the behavior and performance of the UHPC and the HPC girders and were also compared to the American Association of State Highway and Transportation Officials (AASHTO) predicted behaviors. This study is one of the first that compares HPC and non-proprietary UHPC bridge performance subjected to the same environmental conditions and vehicular loading. The findings of the study will aid in the development of recommendations incorporating UHPC into design provisions as well as provide meaningful information of the short and long-term performance between the two materials including durability and load distribution.

Keywords: diagnostic load test, ultra-high performance concrete, high performance concrete, strain measurement, load distribution

INTRODUCTION

Ultra-high performance concrete (UHPC) is an increasingly utilized material that provides high compressive strengths and advanced durability properties. Typically including fiber reinforcement, UHPC provides significantly increased post-cracking strength and ductility, allowing for the reduction or elimination of conventional mild steel reinforcement in structural members. The advantages to structural design, offered by the advanced mechanical and durability properties of UHPC, include the potential for longer lifespans and corresponding reductions in lifecycle

economic impacts. Additionally, UHPC allows for smaller, lighter structural members that require less structural detailing, and facilitate more rapid construction and reduced service-life maintenance (Ahlborn et al., 2011).

Proprietary UHPC mixture proportions are currently available in the United States of America (USA), however, the lack of standardized domestic design specifications and high material costs have limited the widespread use of UHPC. The USA Federal Highway Administration (FHWA) has fostered research to provide a greater understanding of UHPC material properties and promote the use of this advanced structural material (Graybeal, 2008). Research has been focused primarily on commercially available products, although, the use of non-proprietary mixture proportions in structural applications is being investigated in different states of the USA.

Non-proprietary UHPC mixture proportions utilizing unique mixing procedures, curing regimens, and materials typical of precast production and primarily local to New Mexico (NM) have been developed. The resulting material possesses the superior mechanical and durability properties characteristic of UHPC (Muro-Villanueva et al., 2012; Weldon et al., 2012). More recent research has focused on the experimental testing of full-scale structural components and implementation of the non-proprietary UHPC in a local precast-prestressed bridge (Taylor et al., 2013; Giesler et al., 2016; Manning et al., 2016; Giesler et al., 2018; Visage et al., 2019). Based on the results of an extensive research program, the design and construction of the first non-proprietary UHPC bridge in New Mexico were successfully completed in 2017. The bridge is a two-span structure and is fabricated with non-proprietary UHPC (145 MPa) girders for span 1, and conventional high performance concrete (HPC, 65.5 MPa) girders, typical of bridge construction in New Mexico, for span 2. The design and behavior of this non-proprietary UHPC are being validated through short-term and long-term strain monitoring of the bridge. This study reports on the first load tests conducted on the bridge following construction.

To evaluate the behavior of the two-span bridge, the superstructure was equipped with external strain gauges and load tested. In early 2017, a diagnostic load test under a slow moving truck load was completed and ∼9 months later a diagnostic test under incremental, static truck loads was conducted on the bridge in 2018. The diagnostic test using a slow moving load, referred to as stage 1 loading, consisted of one truck moving at ∼8 km/h across the bridge along six load paths. Each path was designed to maximize the response of a single girder and was used to gain an initial understanding of the bridge response and provided guidance for the tests under multiple truck loads. The diagnostic test using incremental static loads, referred to as stage 2 loading, involved the application of the maximum feasible load using up to four trucks statically along several load paths to maximize the response of the bridge. This paper presents the results of the stage 1 and stage 2 load tests conducted on the bridge and compares the responses between the UHPC and HPC spans. Additionally, the measured response of the bridge is compared to the design-based estimated behavior.

BACKGROUND

UHPC is an advanced construction material that provides new opportunities for the future of highway infrastructure. This class of concrete has enhanced properties that address specific problems for highway bridge infrastructure, such as increased service life through improved durability and tensile ductility. Initial material development and structural testing of UHPC began more than two decades ago. The first UHPC traffic bridge was constructed in 2001 in the France's Drome region (Hajar et al., 2004). The first field deployment of UHPC in the USA was the construction of a prestressed concrete girder bridge in Wapello County, Iowa in 2006 (Graybeal, 2008). Since being introduced, more than 100 bridges (motorway and pedestrian) have incorporated UHPC in one or more components including shear keys, overlays, and joint connections (Graybeal, 2010; Brühwiler and Denarié, 2013; Voo et al., 2014; Yuan and Graybeal, 2016).

Proprietary UHPC has been implemented in different applications throughout the world. However, the high cost of the materials, a lack of design code provisions, and low industry familiarization with the material have limited its use, particularly in the USA. With the intention of improving the economic impact and increase sustainability, Weldon et al. (2012) developed and tested non-proprietary UHPC using materials local to New Mexico that has mechanical and durability properties similar to commercially available products. Furthermore, the use of familiar material constituents makes implementation into precast plants, ready-mix applications, and construction practices simpler.

Development of Local UHPC
Mixture Proportions

Allena (2010) investigated the use of material constituents local to New Mexico for the development of UHPC. Mixture proportions included fine aggregate, Type I/II Portland cement, silica fume, high-range water-reducing admixture (HRWRA), and a dosage of steel fibers. To increase sustainability and reduce cost, Lyell (2011) replaced a portion of silica fume with Class F fly ash. Final optimization was conducted by Weldon et al. (2012) by increasing the size and quantity of the aggregates. The final mixture proportions used a fine aggregate with a 4.76 mm nominal top size. Greater economy was achieved by reducing labor costs associated with tedious sieving of fine aggregates without negative effects on the mechanical properties of the UHPC. High strength steel fibers were provided at 1.5% by volume. The UHPC had a design compressive strength of 146 MPa.

Laboratory Testing

Investigation of the flexural behavior of locally developed non-proprietary UHPC began with a parametric study in which small-scale specimens were tested in flexure (Manglekar et al., 2016; Visage et al., 2019). The results showed favorable potential for UHPC made with local materials and research moved to the implementation of UHPC in precast/prestressed

applications. Flexural testing of large-scale prestressed beams by Giesler et al. (2016, 2018) was conducted to further verify the flexural behavior of non-proprietary UHPC and continue the development of structural design models. The scope of the research included modifications to the curing regimen and trial batching for implementing UHPC into precast plant production. Three prestressed concrete beam specimens were designed according to AASHTO (2012) for flexure with modifications made for the improved material properties of UHPC including changes to the modulus of elasticity, compressive strength, and tensile strength. Flexural

testing validated the designs. Manning et al. (2016) designed two full-scale prestressed girders; one using conventional HPC typical of current New Mexico bridge design, and the second designed using the locally developed UHPC. Both sections were designed to provide equal capacities and thus, flexural investigations of the sections provided a direct comparison of the behavior and performance of the two types of concrete. The UHPC girder, with a reduced cross-section and reduced shear reinforcement, provided the same capacity, equal stiffness, and improved post-cracking behavior compared to the HPC girder.

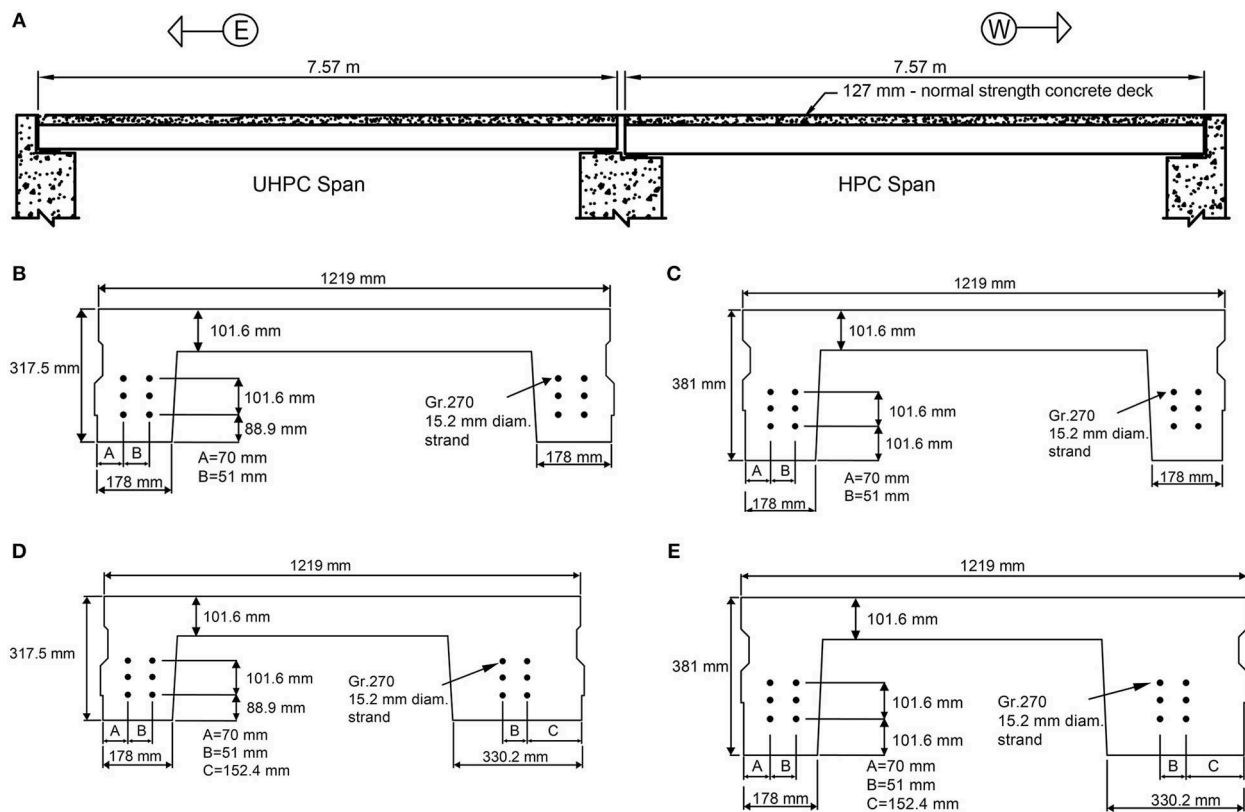FIGURE 1 | Bridge 9706 **(A)** during construction, **(B)** at completion.

FIGURE 2 | Bridge 9706 **(A)** profile, **(B)** UHPC interior girder, **(C)** HPC interior girder, **(D)** UHPC edge girder, and **(E)** HPC edge girder.

Field Testing

Load testing is a proven field method to evaluate the structural capacity, construction quality, and effectiveness of new materials used for bridge construction. The American Association of State Highway and Transportation Officials (AASHTO) recommends load testing to evaluate the *in-situ* bridge response and behavior under loading (AASHTO, 2000). The goal of a load test is to evaluate a bridge's structural response without causing damage to the structure. The measured response can then be compared to theoretical behavior to improve design methods and procedures. Furthermore, load tests can provide information necessary to guide inspections, improve asset management, and identify best repair practices. Load testing is also an effective method for determining load ratings for bridges without plans (Aguilar et al., 2015, 2018; Cuaron et al., 2017). Diagnostic load testing provides an initial measure of the load effects (i.e., moment, shear, deflection, load distribution) in the structure due to applied loads (Phares et al., 2005) and provides a means to identify critical components or load paths for further investigation. Proof load testing determines the magnitude and configuration of loads that cause structural components to approach their elastic limit (Cai et al., 2012), and typically the loads are applied statically using blocks, sandbags, etc. (Lantsoght et al., 2017). In some cases, the proof load test targets critical components rather than testing the full bridge.

Load testing has been used to evaluate and rate bridge response, investigate fatigue life (Alampalli and Lund, 2006) and to evaluate new construction materials and technologies (Hou and Lynch, 2006; Kleinhans et al., 2007). Load testing was used to load rate a bridge in New York, USA that replaced the bridge deck with a fiber reinforced polymer (FRP) deck, that was 80% lower in weight compared to the original concrete deck (Alampalli and Kunin, 2003). Load testing was also used to evaluate the capacity and performance of a bridge strengthened with FRP laminates. Load tests were conducted before and after the installation of the laminates to assess the effectiveness of the strengthening FRP system (Hag-Elsafi et al., 2004). Similarly, in New Mexico a bridge was retrofitted with carbon fiber-reinforced polymer (CFRP) laminates. Load tests were performed before and after retrofitting the bridge and again 9 years after the installation of the laminates to evaluate the immediate and long-term effectiveness of the CFRP retrofit of the bridge (Regalado et al., 2017). The load

tests used in this research were used to validate the use of the non-proprietary UHPC using local materials in bridge design.

DESCRIPTION OF BRIDGE 9706

It should be noted that research conducted by Manning et al. (2016) helped to further improve methods of precast production of UHPC prestressed bridge girders in New Mexico and the analyses of specimens cast from UHPC. The research findings of Manning et al. (2016) and Giesler et al. (2016, 2018) were instrumental in the development and design of the first bridge incorporating locally developed UHPC in New Mexico, Bridge 9706.

Bridge 9706 replaced a structurally deficient bridge in Anthony, New Mexico, USA. The bridge has an 18° skew and is comprised of two 7.62 m spans with a rail-to-rail width of

TABLE 1 | UHPC and HPC available moment and strain parameters.

Variable	UHPC		HPC	
	Edge	Interior	Edge	Interior
k	0.79	0.74	0.79	0.74
f_{pi} (MPa)	1469	1379	1468	1378
Number of strands	12.0	12.0	12.0	12.0
Area per strand (mm^2)	140	140	140	140
P_e (kN)	1,974	1,930	1,946	1,594
S_c (mm^3)	1.8×10^7	1.4×10^7	2.4×10^7	1.8×10^7
S_{nc} (mm^3)	1.05×10^7	7.9×10^6	1.5×10^7	1.14×10^7
A_{nc} (mm^2)	2.3×10^5	2.01×10^5	2.6×10^5	2.2×10^5
I_{nc} (mm^4)	2.02×10^9	1.62×10^9	3.45×10^9	2.78×10^9
E_{design} (MPa)	46,192	46,192	40,968	40,968
e_{nc} (mm)	51.5	65	75	91.7
f'_c girder (MPa)	145	145	65.5	65.5
f'_c deck (MPa)	27.5	27.5	27.5	27.5
f_{cr} (MPa)	5.9	5.9	3.9	3.9
M_{dnc} (kN-m)	66.7	61.1	72.2	65
M_{dc} (kN-m)	7.2	0.00	7.2	0.00
$M_{available}$ (kN-m)	308	293	383	362
$\varepsilon_{available}$*	370	455	389	483

*Available strain using effective flange width of 1,220 mm.

FIGURE 3 | Instrumentation locations at bridge midspan.
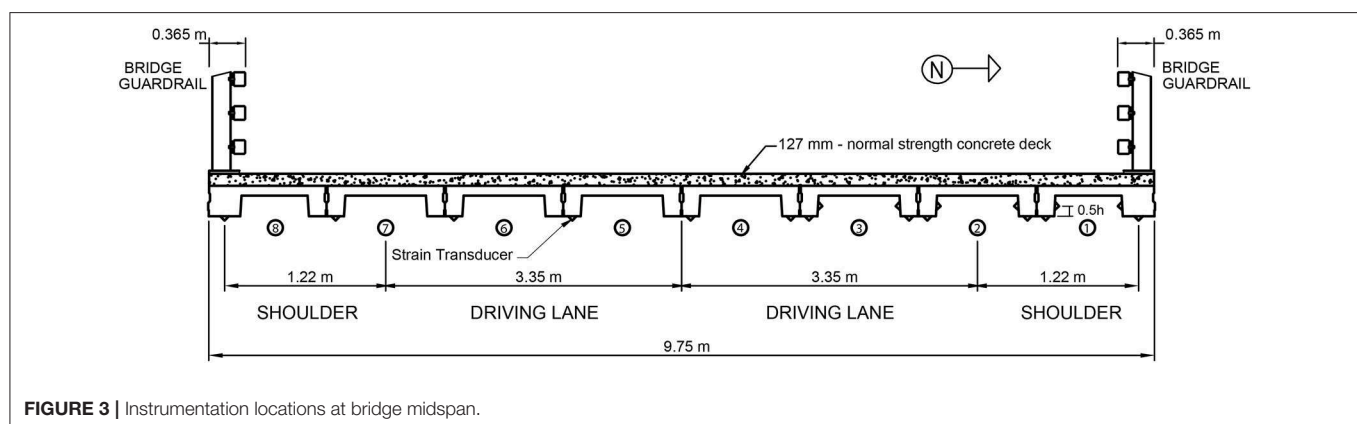
9.14 m (9.75 m out-to-out). The bridge supports two design lanes. The girders in the East span of the bridge were designed with UHPC and the girders in the West span were designed using HPC typically used for prestressed concrete in New Mexico. The UHPC channel girders are 317.5 mm in depth and the HPC channel girders are 381 mm in depth. The resulting span-to-depth ratios are 24:1 for the UHPC span and 20:1 for the HPC span. A stepped abutment was used to accommodate the different depths of the girders. The channel girders are placed directly next to one another and transversely fastened with a threaded rod through the stems at midspan. Embedded 305 mm long steel bearing seats rest on elastomeric bearing pads at the abutments

and middle pier. Additionally, there is a 127 mm composite normal strength concrete (NSC) deck (see **Figure 2A**) and New Mexico Department of Transportation (NMDOT) metal-thrie bridge railings are attached to the edge girders. Overall, the bridge has a length of 15.24 m and carries NM-186 over an irrigation canal. A photo of the Bridge 9706 during construction, completion, and the bridge profile and interior and edge girder cross-sections are shown in **Figures 1**, **2**, respectively. The girders were designed with twelve straight Grade 270, seven wire low relaxation prestressed strands with a diameter of 15.2 mm (area = 140 mm^2 per strand). Each strand had a designed pre-stress force of 260.6 kN, for a total force of 3,128 kN per girder. The width of the exterior stem of the edge girder was increased to accommodate the bridge rail connection (see **Figures 2D,E**).

INSTRUMENTATION

Bridge 9706 was instrumented with 36 external strain transducers placed at midspan of both spans. For each span, 12 strain transducers were attached to the bottom of the stem and six were attached at mid-height of the stem. The instrumentation layout was the same for the stage 1 and stage 2 load tests. The girder

TABLE 2 | AASHTO live load distribution factors for UHPC and HPC.

Lanes loaded	UHPC			HPC		
	One	Two	Three	One	Two	Three
Edge	0.60	0.50	0.43	0.60	0.50	0.43
Interior	0.340	0.333	0.327	0.341	0.335	0.329

TABLE 3 | Expected strain.

| Truck loading	$\varepsilon_{expected}$ ($\mu\varepsilon$)			
	AASHTO DF		DF = 1	
	UHPC	HPC	UHPC	HPC
Interior single truck	111	95	326	279
Edge single truck	133	112	221	187
Interior double truck side-by-side	174	150	326	280
Edge double truck side-by-side	133	112	221	187
Interior triple truck side-by-side	171	147	326	280
Edge triple truck side-by-side	133	112	221	187
Interior single truck back-to-back	127	109	373	320
Edge single truck back-to-back	152	128	253	214
Interior double truck back-to-back	199	171	373	320
Edge double truck back-to-back	152	128	253	214

FIGURE 5 | Single truck moving on the bridge.
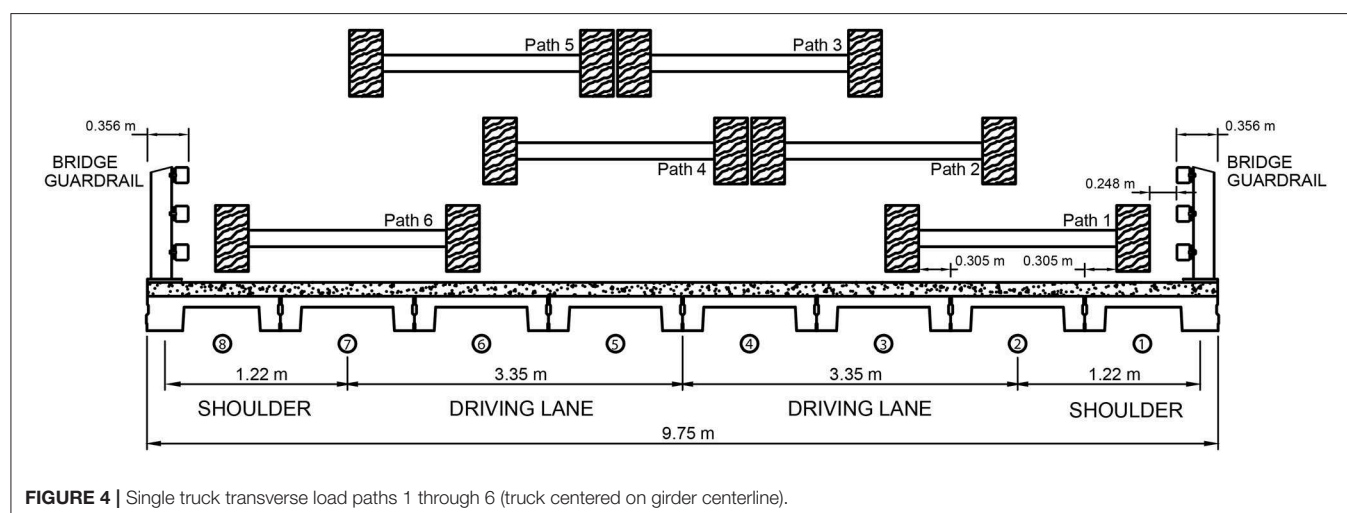
FIGURE 4 | Single truck transverse load paths 1 through 6 (truck centered on girder centerline).

and stem gauges are numbered from North to South and labeled using the notation: N/S—North stem/South stem, B/M—gauge location on bottom or at mid-height of the stem, and G#—girder number. The placement of strain gauges on each span is shown on the bridge cross-section in **Figure 3**.

PREPARATORY CALCULATIONS

Available Moments and Strains

The available strain capacities of the bridge girders were computed and used to monitor the measured strains during the load tests to prevent damage to the bridge. To obtain the available strains, the girder cracking moment was first calculated. The dead load moment was then subtracted to determine the available moment capacity the beam can resist before cracking. The available moment was divided by the product of the section modulus and the design modulus of elasticity to obtain the available strain. The available moment and strain equations are given in Equations (1) and (2).

$$M_{available} = S_c * \left[P_e * \left(\frac{1}{A_{nc}} + \frac{e_{nc}}{S_{nc}} \right) + f_{cr} \right]$$
$$- M_{dnc} * \left(\frac{S_c}{S_{nc}} \right) - M_{dc} \quad (1)$$

where f_{cr} is the modulus of rupture, P_e is the effective prestress determined from the AASHTO Load and Resistance Factor Design (LRFD) Specifications, A_{nc} is the area of the non-composite section, and e_{nc} is the distance between the centroid of the non-composite section to the centroid of the strands. S_c, S_{nc}, M_{dc}, and M_{dnc} are the composite and non-composite section moduli and the composite and non-composite dead load moments, respectively. The available strain capacity for the beam is computed as:

$$\varepsilon_{available} = \frac{M_{available}}{S_c * E_{design}} \quad (2)$$

where E_{design} is the concrete elastic modulus (either for UHPC or HPC). Equation (3) (Grabeal, 2006) and Equation (4) (ACI Committee, 2011) are used to calculate the modulus of elasticity for the UHPC and HPC, respectively:

$$E_{UHPC} = 3840 \sqrt{f'_{c\,(UHPC)}} \, (MPa) \quad (3)$$
$$E_{HPC} = 0.043 \, w_c^{1.5} \sqrt{f'_{c\,(HPC)}} \, (MPa) \quad (4)$$

where $f'_{c\,(UHPC)}$ is the compressive strength of UHPC, $f'_{c\,(HPC)}$ is the compressive strength of HPC, and w_c is the weight of the concrete (2,402 kg/m^3). **Table 1** summarizes the section properties, calculated moments, and strains for the UHPC and HPC girders, where k is the remaining prestress force percentage after all losses, f_{pi} is the actual effective prestressed stress after all losses, I_{nc} is the moment of inertia for the non-composite section, and the other parameters were previously defined.

Live Load Distribution Factor

To calculate the bending moments for the girders, the lateral distribution was calculated in accordance with the current design standard. The AASHTO LRFD Bridge Design Specifications were used for Bridge 9706. Table 4.6.2.2.1–1 in Articles 4.6.2.2.2 and 4.6.2.3 defines the superstructure types. Bridge 9706 was considered as type (h), precast concrete channel sections with shear keys and a cast-in-place concrete overlay, although the bridge has a composite deck instead of an overlay.

Tables 4.6.2.2.2b–1 and 4.6.2.2.2d–1 provide the live load distribution factors for moment in interior and edge beams, respectively, based on the type (h) equations for interior beams and the lever rule calculation for edge beams.

A summary of the calculated AASHTO live load distribution factors for UHPC and HPC girders are presented in **Table 2**.

TABLE 4 | Stage 1 load test: truck weights.

Truck number	Axle weight (kN)		Total weight (kN)
	Front single	Rear tandem	
1	70	209	279
2	63	208	271

TABLE 5 | Maximum stage 1 load test strains of UHPC and HPC.

Gauge location	Path 1	Path 2	Path 3	Path 4	Path 5	Path 6
UHPC STRAIN SINGLE TRUCK LOAD ($\mu\varepsilon$)						
NBG1	81	47	19	8	4	3
SBG1	**89**	62	28	17	9	7
NBG2	81	61	29	19	7	6
SBG2	67	63	42	29	13	10
NBG3	66	65	48	32	15	14
SBG3	61	**66**	64	51	28	26
NBG4	54	55	60	54	32	25
SBG4	45	48	**66**	69	56	48
SBG5	21	23	47	63	60	62
SBG6	13	12	28	44	**64**	71
SBG7	5	5	14	25	46	**86**
SBG8	2	2	5	18	32	85
HPC STRAIN SINGLE TRUCK LOAD ($\mu\varepsilon$)						
NBG1	74	38	12	6	2	2
SBG1	76	50	19	14	6	6
NBG2	**78**	60	28	17	7	7
SBG2	70	**72**	45	29	15	15
NBG3	67	68	44	30	16	13
SBG3	56	61	63	50	30	24
NBG4	56	61	65	55	35	26
SBG4	50	53	**75**	73	60	54
SBG5	25	30	57	72	**74**	73
SBG6	9	12	28	43	70	77
SBG7	2	5	13	22	43	78
SBG8	2	3	7	10	25	**78**

Expected Strains

For comparison to the available moment and strain capacities calculated from Equations (1) and (2), the total expected midspan moment was first calculated for the test truck applied in the stage 1 load test. The total moment was then multiplied by the design-based distribution factor from AASHTO and the "upper bound" distribution factor that represents the worst-case scenario for live load distribution between the girders (i.e., a distribution factor of one). These two factors provide the range of expected girder moments possible for the stage 1 and stage 2 test loads. The expected strains for UHPC and HPC girders were computed using Equation (5) and strain values are presented in **Table 3**.

$$\varepsilon_{expected\ (int.\ or\ edge)} = \frac{DF_{int.\ or\ edge} * Truck\ Moment}{S_c * E_{design}} \quad (5)$$

where $DF_{int.}$ and DF_{edge} are the distribution factors for an interior and edge girder, respectively.

STAGE 1 LOAD TESTING

A moving diagnostic load test (stage 1) was first conducted to gain an understanding of the *in-situ* bridge behavior prior to the load test with larger truck loads (stage 2). The magnitude of the total truck load applied on the bridge during the stage 1 load test was less than the stage 2 target load due to the uncertainties in the bridge response. Load was applied in the stage 1 load test in similar paths used in the stage 2 load test for the single truck paths configurations; however, truck loads and paths were not applied to maximize the loading but to gather information on the behavior, load distribution between adjacent girders, and to compare the initial structural response between the UHPC and HPC spans. Six single truck load paths were conducted as part of the stage 1 load test. A single truck was applied as a slow-moving load along the transverse paths shown in **Figure 4**.
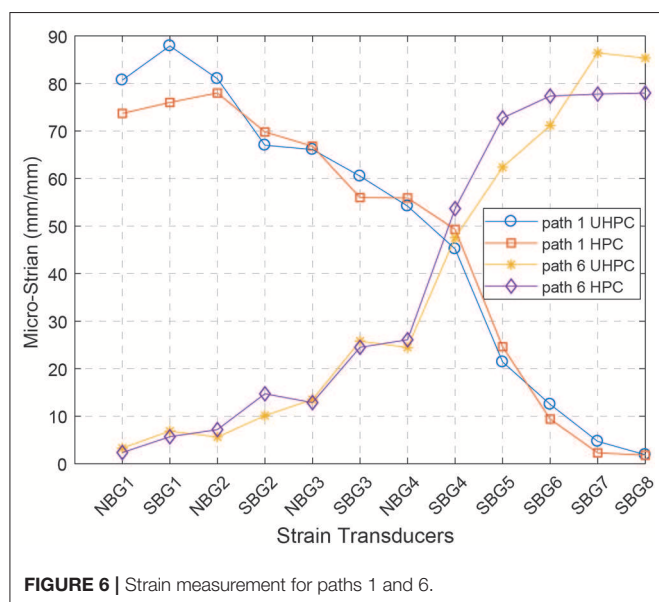

FIGURE 6 | Strain measurement for paths 1 and 6.

On March 30, 2017, the stage 1 load test was performed on Bridge 9706. **Figure 5** shows a photo of a single truck on the bridge. Two load trucks, weighing 275 kN on average, were used during the stage 1 load test. **Table 4** shows the axle weights of the trucks used for the stage 1 load test.

Maximum Strain for UHPC and HPC Spans

The maximum strain for each load path and the corresponding strain transducer and location on the UHPC span and HPC span is shown in **Table 5**. The maximum measured strain for each load path on each span is indicated in bold. The strains measured during the stage 1 load test and bridge behavior are discussed later.

Strain Comparison Between UHPC and HPC Spans

Comparing the strains between the UHPC span and the HPC span for the stage 1 load test, the following was observed:

- The largest measured strains in the UHPC span, were 89 and 86 με for paths 1 and 6, respectively (see **Table 5**). For the HPC span, the largest measured strains were 78 and 78 με during path 1 and path 6, respectively.
- The edge girders for both the UHPC and HPC spans experienced more tensile strains for paths 1 and 6 since the truck wheel loads were positioned over the edge girders. When the truck load was moved toward the interior girders, the tensile strains showed better distribution between adjacent girders, typically resulting in lower strains.
- Strains measured in the UHPC span were higher than strains in the HPC span. The maximum strains for the UHPC span occurred in either girder 1 or 7. The maximum strains for the HPC span occurred in either girder 2 or 7. The HPC girders have a larger cross-sectional area compared to the UHPC girders. Although the UHPC and HPC girders were designed to have the same capacity, UHPC girders measured higher values of strain. Although the modulus of elasticity of the UHPC is greater than that of HPC, the section modulus is smaller. The section and elastic moduli ratio between the UHPC and HPC are 0.7 and 1.2, respectively.
- **Figure 6** shows the strain behavior across the bridge width for load paths 1 (North side) and 6 (South side). More strain transducers were placed on girders 1–4, therefore, additional data points are shown for these girders. The results illustrate

TABLE 6 | Stage 1 load test: expected vs. measured strain.

Truck loading		Strain (με)	
		UHPC	HPC
Interior single	Expected	111	95
	Measured	86	78
	Difference	23%	18%
Edge single	Expected	133	112
	Measured	89	78
	Difference	33%	30%

FIGURE 7 | (A) Single truck back-to-back loading, **(B)** double truck back-to-back loading, **(C)** triple truck side-by-side loading.

the symmetric behavior of the bridge as expected for a newly constructed bridge.

Comparison of Measured and Expected Strains

The maximum measured stage 1 load test strains and the expected strains are tabulated in **Table 6**. The percent difference between the two strain values is also shown. Overall, the measured strains for the UHPC and HPC spans were lower than the predicted behavior, indicating the designed-based load distribution factors to be conservative for the UHPC and HPC bridge girders. The percent difference between the measured and expected strains for the UHPC girders is slightly larger than the HPC girders indicating better load distribution in the UHPC bridge.

STAGE 2 LOAD TESTING

Based on the results from the stage 1 load test, the bridge showed no signs of cracking nor did it exceed the available strain. The measured strains were 24 and 19% of the available strains for edge and interior UHPC girders, respectively. The measured strains were 20 and 16% of the available strains for interior and edge HPC girders, respectively. Consequently, the stage 2 load test was planned and conducted with the goal of applying the largest load

possible to the bridge without exceeding the available moment to investigate the bridge behavior at larger loads. The bridge behavior under the stage 2 truck loading was monitored carefully via strain measurements. For the stage 2 load test, the test vehicles were loaded to the maximum weight and positioned along the paths producing the largest girder strains (critical paths). As the applied loads increased during the stage 2 load test, the measured strains were monitored carefully to ensure they did not exceed the expected or available strains. Single truck, double truck side-by-side, triple truck side-by-side, single truck back-to-back, and double truck back-to-back (i.e., four trucks) loadings were done as part of the stage 2 load test. The loading was applied by moving the trucks incrementally to specified locations along the span. **Figures 7A–C**, show pictures of the bridge being loaded with the single truck back-to-back, double truck back-to-back, and triple truck side-by-side load paths during the stage 2 load test. **Figures 8A,B** show the configurations of the double truck side-by-side and triple truck side-by-side paths for the stage 2 load test. **Figure 9A** shows the bridge profile with the back-to-back truck loadings, which are applied in similar path configurations as illustrated in **Figure 4** (single truck back-to-back) and **Figure 8A** (double truck back-to-back). The back-to-back load path configurations were incrementally loaded, placing the center of the two rear tandem axels at the abutments, quarter-points, mid-points, and pier along the length

FIGURE 8 | (A) Double truck side-by-side transverse load paths 7, 8, and 9, (B) Triple truck side-by-side transverse load path 10.
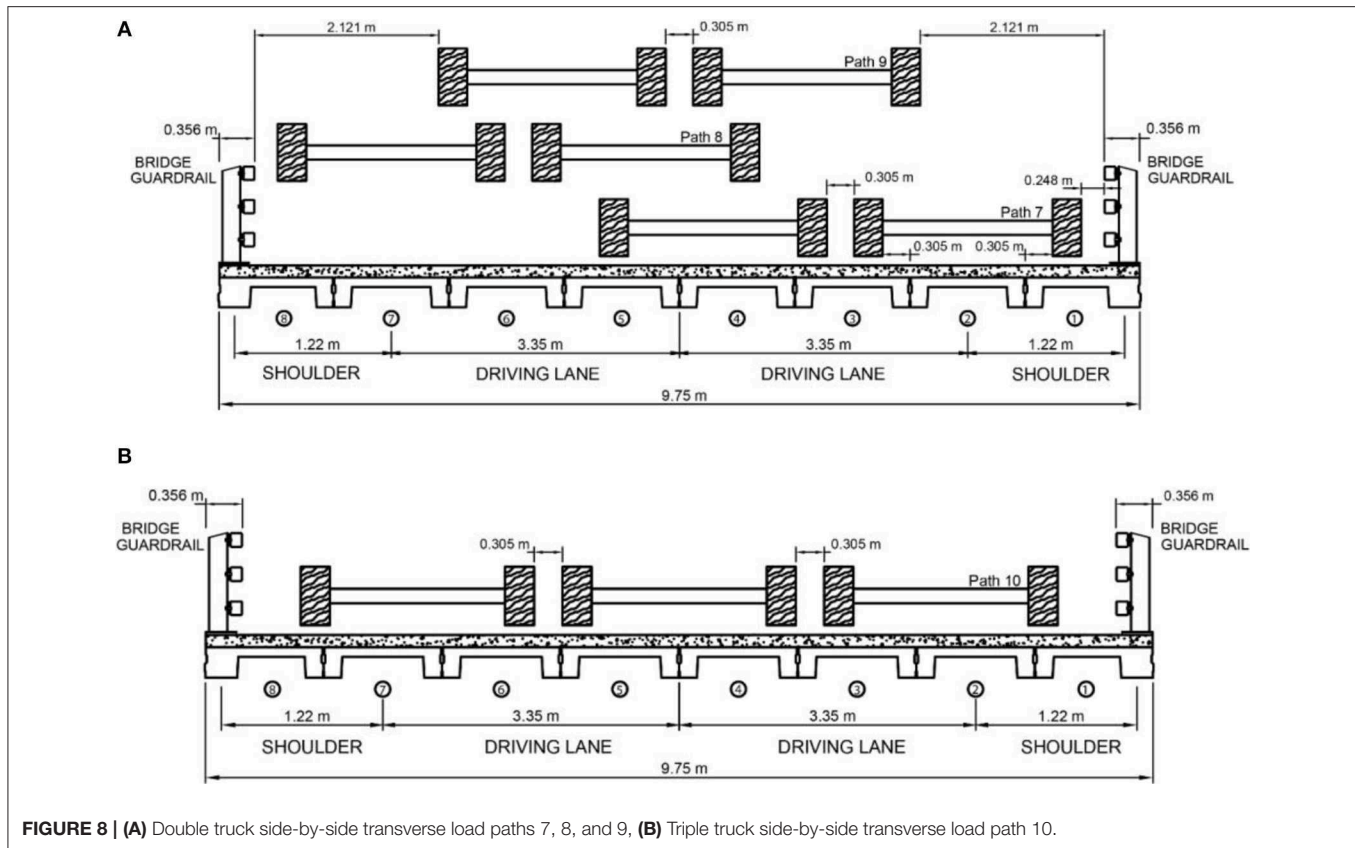
of the bridge. **Figures 9B,C** show the top view of the bridge being loaded with single and double truck back-to-back load path configurations, respectively. It is noted that multiple load paths were used, however, only one example path is shown. For the stage 2 load test, dump trucks were maximized in weight and applied in different configurations to maximize the moment along the length of the bridge. The truck configurations included single truck, single truck back-to-back, double truck back-to-back (four trucks), and triple truck side-by-side. The double truck back-to-back and triple truck side-by-side configurations maximized the number of trucks that could be applied based on the dimensions of the bridge and were used to apply the largest load feasible. The truck moments applied to the bridge during the stage 1 and stage 2 load tests were about 15 and 20% higher than the non-factored standard truck live load moment (HL93), respectively.

From January 29 through January 31, 2018, the stage 2 load test was performed on Bridge 9706, 9 months after the stage 1 load test. Four load trucks, weighing on average 283 kN, were used for the test. **Table 7** shows the axle weights of the trucks used for the stage 2 load test. The stage 2 load test consisted of a preliminary load test in which a few slow-moving and incremental truck load paths were used to calibrate the strain transducers and ensure the behavior of the bridge had no significant changes since the time of the stage 1 load test. Then, the stage 2 load test was conducted loading the trucks onto the bridge following the designed paths to maximize the total load applied to each span.

Maximum Strains

Table 8 provides the maximum measured strains for each load path configuration on the UHPC span and HPC span. The maximum measured strain for each load path configuration on each span is indicated in bold. The strains measured during the stage 2 load test and bridge behavior are discussed later.

Strain Comparisons Between UHPC and HPC Spans

Comparing the strains between the UHPC span and the HPC span for the stage 2 load test, the following was observed:

- For a single truck load, the maximum strain for the UHPC span was 99 $\mu\varepsilon$, which was higher than the strain measured for the HPC span, 95 $\mu\varepsilon$. Similarly, the strain measured for double truck side-by-side loading for the UHPC span was 126 $\mu\varepsilon$ and for the HPC span was 129 $\mu\varepsilon$.
- For triple truck side-by-side loading, the largest measured strain for the UHPC span was 128 $\mu\varepsilon$. For the HPC span, the largest measured strain was 127 $\mu\varepsilon$. During this loading, the strains were more evenly distributed across all girders.
- The maximum measured strain for single truck back-to-back loading for the UHPC span was 120 $\mu\varepsilon$, and for the HPC span was 120 $\mu\varepsilon$.
- For the double truck back-to-back load path, the largest measured strains for the UHPC span was 154 $\mu\varepsilon$. For the HPC span, the largest measured strain was 143 $\mu\varepsilon$.
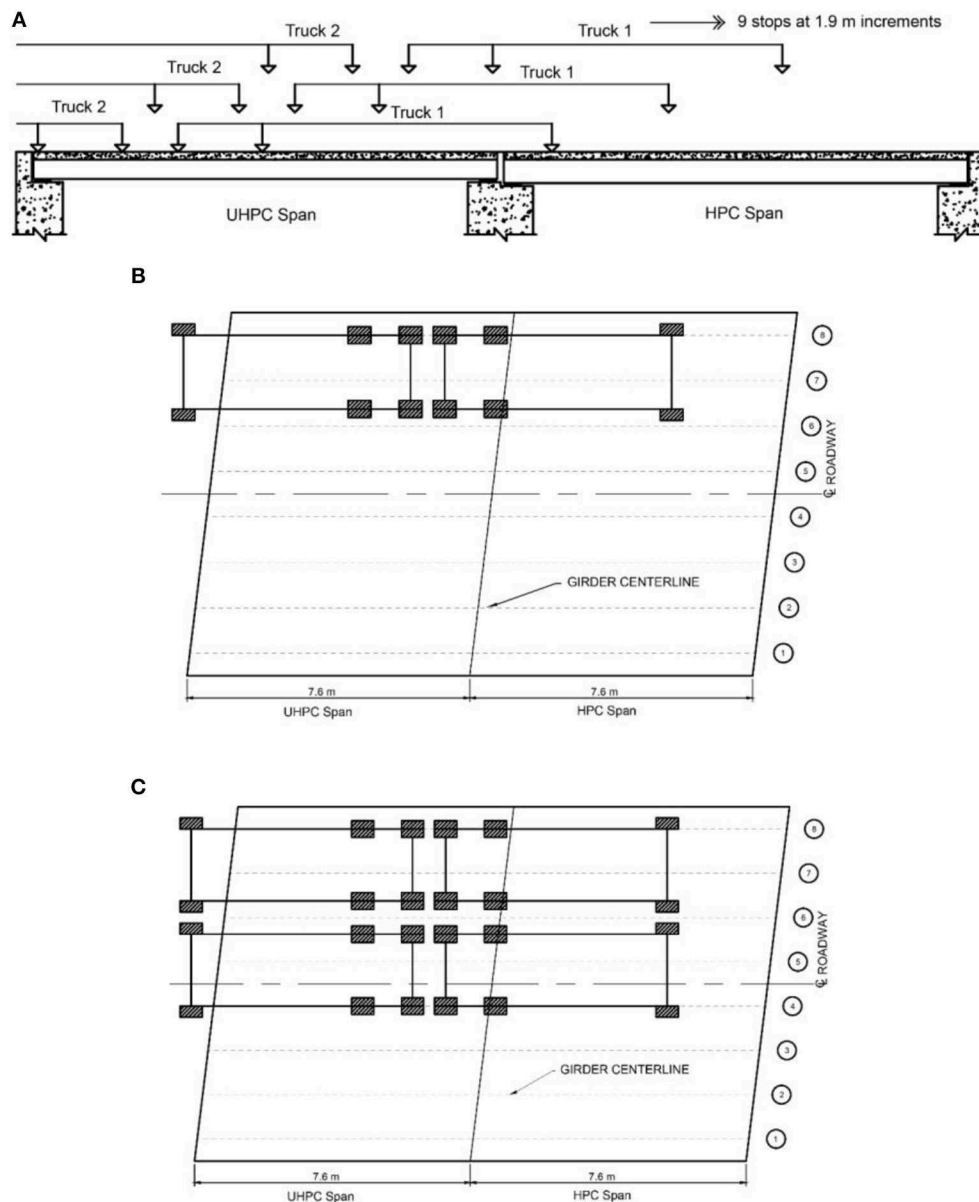
FIGURE 9 | Path configurations **(A)** bridge profile with trucks, **(B)** top view of single truck back-to-back path, **(C)** top view of double truck back-to-back path.

- The maximum strains usually occurred in the UHPC and HPC interior girders. Results show that as the bridge becomes more uniformly loaded, measured strains between the HPC and UHPC spans are more similar.

Comparison of Measured and Expected Strain

The maximum measured stage 2 load test strains and the expected strains are presented in **Table 9**. The percent difference between the two strains is also shown. Overall, the measured strains for the UHPC and HPC spans were lower than the predicted behavior, indicating that the designed-based load

distribution factors are conservative for both the UHPC and HPC bridge girders. Again, in general, the UHPC predicted strains are greater in comparison to the measured strains than those for the HPC span. This indicates better load distributions for the UHPC span compared to HPC span.

CONCLUSIONS

The stage 1 load test of Bridge 9706 was comprised of six single truck load paths (slow-moving). The stage 2 load test was conducted ~9 months after the stage 1 load test, focusing on the behavior of the new concrete material, to provide a

baseline for the bridge behavior, and compare the behaviors of the two different spans. The stage 2 load test was comprised of incremental single truck, double truck side-by-side, triple truck side-by-side, and both single and double truck back-to-back load paths. Overall, the maximum measured strains for UHPC and HPC for both the stage 1 load test and stage 2 load test were similar. A few observations and conclusions from the load tests can be made:

TABLE 7 | Stage 2 load test: truck load weights.

Test date	Truck number	Axel weight (kN)		Total weight (kN)
		Front single	Rear tandem	
Jan 29th	1	70	214	284
	2	70	216	286
	3	65	217	282
	4	76	213	289
Jan 30th	1	70	213	283
	2	68	213	281
	3	64	213	278
	4	75	210	285
Jan 31st	1	70	211	281
	2	68	213	281

- The stage 1 and stage 2 load test results showed that the UHPC span experienced larger strains than the HPC span when loaded with a single truck. The combined effect of a smaller section modulus and an increased modulus of elasticity results in slightly larger expected strains in the UHPC span.
- The stiffness (EI) of the UHPC girders was calculated to be 34% smaller than HPC for both edge and interior beams. However, the measured strains were similar between the two materials. This also may indicate that the estimated E may be overly conservative for the UHPC.
- During the stage 1 and stage 2 load tests, the maximum measured strains for the UHPC and HPC spans did not exceed the expected strains. It is noted that the expected strains presented in this paper are based on the actual truck weights and positioned as measured during the tests. Prior to testing, the expected strains were based on estimated loads and the designed load paths (which were also not exceeded).
- As more trucks were added during the stage 2 load test, more girders were engaged demonstrating better load distribution across the bridge. The distribution was achieved through the composite deck and shear keys between girders.
- To ensure that no damage was done to the bridge during the load tests, the measured and expected strains were shown to not exceed the available strains that were calculated based on the AASHTO specifications for both tests. The maximum percentage of the available strains exhausted for the

TABLE 8 | Maximum stage 2 load test strains for UHPC and HPC.

Gauge location	Single truck	Double truck side-by-side	Triple truck side-by-side	Single truck back-to-back	Double truck back-to-back
UHPC SPAN STRAINS (μɛ)					
NBG1	3	21	78	20	146
SBG1	5	27	92	19	148
NBG2	5	34	88	19	**154**
SBG2	4	40	73	20	127
NBG3	6	52	86	20	150
SBG3	12	75	93	27	143
NBG4	16	88	98	30	141
SBG4	30	103	102	48	136
SBG5	52	109	104	75	88
SBG6	84	103	122	100	67
SBG7	**99**	**126**	**128**	**120**	40
SBG8	90	119	107	105	14
HPC SPAN STRAINS (μɛ)					
NBG1	8	30	69	12	115
SBG1	8	37	79	10	113
NBG2	8	54	93	17	135
SBG2	12	69	97	17	140
NBG3	10	68	110	20	130
SBG3	21	109	111	33	**143**
NBG4	20	105	94	33	124
SBG4	38	127	117	56	138
SBG5	71	**129**	**127**	93	117
SBG6	**95**	122	120	109	80
SBG7	93	120	100	101	51
SBG8	97	105	98	**120**	33

TABLE 9 | Stage 2 load test: expected vs. measured strain.

Girder/load path configuration		Strain (με)	
		UHPC	HPC
Interior/single truck	Expected	111	95
	Measured	99	95
	Difference	11%	0%
Edge/single truck	Expected	133	112
	Measured	90	97
	Difference	32%	13%
Interior/double truck side-by-side	Expected	174	150
	Measured	126	129
	Difference	28%	14%
Edge/double truck side-by-side	Expected	133	112
	Measured	119	105
	Difference	11%	6%
Interior/triple truck side-by-side	expected	171	147
	Measured	128	127
	Difference	25%	14%
Edge/triple truck side-by-side	Expected	133	112
	Measured	107	98
	Difference	20%	13%
Interior/single truck back-to-back	Expected	127	109
	Measured	120	109
	Difference	6%	0%
Edge/single truck back-to-back	Expected	152	128
	Measured	105	120
	Difference	31%	6%
Interior/double truck back-to-back	Expected	199	171
	Measured	154	143
	Difference	23%	16%
Edge/double truck back-to-back	Expected	152	128
	Measured	148	115
	Difference	3%	10%

UHPC span was 40 and 34% for edge and interior girders, respectively. The maximum percentage of available strains exhausted for the HPC span was 31 and 30% for edge and interior girders, respectively.

- The UHPC span experienced better live load distribution compared to the HPC span, validating the expected behavior based on the distribution factor presented in **Table 2**.
- The use of load testing provides measured data to understand the behavior of the different concrete materials used in the bridge. Furthermore, the data can be compared to verify design procedures that incorporated the material properties of UHPC design and provide additional information for the introduction of UHPC into design codes. Based on the results from these load tests, non-proprietary UHPC can be effectively

used in bridge construction with the following advantages: less material, equal or higher capacity with smaller girder cross-section, and more economical compared to proprietary products. The results also demonstrated that the introduction of UHPC into precast production was successful and the construction quality of the bridge was good.

- The information collected from load tests provides essential information for the long-term performance study of the use of UHPC. Over the design-life of the bridge, the two spans can be observed to compare the difference in performance, particularly focusing on the durability and maintenance required. Additionally, future load tests can be utilized to monitor the long-term behavior of this new concrete material by comparing changes in behavior to the baseline data. As changes are observed, the data collected can also be used to guide inspections and denote key areas that require more detailed inspections.

DATA AVAILABILITY STATEMENT

The data models, or code generated or used during the study are available from the corresponding author by request and upon approval from the New Mexico Department of Transportation.

AUTHOR CONTRIBUTIONS

All authors have contributed to the testing, data analysis, and writing of this paper.

REFERENCES

AASHTO (2000). *Manual for Condition Evaluation of Bridges, 1994*. Washington, DC: American Association of State Highway & Transportation Officials.

AASHTO (2012). *American Association of State and Highway Transportation Officials (AASHTO) Load Resistance Factor Design (LRFD) Bridge Design Specifications*. Washington, DC: American Association of State and Highway Transportation Officials.

ACI Committee (2011). *Building Code Requirements for Structural Concrete (ACI 318-11) and Commentary*. Farmington Hills, MI: American Concrete Institute.

Aguilar, C. V., Jáuregui, D. V., Newtson, C. M., Weldon, B. D., and Cortez, T. M. (2015). Load rating a prestressed concrete double T-beam bridge without plans by field testing. *Transp. Res. Record J. Transp. Res. Board* 2522, 90–99. doi: 10.3141/2522-09

Aguilar, C. V., Jáuregui, D. V., Weldon, B. D., and Newtson, C. M. (2018). *Rating of Prestressed Concrete Adjacent Beam Bridges Without Plans*. Farmington Hills, MI: Special Publication, 323, 5–1.

Ahlborn, T. M., Harris, D. K., Misson, D. L., and Peuse, E. J. (2011). "Strength and durability characterization of ultra-high performance concrete under variable curing conditions," in *Presented at 90th Annual Meeting of the Transportation Research Board* (Washington, DC).

Alampalli, S., and Kunin, J. (2003). Load testing of an FRP bridge deck on a truss bridge. *Appl. Compos. Mater.* 10, 85–102. doi: 10.1023/A:1022885728627

Alampalli, S., and Lund, R. (2006). Estimating fatigue life of bridge components using measured strains. *J. Bridge Eng.* 11, 725–736. doi: 10.1061/(ASCE)1084-0702(2006)11:6(725)

Allena, S. (2010). *Ultra high strength concrete using local materials* (Ph.D. dissertation), New Mexico State University, Las Cruces, NM, United States.

Brühwiler, E., and Denarié, E. (2013). Rehabilitation and strengthening of concrete structures using ultra-high performance fibre reinforced concrete. *Struct. Eng. Int.* 23, 450–457. doi: 10.2749/101686613X1362734710 0437

Cai, H., Abudayyeh, O., Abdel-Qader, I., Attanayake, U., Barbera, J., and Almaita, E. (2012). Bridge deck load testing using sensors and optical survey equipment. *Adv. Civil Eng.* 2012:493983. doi: 10.1155/2012/ 493983

Cuaron, A. M., Jáuregui, D. V., and Weldon, B. D. (2017). "Invited Student Paper- A Procedure for Load Rating Reinforced Concrete Slab Bridges without Plans (No. 17–01754), in *Transportation Board 96th Annual Meeting* (Washington, DC).

Giesler, A. J., Applegate, S., and Weldon, B. (2016). Implementing, nonproprietary, ultra-high performance concrete in a precasting plant. *PCI J.* 61, 68–80.

Giesler, A. J., McGinnis, M. J., and Weldon, B. D. (2018). Flexural behavior and analysis of prestressed ultra-high-performance concrete beams made from locally available materials. *PCI J.* 63, 66–80.

Grabeal, B. A. (2006). *Material Property Characterization of Ultra High Performance Concrete*. FHWA-HRT-06-103, Turner-Fairbank Highway Research Center, McLean, VA.

Graybeal, B. A. (2008). "UHPC in the US highway transportation system," in *Proceedings of the Second International Symposium on Ultra High Performance Concrete* (Kassel), 11–17.

Graybeal, B. A. (2010). *Behavior of Field-Cast Ultra-High Performance Concrete Bridge Deck Connections Under Cyclic and Static Structural Loading (No. FHWA-HRT-11-023)*. McLean, VA: Federal Highway Administration.

Hag-Elsafi, O., Alampalli, S., and Kunin, J. (2004). In-service evaluation of a reinforced concrete T- beam bridge FRP strengthening system. *Compos. Struct.* 64, 179–188. doi: 10.1016/j.compstruct.2003. 08.002

Hajar, Z., Lecointre, D., Simon, A., and Petitjean, J. (2004). "Design and construction of the world first ultra-high performance concrete road bridges," in *Proceedings of the International Symposium on UHPC* (Kassel), 39–48.

Hou, T. C., and Lynch, J. P. (2006). "Rapid-to-deploy wireless monitoring systems for static and dynamic load testing of bridges: validation on the grove street bridge," in Nonintrusive Inspection, Structures Monitoring, and Smart Systems for Homeland Security, Vol. 6178, eds A. A. Diaz, H. F. Wu, S. R. Doctor, and Y. Bar-Cohen (San Diego, CA: International Society for Optics and Photonics), 61780D.

Kleinhans, D. D., Myers, J. J., and Nanni, A. (2007). Assessment of load transfer and load distribution in bridges utilizing FRP panels. *J. Compos. Constr.* 11, 545–552. doi: 10.1061/(ASCE)1090-0268(2007)11:5(545)

Lantsoght, E. O., van der Veen, C., de Boer, A., and Hordijk, D. A. (2017). State-of-the-art on load testing of concrete bridges. *Eng. Struct.* 150, 231–241. doi: 10.1016/j.engstruct.2017.07.050

Lyell, E. K. (2011). *Optimization of Ultra High Performance Concrete Mixture Proportions Using Locally Available Materials*. MS thesis, New Mexico State University, Las Cruces, NM.

Manglekar, H. C., Visage, E. T., Ray, T., and Weldon, B. D. (2016). Experimental and analytical investigations of a locally developed ultrahigh-performance fiber-reinforced concrete. *J. Mater. Civil Eng.* 29:04016202. doi: 10.1061/(ASCE)MT.1943-5533.0001732

Manning, M. P., Weldon, B. D., McGinnis, M. J., Jáuregui, D. V., and Newtson, C. M. (2016). Behavior comparison of prestressed channel girders from high-performance and ultrahigh-performance concrete. *Transp. Res. Record J. Transp. Res. Board* 2577, 60–68. doi: 10.3141/2577-08

Muro-Villanueva, J., Newtson, C. M., Allena, S., Weldon, B. D., and Jauregui, D. V. (2012). "Freezing and thawing durability of ultra high strength concrete," in *International Congress on Durability of Concrete* (Trondheim).

Phares, B. M., Wipf, T. J., Greimann, L. F., and Lee, Y. (2005). *Health Monitoring of Bridge Structures and Components Using Smart Structure Technology*, Vol. 2. Washington DC: Wisconsin Highway Research Program.

Regalado, A., Carpenter, B. A., Jáuregui, D. V., and Weldon, B. D. (2017). Performance evaluation of a reinforced concrete slab bridge retrofitted with carbon fiber reinforcement polymer laminate system. *Transp. Res. Record J. Transp. Res. Board* 2642, 68–76. doi: 10.3141/2642-09

Taylor, C. W., Weldon, B. D., Jáuregui, D. V., and Newtson, C. M. (2013). Case studies using ultrahigh-performance concrete for prestressed girder bridge design. *Pract. Period. Struct. Design Constr*, 18, 261–267. doi: 10.1061/(ASCE)SC.1943-5576.0000167

Visage, E. T., Weldon, B. D., Jauregui, D. V., and Newtson, C. M. (2019). Flexural performance of ultrahigh-performance concrete developed using local materials. *J. Mater. Civil Eng.* 31:04019050. doi: 10.1061/(ASCE)MT.1943-5533.0002683

Voo, Y. L., Foster, S. J., and Voo, C. C. (2014). Ultrahigh-performance concrete segmental bridge technology: toward sustainable bridge construction. *J. Bridge Eng.* 20:B5014001. doi: 10.1061/(ASCE)BE.1943-5592. 0000704

Weldon, B., Jauregui, D., Newtson, C., Montoya, K., Taylor, C. Allena, S., et al. (2012). Feasibility Analysis of Ultra High Performance Concrete for Prestressed Concrete Bridge Applications – Phase II. NMDOT Report No. NM09MSC-01, New Mexico State University, Las Cruces, NM.

Yuan, J., and Graybeal, B. (2016). Full-scale testing of shear key details for precast concrete box-beam bridges. *J. Bridge Eng.* 21:04016043. doi: 10.1061/(ASCE)BE.1943-5592. 0000906

Challenges Related to Probabilistic Decision Analysis for Bridge Testing and Reclassification

Jacob Wittrup Schmidt[1]*, Sebastian Thöns[1,2], Medha Kapoor[1], Christian Overgaard Christensen[1], Svend Engelund[3] and John D. Sørensen[4]

[1] Department of Civil Engineering, Technical University of Denmark, Lyngby, Denmark, [2] Department 7: Safety of Structures, BAM Federal Institute for Materials Research and Testing, Berlin, Germany, [3] COWI AS, Lyngby, Denmark, [4] Department of Civil Engineering, Aalborg University, Aalborg, Denmark

This paper reviews historical developments and recent challenges in full scale bridge testing and introduces results- and hypotheses related to an ongoing bridge testing research project. This research project encompasses full scale bridge testing in conjunction with bearing capacity analysis as well as related contact- and non-contact monitoring procedures combined with a decision analytical approach. Results from the first steps of the project, focusing on full scale load testing of bridges, are presented. The next part approaches the interfaces between three project areas namely the bearing capacity analysis, the utilization of monitoring procedures and a decision analytical approach. The proposed probabilistic decision analysis approach is described for two scenarios: (1) The decision support for the actual proof load test providing decision rules for a safe and efficient *in-situ* test and (2) for the identification of efficient strategies for the bridge reclassification accounting for modeling, simulation, and monitoring information. The paper concludes with a summary highlighting deemed challenges in the used approaches.

Keywords: load testing, bridge reclassification, decision analysis, probabilistic analysis, bridges

INTRODUCTION

The road authorities in most countries face problems related to aging bridges and increased traffic intensity and traffic loads. The aging infrastructure was originally designed according to old codes that were developed at a time when the traffic loads were considerably lower than today. Hence, the road authorities must choose between three different options:

1. Impose restrictions to the traffic on the bridge (maximum limit for axle loads or the total weight of the vehicles using the bridge)
2. Strengthen the bridge
3. Perform tests and analyses that demonstrate that the load carrying capacity of the bridge is acceptable.

The costs related to traffic restrictions or a bridge strengthening are usually relatively high compared to the cost of the tests and analyses that may demonstrate that the load carrying capacity of the bridge is acceptable. Therefore, the road authorities will usually choose the third option.

The road authorities may perform tests to determine the properties of materials such as concrete, reinforcement or steel. The results of these tests may be used to determine more accurate estimates of the relevant material properties.

In addition, one of the tests available to the road authorities is full scale bridge testing. Full scale bridge testing has the advantage that it provides increased information accuracy with respect to the actual response and load carrying capacity of the considered bridge. There are two different approaches to full scale bridge testing:

(1) Proof loading, which is performed in the linear elastic regime up to a pre-defined proof load magnitude. As large loads are needed for proof load testing, the associated risks can be large. Therefore, the structural response must be followed closely during testing. If the bridge can withstand the pre-defined proof load without signs of distress, the capacity is experimentally proven. Normally pre-defined stop criteria and target load are decided upon in order to ensure that no permanent damage occurs. If the structural response exceeds the pre-defined stop criteria or target load, the proof load test must be terminated and no further loading is allowed.

(2) Failure loading, where loading is applied to evaluate the full response of a certain bridge type. More information concerning the boundary conditions, governing failure modes, interaction between structural elements etc. can be evaluated by using this approach. However, permanent damage of the bridge structure is the outcome of such testing and, as a result, demolishing of the structure.

Often failure loading shows that the capacity is higher than expected in the tested bridge structures, since uncertainties related to the overall structural behavior, materials, modeling approach etc., are reduced compared to prior models.

However, the real ultimate capacity of tested bridges is often up to discussion, since testing of bridges intended for continued service do not allow permanent damage. Consequently, the margin between the predicted capacity and real ultimate capacity is unknown and can differ depending on the bridge type.

Historical Developments

Bridge load testing to failure was already initiated in 1913, where testing was performed on a flat arch bridge (Elmont, 1913). The highest value of the compressive stresses was reached via a concentrated load over the center of one part of the arch.

Later, in 1952, a three span concrete bridge was tested to failure in the UK. The bridge was a pre-stressed three span pedestrian foot bridge located at the South Bank. Failure occurred at a dead load of approximately 2.4 times the design load and lasted for ~3 days (Civil Engineering Review, 1952).

Dead loading was the main loading type until 1963, where Rösli (1963) used hydraulic jacks. This was one of the first applications, where such loading method was used and it was reported that the ultimate failure load reached the same level as foreseen in the theoretical evaluations.

In 1968, Gosbell and Stevens (1968) loaded a pre-stressed I-beam bridge with an *in-situ* cast concrete bridge deck. The ultimate punching shear of the one-span bridge was stated to correlate well with theory. It was however reported that a three time higher cracking load, than predicted, was applied to initiate cracking.

Load simulating different wheel pressures was performed in 1973 by Goodpasture and Burdette (1973). It was stated that the applied theory correlated well with the measured results. Additionally the AASHO showed predictions, which were approximately half of the measured values. Jorgenson and Larson (1976) however reported loads which reached nearly 5.5 times the characteristic traffic load. Furthermore, load testing was performed by Nanni et al. (1999), Alkhrdaji et al. (2001), Zhang et al. (2011, 2013), and Lantsoght (2013).

It is seen from the literature that the aim of the research projects differ greatly. Most of the projects succeeded in testing the bridges to failure but the ultimate failure testing approaches are fragmented. Consequently, the approaches and results are based on separate assumptions depending on the actual project and bridge design.

Some of the research programs aimed at implementing the obtained knowledge into national codes. However, it is normally not reported if they succeeded in this, which could be dedicated to the fact that only a limited number of bridges were tested and reported together (mostly only 1 bridge per publication).

Additionally no sufficient method to find the link between material testing, sub component testing and full scale testing, seem to exist.

A number of suggestions were given to explain a higher test capacity when comparing with theory (Strain hardening, conservative load distribution etc.). The research projects do, however, not include any evaluations of the magnitude of these contributions.

Several types of monitoring approaches were used in the described research projects to evaluate the response until failure. Mostly contact monitoring methods were used, whereas application of more novel approaches such as acoustic emission, laser-, radar-, DIC systems, etc. are limited, all though research is ongoing in this regard.

It is seen that monitoring plays an essential role when performing bridge testing, since global and local thresholds have to be evaluated as a mean to find the stop criterion. In addition, results from the applied measurement equipment can be used to verify- or falsify the theoretical evaluations and thus for calibration. Consequently, the evaluation of a bridge structure seems to be an iterative process, where several parameters can influence and potentially change the final decision regarding a stop criterion. This depends on the monitored responses and calibrated theoretical models.

For diagnostic and proof load testing, a number of national guidelines exists. In North America the Manual for Bridge Evaluation (AASHTO, 2011), based on the Manual for Bridge Rating through Load Testing (NCHRP, 1998) gives recommendations for diagnostic testing and for determining the target proof load in proof load tests of bridges, however no stop criteria are defined. The ACI 437.2M-13 (ACI Committee 437, 2013) define both loading protocol and stop criteria ("acceptance criteria" in ACI) for buildings, but not for bridges. In Europe, Germany (DAfStb, 2000), Ireland (NRA, 2014), and Great Britain (ICE, 1998) among others have national guidelines for load testing, but only the German guideline prescribe stop criteria, again for buildings.

Since bridges are complex structures to evaluate, it is still up to discussion how stop criteria can be defined. Additionally, such thresholds should be evaluated to an extent that provides comfort in a final decision taking regarding the target load magnitude—the bridge might not behave as expected when loading is applied *in-situ*.

Motivated by the absence of applicable guidelines (Lantsoght et al., 2018) presents a proposal for stop criteria in proof load testing of reinforced concrete slab bridges. The proposal provides a solid base for further development, but the thresholds seems not yet evaluated to a satisfactory extent in regards to decision taking.

Some of the outlined challenges are addressed in an ongoing research project. This project is so far focussed on the development of an efficient *in-situ* full scale testing procedure and will be extended to address the combination of proof loading and the realistic simulation of the ultimate capacity behavior (Serviceability limit state- and ultimate limit state) and decision approaches.

This paper provides an overview of the current project achievements in regard to the testing procedure and test results and contains a proposal relating to a probabilistic decision approach as an iterative process, where two scenarios can be described and analyzed: (1) The decision support for an actual proof load test providing decision rules for a stop criterion and thus safe and efficient *in-situ* testing, and (2) for the identification of efficient strategies for the bridge reclassification accounting for modeling, simulation, and monitoring information.

RESEARCH FOR RECLASSIFICATION OF BRIDGES

The research project considered for the probabilistic and theoretical decision approach is a part of an ambitious research project initiated in 2016 in Denmark concerning full-scale testing of one-span concrete slab bridges with maximum span of 12 m (39.4 feet). Some of the initial main milestones as well as related research questions of the project are the following:

- *Development of a full-scale test method:* Is it possible to construct a test rig, which meets the demands to a high loading magnitude combined with a fast and precise *in-situ* full-scale test?
- *Simplified monitoring:* Is it possible to optimize advanced monitoring to a level, where measurements are performed in a fast- and simplified way, and at the same time reveal governing thresholds related to the needed stop criterions?
- *Calibration of theoretical models:* Can advanced theoretical models be presented in a more abridged way, where it is calibrated, via input from *in-situ* testing, to the developed monitoring method?

In the following, the development of a full-scale test method is described together with a conceptual approach of how to address a systematic reclassification of bridges as decision analysis combined with monitoring and further evolution of theoretical models.

A reclassification can be relevant to perform when there are uncertainties associated with the original capacity evaluation or the current state of an aging bridge. From a bridge owner's perspective, the goal usually is to verify the current bridge class or to obtain a higher class to meet a higher traffic demand.

In-situ Testing

When performing full-scale load testing, the loading setup should comply with national guidelines. One of the challenges in this approach, is to apply load configurations that accurately reflects axle- and wheel loading described in the Danish bridge classification system (Danish Road Directorate, 2009). **Figure 1** shows an example of a classification vehicle (class 100 ton vehicle) with related axle load magnitudes, distances and geometries and with a distributed surface load, p.

The classification system describes the vehicle class with related axle configurations and load magnitudes. It is seen that a vehicle A- and B should be placed adjacent to each other and in the most undesirable way when applied to a given bridge structure.

When the load configurations are applied to short span bridges, it is often seen that the vehicle is too long for the bridge. Consequently, the rear axle represent the loading from the vehicle, since it provides the highest load magnitude. The combination of vehicle A- and B including safety factors should be less than the bridge capacity and as a result the bridge class is found.

Vehicle B always represents a fixed load. For the highest bridge class, vehicle B can reach an axle load of 11.8 tons. Vehicle A can reach an axle load up to 23.7 tons (without safety factors).

A novel test rig was developed specially to comply with these demands, and thereby enabled loading precisely as described in the Danish classification system. The loading rig is depicted in **Figure 2**. The rig applies an accurate vehicle A- and B load, by use of hydraulic jacks and dead loading. The hydraulic jacks are placed between the loading frames and main girder, whereas the dead load is applied directly on the vehicle A- and B loading frames. This configuration ensures a flexible high magnitude loading and enable a precise semi-deformation controlled loading (Schmidt et al., 2018).

The precision of the loading application is paramount for the probabilistic- and theoretical decision approach, which is dependent on the two components of load and resistance. With a precise loading application, the uncertainties connected with the load component are small, consequently resulting in a significant reduction of the overall model uncertainty. In addition, the code prescribes load values, but do not define the frequency of the load occurrence. When performing life cycle oriented decision analyses, such input is extremely relevant as well. So far, several one span bridges have been tested using the developed test rig. Two of the bridges had a span of ∼11 m, for which the monitoring setup consisted of a land surveyor, LVDTs, distance lasers, digital image correlation (DIC) as well as output from the separately controlled hydraulic jacks and deformation measurements between the test rig parts (see Halding et al., 2017; Schmidt et al., 2018).
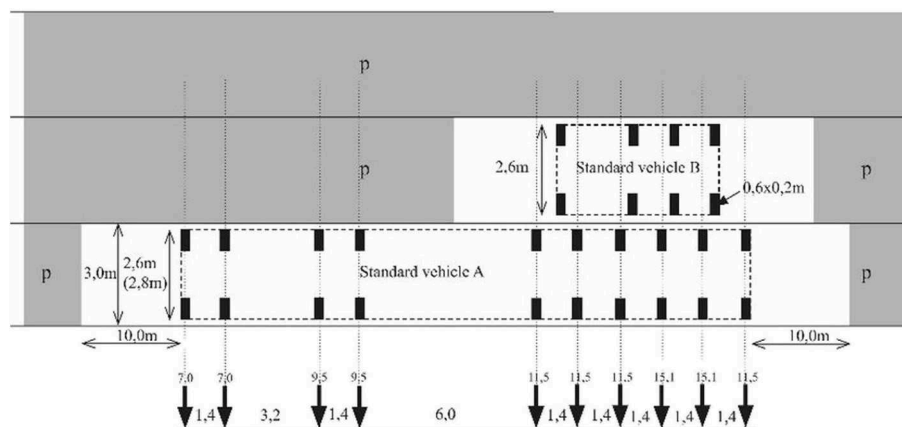
FIGURE 1 | Example of a classification vehicle—in this case a class 100-ton vehicle.
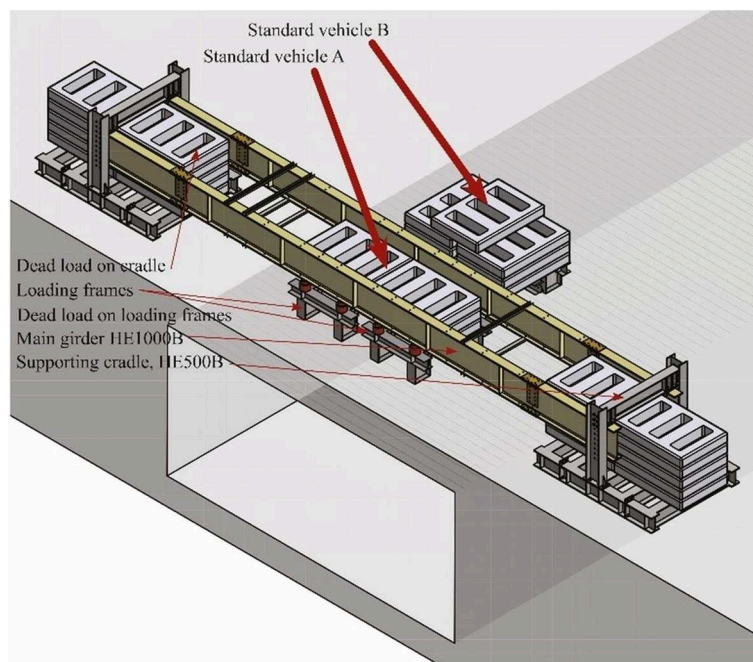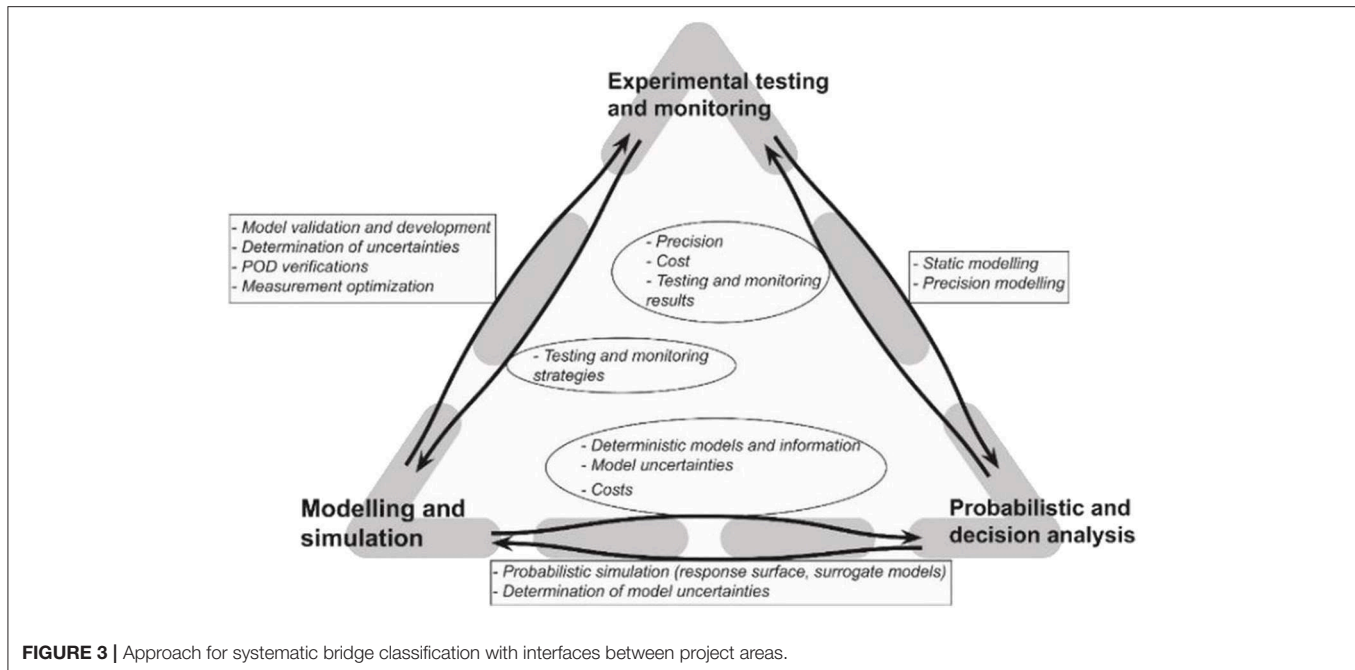

FIGURE 2 | Loading rig.

The bridges consisted of pre-stressed OT-beams (overturned T-beams) with *in-situ* concrete cast on top, a bitumen layer, protective concrete layer and finally asphalt.

Testing was performed within 1 day and the test rig applied an axle load of approximately 100 ton (test rig limit) without reaching failure, which is more than four times the highest axle load described in the classification system.

It was observed that *in-situ* monitoring during testing can be challenging. Most of the monitoring equipment are originally intended for controlled laboratory use and thus susceptible to *in-situ* environment and challenges related to a tight time schedule. However, it was still possible to obtain promising results and

strong indications. The usability and precisions of the monitoring methods on larger structures and in *in-situ* conditions are presently being evaluated in detail.

As for the load application, a good precision of the monitoring equipment is essential as a mean to calibrate the theoretical model and as input in the probabilistic model. Another important monitoring output is indicative occurrences, which can be used as both stop criteria and/or input in theoretical models, which can be updated during testing. An example of an indicative occurrence could be the detection of a crack in a certain zone or indications of initial damage occurrence. When deciding if further loading should be applied during testing, the upcoming

FIGURE 3 | Approach for systematic bridge classification with interfaces between project areas.

loading step would then be concluded upon by the use of several input parameters and not a single threshold alone. In addition, it is in this case assumed that the load-deformation relationship (i.e., ductile or brittle behavior) is evaluated and decided upon. This concept is proposed as a first step toward a systematic bridge classification method, where (1) an iterative calibration of the theoretical model, (2) close monitoring of stop criteria including continuous updating from the theoretical model, and (3) probabilistic models continuously updated with input from the theoretical model and from monitoring, which consequently provides approval for an upcoming load step during testing.

SYSTEMATIC BRIDGE CLASSIFICATION

A systematic and network-wise reclassification may be achieved by a combination of methods, approaches and technologies with a linked research synergy, **Figure 3**. This includes development of (1) modeling and simulation techniques especially for more realistic models of the structural behavior, (2) tailored testing strategies in combination with advanced monitoring and (3) probabilistic and decision analyses to combine modeling, testing, and performance information as well as to identify efficient strategies for next load step approval and thus reclassification. The interfaces between the project areas "Modeling and simulation," "Testing and monitoring," and "Probabilistic and decision analyses" are very relevant for the success of the overall and the individual project areas. **Figure 3** contains the approach and lists keywords for interactions between the linked research areas.

The area "Probabilistic and decision analyses" can support "Modeling and simulation" and "Testing and monitoring" with expertise on:

(1) statistical, probabilistic and uncertainty (or precision) modeling to analyze measurement results,
(2) how to combine probabilistic and simulation models and
(3) how to determine model uncertainties.

The project area "Probabilistic and decision analyses" needs support from "Modeling and simulation" in terms of:

(1) the integration of the information type (e.g., model parameter, random variable, indication or capacity) in the probabilistic models,
(2) the monetarization of the human, software and hardware resources
(3) the quantification of the model- and physical structural uncertainties.

The project area "Probabilistic and decision analyses" needs support from "Testing and monitoring" in terms of:

(1) the experimental outcomes and related precision,
(2) the quantification of the testing, monitoring and operational uncertainties
(3) the monetarization of the needed analyses, human and testing resources.

The interface between "Probabilistic and decision analyses" and "Testing and monitoring" are here further elaborated upon, for explanatory purposes.

The experimental outcomes are the overall result of testing, which can roughly be described as: (1) Brittle collapse, without warning, (2) Occurrence of irreversible damage, which is not detected by monitoring in time, and (3) A successful test, where the target load is reached or the loading is stopped in time to prevent irreversible damage.

TABLE 1 | Recommendations for stop criteria for proof load testing (Lantsoght et al., 2018).

Failure mode	Cracked in bending or not	
	Not cracked in bending	Cracked in bending
Bending moment	$\varepsilon_c < \varepsilon_{c,lim} - \varepsilon_{c0}$	$\varepsilon_c < \varepsilon_{c,lim} - \varepsilon_{c0}$
	$w_{max} \leq 0.5\ mm$	$w_{max} \leq 0.5\ mm$
	$w_{res} \leq 0.3\ w_{max}$, min 0.05 mm	$w_{res} \leq 0.2\ w_{max}$, min 0.05 mm
	25% reduction in stiffness	25% reduction in stiffness
	Deformation profiles	Deformation profiles
	Load-deflection diagram	Load-deflection diagram
Shear	$\varepsilon_c < \varepsilon_{c,lim} - \varepsilon_{c0}$	$\varepsilon_c < \varepsilon_{c,lim} - \varepsilon_{c0}$
	$w_{max} \leq 0.3\ mm$	25% reduction in stiffness
	25% reduction in stiffness	Deformation profiles
	Deformation profiles	Load-deflection diagram
	Load-deflection diagram	

The quantification of the testing, monitoring and operational uncertainties are comprehensive to describe, but considers essential input parameters for the probabilistic model. Considering stop criteria and measurement equipment, the stop criteria recently proposed in Lantsoght et al. (2018) are shown in **Table 1**. Criteria are proposed for both bending and shear failure, though it is stated that the criteria for shear needs further research. However, the uncertainties connected to the criteria are not quantified toward probabilistic model input based on the applied monitoring equipment. When considering strain levels or crack widths in a test and the criteria values are reached, it is paramount to know the probability, that the measured value is equal to the true value. In an *in-situ* environment, this can sometimes be a significant challenge. In connection with the proposed stop criteria it is also stated, that in bridge tests performed to failure, the loading would have been stopped at 60–70% of the maximum applied load when applying the proposed criteria. The safety/risk in this is described as being "not overly conservative," which seems to reveal a need for a quantification to an input value applicable in a decision analysis. Input for this could be the generated from the "Modeling and simulation" area.

An alternative stop criteria could be the detection of crack formation, which also presents a need for quantification of two parameters needed in the probabilistic analysis; (1) the probability of detection of a crack, and (2) the probability that the detected actually is a crack and not a false positive, both given a pre-defined threshold.

The monetarization of the needed analyses in terms of human and testing resources are needed in the decision analysis to match risk with cost for the most profitable decision.

PROBABILISTIC AND DECISION ANALYSIS APPROACH

In the context of probabilistic and decision analyses, this section provides a starting point for a decision analytical approach for bridge reclassification, i.e., for the combination of all relevant information to reduce uncertainties related to the performance of bridges and the identification of cost- and risk efficient reclassification strategies building upon Thöns (2018). The decision analytic approaches takes basis in the Bayesian decision theory, see e.g., Raiffa and Schalifer (1961) and Benjamin and Cornell (1970), and the utility theory, see Von Neumann Morgenstern (1947). The framework encompasses (1) proof loading information on component and system level, (2) outcomes of laboratory tests on component and subsystem level, (3) modeling and simulation information with various refinement levels and (4) a combination of these strategies. In the scientific literature, the stated elements of the framework have been analyzed separately and not integrally [see e.g., Yang (1976), Lin and Nowak (1984), Rackwitz and Schrupp (1985), Diamantidis (1987), Fu and Tang (1995), Saraf and Nowak (1998), Faber et al. (2000), Ersdal et al. (2003), Nishijima and Faber (2007), Sørensen and Toft (2010), Thöns et al. (2011), Casas and Gómez (2013), Gutermann and Schröder (2015), Brüske and Thöns (2016), Lantsoght et al. (2016, 2017)].

Description of Decision Processes

The decision process is subdivided into two interconnected decision situations. Decision situation 1 constitutes the efficient planning and performance of the proof loading and the prevention of bridge damage. Decision situation 2 constitutes decision about the most efficient bridges reclassification strategy encompassing proof loading, laboratory testing and advanced modeling and simulation.

For decision situation 1, the decision maker is the planner of the proof loading. The decision maker chooses the loading level, the monitoring technologies and methods as well as the stop criteria to minimize the expected costs of the test and to comply with the acceptable risks.

The decision tree in **Figure 4** illustrates the decision process with decision nodes (rectangles) which refer to the choices. The chance nodes (circles) represent the most relevant uncertainties associated to the choices, i.e., the decision variables, and encompass testing, monitoring, operational, model, statistical, and structural uncertainties. The temporal dimension added to the decision scenario illustrates the effects of the proof load testing on the expected life cycle costs of the bridge through the updated failure probabilities and subsequent risk reduction. The connections in the decision tree are representative of the effect of the proof loading survival outcome on the bridge probability of failure in the year(s) following the testing. The optimization is performed with consideration to the target reliability levels recommended by for e.g., the probabilistic model code [Joint Committee on Structural Safety (JCSS), 2001], which serve as boundaries for the decision analysis.

Decision situation 2 is subdivided into the information acquirement phase and the bridge utilization phase. The decision maker is here the planner of the reclassification and can select the combination of the *in-situ* proof loading, experimental testing and simulation strategies. The objective is the maximization of the expected benefits with the reclassification of a bridge in
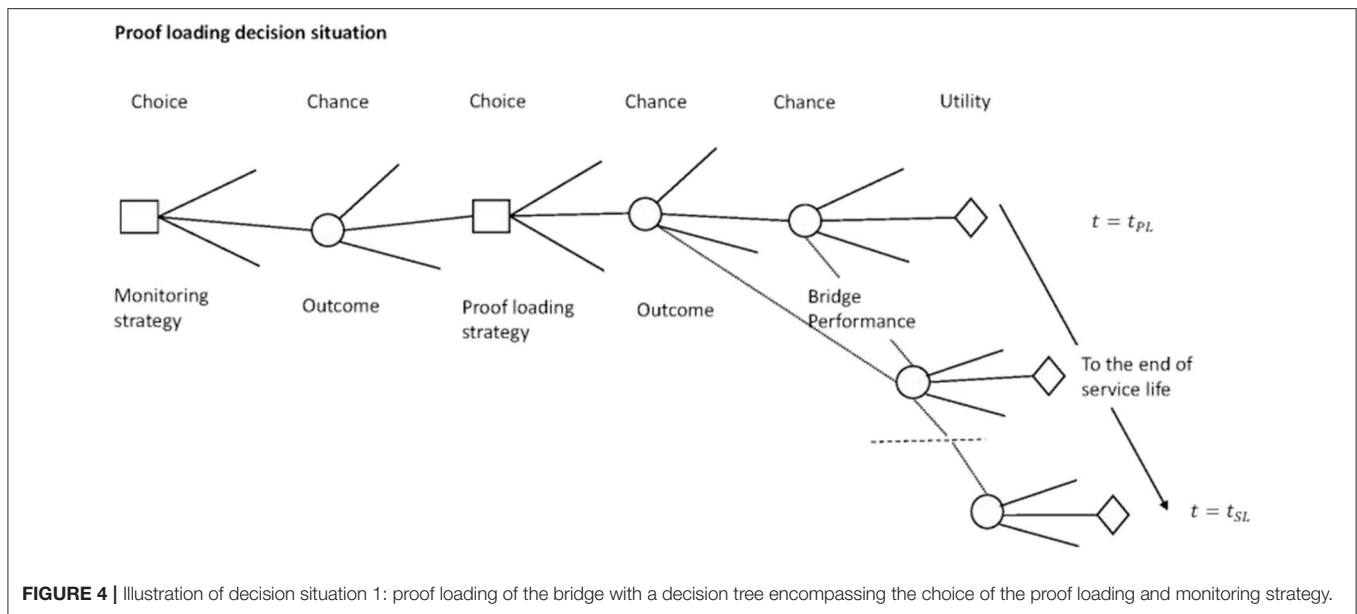
combination with the least expected costs for the proof loading, laboratory testing and the modeling information.

The information acquirement phase encompasses the modeling and simulation, experimental testing and proof loading approaches. For modeling and simulation, the decision variables are represented by the modeling approaches and simulations with various refinement levels. The precision of these models and simulations are described with model uncertainties. The experimental testing includes different strategies such as e.g., laboratory testing of sub-systems and components as well as material parameters as decision variables. The outcomes of the experimental testing are described with the uncertainties associated to the experiments and tests accounting for the measurement uncertainties and the operational uncertainties. Proof loading encompasses various proof loading strategies on system, sub-system and component level and the associated uncertainties together with monitoring during the proof loading test (see decision scenario 1).

The utilization phase contains the load bearing capacity, i.e., the classification of the bridge, as the decision variable and the uncertain performance in the remaining service life including e.g., the gathered information and degradation. The bearing capacity choice includes e.g., the choice of an increased load rating for the bridge. Utilities, i.e., expected benefits and expected cost as well as risks are associated to the decision variables, i.e., the information acquirement strategies, and the bearing capacity class and the operational costs throughout the service life. For a full-scale proof load test, the risk of structural failure is part of the consequence and follow-up consequence modeling.

Illustration

As an illustration, decision situation 1 is expanded upon with an example to demonstrate the probabilistic and decision framework and the interface between project areas of "Probabilistic and decision analyses" and "Testing and monitoring." Let us consider a deteriorated bridge at an advanced age, having completed 85 years of its' planned service life of 100 years (t_{SL}). It is planned to perform a full scale proof loading of the bridge in order to assess the reliability of the structure. The decision scenario considers the proof load test planner who seeks to identify the optimal proof loading strategy, monitoring method and technology as well as the stop criteria that lead to an efficient and safe testing. The decision situation is considered in the following sections first with a prior decision analysis where the benefit gain from performing a full-scale proof loading is assessed. Here, the performance of the bridge is modeled by calculating its annual probability of failure. The outcome of a proof load testing with different proof load levels is predicted and a decision analysis is performed to identify the optimal proof load level as the one leading to the highest expected benefit gain. The expected benefit gain is quantified as the difference between the optimal expected utility with and without any proof load testing. A pre-posterior decision analysis with additional predicted information is illustrated with the consideration of monitoring information during proof load testing. In the pre-posterior decision analysis, the outcome of the proof load testing as well as the information obtained from the monitoring system during the testing is predicted. The decision analysis enables the identification of the optimal information choice (monitoring system) and the optimal choice of stop criteria. This is achieved by maximizing the value of information and actions i.e., the difference between the optimal expected utility with and without additional information (from the monitoring) and actions (proof load testing).

Prior Decision Analysis

The performance of the bridge in the ultimate limit state is described with the quantification of its reliability level or probability of failure. For this purpose, limit state functions of the variables influencing the bridge reliability e.g., the resistance,

deterioration, loading etc., are formulated. The methods for calculation of the reliability level or failure probability from the limit state function are well-documented in literature, see e.g., Ditlevsen and Madsen (2005). The bridge is modeled as a structural system with n_c number of components and the system failure probability is computed by modeling the bridge as a ductile Daniels' system (Daniels, 1945). This is considered keeping in view the system redundancy—failure of a bridge component does not lead to failure of the whole system as the loads may be redistributed among the remaining components. It should be noted that the systems model used is a generic model and not based on an actual structure. The annual probability of failure for the system and a component in any year t is calculated with the following limit state functions,

$$P\left(F_{sys}\left(t\right)\right) = P\left(g_{f,sys}\left(\mathbf{X}, t\right) \leq 0\right)$$

$$= P\left(\sum_{i=1}^{n_c} M_{R_{c,i}} R_{c,i}\left(t\right) - M_S(S_D + S_L) \leq 0\right) \quad (1)$$

$$P\left(F_{c,i}\left(t\right)\right) = P\left(g_{f_{c,i}}\left(\mathbf{X}, t\right) \leq 0\right) \quad (2)$$

$$= P\left(M_{R_{c,i}} R_{c,i}\left(t\right) - M_S\left(S_D + S_L\right) \cdot \left(\frac{1}{n_c}\right) \leq 0\right)$$

$$R_{c,i}(t) = R_{c,i}\left(1 - D_{c,i} \cdot t\right) \quad (3)$$

In the formulations above, $R_{c,i}$ represents the resistance or capacity of the component, S_L represents the annual maximum live load, S_D represents the dead load (self-weight and other permanent fixtures), $M_{Rc,i}$ and M_{S_L} represent the associated model uncertainties, $D_{c,i}$ represents the deterioration and n_c is the number of components. The mean of the resistance distribution is calibrated assuming that the system reliability is 4.7 (reference period 1 year) in the Ultimate Limit State in the first year of service i.e., without any deterioration. This corresponds to the recommended target reliability level for a structure with large consequences of failure and small relative costs of safety measure, based on a monetary optimization [Joint Committee on Structural Safety (JCSS), 2001]. The annual maximum live load with a return period of 1 year is used for this calibration. The probabilistic models of the resistance and resistance model uncertainties are based on assumptions and will be further developed with further information and research in the project. The probabilistic model for the structural properties used is provided in **Table 2**. Further, the system is modeled with 5 components, considering correlation between component resistances' and resistance model uncertainty ($\rho_{R_iR_j} = 0.7$, $\rho_{M_{Ri}M_{Rj}} = 0.5$), and component deterioration ($\rho_{D_iD_j} = 0.8$).

In the decision scenario of the testing, the application of the loading is defined as the action available to the decision maker. The choice of the loading level can then be modeled as the set of actions. The choice of different load levels varying from 0.5 to 2 times the characteristic value of the annual maximum live load S_k is considered. The characteristic value S_k is here defined as the load with a probability of non-exceedance of 0.98 in a reference

TABLE 2 | Probabilistic Model of structural properties.

Parameter	Distribution type	Mean	Standard deviation
$R_{c,i}$	Lognormal	Calibrated	10% of mean
S_D	Normal	1	0.05
S_L	Gumbel	1	0.10 (Faber et al., 2000)
S_{PL}	Deterministic	0.5 to 2 S_k	–
$M_{R,i}$	Lognormal	1.2	0.15 [Joint Committee on Structural Safety (JCSS), 2001]
M_{SL}	Lognormal	1	0.20
M_{SPL}	Lognormal	1	0.20
$D_{c,i}$	Lognormal	0.001	0.001 (Thöns et al., 2018)

period of 1 year.

$$P\left(F_{PL}\left(S_{PL_j}, t_{PL}\right)\right) = P\left(g_{f_{PL}}\left(\mathbf{X}, S_{PL_j}, t_{PL}\right) \leq 0\right)$$

$$= P\left(\sum_{i=1}^{n_c} M_{R_{c,i}} R_{c,i}\left(t_{PL}\right) - M_{S_{PL}}\left(S_D + S_{PL_j}\right) \leq 0\right) \quad (4)$$

Following a successful outcome of the testing, the updated probability of failure of the bridge in any year t is calculated using Bayes' theorem,

$$P\left(F_{sys,u}\left(S_{PL_j}\right), t)\right) = \frac{P\left(g_{f,sys}\left(\mathbf{X}, t\right) \leq 0 \cap g_{f_{PL}}\left(\mathbf{X}, S_{PL_j}, t_{PL}\right) > 0\right)}{P\left(g_{f_{PL}}\left(\mathbf{X}, S_{PL_j}, t_{PL}\right) > 0\right)} \quad (5)$$

It may be expected that the higher the proof load level, the higher would be the updated reliability of the bridge, leading to higher benefit gain from performing the testing but, at the same time, high proof loads may end up damaging the bridge or, worst, cause the bridge to collapse during testing. This is illustrated in **Figures 5**, **6**. The updated annual reliability level of the bridge for the different proof load levels, calculated from Equation 5, is plotted in **Figure 5**. As a reference, the annual reliability level without any proof loading, calculated using Equation 1, is also plotted. It is observed that load levels higher than 1.0 S_k are needed to demonstrate a reliability level higher than the target reliability level of 4.7. The reliability level of the bridge due to the applied proof load (during the test) is plotted in **Figure 6** (refer Equation 4).

In the year of performing the proof load test, the bridge may either fail due to the annual maximum live load or due to the proof loading test. The failure probability in the year of testing t_{PL} then is obtained as the union of the events of failure due to test or due to annual maximum live load.

$$P\left(F_{sys}\left(S_{PL_j}, t_{PL}\right)\right) =$$
$$P\left(g_{f,sys}\left(\mathbf{X}, t_{PL}\right) \leq 0 \cup g_{f_{PL}}\left(\mathbf{X}, S_{PL_j}, t_{PL}\right) \leq 0\right) \quad (6)$$
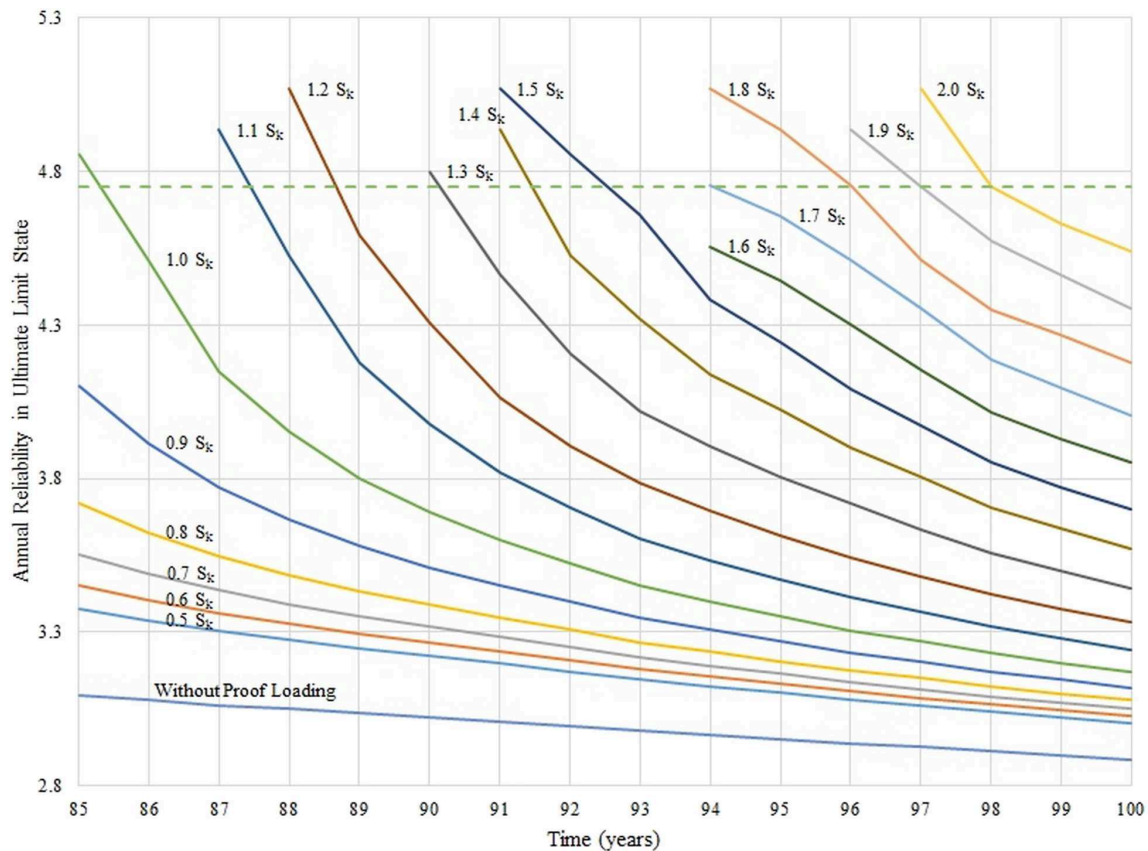
FIGURE 5 | Illustration of the updated annual reliability levels following load testing with the different proof load levels (indicated next to the curves). The annual reliability level without any proof loading is also plotted along with the target annual reliability level of 4.7 (dotted curve).
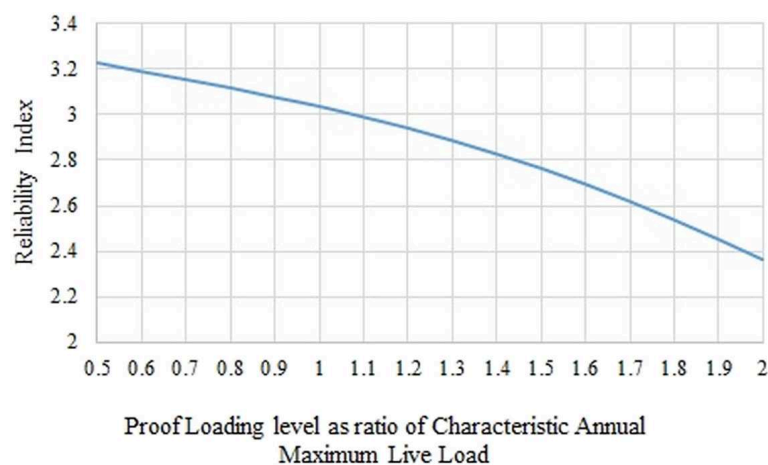

FIGURE 6 | Reliability level of the bridge during testing as a function of the proof load levels.

The expected utility is calculated with the aggregation of the expected costs from the structural performance over the remaining service life of the bridge (the costs are modeled as negative utilities). The total expected costs over the remaining service life of the bridge is obtained with the summation of the annual risks. The annual risk of structural failure is computed as the product of the annual probability of failure and the cost incurred as a consequence of failure. In the year of the testing,
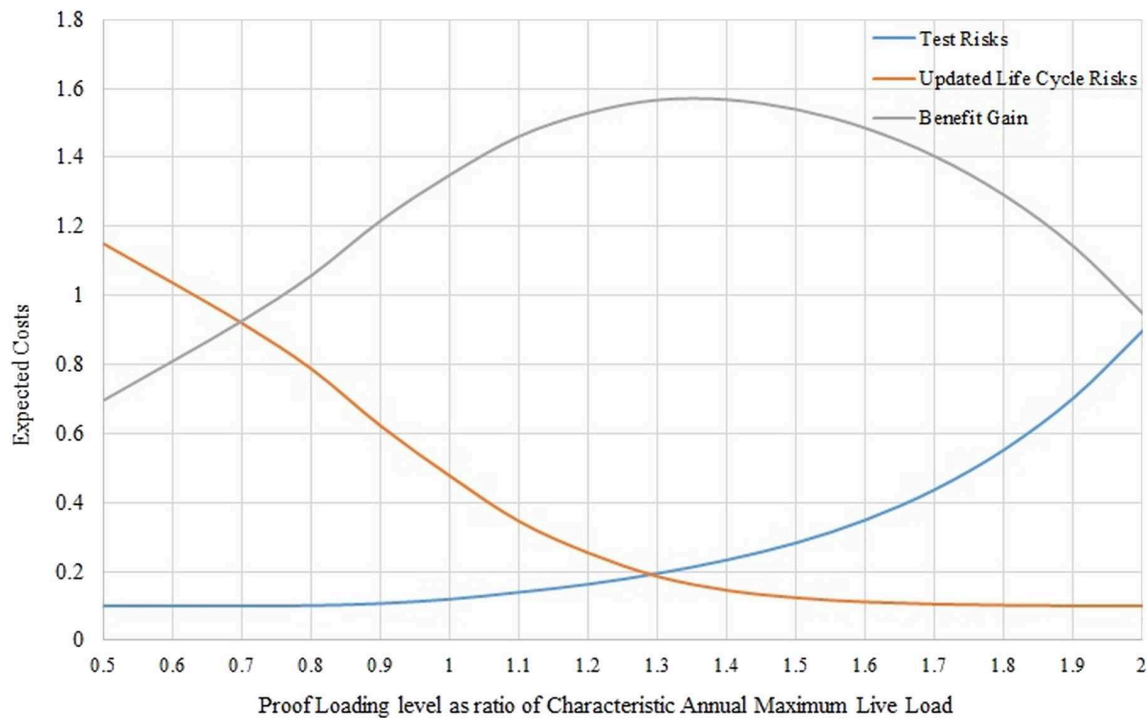
FIGURE 7 | Illustration of expected costs (test risks in blue and life cycle risks in orange) and benefit gain (in gray) from the proof loading as a function of the proof load level.

the risk due to the test performance is taken into account by calculating the annual failure probability according to Equation 6. The consequence of failure is modeled as a cost $C_f = 100$ monetary units. In computing the total expected costs with the testing, the cost of performing the proof loading test, $C_{PL} = 0.1$ monetary units, is also added. A depreciation in the modeled costs is considered to discount the future costs to present value, with a discount rate of $r = 2\%$. The calculation of the expected utility without any proof load testing, U_0, is presented in Equation 7. The expected utility corresponding to proof load testing with the jth proof load level, $U_1 \left(S_{PLj} \right)$, is calculated using Equation 8.

$$U_0 = \sum_{t_{PL}}^{t_{SL}} P \left(F_{sys} (t) \right) \cdot C_f \cdot (1 + r)^{-t} \tag{7}$$

$$
\begin{aligned}
U_1 \left(S_{PLj} \right) &= C_{PL} + P \left(F_{sys} \left(S_{PLj}, t_{PL} \right) \right) \cdot C_f \cdot (1 + r)^{-t_{PL}} \\
&\quad + P \left(\overline{F_{PL}} \left(S_{PLj}, t_{PL} \right) \right) \sum_{t_{PL}+1}^{t_{SL}} P \left(F_{sys,u} \left(S_{PLj}, t \right) \right) \cdot \\
&\quad C_f \cdot (1 + r)^{-t}
\end{aligned}
\tag{8}
$$

It may be expected that the higher the proof load level, the higher would be benefit gain from performing the testing on account of the reduced life cycle risks, but, at the same time, high values of the loading also lead to higher risks from the testing. This is clearly observed in **Figure 7** where the risks in the year of

testing show an upward trend but the updated risks in the year following the testing decrease with increasing proof load levels. Subsequently, the expected benefit gain "$U_1 \left(S_{PLj} \right) - U_0$" shows an increase due to the risk reduction up to a certain level beyond which the risks from the testing cause a drop.

From the prior decision analysis, it is found that the optimal loading level is 1.3 S_k which leads to the maximum expected benefit gain of 1.56 monetary units (see **Figure 7**). The updated reliability index with this load level is plotted in **Figure 5** and is observed to satisfy the target reliability criteria. Further, with the deterioration model assumed, it is observed (from **Figure 5**) that the reliability level of the bridge is above the target for up to year 90 of the service life of the bridge. The bridge operator can use this information to schedule repair and maintenance activity.

Pre-posterior Decision Analysis

The decision situation considers the proof load test planner who seeks to identify the optimal strategies for a successful full-scale proof loading test. These include selection of the stop criteria, the optimal method and type of monitoring and the optimal loading level. To achieve this, a pre-posterior decision analysis is performed where the optimal choices are identified with the consideration of yet unknown additional information. The information is acquired from the monitoring system deployed during the proof load testing which measures the structure response to the loading i.e., deformations, strains etc.

The information acquirement leads to knowledge of the realization of the loading model uncertainty related to the load
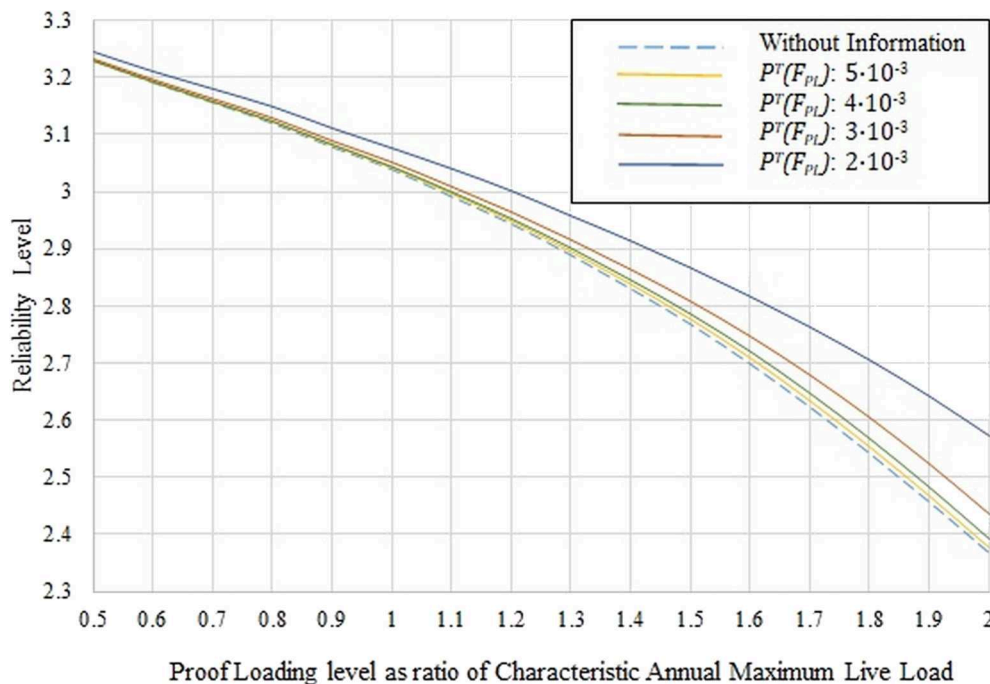
FIGURE 8 | Reliability level of the bridge during testing following indication event $\mathbf{Z_1}$ with the different stop criteria ($\mathbf{P^T}$ ($\mathbf{F_{PL}}$)) used.

effect i.e., by loading the structure a realization of the model uncertainty is manifested and this can be measured by the monitoring system. Hence, the model uncertainty on the loading is updated,

$$M''_{S_{PL}} = U_{meas} \cdot \hat{M}_{S_{PL}} \qquad (9)$$

Here, U_{meas} is the measurement uncertainty of the monitoring system modeled with a normal distribution and $\hat{M}_{S_{PL}}$ is the realization of the model uncertainty. The realization of the model uncertainty may be higher or lower than the expected value. A high realization could lead to higher risks of damage to the structure and thereby to the actions of stopping the loading whereas a lower realization could be beneficial as the loading could be continued. Agusta and Thöns (2018) proposed a method for categorizing the realizations of the model uncertainties in connection with target probabilities. Here, the target failure probability for the proof loading is considered as the stop criteria. The value for model uncertainty realization at the threshold $\hat{M}_{S_{PL},th}$ is derived using the following:

$$P\left(g_{f_{PL,c,i}} \leq 0 \Big| \hat{M}_{S_{PL},th}\right) = P^T(F_{PL}) \qquad (10)$$

In the equation above, $g_{f_{PL,c,i}}$ models the ith component's performance in a load testing and $P\left(g_{f_{PL,c,i}} \leq 0 \Big| \hat{M}_{S_{PL},th}\right)$ is the probability of failure of the ith component during the load testing given that the loading model uncertainty is equal to the threshold value. The outcomes of the structural measurement can be defined in reference to the threshold value as two

indication events: event Z_1 where the monitoring indicates that the component has adequate performance (i.e., the realization of the loading model uncertainty is lower than the threshold value) and event Z_2 where the monitoring indicates that the component has inadequate performance. The target probability of proof loading failure $P^T(F_{PL})$ (or the stop criteria) is treated as a decision parameter to be optimized.

In the following, the loading model uncertainty value at the threshold $\hat{M}_{S_{PL},th}$ is derived by modeling the component performance at load level $0.5\ S_k$ and using target probabilities $5 \cdot 10^{-3}$ to $2 \cdot 10^{-3}$ (Equation 10). The indication events are modeled with the distribution of the loading model uncertainty $f_{M_{S_{PL}}}\left(m_{S_{PL}}\right)$ and a threshold value corresponding to a target failure probability (Equations 11 and 12).

$$P(Z_1) = \int_0^{\hat{M}_{S_{PL},th}} f_{M_{S_{PL}}}\left(m_{S_{PL}}\right) dm_{S_{PL}} \qquad (11)$$

$$P(Z_2) = \int_{\hat{M}_{S_{PL},th}}^{\infty} f_{M_{S_{PL}}}\left(m_{S_{PL}}\right) dm_{S_{PL}} \qquad (12)$$

The expected utility is calculated for each of the stop criteria with consideration of the information and the decision rule that the action of a higher proof loading level is performed only if indication Z_1 is obtained. The calculation is inclusive of the costs of monitoring and testing. The monitoring system is modeled with a cost $C_i = 0.01$ monetary units and precision $U_{meas} \sim N(1, 0.01)$. **Figure 8** illustrates the effect of the indication event Z_1, on the reliability during the proof load testing. A risk reduction can be achieved with the information of adequate performance during the proof load testing (indication event Z_1).
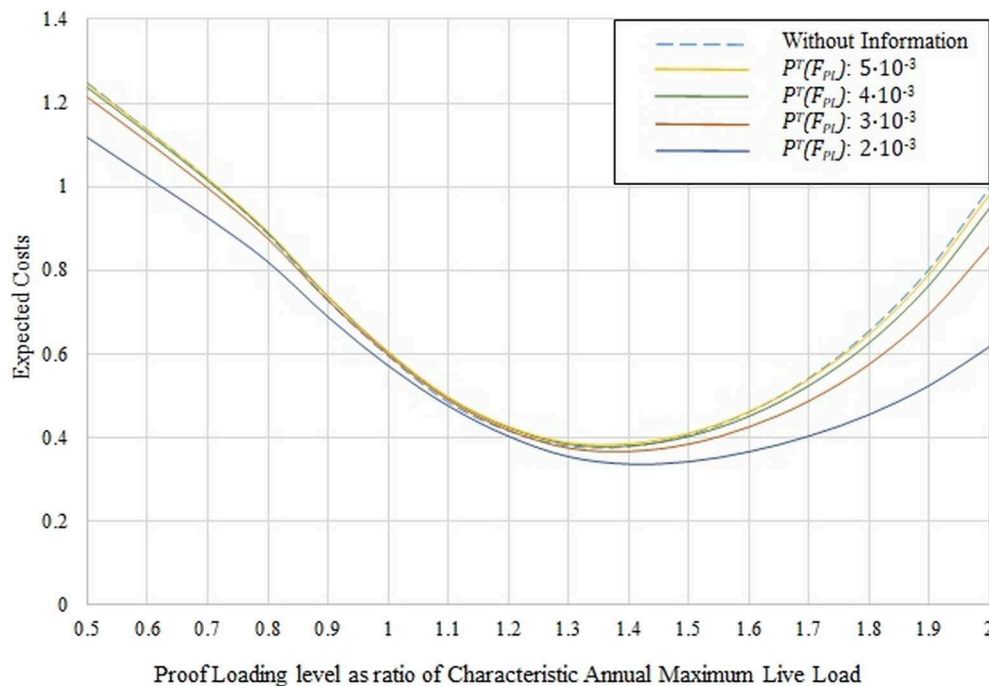
FIGURE 9 | Expected remaining service life costs (inclusive of test risks) as a function of the proof loading level (conditional on indication event Z_1).
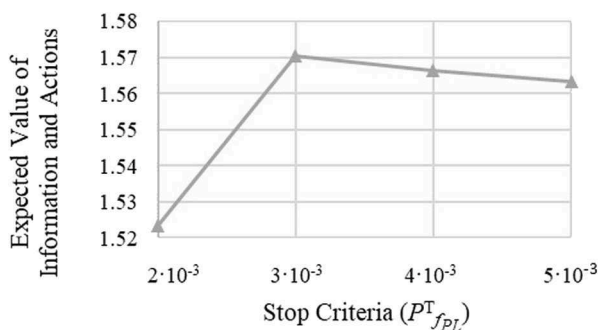

FIGURE 10 | Expected Value of Information and Actions considering the different stop criteria ($\mathbf{P}^T$ ($\mathbf{F}_{PL}$)) used.

This can be observed in **Figure 9** where the expected life cycle costs conditional on the indication event Z_1, are plotted.

The Value of Information and Actions is calculated as the difference between the optimal expected utility with proof load testing and monitoring information and the expected optimal utilities without any proof load testing and monitoring. The results are presented in **Figure 10** for the different stop criteria considered. It is observed that using the stop criteria with $P^T(F_{PL})$: $3 \cdot 10^{-3}$ leads to the highest expected Value of Information and Actions. The loading level leading to the highest expected utility with this stop criteria is 1.4 S_k.

The analysis may be repeated for monitoring systems with different precision and costs to identify the optimal

monitoring system, and the associated optimal choices of stop criterion and load level, with the comparison of the expected Value of Information and Actions from different monitoring systems (Kapoor et al., 2019).

Summary and Outlook

For the reclassification of bridges, two decision support approaches have been identified namely (1) for the efficient planning and performance of the proof loading and the prevention of bridge damage and (2) for the identification of an efficient bridge reclassification strategy encompassing proof loading, laboratory testing and advanced modeling and simulation. An exemplary decision analysis has been performed to demonstrate how the optimal proof loading level can be identified and how monitoring based stop criteria may be identified with the utilization of the probabilistic design and decision analysis models.

Both, the decision support approaches and the exemplary decision analysis constitute a first step and will be further substantiated and further developed to align the decision scenarios and the structural and structural information modeling to specific bridges and the specific bridge integrity management processes. One of the challenges related to the decision analyses seem to relate to the precision of the theoretical model related to the structural behavior. It seems to be a precondition that there are a number of unknown contributions to the actual capacity of the structure that cannot be sufficiently modeled analytically. A reduction in the uncertainties related to the models is achieved when applying proof loading. If, however, an extremely accurate model for the capacity is used as a basis, proof loading may not serve as an efficient means for

the reclassification. It therefore seems important to provide the information interaction between the disciplines described in **Figure 3**. However, we cannot abstain from using the basis theoretical model, because we need to use a model of the structural behavior in order to determine the critical failure mode and the critical load configuration. This is why the illustration in **Figure 3**, which indicates that there is an important information interaction back and forth between all the three different disciplines.

SUMMARY AND CONCLUSIONS

This paper summarizes recent challenges advances in proof loading of bridges and introduces an approach of the systematic reclassification of bridges. The development of a full-scale test method is described in detail addressing the demands of a high loading magnitude combined with a fast and precise load application.

The systematic and network wise reclassification of bridges maybe achieved by a combination of methods, approaches and technologies with directed research. This includes the further development of (1) modeling and simulation techniques, (2) of tailored testing strategies in combination with monitoring, and (3) probabilistic and decision analyses to combine modeling, testing and performance information and to identify efficient strategies for reclassification.

DATA AVAILABILITY STATEMENT

All datasets generated/analyzed for this study are included in the article/supplementary material.

AUTHOR CONTRIBUTIONS

All authors have agreed on the content of this paper. Consequently, it includes a result of the author's discussions and portions of their expertise in the paper sections. However, ST, MK, SE, and JDS have worked mostly on the probabilistic part with ongoing discussions with JWS who have worked on the remaining parts (i.e., testing, systematic re-classification etc.) with assistance from CC. However, it is difficult to separate the contributions sharply, which has not been the scope of the collaborating authors.

ACKNOWLEDGMENTS

REFERENCES

AASHTO (2011). *The Manual for Bridge Evaluation*. Washington, DC: American Association of State Highway and Transportation Officials.

ACI Committee 437 (2013). *Code Requirements for Load Testing of Existing Concrete Structures (ACI 437.2M-13)*. Farmington Hills, MA: ACI Committee 437.

Agusta, A., and Thöns, S. (2018). "Structural monitoring and inspection modeling for structural system updating," in *Sixth International Symposium on Life-Cycle Civil Engineering* (Ghent).

Alkhrdaji, T., Barker, M., Chen, G., Mu, H., Nanni, A., and Yang, X. (eds.). (2001). "Destructive and non-destructive testing of bridge J857," in *Strengthening and Testing to Failure of Bridge Decks, Vol. 1* (Phelps County, MO: Center for Infrastructure Engineering Studies), 1–131.

Benjamin, J. R., and Cornell, C. A. (1970). *Probability, Statistics and Decision for Civil Engineers*. New York, NY: McGraw-Hill Book Company.

Brüske, H., and Thöns, S. (2016). "Value of information by updating of model uncertainties utilising proof loading in the context of series and Daniels systems," in *Proceedings of the International RILEM Conference Materials, Systems and Structures in Civil Engineering* (Lyngby), 52–61.

Casas, J. R., and Gómez, J. D. (2013). Load rating of highway bridges by proof-loading. *KSCE J. Civil Eng.* 17, 556–567. doi: 10.1007/s12205-013-0007-8

Civil Engineering Review. (1952). Destruction of the Prestressed Concrete Footbridge at the South Bank. 6, 33.

DAfStb (2000). *DAfStb-Guideline: Load Tests on Concrete Structures*. Berlin: Deutscher Ausschuss für Stahlbeton.

Daniels, H. E. (1945). "The statistical theory of the strength of bundles of threads," in *Proceedings of the Royal Society of London. Series A, Mathematical and Physical Sciences*, Vol. 183, 405–435. Available online at: http://www.jstor.org/stable/97823 (accessed January 13, 2017).

Danish Road Directorate (2009). *EN 1991-2 DK NA:2009 - Annex A*.

Diamantidis, D. (1987). Reliability assessment of existing structures. *Eng. Struct.* 9, 177–182. doi: 10.1016/0141-0296(87)90013-7

Ditlevsen, O., and Madsen, H. O. (2005). *Structural Reliability Methods*. Available online at: http://www.mek.dtu.dk/staff/od/books.htm (accessed January 17, 2017).

Elmont, V. J. (1913). "Test-loading until breaking point of a 100-foot arch bridge," in *Canadian Engineer*.

Ersdal, G., Sørensen, J. D., and Langen, I. (2003). "Updating of structural failure probability based on experienced wave loading," in *International Offshore and Polar Engineering Conference*, Vol. 5 (Honolulu, HI), 461–468.

Faber, M. H., Val, D. V., and Stewart, M. G. (2000). Proof load testing for bridge assessment and upgrading. *Eng. Struct.* 22, 1677–1689. doi: 10.1016/S0141-0296(99)00111-X

Fu, G., and Tang, J. (1995). Risk-based proof-load requirements for bridge evaluation. *J. Struct. Eng.* 121, 542–556. doi: 10.1061/(ASCE)0733-9445(1995)121:3(542)

Goodpasture, D. W., and Burdette, E. G. (1973). Full scale tests to failure of four highway bridges. *Am. Railway Eng. Assoc.* 74, 454–473.

Gosbell, K. B., and Stevens, L. K. (1968). Test loading of a full scale bridge. *ARRB Proc.* 4, 2018–2041.

Gutermann, M., and Schröder, C. (2015). Loading vehicle BELFA development and experience gained in 10 years of practice. *Bridge Struct.* 11, 19–31. doi: 10.3233/BRS-150081

Halding, P. S., Schmidt, J. W., Jensen, T. W., and Henriksen, A. H. (2017). "Structural response of full-scale concrete bridges subjected to high load magnitudes," in *4th Conference on Smart Monitoring, Assessment and Rehabilitation of Civil Structures* (Zürich).

ICE (1998). *Guidelines for the Supplementary Load Testing of Bridges*. London: The Institution of Civil Engineers - National Steering Committee for the Load Testing of Bridges.

Joint Committee on Structural Safety (JCSS) (2001). *Probabilistic Model Code*. Joint Committee on Structural Safety (JCSS)

Jorgenson, J. L., and Larson, W. (1976). Field testing of a reinforced concrete highway bridge to collapse. *Transport. Res. Rec.* 66–71.

Kapoor, M., Schmidt, J. W., Sorensen, J. D., and Thöns, S. (2019). "A decision theoretic approach towards planning of proof load tests," in *13th International*

Conference on Applications of Statistics and Probability in Civil Engineering (ICASP13) (Seoul), 1715–1722.

Lantsoght, E. O. L. (2013). Shear in reinforced concrete slabs under concentrated loads close to supports. *ACI Struct. J.* 110, 275–284.

Lantsoght, E. O. L., Veen, C. V. D., Boer, A. D., and Hordijk, D. A. (2017). "Proof load testing of reinforced concrete slab bridges in the Netherlands," in *96th Annual Meeting of the Transportation Research Board* (Washington, DC).

Lantsoght, E. O. L., Yang, Y., Tersteeg, R. H. D., Van Der Veen, C., and De Boer, A. (2016). "Development of stop criteria for proof loading," in *Life-Cycle of Engineering Systems: Emphasis on Sustainable Civil Infrastructure*, eds J. Bakker, D. M. Frangopol, and K. van Breugel (Delft: Taylor & Francis), 1064–1071.

Lantsoght, E. O. L., Yang, Y., Van Der Veen, C., and Hordijk, D. A. (2018). "Stop criteria for proof load tests verified with field and laboratory testing of the Ruytenschildt Bridge Ruytenschildt field test," in *IABSE Conference* (Copenhagen), 1–8.

Lin, T. S., and Nowak, A. S. (1984). Proof loading and structural reliability. *Reliabil. Eng.* 8, 85–100.

Nanni, A., Alkhrdaji, T., Chen, G., Barker, M., Yang, X., and Mayo, R. (1999). "Overview of testing to failure of a highway bridge strengthened with FRP composites," in *4th International Symposium on FRP for Reinforcement of Concrete Structures (FRPRCS4)* (Baltimore, MD), 69–80.

NCHRP (1998). *Manual for Bridge Rating Through Load Testing*. Washington, DC: NCHRP.

Nishijima, K., and Faber, M. H. (2007). Bayesian approach to proof loading of quasi-identical multi-components structural systems. *Civil Eng. Environ. Syst.* 24, 111–121. doi: 10.1080/10286600601159172

NRA (2014). *Load Testing for Bridge Assessment*. Dublin: NRA.

Rackwitz, R., and Schrupp, K. (1985). Quality control, proof testing and structural reliability. *Struct. Safety* 2, 239–244. doi: 10.1016/0167-4730(85)90030-X

Raiffa, H., and Schalifer, R. (1961). *Applied Statistical Decision Theory*. Boston, MA: Harvard University Press.

Rösli, A. (1963). *Die Versuche an der Glattbrücke in Opfikon*. Eidgenössische Materialprüfungs- und Versuchsanstalt für Industrie, Bauwesen und Gewerbe, 192, 85.

Saraf, V., and Nowak, A. S. (1998). Proof load testing of deteriorated steel girder bridges. *J. Bridge Eng.* 3, 82–89. doi: 10.1061/(ASCE)1084-0702(1998)3:2(82)

Schmidt, J. W., Halding, P. S., Jensen, T. W., and Engelund, S. (2018). High magnitude loading of concrete bridges. *ACI Struct. J.* 323, 9.1–9.20.

Sørensen, J. D., and Toft, H. S. (2010). Probabilistic design of wind turbines. *Energies* 3, 241–257. doi: 10.3390/en3020241

Thöns, S. (2018). On the value of monitoring information for the structural integrity and risk management. *Comp. Aided Civil Infrastruct. Eng.* 33, 79–94. doi: 10.1111/mice.12332

Thöns, S., Döhler, M., and Long, L. (2018). On damage detection system information for structural systems. *Struct. Eng. Int.* 28, 255–268. doi: 10.1080/10168664.2018.1459222

Thöns, S., Faber, M. H., and Rücker, W. (2011). "On the utilization of monitoring data in an ultimate limit state reliability analysis," in *11th International Conference on Applications of Statistics and Probability in Civil Engineering (ICASP)* (Zurich).

Von Neumann and Morgenstern (1947). *Theory of Games and Economical Behavior*. Princeton, NJ: Princeton University Press.

Yang, J. N. (1976). Reliability analysis of structures under periodic proof tests in service. *AIAA J.* 14, 1225–1234. doi: 10.2514/3.7214

Zhang, J., Peng, H., and Cai, C. S. (2011). Field study of overload behavior of an existing reinforced concrete bridge under simulated vehicle loads. *J. Bridge Eng.* 16, 226–237. doi: 10.1061/(ASCE)BE.1943-5592.0000140

Zhang, J., Peng, H., and Cai, C. S. (2013). Destructive testing of a decommissioned reinforced concrete bridge. *J. Bridge Eng.* 18, 564–569. doi: 10.1061/(ASCE)BE.1943-5592.0000408

Non-destructive Testing of a 100-Year-Old Reinforced Concrete Flat Slab Bridge

Patryk J. Wolert[1]*, Marek K. Kolodziejczyk[2], J. Michael Stallings[3] and Andrzej S. Nowak[3]

[1] COWI North America, Seattle, WA, United States, [2] PRIME AE, Richmond, VA, United States, [3] Department of Civil Engineering, Auburn University, Auburn, AL, United States

Non-destructive tests and field measurements were used to establish the structural details and behavior of a 100-year-old reinforced concrete flat slab bridge. There are no structural drawings of the bridge, its reinforcing details, or records from the time of its original construction. The purpose of this project was to identify the structural details necessary to model the bridge for a determination of its ultimate load capacity. This paper discusses the methods used to accomplish this purpose. Live load tests were performed to investigate the overall behavior of the bridge. A finite element model of a single span of the 11-span bridge was developed in ABAQUS. FE model calibration was performed based on measured strains and deflections. Comparison of the finite element analysis and live load test results are presented herein.

Keywords: flat slab concrete bridge, non-destructive testing, live load testing, finite element modeling, numerical non-linear material models

INTRODUCTION

The highway infrastructure is exposed to an increasing number of vehicles and heavier loads. Existing bridges often carry trucks that are significantly heavier than the original design loads. There is not enough money to strengthen or replace deficient structures. To save limited resources, there is a need for accurate evaluation of the bridges and determination of their actual resistance. Knowledge of the resistance as well as the predicted maximum expected loads, can serve as basis in important decision-making process about prioritization for repair or replacement. Therefore, the State Departments of Transportations that are responsible for maintenance of roads and bridges, can benefit from having efficient bridge evaluation procedures. The objective of the present study sponsored by the Alabama Department of Transportation (ALDOT), is to develop an approach for the evaluation of a reinforced concrete rigid frame bridge without any prior technical documentation.

RESEARCH SIGNIFICANCE

US Bridge Inventory contains a large portion of flat slab bridges that were built in the first half of 20th century. Flat slab bridges were not designed to carry current traffic that has increased in volume and weight over the years. The bridge considered herein is an example of an old reinforced concrete flat slab structure for which there are no existing technical drawings nor other details. Currently the bridge carries unrestricted traffic, which is allowed by AASHTO's Manual for Bridge

Evaluation (AASHTO, 2011) for a reinforced concrete bridge of unknown details that has carried unrestricted traffic without developing signs of distress. Such behavior phenome is typical for this type of bridges. Research on flat slab bridges conducted up to date often involved overly conservative rating analyses based on effective width strip that in recent years were derived from FEA of slabs using shell elements.

There is no publication available that would comprehensively describe all the steps necessary to conduct non-destructive tests (NDTs) and to determine essential inputs for non-linear FE Model of a flat slab bridge. This paper illustrates how current NDT methods can be used to develop a state-of-art FE model using solid elements that can be further utilized in more accurate assessment of ultimate capacity of the flat slab bridge.

CONSIDERED STRUCTURE

The considered structure is an 11-span flat slab reinforced concrete bridge with no existing technical drawings nor other details. The bridge goes over Barnes Slough and Jenkins Creek on the northbound side of US Highway 82/231 at milepost 162.56 (**Figure 1**) in the State of Alabama, United States. According to archival research conducted by the research team, the bridge was constructed between 1914 and 1916, and ALDOT's records showed that it was widened by approximately 4 ft (1.20 m) in 1930. Visual inspection of the bridge indicates that it was widened twice. It was not established when the second widenings were added.

Currently ALDOT allows unrestricted traffic on the bridge based on AASHTO Manual for Bridge Evaluation (AASHTO, 2011) provisions in cases where a reinforced concrete bridge of unknown details has carried unrestricted traffic without developing signs of distress. However, because the structural details of the bridge are unknown, ALDOT cannot issue permits to overweight and non-standard trucks because this requires analytical justification.

In order to determine some of the structural parameters, the bridge was inspected and measured using field testing
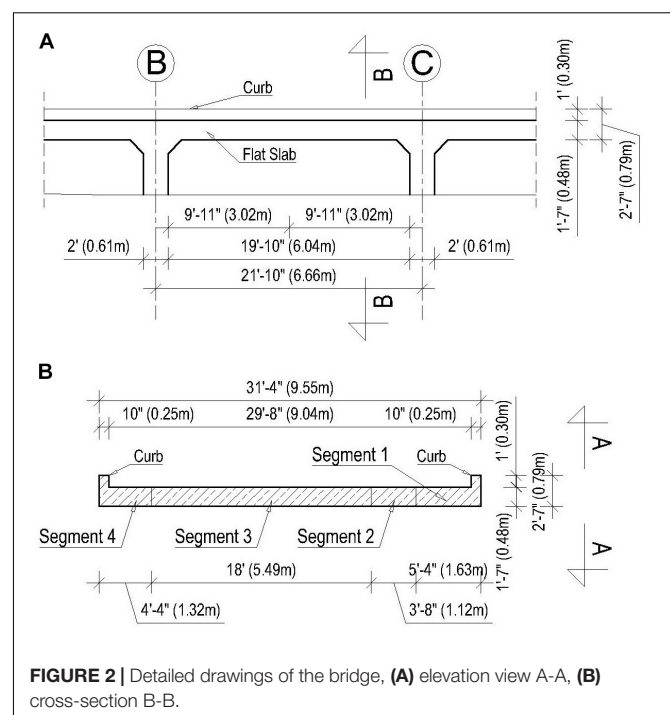
instruments, involving a series of destructive and non-destructive tests described in the following sections of this paper.

All 11 spans are equal, and the center-to-center span length is 21 ft – 10 inch (6.65 m), while the total width is 31 ft – 4 inch (9.53 m). Pier wall thickness is 2 ft (0.61 m). Total cross-sectional width for each span of the bridge consists of four segments: the original one and three additions. The width of the oldest segment (segment 3) is 18 ft (5.49 m). First, the bridge was widened by 3 ft – 8 inch (1.12 m) on the East side (segment 2) (**Figure 2**). Then it was widened on both sides by 5 ft – 4 inch (1.63 m) on the East side (segment 1) and by 4 ft – 4 inch (1.32 m) on the West side (segment 4).

FIELD MEASUREMENTS

Bridge location required the field measurements to have minimal to no impact on busy highway traffic. The measurements performed involved measurements of span dimensions, slab thickness, as well as detection and measurement of slab's reinforcing bars. The research team used traditional tape measure, laser distance meter, a thickness measuring device, which utilizes ultrasonic pulse velocity (UPV) technology, and an advanced concrete cover meter (ACCM) that detects rebars and measures their diameters and spacings. These two high-tech instruments were operated from underneath the span and allowed to inspect the bottom reinforcement without interference with traffic. Top reinforcement was scanned with ground penetrating radar (GPR) and required lane closure. ALDOT's qualified personnel was responsible for lane closure and top surface tests that were co-instructed by the research team. ALDOT's certified equipment was used to obtain concrete

FIGURE 1 | Side view of the bridge.

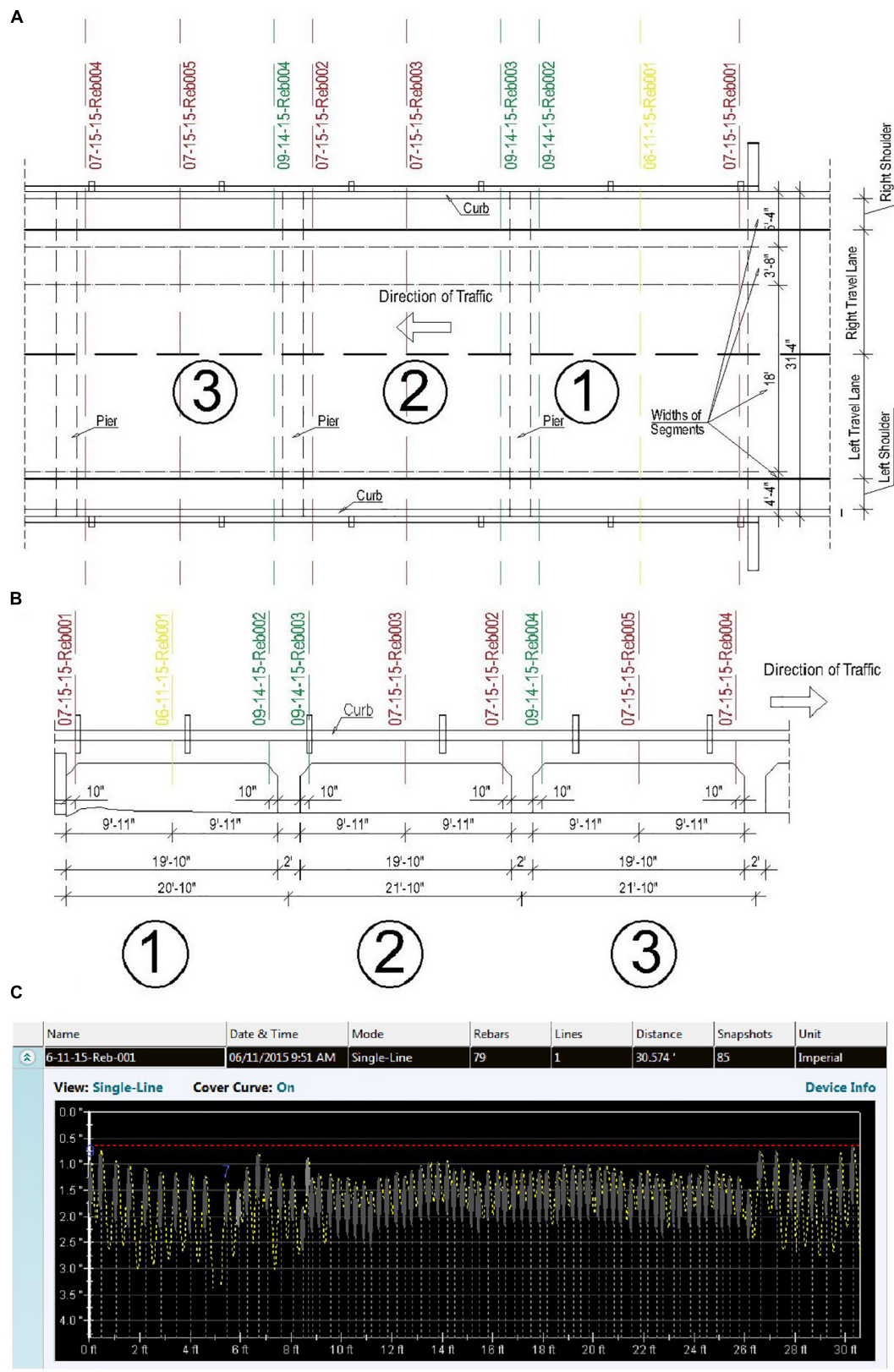**FIGURE 2 |** Detailed drawings of the bridge, **(A)** elevation view A-A, **(B)** cross-section B-B.

FIGURE 3 | (A) Location of the reinforcement measurements – plan view, (B) location of the reinforcement measurements – NE elevation, (C) line measurement of reinforcing bars – scan 06-11-15-Reb001 (1 ft = 0.305 m, 1 inch = 25.4 mm).

core samples, expose bottom rebars for visual size verification, and GPR testing.

Slab Thickness

The goal in using the UPV device was to measure the thickness of concrete slab under regular traffic. Due to relatively low clearance under all the spans, ranging from about 4 to 10 ft (1.2 to 3.0 m), the measurements were taken without additional equipment required for elevated works. Multiple locations under first and second span were scanned with UPV device at original and newer widened parts of the slab. Due to the nature of the UPV technology, the measurements allowed to confirm that the concrete at all examined locations was sound with minor pulse velocity distortions near the top surface of the slab. This was an indication of roughened concrete at the interface with hot mix asphalt (HMA) Layer. Results of UPV thickness measurements showed that slab was 19 inch (48.3 cm) thick. This value was confirmed with measurements taken from bridge's drainage holes with tape measure and later used in FE modeling.

Reinforcement

The location and size of bridge's existing reinforcement was investigated using advanced detecting devices. Bottom surface of the bridge was scanned with ACCM, an instrument using electromagnetic pulse induction technology. The ACCM precisely detected locations of the bottom rebars, measured their diameters and cover thickness. A series of nine line-scans (**Figures 3A,B**) showed the same rebar distribution for all the scanned spans. A sample of the ACCM's reading is shown in **Figure 3C**, where four different reinforcement distributions, corresponding to four slab segments, are clearly notable. Concrete cover of individual rebars detected is shown on vertical axis in **Figure 3C**. A summary of the bottom reinforcement found, is presented in **Table 1**.

The cover of 1.25 inch (3.2 cm) was chosen as it conservatively represents maximum clear cover read for few instances. Similar approach has driven the choice of rebars' size, where the minimum observed diameter was selected as representative for each segment. In order to confirm ACCM's readings the reinforcing bars were exposed in two segments. Accuracy of detecting and measuring capabilities were confirmed to be good, and interestingly, the exposed rebars turned out to be cupped. Such bar was not expected to be noticed, as around the time of bridge construction square plain bars were widely used worldwide. Additional research on old rebar types confirmed that the cupped bars were introduced to the construction industry around 1914. It was concluded that lack of bond between reinforcing bars and concrete was not an issue.

Top surface of the bridge is a 2 inch (5 cm) layer HMA, and it was investigated using the GPR. The GPR provided information on the top reinforcement distribution and detected transverse cracks in the slab over the support locations. This was also confirmed visually as presence of hair-cracks on side edges of the slab was observed. Transverse spacing of top longitudinal rebars turned out to be 12 inch (30 cm). One concrete core was drilled thru a top reinforcing bar to verify its diameter that turned out to be #4 (12 mm), as shown in **Figure 4**.

All the transverse line-scan readings obtained with ACCM were thoroughly processed and analyzed, confirming that the bottom longitudinal reinforcement is extended into the supports in the three segments added to widen the bridge – Segment numbers 1, 2, and 4. For the original segment no. 3 it was found that two-thirds of the reinforcement was extended into supports and one-third was either terminated or bent up. The GPR did not detect any #8 (25 mm) or #7 (22 mm) bars at the top of the slab. Hence, it was concluded that the missing one-third of the bars were not bent up and were terminated 3.5 ft (1.06 m) from each support. Also, the core drilled from the top of the slab at the support location, showed only #4 (12 mm) rebars without any evidence of bottom bars that were bent up. With this evidence it was possible to check the development length of the one-third of the bars in the original segment. All the bottom bars were concluded to be developed based on simple span moment analysis.

Based on these findings it was concluded that the bridge was reinforced as if it is a series of simple spans, and in subsequent load capacity calculations simple support conditions were assumed with top reinforcement neglected entirely. The AASHTO Manual (AASHTO, 2011) specifies yield strength for reinforcing bars by considering the date of construction. For unknown steel constructed prior to 1954, the yield strength F_y is given as 33 ksi (227 MPa).

TABLE 1 | Details of the bottom reinforcing bars.

Segment no.	Rebar size (mm)	Cover inch (mm)	Number of rebars in segment
1	#8 (25)	1.25 (32.0)	10
2	#7 (22)	1.25 (32.0)	9
3	#8 (25)	1.25 (32.0)	53
4	#8 (25)	1.25 (32.0)	7

FIGURE 4 | Cylindrical concrete sample drilled (1 inch = 25.4 mm).

Concrete

At least three different concrete mixes were used in the bridge. Due to restrictions on the number of cores that could be drilled, only three concrete samples were available. One core was drilled in original segment no. 3 (**Figure 2**), in the oldest concrete, at over the support location. Additional two cores were taken from segment no. 1 with the newest concrete, at over support and mid-span locations. Concrete cylinder compressive strength values obtained in ALDOT's material laboratory are presented in **Table 2**. For superstructure components constructed prior to 1959 AASHTO Manual (AASHTO, 2011) recommends a minimum compressive strength value of 2500 psi (17.2 MPa), which turned out to be under conservative for segment 1.

LOAD TESTS

Bridge load testing program should be planned ahead and consider individual conditions related to the structure as well as its site specifics (Amer et al., 1999; Chajes and Shenton, 2006; Sanayei et al., 2012; Davids and Tomlinson, 2016). Flat slab bridges usually are supported on maximum 15–20 ft (4.5–6.0 m) tall piers and provide enough clearance to inspect the bottom of the slab span. Investigated bridge carries traffic of a busy highway and closure of the bridge to conduct live load tests was not permitted. Instead, one lane was closed to commence the tests. Low clearance under the bridge allowed to easily instrument the bridge with sensors measuring strains and deflections.
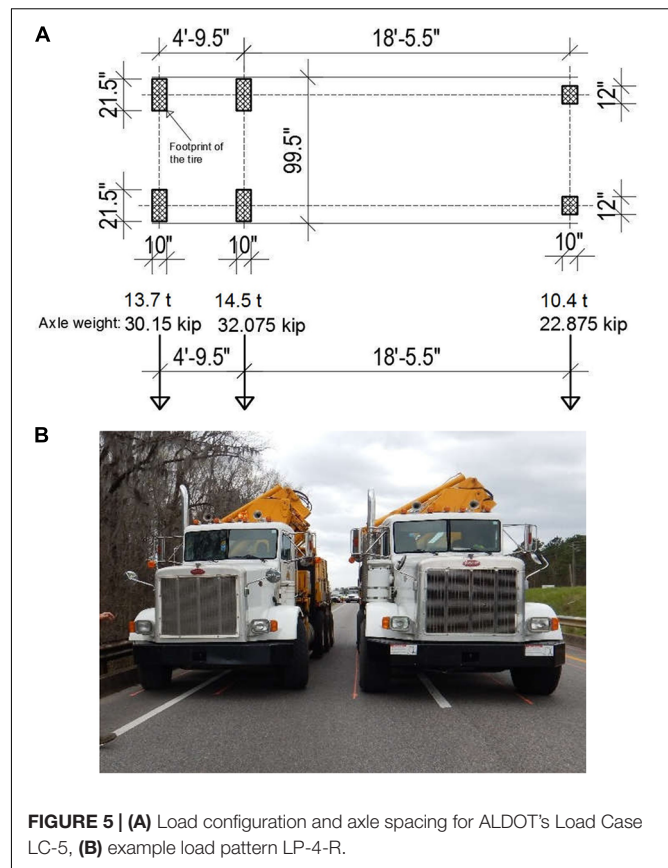
Testing Plan

To investigate the behavior of a hybrid structure consisting of four concrete segments (**Figure 2**), three kinds of load tests were conducted. The first test was conducted for determining the static response under multiple load patterns. This test was performed with a truck placed on the bridge without any movement. Then, selected load patterns were repeated with the trucks moving at a crawling speed. Finally, the trucks moved over the bridge with a speed of 61 mph (98 km/h), to check the dynamic response of the bridge.

Two 85.1-kip (38.6-ton) test trucks configured according to ALDOT's LC-5 Load Case (**Figure 5A**) were used as the live load and were placed on the bridge in configurations as listed below:

(1) LP-1-R: Static loading. One truck placed in the middle of right traffic lane*

FIGURE 5 | (A) Load configuration and axle spacing for ALDOT's Load Case LC-5, **(B)** example load pattern LP-4-R.

(2) LP-1-L: Static loading. One truck placed in the middle of left traffic lane*

(3) LP-2-R: Static loading. One truck placed 1 ft (0.3 m) from right curb*

(4) LP-2-L: Static loading. One truck placed 1 ft (0.3 m) from left curb*

(5) LP-3-R: Crawling speed. LP-1-R truck passing at crawling speed, no stops**

(6) LP-3-L: Crawling speed. LP-1-L truck passing at crawling speed, no stops**

(7) LP-4-R: Static loading. Two trucks placed side-by-side 1 ft (0.3 m) from right curb* (**Figure 5B**)

(8) LP-4-L: Static loading. Two trucks placed side-by-side 1 ft (0.3 m) from left curb*

(9) LP-5-R: Speed = 61 mph (98 km/h). LP-1-R truck passing at speed of 61 mph (98 km/h), no stops**

* For all static load patterns, second axle of truck/trucks located at midspan.

** Non-static load patterns are not presented in this paper due to insignificant differences with results obtained for static cases.

The trucks were placed in both lanes of the bridge to produce heavy loading in the critical locations corresponding to design by AASHTO (AASHTO, 2001).

Strains and deflections are the two most common measurements taken during live load testing of the bridges.

TABLE 2 | Compressive test results for concrete cores.

Sample	1	2	3	AASHTO recommended
Compressive strength, psi (MPa)	3340 (23.0)	1937 (13.4)	1760 (12.1)	2500 (17.2)
Location	Original segment 3 – over support	East segment 1 – over support	East segment 1 – midspan	–

For the flat slab bridges strains and deflections are two most effective measurements as per AASHTO Manual (AASHTO, 2011). BDI equipment was chosen for these tests because of its good reputation and performance in similar research projects.

For measurements of the strains, strain transducers (ST) with special extensions were mounted at the bottom of the slab and covered with aluminum foil to reduce "drift" effect due to the change of the temperature (BDI, 2016b). Due to small values of expected strains, the aluminum extensions for STs were used for more precise measurements. The deflections were measured with Linear Variable Differential Transformers (LVDT) (BDI, 2016a). Total of 12 STs and four LVDTs were used and installed under the bridge as shown in **Figure 6**. The measuring system consisted of Base Station, Access Point, Data Acquisition Nodes and Sensors. The sensors were connected with a cable to the Data Acquisition Nodes, which sent data over WiFi to the Access Point and Base Station. The data was recorded at frequency of 100 Hz and required further post-processing.

Analysis of Field Data

Data recorded during the live load tests was further analyzed and summarized. Numerous comparisons between load cases were conducted. Transverse behavior of the bridge was verified for symmetry and consistency in measured values of strains and deflections. After the analysis of the results, data recorded by three STs (S-T 5488, S-T 5490, and S-T 5496) appeared to be incorrect and it was excluded from the database (see crossed-out sensors in the **Figure 6**). Since 18-inch (45.7 cm) long extensions were used with 3 inch (7.6 cm) long STs, the recorded values of strains had to be divided by 6.

Manufacturer of the diagnostic system provided calibration factors for each ST as well as specified an adjustment factor of 1.1 (BDI, 2016b), which relates to aluminum extensions. These two factors were applied as multipliers to all the recoded values of strains.

For all the static load cases measured strain values from spans 1 and 2 were compared. For span 1, the pattern of strains measured in the oldest segment of the bridge is consistent with expected linear increase (**Table 3**). Strains measured under span 2 (**Table 3**) were also reasonably symmetric. This was an indication of symmetric behavior of the slab in transverse direction. The largest measured strain value was 34.3 με, recorded under span 2 for the load pattern LP-4-R being the most critical.

Summary of the deflections recorded during load tests is shown in **Table 4**. Comparison of measured deflections for spans 1 and 2 at mid-width locations showed good agreement between spans, as well as reasonable symmetry for span 1. The largest deflection of 0.598 mm (0.024 inch) was recorded at the west side of span 1. This deflection was recorded under load case LP-4-L with two trucks placed side-by-side close to the curb on the west side of the bridge.

FINITE ELEMENT MODEL

Bridge testing often follows a computer model development for additional analysis of the structure. Depending on the bridge type, ones' consideration often is limited to beam-shell models for girder bridge types or shell/grillage models for flat slabs. Regardless of the modeling technique, flat slab
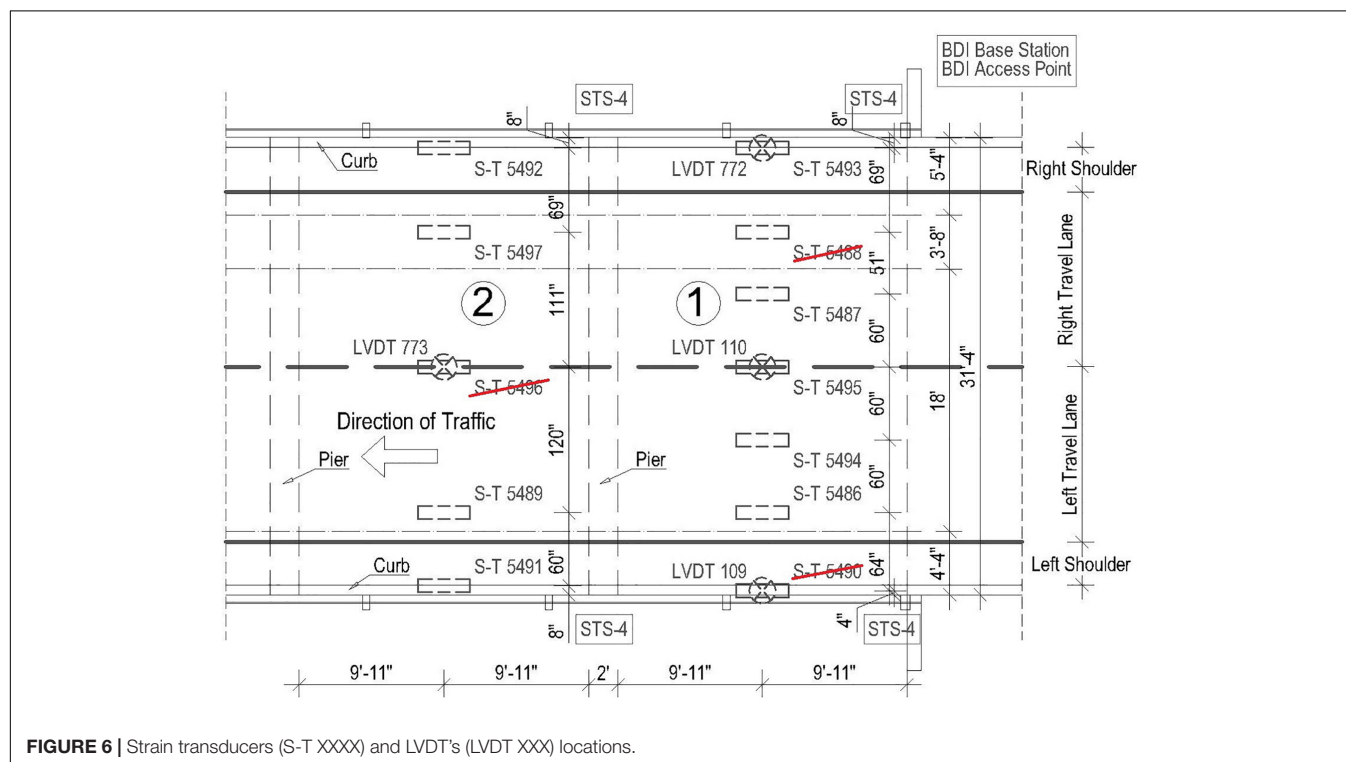

FIGURE 6 | Strain transducers (S-T XXXX) and LVDT's (LVDT XXX) locations.

TABLE 3 | Summary of strains for each static load pattern (με) – span 1 and 2.

	SPAN 1						
S-T	5490	5486	5494	5495	5487	5488	5493
Distance along the width (inch)	4	68	128	188	248	299	368
Distance along the width' (inch)	372	308	248	188	128	77	8
LP-1-R	–	3.7	7.1	12.4	16.3	–	11.9
LP-1-L	–	18.3	17.8	12.4	7.1	–	0.7
LP-2-R	–	2.0	4.5	8.7	16.5	–	22.1
LP-2-L	–	19.7	15.8	8.8	4.9	–	0.8
LP-4-R	–	11.4	20.5	26.0	**31.2**	–	26.9
LP-4-L	–	28.2	29.9	25.4	20.7	–	6.1
	SPAN 2						
S-T	5491	5489	N/A	5496	N/A	5497	5492
Distance along the width (inch)	8	68	-	188	-	299	368
Distance along the width' (inch)	368	308	-	188	-	77	8
LP-1-R	2.2	3.8	–	–	–	19.4	13.1
LP-1-L	13.6	20.5	–	–	–	3.5	1.5
LP-2-R	1.1	1.9	–	–	–	22.1	26.2
LP-2-L	24.7	21.7	–	–	–	2.1	0.7
LP-4-R	7.6	12.8	–	–	–	32.5	**34.3**
LP-4-L	28.6	30.6	–	–	–	11.3	6.3

Bold values indicate maxima for each subcase.

TABLE 4 | Summary of deflections for each static load pattern (mm) (1 inch = 25.4 mm).

	First span				Second span	
LVDT	109	110	772	LVDT		773
Distance along the width (inch)	4	188	368	Distance along the width (inch)		188
LP-1-R	−0.046	−0.248	−0.273	LP-1-R		−0.376
LP-1-L	−0.286	−0.250	−0.033	LP-1-L		−0.295
LP-2-R	−0.011	−0.193	−0.442	LP-2-R		−0.287
LP-2-L	−0.458	−0.198	−0.018	LP-2-L		−0.253
LP-4-R	−0.162	−0.524	−0.592	LP-4-R		**−0.566**
LP-4-L	**−0.598**	−0.515	−0.167	LP-4-L		−0.558

Bold values indicate maxima for each subcase.

bridges are proven to have capacities far exceeding theoretically derived values that base on flexural strength of a unit-width member (Saraf, 1998; Jáuregui et al., 2010; Davis et al., 2013). For the purpose of the research project, it was decided to develop a state-of-art FE model of the examined bridge to accurately trace stress distribution and to use it later for ultimate strength evaluation.

Based on the findings from field measurements, a FE model of a single span of the bridge (**Figure 7**) was developed in Simulia Abaqus FE Software. FE model was first used to predict behavior and magnitudes of stresses, strains, and deflections expected during the load tests. After the live load testing commenced the FE model was calibrated to serve as basis for further analysis.

This section presents all the input variables and their calibrated values that yielded results best matching the measured values. A three-dimensional FE model was developed with usage of solid and beam elements. The application of solid elements allowed for a detailed investigation of local stress and strain distributions as well as overall bridge behavior. The model contains upper portions of the piers, slab segments, bottom reinforcing bars, and curbs of dimensions as shown in **Figure 2**. The curbs have cross-sectional dimensions of 8 × 10 inch (20 cm × 25 cm). Four different width segments, fully bonded with each other, create each of the simple span slabs.

Static wheel loads on the bridge were modeled as flat rigid load transferring plates with a uniform load applied.

Element Types

Among various element types available in the finite element method (FEM) only selected elements are presented. The concrete elements – curbs, slab segments, and piers were modeled with 8-noded linear brick elements with reduced integration (C3D8R). Reduced integration element was chosen due to its computational cost, which is less than for a full-integration element. The element type used for reinforcing bars is a 2-node linear beam element (B31). The advantage of the beam over widely used link elements in FE modeling of reinforcement is its ability to act in compression as well as in tension. Both element types selected, C3D8R and B31, are suitable for stress/displacement simulations. Brick elements have three degrees of freedom active at each node – translations in the nodal x, y, and z directions. For the beam elements all six degrees of freedom (rotations and translations) at each node are computed. For this particular bridge model, the application of solid finite elements for concrete members allowed to control the contact definitions between concrete segments and resulted in more detailed investigation of localized stress and strain distributions.

The reinforcing bars were modeled as embedded into slab. From the numerical method point of view an embedded rebar acts as fully bonded with concrete slab, which was concluded from field measurements. Although, the rebars are present in all concrete members they were modeled in the slab segments only. Reinforcement in the piers was neglected due to their large dimensions and lack of detection capabilities of the sensing instrument.

One of the most important parameters that impacts accuracy of results and analysis time is FE mesh size (Logan, 2017). A mesh density study was performed by monitoring three key parameters: mesh size, convergence of results, and non-linear analysis time. This study showed that the most effective mesh size, in terms of accuracy and computing time, is 4 × 4 × 3.8 inch (10 cm × 10 cm × 9.7 cm) for the brick elements and 4 inch (10 cm) of length for the beam elements.

Numerical Material Models

In order to develop numerical material models all collected data and available literature was reviewed. FEM material models require specification of basic material parameters such as
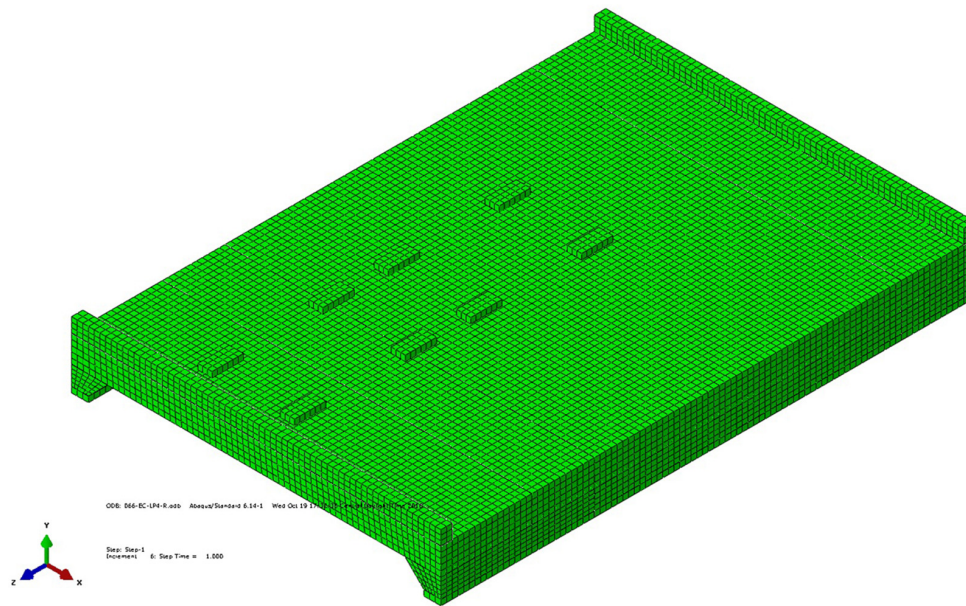
FIGURE 7 | Isometric view of the FE Model of the Bridge. ALDOT Test Trucks footprint pattern presented.

modulus of elasticity, Poisson's ration as well as stresses with corresponding strains in inelastic stress ranges for more advanced analyses. Two non-linear material models, concrete damage plasticity (CDP) for concrete and elasto-plastic for steel, were implemented into the FE model. At the time of selection of numerical material materials benefits coming from non-linear analysis were justified by need for accurate stress investigation for loads causing concrete cracking and compressive stresses reaching their ultimate values.

Concrete Material Model

Among smeared crack and brittle crack concrete models available in Abaqus software, the CDP model was selected due to its potential to represent complete inelastic behavior of the concrete bridge elements in tension and compression and their damage characteristics. All concrete material models have their pros and cons, but for this application CDP was justified because of lack of numerical convergence issues during the analysis, overall good agreement with the test results (Chaudhari and Chakrabarti, 2012), and macro-scale of the structure for which investigation of crack development was not required. Furthermore, the CDP can be used both in Abaqus/Standard and Abaqus/Explicit, which at the time of numerical material model considerations was a valuable advantage allowing for bridge collapse simulation.

The CDP model available in Abaqus requires input of parameters associated with simplified Drucker-Prager concrete strength hypothesis. The dilation angle ψ, flow potential eccentricity ε, f_{b0}/f_{c0} ratio (point in which the concrete undergoes failure under biaxial compression), K_c parameter (ratio of the distances between compression and tension meridians in the deviatoric cross-section) as well as Viscosity parameter describe behavior of concrete in biaxial stress state. Description and

recommended values for these parameters are available in Abaqus Manual (ABAQUS, 2014) and research papers (Kamiński and Kmiecik, 2011). Plasticity parameters used were set at recommended by Abaqus Manual values: $\psi = 36°$, $\varepsilon = 0.1$, $f_{b0}/f_{c0} = 1.16$, $K_c = 0.667$, Viscosity parameter = 0.

In addition to concrete plasticity parameters, the CDP material model definition requires stress-strain data within inelastic region for compressive and tensile behavior. These can be determined from strain-stress curve for a concrete sample. Due to lack of stress-strain data for the concrete samples taken, the relationship curves had to be developed with approximate equations.

ACI 318-14 (American Concrete Institute, 2014) provides the formula, where modulus of elasticity, E_c is a function of concrete compressive strength, f'_c.

$$E_c = 57000\sqrt{f'_c}$$

Where:

E_c = Initial Modulus of Elasticity (output in psi),

f'_c = Compressive Strength of concrete (input in psi).

During the calibration process it was found that Eurocode formula (European Committee for Standarization, 2004) for the modulus of elasticity adopted to the FE model produces values of strains and deflections better matching the measured values. Hence, the Eurocode formula presented below was used in the material model.

$$E_c = 22000(f'_c)^{1/3}$$

Where E_c and f'_c in MPa.

TABLE 5 | Parameters of concrete for each of the slab's segments.

Segment	4 (West)	3	2	1 (East)
f'c, psi (MPa)	1850 (12.8)	3340 (23.0)	1760 (12.1)	1940 (13.4)
E, ksi (GPa)	3432.5 (23.7)	4098.1 (28.2)	3381.5 (23.3)	3481.7 (24.0)

The compressive stress-strain relationship curves were derived using Desayi and Kirshnan (1964) equation.

$$\sigma_c = \frac{E_c \varepsilon_c}{1 + \left(\frac{\varepsilon_c}{\varepsilon_0}\right)^2}$$

Where:

σ_c = Compressive Stress,

ε_c = Compressive Strain,

ε_0 = Strain at maximum Stress,

E_c = Initial tangent modulus, assumed to be twice the secant modulus at maximum stress f'_c.

It was assumed that numerical concrete material models perform linearly up the stress of $0.4f'_c$. The three presumptions on initial tangent modulus of elasticity: being a function of f'_c, being equal to twice the secant at f'_c, and it's linearity within 0.4 f'_c allowed to derive the compressive stress-strain relationships for concrete segments based only on one input variable f'_c. Due

to lack of stress-strain data from compressive tests of the samples the presented approach was considered appropriate.

The tensile stress-strain relationship was developed using the Wang and Hsu formula (Wang and Hsu, 2001), which among many other formulas is considered to most accurately describe concrete tension stiffening (Kamiński and Kmiecik, 2011).

$$\sigma_t = \begin{cases} E_c \varepsilon_t & \text{if } \varepsilon_t \leq \varepsilon_{cr} \\ f'_c \left(\frac{\varepsilon_{cr}}{\varepsilon_t}\right)^{0.4} & \text{if } \varepsilon_t > \varepsilon_{cr} \end{cases}$$

Where:

σ_t = Tensile Stress,

ε_t = Tensile Strain,

ε_{cr} = Cracking Strain,

In order to establish cracking strain, the modulus of rupture needs to be known. The AASHTOs' formula (AASHTO, 2001) was used to establish the tensile strength of the concrete.

$$f_r = \begin{cases} 7.5\sqrt{f'_c} & \text{(US units)} \\ 0.623\sqrt{f'_c} & \text{(SI units)} \end{cases}$$

Four different compressive strengths of concrete were taken for each of the four slab segments to develop stress-strain relationships for compressive and tensile behavior. Compressive strengths used as well as the values of corresponding moduli of
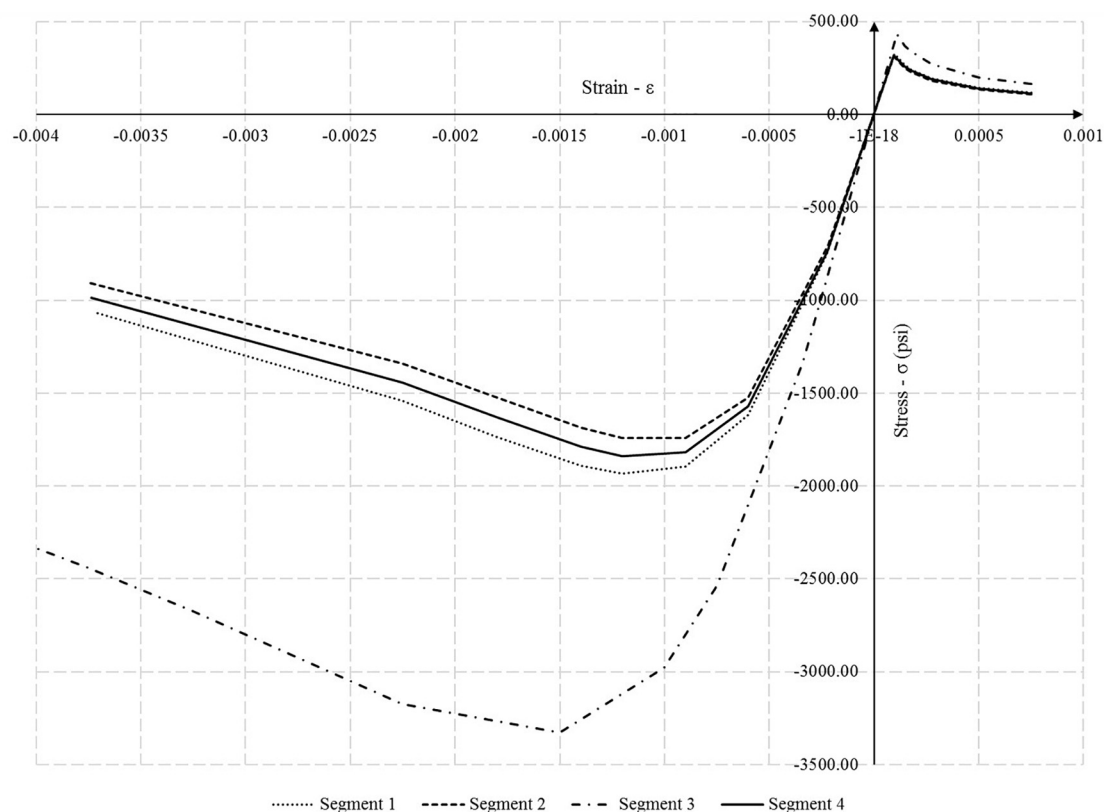
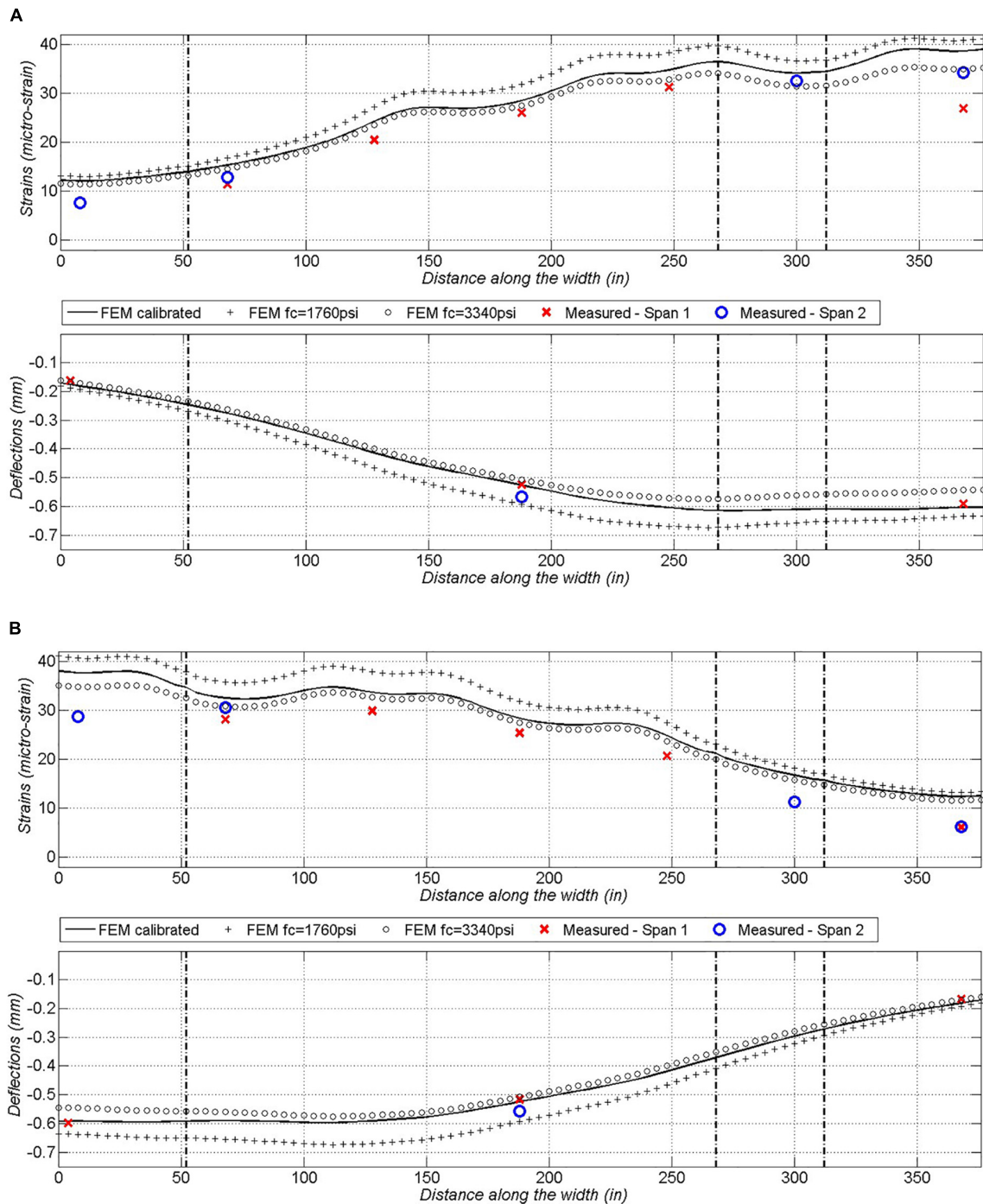**FIGURE 8 |** FEM input Stress-strain curves for segments 1–4 (100 psi = 0.69 MPa).

FIGURE 9 | Comparison plot of strains and deflections for **(A)** LP-4-R, **(B)** LP-4-L (1 inch = 25.4 mm, 1 mm = 0.02 inch).

elasticity are shown in **Table 5**. Developed curves for each of the slab's segment are shown in **Figure 8**.

Steel Material Model
Provisions from AASHTO Manual (AASHTO, 2011) allowed to develop the material model for reinforcing steel bars. The Manual recommends the yield strength of steel of 33 ksi (227 MPa) for

unknown reinforcing steels built prior to 1954. The ultimate tensile strength of steel was assumed to be 58 ksi (400 MPa) with slope of 2.5% of initial modulus of elasticity within inelastic region. This strain hardening of steel was input purely for numerical analysis stability purposes. The reinforcing bars reach yielding at strain value of 1.14E-3 based on assumed modulus of elasticity of 29000 ksi (200 GPa).
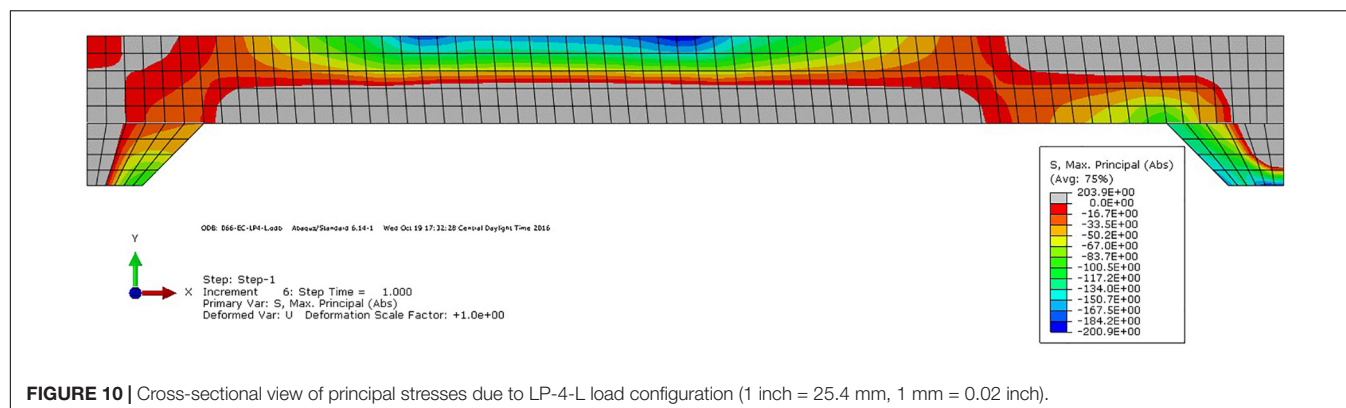
FIGURE 10 | Cross-sectional view of principal stresses due to LP-4-L load configuration (1 inch = 25.4 mm, 1 mm = 0.02 inch).

Boundary Conditions and Loads

The first supporting pier, at the abutment location, has restrained displacements in Y and Z directions. Unrestrained displacement in X direction allows it to move in longitudinal direction, parallel to direction of traffic. Second pier has all the displacements restrained. The rotations for both piers are allowed in all the directions.

Slab end edges were unrestrained to imitate its discontinuity due to the transverse cracks detected over the supports during the field measurements (**Figure 7**). Contact conditions specified in the model are as follows: full bond of reinforcing bars with concrete in all segments, full connection between side surfaces of the adjacent segments, pressure transfer interaction between tire footprint elements and concrete segments.

Load applied to the model during calibration process was the actual truck used during the live load tests. ALDOT's LC-5 Test Truck axle spacing, footprint area, and axial loads are presented in **Figure 5A**.

RESULTS

Initially developed FE model, before the load testing commenced, correctly predicted lack of concrete rupture and very small values of deflections. It was confirmed that stresses in concrete segments and reinforcing bars would remain in elastic range.

Field measured strains and deflections, for the most severe static load cases, were plotted with FEA obtained values from a calibrated model (**Figures 9A,B**). FEA were performed for two additional models assuming all the slab's segments have the same compressive strength of concrete, which results in the same concrete material model throughout the slab. Plots show FEA results for the calibrated model and two models with strength of concrete of 1760 psi (12.1 MPa) and 3340 psi (23.0 MPa). Values on the horizontal axis correspond to the total width of the bridge and limits of adjacent segments (**Figure 2B**) are indicated with vertical dash-dotted lines.

Due to the shape of the piers and span-to-thickness ratio, it was expected to see compressive stresses in the slab distribute in a shape of an arch. **Figure 10**, confirms this argument and shows a map of compressive stresses with tensile stress regions grayed-out.

CONCLUSION

This project illustrates how field measurements from GPR, UPV testing device, ACCM, core tests and live load tests were performed and used to define the structural details of a flat slab bridge. These details allowed to develop state-of-art non-linear FE model to determine the load capacity of the structure. Based on the field measurements it was found that cupped reinforcing bars were used in the oldest, original segment 3, back in 1915. For this segment it was established that one-third of the reinforcement was terminated at 3.5 ft (1.06 m) from each support. Values of deflections and strains recorded during the load tests were very small, as expected. Even for the most critical load pattern with two test trucks together in one span, the bridge did not crack. This confirms the overall good condition of the structure and its reserve flexural capacity. Measured values of strains and deflections show reasonable symmetry in bridge's behavior, especially for the oldest part of the slab. The FE Model developed showed overall good correlation with the measured values of strain and deflection. FE Model confirmed that the strength of the structure, resulting in small values of strains and deflection under live load, comes from arching action which is strictly associated with the geometry of the bridge. Non-linear material model definitions allow the model to be used in numerical simulations of load carrying capacity.

DATA AVAILABILITY STATEMENT

All datasets generated for this study are included in the article/supplementary material.

AUTHOR CONTRIBUTIONS

PW: main author of the manuscript, conducted analytical modeling, and field studies. MK: performed live load measurements and preliminary analysis of the results. JS: co-PI on the research project and the lead professor. AN: was a PI of the research project.

FUNDING

ACKNOWLEDGMENTS

REFERENCES

AASHTO, (2001). *AASHTO Standard Specifications for Highway Bridges*. Washington, DC: AASHTO.

AASHTO, (2011). *AASHTO Manual for Bridge Evaluation*. Washington, DC: AASHTO.

ABAQUS, (2014). *Abaqus Analysis User's Manual, Version 6.14*. Vélizy-Villacoublay: Dassault Systèmes.

Amer, A., Arockiassmy, M., and Shahawy, M. (1999). Load distribution of existing solid slab bridges based on field tests. *J. Bridge Eng*. 4, 189–193. doi: 10.1061/(asce)1084-0702(1999)4:3(189)

American Concrete Institute, (2014). *ACI 318-14 Building Code Requirements for Structural Concrete and Commentary*. Farmington Hills, MI: American Concrete Institute.

BDI, (2016a). *LVDT – Displacement Sensor: Specification*. Available online at: https://bditest.com/wp-content/uploads/LVDT (accessed August 13, 2019).

BDI, (2016b). *ST350 – Strain Transducer: Operations Manual*. Available online at: https://bditest.com/wp-content/uploads/ST350-Strain-Transducer-Operations-Manual-v3.0.pdf (accessed August 13, 2019).

Chajes, M. J., and Shenton, H. W. (2006). Using diagnostic load tests for accurate load rating of typical bridges. *J. Bridge Struct*. 2, 13–23. doi: 10.1080/15732480600730805

Chaudhari, S. V., and Chakrabarti, M. A. (2012). Modeling of concrete for nonlinear analysis using finite element code abaqus. *Int. J. Comput. Appl*. 44, 14–18. doi: 10.5120/6274-8437

Davids, W., and Tomlinson, S. (2016). *Instrumentation During Live Load Testing and Load Rating of Five Reinforced Concrete Slab Bridges*. Report 16-23-1332.3. Orono, ME: University of Maine.

Davis, W. G., Poulin, T. J., and Goslin, K. (2013). Finite-Element Analysis and load rating of flat slab concrete bridges. *J. Bridge Eng*. 18, 946–956. doi: 10.1061/(asce)be.1943-5592.0000461

Desayi, P., and Kirshnan, S. (1964). Equations for the stress-strain curve of concrete. *J. Amer. Concr. Inst*. 61, 345–350. doi: 10.3390/ma9050377

European Committee for Standarization, (2004). *EN 1992-1-1: Design of Concrete Structures – Part 1-1: General Rules and Rules for Buildings*. Brussels: European Committee for Standardization.

Jáuregui, D., Licon-Lozano, A., and Kulkarni, K. (2010). Higher level evaluation of a reinforced concrete slab bridge. *J. Bridge Eng*. 15, 93–96.

Kamiński, M., and Kmiecik, P. (2011). Modelling of reinforced concrete structures and composite structures with concrete strength degradation taken into consideration. *Arch. Civil Mech. Eng*. 11, 623–636. doi: 10.1016/s1644-9665(12)60105-8

Logan, D. L. (2017). *A First Course in the Finite Element Method*, 6th Edn. Boston, MA: Cengage Learning.

Sanayei, M., Phelps, J., Sipple, J., Bell, E. S., and Brenner, B. R. (2012). Instrumentation, nondestructive testing and finite-element model updating for bridge evaluation using strain measurements. *J. Bridge Eng*. 17, 130–138. doi: 10.1061/(asce)be.1943-5592.0000228

Saraf, V. (1998). Evaluation of existing RC slab bridges. *J. Perform. Const. Facil*. 12, 20–24. doi: 10.1061/(asce)0887-3828(1998)12:1(20)

Wang, T., and Hsu, T. T. C. (2001). Nonlinear finite element analysis of concrete structures using new constitutive models. *Comput. Struct*. 79, 2781–2791. doi: 10.1016/s0045-7949(01)00157-2

Bridge Load Testing for Identifying Live Load Distribution, Load Rating, Serviceability and Dynamic Response

Chuanzhi Dong[1], Selcuk Bas[1,2], Marwan Debees[1], Ninel Alver[1,3] and F. Necati Catbas[1]*

[1] Civil, Environmental and Construction Engineering Department, University of Central Florida, Orlando, FL, United States, [2] Department of Civil Engineering, Bartin University, Bartin, Turkey, [3] Department of Civil Engineering, Ege University, İzmir, Turkey

In this article, dynamic and static load tests of a concrete highway bridge, which is a deteriorated and repaired, are presented depending on displacement and strain data for engineering decision making about the operation of a critical bridge. Static load test was carried out to determine the live load distribution factor (DF) and load-rating factor (RF) as well as serviceability by means of deflection limits. Modal characteristics in terms of structural frequencies and mode shapes and impact factor (IM) were identified from the dynamic load test for different truck-load and speed cases, and finite element (FE) model. The DF and rating factor (RF) were also compared with those calculated according to AASHTO standard and FE model. The results showed that the DF calculated by American Association of State Highway and Transportation Officials (AASHTO) standard gave more conservative results when compared with the experimental and FEM approaches. Similarly, the load-rating factor (RF) calculated by AASHTO standard yielded to more conservative results comparing with the experimental FEM approaches using practical DFs. Maximum deflections in static cases and dynamic cases were found to be within the limit calculated by (L/800) given in the AASHTO code. Impact factors among all the cases were obtained much smaller than the one recommended by AASHTO standard (33%). The modal properties were obtained to track changes in dynamic behavior due to stiffness and boundary effects as well as for finite element model calibration. The calibrated FE model of the bridge also indicated that the load carrying capacity of the bridge is adequate after repair. Finally, the results from the current study reveal that use of experimental data can be utilized to obtain load rating with minimum interruption to bridge operations through computer vision technology and methods.

Keywords: concrete bridge, load testing, load rating (RF), distribution factor (DF), impact factor (IM), modal characteristics

INTRODUCTION

Bridge load testing is commonly employed to determine issues that cannot be easily resolved by visual inspection or simple analysis. Visual inspection, load-testing, structural health monitoring (SHM), non-destructive testing (NDT) and finite element (FE)-based structural modeling are commonly utilized to address issues related to a bridge

or a population of bridges. For example, AASHTO-MBE (2018) recommends load testing for structural condition rating of highway concrete deck bridges. The load test objectives may vary from case by case, and such a test may be needed on particular bridge or a population of similar bridges in question to make decisions such as bridge closure, bridge load posting, replacement, and retrofit.

A general structural identification framework that also encompasses bridge testing was presented in detail along with utilization of field experimental and analytical studies for decision making (Catbas et al., 2013). A particular bridge can be tested to understand critical issues, and sometimes a sample representative bridge can be tested to address issues related to the similar bridge population (Gokce et al., 2011). Similarly, a representative bridge population sample can be tested to be able to make decisions on the entire bridge population (Catbas et al., 2005). In order to conduct rapid experimental test on a reinforced concrete bridge population, the researchers proposed a method to determine the moment DFs for single-span-T-beam bridges (Catbas et al., 2012). They presented that the new approach could be predicted live load reasonably well when compared to standard girder analysis given in the (AASHTO, 2017) code. Based on the load and resistant factor rating (LRFR) approach, load rating factors were obtained for a fully instrumented bridge for three different methods (standard, experimental strain data, and FEM) (Sanayei et al., 2016). Standard approach resulted lower rating factors than the others. Static and dynamic testing was also carried out by Catbas et al. (2006) for a concrete T-Beam bridge taking into account before and after retrofit of the bridge through carbon fiber–reinforced polymer (CFRP) material. According to the results of experimental data for both cases, they clearly showed that the CFRP retrofit had an ability to improve structural response of the concrete bridge. In order to quantify the effect of deterioration on live-load response of an existing concrete bridge, Torres et al. (2019) performed experimental and numerical study. Based on the results from load-test as well as visual inspection, they found heavily deteriorated deck, undamaged girders and moderate connection problems at the longitudinal joints. By performing a parametric study on the calibrated the FE model of the bridge, the moment and shear girder distribution factor (DF) equations were developed in that study. Tawadrous et al. (2019) carried out live load-testing on two concrete bridges with different deck systems: (i) newly developed precast concrete deck and (ii) standard cast-in-place (CIS) deck to compare their performances on the basis of strain and deflection. The influence of foundation movements and geohydraulic hazards on load rating of a highway bridge was also investigated by Davis et al. (2018). The proposed load rating approach was obtained to give more conservative RF values than those of the standard method if foundation movements were considered. More recent load-test implementations to concrete bridge can be found in the study of Omar and Nehdi (2018). On the other hand, some researchers also recently demonstrated that more effective bridge condition assessments could be done through other technologies (computer vision, image, thermal camera, etc.) (Agdas et al., 2016; Zaurin et al., 2016; Hiasa et al., 2018; Dong and Catbas, 2019). In these studies, these technologies were determined to be an

effective complementary tool. More recently, civil infrastructure technologies were grouped to be utilized for commonly seen bridge failures (Bas and Catbas, 2019).

The main objective of this paper is to present a bridge load test with particular engineering objectives regarding a multi-span bridge with several spans of the same geometry and material properties. The span under consideration is the worst condition span and acceptable performance from this span will be favorably extrapolated to the entire bridge. The specifics goals of the load test are as follows: (i) obtain impact factors (IM) under different loads and speeds, (ii) obtain dynamic responses in terms of structural frequencies and mode shapes, and (iii) obtain load distribution of the bridge and evaluation of the load carrying capacity of the bridge. During the bridge test, the strain/stress responses, displacements and accelerations under different truck loads were collected by using proper sensors and data acquisition systems. For this aim, instrumentation plan and truck load configuration for the bridge were given. From static load-test with different truck loads, distribution (DF) and load rating (RF) factors, and deflection check of the bridge were determined. Dynamic load-testing with different truck loads and speeds were carried out to calculate the IM and dynamic characteristics of the bridge. The DF results from the experimental field test and FEM were compared with the standard formulation given in AASHTO (2017).

GENERAL FEATURES OF THE BRIDGE

As shown in **Figure 1A**, the bridge considered in the study is a multi-span concrete bridge with a bascule section in the middle, located in Florida, United States. The bridge was constructed in 1964 and has a total length of 912 m. Each span consists of five pre-stressed I-beam spans, two flanking spans, and a steel double leaf bascule main span, which is 39.5 m between trunnion centers. AASHTO Type II Girders are spaced at 2.4 m with an 18 cm cast in place deck and 5.1 cm wearing surface. All approach spans are 15.9 m each. The substructure is composed of two cast in place reinforced concrete end bent caps founded on 61 cm square pre-stressed concrete piles with rubble riprap slope protection retained by a seawall system, 53 intermediate reinforced concrete bent caps founded on 61 cm square pre-stressed concrete piles. The aged bridge underwent a retrofit of the deteriorated girders, including removal of all spalled and delaminated concrete, cleaning the corroded steel and rebar, installing special splice when a strand was severed or has more than 50% sectional loss, repairing hairline cracks. The load test here would explore if the load carrying capacity is adequate.

INSTRUMENTATION PLAN

As shown in **Figure 1B**, three types of sensors were installed on the bridge. Totally, 15 accelerometers were installed at the 1/4 span, mid span and 3/4 span of five girders (G1–G5) to test the dynamic responses during load test.

Five displacement sensors (i.e., potentiometers) were installed at the mid span of each girder to measure the displacement.
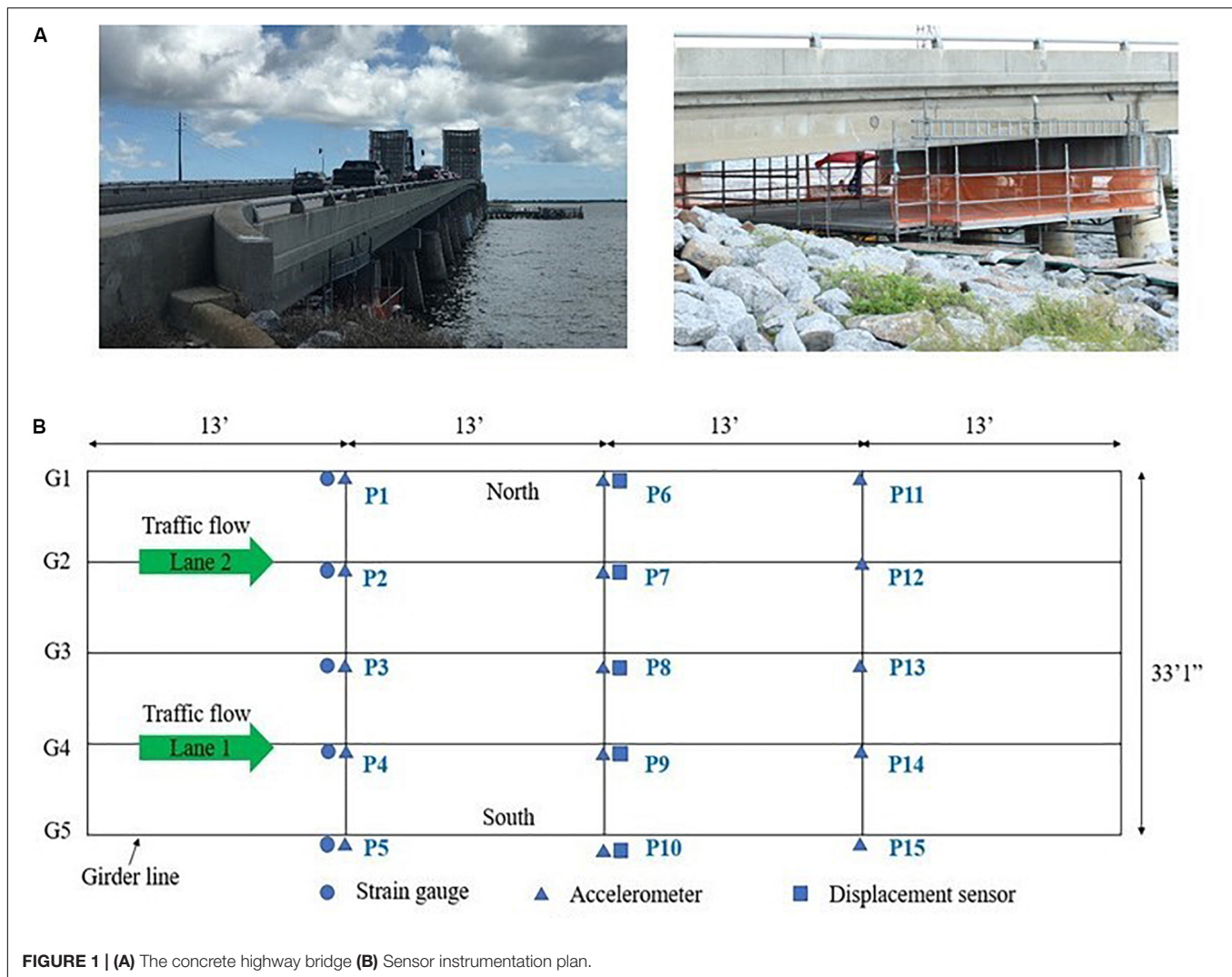
Three cameras were employed to measure the displacements at the same location. The camera-based monitoring and computer vision implementation will be presented separately in other publications. Five strain gauges were installed at the 1/4 span of each girder. One camera was employed to record the traffic footage. Details of the sensors and cameras are shown in **Table 1**. All the sensors were installed at the bottom of the girders as shown in **Figure 2A**.

LOADING PLAN

The truck loading test plan consisted of static and dynamic loads with two different trucks separately. Two types of trucks, Truck 1 (T1) and Truck 2 (T2) were operated to conduct the load test. The trucks and loading plan are shown in **Figures 2B**, **3A,B**.

In the static test, the truck (T1 or T2) was stopped and remained at four different locations of each lane (Lane 1 and Lane 2), and it took four steps for one test round. According to the types of the truck and the lanes, **Table 2** summarizes

the static loading cases. In this study, to point out the loading location or step, S_i (i = 1, 2, 3, 4) is added at the end of the case name. For example, the load location in **Figure 3A** is represented by T1L1S1.

In the dynamic test, the load configuration was similar to the static test. The difference is instead of putting the trucks statically in all four locations, the trucks moved in the lane with different speeds. According to the types of the truck, moving speeds and the lanes, **Table 3** summarizes the dynamic loading cases.

STATIC LOAD-TEST

General

Figure 4A shows the displacement results of T2L1. This figure shows both the displacement results from cameras and potentiometers. The results from the cameras and the potentiometers are very consistent with each other and the maximum difference is within 2.5% range. Only small motions of the potentiometers installed at the two exterior girders (P6 and

TABLE 1 | Specifications of sensors and cameras.

|	Sensor	Specifications
Accelerotneter		ModelNo.:PCB603C01 Weight: 1.8 gz,(51 g) Sensitivity: (=10%) 100 mV/g (10.2 mV/(m/s^2) Frequency Range: (±3dB) 30–600,000 cpm (0.5–10,000 Hz) Sensing Element: Ceramic Measurement Range: ±50 s (=490 m/s^2^{2})
Strain gauge		Model No.: KYOWA-kc-120-120-Al-ll Gauge factor: 2.13±1.0% Gauge length: 120 mm Gauge resistance (24°C, 50%RH): 119.8±0.2 Ω
Displacement sensor		Model No.: BEl9615 potentiometer Linearity: ±0.35%; Full scale: 38 mm
Camera		(1) Camera for displacement: Z Camera El Resolution: 4K (3840 × 2160 pixels) Speed: 30 frame per second Lens: Olympus 75–300 mm zoom lens (2) Camera for traffic: Canon VDOA HF R42 Resolution: lOSOp (1920 × 1080 pixels) Speed: 60 frame per second Lens: built-in 32× zoom 2.8–89.6 mm lens
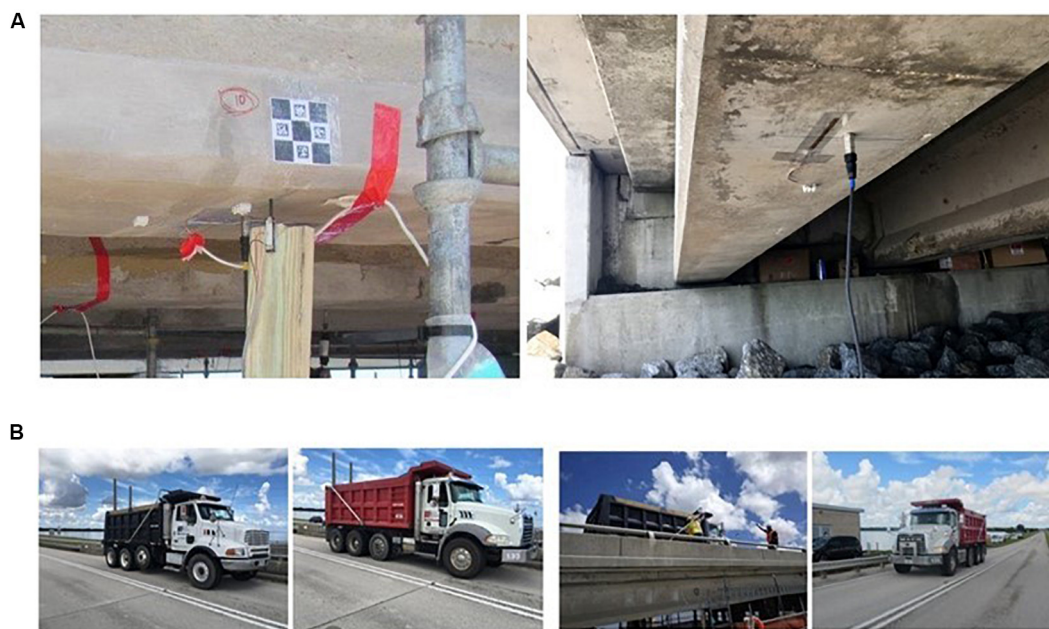
FIGURE 2 | (A) Sensors installed on the bottom of the girders **(B)** Loading trucks.

P10) were observed during the load test. Therefore, only results from cameras are shown in **Figure 4A** and only these results were used for assessment. Details of the test and use of computer vision based implementation are given by Catbas et al. (2019) and will be presented in other presentations. From **Figure 4A**, it can be seen that the displacement gives a flat level at each test step and when the truck was loaded on L1, the girder under the truck has the largest displacement response. For example, here P9 is the mid span of Girder 4 and it gives the largest displacement, 2.76 mm at step 3 (S3) among all the girder measurement points. The displacement of P6, P7, P8, and P10 at step 4 is 0.41, 1.48, 2.69, and 1.49 mm, respectively.

Case no.	Case name	Truck	Lane
1	T1L1	TI	LI
2	T1L2	TI	L2
3	T2L1	T2	LI
4	T2L2	T2	L2

FE Model of the Bridge

As shown in **Figure 5**, FE model of the bridge was established using beam elements and shell elements for the reinforced concrete prestress girders and deck, respectively. Besides, tendon elements was utilized to consider the prestress effect in the analyses. All considerations for FE model of the bridge were obtained according to its calculation report and project drawings. For this aim, structural analysis software, SAP2000 (CSI, 2019),
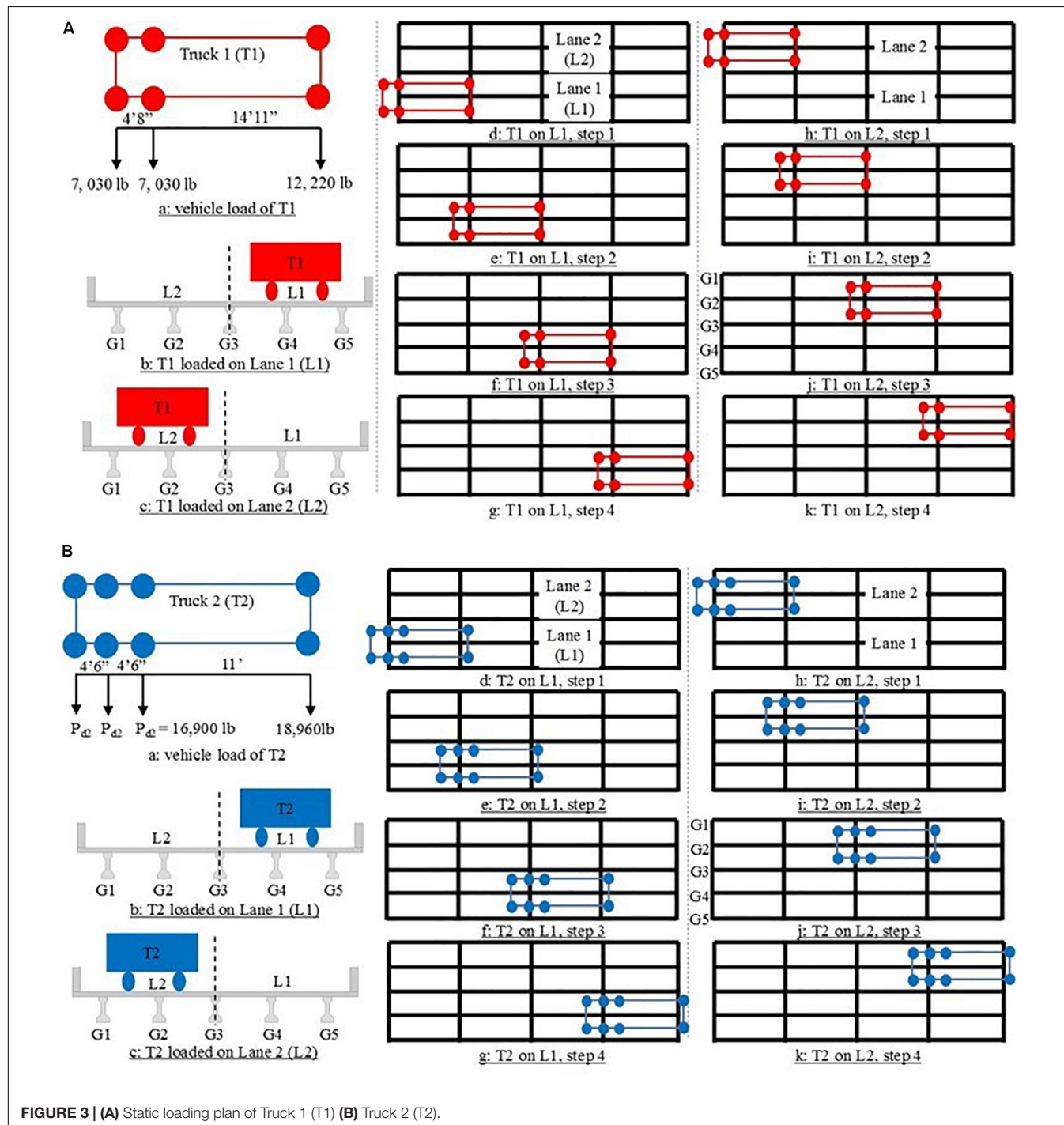

FIGURE 3 | (A) Static loading plan of Truck 1 (T1) (B) Truck 2 (T2).

Case no.	Case name	Truck	Speed (mph)	Lane
5	T1L1-35	TI	35	LI
6	T1L2-35	TI	35	L2
7	T2L1-35	T2	35	LI
8	T2L2-35	T2	35	L2
9	TILI-55	TI	55	LI
10	T1L2-55	TI	55	L2
11	T2L1 -55	T2	55	LI
12	T2L2-55	T2	55	L2

was utilized. The bridge was then updated as per the modal characteristics and displacement results obtained from the experimental field test. The live load DF and load-rating (RF) of the updated FE model are also taken into account for the sake of the comparison of experimental and AASHTO (AASHTO, 2017) calculation.

Linearity Check

The linearity check of the bridge was carried out mainly for two reasons. First, it is to determine the load rating with larger load levels and secondly to be able to calculate multiple presence factors by combining separate test results. Under regular operational loads, the bridge response should not reach ultimate response levels. As such, it would be possible to observe linear behavior under given increasing load conditions. To check the linearity of the bridge, the girders with the largest responses were selected and here it is for the case the truck loaded on L1, the girder is G4. Two loading cases T1L1 and T2L1 were taken as an example to check the linearity (**Figure 6**). The load increase is observed to be 2.65 due ratio of the weight of T2 to T1 as shown in **Figure 6**. It should be noted that the axle number and total length of truck are not exactly the same. In addition, the placement of the trucks in real life are somewhat different as one truck has two and the other has three rear axles as shown in **Figure 3**. From **Figure 6**, it can be seen that the displacement and the strain increase ratios are quite consistent and gives 3.16 and 3.08, respectively. Considering the change of axle number and total length of truck, and also the similar trend between displacement and strain (both in the range of $15 \pm 1\%$ to the difference of weight increase), it is fair to say that the linearity is validated. This provides proof that the bridge behaves linearly under operational loads in the range of 26–70 kip range.

Distribution Factor Using Experimental Data and FEM

Using the responses across the bridge, we can obtain bridge load distribution, which is critical for bridge response and load rating. With the displacement results of each girder, the DF can be calculated based on Eq. (1) below:

$$DF_i = \frac{\alpha_i}{\sum_{j=6}^{10} \alpha_j} \qquad (1)$$

where i and j are the girder numbers with the range from 6 to 10 and a_i or a_j are the strain or displacement of the girder

at the same section depending on the data being used. The DFs calculated from the experimental displacement results are shown in **Figure 4B** for T2L1 load case. It should be noted that **Figure 4B** has two vertical axes and the left vertical axis represents the displacement and the right one is for DF. The DF can also be calculated from the strain data. **Figure 7A** shows the strain result of each girder at 1/4 span. Due to the signal noise and the small strain measurements, the raw data (in red line) was filtered and the filtered data was shown in blue line. The DF results are very similar to those obtained from displacements. The strain of Girder 4 (G4) gives the largest value due to the loading also shown in **Figure 7A**. **Figure 7B** illustrates the DFs obtained from the load test with Truck 2 (loaded truck T2) on Lane 1 (L1). It is observed that the max DF is 0.4 right under the truck load. This DF of 0.4 is indicating that there is good load distribution across the bridge. This fully loaded truck DF results can be predicted due to T2 on L2, and this will allow addition of the DFs to obtain multi-load case, which is more conservative than the multi-presence factor given in AASHTO (2017). Similar calculations for DF were carried out based on the results from the FE analysis as given in **Figure 7A** and almost similar DF values to the experimental test were yielded.

AASHTO (2017) utilizes a multi-parameter formulation for the load distribution. The DF was employed for the load rating of the bridge by means of girder line analysis. The detailed formulation for DF calculation can be seen in **Table 4**. It should be noted that the DF calculations by using displacement or strain only consider one single truck in one of the two lanes. In real cases, there is still a chance that multiple vehicles are present in multiple lanes at the same time. AASHTO (2017) code considers this scenario and use the larger value of DFs between the multiple design lanes loaded and single one.

In this study, due to the symmetry of this bridge, the DFs of multiple lanes (two vehicles here) were also calculated and shown in **Figure 8A**. The unit of displacement in the results is millimeter and the unit of strain is $\mu\varepsilon$. From **Figure 8A**, it can be seen that the DFs calculated by experimental displacement and strain at Girder 3 (G3) are very close to the ones calculated by AASHTO (2017). Similarly, this agreement was also seen for the DF results from FEM as shown in **Figure 8A**. It should be mentioned again that the multi girder DFs were calculated under two heavy loaded truck side by side and this would create a load case more conservative than the AASHTO (2017) based DF results. In other words, considering a combined DF of 0.6 can be regarded to be conservative. While the DFs of the other girders calculated by experimental and FEM displacement and strain are much smaller than those calculated by AASHTO (2017). It means that AASHTO (2017) gives more conservative DF, especially for the girders away from the boundary of two adjacent lanes, e.g., G1, G2, G3, and G4. For the girder close to the boundary of two adjacent lanes, e.g., G3, the DFs calculated from displacement and strain are close to those calculated by AASHTO (2017), but still smaller.

Load Rating

By utilizing the results of DFs from the experimental study and FE model, a simple method yet widely used the load rating
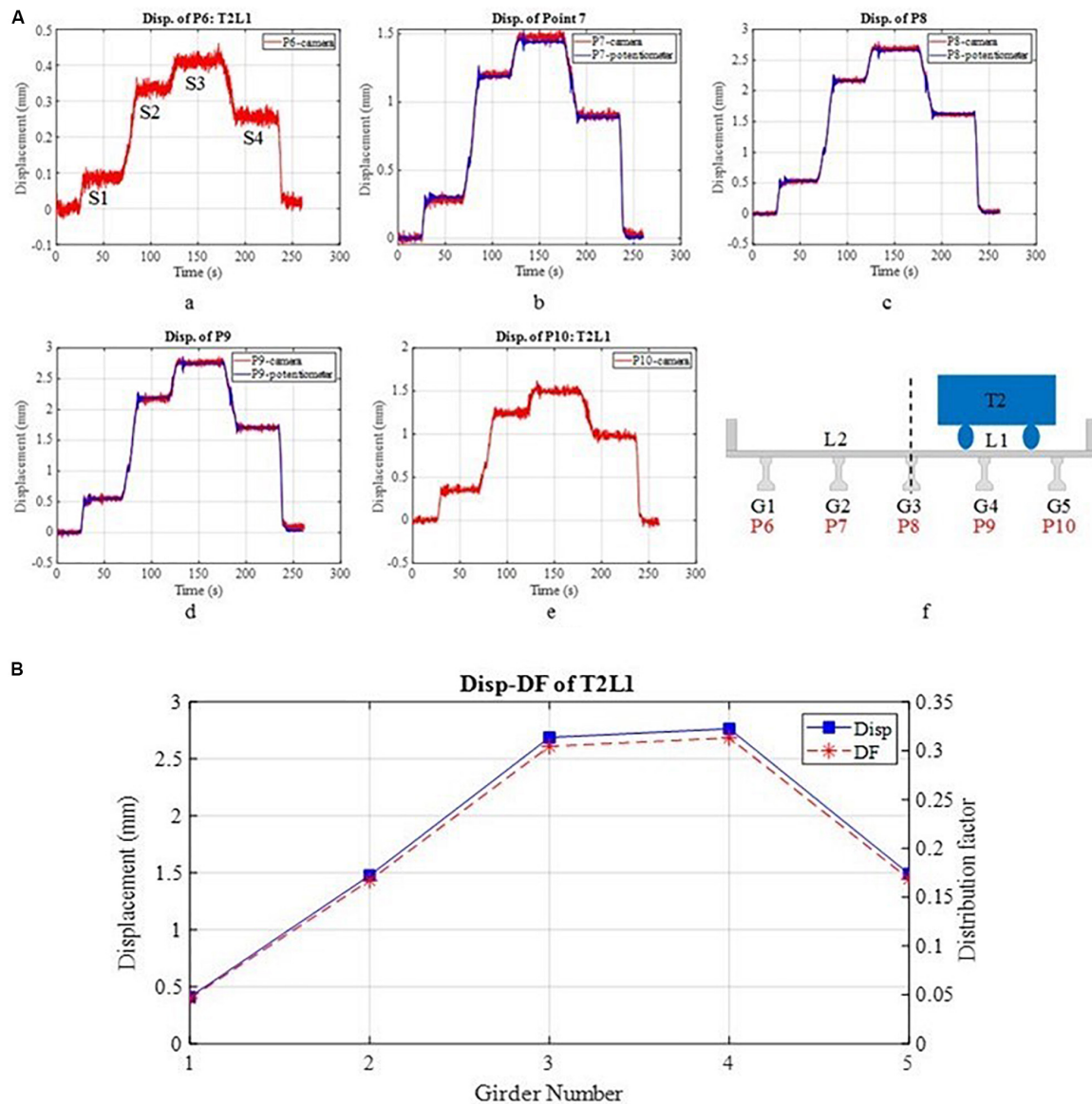
FIGURE 4 | (A) Displacement results of static load case T2L1 **(B)** Distribution factor calculated from displacement results.

factor can be calculated using formulations given in AASHTO (2017). The rating factors (RF) calculated by using different DFs and HL 93 truck for Strength Limit I are listed as shown in **Figure 8B**. General formulation for load rating from AASHTO (2017) is given with Eq. (2). The load factors such as φ, φ_s, $\varphi_c, \gamma_{DC}, \gamma_{DW}, \gamma_p, \gamma_L$ can be found in AASHTO (2017) standard.

$$\text{RF} = \frac{\varphi_c \varphi_s \varphi R - \gamma_{DC}\text{DC} - \gamma_{DW}\text{DW} \mp \gamma_p P}{\gamma_L (\text{LL} + \text{IM})} \quad (2)$$

As stated in the calculation of DF, the load rating using the DF calculated from AASHTO (2017) also indicates that AASHTO codes give the more conservative rating factors than the ones obtained by experimental and FEM method (RF-disp and RF-strain), especially for the girders away from the boundary of two

adjacent lanes, e.g., G1, G2, G3, and G4. For the girder close to the boundary of two adjacent lanes, e.g., G3, the RFs from displacement and strain are close to those calculated by AASHTO (2017), but still larger. The experimental case also presents a more conservative case due to low probability of having two such heavy trucks side by side creating the most critical load case. As a result, it can be concluded that the RFs in real life can even be considered to be even higher than reported in **Figure 8B**.

Deflection of Limit Check

The deflection limit check is to check whether the maximum displacement of mid span is larger than the value calculated by (L/800). This limit is commonly used to evaluate the serviceability of the bridge. Here L is the length of span, which is 15,849.61 mm
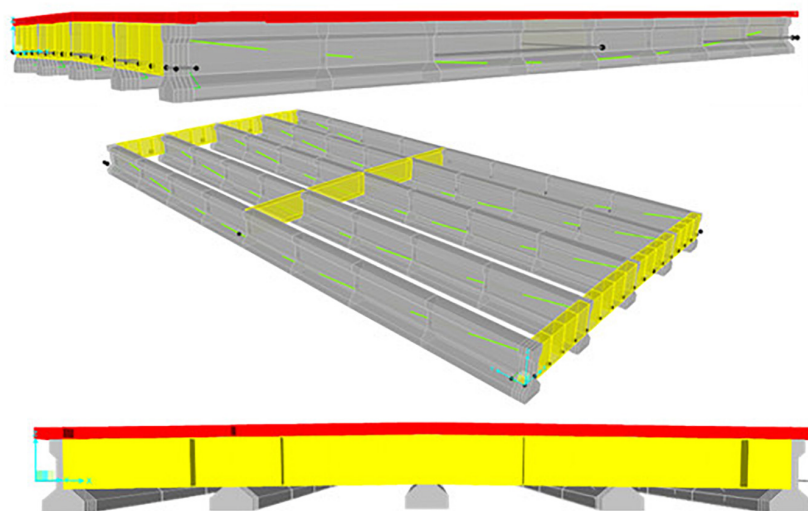
FIGURE 5 | FE Model of the bridge.

Case name	Truck	Total weight (lb)	Displacement (mm)	Strain ($\mu\varepsilon$)
T1L1	T1	26, 280	0.87	25.46
T2L1	T2	69, 660	2.75	78.54
Ratio		2.65	3.16	3.08

FIGURE 6 | Trucks loaded the left lane Truck-1 and Truck-2.

(52 ft). Here (L/800 = 52/800 = 0.065 ft) is 19.81 mm. As demonstrated in **Figure 6**, the maximum displacement of mid span of Girder 4 in loading case T2L1 under static vehicle load is 2.75 mm, which is considerably less than the serviceability deflection limit. This finding can be somewhat expected due to the number of AASHTO girders and the span length of the bridge. In conclusion, the bridge fulfills AASHTO (2017) serviceability requirement.

DYNAMIC LOAD-TEST

Modal Testing

To estimate the dynamic properties of the bridge, the accelerations versus time histories collected by fifteen accelerometers installed on the bridge were processed. One

of the other objective of the modal testing is to use its results to update the FE model of the bridge as developed in the previous section above. These dynamic results can be tracked over time to determine any global changes. They were employed to validate or calibrate FEM of the bridge. Here load case T2L1-55 (Truck 2 moved on Lane 1 with a speed of 55 mph = 80.7 ft/s) is considered for the dynamic analysis. It is seen based on the speed of the truck it takes about 0.64 s to cross the bridge. **Figure 9A** shows the acceleration time histories of each measurement point for load case T2L1-55. **Figure 9B** shows the FFT analysis of acceleration at P4 and possible modal frequencies were marked. Based on all the collected time histories, operational modal analysis methods, enhanced frequency-domain decomposition (EFDD) and stochastic subspace identification-unweighted principal component (SSI-UPC) as shown in **Figure 9C**, is employed to identify the modal frequencies, damping ratio and mode shapes
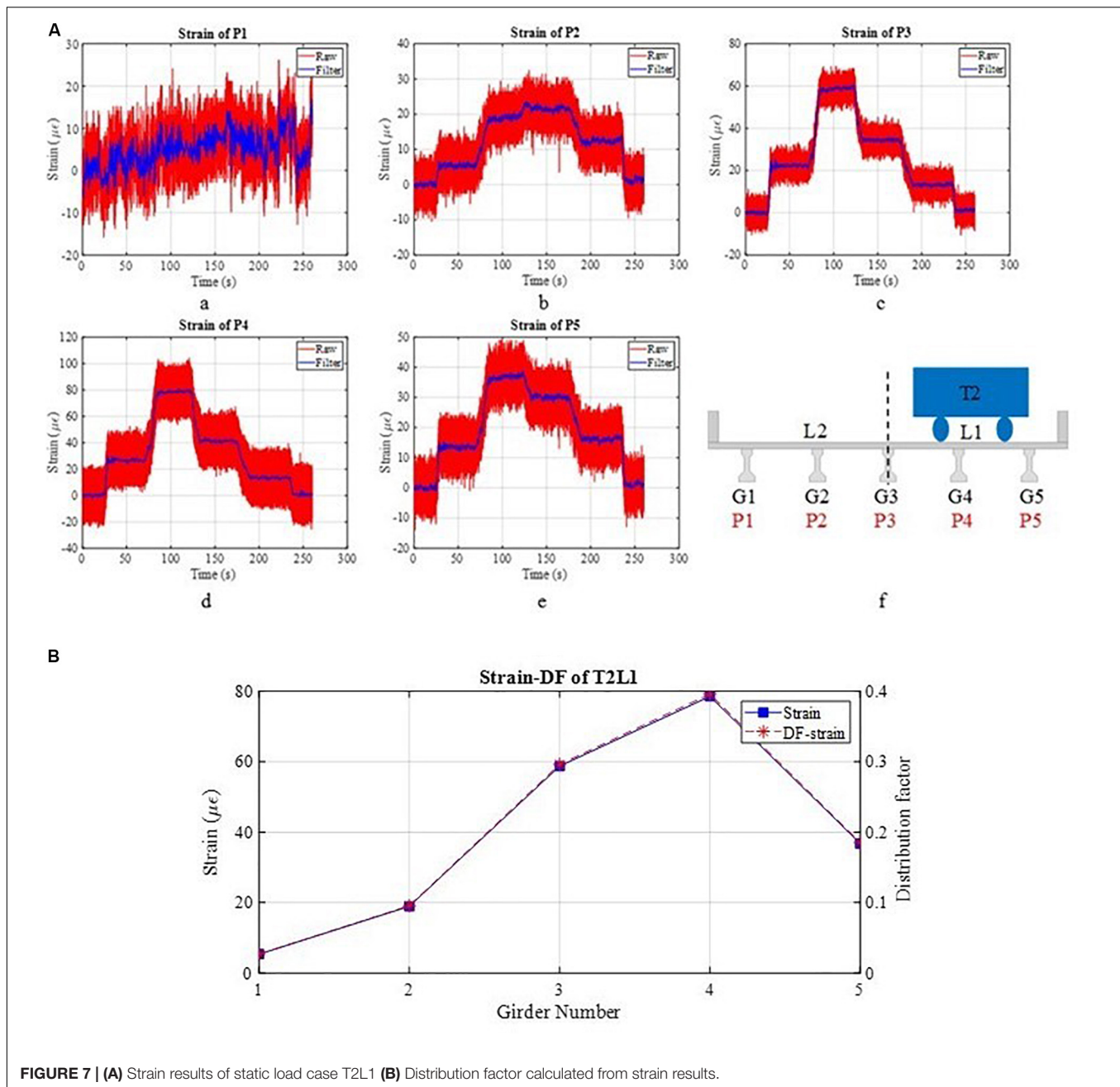
FIGURE 7 | (A) Strain results of static load case T2L1 (B) Distribution factor calculated from strain results.

TABLE 4 | Distribution factor calculation in AASHTO (2017).

DF for moment, interior girder	DF for moment, exterior girder
One design lane loaded: $mg^{SI}_{moment} = 0.06 + \left(\frac{S}{14}\right)^{0.4} \left(\frac{S}{L}\right)^{0.3} \left(\frac{K_g}{12Lt_s^3}\right)^{0.1}$	One design lane loaded: $mg^{SE}_{moment} = \frac{S}{5.5}$
Two or more (multiple) design lanes loaded: $mg^{MI}_{moment} = 0.075 + \left(\frac{S}{9.5}\right)^{0.6} \left(\frac{S}{L}\right)^{0.2} \left(\frac{K_g}{12Lt_s^3}\right)^{0.1}$	Two or more (multiple) design lanes loaded: $mg^{ME}_{moment} = e(mg^{MI}_{moment})$ $e = 0.77 + \frac{d_e}{9.1} \geq 1.0$ d_e is positive if girder is inside of barrier, otherwise negative
AASHTO 4.6.2.2.2b-I	AASHTO 4.6.2.2.2.1d-I

S = girder spacing (ft); L = span length (ft); t_j, = slab thickness (in.); $K_g = n(I_g + e_g^2 A)$; n = modular ratio of girder and deck; I_g = moment of inertia of girder (in.*), e_g = girder eccentricity which is the distance from girder centroid to middle centroid of slab, (in.); A = girder area (in.^{2}).

Girder No	Exp. Disp. of S3	Exp. Strain of S3	Exp. DF-Disp.- single	Exp. DF-Strain- single	Exp. DF-Disp.- multiple	Exp. DF-Strain- multiple	AASHTO
1	0.41	5.33	0.046	0.027	0.22	0.21	0.53
2	1.48	18.94	0.167	0.096	0.48	0.49	0.62
3	2.69	58.74	0.304	0.296	0.61	0.59	0.62
4	2.76	78.54	0.313	0.396	0.48	0.49	0.62
5	1.49	36.75	0.169	0.185	0.22	0.21	0.53
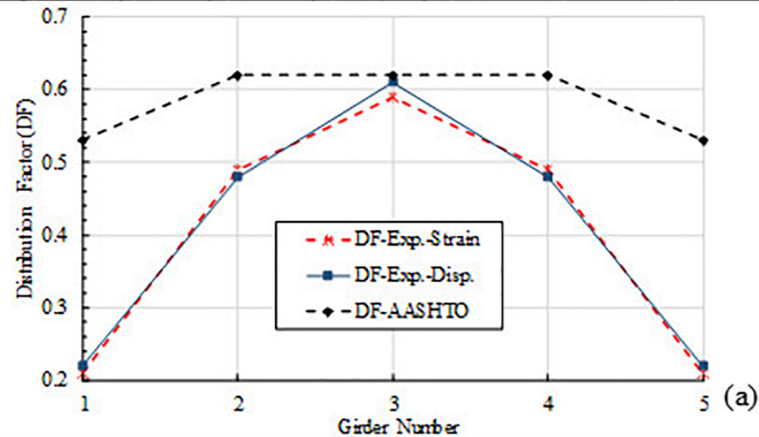
Girder No.	Experimental				RF FEM	RF AASHTO
	RF-disp		RF-strain			
	single lane	multi lane	single lane	multi lane		
1	14.63	3.06	24.93	3.21	3.84	1.27
2	4.01	1.4	6.98	1.37	3.12	1.08
3	2.2	1.1	2.26	1.13	2.78	1.08
4	2.14	1.4	1.69	1.37	3.12	1.08
5	3.98	3.06	3.64	3.21	3.84	1.27

RF-disp and RF-strain: Rating factor using displacement and strain based distribution factors, respectively. RF-AASHTO: Rating factor based on AASHTO (2017)
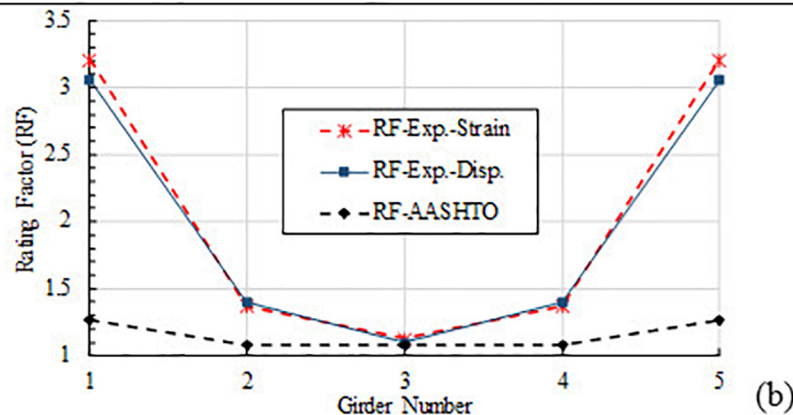

FIGURE 8 | Comparison **(A)** DF **(B)** RF results.

(Artemis-Modal, 2015). Both methods are generally used to identify modal parameters of linear systems using output-only measurements. In the SSI method, dynamic response of a structural system is assumed to consist of state and observation parts. The philosophy of this approach is to represent dynamics of a structure is modeled as $n \times n$ state matrix (n: state space dimension). Observation matrix can be estimated from a part of the state matrix. Thus, the system response vector that includes
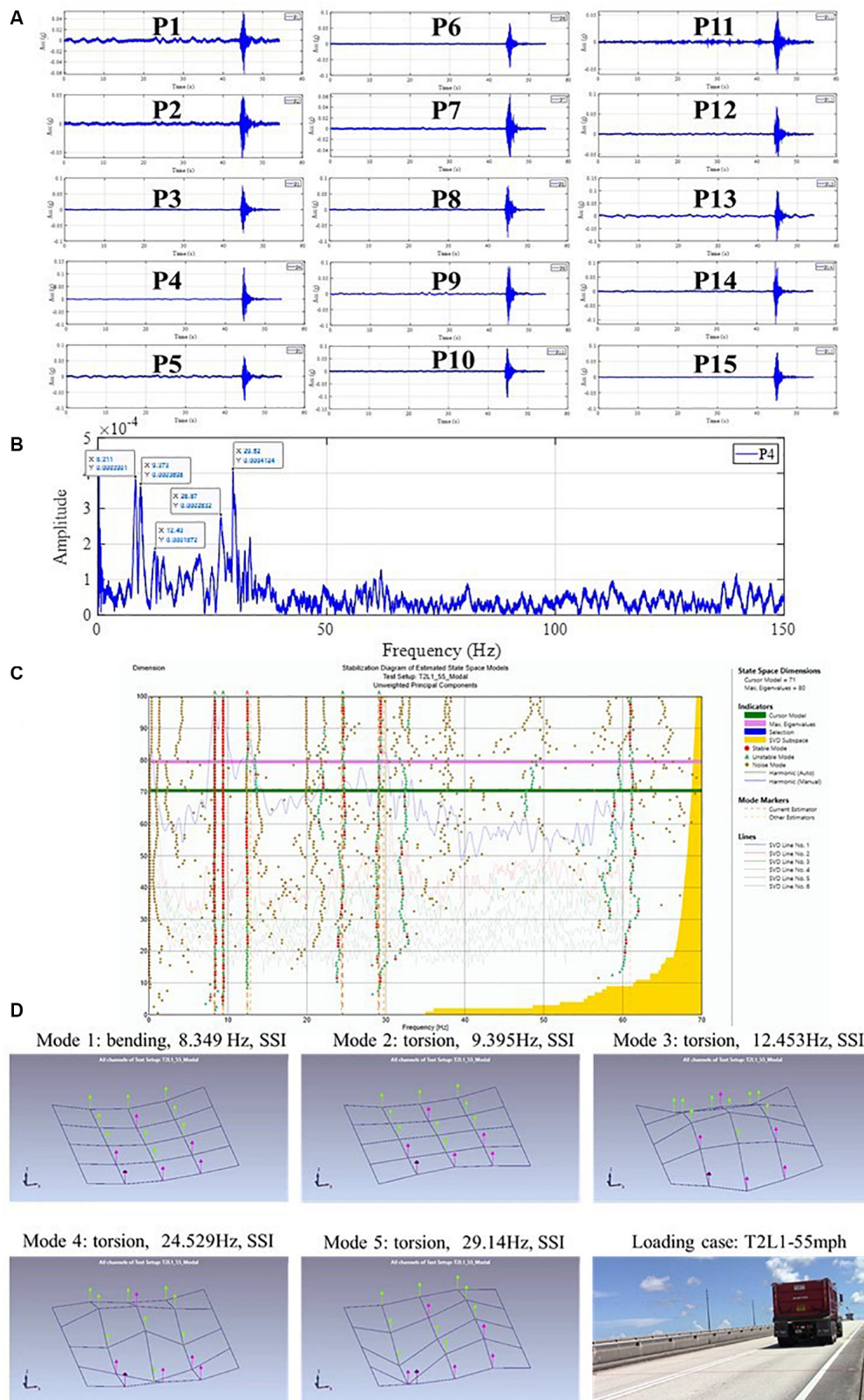
FIGURE 9 | (A) Acceleration time-histories **(B)** FFT analysis of P4 acceleration **(C)** Stabilization diagram for SDDD **(D)** Estimated modal characteristics.

TABLE 5 | Comparison of modal frequencies.

No	Type	Experimental (Hz)		FEM (Hz)	Difference (%)	
		SSI	EFDD		FEM-SSI	FEM-EFBD
1	Bending	8.349	8.307	7.97	4.54	4.06
2	Torsional	9.395	9.235	9.03	3.89	222
3	Torsional	12.453	12.879	15.56	24.95	20.82
4	Torsional	24.529	26.821	28.96	18.06	7.98
5	Bending	29.14	29.888	29.34	0.69	1.83

TABLE 6 | (a) Impact factor Truck 2 for displacement **(b)** Truck 1 for strain.

(a)					
Girder no.	Disp (static)	Disp (35mph)	Disp (55mph)	IM-35 (%)	IM-55 (%)
G2	2.6489	2.7139	2.9762	2.45	12.36
G3	2.1229	2.1698	2.4613	2.21	15.94
G4	1.0646	1.128	1.2075	5.96	13.42

(b)					
Girder no.	Strain (static)	Strain (35 mph)	Strain (55 mph)	IM-35	IM-55
G2	6.98	8.53	7.71	22.3%	10.5%
G3	19.S5	20.45	20.47	3.0%	3.1%
G4	25.46	23.83	22.55	−6.4%	−11.4%

the modal characteristics of structure considered is obtained as different version of observable part of the state matrix. More details can be found in Van Overschee and De Moor (1996). The main idea of EFDD approach is to decompose appropriately the system response into a certain number of independent single degree of freedom systems (SDOF). First, spectral density matrices are predicted from raw experimental data. Singular value decomposition of the estimated spectral density matrices is then performed. The average singular values and corresponding singular vectors present modal frequencies and mode shapes of structural system, respectively. More details can be reached to the study of Brincker et al. (2000).

Figure 9D presents the estimated modal parameters and modes shapes. The frequency of the first bending mode (Mode 1) is 8.35 Hz and the frequency of the second bending mode (Mode 5) is 29.14 Hz. The others are torsion modes. The outcomes from FE analysis of the bridge were also given in **Table 5** with the comparison of those from the experimental. When compared with the updated FE model of the bridge, it was observed to be difference only for the 3rd mode. However, the modal participation mass ratio of this mode (3rd mode) was obtained to be relatively lower, which means that the importance of this mode on a dynamic load can be neglected. Such data and dynamic response can be collected efficiently under operating traffic and can be evaluated to track any stiffness or boundary condition change.

Impact Factor

Identification of the IM can be important for bridge operation to possibly reduce live load effects on the bridge. This can be achieved by improving the bridge surface, smooth expansion joints, or limiting the traffic speed. As a result, it is critical to determine the IM. In this study, the most conservative cases were selected to obtain the impact effect caused by moving loads. **Table 6a** shows the IM of three girders (G2, G3, and G4) calculated by the displacement data of T2L2, T2L2-35, and T2L2-55. Here, the speed of the truck increased from static cases to 35 and 55 mph. From **Table 6a**, it can be seen that with the increase of the speed, the IM also increases. The maximum IM obtained from all data sets is 15.94%, (Girder 3, 55 mph), which is much smaller than the value (33%) recommended by AASHTO (2017).

Table 6b shows the IM of three girders (G2, G3, and G4) calculated by the strain data of T1L1, T1L1-35, and T1L1-55. One should note that the strain data has more signal noise than displacements. In addition, the displacement data were cross-validated using computer vision data. Nevertheless, the IM from strain measurements were also obtained. The maximum IM is 22.3%, (Girder 2, 35 mph), which is also much smaller than the value (33%) recommended by AASHTO (2017). While the impact factor of IM-35 of Girder 2, 22.3%, is larger than that of IM-55, 10.5%, which is not reasonable as one would expect a higher IM under higher speed vehicle, as also shown in **Table 6a** with deflections. For Girder 3, the IM are almost the same and for Girder 4, they are negative. The abnormal values here might be caused by the signal noise received by the strain gauges.

Combining **Table 6a** and **Table 6b**, the author recommends that the IM using deflections can be utilized. For the truck with 35 mph velocity, the IM is 5.96% and the truck with 55 mph velocity, the IM is 15.94%.

SUMMARY AND CONCLUSION

In this study, static and dynamic load test were conducted for an existing in-service concrete pre-stressed girder bridge through the field test. Thus, the DF, load rating (RF), deflection limit check, modal characteristics and IM were obtained and compared with those from the conventional calculation methods and FE model. Bridge behavior characterized with these indices (e.g., DF, RF) are to be obtained as summarized in this paper to be able to make decisions about load posting, repair effectiveness, reducing traffic speed and ultimately major retrofit or replacement. A general framework for such a field study is presented along with an example on a typical highway bridge. Some of the specific findings for this bridge are summarized in the following:

- The DF of live load calculated by AASHTO standards gives more conservative results when compared with the experimental and FEM approaches. The DF for a single load case is 0.4. The conservative experimental DF with two heavy truck loads side by side gives 0.59, which is less than 0.62 of AASHTO code. This value was obtained as 0.52 from the updated FE model.

- The load-rating factor (RF) of live load calculated by AASHTO standards gives more conservative results comparing with the experimental and FEM approaches using practical DFs. Rating factors of Strength Limit I are all larger than "2.0" for HL93 trucks for single lane and RF for multilane is 1.10 which is slightly larger than AASHTO code.
- Maximum deflections in static cases and dynamic cases are within the limit calculated by (L/800) and deflections are much less than the AASHTO code based L/800.
- Impact factors among all the cases are much smaller than the one recommended by AASHTO standards (33%). We observe 16%, which was observed under fully loaded truck at 55 mph on the bridge.
- Modal testing results were obtained through the experimental data. These results were used for developing updated FE model of the bridge. The DF and RF outcomes from the updated FE model were obtained to be good agreement with those form the field test. Hence, the updated FE model can be adopted reliably for advanced analysis of the bridge.
- The study showed that bridge condition assessment could be conducted reliably fast with no need for blocking traffic/interrupting bridge's operation. Therefore, the framework given in the study can be practically implemented to a bridge in the same bridge population. Computer vision methods and technology (camera, image, etc.) can be considerably effective for this aim.
- Based on the findings, it is shown that the bridge has sufficient load carrying capacity and the retrofitted bridge can carry large truck loads. The full truck is ~70 kips, very comparable to 72 kips HL-93 AASHTO truck. For the load rating under multiple vehicles, the 70 kip truck was employed by means of superposition due to linearity to obtain the rating factor for the most critical condition. It is shown the AASHTO based formulations satisfy the rating factor, and even the calibrated FE based load rating is even higher. As a result, the bridge can continue to serve and no load posting is necessary based on the results given in this paper.

DATA AVAILABILITY STATEMENT

The datasets generated for this study are available on request to the corresponding author.

AUTHOR CONTRIBUTIONS

FUNDING

ACKNOWLEDGMENTS

REFERENCES

AASHTO (2017). *LRFD Bridge Design Specifications*. Washington, DC: American Association of State Highway and Transportation Officials.

AASHTO-MBE (2018). *The Manual for Bridge Evaluation (MBE)*, 3rd Edn. Washington, DC: American Association of State Highway and Transportation Officials.

Agdas, D., Rice, J. A., Martinez, J. R., and Lasa, I. R. (2016). Comparison of visual inspection and structural-health monitoring as bridge condition assessment methods. *J. Perform. Const. Facil.* 30:04015049. doi: 10.1061/(ASCE)CF.1943-5509.0000802

Artemis-Modal (2015). *User's Guide, Structural Vibration Solutions*. Aalborg: Artemis-Modal.

Bas, S., and Catbas, F. N. (2019). "Bridge failures and mitigation using monitoring technologies," in *Developments in International Bridge Engineering*, eds A. Caner, P. Gülkan, and K. Mahmoud (Cham: Springer).

Brincker, R., Zhang, L., and Andersen, P. (2000). "Modal identification from ambient responses using frequency domain decomposition," in *Proceedings of the 18th International Modal Analysis Conference (IMAC)*, San Antonio, TX.

Catbas, F. N., Ciloglu, K., and Aktan, A. E. (2005). Strategies for condition assessment of infrastructure populations: a case study on T-beam bridges. *Struct. Infrastruct. Eng. J. SIE* 1, 221–238. doi: 10.1080/15732470500031008

Catbas, F. N., Dong, C., Bas, S., and Alver, N. (2019). *Indian River Bridge Test, Final Project Report by UCF CITRS*. Fort Lauderdale, FL: Sanalil Construction Inc.

Catbas, F. N., Gokce, H. B., and Gul, M. (2012). Practical approach for estimating distribution factor for load rating: demonstration on reinforced concrete T-beam bridges. *J. Bridge Eng.* 17, 652–661. doi: 10.1061/(ASCE)BE.1943-5592. 0000284

Catbas, F. N., Grimmelsman, K. A., Ciloglu, S. K., Burgos-Gil, I., and Coll-Borgo, M. (2006). Static and dynamic testing of a concrete T-beam bridge before and after carbon fiber–reinforced polymer retrofit. *Transport. Res. Rec.* 1976, 76–87. doi: 10.1177/0361198106197600109

Catbas, F. N., Kijewski-Correa, T., and Aktan, A. E. (2013). *Structural Identification of Constructed Systems: Approaches, Methods, and Technologies for Effective Practice of St-Id*. Reston: American Society of Civil Engineers.

CSI (2019). *SAP2000: Integrated Finite Element Analysis and Design of Structures*. Berkeley, CA: Computers and Structures Inc .

Davis, N. T., Hoomaan, E., Sanayei, M., Agrawal, A. K., and Jalinoos, F. (2018). Integrated superstructure-substructure load rating for bridges with foundation movements. *J. Bridge Eng.* 23:04018022. doi: 10.1061/(ASCE)BE.1943-5592. 0001232

Dong, C.-Z., and Catbas, F. N. (2019). A non-target structural displacement measurement method using advanced feature matching strategy. *Adv. Struct. Eng.* 22, 3461–3472. doi: 10.1177/136943321985 6171

Gokce, H. B., Catbas, F. N., and Dan, M. F. (2011). System reliability and load rating evaluation of a movable bridge. *Transp. Res. Rec. J. Transp. Res. Board* 2251, 114–122. doi: 10.3141/2251-12

Hiasa, S., Karaaslan, E., Shattenkirk, W., Mildner, C., and Catbas, F. N. (2018). "Bridge inspection and condition assessment using image-based technologies with UAVs," in *Proceedings of the Conference on Structures Congress*, (Reston: ASCE), 217–228.

Omar, T., and Nehdi, M. L. (2018). Condition assessment of reinforced concrete bridges: current practice and research challenges. *Infrastructures* 3:36. doi: 10.3390/infrastructures3030036

Sanayei, M., Reiff, A. J., Brenner, B. R., and Imbaro, G. R. (2016). Load rating of a fully instrumented bridge: comparison of LRFR approaches. *J. Perform. Construct. Facil.* 30:04015019. doi: 10.1061/(ASCE)CF.1943-5509.0000752

Tawadrous, R., Morcous, G., and Maguire, M. (2019). Performance evaluation of a new precast concrete bridge deck system. *J. Bridge Eng.* 24:04019051. doi: 10.1061/(ASCE)BE.1943-5592.0001422

Torres, V., Zolghadri, N., Maguire, M., Barr, P., and Halling, M. (2019). Experimental and analytical investigation of live-load distribution factors for double tee bridges. *J. Perform. Construct. Facil.* 33:04018107. doi: 10.1061/ (ASCE)CF.1943-5509.0001259

Van Overschee, P., and De Moor, B. (1996). *Subspace Identification for Linear Systems: Theory - Implementation - Applications*. Dordrecht: Kluwer Academic Publishers.

Zaurin, R., Khuc, T., and Catbas, F. N. (2016). Hybrid sensor-camera monitoring for damage detection: case study of a real bridge. *J. Bridge Eng.* 21:05016002. doi: 10.1061/(ASCE)BE.1943-5592.0000811

Bridge Load Rating Through Proof Load Testing for Shear at Dapped Ends of Prestressed Concrete Girders

Y. Edward Zhou[1]* and Mark R. Guzda[2]*

[1] *Bridge Instrumentation & Evaluation Lead, North America, AECOM, Germantown, MD, United States,* [2] *Bridge Engineer, AECOM, Hunt Valley, MD, United States*

Load ratings of the 1967 built I-195 westbound bridge over Seekonk River in Rhode Island are governed by shear at the dapped ends of prestressed concrete (PSC) girders. Insufficient analytical load ratings, in combination with visible shear cracks at the dapped ends, prompted the need for a refined method of load rating through load testing. The proof load testing method was chosen over diagnostic testing for a higher level of reliability due to uncertainties involved in calculating shear capacities of the dapped ends. A proof load test was successfully completed with a maximum proof load of two test trucks of approximately 100,000 lbs each crossing the bridge side-by-side without any signs of distress or non-linear behavior observed. Vehicle loading dynamic impact was also assessed during the load test. Test measurements indicated full composite action between the bridge deck and the PSC drop-in girders, which was not accounted for in the analytical rating of the dapped ends. Test results suggested that the strut-and-tie and shear-friction analysis methods underestimate the shear resistance of the dapped ends by considering only the stirrup reinforcement and draped prestressing strands within the PSC girder. This paper provides detailed information on bridge proof load testing in general concept and procedure, comparisons with the diagnostic load testing method, field operation, examination of test measurements for linear elastic structural behavior, and determining bridge load ratings based on test results per *The Manual for Bridge Evaluation* of AASHTO.

Keywords: bridge, load rating, prestressed concrete, dapped end, proof load test

INTRODUCTION

The I-195 westbound (WB) bridge over Seekonk River in Providence, Rhode Island was built in 1967 and consists of 13 prestressed concrete (PSC) girder spans and five steel plate girder spans. The bridge carries five traffic lanes before an exit ramp and four traffic lanes plus a full-width right shoulder after the exit ramp. The superstructure of the PSC spans is of the cantilevered and drop-in girder construction and consists of six lines of girders equally spaced at a distance varying from 13 ft in the five lane section to 11.4 ft in the four lane section. The drop-in girders are the PSC Type IV AASHTO girders with dapped ends resting on elastomeric bearings at the end of the cantilevered girder sections.

Figure 1 shows a typical PSC girder span of the I-195 WB bridge, which has a reinforced concrete arch wall on each side as an aesthetic feature. In the photograph, the arch span at the lower-left corner in the background is an exit ramp, and the steel girders at the upper-right corner in the foreground are part of the I-195 eastbound (EB) bridge. Load ratings of the PSC girder spans were found to be governed by shear at the dapped end of the drop-in girders. **Figure 2** is a close-up view of the drop-in girder dapped end supported by a cantilevered girder section from the pier. **Figure 3** is from the 1967 bridge plans depicting the drop-in section of the PSC girders including the path of deflected prestressing strands as well as reinforcing details at the dapped end.

Analytical load ratings for the dapped ends were calculated significantly insufficient for most rating vehicles from the strut-and-tie and shear friction analysis methods with the shear capacity based on the resistances from the stirrup reinforcement and draped prestressing strands within the PSC girder. Diagonal concrete cracks initiated from the re-entrant corner of the dapped end have been observed in multiple girders. However, no correlations were found between the degree of field observed diagonal cracking and the level of analytical load effects at the dapped ends. The insufficient analytical load ratings, in combination with the apparent shear cracks observed at the dapped ends, prompted the need for a refined method of load rating through load testing. The bridge has been carrying interstate highway loads without any weight restrictions.

SELECTION OF LOAD TESTING METHOD

Load ratings measure a bridge's load carrying capacity for specific loading vehicles in addition to its self-weight. Bridge load ratings are defined with different levels of reliability in AASHTO's *The Manual for Bridge Evaluation* (MBE) (AASHTO, 2018) and provide a basis for decisions on weight posting, overweight vehicle permits, and structural strengthening or replacement. Engineering experience indicates that the conventional methods of analysis may yield overly conservative load ratings in some circumstances. Load testing has proven to be a reliable and efficient method for determining more accurate load ratings that reflect the actual structural behavior and physical condition of the bridge (TRB, 1998; TRB, 2019). Field measurements help identify inherent mechanisms that assist in carrying live load, such as unintended composite actions between primary load-carrying members (girders, trusses, arch ribs, etc.) and secondary components (deck, flooring frames, barriers, etc.). Load test results also provide quantitative measurements for actual live load distribution among multiple structural elements as well as the effects of *in situ* conditions of connections and supports.

The AASHTO MBE prescribes two load testing methods for bridge load rating purposes: the diagnostic load test and the proof load test. Diagnostic load testing determines the actual responses of key structural components, generally in terms of measured strains and deflections, to known test loads. An analytical model is usually established based on best available

information and compared with the load test results. After being adjusted and validated with test results, the analytical model is used to assess the maximum load effects of dead load and all required rating vehicles. In order to calculate refined bridge load ratings through a diagnostic load test, member capacities must be quantified based on section and material properties per construction documents, field measurements, or through *in situ* material testing.

Alternatively, proof load testing physically proves the bridge's ability to carry its full dead load plus some magnified live load. Test loads are applied to the bridge in a multiple-step loading and unloading process in a progressively increasing manner toward a predetermined target proof load. The target proof load is established to be sufficiently higher than the rating vehicles in order to include a live load factor for the required margin of safety and to account for the effects of dynamic impact. During each loading and unloading step, key responses of the structure are measured and monitored for possible signs of distress or non-linear-elastic behavior. Upon successful completion of a proof load test, the highest applied load provides a lower bound on the true strength capacity, which leads to a lower bound bridge load rating after incorporating proper load factors and dynamic load allowance.

Compared with diagnostic load testing, proof load testing requires a reduced level of structural analysis without the necessity for calculating section capacities or the maximum force effects of dead and live loads. The direct result from a proof load test is to conclude whether the rating factor for a specific vehicle type (the test vehicle) exceeds 1.0 at the Operating level of reliability, which is lower than the Inventory level of reliability as in bridge design. Load ratings for other vehicle types can be determined from a simple structural analysis by comparing the governing force effects of the rating vehicles with those of the test vehicle. Despite having been available for over two decades (Fu and Tang, 1995; TRB, 1998), the proof load testing method still lacks a definitive procedure for interpreting and translating the test results into bridge load ratings (Lantsoght et al., 2017; Lantsoght, 2019; TRB, 2019).

For the I-195 WB bridge, proof load testing was chosen over diagnostic testing for a higher level of reliability because calculating the shear capacity of the dapped end involves multiple uncertainties including quantification of the contributions of vertical and horizontal reinforcing bars as well as prestressing strands at the dapped end, effects of existing cracks, etc. Additionally, the effect of the reinforced concrete bridge deck in distributing and resisting shear at the dapped end is difficult to quantify in any analytical model.

INSTRUMENTATION PLAN

One span (Span 2) was chosen for load testing to represent all 13 PSC girder spans of the bridge that have similar analytical load ratings. The selected span has easy access from the ground and was representative of the worst condition in diagonal cracking and concrete spalling at the dapped end throughout the bridge. **Figure 4** depicts the instrumented span including the layout of

FIGURE 1 | Overview of a typical PSC girder span of I-195 WB bridge over Seekonk river.

FIGURE 2 | Dapped end of drop-in girder supported by cantilevered girder section from pier.

32 strain sensors in the plan view and cross section view. Of these strain sensors, 26 measure the effects of shear at the dapped end of all six (6) drop-in girders (four on each east end of all six girders and two on west end of Girder F), four (4) measure the effects of

flexure at the mid-span of Girders E and F, and two (2) measure the effects of flexure near the east end of Girder F.

Placement details of strain transducers on concrete surface for shear at the dapped end are described in **Figure 5**, along
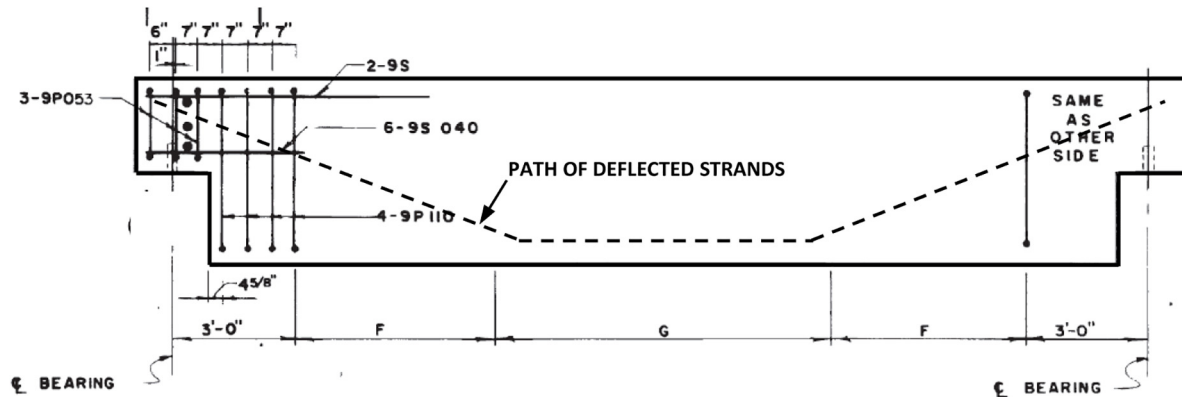
FIGURE 3 | Reinforcing details at dapped end and prestressing strand path of drop-in girder.
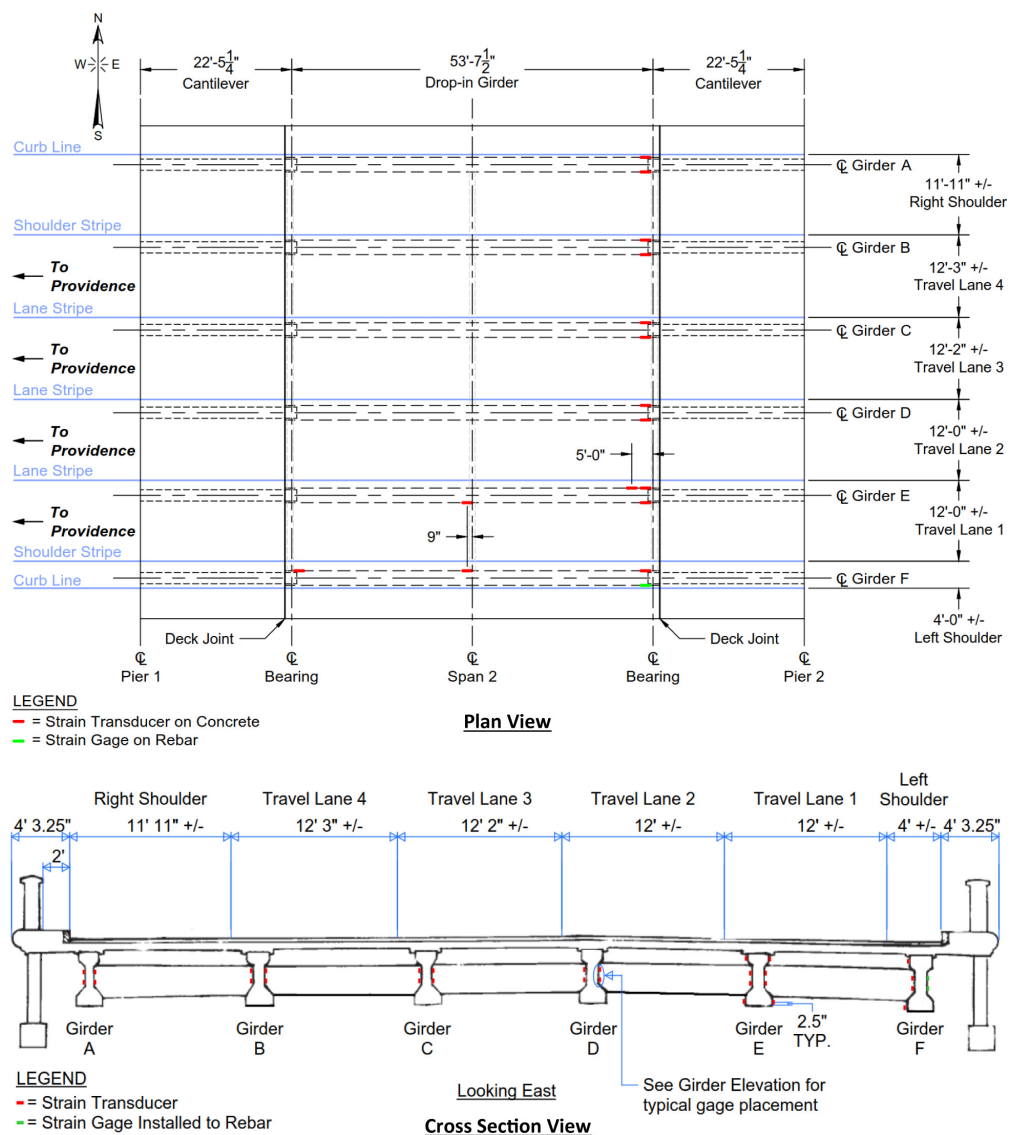
FIGURE 4 | Layout of 32 strain sensors on six drop-in girders.
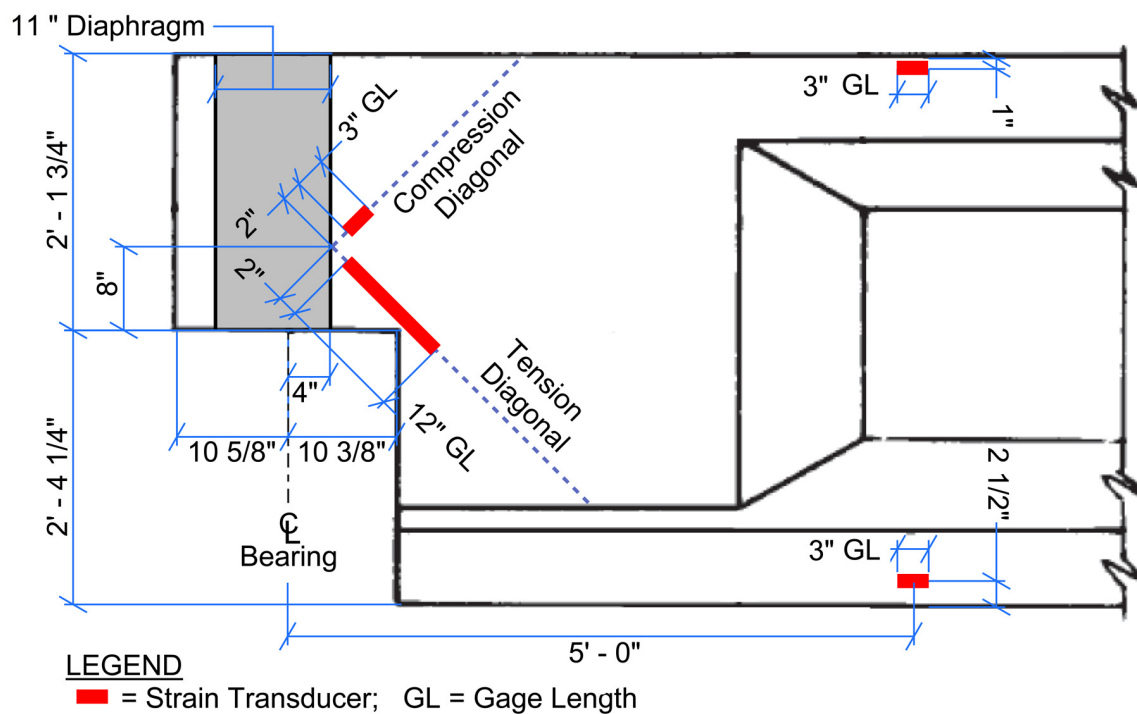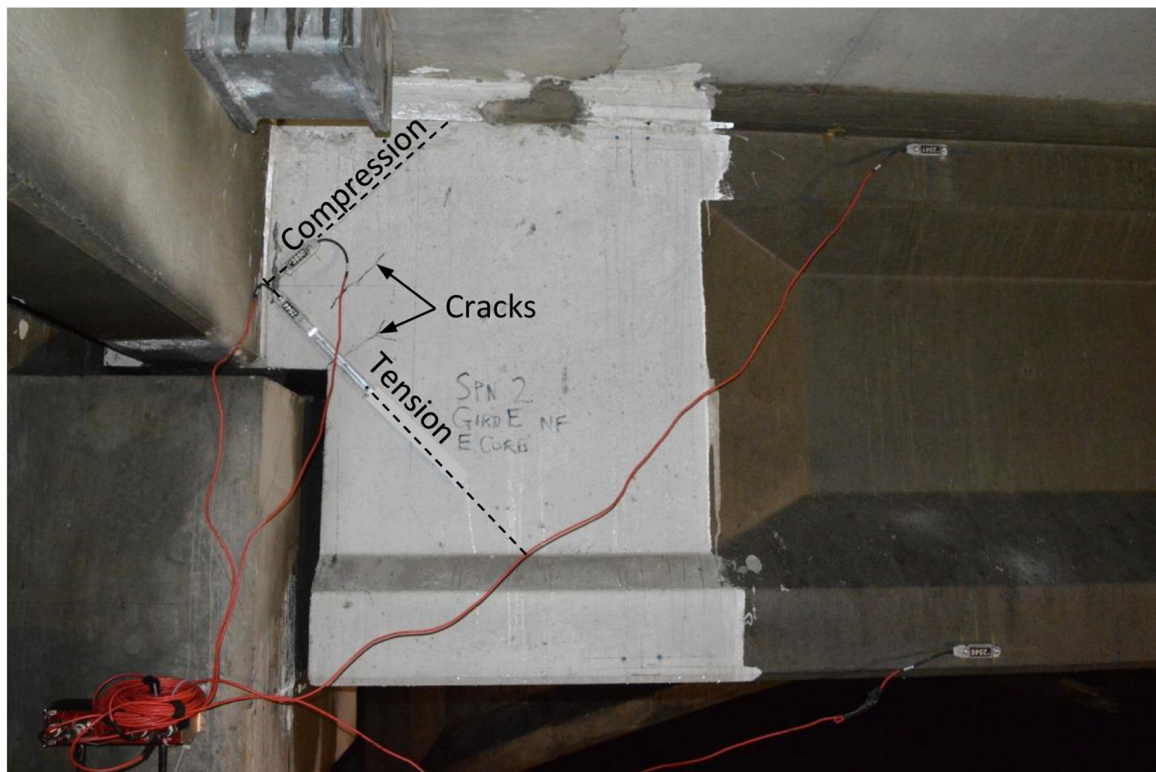
FIGURE 5 | Strain transducers on concrete surface at dapped end.

the compression and tension diagonals at a 45-degree angle, respectively. Strain transducers installed along the compression diagonal had a 3″ gage length, while those along the tension

diagonal were extended to a 12″ or 15″ gage length to span over any existing cracks or spalls. The east end of all six (6) drop-in girders were instrumented with two (2) strain transducers for

FIGURE 6 | Weldable strain gauges on exposed rebars at dapped end.
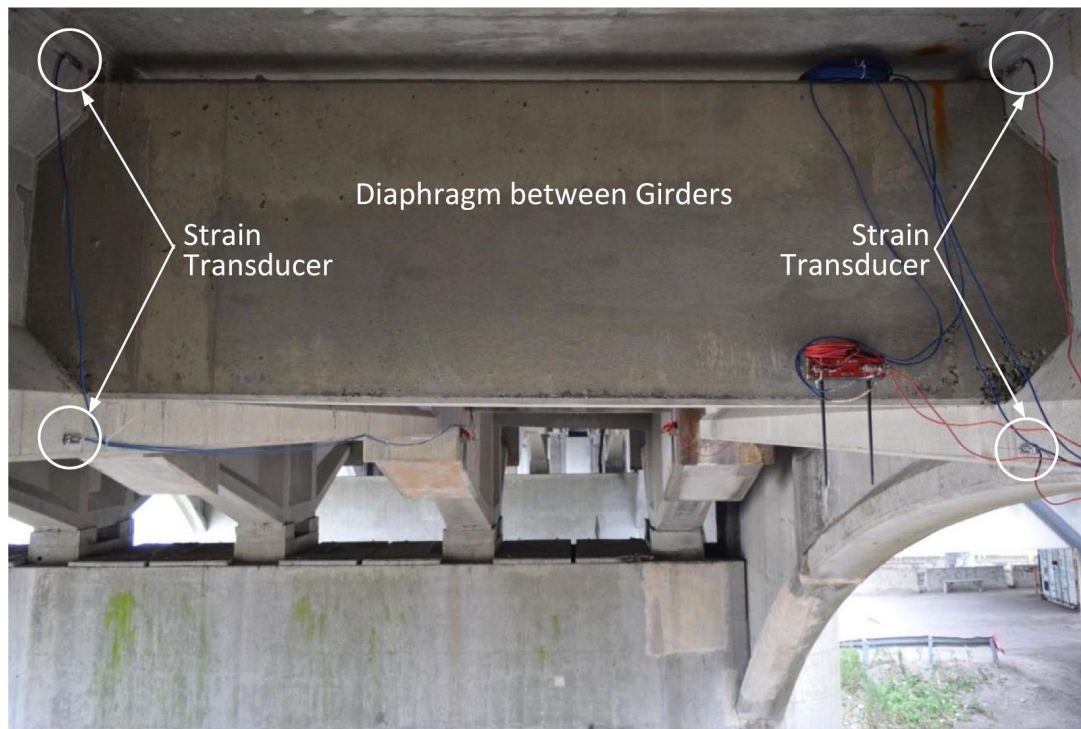
FIGURE 7 | Strain transducers on top and bottom flanges of drop-in girder at mid-span.

shear on each side of the web, with the exception of the south face of Girder F, which had two (2) weldable strain gages installed to exposed steel reinforcement as shown in **Figure 6**. The west end of Girder F was also instrumented with two (2) strain transducers for shear on its north web surface only.

Strain transducers on concrete surface for flexural effects were installed to the top and bottom flanges of drop-in Girders E and F near the mid-span, as shown in **Figures 4, 7**. Girder E was also instrumented with two strain transducers on the top and bottom flanges near its east end, at $5'$-$0''$ (greater than the girder depth) from the centerline of bearing as shown in **Figure 5**. These sensors provide information for assessment of the deck-girder composite action at a high shear location in addition to flexural strains in the PSC girders. All sensors were connected to a wireless digital data acquisition system that records sensor responses and allows real-time review of test results during the load test.

TARGET PROOF LOAD

The target proof load needs to be sufficiently high to appropriately encompass an evaluation live load factor (γ_{LL}) and a dynamic load allowance (*IM*) for load rating. *The Manual for Bridge Evaluation* (MBE) (AASHTO, 2018) specifies the values of γ_{LL} that vary with the method and level of bridge load rating. Different load rating methods include the Load and Resistance Factor Rating (LRFR), Load Factor Rating (LFR), and Allowable Stress Rating (ASR). LRFR includes Design load rating at the Inventory and Operating levels, as well as Legal load rating and

Permit load rating. LFR and ASR each includes load ratings at the Inventory and Operating levels. It is important to note that proof load testing should only be expected to verify a lower bound load rating at the LRFR Design Operating, Legal or Permit level, or the LFR Operating level.

The MBE (AASHTO, 2018) prescribes the following for establishing the target proof load (L_T):

$$L_T = X_{pA} L_R (1 + IM) \qquad (1)$$

where:

> X_{pA} = adjusted target live load factor.
> L_R = comparable unfactored live load due to the rating vehicle for the lanes loaded.
> *IM* = dynamic load allowance.

In accordance with the MBE, the target live load factor (X_P) has a base value of 1.40 but should not be less than 1.3 or more than 2.2 after adjustments (X_{pA}) considering the number of loaded lanes, structural redundancy, presence of fracture critical details, *in situ* condition, average daily truck traffic (ADTT), etc. (AASHTO, 2018). Values of the adjustments provided were calibrated to provide a comparable level of reliability as the calculated load capacity.

In LRFR Legal load rating, the generalized live load factor (γ_{LL}) for the Strength I limit state is 1.30 for ADTT $\leq$ 1,000 and 1.45 for ADTT $\geq$ 5,000 in one direction. The γ_{LL} values account for multiple-presence of two heavy trucks side-by-side on a multi-lane bridge as well as the probability of truck weights exceeding

the legal limits. If warranted, γ_{LL} may be increased by a multiplier of up to 1.3. If the purpose of the test is solely to verify a rating for a permit load, X_p may be reduced in correspondence with the permit load factors that range from 1.10 to 1.40 (AASHTO, 2018).

It must be noted that the L_T or L_R used in the AASHTO *MBE* for prescribing the target proof load is the force effect governing the bridge load rating. For a bridge proof load test using vehicles for load application, the test load needs to be defined by the type and number of test trucks to be used, their initial and target weights, as well as their weight increases and combinations during the multiple-step loading and unloading process.

For this bridge, the maximum shear force (V_{max}) at the dapped end of the drop-in girder was used as the key parameter to establish the target proof load since it governs the bridge load rating. **Table 1** lists the V_{max} in the 53′-71/2″ test span from a simple beam analysis for the HL93 design truck plus eight (8) different legal vehicles for load rating. Among the legal vehicles, the SU7 vehicle (SU7) produces the highest V_{max} of 58.76 kips, which is very close to (98.81% of) that of the HL93 design truck (59.47 kips).

Two three-axle dump trucks were chosen for the proof load testing based on the availability of test vehicles as well as the span length (53′-71/2″) and girder spacing (12′-3″) of the concerned structure where load rating is governed by shear at the dapped end. The axle configurations of the test trucks are similar to, but slightly longer than, the AASHTO Type 3 vehicle (Type 3). Therefore, Type 3 was used to estimate the target weight of the test vehicles.

Based on **Table 1**, the gross vehicle weight (GVW) of Type 3 for producing an equivalent maximum shear due to SU7 is: (58.76K/43.06K) (50K) = 68.23K. Using the 1.40 base value of the target live load factor (X_p) without dynamic load allowance, the target proof weight for Type 3 is: (1.40) (68.23K) = 95.52K. This was used as the approximate target weight for the test vehicles due to their similarity to Type 3. It should be realized that the wheel and axle weights of a truck for a GVW vary with the loading material and equipment employed, and cannot be predicted beforehand.

PROOF TESTING PROCEDURE AND OPERATION

A detailed proof load testing procedure was developed for applying test loads in a progressively increasing manner aiming to accomplish the target proof load. The test plan considered: a) applying direct and similar test loads to each of the six girders in the instrumented span; b) at each truck weight level, running multiple single truck and two-truck side-by-side crossings at varying lateral positions for different load effects; c) repeating the same crossing patterns at all weight levels, and d) when possible, making pairs of slow speed and highspeed runs using the same truck at the same lateral position for assessing dynamic impact. Measures were also prepared for aborting the load test at any intermediate step if deemed necessary based on possible signs of distress or non-linear behavior. In addition, deliberate considerations were given to safety as well as operation issues

such as maintenance of traffic, entrance and exit points on the interstate highway for the test trucks, etc.

The proof load test consisted of 44 test runs using two test trucks at four (4) different weight levels as shown in **Figure 8**. The actual truck weights at the highest weight level ended up to be 101.72K and 100.38K, slightly higher than the target proof load of 95.52K for Type 3.

The 44 test runs included 13 each at weight levels No. 1 (WL#1) and No. 2 (WL#2), and nine (9) each at WL#3 and WL#4. **Table 2** describes the 13 test runs at WL#2, including five (5) single truck crossings at a crawl speed (about 5 MPH), four (4) two-truck side-by-side crossings at a crawl speed, and four (4) single truck crossings at the speed limit (about 55 MPH). WL#1 had similar test runs as WL#2; WL#3 and WL#4 each had only the nine (9) crawl speed runs since highspeed runs at such weights are unsafe if even possible.

The proof load test was performed in two consecutive nights between 10 PM and 4 AM. During the testing period in each night, the two left lanes of I-195 WB were closed to traffic and used as a staging area for the test trucks and the load testing staff for approximately one mile beyond each end of the test span. The two right lanes remained open except for during the test runs when the entire bridge was closed to traffic intermittently. **Figure 9** depicts the load test operation including loading and weighing a test truck and running a single truck and a two-truck side-by-side test runs.

Upon completion of each test run, measurement results from all sensors were reviewed for magnitudes, linearity of strain increase vs. load increase, and zero turns. Visual observations were also made for possible signs of distress or condition changes.

STRAIN RESPONSES VS. INCREASING TEST LOAD FOR LINEAR ELASTIC BEHAVIOR

For the purpose of investigating linear-elastic behavior of the PSC drop-in girders, results of the proof load test were plotted in terms of increasing test load vs. peak strain measurements from all the sensors for all test runs. Based on the sensor locations as depicted in **Figures 4–7**, strain responses include shear induced tension, shear induced compression, and flexure induced tension and compression. For the concerned dapped-end, measurements from strain sensors placed along shear induced tension diagonal were chosen as the parameter for capturing possible non-linear behavior or onset of failure due to shear. **Figure 10** illustrates plots of total test load vs. peak strain along shear-induced tension diagonal at the dapped end for single truck and two-truck side-by-side test runs. The test load is represented in gross vehicle weight (GVW) in the left plot and tandem axle weight (TAW) in the right plot. In general, TAW requires separate examination for short spans with respect to the vehicle length and where key responses of concern, such as shear (or reaction) at the support, are sensitive to axle loads.

In the load vs. response plots, the slope of the line between any two adjacent data points represents the girder stiffness in terms of load increase relative to strain increase. For linear-elastic

TABLE 1 | Maximum shear force (V_{max}) in a 53'-71/2'' simple span due to different rating vehicles.

Vehicle	Type	GVW	Axle configuration (weight in K = kips & spacing in ' = ft)	V_{max} (K)
HL93 (Truck)	Design	72K	8K (14.0') 32K (14.0') 32K	59.47
H20	Legal	40K	8K (14.0') 32K	37.91
Type 3	Legal	50K	16K (15.0') 17K (4.0') 17K	43.06
Type 3S2	Legal	72K	10K (11.0') 15.5K (4.0') 15.5K (22.0') 15.5K (4.0') 15.5K	47.01
Type 3-3	Legal	80K	12K (15.0') 12K (4.0') 12K (15.0') 16K (16.0') 14K (4.0') 14K	44.43
SU4	Legal	54K	12K (10.0') 8K (4.0') 17K (4.0') 17K	47.51
SU5	Legal	62K	12K (10.0') 8K (4.0') 8K (4.0') 17K (4.0') 17K	52.83
SU6	Legal	69.5K	11.5K (10.0') 8K (4.0') 8K (4.0') 17K (4.0') 17K (4.0') 8K	55.94
SU7	Legal	77.5K	11.5K (10.0') 8K (4.0') 8K (4.0') 17K (4.0') 17K (4.0') 8K (4.0') 8K	58.76

Test Truck 'A' Weights

No.	Axle (lbs)			Vehicle (K)
1	18,760	25,020	25,060	68.84
2	21,960	28,460	28,600	79.02
3	24,180	31,640	32,420	88.24
4	27,100	38,440	36,180	101.72

19'-6"   4'-6"

Test Truck 'B' Weights

No.	Axle (lbs)			Vehicle (K)
1	22,630	23,800	21,860	68.29
2	24,640	27,960	26,840	79.44
3	23,160	33,540	31,660	88.36
4	25,140	43,060	32,180	100.38

20'-8"   4'-4"
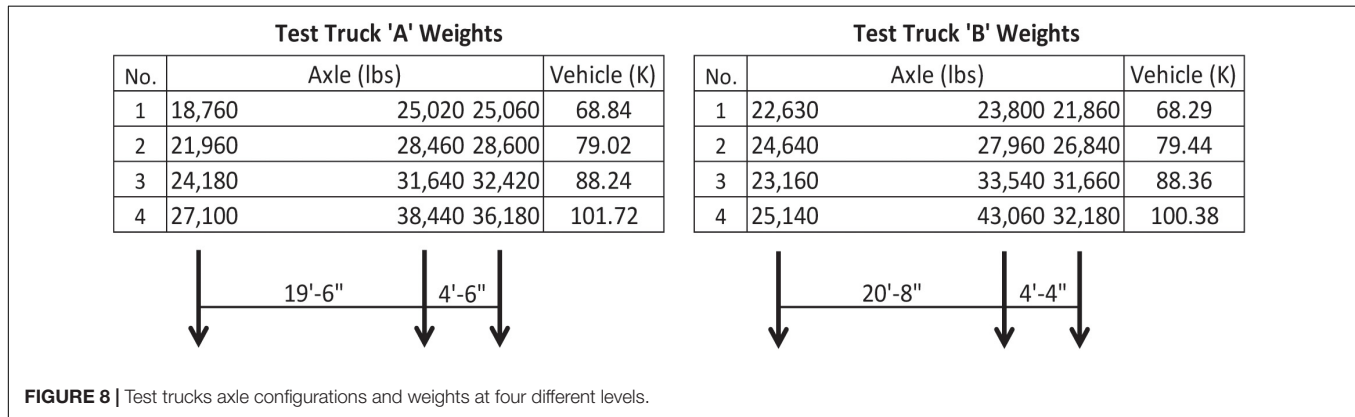
FIGURE 8 | Test trucks axle configurations and weights at four different levels.

TABLE 2 | Descriptions of 13 test runs at weight level no. 2 (WL#2).

Test run no.	Weight level	Test truck position and combination					Speed	Travel direction
		Lane 1	Lane 2	Lane 3	Lane 4	R. Shldr		
14	No. 2	Truck A					Crawl (5 MPH)	Forward WB
15			Truck B					
16				Truck A				
17					Truck B			
18						Truck A		
19		Truck A	Truck B					
20			Truck A	Truck B				
21				Truck A	Truck B			
22					Truck A	Truck B		
23		Truck A					Speed Limit (55 MPH)	
24			Truck B					
25				Truck A				
26					Truck B			

structural behavior, strain responses are expected to increase linearly with load increase. Particular attention should be paid to any noticeable decrease of the slope with the increase of test load, as this may be an indication of structural stiffness decrease due to non-linear structural behavior, distress, or onset of failure.

In bridge field testing, the test vehicles actual lateral position may change slightly among comparable test runs at different weight levels. This results in slightly different load distribution among girders as reflected in some sensor plots in **Figure 10**, where the slope of the line changes between load increments.

Lateral shifting of test vehicle position at different weights generally causes opposite slope changes in adjacent girders. Non-linear structural behavior or onset of failure would cause consistent slope decreases from multiple sensors which may worsen with further load increase. An effective method for canceling the effect of test vehicle lateral shifting is to plot an average response of multiple sensors mounted on adjacent girders directly under the test load. The red dashed lines in **Figure 10** (Top) are the average of four strain sensors on both webs of Girders B and C; the red dashed lines in **Figure 10** (Bottom) are

FIGURE 9 | Photos of loading and weighing test trucks and operating test runs.

the average of six strain sensors on both webs of Girders B, C and D. Each of the average plots clearly indicated linear response with increasing test load.

Confirmation of linear elastic structural behavior for a proof load test also requires examining the zero return of all sensors after each unloading and the magnitudes of strain and deflection measurements in comparison of material properties or analytical predictions. The strain time histories of all 44 test runs exhibited smooth and distinctive responses to the crossings of the test vehicles and their axles. All strain responses returned to zero after unloading at the end of each test run. The maximum measured strain was 198 micro-strain (corresponding to 798 psi for the concrete compressive strength of $f'_c = 5{,}000$ psi) along the tension diagonal on the north face of Girder E during Test Run 41 with two-truck side-by-side crossing Lanes 1 and 2.

VEHICLE LOADING DYNAMIC IMPACT

Dynamic impact due to vehicle loading was assessed by comparing strain responses from the same sensors between the crawl speed and highspeed test runs of the same test truck of the same weight in the same lateral position. An impact factor (I) was calculated by dividing the peak response from a highspeed run by that from the corresponding crawl speed run. Field measured I values were calculated for the most heavily loaded girders within each pair of test runs from the sensors measuring the

effects of shear and flexure, respectively. For shear effects at the dapped end, the average of strain measurements on both sides of the girder web along the respective compression (Com) and tension (Ten) diagonal was used for assessing vehicle dynamic impact. Highspeed runs were conducted in all four travel lanes at WL#1 and WL#2 but not at WL#3 and WL#4 for safety reasons and not to cause damages to the test trucks. Results of field measured impact factors (I) from the load test are summarized in **Table 3**.

As shown in **Table 3**, the highest I value was 1.08 for shear and 1.15 for flexure in the test span, respectively, from strain sensors along the compression diagonal at the dapped end of Girder E and on the bottom flange at the mid-span of Girder E. Many I values were calculated less than 1.0 from field measurements due to possible reasons of lateral vehicle position shifting between the crawl and highspeed runs, effects of vibration, etc. In order to properly assess vehicle loading dynamic impact, it is important to use sensor measurements from bridge elements directly loaded by the test vehicles and repeat highspeed runs when possible.

Based on field observed good condition of the deck and joints throughout the bridge, it was recommended to use an impact factor (I) of 1.10 for shear and 1.20 for flexure for load rating in its current condition. These values are in agreement with the AASHTO MBE for reducing the Dynamic Load Allowance (IM) to 10% for smooth riding surface at approaches, bridge deck, and expansion joints and 20% for minor surface deviations or depressions.
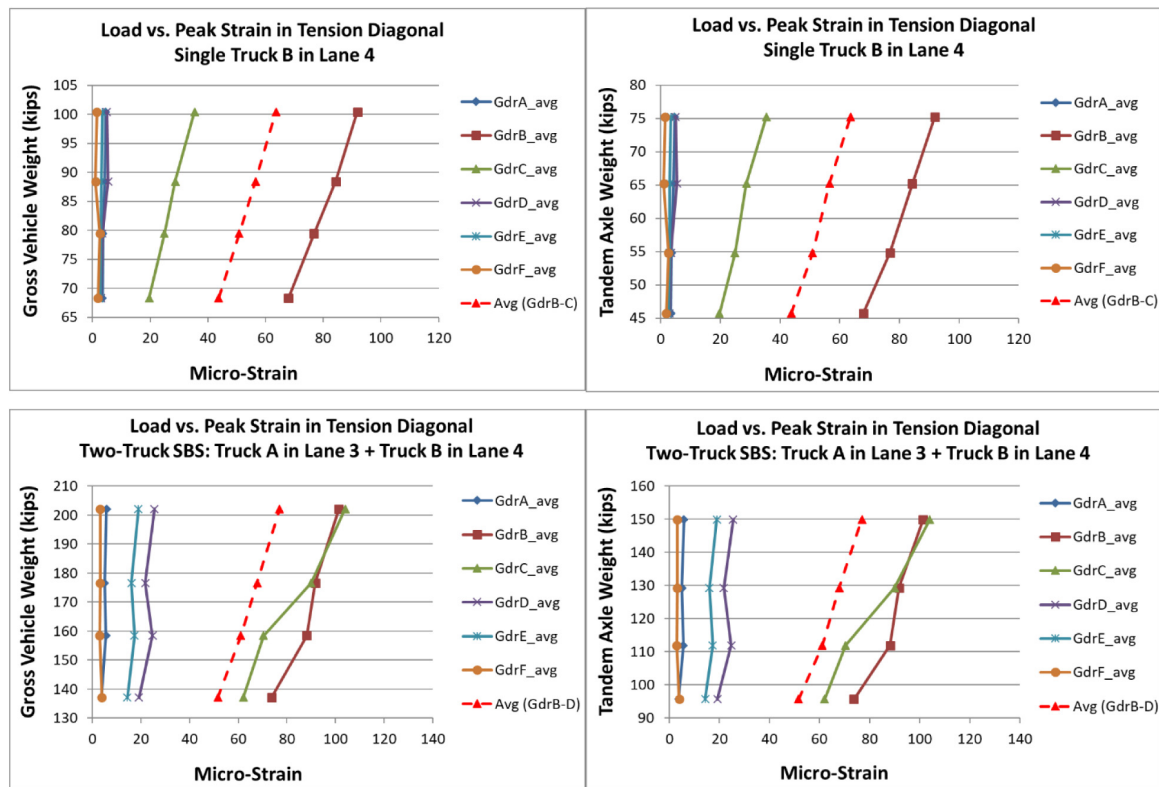
FIGURE 10 | Load vs. peak strain in tension diagonal of dapped end: single truck B in lane 4 test runs **(top)** and two-truck side-by-side test runs, truck A in lane 3 & truck B in lane 4 **(bottom)**.

DECK-GIRDER COMPOSITE ACTION

Strain measurements from the sensors installed on the girder top and bottom flanges for flexural effects showed very low compressive strains in the top flange compared to the tensile strains in the bottom flange of the same girder section throughout the load test at both the mid-span and a section 5 ft from the support. This clearly indicated full deck-girder composite action, including in the dapped-end region, at all the test load levels. This finding is important because it disapproved an assumption in the rating analysis which assumes the shear resistance in the dapped end is supplied by the stirrup reinforcement and draped prestressing strands in the girder without any participation of the deck or the reinforcing steel in and surround it.

BRIDGE LOAD RATING BASED ON PROOF TEST RESULTS

A lower-bound bridge load rating for a rating vehicle, depending on the load rating method and level, can be determined using the following equation based on the proof test results:

$$RF_P = (k_O)(W_P/W_R)(f_V)/[(\gamma_{LL})(1 + IM)] \qquad (2)$$

where:

RF_P = a lower-bound rating factor for a rating vehicle based on a proof load test.

k_O = proof load test termination factor per AASHTO *MBE* (1.00 for reaching target load without distress; 0.88 for test aborted due to distress before reaching target load).

W_R = gross vehicle weight (GVW) of rating vehicle.

W_P = final GVW of test vehicle upon completion of proof load test.

f_V = vehicle adjustment factor = W_{eq}/W_P, where

W_{eq} = equivalent GVW of rating vehicle for the same force effect of test truck.

γ_{LL} = live load factor for specific load rating levels per AASHTO *MBE* (see **Table 4**).

IM = dynamic load allowance per AASHTO *MBE*.

Bridge load ratings derived from a proof load test vary with the live load factor (γ_{LL}) of the load rating method and level as shown in **Table 4**. **Table 5** illustrates calculated lower-bound load ratings (RF_P) of the I-195 WB bridge based on the proof test results for four different legal vehicles using Eq. (2), **Table 4**, and the dynamic load allowance discussed previously. The upper and lower portions of **Table 5** provide LRFR Legal load ratings for ADTT $\leq 1,000$ ($\gamma_{LL} = 1.30$) and ADTT $\geq 5,000$ ($\gamma_{LL} = 1.45$), respectively; linear interpolations can be made for any ADTT in between. In **Table 5**, $W_P = 101.7$ kips upon successful completion of proof load test without any signs of distress, thus $k_O = 1.00$. For

TABLE 3 | Vehicle loading impact factor (I) from field measurements.

Test Run Pair No.	Vehicle ID	Lateral Position	GVW (K)	Speed (MPH)	Girder A Com	Girder A Ten	Girder B Com	Girder B Ten	Girder C Com	Girder C Ten	Girder D Com	Girder D Ten	Girder E Com	Girder E Ten	Girder F Com	Girder F Ten	E End	Girder E Mid-Sp	Gdr F Mid-Sp
1 & 10	Truck A	Lane 1	68.84	45	–	–	–	–	–	–	–	–	0.96	0.95	0.97	0.96	0.87	0.96	0.92
14 & 23			79.02	55	–	–	–	–	–	–	–	–	0.92	1.00	0.82	0.87	0.93	1.01	0.87
2 & 11	Truck B	Lane 2	68.29	55	–	–	–	–	–	–	0.97	0.99	**1.08**	1.04	–	–	0.93	**1.15**	–
15 & 24			79.44	55	–	–	–	–	–	–	1.00	0.98	0.88	0.94	–	–	0.97	0.93	–
3 & 12	Truck A	Lane 3	68.84	35	–	–	–	–	1.03	1.01	0.81	0.85	–	–	–	–	–	–	–
16 & 25			79.02	55	–	–	–	–	1.06	1.04	0.66	0.73	–	–	–	–	–	–	–
4 & 13	Truck B	Lane 4	68.29	55	–	–	0.97	0.96	0.94	0.93	–	–	–	–	–	–	–	–	–
17 & 26			79.44	55	–	–	0.98	1.05	0.57	0.65	–	–	–	–	–	–	–	–	–

Bold values indicate maximum value of I due to Flexure and Shear.

TABLE 4 | Live Load Factor (γ_{LL}) for AASHTO LRFR and LFR Methods.

Load Rating Method	Load Rating Level	Live Load Factor γ_{LL}	AASHTO MBE
Load and resistance factor rating (LRFR)	Design inventory	1.75	Table 6A.4.3.2.2-1
	Design Operating	1.35	
	Legal	1.45 (ADTT ≥ 5,000)	Table 6A.4.4.2.3a-1 (linear interpolation)
		1.30 (ADTT ≤ 1,000)	
	Permit	1.10 to 1.40	Table 6A.4.5.4.2a-1
Load factor rating (LFR)	Inventory	2.17	Article 6B.4.3
	Operating	1.3	

each rating vehicle, an equivalent gross vehicle weight W_{eq} was calculated for producing the same maximum bending moment (M_{max}) and maximum shear force (V_{max}), respectively, from a line beam structural analysis of 53′-7″ simple span.

Based on the proof load test results discussed, the bridge was physically proven to have load ratings equal to or higher than the lower-bound load ratings as shown in **Table 5**.

ANALYTICAL ASSESSMENT OF SHEAR RESISTANCE OF DAPPED END

Two analytical methods were used to assess the nominal shear resistance of the dapped end: the strut-and-tie (S-T) and the shear-friction (S-F) methods.

Strut-and-Tie (S-T) Method

The S-T method models the flow of forces in 'D-regions' near discontinuities for the design of reinforced or prestressed concrete members (Collins and Mitchell, 1986; Schlaich et al., 1987). Discontinuities may be caused by abrupt changes in member geometry (e.g., dapped ends or openings) or by concentrated forces such as reactions or post-tension anchorages. In contrary, 'B-regions' are for bending where planar sections can be assumed to remain plane after loading and shear stresses reasonably uniform over the effective web area. For B-regions, the conventional sectional design approach is sufficient without addressing how the forces are introduced into the member. In D-regions, however, the stress flows are disturbed; planar sections do not remain plane and shear stresses are not uniform over the effective shear area; and S-T modeling serves as an effective design method (Mitchell et al., 2004; AASHTO, 2017).

It is important to understand that strut-and-tie (S-T) modeling is a conservative design method when the conventional sectional models become invalid. It is a "lower bound approach" for minimizing the amount of reinforcement through postulating a number of different S-T models that all provide safe paths for the loads to reach the supports (Mitchell et al., 2004). S-T modeling simplifies the highly complicated load paths

TABLE 5 | Lower-bound bridge load ratings derived from proof test results.

Load Ratings of LRFR Legal ADTT < 1,000

$k_0 = 1.00$		$\gamma_{LL} = 1.30$		Flexure					Shear				
Rating VehicleType		W_R (kips)	RF_P	M_{max} (k-ft)	W_{eq} (kips)	f_V	IM	$(RF_p)_M$	V_{max} (kips)	W_{eq} (kips)	f_V	IM	$(RF_p)_V$
'Truck A'	Testing	101.7		1019.8	101.7	1.00			86.1	101.7	1.00		
H-15	Legal	30	1.96	361.0	84.7	0.83	10%	1.98	28.2	91.7	0.90	20%	1.96
Type 3		50	1.29	518.8	98.3	0.97	10%	1.37	42.8	100.7	0.99	20%	1.29
HS-20		72	0.94	689.6	106.5	1.05	10%	1.03	58.9	105.3	1.04	20%	0.94
SU7		77.5	0.92	774.8	102.0	1.00	10%	0.92	58.9	113.2	1.11	20%	0.94

Load Ratings of LRFR Legal ADTT = 5,000

$k_0 = 1.00$		$\gamma_{LL} = 1.45$		Flexure					Shear				
Rating VehicleType		W_R (kips)	RF_P	M_{max} (k-ft)	W_{eq} (kips)	f_V	IM	$(RF_p)_M$	V_{max} (kips)	W_{eq} (kips)	f_V	IM	$(RF_p)_V$
'Truck A'	Testing	101.7		1019.8	101.7	1.00			86.1	101.7	1.00		
H-15	Legal	30	1.76	361.0	84.7	0.83	10%	1.77	28.2	91.7	0.90	20%	1.76
Type 3		50	1.16	518.8	98.3	0.97	10%	1.23	42.8	100.7	0.99	20%	1.16
HS-20		72	0.84	689.6	106.5	1.05	10%	0.93	58.9	105.3	1.04	20%	0.84
SU7		77.5	0.83	774.8	102.0	1.00	10%	0.83	58.9	113.2	1.11	20%	0.84

in D-regions into a straight-line truss model consisting of concrete compressive struts, steel tension ties, and nodes. It then determines their respective factored resistances based on the geometrical and strength properties of reinforcing steel, prestressing steel, concrete, as well as development or anchorage of steel elements in concrete. The S-T method is subjective to some degree as it requires visualization of stress flows and discretion in assembling and detailing an idealized truss model.

Figure 11 illustrates a strut-and-tie model for the I-195 WB bridge dapped end, where the blue lines represent compression struts and red lines for tension ties. Shear resistance of the dapped end is governed by the tension resistance of vertical tie BC, which consists of contributions from non-prestressed stirrup reinforcement made of ASTM standard No. 9 reinforcing bars of 40 ksi yield strength and draped prestressing strands made of ASTM standard Grade 250, 0.5 in. diameter seven-wire prestressing strands.

Nominal shear resistance of the dapped end (R_{nV}) from the S-T method is calculated as follows (AASHTO, 2018):

$$R_{nV} = R_{nV,st} + R_{nV,ps} \tag{3}$$

$$R_{nV,st} = f_y A_{st} \tag{4}$$

$$R_{nV,ps} = (A_{ps})(f_{pe} + f_y) sin(\beta) \tag{5}$$

where:

$R_{nV,st}$ = nominal tension resistance of stirrup reinforcement.
$R_{nV,ps}$ = vertical component of compression force from draped prestressing strands.
A_{st} = area of four (4) sets of double-leg stirrups = (4) (2) (1.00 in^2) = 8.0 in^2.
A_{ps} = area of prestressing steel = (2) (0.144 in^2) = 0.288 in^2.

f_y = yield strength of non-prestressed reinforcement (ksi) = 40 ksi.
f_{pe} = effective stress in prestressing steel after losses = (0.6) (250 ksi) = 150 ksi.
β = angle of draped prestressing strands with respect to horizontal axis = 7°.

Thus, $R_{nV,st} = (8.0\ in^2)\ (40\ ksi) = 320$ kips

$R_{nV,ps} = (0.288\ in^2)\ (150\ ksi + 40\ ksi)\ sin(7°) = 6.67$ kips
$R_{nV} = R_{nV,st} + R_{nV,ps} = 320$ kips $+ 6.67$ kips $= 326.67$ kips

Shear-Friction (S-F) Method

The S-F method is used to determine the shear strength along a specific shear failure plane such as an existing or potential crack in monolithic concrete or an interface between two concretes cast at different times (Birkeland and Birkeland, 1966; Mattock and Hawkins, 1972). The S-F concept assumes the shear resistance to be provided by the dowel action of the reinforcement across the shear failure plane and the friction resulting from the sliding movement of the crack faces under the clamping force from the reinforcement in tension to its yield strength. Any permanent net compression due to properly developed prestressing strands across the shear plane is also added to the force in the shear-friction reinforcement.

For the I-195 WB bridge dapped end, the shear-friction crack plane may be assumed at a 45° angle initiating from the re-entrant corner, as shown by the purple dashed line in **Figure 11**. Similar to Equation (3), nominal shear resistance of the dapped end (R_{nV}) consists of the vertical component of shear resistance along the assumed shear plane due to shear-friction of vertical stirrups ($R_{nV,st}$) and that due to the draped prestressing
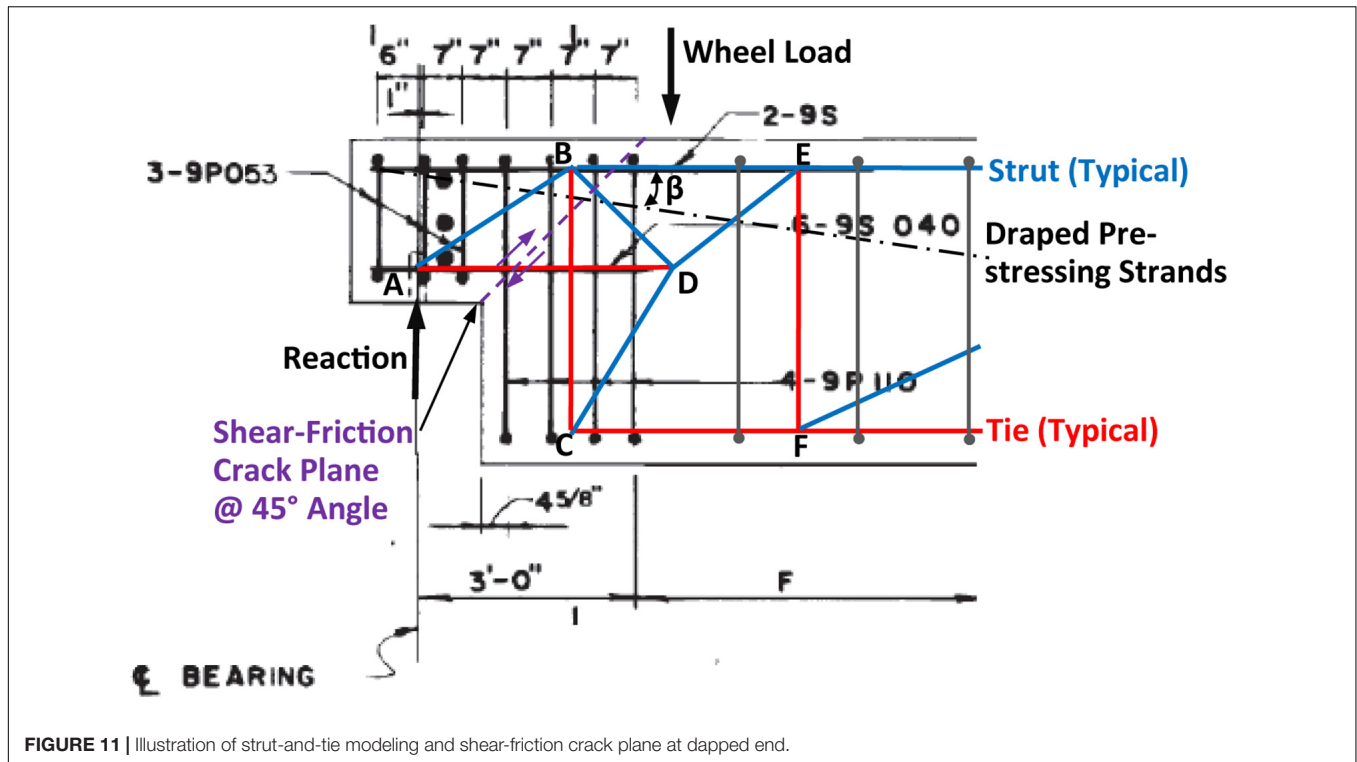
FIGURE 11 | Illustration of strut-and-tie modeling and shear-friction crack plane at dapped end.

strands ($R_{nV,ps}$) (Mattock, 1974; Mattock, 1977; AASHTO, 2002; ACI, 2019):

$$R_{nV,st} = A_{vf}f_y[\mu sin(\alpha) + cos(\alpha)]sin45° \quad (6)$$

$$R_{nV,ps} = A_{ps}f_{pe}[\mu sin(45° + \beta) + cos(45° + \beta)]sin45° \quad (7)$$

where:

A_{vf} = Area of three (3) sets of double-leg stirrups = (6) (1.00 in^2) = 6.0 in^2.
α = angle between shear-friction reinforcement and shear plane = 45°.
45° + β = angle between prestressing strands and shear plane = 45° + 7° = 52°.
μ = coefficient of friction depending on contact surface condition.
 = 1.4λ for concrete placed monolithically (λ = 1.0 for normal weight concrete) = 1.4.

Thus, $R_{nV,st}$ = (6.0 in^2) (40 ksi) [(1.4) (sin45°) + cos45°] sin45° = 288 kips

$R_{nV,ps}$ = (0.288 in^2) (150 ksi) [(1.4) (sin52°) + cos52°] sin45° = 52.51 kips
R_{nV} = $R_{nV,st}$ + $R_{nV,ps}$ = 288 kips + 52.51 kips = 340.51 kips

Comparing the results from the two analytical methods indicates: (1) the S-F method yields slightly (4%) higher shear resistance than the S-T method; (2) shear resistance

from the S-T method has a higher contribution from non-prestressed reinforcement because vertical tie BC consists of four sets of stirrups while the shear-friction crack plane only involves three sets of stirrups; and (3) shear resistance from the S-F method has a higher contribution from the draped prestressing strands. In the S-F method, both layers of horizontal reinforcement across the shear plane cannot be included for shear resistance because they are subject to compression due to shear slippage (ACI, 2019).

It is important to point out that each method establishes an analytical shear resistance based on a hypothetical failure mode and resistance mechanism. Neither method considers the effects of an 8.5 in. thick reinforced concrete deck in distributing and resisting shear, which are likely the main reason for why analytical load ratings underestimated the shear capacity of the dapped end.

SUMMARY AND CONCLUSION

For a prestressed concrete girder bridge with insufficient analytical load ratings governed by shear at the dapped ends, a proof load test was successfully completed in four loading and unloading steps with a maximum proof load of two test trucks of approximately 100,000 lbs each crossing the bridge side-by-side. The load test consisted of 44 test runs with the use of 32 strain sensors. No signs of distress or non-linear behavior were observed throughout the process.

The following findings and conclusions are made from this study:

(1) Proof load testing has a higher level of reliability than diagnostic testing in assessing structural capacity because it includes the effects of full dead load plus a magnified live load and minimizes uncertainties in calculating structural capacities. However, proof testing requires more complex field operations and involves a higher level of risks.

(2) In a proof load test, sensors must be placed at locations that can capture possible signs of distress, non-linear behavior, or onset of failure of the structure.

(3) Key factors in determining a target proof load include a desired or target load rating, available test vehicles, comparison of the governing force effect between the rating vehicle and the test vehicle, number and weight capacities of test vehicles to be used, etc.

(4) Test runs of increasing load need to be arranged to apply direct loads to all primary load carrying elements, utilize a variety of crossing patterns for different load effects, repeat the same crossing patterns at all weight levels, and make pairs of slow speed and highspeed test runs for assessing vehicle loading dynamic impact.

(5) Plots of key sensor responses vs. increasing test load, in combination with examination of zero returns and the magnitudes of strain and deflection measurements, serve as an effective method for assessing linear elastic behavior of the structure and capturing possible signs of distress or onset of failure.

(6) Vehicle dynamic impact can be assessed by comparing strain responses from the same sensors between the crawl speed and highspeed test runs of the same test truck of the same weight in the same lateral position. Only sensor measurements from bridge elements directly loaded by the test vehicles should be used for this purpose. Highspeed test runs should be repeated when possible for increased reliability.

(7) Lower bound bridge load ratings can be derived from the results of a proof load test using Eq. (2) depending on the load rating method and level as needed.

(8) Test results suggested that analytical methods of strut-and-tie and shear-friction underestimate the shear resistance of the dapped ends by considering only the stirrup reinforcement and draped prestressing strands within the PSC girder. Effects of a composite reinforced concrete deck in distributing and resistant shear are likely the main reason for why analytical load ratings underestimated the shear capacity of the dapped end.

(9) *The Manual for Bridge Evaluation* of AASHTO contains conceptual guidelines for determining bridge load rating through proof load testing. This paper provides detailed procedures for field implementation, test results interpretation, and load rating derivation.

(10) It is important to note that proof load test results are valid only upon the structural condition at the time of load test. A re-evaluation may be required if any significant changes or deteriorations occur in the superstructure or the substructure.

DATA AVAILABILITY STATEMENT

The raw data supporting the conclusions of this article will be made available by the authors, without undue reservation, to any qualified researcher.

AUTHOR CONTRIBUTIONS

YZ and MG performed all the testing and analytical work discussed in this manuscript. YZ wrote the majority of the manuscript with assistance from MG for the development of tables and figures. Both authors contributed to the article and approved the submitted version.

ACKNOWLEDGMENTS

The authors would like to express their acknowledgments to Mr. Corey Richard of AECOM for his efforts in project management and field testing coordination; Mr. Michael Sullivan, formerly of AECOM, for his efforts during field testing and data processing; and Mr. Stephen Matty of AECOM for his supports in the strut-and-tie and shear friction methods of analysis.

REFERENCES

AASHTO (2002). *Standard Specifications for Highway Bridges*, 17th Edn, Washington, DC: American Association of State Highway and Transportation Officials.

AASHTO (2017). *AASHTO LRFD Bridge Design Specifications*, 8th Edn, Washington, DC: American Association of State Highway and Transportation Officials.

AASHTO (2018). *The Manual for Bridge Evaluation*, 3rd Edn, Washington, DC: American Association of State Highway and Transportation Officials.

ACI (2019). *Building Code Requirements for Structural Concrete, ACI 318-19*. Naples, FL: American Concrete Institute.

Birkeland, P. W., and Birkeland, H. W. (1966). Connections in precast concrete construction. *ACI J. Proc.* 63, 345–368.

Collins, M. P., and Mitchell, D. (1986). A rational approach to shear design – the 1984 canadian code provisions. *ACI J.* 83, 925–933.

Fu, G., and Tang, J. (1995). Risk-based proof-load requirements for bridge evaluation. *J. Structut. Eng.* 121, 542–556. doi: 10.1061/(asce)0733-9445(1995)121:3(542)

Lantsoght, E. O. L. (ed.) (2019). *Proof Load Testing and the Future of Load Testing, (Structures and Infrastructures)*. Boca Raton, FL: CRC Press.

Lantsoght, E. O. L., van der Veen, C., Hordijk, D. A., and de Boer, A. (2017). Development of recommendations for proof load testing of reinforced concrete slab bridges. *Eng. Struct.* 152, 202–210. doi: 10.1016/j.engstruct.2017.09.018

Mattock, A. H. (1974). Shear Transfer in Concrete Having Reinforcement at an Angle to the Shear Plane, Shear in Reinforced Concrete, SP-42. Farmington Hills, MI: American Concrete Institute.

Mattock, A. H. (1977). Discussion of considerations for the design of precast concrete bearing wall buildings to withstand abnormal loads, by

PCI committee on precast concrete bearing wall buildings. *PCI J.* 22, 105–106.

Mattock, A. H., and Hawkins, N. M. (1972). Shear transfer in reinforced concrete—recent research. *PCI J.* 17, 55–75. doi: 10.15554/pcij.03011972.55.75

Mitchell, D., Collins, M. P., Bhide, S. B., and Rabbat, B. G. (2004). *AASHTO LRFD Strut-and-Tie Model Design Examples.* New York, NY: Portland Cement Association.

Schlaich, J., Shafer, K., and Jennewein, M. (1987). Towards a consistent design of reinforced Concrete Structures. *PCI J.* 32, 77–150.

TRB (1998). *Manual for Bridge Rating through Load Testing. NCHRP Research Results Digest No. 234.* Washington, DC: Transportation Research Board.

TRB (2019). *Primer on Bridge Load Testing. Transportation Research Circular E-C257.* Washington, DC: Transportation Research Board.

Advantages of publishing in Frontiers

OPEN ACCESS
Articles are free to read
for greatest visibility
and readership

FAST PUBLICATION
Around 90 days
from submission
to decision

HIGH QUALITY PEER-REVIEW
Rigorous, collaborative,
and constructive
peer-review

TRANSPARENT PEER-REVIEW
Editors and reviewers
acknowledged by name
on published articles

Frontiers
Avenue du Tribunal-Fédéral 34
1005 Lausanne | Switzerland

Visit us: www.frontiersin.org
Contact us: info@frontiersin.org | +41 21 510 17 00

REPRODUCIBILITY OF RESEARCH
Support open data
and methods to enhance
research reproducibility

DIGITAL PUBLISHING
Articles designed
for optimal readership
across devices

FOLLOW US
@frontiersin

IMPACT METRICS
Advanced article metrics
track visibility across
digital media

EXTENSIVE PROMOTION
Marketing
and promotion
of impactful research

LOOP RESEARCH NETWORK
Our network
increases your
article's readership